University of Fort Hare
Together in Excellence

SEDIMENTARY, GEOCHEMICAL AND GEOPHYSICAL STUDY OF THE ECCA GROUP, KAROO SUPERGROUP AND ITS HYDROCARBON POTENTIAL IN THE EASTERN CAPE PROVINCE, SOUTH AFRICA

By

CHRISTOPHER BAIYEGUNHI

Thesis submitted in fulfilment of the requirement for the degree of
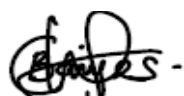
DOCTOR OF PHILOSOPHY

In

GEOLOGY

FACULTY OF SCIENCE AND AGRICULTURE
UNIVERSITY OF FORT HARE, SOUTH AFRICA

SUPERVISOR: PROFESSOR KUIWU LIU
CO-SUPERVISOR: PROFESSOR OSWALD GWAVAVA

SEPTEMBER, 2017

DECLARATION

I, Christopher Baiyegunhi, declare that this thesis entitled "Sedimentary, geochemical and geophysical study of the Ecca Group, Karoo Supergroup and its hydrocarbon potential in the Eastern Cape Province, South Africa" to be my own unaided work. The research reported in this thesis, except where otherwise indicated, contain the original research results and has not been previously accepted or concurrently submitted to any other university for any degree award or examination purposes.

24/08/2017

…………………………………….   ………………….

      Christopher Baiyegunhi   Date

   University of Fort Hare, Alice

DECLARATION ON PLAGARISM

I, Christopher Baiyegunhi with student number 201201530 declare that I am fully aware of the University of Fort Hare's policy on plagiarism and I have taken every precaution to comply with the regulations. Where other written sources have been quoted, their words have been cited and the general information attributed to them is appropriately referenced.
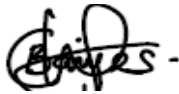
24/08/2017

………………………………………….   ………………….

Christopher Baiyegunhi   Date

University of Fort Hare, Alice

DECLARATION ON RESEARCH ETHICS CLEARANCE

I, Christopher Baiyegunhi with student number 201201530 declare that I am fully aware of the University of Fort Hare's policy on research ethics, and I have taken every precaution to comply with the regulations. I confirm that my research constitutes an exemption to Rule G17.6.10.5 and an ethical certificate with a reference number is not required.

24/08/2017

……………………………………….   ………………….

Christopher Baiyegunhi   Date
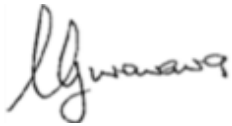
University of Fort Hare, Alice

CERTIFICATION

This thesis titled "Sedimentary, geochemical and geophysical study of the Ecca Group, Karoo Supergroup and its hydrocarbon potential in the Eastern Cape Province, South Africa" meets the regulation governing the award of degree of Doctor of Philosophy of the University of Fort Hare and is approved for its contribution to scientific knowledgement.

25/08/2017

…………………………………………….   ………………….

Prof Kuiwu Liu (Main Supervisor)   Date

25/08/2017

…………………………………………..   ………………….

Prof Oswald Gwavava (Co-supervisor)   Date

DEDICATIONS

This research work is dedicated to God Almighty (giver of life and wisdom) and in blessed memory of my wonderful parents, Late (Mr) and Late (Mrs) D. F. Baiyegunhi.

"A man's heart plans his way, but the LORD directs his steps"

Proverbs 16:9 (KJV)

ACKNOWLEDGEMENTS

First and foremost, I would like to acknowledge God Almighty for His constant source of strength, wisdom, guidance, inspiration and immeasurable blessings, without Him this would not have been possible.

I would also like to express my profound gratitude to my main supervisor, Prof K. Liu for his constructive and insightful comments, remarks and engagements through the learning process in this study. I could not have imagined having a better supervisor for my PhD program. Your persistence, understanding and kindness have really thought me so many things in life. In addition, your guidance has helped me throughout the period of my research and write-up. I wish I could express my heartfelt thankfulness beyond what pen could write and what mouth could say. Likewise, I will forever be indebted and grateful to Prof O. Gwavava for providing me with the opportunity to join this prestigious, dynamic and renowned department (Geology Department) and for his motivation, enthusiasm, immense knowledge and contribution towards my success in life. Without your unalloyed support and unparalleled supervision, this great feat would not have been attained. In it all, I owe my supervisors eternal gratitude.

"A teacher affects eternity; he can never tell where his influence stops"

Special thanks to Dr K. Madi (HOD), Mr C.J. Gunter, Mrs V. Mazomba, Mr L. Sigabi, Mr M. Katwire and to all the Geology postgraduate students (2015-2017), especially Zusakhe, Siphokazi, Washington, Nemanashi, Ndlovu, Chima, Nike, Sinesihle, Mimi, Liso, Sipo and Takalimana (PC), just to mention a few, you all are appreciated.

I am indeed grateful and appreciative to all my family members particularly Dr/Dr (Mrs) L.J.S. Baiyegunhi for showing me the road to South Africa, Mr/Mrs Johnson Baiyegunhi, Mr/Mrs Oluwole Owoleke, Mr/Mrs Peter Baiyegunhi, Bidemi Baiyegunhi and Mrs B.B. Asiwaju for their love, care and support at all time. Praise, Melody, Victor, Victory, Desmond and Favour are also appreciated. I am equally grateful to my cousin Dr F.K. Okaiyeto for his encouragement and setting the pace; thanks for always been there for me both in the desert and forest. Thanks to Mrs Florence Okaiyeto for taking very good care of my cousin. This section would not be complete without a special and golden appreciation to my one and only jewel (my wife), Mrs Temitope Love Baiyegunhi for her immeasurable love, encouragement, patience and support. You are indeed a source of inspiration and

ABSTRACT

The Ecca Group of Karoo Supergroup is a sedimentary rock sequence that deposited between the Late Carboniferous (Dwyka Group) and the Late Permian-Middle Triassic (Beaufort Group). The Ecca Group investigated in this study is situated in the Eastern Cape Province of South Africa and it comprises mainly of shales, mudstones, siltstones and sandstones. The Ecca Group sequence contains considerable carbon content and suitable thickness to make it an ideal target for shale gas exploration. Previous studies put more emphasis on the geology and stratigraphy of the Ecca Group, this study revised the stratigraphy, and put new insight on the petrography, depositional processes, sedimentary facies, provenance, paleoweathering, tectonic setting, subsidence rates and history, electrical resistivity, source rock characteristics and diagenesis of the potentially feasible sandstone and mudrock reservoir rocks of the Ecca Group.

Based on the lithological features, sedimentary structures and facies characteristics, the stratigraphy of the Prince Albert, Whitehill, Collingham and Fort Brown Formations of the Ecca Group is now subdivided into two informal members each, i.e. Lower Member and Upper Member. Furthermore, the Ripon Formation is now subdivided into three informal members. Each member has been asigned a lithological name.

The grain size parameters show that most of the Ecca Group sandstones are very fine to fine grained, poorly to moderately well sorted, mostly near-symmetrical and mesokurtic in grain-size distribution. The linear discriminant function analysis is dominantly indicative of turbidity current deposits under deep marine environment for Prince Albert, Whitehill and Collingham Formations, shallow marine environment for Ripon Formation, while the Fort Brown Formation is lacustrine-deltaic deposits.

Modal composition analysis and petrography studies revealed that the detrital components of the sandstones are dominated by monocrystalline quartz, feldspar and lithic fragments. The sandstones are compositionally and texturally immature and can be classified as feldspathic wacke and lithic wacke. The provenance analysis revealed plutonic and metamorphic terrains as the main source rocks with minor debris derived from recycled sedimentary rocks. The detrital modal compositions of these sandstones are related to back arc to island and continental margin of tectonic setting.

Based on the detailed sedimentological analyses of outcrop and borehole data, fourteen lithofacies were identified and seven facies associations (FAs) were recognised. The facies

associations are: FA 1: Shale and mudstones intercalated with siltstones, FA 2: Carbonaceous shale, mudstone with subordinate chert and sandstone, FA 3: Mudstones rhythmite with thin bedded mudstone and lenticular siltstone, FA 4: Greyish medium bedded sandstone intercalated with laminated mudstone, FA 5: Dark-grey medium to thick bedded mudstone and siltstone, FA 6: Thin to medium bedded sandstone alternated with thin bedded carbonaceous mudstone, and FA 7: Varved mudstone rhythmite intercalated with siltstone and minor sandstone. Sedimentological characteristics of the identified facies associations indicate four deposition environments, namely, deep marine basin, turbidite, shallow marine and lacustrine environments, which constitute a gradually regression sequence as a result of sea-level dropping and shallowing of the basin during the developmental processes.

Geochemical analysis of the Ecca mudrocks and sandstones revealed that the rocks are of quartzose sedimentary provenance, suggesting that they were derived from a cratonic interior or recycled orogen. The petrography and geochemistry of the sandstones indicated that the source areas are composed of plutonic and metamorphic rocks with a minor component from sedimentary rocks. The geochemical diagrams and indices of weathering suggested that the granitic source rocks underwent moderate to high degree of chemical weathering. The tectonic setting discrimination diagrams support passive continental margin setting of the provenance.

The organic geochemistry results show that the shales have TOC ranging from 0.11 wt.% to 7.35 wt.%. About 98% of the samples have hydrogen index (HI) values of less than 50 mg HC/g TOC, indicating Type-IV kerogen, which is mostly derived from reworked organic matter with little or no potential for hydrocarbon generation. Tmax values range from 318 ℃ to 601℃, indicating immature to over-maturity of the samples. The vitrinite reflectance (Ro) values range from about 2.22% to 3.93%, pointing to over-maturity of the samples. Binary plot of HI versus Tmax and van Krevelen diagram shows that the shales are of Type II and mixed Type II-III kerogen, which are capable of generating both gas and minor oil.

The main diagenetic processes that have affected the rocks of the Ecca Group are cementation, mechanical compaction, recrystallization, replacement and dissolution. These processes are grouped into three stages, namely, early diagenesis, burial diagenesis and uplift-related diagenesis. The rocks of Ecca Group were subjected to moderate-intense mechanical and chemical compaction during its progressive burial. Intergranular pores, secondary dissolution and fractured pores are well developed in the Ecca Group. The

presence of fractured and dissolution pores tend to enhance reservoir quality. However, the isolated nature of the pore linkage makes them unfavourable producers of hydrocarbons, which at best would require stimulation and fracking.

The horizontal resistivity profiling (HRP) reveals that the resistivity of the subsurface varies laterally between 2 Ωm and 500 Ωm. The vertical electrical sounding (VES) curves indicate four to five geoelectric layers. The 2-D resistivity pseudosections reveal that the lower Ecca Group rocks are generally characterised by low resistivity compared to the upper Ecca Group rocks. With the exception of the Cookhouse section, all the measured sections have been intruded by dolerites. These dolerite intrusions could possibly act as barriers for fluid/groundwater migration as well as introduce technical difficulty in the drilling stage of the hydraulic fracturing process.

The average rate of sedimentation in the Prince Albert, Whitehill, Collingham, Ripon and Fort Brown Formations are calculated to be 0.017 mm yr^{-1}, 0.035 mm yr^{-1}, 0.03 mm yr^{-1}, 0.125 mm yr^{-1}, and 0.088 mm yr^{-1}, respectively. Three major subsidence episodes characterise the Ecca Group namely: (1) rapid subsidence in an extensional regime, (2) slow subsidence in the middle of basin development, and (3) another rapid subsidence in a compressional regime. The subsidence of the basin is believed to have been initiated and mainly controlled by mechanical (gravitational) loading and tectonic events, with little contribution of thermal events. The average rate of tectonic subsidence in the Prince Albert, Whitehill, Collingham, Ripon and Formations are 63 mMa^{-1}, 28 mMa^{-1}, 25 mMa^{-1}, 215 mMa^{-1}, and 180 mMa^{-1}, respectively. It is inferred that the southeastern Karoo Basin evolved from a passive continental margin into an Andean-type continental foreland basin; thus portraying a completely evolved post-rift setting along the southeastern Gondwana margin.

Keywords: Sedimentary, geochemical, geophysical, Ecca Group, hydrocarbon potential.

RESEARCH OUTPUT

The research outputs associated with this work are as follows:

1. **Christopher Baiyegunhi**, Kuiwu Liu and Oswald Gwavava (2017). Sedimentation rate and subsidence history of the Southeastern Karoo Basin, South Africa, using 1D backstripping method. Arabian Journal of Geosciences, 225 (10), 1379-1402. Doi: 10.1007/s12517-017-3009-x.

2. **Christopher Baiyegunhi**, Kuiwu Liu and Oswald Gwavava (2017). Diagenesis and reservoir properties of the Permian Ecca Group sandstones and mudrocks in the Eastern Cape Province, South Africa. Minerals, 88 (7), 1-26. Doi: 10.3390/min7060088.

3. **Christopher Baiyegunhi**, Kuiwu Liu and Oswald Gwavava (2017). Grain size statistics and depositional pattern of the sandstones of the Ecca Group, Karoo Supergroup in the Eastern Cape Province, South Africa. Open Geosciences. **Accepted (In press)**.

4. **Christopher Baiyegunhi**, Kuiwu Liu and Oswald Gwavava (2017). Modal composition and tectonic provenance of the sandstones of Ecca Group, Karoo Supergroup in the Eastern Cape Province, South Africa. Open Geosciences. **Accepted (In press)**.

5. **Christopher Baiyegunhi**, Kuiwu Liu and Oswald Gwavava (2017). Geochemistry of sandstones and shales from the Ecca Group, in the Eastern Cape Province of South Africa: Implication for provenance and tectonic setting. Open Geosciences. **Accepted (In press)**.

6. **Christopher Baiyegunhi**, Kuiwu Liu, Nicola Wagner and Oswald Gwavava (2017). Geochemical evaluation of the Permian Ecca shale in the Eastern Cape Province, South Africa: Implications for shale gas potential. Arabian Journal of Geosciences. **Accepted (In press)**.

7. **Christopher Baiyegunhi**, Kuiwu Liu and Oswald Gwavava (2017). Sedimentary facies and depositional environment of the Ecca Group, Karoo Supergroup in the Eastern Cape Province, South Africa. Open Geosciences. **Under Review**.

TABLE OF CONTENTS

LIST OF FIGURES

LIST OF TABLES

LIST OF ABBREVIATIONS AND ACRONYMS

Acc: Accessory minerals

ACM: Active Continental Margin

ASTM: American Society for Testing Materials

BSE: Back Scattered Electron

CFB: Cape Fold Belt

CIA: Chemical Index of Alteration

CIA: Continental Island Arc

CIW: Chemical Index of Weathering

EDX: Energy Dispersive X-ray Microanalysis

ENS: Effective Non-Source Field

FA: Facies Association

GPS: Global Positioning System

HFSE: High Field Strength Elements

HI: Hydrogen Index

HRP: Horizontal Resistivity Profiling

ICV: Index of Compositional Variability

LDF: Linear Discriminant Function

L: Lithic fragments

LILE: Large Ion Lithophile Elements

LOI: Loss on ignition

Ma: Million years

Mx: Matrix

NASC: North American Shale Composite

NNMB: Namaqua Natal Metamorphic Belt

OI: Oxygen Index

PAAS: Post Archaean Australian Shale

Pd: Potential Difference

PI: Production Index

PIA: Plagioclase Index of Alteration

PM: Passive Continental Margin

QFL: Quartz Feldspar Lithic fragments

QmFLt: Monocrystalline quartz Feldspar Total lithic fragments

QtFL: Total quartz Feldspar Lithic fragments

Qm: Monocrystalline quartz

Qp: Polycrystalline quartz

RMS: Root Mean Square

Ro: Vitrinite reflectance

Ro_c: Calculated Vitrinite Reflectance

Ro_m: Measured Vitrinite Reflectance

SACS: South African Committee of Stratigraphy

SEM: Scanning Electron Microscopy

SP: Hydrocarbon Potential

Tmax: Maximum Temperature

TOC: Total Organic Carbon

TTE: Transition Trace Elements

UCC: Upper Continental Crust

VES: Vertical Electrical Sounding

XRD: X-Ray Diffraction

XRF: X-Ray Fluorescence

CHAPTER 1
GENERAL INTRODUCTION

1.1 Location of the study area

The area investigated in this study is situated in the Eastern Cape Province of South Africa. Geographically, it lies between longitudes 24 ^{o} and 29 ^{o} E and between latitudes 32° and 34° S. The area is linked by two national roads (N2 and N10) and four regional roads (R67, R335, R344 and R350). The National road N2 between Grahamstown and East London connects to Peddie and N10 connects Paterson to Cookhouse. The Regional road R350 between Grahamstown and Bedford connect to Adelaide via Regional road R344 and the National road N2 between Grahamstown and East London connect to Fort Beaufort via Regional road R67 (Figure 1.1). The rocks outcropping in the study area mostly belong to the Cape and Karoo Supergroups. On vertical profiling, the former extends from sea shore to inland, whereas the latter unconformably overlies the Cape Supergroup, extending further into the inland area on the geological map (Figure 1.1).

The exposure quality of the outcrops is considerably better along road cuttings and is easily accessible when compared to outcrops in private farms and game reserves. Thus, this research was targeted at the Ecca Group of the Karoo Supergroup, which is well exposed along National roads N2 (between Grahamstown and Peddie) and N10 (between Cookhouse and Paterson), and Regional roads R67 (between Grahamstown and Fort Beaufort; Ecca Pass), R335 (between Somerset East and Kirkwood), R344 (between Grahamstown and Adelaide) and R350 (between Grahamstown and Bedford) (Figure 1.1). The climatic condition of the study area is temperate to subtropical, with a winter (cold and dry winter) and summer (hot and wet summer) season. The black Xhosa people are the dominant race in the area, while the Whites and Indians are minority races. Generally, the area can be subdivided into several sparsely inhabited farms, with few settlements. Most of the farms function either as game hunting areas, farming areas or as game reserves whereas the settlement is mostly rural with many small towns and villages.
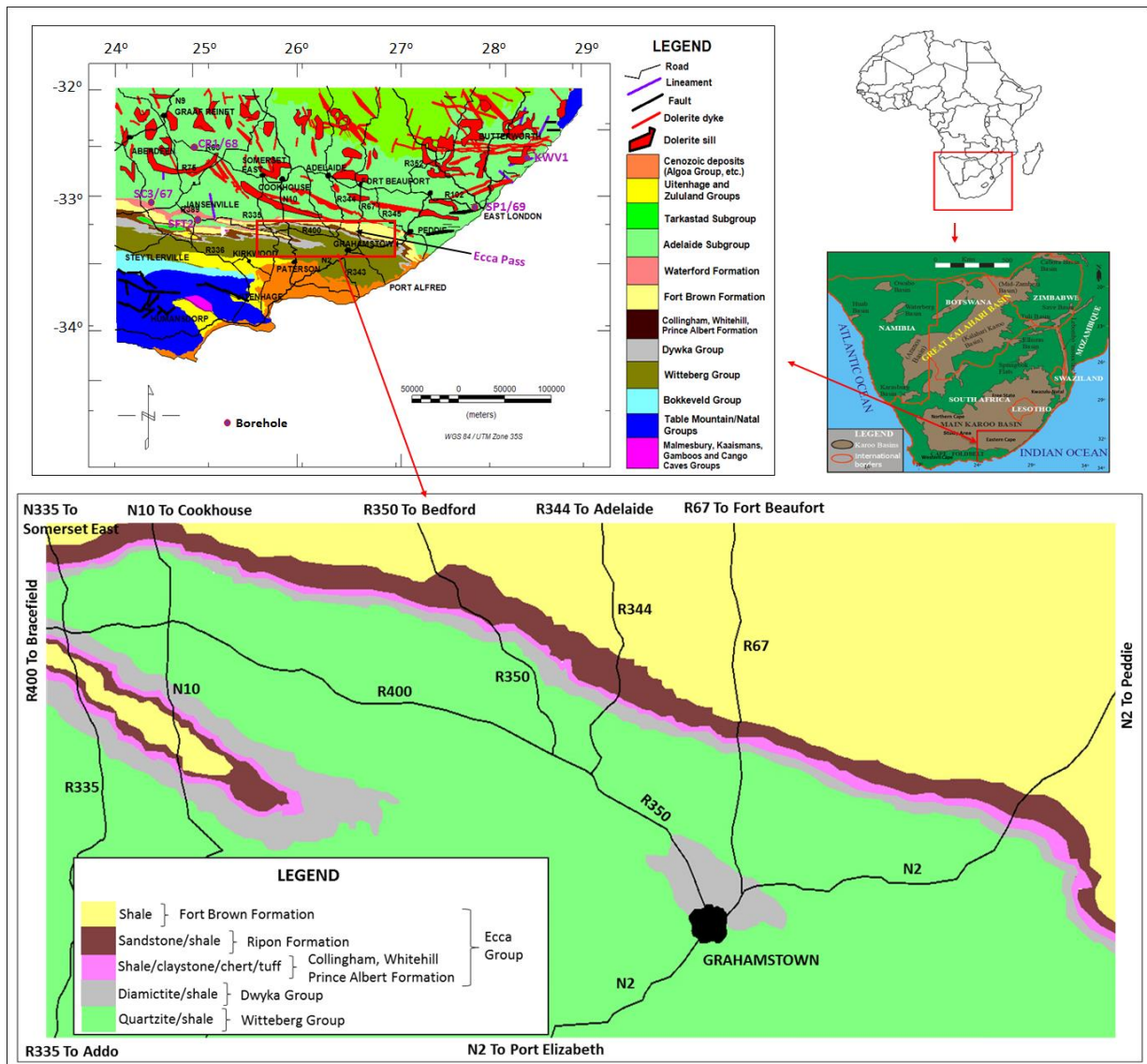
Figure 1.1: Location of the study area (Modified from Council for Geoscience, 1995).

1.2 Problem statement

The geology of the Main Karoo Basin in South Africa is quite complex considering the fact that the basin was intruded by multiple dolerite sills and dykes at about 183 Ma. These dolerite intrusions could impact the quality of the shale resources and increase the risks of shale gas exploration. Nonetheless, the Ecca formations in the study area are thought to have a considerable carbon content and suitable thickness to make it an ideal target for shale gas development. Despite the fact that published data gives a vast amount of information on the geology, stratigraphy and lithostratigraphy of the Ecca Group that host the purported shale gas, so far, the Ecca Group in the area received a very casual attention for its sedimentological details, in spite of the excellent preservation of the stratigraphic sequence, sedimentary structures and variation in lithological characteristics. Despite the fact that

2

Kingsley (1977) carried out detailed stratigraphic analysis of the Ecca Group in the Eastern Cape Province of South Africa, to date, little is known of the source rock characteristics, depositional processes, sedimentation mechanisms, hydrodynamic energy conditions, sedimentary facies, provenance, paleoweathering, tectonic setting, subsidence rates, shale gas potential and diagenesis of the potentially feasible shales and sandstones of the Ecca Group. Also, the identified sedimentary facies have not been thoroughly mapped in order to further subdivide the formations into stratigraphic members and there is an absence of integrated analysis of sedimentary and geochemical data of the mudstones and sandstones of the Ecca Group. While focusing on the purported challenges that are related to hydraulic fracturing of the Karoo for shale gas, there is urgent need to use sedimentological, geochemical and geophysical techniques to identify characteristics that would classify the Ecca shales as a potential unconventional gas reservoir in the Eastern Cape Province of South Africa.

1.3 Aim and objectives

The purpose of this research work is to better define the depositional and diagenetic history of the Ecca Group and identify characteristics that would classify the Ecca rocks as a potential unconventional gas reservoir. For this purpose, the following was investigated:

- Stratigraphy;
- Grain size distribution and depositional pattern;
- Modal composition and petrography
- Sedimentary facies and depositional environments;
- Geochemistry, provenance and tectonic setting
- Source rock potential (organic geochemistry)
- Diagenesis
- Electrical resistivity;
- Subsidence analysis

1.4 Methodologies

To achieve the aim and objectives of this project, the following method and procedures were carried out systematically:

1.4.1 Literature review and data collection

A review of literature on the Karoo Basin, as well as shale gas evolution was consulted in order to have an overview of the geology and economic potential of the area. The literature consulted include scientific articles, technical reports, exploration data, existing borehole logs, geological (stratigraphic) and geophysical data.

1.4.2 Geological fieldwork and sampling

Geological fieldwork in the study area was limited to road-cut exposures of the Ecca Group formations. This is due to the lack of well exposed outcrops of the Ecca Group within the area, and the difficulty to access private game reserves and farms. The geological fieldwork was conducted between the month of April to June 2015 and March 2016. The instrument used during the fieldwork include global positioning system (Garmin eTrex-10), compass, digital camera, measuring tape, grain size charter, sample bags, hand lens, permanent marker, masking tapes, pencils and field notebook. The area investigated was carefully mapped by observing and identifying different lithologies, sedimentary structures, vertical packing styles and the colour of rocks. The observed sedimentary structures on the outcrops were described and measured with a tape and where necessary, photographs were taken using a digital camera. Thicknesses of the stratigraphic units were measured perpendicular to the strike of the outcrop using a measuring tape. Rock samples of mudrocks and sandstones were collected in well labelled sample bags for further petrographic studies and geochemical analysis.

1.4.3 Geophysical fieldwork

Geophysical fieldwork was carried out between April and May 2016. A Geotron resistivity meter (Model G41) was used to carry out 37 vertical electrical soundings (VES) and 32 horizontal resistivity profiling (HRP) along the road-cut exposures of the Ecca Group in the study area (Figure 1.1). The VES and HRP surveys were carried out using the Schlumberger and Wenner electrode configurations, respectively. Other materials used in the survey includes 4 steel electrodes (2 potential and 2 current electrodes), insulated cables, measuring tape, hammers, global positioning system (GPS) and distance markers. Both VES and HRP methods were employed in order to determine the vertical and horizontal variations in subsurface resistivity that might exist in the survey area. The survey data were processed using Microsoft Office Excel, Geosoft Oasis Montaj, IPI2WIN and RES2DINV inversion

software, and the results were displayed as isoapparent resistivity map, sounding curves and pseudosections.

1.4.4 Stratigraphy

A detailed review of the spatial stratigraphic changes of the sedimentary successions of the Ecca Group, including the analysis of facies changes based on field observations and borehole logs were performed. Existing Karoo borehole cores VR 1/66, SC 1/67, CR 1/68 and SP 1/69 were logged at the Council for Geoscience core library in Pretoria (South Africa). Stratigraphic subdivision of the formations into members was based on similarities in lithological features. The stratigraphic data was processed using Strater Software and Microsoft Office PowerPoint and the results were expressed in form of stratigraphic sections.

1.4.5 Petrographic studies

A total of 194 thin sections were prepared and analysed using a petrographic light microscope. At least 30 representative thin sections of the Prince Albert, Whitehill, Collingham, Ripon and Fort Brown Formations were studied. While varying the magnification of the microscope (i.e. using the low and high magnification), authigenic and detrital minerals were identified under plane and cross polarized light by their optical properties. Petrological textures of the identified minerals were studied in order to ascertain/determine variation in the grain sizes, degree of sorting and roundness, mineral composition and rocks types.

Grain size measurements of the sandstones were conducted on the thin sections under petrographic microscope using an ocular with a millimetre scale. At least 500 grains per thin section were measured for each sample using the conventional method of grain's longest axis measurement (Adams, 1977; Johnson, 1994; Liu and Greyling, 1996). The frequencies of grain size ranges were calculated and the grain size classes were determined using the Udden-Wentworth grade scale (Udden, 1914; Wentworth, 1922). The dimension of grain sizes (mm) was converted to a phi scale. The statistical parameters of grain size distribution were calculated using equations proposed by Folk and Ward (1957). Bivariate scatter plots were employed to discriminate between depositional settings based on their textural variation. Sahu (1962, 1964) linear discriminant function (LDF) was modified and used to determine the process and environment of deposition. In addition, C-M plots and log-probability curves were used to reveal the different depositional processes, mechanism of sedimentation and energy condition of the transporting medium (Passega, 1964; Visher, 1969).

Quantitative detrital modes of the sandstones were also calculated from point counts of thin sections (Dickinson, 1985). The Gazzi-Dickinson's point-count method was applied for quantitative compositional analysis. In the point count method, grains were grouped as monocrystalline quartz (Qm), polycrystalline quartz (Qp), plagioclase (P), K-feldspar (K) and lithic fragments (L). The detrital modes were then recalculated to 100%, excluding matrix, cement, micas, heavy minerals and carbonate grains (Dickinson, 1985). The recalculated or normalised values were plotted on quartz-feldspar-lithics (QFL) ternary diagrams of Dickinson and Suczek (1979), Dickinson et al. (1983), Yerino and Maynard (1984), Dickinson (1988) and Kumon et al. (1992) which shows compositional fields associated with different provenances (i.e., continental block provenances, recycled orogeny, magmatic arc provenances and collision suture sources). Furthermore, the values were also plotted on QFL ternary diagrams of Folk (1980) which show different sandstone types. For modal analysis, 500 points were counted per thin section.

1.4.6 Sedimentary facies

Sedimentary facies analysis was performed using both field and borehole data. The field data mostly consisted of lithological features, sedimentary structures (primary and secondary structures) and colour of the rocks. The primary sedimentological features were documented for the identification of sedimentary facies in order to try and correlate strata in different parts of the study area, as well as to characterise the different depositional conditions/environment. Detailed facies analysis was carried out using a modified version of lithofacies classification scheme by Miall's (1988a, 1988b, 1996). The identified lithofacies were grouped into facies associations which represent different kinds of depositional environments of the Ecca Group.

1.4.7 Geochemical analysis

Mineral compositions of the shales, mudstones and sandstones were determined by XRD, while major and trace element geochemistry was determined by XRF. Both XRD and XRF were performed at the Council for Geoscience laboratory in Pretoria (South Africa). The XRD result is presented in tabular form. Major element geochemistry of sedimentary rocks are influenced by various factors such as source material, sedimentary processes within the depositional basin, transportation, diagenesis, physical sorting and weathering (Bhatia, 1983; Bhatia and Crook, 1986). Major and trace element geochemistry of sandstones and shales can be used as a powerful tool to determine provenance and tectonic setting of sedimentary basins (Bhatia, 1983; Bhatia and Crook, 1986; Roser and Korsch, 1986). In this study, major and

trace element geochemistry of the sandstones and shales were used to determine provenance and tectonic setting of the Main Karoo Basin using major element discriminant function diagrams (After Roser and Korsch, 1988), binary plots of TiO_2 versus Zr, TiO_2 against Ni, Th/Co versus La/Sc, La/Th against Hf, Cr versus Ti, TiO_2 against $Fe_2O_3 + MgO$, Al_2O_3/SiO_2 versus $(Fe_2O_3 + MgO)$, K_2O/Na_2O versus Fe_2O_3+MgO, $Al_2O_3/(CaO + Na_2O)$ versus (Fe_2O_3+MgO) and K_2O/Na_2O versus SiO_2 (After Hayashi et al., 1977; Bhatia, 1983; Roser and Korsch, 1986; Floyd and Leveridge, 1987; Floyd et al., 1989; McLennan et al., 1993; Cullers, 2002) and ternary plots of V-Ni-Th×10, A-CN-K, Na_2O-CaO-K_2O, Th-Sc-Zr/10 and La-Th-Sc (After Nesbitt and Young, 1984; Bhatia and Crook, 1986; Toulkeridis et al., 1999; Cullers, 2002; Bracciali et al., 2007). In addition, indices of weathering (CIA, CIW and PIS) were calculated from the major elements using the formulas proposed by Nesbitt and Young (1982), Harnois (1988) and Fedo et al. (1995). Chemical maturity of the sandstones and shales were determined using the binary plot of ICV against CIA, and SiO_2 versus $Al_2O_3+K_2O+ Na_2O$ (After Suttner and Dutta, 1986).

1.4.8 Total organic carbon and rock-eval analysis

Total organic carbon (TOC) content was determined first, to screen the samples before they were sent to different laboratories for vitrinite reflectance (Ro) and rock-eval analyses. A total of 82 outcrop samples of shale presumed to be rich in organic matter were collected from road-cut the exposures of the Ecca Group (Figure 1.1). In addition, 38 core samples of Ecca shale from boreholes CR 1/68, SC 3/67, SP 1/69 and KWV 1 were collected from the Council for Geosciences core library in Pretoria, making a total of 120 shale samples that were tested for TOC content. 28 organic-rich shale samples were analysed using Rock-eval 6 pyrolyser at GeoMark Research Laboratory in the United States to determine the hydrocarbon generation potential, maturity, kerogen type and hydrogen richness. The 19 samples out of the 28 organic rich samples were further analysed for vitrinite reflectance (Ro) by Professor Nicola Wagner at the University of Johannesburg, South Africa. The TOC, Ro and rock-eval analyses result were geochemically evaluated to identify characteristics that would classify the shales as a potential unconventional gas reservoir.

1.4.9 Diagenesis

The description of primary and authigenic minerals in mudstones and sandstones of the Ecca Group was based on petrographic study and scanning electron microscopy (SEM). SEM was employed because it has a wide range of magnification for the identification of fine grained

minerals. The used SEM was aided with energy dispersive X-Ray (EDX), which makes identification of the mineral compositions possible. The SEM+EDX were used to determine the rock textures, cement types, minerals composition, as well as their percentages. Rock samples for SEM analysis were broken into rock chips that have natural flat surfaces with a hammer and were mounted on glass slides using Canadian slide glue. The samples were then carbon coated in a Cressington 108 carbon/a carbon coater and kept in an air tight container to prevent moisture from the air. Subsequently the carbon coated samples were analysed using a Jeol JSM-6390 LV model (SEM) equipped with a link system energy dispersive X-Ray micro-analyser (EDX). The samples were examined in Secondary Electron Image (SEI) and Back Scattered Electron (BSE) modes of imaging. Both SEM and petrographic microscopy were performed at the University of Fort Hare, South Africa.

1.4.10 Subsidence analysis

The subsidence history of the Ecca Group was reconstructed by a tectonic subsidence analysis involving the backstripping technique. The tectonic subsidence computation was done with the OSXBackstrip program which was developed by Cardozo in 2012 (University of Stavanger, Norway). The program performs a "1D Airy backstripping" based on the approach by Watts (2001) and Allen and Allen (2004).

1.5 Structure of the thesis

This thesis consists of twelve chapters. Chapter 1 outlines the research area, problem statement, aim and objectives, methodologies and structure of the thesis. The geological setting of the Karoo Basin is presented in Chapter 2. In Chapter 3, a stratigraphic analysis was carried out on the Permian deposits of the Ecca Group in order to unravel the stratigraphic framework. Chapter 4 deals with grain size analysis and depositional pattern of the Ecca sandstones. The modal composition and petrography of the Ecca Group rocks is documented in Chapter 5. Sedimentary facies and depositional environments of the Ecca Group deposits are presented in Chapter 6. Chapter 7 deals with geochemistry, provenance and tectonic setting of the Ecca Group rocks. Source rock potential of the Ecca Group rocks is documented in Chapter 8. Chapter 9 provides a general account of the diagenesis of sandstones and mudrocks of the Ecca Group. Chapter 10 deals with geophysical characterization of the Ecca Group using electrical resistivity method. Sedimentation rate and subsidence history of the Ecca Group are reported in Chapter 11, while Chapter 12 gives the summary of the results presented in the different chapters.

CHAPTER 2
GEOLOGICAL SETTING OF THE KAROO BASIN

2.1 Geological background

The Karoo is a semi-desert region of southern Africa with vast distribution of sedimentary rocks. The word "Karoo" was derived from the Main Karoo Basin of South Africa to describe sedimentary fill of all basins of akin age across Gondwana. The Main Karoo Basin is a large sedimentary depository lying north of the Cape Fold Belt in South Africa. The basin developed within the continental interior of southwest Gondwana (Milani and de Wit, 2008; Linol et al., 2015) and covers up to 700, 000 km^2. But it was much more extensive during the Permian (Aarnes et al., 2010) and represents about 117 Ma of sedimentation spanning from 300 Ma to 183 Ma (Catuneanu et al., 2005). In addition, the basin is underlain by a stable basement comprising the Kaapvaal Craton in the north (Catuneanu et al., 1998; James et al., 2003), the Namaqua-Natal Metamorphic Belt (NNMB) in the south (Cornell et al., 2006) and the Cape Fold Belt (CFB) along its southern margin (Johnson et al., 2006). Thomas et al. (1993) defined the NNMB is as those terranes in southern Africa that acquired a pervasive structural fabric during the ca. 1.1 Ga Kibaran tectono-magmatic event. The Natal Belt makes up the eastern section of the NNMB and lies adjacent to the south-eastern margin of the Kaapvaal Craton. The Main Karoo Basin of South Africa is a unique type of basin of all the Karoo basins in southern Africa because it contains the thickest and stratigraphically most complete mega-sequence of several depositories of the Permo-Carboniferous to Jurassic age sediments in southwestern Gondwana continent (Catuneanu et al., 1998). Furthermore, it serves as a datum for classifying Karoo basins in central and southern Africa (Figure 2.1).

The Karoo Basin preserve a long history of sedimentation that span from the Paleozoic to the Middle Mesozoic and bulk of the Karoo strata occurs in the Main Karoo Basin, with maximum cumulative thickness of about 12 km along the southern margin of the basin; a large erosional remnant of the Karoo Supergroup that now covers approximately two-third of South Africa (Linol et al., 2015). The basin is a retroarc foreland system (de Wit et al., 1988; Catuneanu et al., 1998) that developed in front of the Cape Fold Belt in response to crustal shortening and thickening that resulted from the Late Paleozoic-Early Mesozoic subduction episode of the palaeo-Pacific plate beneath the Gondwana plate (de Wit and Ransome, 1992; Pysklywec and Mitrovica, 1999). Subsequently, the associated foreland basins fragmented due to the break-up of Gondwana, and are preserved today in southern Africa (Karoo Basin),

South America (Parana Basin), Australia (Bowen Basin) and Antarctica (Beacon Basin) (Figure 2.2). The Karoo basin, as well as other major Gondwana foreland basins (i.e. Paraná, Beacon and Bowen Basins) is believed to have been formed as a result of accretion tectonics along the southern edge margin of Gondwana during the Late Paleozoic (de Wit and Ransome, 1992; Veevers et al., 1994; Turner, 1999; Catuneanu, 2004; Lopez-Gamundi, 2006; Flint et al., 2009). The northward subduction of the Panthalassan underneath the Gondwana plate resulted in the development of a magmatic arc located between the Karoo basin and the southern margin of Gondwana (Visser, 1993; Visser and Praekelt, 1996).
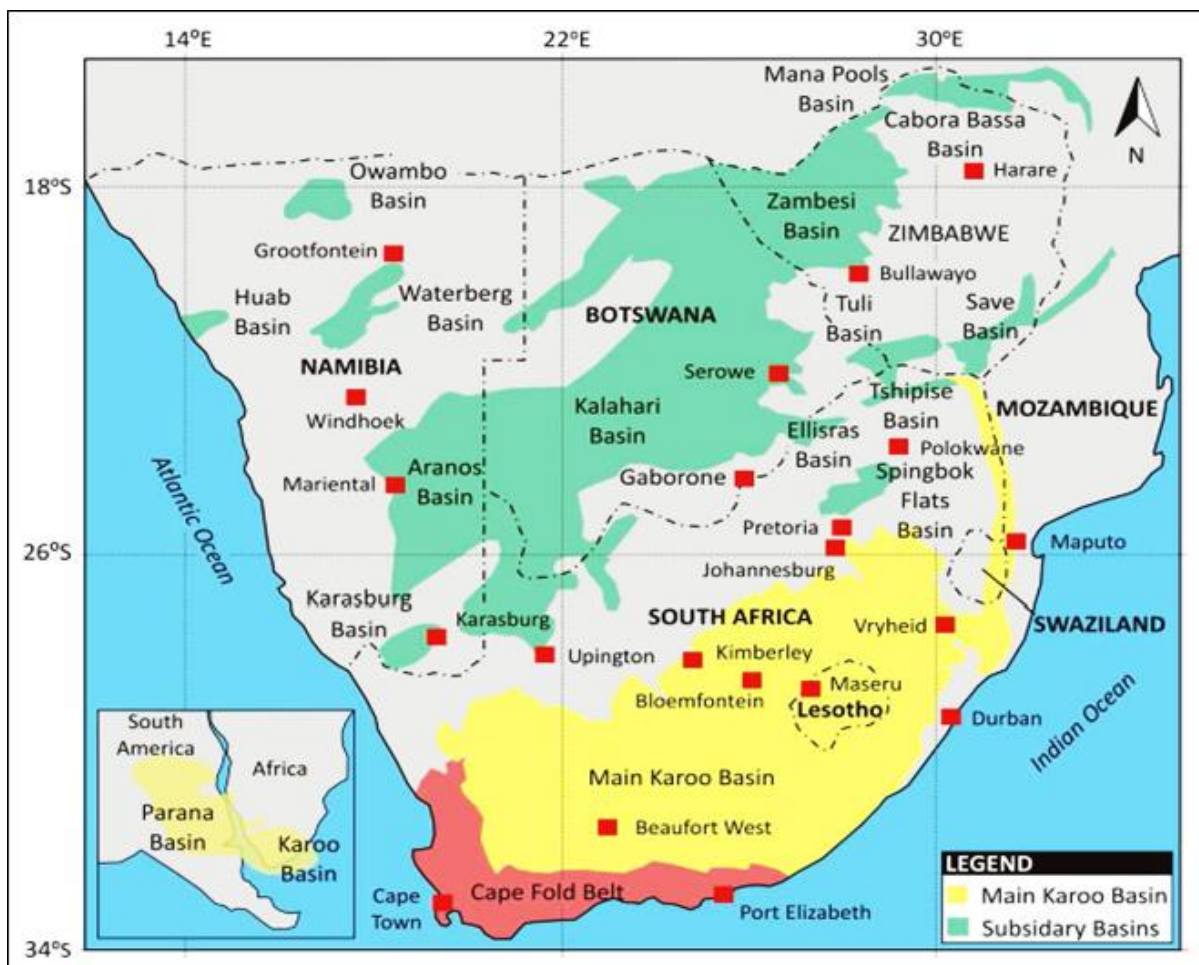
Figure 2.1: Location of the Main Karoo Basin and subsidiary basins in southern Africa. Insert: location of the Karoo Basin and other continent blocks during Gondwana times (After Johnson et al., 1996; Andersson et al., 2003).
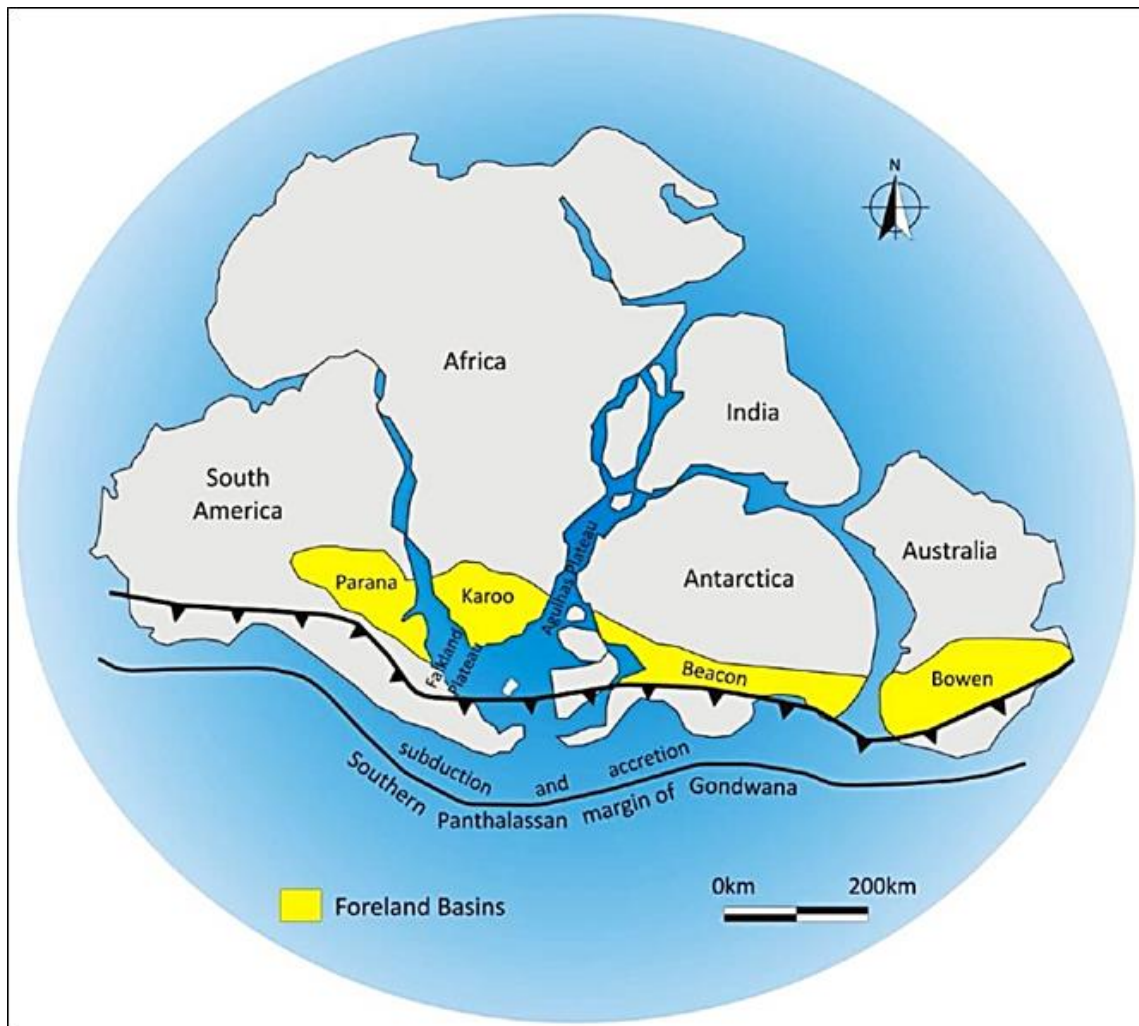
Figure 2.2: Palaeogeography reconstruction of the Karoo basin and Gondwanaland during the Late Paleozoic showing accretionary foreland basins (After Turner, 1999; Lewis, 2008).

The sedimentation that occurred in the retroarc foreland setting (Karoo Basin) was controlled by the orogenic cycles of loading and unloading in the Cape Fold Belt (Catuneanu et al., 1998). As documented by Johnson et al. (2006), the sedimentary part of the Main Karoo Basin comprises of the Dwyka (Late Carboniferous-Early Permian), Ecca (Permian), Beaufort (Late Permian-Triassic) and the Stormberg Group (Late Triassic-Early Jurassic). The Karoo sedimentary sequence was subsequently intruded by several Early Jurassic sills and dykes (about 183 Ma), with the widest and thickest sills located within the Ecca Group (Chevallier and Woodford, 1999). The Karoo sedimentary fill generally thins northward, producing a highly asymmetrical basin. The geometry of the sedimentary fill is said to be a wedge shape, which is usually associated with foreland successions (Catuneanu et al., 2002).

The palaeoenvironmental settings of the Karoo succession revealed changing climatic conditions as Gondwanaland drifted from high latitudes towards the equator (Johnson et al.,

11

1996; Tankard et al., 2009), varying from glacial and partly marine in the Dwyka Group, to marine in the Ecca Group, then to fluvial and aeolian in the overlying Beaufort and Stormberg Groups, respectively (Smith, 1993). During the deposition of the Dwyka and Ecca Groups, an interior seaway transgressed the Karoo Basin, but it totally regressed from the confines of the preserved basin at the end of Ecca time (Catuneanu et al., 2002). Several researchers including Kingsley (1981), Halbich (1983), and Cole (1992) have proposed that bulk of the Ecca and Beaufort Group sediments in the southern foredeep part of the basin were derived from the magmatic arc during the Permian, but the rapidly rising Cape Fold Belt along the basin margin contributed significantly to the basin fill during the Triassic and was the predominant source for the Molteno and Elliot Formations. This interpretation was contested by Johnson (1991), who envisaged that a southern magmatic arc located south of Cape Fold Belt also serve as an additional source area for the successions during the Triassic.

2.2 Geodynamic setting

The Carboniferous Period was a time of mountain building when the collision of the Laurasia and Gondwanaland land masses started to form a supercontinent. By the Permian time, plate movements had brought together all the world's land masses into a single supercontinent, Pangea. This assemblage was a direct result of continental collisions that occurred between Gondwana and Laurasia, as well as collision between Laurasia, Kazakhstania and Siberia (Cairncross, 2001). The collision between Laurasia and Siberia-Kazakhstania and China finalized assembly of Pangea by end of Permian (Linol et al., 2014). This was the first time since the Late Proterozoic supercontinent of Rodinia that such a landmass had formed. At this time, the shape of the Pangea looks like a giant "Pack man", with a huge mouth facing eastward across the equator. The large open mouth becomes the Tethys Ocean, which covered much of what is now the southern and central Europe (Figure 2.3). Prior to the break-up of Pangea, the super-ocean that surrounded the supercontinent Pangea is known as the Panthalassa. Suturing that was related to Pan-African-Brasiliano orogenic belts of western Gondwana and collision of eastern Gondwana along the Mozambique Belt led to the formation of Gondwana over a period of ~390 Ma, spanning from the Late Neoproterozoic (~550 Ma) to Early Jurassic (~160 Ma). The Mid-Carboniferous (330-310 Ma) was a period of orogeny (mountain-building event) along the palaeo-Pacific margin, where the southern Tethyan margin was characterised by shallow marine sedimentation (Tankard et al., 2012).
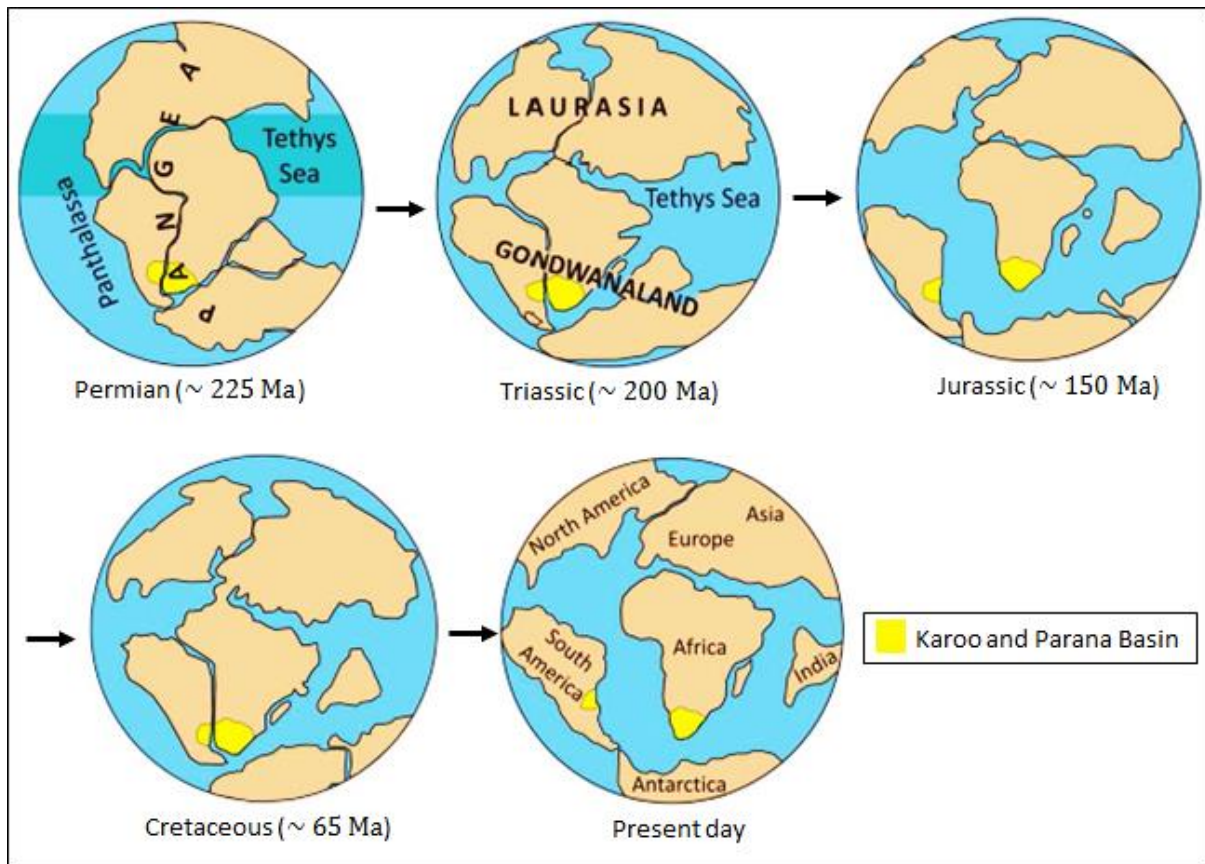
Figure 2.3: Pangea supercontinent schematic showing the break-up from the Early Permian to present day (After Blakey, 2008).

During the Early Paleozoic, most of the continents gathered around the equator, with Gondwana (representing majority of the old Rodinia) slowly drifting south across the South Poles. This resulted in two episodes of glaciation, the latest which occurred during the Carboniferous led to the deposition of tillite (Dwyka glaciation) (Linol et al., 2014). The glaciation was related to the formation of ice-caps on elevated coastal ranges and in high lying interior regions. These regions were thought to be "ice spreading centres" for Gondwana ice sheets in the Late Carboniferous, signifying the onset of sedimentation in the Karoo Basin (Visser and Praekelt, 1996; Smith et al., 1993; Johnson et al., 2006). By the Mid Carboniferous, the ice-caps were located on the uplifted Pampean-North Patagonian-Deseado massif from where glacial sediment was shed towards the south. During this time, the interior of the supercontinent uplift axes were located in the Damara and Mozambiquan Mobile Belts, perhaps pointing to the existence of a major stress regime. The accreting Panthalassan terrane joined with the mainland and formed a transtensional foreland basin that may have led to a reversal in sediment supply (Visser and Praekelt, 1996).

In the Late Carboniferous to Early Permian, there was a change from an elevated landscape to large scale subsidence in the south. Large, interconnected basins formed adjacent to palaeo-Pacific coastal ranges; while smaller ones were confined to the interior. The location of these near linear basins has been shown to correspond to the location of a seaway that spanned across Africa, nearly linking the Tethys Sea to the palaeo-Pacific Ocean (Visser and Praekelt, 1996). Rifting that is associated with magmatic activity as well as marine transgressions dominated the southern Tethyan margin. Furthermore, active Gondwana plate tectonism associated with the palaeo-Pacific magmatic arc existed to the south of the present day continental margins during the Late Carboniferous and Early Permian. The presence of volcanic ash beds in shales, at about 100 m from the base of the Dwyka Group support or point to the existence of this magmatic arc (de Beer, 1992; Visser and Praekelt, 1996). Accumulation of Karoo aged successions in Africa can be linked or related to the Pangean first-order phase of supercontinent assembly and break-up. The beginning of sedimentation in the Karoo (referred to as Karoo first-order depositional sequence) is usually placed in the Late Carboniferous (about 300 Ma) after a major inversion tectonics events that occurred along the southern margin of the supercontinent and resulted in the assembly of the Pangea (Catuneanu et al., 2005).

Sedimentation in the Karoo Basin continued across Gondwana until the Early Jurassic (about 183 Ma) when formation of sediment was replaced with the emplacement and extrusion of the Karoo large igneous province (LIP), which includes the outpouring of about 1.4 km of basaltic lavas (the Drakensberg Group) from a large feeder network of dolerite sills and dykes at multiple levels within the basin (Svensen et al., 2012). These intrusions change from dominantly dykes and saucer-shaped sills within the upper and mid-stratigraphic levels (Stormberg and Beaufort Groups), to extensive sub-horizontal sills and sheets within the lower stratigraphic levels (Ecca and Dwyka Groups and basement) (Chevallier and Woodford, 1999; van Zijl, 2006a; 2006b). During the post-Gondwana time, the upper section of the Karoo sequence was exposed to physical processes like erosion, thus the age of the youngest (newest) preserved Karoo deposits generally varies from Triassic to the Middle Jurassic (Catuneanu et al., 2005). The source of most of the Karoo sediments are thought to be from the south, sources include the Cape Fold Belt and a magmatic arc that formed by the convergence of Panthalassa and Pangea (Veevers et al., 1994). Late isostatic uplift of the Cape Fold Belt may have provided an important southerly sediment source for the Main Karoo Basin until the end of the Middle to Late Triassic when Drakensberg lavas were

emplaced. The lavas represent the termination of Karoo sedimentation and the early rifting of Gondwana prior to break-up (Turner, 1999).

Gondwana later collided with Eurasia in the Early Cretaceous, forming a subduction zone (Tethyan Trench). As a result of rifting and extensional tectonics, Gondwana was later separated into present day continents. Turner (1999) documented that the break-up of Gondwana was initiated in the Early Jurassic through the clockwise rotation of East Gondwana against West Gondwana that lasted for ∼ 40 Ma. The rifting of Gondwana resulted in the extrusion of the Drakensburg basalts and the injection of the Karoo dolerites (Riley and Knight, 2001). Gondwana broke up through the process of marginal rift faulting involving tilted fault blocks as well as horst and graben structures that formed due to extensional rifting. Along the east coast of southern Africa, the break-up occurred at ∼ 160 Ma, while the break-up along the west occurred at ∼ 130 Ma. The characteristics of the south western coast of South Africa were determined by the linear strike-slip or transform fault associated Agulhas-Falkland Fracture Zone (Lewis, 2008). The summary timescale related to the geodynamic setting and formation of Karoo Basin is presented in Table 2.1.

Table 2.1: Summary of time scale related to the geodynamic setting of the Karoo Basin (After Lewis, 2008).

Period	Epoch	Major event
Jurassic	Early-Middle	Sedimentation terminated Igneous Province emplaced
Triassic	Late	Lava emplacement terminates Karoo sedimentation Rifting of Gondwana
	Middle	Sedimentation interrupted Drakensberg Lava emplacement
	Early	Basin formation continues
Permian	Late	Basin formation continues Plate related tectonism
	Middle	Pangea rifts from Tethys Ocean Landscape predominantly related to subsidence
	Early	Pangea fully assembled Gondwana and Laurasia formed
Carboniferous	Late	Gondwana and Laurasia begin to form Change from elevated landscape to subsidence Formation of basins Plate tectonism 1st order deposition and sedimentation
	Middle	Assembly of Pangea begins Continental uplift Orogeny (Palaeo-Pacific margin) Rifting (Tethys Ocean and Pangea) Formation of Gondwana and Laurasia Ice caps in uplifted regions Formation of initial foreland basin
	Early	Gondwana Uplifted Gondwana drifts over pole Formation of ice caps Deposition of the Dwyka Group Initiation of the Karoo sedimentation

2.2.1 Karoo Basin development

In Africa, the most widespread and thick Phanerozoic deposits are those of the Karoo Supergroup, which are well-preserved throughout southern Africa. The deposition and accumulation of Karoo successions in southern Africa was in response to the Pangean first-order cycle of supercontinent assembly and subsequent break-up (Catuneanu et al., 2005). Therefore, the Karoo Basin represents episodes of subsidence and sedimentation within the

interior of Gondwana (Tankard et al., 2009; 2012), with depocentres changing from a passive continental margin in the Early Paleozoic to a landlocked foreland basin during the Permo-Triassic (Smith et al., 1993). To date, there is controversy surrounding the development of the Karoo Basin. Several models have been proposed for the formation of the Late Carboniferous-Middle Jurassic Karoo Basin. Recently, the interpretation of the evolution and tectonic setting of the Karoo Basin vary from a retro-arc foreland basin formed as a result of shallow angle subduction of the palaeo-Pacific plate underneath the Gondwana supercontinent (Catuneanu et al., 1998; 2002; Catuneanu, 2004; Johnson et al., 2006), a transtensional foreland system formed as a result of subsidence and tilting in a strike-slip regime (Tankard et al., 2009; 2012), a thin-skinned fold belt that developed from collisional tectonics and distant subduction to the south (Lindeque et al., 2011; Pangaro and Ramos, 2012), to a transient hypothetical mantle plume related model (Turner, 1999). Veevers et al. (1994) envisaged that the continued subduction of the Panthalassan (palaeo-Pacific Ocean) beneath the Gondwana plate led to northward compression as well as the eventual development of a fold-thrust belt inboard of the magmatic arc.

Several researchers (i.e. Tankard et al., 1982; de Wit and Ransome, 1992; Hälbich, 1993; Paton et al., 2006) documented that the tectonic evolution of southern South Africa involve series of compressional and extensional deformation episodes over the last 650 Ma. Thomas et al. (1993) envisaged that the Namaqua-Natal Mobile Belt (NNMB) that developed as a result of compression of the passive margin at the southern edge of the Kaapvaal Craton during the Namaqua-Natal Orogeny (950-900 Ma) is one of the main factors that controls the development of the region. After the termination of compression, a series of east-west trending extensional basins developed from about 900-600 Ma, within which the sediments of the Pre-Cape Group were deposited, these basins were later overturned during the Pan African Orogeny (600-450 Ma) (Tankard et al., 1982). According to McCarthy and Rubidge (2005), at about 500 Ma, the supercontinent Gondwana had consolidated and the mountains ranges that developed along its suture were being eroded, thus exposing the Pan-African metamorphic rocks that had formed deep below the surface.

By 450 Ma, rifting began across what is today the southern Cape (probably as a result of internal tension experienced by the supercontinent), causing thinning of the crust and invasion by the sea. Rivers were said to have diverted into the rift and began to deposit its sediment (mainly sand and gravel) to form the Klipheuwel Group (McCarthy and Rubidge, 2005). A major rift was created by the continued stretching of the present deeply eroded Pan-

African belts. McCarthy and Rubidge (2005) documented that this rifting extended eastward across the southern part of South Africa to beyond the present position of Port Elizabeth (Figure 2.1). The north-easterly part of the rifting extends into the present-day KwaZulu-Natal (around Durban Figure 2.1). The rift was flooded rapidly by the sea and thus resulted in the formation of a seaway across the southern Cape (called the Agulhas Sea; Figure 2.4) as the crust thinned and subsided. The rocks of the Klipheuwel Group and the eroded Pan-African rocks (Cape granites and associated metamorphosed sedimentary rocks of the Malmesbury, Kango and Kaaimans Groups) floored the sea in the west and east, respectively. As the rifting continued, the depression widened and more sediment were transported and deposited in the depressions forming the Cape Supergroup (Figure 2.4).
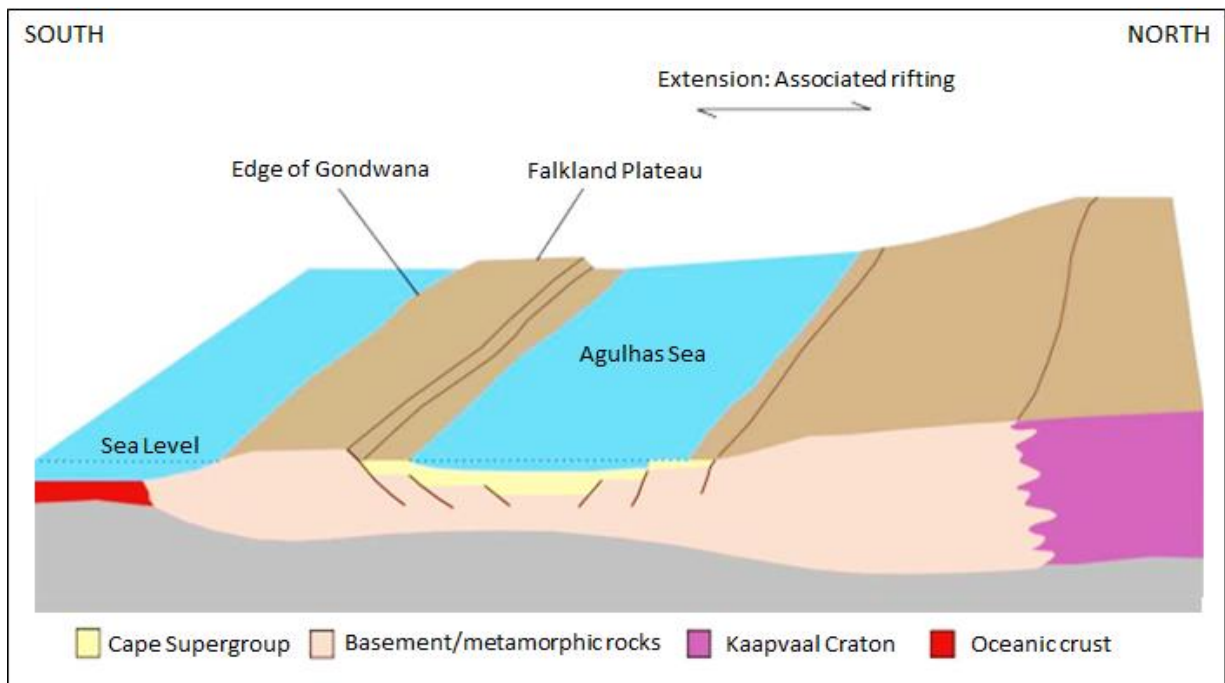
Figure 2.4: Extensional tectonic setting for the deposition of Cape Supergroup sediments (After Lewis, 2008).

Deposition during the initial phases of the Cape basin, subsidence has been interpreted as being tectonically controlled by faulting of the basement (Tankard et al., 2009). The rocks of the Cape Supergroup can be subdivided into three groups (Witteberg, Bokkeveld and Table Mountain Groups) of varying age, depositional environment and fossil content. The top of the Witteberg Group signifies the end of sedimentation in the Agulhas Sea. The end of sedimentation in the Agulhas Sea is marked by a change from an environment of stretching, thinning and subsidence of the crust, to an environment of compression, crustal shortening and thickening (McCarthy and Rubidge, 2005). Generally, the rocks of the Cape Supergroup

were deposited over a period ranging from the Ordovician to the Carboniferous (about 500-330 Ma). The Cape Supergroup is believed to have been deposited in a passive margin basin after "the Late Precambrian to Early Cambrian Saldanian orogeny and Pan-African depositional cycles had completed in the Gondwana" due to extensional processes (Catuneanu, 2004).

At about 310 Ma, a subduction zone developed along the southern margin of Gondwana due to closure of the rift valley that started at about 330 Ma, and the internal part of the supercontinent began to experience compression (McCarthy and Rubidge, 2005). This caused the sedimentary rocks of the Cape Supergroup to begin to fold or buckle, the crust thickened, forming a mountain range in the place where the Agulhas Sea formerly existed. Thus, the earlier known Agulhas Sea became the Cape Mountains. Due to the load (weight) of this mountain range, the continental crust of southern Africa began to sag, resulting in a basin development on the northern flanks, into which the sediments of the Karoo Supergroup were deposited over a period that span from the Late Carboniferous to the Middle Jurassic (about 310-183 Ma). The development of the Gondwanian orogeny in the Permian led to the termination of Cape Supergroup deposition (Paton et al., 2006). Deformation of the Cape Supergroup margin deposits into the Cape Fold Belt as well as the formation of the Karoo foreland basin to the north are manifestation of the compression in South Africa (Veevers et al., 1994; Figure 2.5). Paton et al. (2006) concluded that the Cape Fold Belt cannot be classified as a thin skinned nor thick-skinned tectonic end-member but their deformation can be said to be controlled by a south dipping mega-decollement that shows features of both end-members. With time, much of the Cape Supergroup rocks became buried under the Karoo deposits, but later re-surfaced as mountains during the upliftment of the subcontinent at about 180 Ma (coincides with the intrusion of dolerites), and again at about 20 Ma, which initiated an episode of continuous erosion that removed some of the surface deposits from southern Africa.
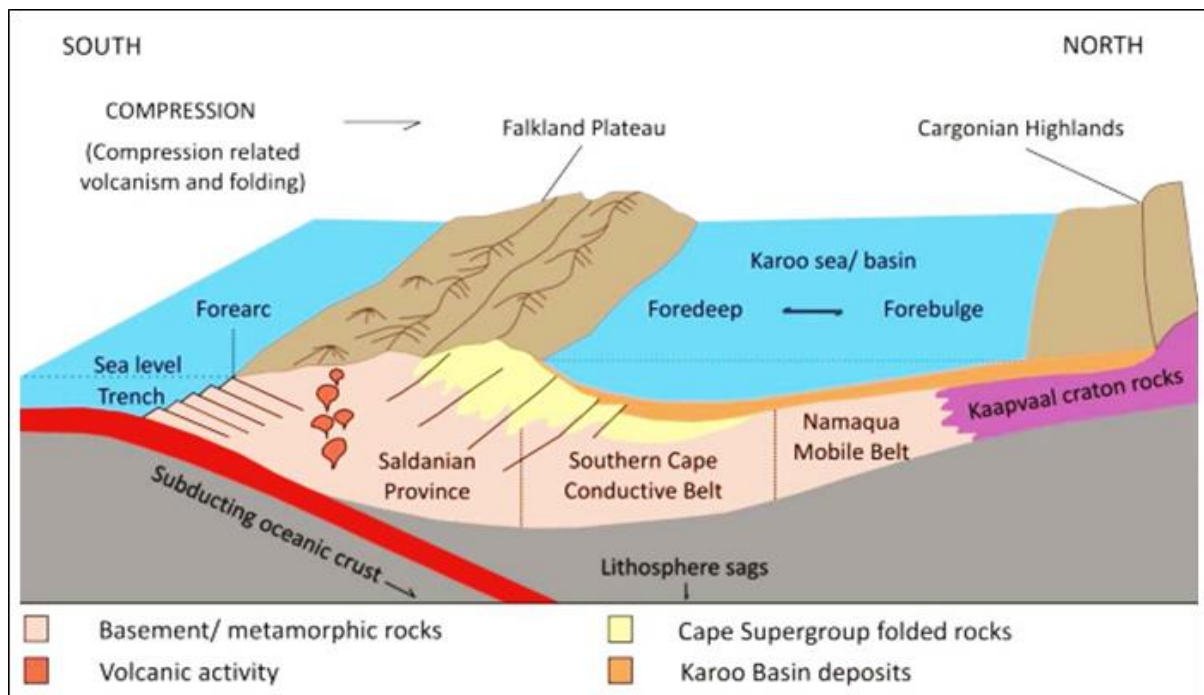
Figure 2.5: Cape Fold Belt and Karoo sea development (After Lewis, 2008; Turner, 1999).

According to McCarthy and Rubidge (2005), at the time of formation of the Cape Mountain, South Africa was believed to be located over the South Pole due to the steady northward drifting of Gondwana. The ice sheet that covered the southern Gondwana (i.e. Africa) was probably of several kilometres thick. The glacial deposits from the ice sheet were the first of the sediments to be deposited in the developing Karoo depression, thus making the Dwyka Group as the earliest and lowermost of the sedimentary deposits of the Karoo Supergroup. The basin in which the sediments were deposited was deepest in the south along the Cape Mountain front, thus the ice sheet floated on an inland lake, also known as the Karoo inland sea (McCarthy and Rubidge, 2005). Subsequently, the glaciers that emerged from the mountains floated out of the sea as icebergs, they seasonally melted and retreated leaving an enormous quantities of unsorted mud and large fragments of rock that characterised the Dwyka Group. Catuneanu (2004) envisaged that the earliest Karoo sedimentary rocks (about 330-300 Ma) must have been over-thrusted, "cannibalized" and included within the structures of the Cape Fold Belt. According to Tankard et al. (2009), the Cape orogeny is pre-dated by the dynamic phase of subsidence experienced by the early Karoo basin during the Permian. They suggested rapid rate of collapse of the Carboniferous high plateau due to the lack of marked transition to the Dwyka basement high and platform facies associations. Vertical displacement of rigid basement blocks decoupled along crustal-scale boundary was the main subsidence that occurred, which is revealed in the distribution of the Dwyka facies

associations (Tankard et al., 2009). The rate of subsidence of the Namaqua and Natal blocks exceeded the rate in which sediment were supplied, and thus led to the underfilled basin of the platform facies association. The different types of glacial deposits in the Dwyka Group are attributed to the several episodes of advance and retreat of the ice sheets (McCarthy and Rubidge, 2005).

Continued northward drifting of the Gondwana away from the polar region, caused all the ice to melt, after all the ice had melted, a vast inland water body (inland sea) remained, this water body extended across South Africa and the neighbouring regions of Gondwana. According to McCarthy and Rubidge (2005), this inland sea might have had an opening to the ocean but with a lesser or small tidal effects (probably, it is similar to the Black Sea). The Cargonian Highlands that formed the high ground, north of the sea, and the rivers draining the mountains that are north of the Karoo Sea, deposited their sediments along the northern shoreline, forming large swampy deltas. However, some of the sediments deposited into the Karoo Sea were derived from the Cape Mountain to the south of the basin. These latter deposits make up the Ecca Group of the Karoo Supergroup, consisting mostly of shales. The style of subsidence in the Dwyka Group continued into the Ecca Group which is an underfilled basin, dominated by argillaceous sedimentation (Tankard et al., 2012). The transition from the Dwyka glacially affected sedimentation in the post-glacial early Ecca.

During the Ecca time, the Falklands Plateau collided and was later joined with the southern Africa, resulting in the range of mountains that is seen south of the Cape Fold Belt. The Karoo Basin subsidence resulted from mantle flow but becomes complex due to variable degrees of foundering of the basement blocks (Tankard et al., 2009). These basement blocks are coincident with the Hex River area oroclinal bend in the present day Cape Fold Belt and possibly behaved as a buried basin boundary during the Ecca Group time, probably influencing the position of the shelf edge in a way that is similar to a passive margin (Tankard et al., 2009). With the continued accumulation or deposition of sediments into the Karoo Sea as well as formation of the Falkland Plateau and Cape Fold Mountain ranges, the Karoo Sea gradually got filled with sediments that were mostly derived from the Cape Mountains in the south. By this time, the highlands that were formed, north of the Karoo Sea had been probably levelled by erosion and subsequently buried beneath the newer sediments, and the Mississippi-like rivers flowed over the filled-up Karoo Basin from the south, providing new habitats for a variety of flora and fauna. These newer sediments form the overlying Beaufort Group.

During deposition of the Beaufort Group, the climate had warmed sufficiently to become semi-arid such that the Ecca seaway regressed (Johnson et al., 2006). This led to the establishment of a fully non-marine environment and resulted in the accumulation of the fluvio-lacustrine Beaufort Group. The Karoo Sea later became a lake with time (McCarthy and Rubidge, 2005). This transition into the terrestrial marine environment marks the boundary between the Ecca Group and the Beaufort Group, which occurred over a period of about 250 Ma. Johnson et al. (2006) reported that subsequent orogenic activity at the beginning of the Triassic, with associated uplift, resulted in the influx of Beaufort and Stromberg Group sediments which extended throughout the basin. Prior to the Middle Jurassic period, the environmental conditions in the Karoo Basin changed rapidly, coupled with the large movement of the Earth's mantle, the crust experienced a large-scale lifting, and eruption of massive volumes of basaltic lava that constitute the Drakensberg Group. The outpourings of the basaltic lava spread across much of Gondwana about 180 Ma indicating the start of Gondwana break-up. The magma made its way to the surface along a complex system of fractures. Crystallization of the magma within these fractures resulted in the dolerite sills and dykes (about 183 Ma). The presence of numerous sills in the Karoo Basin fed the erupted lava and these sills were linked to the break-up of Gondwana (Johnson et al., 1996). The extrusive equivalents of these dolerites are present as an erosional remnant of continental flood basalt to the northeast of the study area.

The main deformation that took place in the Cape Fold Belt at about 250 Ma affected the Proterozoic meta-sediments, as well as the overlying Paleozoic cover (Weckmann et al., 2012). The Karoo Basin was first referred to as a passive margin (Smith, 1995). Subsequently, it was generally referred to as a retroarc foreland basin, with fills in front of the Cape Fold Belt situated in southwestern Gondwana (Dickinson, 1974; Johnson and Beaumont, 1995). The rocks of the Cape Supergroup are more resistant to erosion when compared to the softer rocks of the Karoo Supergroup. The sedimentary fill of the Karoo Basin are result of crustal uplift, fault-controlled subsidence, and long periods of regional subsidence during which faulting was subordinate (Tankard et al., 2009; 2012). Hälbich (1993) envisaged that the lower units of the Karoo Basin, as well as the Cape Supergroup rocks were deformed at about 250 Ma, with the formation of north-vergent asymmetric or overturned folds and thrust faults. The development of the Cape Fold Belt during the deposition of sediments within the Karoo Basin greatly influenced the depositional environments within the basin and is in turn considered as the major source of detritus to the

Karoo Supergroup. The intense deformation of the Cape Supergroup strata and some lower units of the Karoo Supergroup along the southern margin of the basin are considered to be a direct consequence of the orogeny (Johnson et al., 2006). The source of the sedimentary fill in the Karoo Basin is related to the mountain belt in the paleo-Pacific southwestern Gondwana when rifting of the Gondwana supercontinent began, also referred to as the flexural subsidence stage (Johnson, 1991; Cole, 1992; Duncan et al., 1997).

2.3 Tectonic setting

The tectonostratigraphic development of southern Africa that span from the Paleozoic to Early Mesozoic can be likened to the evolution of western Gondwana (Catuneanu et al., 1998). The several lithospheric plates that separated to form the current Southern Hemisphere continents and India was once together as the Gondwana supercontinent. The southern African remnant of these continents contain the Karoo basins that include the Main Karoo Basin and Great Kalahari Basin (Kalahari Karoo, Aranos, and Mid-Zambezi Basins), as well as other smaller basins in South Africa, Namibia, Zimbabwe and Mozambique (Figure 2.1). Detailed record for southern Africa is still less complete when compared to South America and Antarctica, as a result of the major Mesozoic regional strike-slip and extensional tectonics that removed most of the Late Paleozoic record to the south of the present day South Africa (Flint et al., 2011). Tankard et al. (2009) interpreted the tectono-sedimentary evolution of the Karoo Basin by dividing it into a pre-foreland and foreland phase. According to Tankard et al. (2009), the pre-foreland Karoo Basin that comprises of the Dwyka, Ecca and lower Beaufort Groups developed within the continental interior of Gondwana due to vertical movement of rigid or firm blocks and intervening crustal faults. The foreland Karoo Basin (comprising of the upper Beaufort Group) developed as a response to the uplift of the Cape Fold Belt during the Early Triassic.

The tectonic regime during the Karoo time was related to compression and accretion that occurred along the southern margin of Gondwana coeval with extension promulgating into the supercontinent from its Tethyan margin (Wopfner, 2002). From the start of the Late Carboniferous, tensional stresses propagated gradually to the south from the Tethyan margin, controlling the deposition of Karoo sediments in grabens and subsequent rift structures. The unique combination of the tectonic stresses that were sourced from the convergent and divergent boundaries of Gondwana led to the development of several basin types throughout Africa. Tectonic and dynamic loads created accommodation in the south, while rifting

generated accommodation to the north. Pysklywec and Mitrovica (1999) proposed that the subsidence was partially controlled by dynamic topography in relation to the subducting slab. Their numerical models estimate that 20-30% of sediment accumulation space in the Karoo could have been created by mantle flow (with the subducting slab dipping at 25° to 40°, and a distance to the trench of between 600 km and 1300 km). Geological and geophysical study by Tankard et al. (2009) attributes both Cape and Karoo Basin formation to fault-controlled subsidence of crustal blocks, followed by long periods of regional subsidence due to subduction-driven mantle flow (Pysklywec and Mitrovica, 1999). These thick skinned tectonic models involve basement deformation and movement along crustal-scale structures (Coward, 1983). Halbich (1992) and Gresse et al. (1992) recognised and dated eight coaxial compressional deformations (tectonic paroxysms) in the foreland setting. These tectonic events resulted in varying sedimentary responses (Catuneanu et al., 1998), which was previously inferred to have occurred within a single subsiding basin typified by incessant rise in the base-level in any part of the foreland setting (Rust, 1975; Turner, 1975; Cole, 1992). The two major periods of recurrent subsidence and sedimentation within the interior of Gondwana are represented by the Cape and Karoo basins (Tankard et al., 2009).

The Cape basin that span from the Early Ordovician to Early Carboniferous (about 160 Ma) is believed to have developed due to extensional processes that occurred in an episutural setting (Cloetingh et al., 1992). After about 30 Ma hiatus, the Late Carboniferous to Jurassic Karoo basin was formed as a tabular cover (Geel et al., 2013). Tankard et al. (2012) suggested that the wide thrust fold belt (Cape Fold Belt) is a strike-slip belt, while the adjacent Karoo Basin is a flexural foreland basin based on the basement architecture, timing of the Cape orogeny, and stratigraphic relationships. The ages of orogenic paroxysms P1, P2, P3, P4, P5, P6, P7, and P8 using the K-Ar and Ar-Ar techniques are documented to be 292 ± 5 Ma, 278 ± 2 Ma, 258 ± 2 Ma, 246 ± 2 Ma, 239 Ma, 230 ± 3 Ma, 223 Ma, and 215 ± 3 Ma, respectively (Halbich et al., 1983; Gresse et al., 1992; Figure 2.4). The orogenic paroxysms ages were determined by dating the final phases of compression and metamorphism that were connected to each pulse of orogenic activity (that is the cooling age of metamorphic minerals), meaning that the dates connote the end of active phases of tectonism. Paroxysms P1 and P2 took place during the deposition of Dwyka Group, P3 was coeval with the distal fluvio-deltaic Vryheid sedimentation (which is the only non-marine formation in the Ecca Group), P4 occurred during Balfour sedimentation, P5 is said to be coeval with the deposition of the Tarkastad Subgroup, P6 matches with the bottom (base) of

the Molteno Formation, P7 coincides with the base of the Transitional Member, and P8 occurred at the base of the Elliot Formation (Figure 2.6).
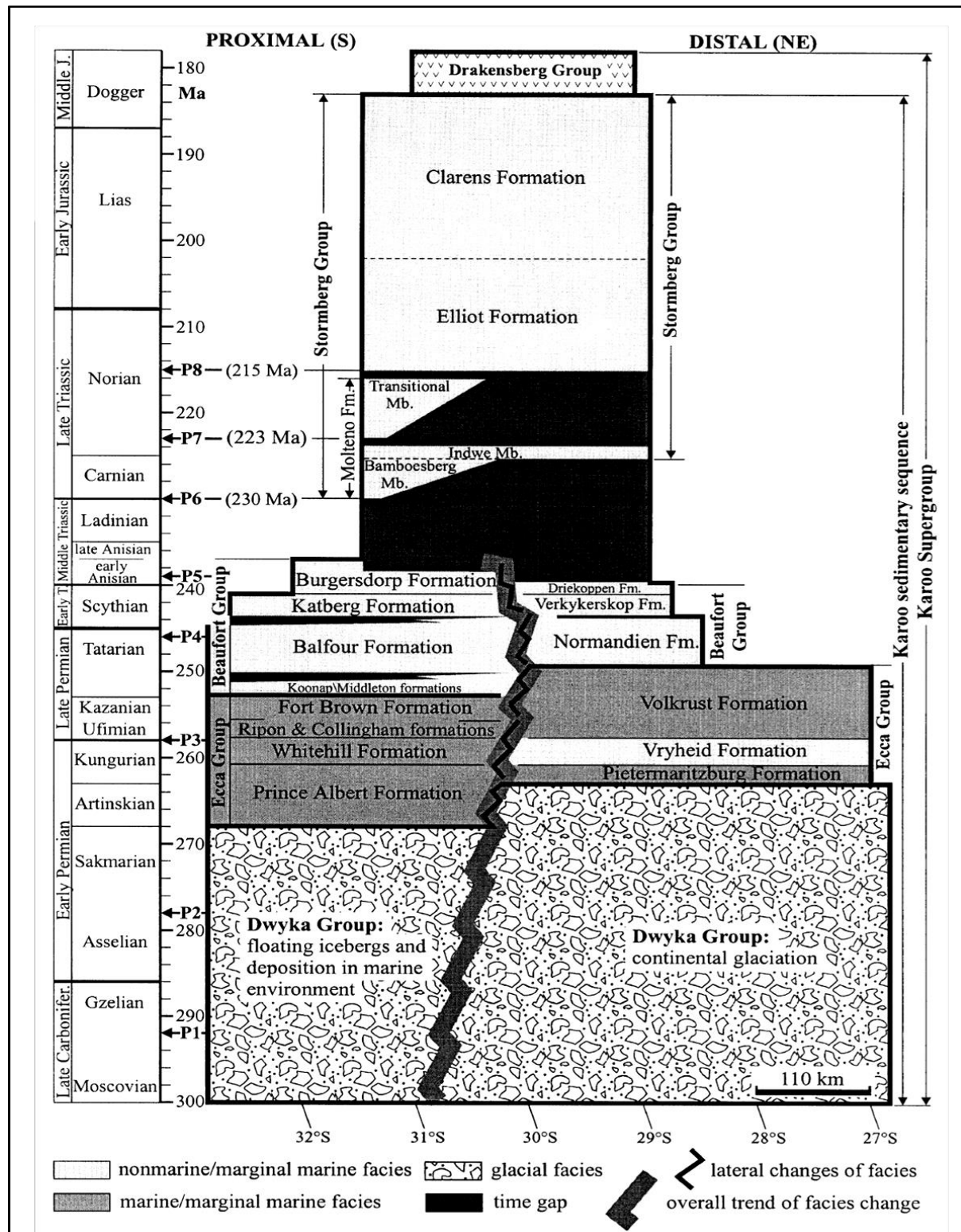
Figure 2.6: Summary of the main stratigraphic subdivisions of the Karoo Supergroup. P1-P8 represents the tectonic paroxysms in the Cape Fold Belt (Modified by Catuneanu et al. (1998) from Halbich (1983) and Gresse et al. (1992)).

The flexural tectonism of the Karoo foreland system ended during the first episode of unloading which occurred during the Late Triassic and lasted until the Middle Jurassic (Catuneanu et al., 2005). However, two other smaller tectonic events in the Cape Fold Belt (P7 final phase approximately 223 Ma and the P8 final phase which is about 215 ± 3 Ma) were documented in addition to the first episode of unloading (Halbich et al., 1983; Catuneanu et al., 1998). During the period of unloading, the proximal area of the system which are close to the Cape Fold Belt were uplifted, eroded and transported into the distal part of the basin that served as a depositional foresag. Orogenic paroxysms were followed by episodes of orogenic unloading. During the development of the Cape Fold Belt, the cycles of orogenic quiescence (unloading) that followed the orogenic paroxysms define the eight cycles of orogenic loading and unloading (Catuneanu et al., 1998; 2002). Within each cycle, the comparative period between the cycles of loading and unloading in the Cape Fold Belt was determined based on the stratigraphic patterns in the Karoo Basin (Catuneanu et al., 1998). Pysklywec and Mitrovica (1999) proposed that all the distal subsidence with a substantial component (about 30%) of the proximal subsidence could be accounted for by the dynamic subsidence that resulted from the deflection of the lithosphere.

Vorster (2013) documented that the detrital zircon age population of samples collected from the Dwyka Group of the lower Karoo Supergroup resembles that of the Cape Supergroup. The ice-flow directions during Dwyka Group glaciation are thought to have been southerly-, northerly- and westerly-directed in relation to the Early Karoo Basin, thus, source regions were considered to be located to the south, north and east of the basin (Cole, 1992). The study conducted by Vorster (2013) on detrital zircon population in Karoo Supergroup shows the presence of Silurian to Carboniferous aged grains within the sediments of the Dwyka Group. This implies that grains of these ages were sourced in the vicinity of the Early Karoo Basin. In addition, there is a possibility that these grains of Silurian to Carboniferous age were sourced from the south during northerly-directed movement of the ice-sheet, since there is Silurian to Carboniferous aged source regions located towards the north of the Karoo Basin. Vorster (2013) reported that there is an abrupt change in the detrital zircon age populations is evident in the Ecca Group formations. As documented by Vorster (2013), the probability density diagrams of the individual samples show a very noticeable peak in the 300 Ma to 250 Ma age ranges, which can be linked to young detrital zircon grains of apparent Permian age constituting ~ 17% to ~ 34% of the total population. Due to the northerly directed Paleocurrent directions recorded in the Ecca Group, these young detrital zircon grains

perhaps originated from a juvenile source region located towards the south. It has long been assumed that an extensive magmatic arc had existed towards the south of the Karoo Basin, given the presence of tuffaceous materials in the Collingham Formation (Cole, 1992). Hence, it is suggested that the young detrital material was sourced from regions within this southern magmatic arc (Vorster 2013). The proportions of age groups among Carboniferous and older zircons in the detrital zircon populations of the samples from the Ecca shows content of similar aged grains within the Cape Supergroup and Dwyka Group. This part of the detrital zircon population (i.e. Permian aged grains) could have been sourced from the underlying sediments of the Dwyka Group and Cape Supergroup. Cole (1992) documented that the deposition of the rocks of the Ecca Group must have occurred during the Mid Permian times. The substantial Permian detrital zircon age component observed by Vorster (2013) in the samples from the Ecca Group also point to the fact that this might be the likely maximum age.

Tectonism and climate are the two main allogenic controls that influenced the sedimentary fill of the Karoo Basin (Tankard et al., 1982; Catuneanu et al., 1998; 2005; Johnson et al., 2006). During the deposition of the Karoo Supergroup, the tectonic regimes changed from mainly flexural in the south, in response to processes of subduction, accretion and mountain building along the Panthalassan (palaeo-Pacific) margin of Gondwana, to extensional in the north, in response to processes of spreading along the Tethyan margin of Gondwana. Catuneanu et al. (2005) envisaged that the tensional episodes initiated during the Karoo time led to the development of the early Tethyan spreading centre. This continued to control deposition in the Karoo basin until break-up of Gondwana in the Middle Jurassic. Propagation of tensional stresses from the Tethyan margin to the south started during the Late Carboniferous, thus controlling the rate of deposition of Karoo sediments in the developed grabens and rift structures. Superimposed of the tectonic control on basin development, changes in climatic conditions also left a mark on the stratigraphic record, showing evidence of an overall shift from cold and semi-arid conditions (marine-delta) during the Late Carboniferous-Early Permian, to warmer conditions and finally hot climates (desert conditions) with changing amount of precipitation during the remaining Karoo time (Johnson, 1976; Stavrakis, 1980; Visser, 1991). The fluctuations in tectonic and climatic conditions from the southern to the northern part of Africa during the Karoo time have led to significant changes in the lithostratigraphic characteristics of the Karoo sequence across the African continent.

2.3.1 Accommodation in the Karoo Basin

The Karoo retroarc foreland system form through the flexural deflection of the lithosphere in relation to a mixture of supra- and sublithospheric loads (Catuneanu et al., 1999). The changes or variations in accommodation within the Karoo Basin were modelled by Catuneanu et al. (1998) and they pointed out that the accommodation is being controlled by the flexural response of the lithosphere to orogenic cycles or episode of loading and unloading. The supracrustal loading orogens led to the subdivision of the Karoo foreland system into flexural provinces (i.e. the foredeep and forebulge; Figure 2.7). The subsequent addition of loads into the orogenic belts by thrusting resulted in subsidence of the foredeep and uplift of the forebulge, but opposite occurred when orogenic load is been removed by extension or erosion. This trend of opposite or reverse vertical tectonics alters the comparative quantity of available accommodation in the two flexural provinces (foredeep and forebulge), and may create out of phase proximal to distal stratigraphies (Catuneanu et al., 2000).

The out of phase history of base level were said to change between the foredeep and the forebulge provinces, thus resulting in different stratigraphies with a timing that correspond to the compressional events that was dated in the Cape Fold Belt (Catuneanu et al., 2000). Together with flexural tectonics, the superimposed effects of the eustasy and dynamic (sublithospheric) loading could also generate or destroy the additional accommodation. Supralithospheric loading usually works at regional scales, and depends on the dynamics and geometry of the processes of subduction beneath the basin (Catuneanu et al., 1997). Sublithospheric loading that is controlled by subduction process beneath the basin triggered the dynamic subsidence (Burgess et al., 1997). Flexural tectonics and dynamic loading are both inferred to have contributed significantly to the total amount of subsidence in the Karoo Basin based on the stratigraphic evidence (Catuneanu et al., 1998). Catuneanu et al. (1998) documented the subdivision of the Karoo foreland system into foredeep and forebulge settings, and mapped the hinge line that separates the two flexural provinces for consecutive time slices. They envisaged that the hinge line moved along the dip relative to load redistribution in the Cape Fold Belt, from the end of the Carboniferous to the Triassic.
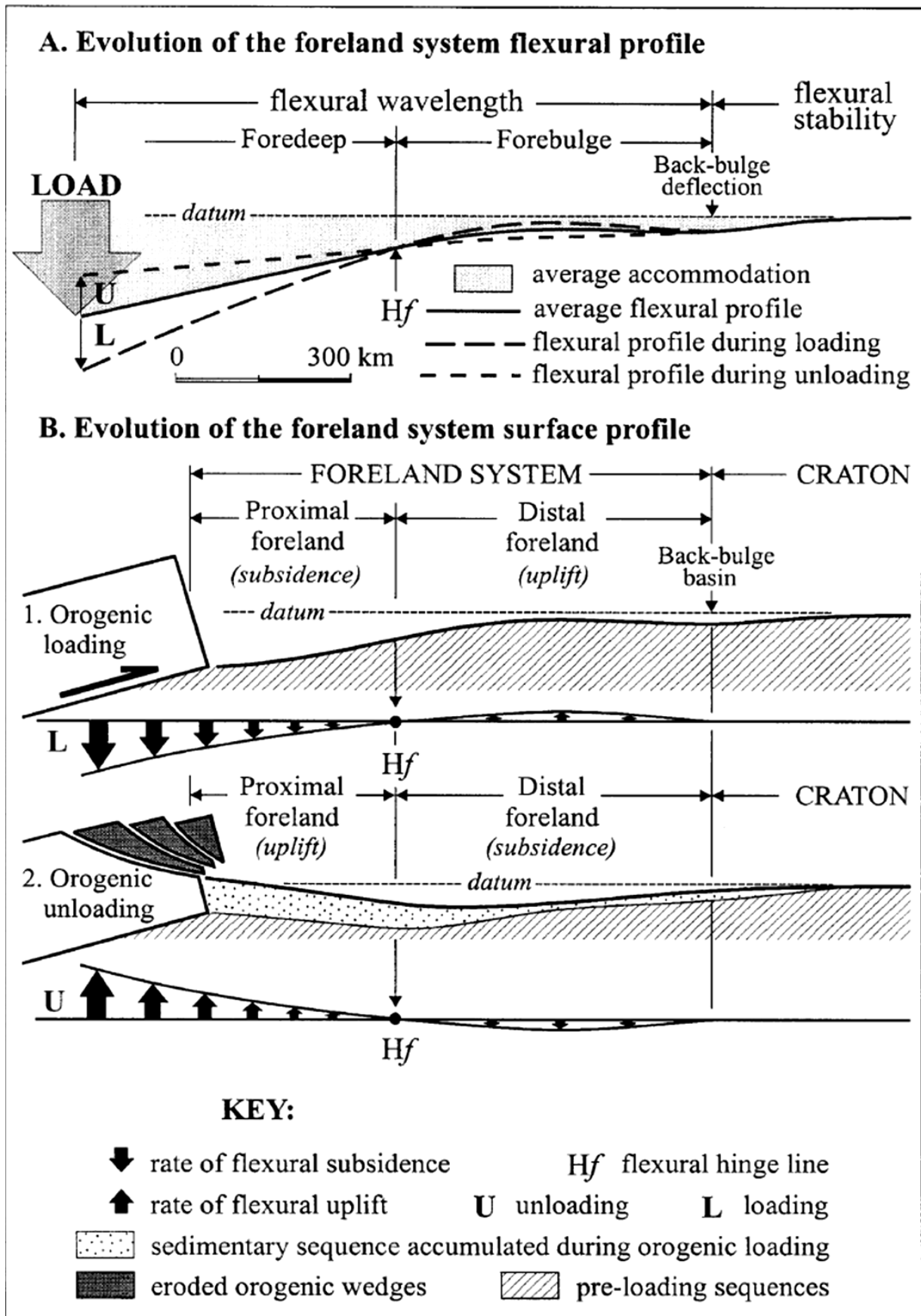
Figure 2.7: Flexural and surface profiles illustrating the evolution of the foreland system during stages of orogenic loading and unloading (After Beaumont et al., 1993).

Miall (1997) reported that the inter-relationship between the base level changes and supply of sediment controls the extent in which the available accommodation was used up by sedimentation. This relationship defines the underfilled, filled and overfilled depositional stages in the evolution of Karoo foreland basin that is dominated by deep marine (Dwyka-lower Ecca), shallow marine (upper Ecca) and fluvial sedimentation (Beaufort-Stormberg) respectively. It is most likely that the Prince Albert and Whitehill Formations were formed in a reducing deep water marine environment, while the Collingham Formation is a tranquil and deep water turbidite deposit. The Ripon Formation was formed in a shallow marine to deltaic environment whereas the overlying Fort Brown Formation was developed in a broad continental margin of lacustrine environment (Figure 2.8).
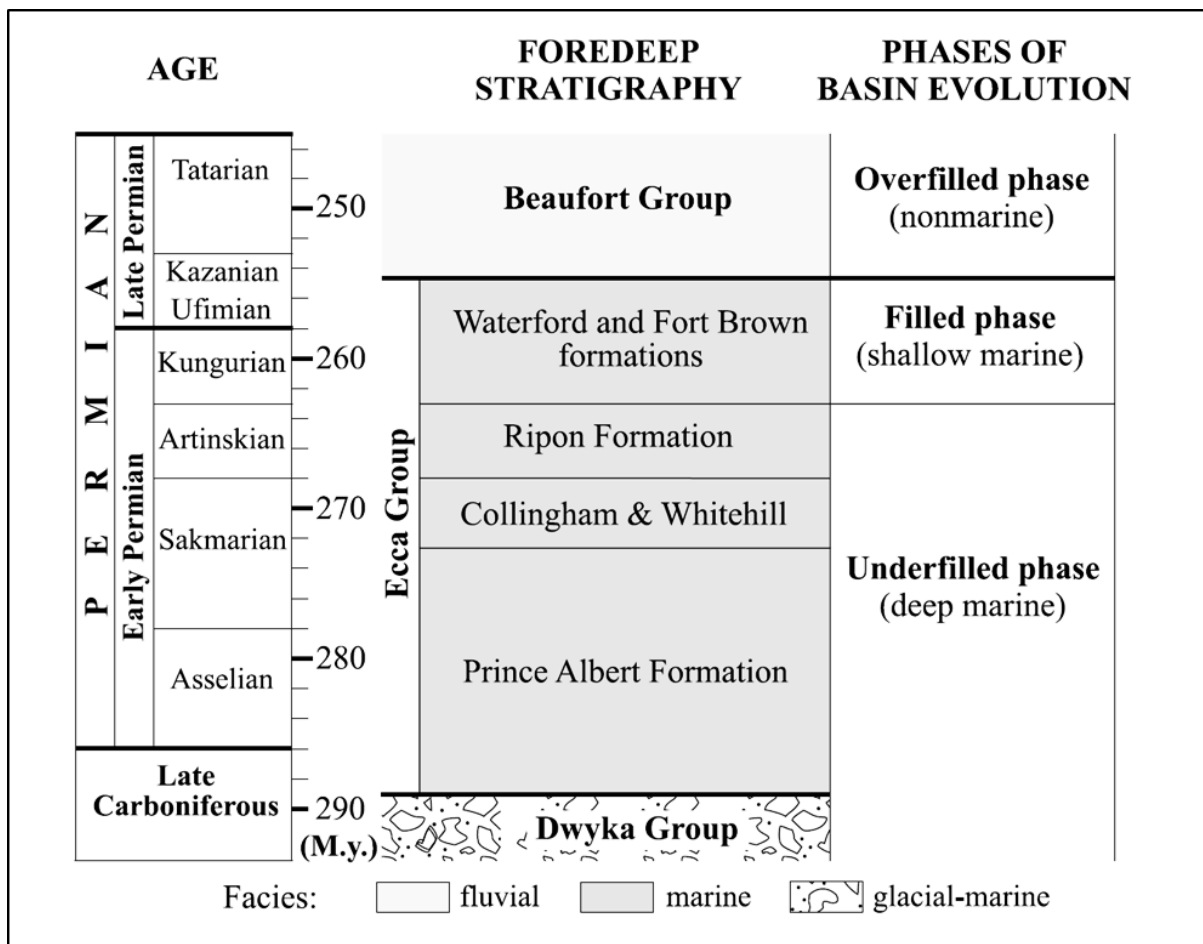
Figure 2.8: Summary of the main stratigraphic subdivisions of the Ecca Group and the stages of evolution of the Karoo foredeep (Catuneanu, 2004; Fildani et al., 2009; Lindeque et al., 2007; Shen et al., 2013).

2.4 Stratigraphy

The Late Carboniferous-Early Jurassic succession of Karoo Supergroup is clearly different in lithology and depositional environment (Catuneanu et al., 2005). These tectono-stratigraphic units are preserved as both fining upward and coarsening upward megacycles forming the basis of the lithostratigraphic sequence (Visser and Dukas, 1979). The succession of the Karoo Supergroup is stratigraphically divided into five main groups, which are, in their ascending stratigraphic order, the Dwyka (Late Carboniferous), Ecca (Early-Middle Permian), Beaufort (Late Permian-Middle Triassic), Stormberg (Late Triassic-Early Jurassic) and Drakensberg Groups (Middle Jurassic) (Damiani, 2004) as shown in Figure 2.9 and Table 2.2, with their aerial distribution depicted in Figure 2.10. SACS (1980) disagrees with the use of Stormberg Group in a formal lithostratigraphic scheme due to insufficient unifying lithologic features. However, it is used here for the sake of convenience. A major stratigraphic gap that coincides with the Late Anisian-Ladinian interval is usually used to separate the underlying Dwyka, Ecca and the Beaufort Groups from the overlying Stormberg and Drakensberg Groups (Catuneanu et al., 1998). With the exception of igneous rocks of the Drakensberg Group, all other Karoo Supergroup is made up of sedimentary rocks and in this research study, it is referred to as Karoo sedimentary sequence.
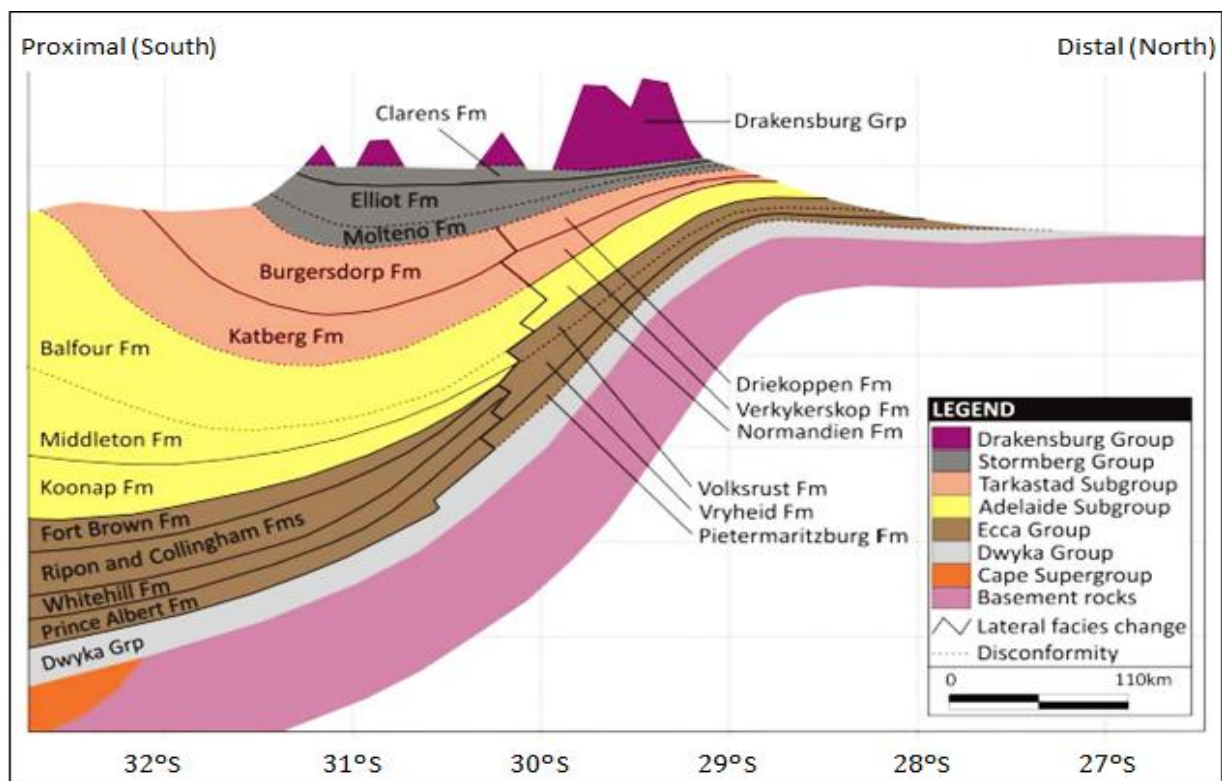
Figure 2.9: Stratigraphic section across proximal south and distal north Karoo Basin (After Catuneanu et al., 1998).

Table 2.2: Lithostratigraphy of the Karoo Supergroup in the Eastern Cape Province as compiled by the Council for Geoscience (Johnson et al., 2006).

SUPERGROUP	GROUP	SUBGROUP	FORMATION	MEMBER	LITHOLOGY	MAXIMUM THICKNESS (M)
KAROO			Drakensberg		Basalt Pyroclastic Deposits	1400
			Clarens		Sandstone	300
			Elliot		Red Mudstone Sandstone	500
			Molteno		Coarse Sandstone Grey & Khaki Shale Coal Measures	450
	BEAUFORT	TARKASTAD	Burgersdorp		Red Mudstone Light Grey Sandstone Grey Shale	1000
			Katberg		Light Grey Sandstone Red Mudstone Grey Shale	900
		ADELAIDE	Balfour	Palingkloof	Red Mudstone Light Grey Sandstone Grey Shale	50
				Elandsberg	Sandstone Siltsone	700
				Barberskrans	Light Grey Sandstone Khaki Shale	100
				Daggaboersnek	Grey Shale Sandstone Siltsone	1200
				Oudeberg	Light Grey Sandstone Khaki Shale	100
			Middleton		Grey & Black Shale Light Grey Sandstone Red Mudstone	1500
			Koonap		Grey Sandstone Shale	1300
	ECCA		Waterford (Not present in Ecca Pass)		Sandstone Shale	800
			Fort Brown		Shale Sandstone	1500
			Ripon		Sandstone Shale	1000
			Collingham		Grey Shale Yellow Claystone	30
			Whitehill		Black Shale Chert	70
			Prince Albert		Khaki Shale	120
			Dwyka		Diamictite, Tillite, Shale	750

32
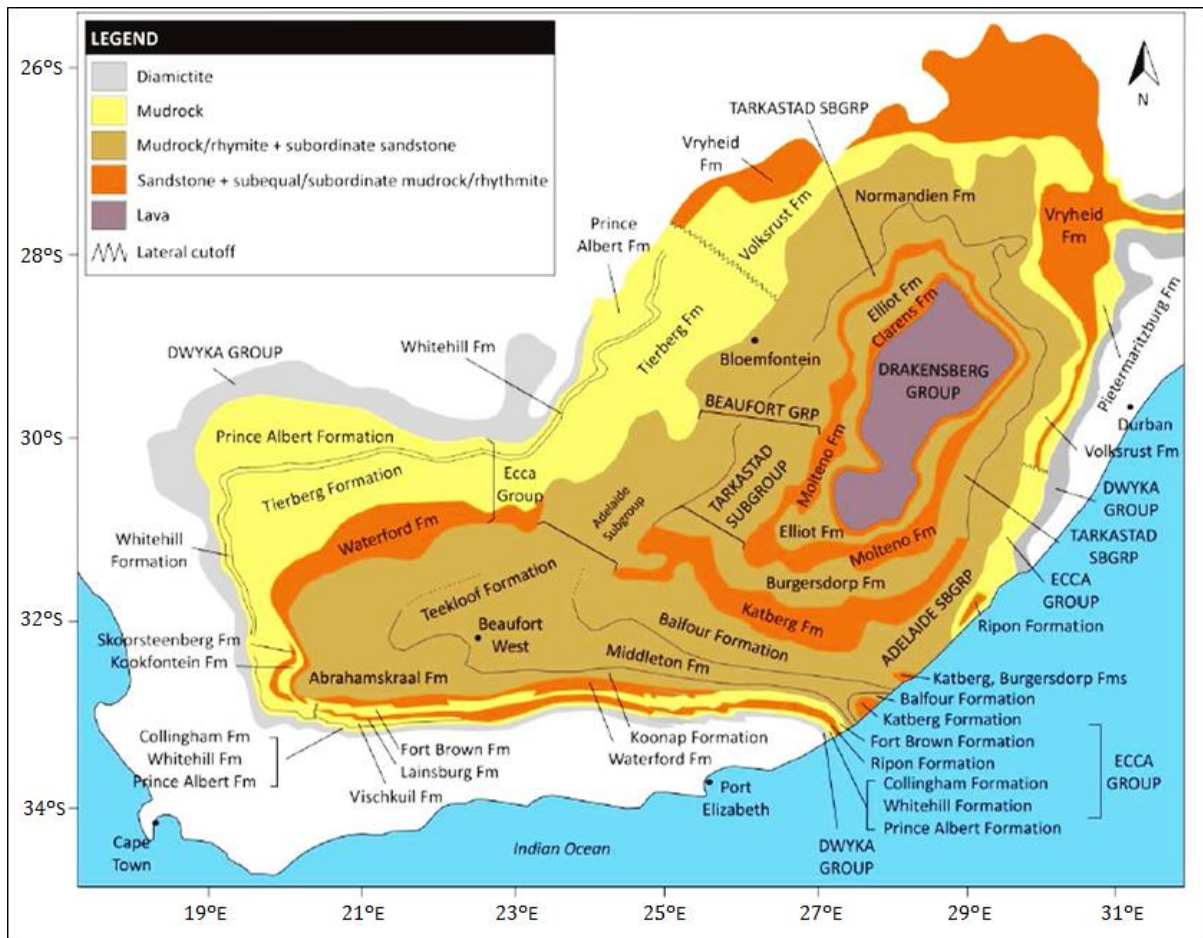
Figure 2.10: Areal distributions of lithostratigraphic units in the Main Karoo Basin (After Johnson et al., 1996; Catuneanu et al., 1998).

The stratigraphy of the Karoo Supergroup generally represents deposition in glacial, marine and terrestrial environments (Damiani, 2004). The filling of the Karoo Basin started with the carbonaceous glaciogenic sediments of the Dwyka Group (Johnson, 1991). Catuneanu and Elango (2001) envisaged that the deeper marine facies of the Dwyka Group and early Ecca Group were accumulated during the under-filled phase of the Karoo foreland system, while the shallow marine facies of the late Ecca Group matches with the filled phase of the basin, and was subsequently followed by fluvial-dominated overfilled phase (Figure 2.8). Damiani (2004) suggested that, from the Late Permian onwards, the non-marine sediments were deposited and provenance primarily from the rising Cape Fold Mountains along the southern margin. Furthermore, the episodic tectonics in the source area, coupled with the foredeep subsidence, led to deposition of the sediments on large prograding alluvial fans. The stratigraphy of the Main Karoo Basin is however complex and this complexity is related to its mode of origin (Catuneanu et al., 2005). Lithostratigraphically, the Karoo Basin can be

33

subdivided into three distinct areas (Catuneanu et al., 1998). The areas are separated from one another by a transitional zone over which lateral facies changes occur (Figure 2.10).

1. The western area: It is located west of 24°E and situated adjacent to the Cape Fold Belt, representing the proximal Karoo Basin facies. The western area is related to the north northwest-south southeast strike of the Cape Fold Belt.

2. The southern area: It is located east of 24°E, situated adjacent to the Cape Fold Belt and represents the proximal Karoo Basin facies. The southern area is related to the west-east strike of the Cape Fold Belt.

3. The north-eastern area: It is situated far away from the Cape Fold Belt and represents the distal Karoo Basin facies.

The stratigraphy of the Karoo Supergroup in the northern (distal) region differs from the stratigraphy in the southern (proximal) region. The stratigraphic variation that was observed within the basin reveals different tectonic/evolutionary histories across the flexural hinge line of the foreland system (Catuneanu et al., 2002). They further reported that a deep marine depositional environment must have controlled the processes of sedimentation in the south, which led to the accumulation of the marine Dwyka tillite with dropstones, as well as the basin floor pelagic sediment of the lower Ecca Group (Prince Albert and Whitehill Formations) and the submarine fans of the Collingham and Ripon Formations. Sedimentation in the southern region (proximal) of the basin continued with the deposition of the shallow marine deposits that include the shelf and marginal marine facies of the upper Ecca Group (Fort Brown and Waterford Formations). In relation to sediment deposition in the south, sediments aggradation occurred in the northern (distal) region of the basin and in the shallow marine and non-marine environments (Catuneanu et al., 2002).

The stratigraphy of the Dwyka-Ecca Group in the distal region of the basin is characterized by the continental tillites of the Dwyka Group, shallow marine facies of the Pietermaritzburg and Volkrust Formations, and the coal-bearing fluvial-deltaic strata of the Vryheid Formation (Figure 2.9). The bathymetric conditions of the interior seaway that was glacial-deep marine during the Dwyka-lower Ecca time, changed to shallow marine condition during the upper Ecca time (Visser and Loock, 1978). Johnson (1976) reported that the change from glacial (Dwyka) to post-glacial (Lower Ecca) sedimentary environments occurred first in the southwestern part of the basin before the northern and eastern parts of the basin. The existence of an environment that is completely non-marine within the confines of the

34

preserved basin was due to the regression of the Ecca seaway, which led to the accumulation of the fluvio-lacustrine Beaufort Group as well as the aggraded fluvial and aeolian Stormberg Group (Smith et al., 1993).

2.4.1 Dwyka Group

The filling of the Karoo Basin commenced with the deposition of the carbonaceous glaciogenic Dwyka Group consisting of glacial tillites and shales, (Johnson, 1991). The Late Carboniferous - Early Permian Dwyka Group in the Main Karoo Basin attained a thickness of about 750 m, and rests on the glaciated Precambrian bedrock surfaces along the northern margin of the basin. But, it unconformably overlies the Cape Supergroup in the south, while it conformably overlies the Natal Group and Msikaba Formation in the east (Johnson, 1991). Generally, the group ranges in thickness from 600-750 m and rests disconformably on the Witteberg Group of the Cape Supergroup (SACS, 1980; Johnson, 1991). Catuneanu and Elango (2001) envisaged that the initiation of sedimentation in the Dwyka Group is estimated at about 300 Ma, following the 30 Ma stratigraphic breaks that took place after the end of Visean, when sedimentation in the Cape basin was terminated. The ice-flow direction signifies origin from the north (Cargonian Highlands), east (Eastern Highlands now in East Antarctica), and southwest (Southern Highlands now in West Antarctica) (Visser, 1997). Cole (1992) also reported that the ice flow markers indicate provenances to the north, east and south with Precambrian rocks dominating the northern and eastern sources, while the southern source is believed to have been a magmatic arc associated with subduction of the palaeo-Pacific plate margin beneath the Gondwana plate. The foreland loads that are associated with the subduction instigated the deposition of the Dwyka Group diamictites (Johnson, 1991; Catuneanu and Elango, 2001).

Visser (1986) recognised seven lithofacies in the Dwyka Group that include the massive diamictites, stratified diamictites, massive carbonate-rich diamictites, conglomerate facies, sandstone facies, mudrock with drop-stone facies and finally the mudrock facies. These lithofacies are thought to have been deposited in a marine setting and they grade upward into finer-grained clastic rocks indicating that the deposition of sediments in the glacial environment is from both grounded and floating ice (Johnson et al., 2006). However, there is no clear contrast between the Dwyka successions in the south (proximal) and the north (distal) (Catuneanu et al., 1998). The massive diamictite facies consist of highly compacted diamictites, generally clast-rich with angular to rounded striated stones of about 2 m across,

and usually reveals the composition of the surrounding or underlying bedrock, thus it can be described as lodgement or melt-out deposits (Johnson et al., 2006).

The stratified diamictites facies consist of argillaceous diamictite comprising of subround to rounded extra-basinal clasts as much as 3 m across. The stratification has faint bedding planes within the diamictite as well as thin interbedded mudrock beds and laminae. These stratified diamictites have been formed by sediment gravity flows, though intermittent reworking of subglacial diamictons and rain-out of glacial debris also occurred during deposition (Johnson et al., 2006). Visser (1991) documented that the massive carbonate-rich diamictite facies are clast-poor diamictites that comprises of thin carbonate beds of about 5 cm, with stringers and concretions forming thick facies units. These facies are believed to have been formed from the rain-out of debris, with the carbonate probably originating by crystallization from interstitial waters (Johnson et al., 2006).

The conglomerate facies range from single layered boulder beds to poorly sorted pebble and granule conglomerate, with boulder beds interpreted as lodgement deposits, whereas the poorly sorted conglomerates are products of water reworking of diamictons by high density sediment gravity flow (Johnson et al., 2006). Large sandstones are found within the massive sandstone diamictite facies. These sandstones can have thickness of up to 30 m. Von Brunn (1994) described these facies as consisting of either very fine to medium grained, massive to ripple-laminated or medium to coarse grained, trough cross bedded, immature sandstones. The ripple laminated sandstones are interpreted as turbidite deposits, whereas the trough cross-bedded sandstones are believed to be tractional fall-out from subaqueous outwash streams. The mudrock with dropstone facies consists mainly of rhythmite. Angular to round detrital stones of varying sizes (maximum $\pm$ 1 m across) are usually seen deforming the rhythmite. These facies signify deposits in a distal iceberg zone (Visser, 1991). The mudstone with stone facies differs from the ordinary mudstone facies because of the absent of detrital stones in the ordinary mudstone facies, the ordinary mudstone facies consist of greenish grey mudstone and black pyrite shale (Visser, 1991) and they are products of suspension settling of mud and tractional fall out of silt from sediment-laden underflows.

Some researchers suggested a marine depositional environment for part of the glacial deposits (Cole, 1992; Johnson et al., 1996; Catuneanu et al., 1998; Rubidge et al., 2000). There is no unequivocal evidence for the marine setting, but there is a possibility that the majority of the Dwyka sequence was deposited in a terrestrial setting (du Toit, 1926 in Rubidge et al., 2000).

The deeper marine glacial facies of the Dwyka Group including those of the early Ecca Group accumulated during the under-filled phase of the foreland basin (Catuneanu et al., 1998). Catuneanu et al. (1998) documented that, in the southern part of the basin, the Dwyka succession has a uniform character with lateral continuity of layers; signifying deposition from floating ice within a large marine basin was a dominant process. Bamford (2004) also agrees with this idea by explaining that the tillites are uniform and laterally extensive, having formed in a glacial marine environment with deposition from both grounded and floating ice, with the latter being dominant.

2.4.2 Ecca Group

The term Ecca was suggested by Rubidge (1858) in Catuneanu et al. (2005) for argillaceous sedimentary strata that are exposed along the Ecca Pass, near Grahamstown in the Eastern Cape Province, South Africa. Hence, the use term "Ecca" outside the Main Karoo Basin is sometimes questionable or inappropriate, because the rock types could be completely different. According to Catuneanu et al. (2005), the Ecca Group is a rock sequence that accumulated between the Late Carboniferous Dwyka Group and the Late Permian-Middle Triassic Beaufort Group. The absolute age of the group is not well-constrained and most age determinations and correlations rely on fossil wood biostratigraphy and palynology (Bamford, 2000). In the study area, the base of the Ecca Group is defined at the top of the glaciogenic succession of the Dwyka Group with varied sequences predominantly of mudstones, siltstones, sandstones, with occasional conglomerates and coal. It is estimated that the Ecca Group attained a thickness of about 3000 m in the southern part of the basin and can be subdivided into six formations, namely, the Prince Albert, Whitehill, Collingham, Ripon, Fort Brown and Waterford Formations, respectively (Johnson et al., 1996; Table 2.2). These formations are partially correlative to the Pietermaritzburg, Vryheid and Volkrust Formations in the northeast of the basin (Catuneanu et al., 1998; Figure 2.9).

The marine clays and mudstones of the Prince Albert Formation were deposited on the diamictites of the Dwyka Group in the southern part of the Karoo Basin. This was followed by the carbonaceous shale of the Whitehill Formation. Subsequently, the Collingham Formation that is made up of persistent grey shales alternating with yellow-claystones, as well as the sandstones and shales of the Ripon, Fort Brown and Waterford Formations were deposited on the submarine fans, shelf and deltas, respectively (Johnson, 1976). The quick lithological change from black carbonaceous shales of the Whitehill Formation to siliciclastic

turbidite deposits that are associated with abundant tuff beds of the Collingham Formation points to a change in the tectonic environment (Johnson et al., 2006). The distal turbidites and volcanic ash layers of the Collingham Formation is the only layer of the Ecca Group that can be directly linked to the southern volcanism with evidence of active volcanic ash. There is likelihood that the tuffs beds in the Collingham Formation are products of the Permian silicic-andesitic and plutonic rocks volcanoes (Veevers et al., 1994; Wickens, 1994). The presence of ash beds in the Collingham Formation indicates volcanism in the source area (Viljoen, 1994).

Williamson (1996) partitioned the Ecca Group into the lower, middle and upper parts. The lower part of the Ecca Group with maximum thickness of about 107 m consists of a succession of fine-grained arenaceous to silty beds that are typically dark-coloured (Johnson et al., 2006). The middle part of the Ecca Group with maximum thickness of approximately 165 m is characterized by the development of yellow and white, medium to coarse-grained feldspathic sandstones (Johnson et al., 2006). The sandstone bands become thinner upward and eventually disappear completely, leaving an entirely argillaceous and carbonaceous succession which is known as the upper part of the Ecca Group with maximum thickness of approximately 138 m (Johnson et al., 2006). The Ecca Group rests directly on the pre-Karoo surface in some places, indicating a significant post-Dwyka Group topography and localized pre-Ecca erosion, such as non-deposition or erosion of the Dwyka Group (Smith, 1984; Williamson, 1996; Segwabe, 2008). The non-carbonaceous that is usually silty and calcareous mudstones with small amounts of fine- to coarse-grained sandstones and siltstones marks the start of the upper part of the Ecca Group (Williamson, 1996; Johnson et al., 1996). The three types of sedimentary structures that have been used to provide dependable palaeo-current data in the Ecca Group are sole clasts, current lineation and micro-cross lamination (Kingsley, 1977). Generally, sole marks, cross bedding and parting lineation are typically used in palaeo-current analysis. Kingsley (1977) envisaged that the even distribution of current directions in the Ecca Group suggests the existence of a large mountainous source area to the south and south east of the current coast line during the Permian-Triassic times.

2.4.3 Beaufort Group
Most of the continental deposits of the Karoo Supergroup are grouped in the aerially broad Beaufort Group that developed from a large quantity of the sediments, produced from the fast rising Cape Fold Belt (Johnson et al., 1997). The Beaufort Group consists of fine-grained

sandstones and mudstones that show fining-upward sequence (Visser, 1995). The group can be divided into two subgroups, namely, the Adelaide and Tarkastad Subgroups (Table 2.2). The Late Permian Adelaide Subgroup that forms the lower part of the group comprises of the Koonap, Middleton and Balfour Formations in the southeastern part of the basin. The Abrahamskraal and Teekloof Formations in the western part are approximately equivalents of the Koonap and Middleton Formations, and a single Normandien Formation in the northern part (Johnson et al., 1996; Catuneanu et al., 1998). The Koonap Formation consists of greenish silty-mudstones and sandstones in a fining upward sequence deposited when a high energy braided river system graded into a lower energy meandering river system (Bamford, 2004). The Middleton Formation has dark red and greenish grey mudstones interbedded with sandstones in an overall fining upward sequence. The Balfour Formation is a fining upward sequence of greenish-grey sandstones with bands of darker mudstones. The formation is thought to have been deposited when braided rivers graded upwards into meandering stream systems (Bamford, 2004). The Oudeberg, Daggaboersnek, Barberskrans, Elandsberg, and Palingkloof Members are the five members that make up the Balfour Formation. These members are distinguished based on the lithological variation, which is dominated and characterised by an alternating sequence of sandstones and mudstones.

Generally, the Adelaide Subgroup reaches a maximum thickness of about 5,000 m in the southeastern part and consists of a succession of bluish-grey, reddish-maroon and greenish-grey mudstones and subordinate fine-to medium-grained, tabular and lenticular sandstone. Though, the thickness decreases to about 800 m in the centre of the Main Karoo Basin. Subsequently, the thickness gradually decreases to around 100-200 m in the far north of the basin (Catuneanu et al., 1998). The Koonap, Middleton and Balfour Formations attain a maximum thickness of approximately 1,300 m, 1,600 m and 2,000 m, respectively (Johnson et al., 1996). In the western part of the basin, the lower Abrahamskraal Formation attained a maximum thickness of about 2,500 m, while the upper Teekloof Formation attained a thickness of approximately 1,400 m with its upper contact being eroded (Johnson et al., 1996). Cole and Smith (2008) used the presence of chert beds with more abundant sandstone and a paucity of reddish-maroon mudrock to distinguish between the Abrahamskraal and Teekloof Formations.

The Early Triassic Tarkastad Subgroup forms the upper part of the Beaufort Group. The subgroup comprises of the Katberg and Burgersdorp Formations, which are restricted to the southern margins of the Karoo Basin from south of Queenstown to north of Aliwal North

(Rubidge, 1995).The tectonic rejuvenation of the source area that occurred during the Early Triassic time led to steeper gradients, as well as a sharp increase in the supply of coarser grained detritus (Johnson et al., 2006). Consequently, alluvial fans were formed in areas adjacent to the source terrain and river channels became braided, depositing only sands that formed the Katberg sandstone, while mud and silts were further transported into the distal parts of the flood plain to give the Burgersdorp Formation (Nyathi, 2014). The Tarkastad Subgroup reaches a maximum thickness of approximately 2,000 m in the south and decreases to around 150 m or less in the far north (Johnson et al., 1996). Smith (1995) reported that the major coarsening upward sequence begins in the Balfour Formation and ends at the top of the Katberg Formation. The upper member of the Balfour Formation is characterized by red and maroon mudrocks as opposed to the dark grey and greenish grey mudrocks of the underlying strata (lower members), and this primarily argillaceous unit coarsens upwards into the arenaceous Katberg Sandstone Formation that is composed of fine to medium grained pinkish grey sandstone with subordinate greenish grey mudstone.

The Katberg Formation overlies the Palingkloof Member of the Balfour Formation. It is characterised by a high abundance of fine to medium grained, light grey sandstoneswith subordinate shale and red mudstones. The reddish-yellowish colour with massive bedding indicates oxidizing environment. The Burgersdorp Formation that conformably overlies the Katberg Formation consists of dark reddish-brown mudstones with subordinate red-maroon siltstones and occasionally, fine to medium grained grey sandstones. The Burgersdorp Formation is the youngest formation of the Permo-Triassic Beaufort Group, the sedimentary unit shows fining upward sequence representing a mixed load meandering river and aggrading floodplain deposit that preserve a fauna assignable to the Cynognathus Assemblage Zone. Smith (1980) envisaged that the strata of the Burgersdorp Formation are predominantly alternating mudstones and siltstones with subordinate lenticular and tabular channel sandstone deposited by a variety of fluvial systems. This resulted in fining-upward sequences of fluvial systems which prograded into the Karoo Basin at the time of basin fill (Smith, 1987; Rubidge, 1995; Smith and Ward, 2001). Almond (2013) also documented that the rocks of the Burgersdorp Formation were laid down within the Main Karoo by north-westwards flowing meandering rivers during a warm, arid to semi-arid climatic conditions and interpreted the well-laminated reddish mudrock with pedocrete layers (cemented soil) as playa lake deposits.

The Permo-Triassic (P-T) boundary is discernable at the base of the Palingkloof Member (Balfour Formation in the Adelaide Subgroup) along the Regional road R61 between Cradock and Tarkastad towns. This placement was based on vertebrate biostratigraphy, with the Permian fauna of the Dicynodon Assemblage Zone occurring in the Elandsberg Member and the overlying Early Triassic Lystrosaurus Assemblage Zone fossils restricted to the Palingkloof Member in the south (Gastaldo et al., 2009). The exact placement of the P-T boundary within this sequence is still a matter of debate. Presently, the boundary is placed at the terrestrial, time equivalent extinction event of the marine faunal crisis. In the Karoo Basin this event is marked by a major extinction of herbivorous dicynodonts and large amphibians (Smith and Ward, 2001). According to Smith (1995), below the P-T boundary, the sediments consist of drab greenish grey mudrocks with a few multi-storied, laterally accreted fine grained sandstone bodies, and above this boundary, the strata changed into reddish brown mudrocks with numerous thin ribbon sandstone bodies and more continuous sheet sandstones. These changes possibly came as a result of the changing depositional environments from marine to fluvial (Smith, 1995). The end-Permian extinction event is recorded at the base of the Palingkloof Member, the uppermost subunit of the Balfour Formation (Ward et al., 2005). However Gastaldo et al. (2009) argue that, it will be difficult to identify the exact stratigraphic position of the P-T boundary at the base of the Palingkloof Member in the basin; thus places doubt on the stratigraphic position of the P-T boundary.

The Beaufort Group is exposed almost over the entire Karoo Basin and is extensively intruded by dolerites. Duncan and Marsh (2006) envisaged that the dolerite intrusions were emplaced during crustal doming and stretching that preceded the break-up of Gondwana at about 180 Ma. The dolerites are not all of the same rock type, they differs and usually vary from being olivine-rich through tholeiitic composition to granophyre. Based on the minerals within the rocks, they are recognised by their differences in colour (Karpeta et al., 1979), with the sills usually depicting grading upwards through olivine, hyperite into gabbro. The ratio of the dolerites to the host rock usually varies across the formations that make up the Beaufort Group. The dolerites are more than the host rocks in some areas and vice versa. This could be due to the fact that some areas experienced much of magmatic activity than other areas. The dolerite intrusions (sills and dykes) created distinctive flat-top hills and mountains in the Karoo, which are the most visible remnant of the dolerite's sill that protect or covers the underlying sandstone from physical processes like weathering and erosion. The dolerite

sills and dykes created fractures or cracks in the Karoo that became water reservoir, thus dolerites are used as groundwater localiser in the Karoo (Chevallier et al., 2001).

2.4.4 Stormberg Group

The Stormberg Group is made up of fluvial and aeolian-lacustrine successions of the Molteno, Elliot and Clarens Formations (Johnson et al., 1996; Table 2.2). A major stratigraphic gap that corresponds to the Late Anasian Ladinian separates the Stormberg Group from the underlying Tarkastad Subgroup (Cole, 1992). This stratigraphic gap denotes the erosional boundary between the Beaufort Group and the overlying Stormberg Group. The Late Triassic-Early Jurassic age Stormberg Group in the southwestern region was deposited as a result of the final deformational phase in the Cape Fold Belt and subsidence of the southwestern Karoo Basin. The deposition occurred because the compressive nature of tectonic regime of the Karoo Basin was still active during the Late Triassic-Early Jurassic time (Hälbich et al., 1983). According to Turner (1975), in the southern outcrop area, the Late Triassic Molteno Formation attained a maximum thickness of about 600 m and can be subdivided into five members, namely, the Bamboesberg Member, Indwe Member, Mayaputi Member, Qiba Member and Tsomo Member. The thickness of the whole succession is less than 10 m in the far north of its outcrop area (Johnson et al., 1996).

The Molteno Formation is made up of medium to coarse grained sandstones that alternate with grey mudstones. The Molteno Formation involves two main coarsening-upward sequences in the southern region of the basin. The Bamboesberg Member and Indwe Sandstone Members form the basal sequence while the upper sequence consists of the Transitional Member (Johnson et al., 1996). The formation is dominated by horizontal tabular sheets of cross- stratified medium to coarse grained sandstones, which were deposited by braided streams (Catuneanu et al., 1998; Bamford, 2004). Likewise, Turner (1975) documented that the deposition of the Molteno Formation was predominantly by bed-load dominated rivers flowing across extensive braid plains. Siltstone, mudstone and coal are also present, but the coal is far less abundant when compared to the coal in Ecca Group. These deposits are interpreted as the fills of abandoned channel tracts and within ponded bodies of water on the braid plain (Turner, 1975). The relatively quartz-rich nature of the Molteno Formation sandstones coupled with the absence of clasts other than quartzite, inherently shows that the rocks of the Cape Supergroup that were uplifted in the Cape Fold Belt had replaced the magmatic arc as the main provenance for the Karoo Basin (Johnson, 1991). The

northward-tapering wedges in the Molteno Formation are due to fault-controlled uplift of granitic provenance along the southeastern basin margin (Turner, 1980; Figure 2.7). The Late Triassic Elliot Formation was deposited by high- meandering (sinuosity) rivers (Cole, 1992). The formation is a typical "red bed" fluvial deposit and consists of alternating sequence of mudstone and subordinate fine to medium-grained sandstone, with sandstones dominating in the east and south, and mudstones in the northwest (Johnson et al., 1996; Catuneanu et al., 1998). The red floodplain mudstones with subordinate channel and crevasse splay deposits that dominated the Elliot Formation were interpreted as mixed loads that control the meandering system in an increasing arid setting (Catuneanu et al., 1998 and 2002; Bordy et al., 2005; Katemaunzanga and Gunter, 2009). The meandering streams deposited the sediments under highly oxidizing conditions with reduced energies (Eriksson, 1984). The formation attained a maximum thickness of approximately 500 m in the south and deposited when the climate was changing to arid conditions, hence the reddish mudstones (Johnson et al., 1996). The climate was hotter and drier than in any of the preceding ages (Visser and Botha, 1980). The uppermost part of the Elliot Formation contains evidence of aeolian conditions (Johnson et al., 2006).

The final stage of the Karoo sedimentation is represented by the Late Triassic - Early Jurassic Clarens Formation, consisting of fine-grained sandstones and sandy siltstones (Catuneanu et al., 1998). The formation was deposited in a desert environment and shows high dip angle cross-bedding structures. The succession attained a thickness of about 100 m in the north and approximately 300 m in the south of its outcrop area (Johnson et al., 2006). Beukes (1970) envisaged that the climate was progressively dry and warming, as depicted by fine grained aeolian sand dunes and associated playa lakes, as well as sheet floods and ephemeral stream deposits. The formation comprises of a central zone showing a true desert condition dominated by an aeolian dune environment and the sand is been transported by a westerly wind (Johnson et al., 1996). Smith (1990) also documented that towards the final stage of deposition of the Clarens Formation, the climate became fairly moderate and wet desert processes of stream and sheet flood became more dominant.

2.4.5 Drakensberg Group
This group has no sedimentary deposits, but it is made up of pure mafic volcanic rocks, basaltic in nature with minor felsic rhyolite in later stage. These Karoo igneous rocks have similar chemical compositions, and are part of a larger world-class continental flood basalt

province that stretches across southern Africa (Cox, 1988; Duncan and Marsh, 2006), Antarctica and Tasmania/Australia as part of the Karoo-Ferrar Large Igneous Province (LIP). The Drakensberg Group lava overlies the Clarens Formation and is believed to have terminated sedimentation within the Karoo Basin in the Middle Jurassic, signifying the breaking up of the Gondwana Continent (Catuneanu et al., 1998; Johnson et al., 1996; 2006; Cole and Smith, 2008). The Drakensberg lava that form the upper parts of the Drakensberg Mountain is made up of a thick succession of basalts that caps the Karoo sedimentary succession and covered a large area of central South Africa and Lesotho. This succession of lavas attained a thickness of about 1,370 m which is preserved in Lesotho (Smith et al., 1993; Johnson et al., 1996).

2.5 Karoo dolerite suite

Chevallier and Woodford (1999) documented that the Karoo dolerite, which comprises of several petrological facies (ranging from a leucogabbro to a dolerite-pegmatite) consists of interconnected networks of dykes and sills and it is very difficult to single out any particular intrusive or tectonic event. This is due to the fact that, an individual sill can be fed by many dykes of different orientations or a dyke can act as a feeder to two different sills or more. Chevallier and Woodford (1999), and Svensen et al. (2007) documented that during the intrusive phases, the molten magma concurrently filled in the numerous fractures, and that the dolerite intrusive network probably behaved as a shallow stockwork-like reservoir or storage system where molten magma of different viscosities intruded the fractures. It appears that there is a lithological control on the emplacement of dykes within the Western Karoo Basin, as the bulk of the dykes are strata bound and concentrated in the Upper Ecca and Beaufort Groups (Woodford and Chevallier, 2002). The Carboniferous-Permian Karoo sediments were intruded by the Jurassic Karoo volcanics (183 Ma) during a period of prolonged magmatic activity that covers almost the whole of the southern African subcontinent during one of the phases of the Gondwana break-up (Hunter and Reid, 1987). This resulted in one of the four major preserved continental flood basalts in the world (White, 1997). The igneous products of the Main Karoo Basin show a larger extent of dolerite dykes and sills when compared to the extrusive (Lesotho basalt) (Chevallier et al., 2001). The geographical distribution of the Karoo dolerite sills and ring-complexes are the same as the dolerite dykes and they are the most common type of intrusion (sills) in the Karoo Basin (Chevallier et al., 2001; Figure 2.11).

The dolerite sills occur throughout the basin, the thickest sills is about 200 m thick, and it represents mainly the extensive (> 200 km) sheets emplaced in the carbonaceous shale of the Permian Ecca Group (Svensen et al., 2007). In the Beaufort Group, the sills form nested saucer-shaped intrusions with thickness of about 100 m (Woodford and Chevallier, 2002). The sills are less common in the uppermost part of the basin (Stormberg Group) when compared to the dykes that form about 120-180 km long lineaments (i.e. the 100-200 m wide gap dykes) (Johnson et al., 1996; Catuneanu et al., 2005). The absence of sills in the Drakensberg Group lavas indicates that the sills were emplaced prior to the main phase of flood volcanism or that sills emplacement within the lava was prevented (Svensen et al., 2007). The Karoo sills are mostly tholeiitic basalts to basaltic andesite, however, some present-day sills evolved locally (Galerne et al., 2011). One of the most noticeable features of the present Karoo landscape is the numerous dolerite sills and ring-complexes. These structures usually show a sub-circular saucer-like shape, the rims of which are mostly seen as topographic highs and form ring-like outcrops (Svensen et al., 2007).
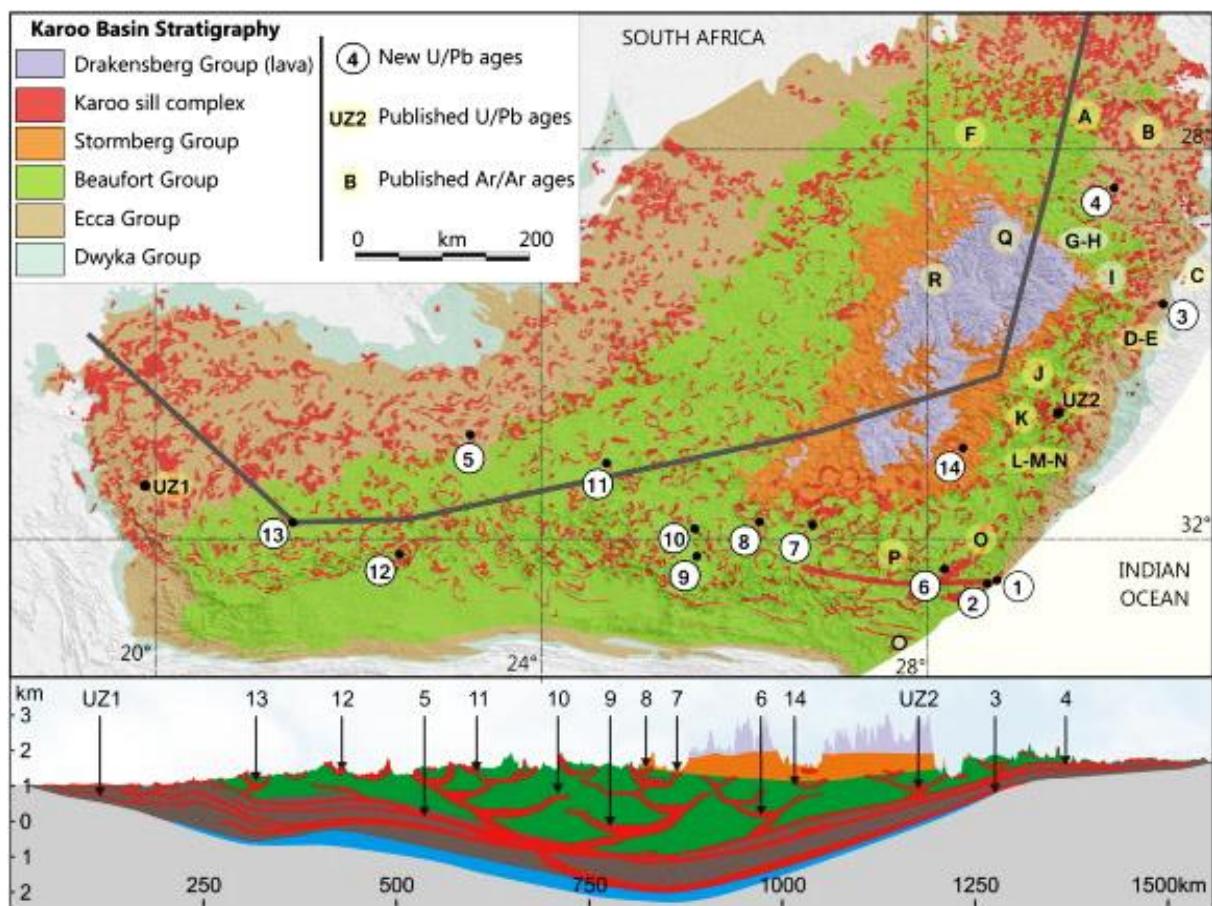
Figure 2.11: The geographical distribution of the dolerite intrusions throughout the Karoo Basin of South Africa (http://karoospace.co.za/dolerite-karoos-fracking-game-changer).

According to Chevallier et al. (2001), three major structural domains that are indicated by dyke distribution have been identified in the Main Karoo Basin (Figure 2.12). These domains are:

- The Western Karoo Domain: It extends from Calvinia to Middelburg and is characterised by two distinctive structural features; east west trending zone of long and thick dykes associated with right lateral shear deformation and north northwest dykes.

- The Eastern Karoo Domain: It extends from Middelburg to East London and comprises two major dyke swarms, namely; a major curvi-linear swarm of extensive and thick dykes diverging from a point offshore of East London and minor north-northeast trending dykes.

- The Transkei-Lesotho-Northern Karoo Domain: It consists of two swarms; northwest trending dykes in the Transkei Region, curving to east-west in the Free State and northeast trending dykes mainly occurring within and alongside the Lesotho basalt.
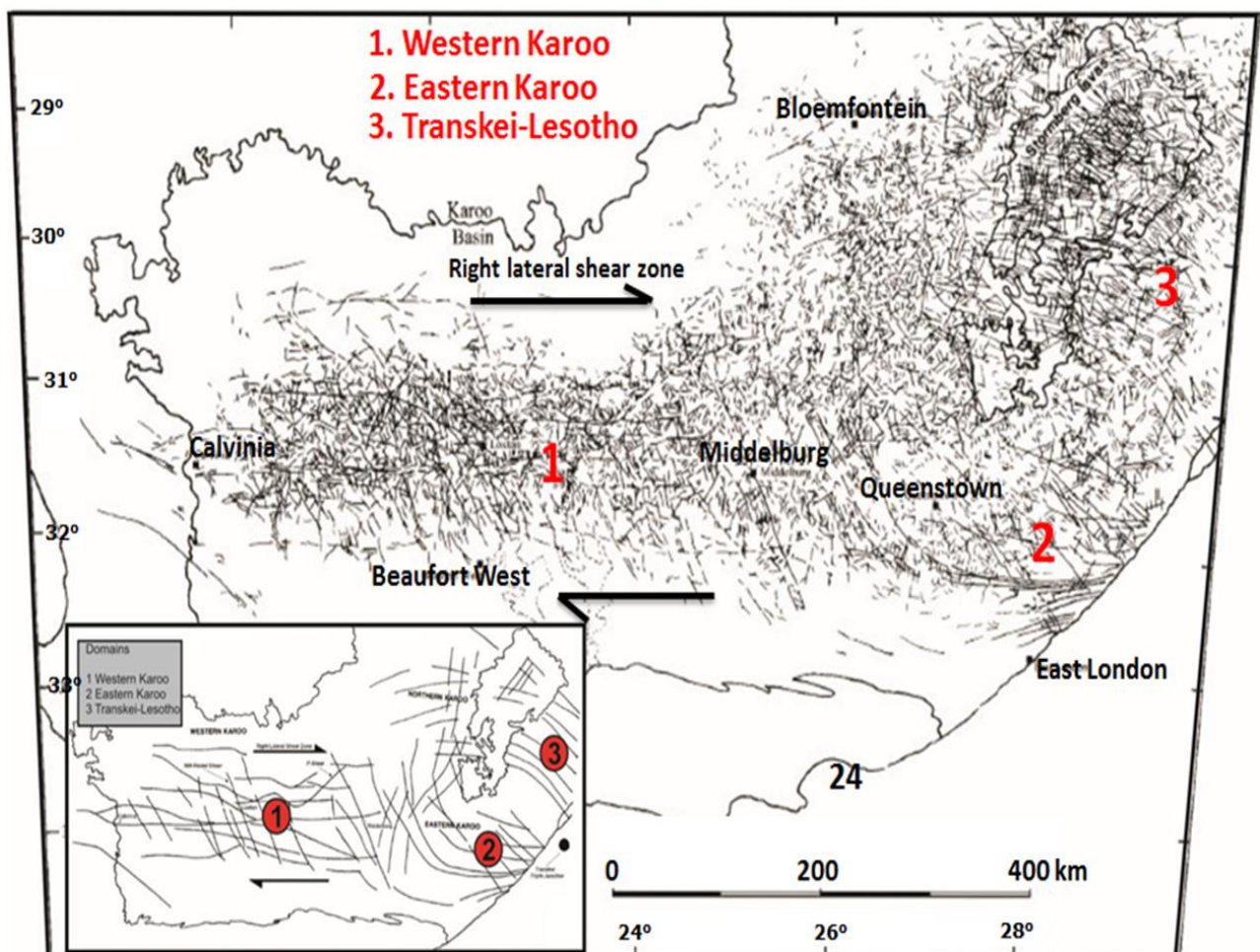
Figure 2.12: Dolerite dykes of the Main Karoo Basin. Insert is a simplified structural map showing the three structural domains (After Woodford and Chevallier, 2002).

The geographical distribution of these structures (sills) are more than the dykes, thus they are the major tectonic style that possibly controls the geomorphology and drainage system of the Main Karoo Basin (Chevallier et al., 2001; Woodford and Chevallier, 2002). This variation is most likely to be due to changes in stress conditions in the crust at the time of emplacement (Stettler et al., 1989). These northern Karoo dykes are those associated with triple junction studies (Burke and Dewey, 1973). From these domains (Figure 2.12), it is obvious that the dominant trend of the dykes in the basin is east-west and north-northwest. These trends are linked to a dominant NW compressive stress field at the beginning of Gondwana break-up, while the east-west dykes are attributed to a similarly oriented shear/dislocation zone linking inferred rifts off the west and east coasts (Chevallier et al., 2001; Woodford and Chevallier, 2002; Scheiber-Enslin et al., 2014). The rift off the east coast is proposed to be a triple junction and represents the source of the Main Karoo magmas (Chevallier et al., 2001). These observations of dyke trends reveal that the event cannot be oversimplified to one magma source. Though, substantial amount of work has been done in this field to better understand the magma source, more studies still need to be carried out, focusing on the southern part of the basin to gain a full understanding of the Karoo magmatic event.

The relationship between the dykes and sill or ring complexes is very complex. The dykes are characteristically encountered in massive arenaceous rocks, while the sills are more common in laminated argillaceous rocks of the Karoo Supergroup (Lurie, 1981). Du Toit (1920) referred to the dolerite injections as ubiquitous, but explained that the intrusion of dolerite is usually along a preferential horizon, such as the contacts between the Dwyka-Ecca Group, the Prince Albert-Whitehill Formation, Upper Ecca-Lower Beaufort Group as well as other lithological boundaries within the Beaufort Group. This was investigated and later confirmed by the deep oil-exploration drilling in the Karoo Basin (Winter and Venter, 1970). Van Zijl (2006a) divided the Karoo dolerites into lower, middle and upper dolerite zones (Table 2.3). The lower zone consists of flat extensive sills ($\sim$ 30 km) in the Dwyka and lower Ecca Groups. The second zone is thought to have the highest number of dolerite intrusions. These intrusions occur within the Upper Ecca and Beaufort Groups, and in some instances, into the Stormberg Group. This abundance is alleged to correspond to the first thick sandstone unit, stressing the importance of horizontal and vertical transport of magma in the system (Scheiber-Enslin et al., 2014). This second group of intrusions is mostly saucer- or basin-shaped, with these structures usually coalescing to form ring complexes (du Toit, 1920). The third dolerite zone intruded the Stormberg Group. It is the most dolerite-poor and consists

mainly of dykes that are assumed to feed the overlying lavas (i.e. northern domain from Chevallier et al. (2001)). Van Zijl (2006a; 2006b) envisaged that due to the low overburden pressure in this zone the intrusion style is independent of lithology.

Table 2.3: Dolerite zones within the Main Karoo Basin of South Africa (van Zijl, 2006a).

Zones	Dominant dolerite geometry	Occurrence	Stratigraphy
Lower	Flat extensive sills (~30 km)	Dolerite-poor	Dwyka Group Lower Ecca Group
Middle	Saucer- or basin-shaped, usually coalescing to form ring complexes	Dolerite-rich	Upper Ecca Group Beaufort Group
Upper	Dykes (and smaller basin structures)	Dolerite-poor	Molteno, Elliott and Clarens Formations

2.6 Conclusions

The lithostratigraphy of the Karoo Supergroup in South Africa indicates gradual change in environmental condition from glacial to continental slope-deltaic, then fluvial and finally aeolian (Johnson et al., 2006). The underlying processes and order of geologic events are revealed in each formation, the order started with diamictites and other glacigene rock types, followed by the shale, sandstones and mudstones of the Ecca and Beaufort Groups, respectively (Johnson et al., 2006). Sedimentation in the Karoo Basin is closely controlled by the orogenic cycles of loading and unloading in the Cape Fold Belt (Johnson et al., 2006). Karoo Basin's rocks potentially host majority of South Africa's onshore fossil fuel reserve. Petroleum exploration in the Karoo is presently focused on the shale gas, coal-bed methane gas and biogenic gas of the Ecca Group and if viable, it will be the main alternate source of energy in South Africa.

CHAPTER 3
STRATIGRAPHY OF THE ECCA GROUP

Abstract

The stratigraphy of the Ecca Group, Karoo Supergroup in the Eastern Cape Province of South Africa has been subdivided into the Prince Albert, Whitehill, Collingham, Ripon, Fort Brown and Waterford Formations. To date, no correlateable stratigraphic sections of the Ecca Group have been documented within the area. In this chapter, we present detailed five stratigraphic sections of borehole logs and road-cut exposures of the Ecca Group, which are stratigraphically correlated in order to elucidate the changes in vertical and lateral facies within the formations and subdivide the formations into members. Based on the lithological features, sedimentary structures and facies characteristics, the stratigraphy of the Prince Albert, Whitehill, Collingham and Fort Brown Formations is subdivided into two members each, while the Ripon Formation is subdivided into three members. Each member has been assigned a lithological name. The Prince Albert Formation is subdivided into the Lower Grey Mudrock Member and Upper Khaki Mudrock Member. The Whitehill Formation is made up of the Lower Black Shale-Chert Member and Upper Grey Mudrock Member. The Collingham Formation consists of the Lower Black Rhythmite Member and Upper Grey Mudrock Member. The stratigraphy of the Ripon Formation is subdivided into the Lower Greywacke-Mudrock Member, Middle Black Mudrock Member, and Upper Black Mudrock-Sandstone Member. The Fort Brown Formation is made up of the Lower Varved Rhythmite Member and Upper Grey Mudrock-Sandstone Member. From west to east, the thickness of the Ecca Group is measured as 1893 m, 1909.6 m, 1625.3 m, 2057 m, and 1738.2 m for the five sections. The stratigraphic correlation shows that the thickness of the Ecca Group in the Eastern Cape Province generally undulate as a result of deformation.

Keywords: Stratigraphy, Ecca Group, Karoo Supergroup, depositional environment.

3.1 Introduction

The stratigraphy of the Ecca Group has been previously investigated on a regional scale by several authors like Rossouw (1953), Ryan (1967), Johnson (1976), Kingsley (1977, 1981), Smith (1990), Smith et al. (1993), Viljoen (1994), Johnson et al. (1996, 2006), Catuneanu et al. (1998, 2005) and Trewin et al. (2002), this led to the subdivision of the Ecca Group into the Prince Albert, Whitehill, Collingham, Ripon, Fort Brown and Waterford Formations.

With the exception of the Waterford Formation, these formations outcrop in the study area and despite the vast amount of available information on the Ecca Group, no correlateable stratigraphic section of the Ecca Group has been produced or established within the study area which is part of the targeted area for shale gas exploration in South Africa. A relatively detailed stratigraphic sequence of the Ecca Group is well exposed in the study area (Figure 1.1), although there is relatively lack of detailed paleontological information in the sequence, stratigraphic correlations can still be established based on physical characteristics of the rocks like similarities in lithology, colour, thickness and sedimentary structures that are manifested in the sequence. The exposure quality of the Ecca sequence is considerably better along road cuttings and easily accessible when compared to outcrops in private farms and game reserves. Thus, in this study, we carried out a much detailed stratigraphic analysis on the road-cut exposures of the Ecca Group formations (Figure 1.1) in order to reveal the lateral and vertical changes in lithological features within each formation and subdivide the formations into members and correlate the measured stratigraphic sections in the area.

3.2 Materials and method

The area investigated was carefully mapped by observing and identifying different lithologies, sedimentary structures, vertical packing styles and colour of the rocks. The observed sedimentary structures in the outcrops were described, measured with a tape and where necessary, photographs were taken using a digital camera. The thickness of the stratigraphic units was measured perpendicular to the strike of the outcrop using a measuring tape. Stratigraphic subdivision of the formations into members was based on similarities in lithological features. Fieldwork was limited to road-cut exposures, because of the quality of the road-cut exposures is considerably better than those exposures in private farms and game reserves and the difficulty in accessing exposures in game reserves/farms. The road-cut exposure of the Ecca Group along Regional road R67 (Ecca Pass; Figure 1.1) give the most complete section of the Ecca Group, however the lower part of Prince Albert and the upper part Fort Brown Formation are only partly exposed. Sedimentary structures are present in the outcrop of the Ecca Group along Regional road R344 (Grahamstown-Adelaide) and National road N10 (Olifantskop Pass; Paterson-Cookhouse). The outcrop of the Ecca Group along National road N2 (Grahamstown-Peddie) are fair to good but have been intruded by dolerites. The road-cut exposure of the Ecca Group along Regional road R350 (North of Kirkwood-Somerset East) are partially covered by soil (poorly exposed); however the stratigraphic thickness was carefully measured along the drainage system. Detailed explanations of all the

five sections in this chapter will be repetitious. Therefore, the stratigraphic section along Regional road R67 (Ecca Pass) will represent the overall description for the formations of the Ecca Group, which is the type locality for the Ecca Group stratigraphy; although references would be made to other locations where interesting or important features and lithological changes were observed. The sections in this chapter were measured in fine detail and stratigraphically correlated in order to reveal the changes in vertical and lateral facies as well as thickness of the formations across the study area. In addition, borehole log studies were undertaken in order to understand lithostratigraphic correlations and ascertain the thickness change of the Ecca Group across the study area. A total of four boreholes that include the Cranemere borehole (CR 1/68), Soekor borehole (SP 1/69), Vrede borehole (VR 1/66) and Schietfontein borehole (SC 3/67) (Figure 1.1) were logged and stratigraphically correlated. The borehole log for the Vrede borehole (VR 1/66) is not complete or missing, thus lack detailed stratigraphic information, and only the available part of the borehole data could be applied to stratigraphic studies. Generally, the borehole core log descriptions give little information on the sedimentary structures and characteristics of the rock sequences; therefore they were only used for stratigraphic correlation and thickness determination.

3.3 Stratigraphic subdivision of the Ecca Group

The stratigraphic sequence of the Ecca Group in the Eastern Cape Province consists of dark grey shale, sandstones and mudrock with subordinate chert and yellowish claystones (tuff). The Ecca Group has been subdivided into five formations, namely; the Prince Albert, Whitehill, Collingham, Ripon, Fort Brown and Waterford Formations. These formations were distinguished from each other and further subdivided into members based on the rock types, sedimentary structures, changes in facies as well as other lithological features such as fossil contents. The members were named after the main lithologies because the studied sites or sections are situated in remote areas and the nearby locality (village) have been used when subdividing the Ecca Group into different formations by previous researchers. The Waterford Formation is absent in the study area. The marker units for subdividing the Ecca Group are the white bands in the Whitehill Formation, yellowish material that are assumed to be ash-fall tuffs in the Collingham Formation, rhythmite units in the Ripon Formation and the varved rhythmite unit of the Fort Brown Formation.

3.3.1 Prince Albert Formation

The Prince Albert Formation is present along Regional road R67 (Ecca Pass; Grahamstown – Fort Beaufort) and is the basal formation of the Ecca Group. It consists predominantly of mudrock and has a measured thickness of about 142.7 m. The Prince Albert shale disconformably overlies the diamictites of the Dwyka Group. The shales are thin bedded or well laminated and shows pencil cleavage. The strata generally have dip angle of about 38° and dip direction of 22°. The lower part of the formation (0 to 112.5 m) is mainly made up of weathered greenish-grey shale (Figure 3.1). Khaki shale and arenaceous mudstones with some silty layers are seen at the upper part of the formation (112.5 m to 142.7 m). The arenaceous mudstones are steep bedded and deformed (folded). It is believed that the deformation is associated with the faulting that cut through the overlying Whitehill Formation.

Figure 3.1: Photograph showing weathered grey shale at the lower part of the Prince Albert Formation along the Ecca Pass (Elevation: 461 m; Longitude E 26º 37′ 38.1″; Latitude S 33º 12′ 49.5″).

Better exposure of the Prince Albert shale occurs along National road N2 (Grahamstown-Peddie). This shale looks like those in the exposure along Regional road R67 (Ecca Pass). However, they are darker in colour (dark-grey) and have been intruded by dolerites which present difficulty when measuring the thickness of the section (Figure 3.2). The formation has a measured thickness of up to 250 m along road cutting. The lower part of the formation (0 to 51.6 m) consists of laminated, greenish dark-grey and micaceous shale. Higher up the formation (51.6 m to 173.2 m), the colour of the shale change to olive-grey and has some

plant rootlets (about 1.2 cm wide) as well as thin black chert layers. Khaki coloured shale and mudstone with silty layers is also seen at the upper part of the formation (173.2 m to 250 m).

Figure 3.2: Photograph showing intrusions of dolerite in the dark-grey shale of the Prince Albert Formation along National road N2 between Grahamstown and Peddie.

The outcrop of the Prince Albert Formation along National road N10 (Olifantskop Pass; Paterson-Cookhouse) is made up of weathered greenish-grey shale of about 64.6 m thick. The Prince Albert shale crumbles easily and overlies on the diamictite of the Dwyka Group. Three lenticular black chert layers are present in the lower part of this formation. From the base of the formation, the first, second and third chert layers are seen at 3.8 m, 9.0 m, and 18.7 m, respectively. The average thickness of the chert layer is approximately 15.6 cm thick and about 3.1 m in length. Weathered phosphorous and calcareous lenses/concretions of varying shapes and sizes (between 5cm and 13 cm thick) are scattered in the basal part of the formation. The upper part of this formation (48.6 m to 64.6 m) is made up of khaki shale and arenaceous mudstones with some grade bedded silty mudstone layers. The shale has significant amount of iron-rich minerals such as illite, pyrite and chlorite, thus hematite is produced after weathering. Along Regional road R350 (North of Kirkwood-Somerset East), the Prince Albert shale is greenish-grey in colour and has a measured thickness of about 72 m. The lower part of the shale (roughly 42 m from the base) has phosphorite lenses (the thickness ranges between 11.6 cm and 23.9 cm), and yellow powdery specks that are possibly of pyritic origin. Khaki colour shale and mudstone with siltstone layers is seen at the upper

part of the shale (between 42 m and 72 m). Generally, at the bottom of the formation, the mudstones are mostly thin bedded and usually less than 10 cm for a single layer in all the section, although sometimes it is well laminated. The khaki colour shale that is mostly encountered at the upper part of the formation was the product of intense weathering that occurred as a result of tectonic uplift and exposure of the rock to the Earth's surface leading to the alteration of the original greyish-black colour to khaki colour. At the upper most part of the formation along the Regional road R67 (Ecca Pass), reddish brown stained were observed in the shales which is believed to be due to leaching of iron-rich minerals resulting in the red colouration (Figure 3.3).

Folded and laminated red stained shale
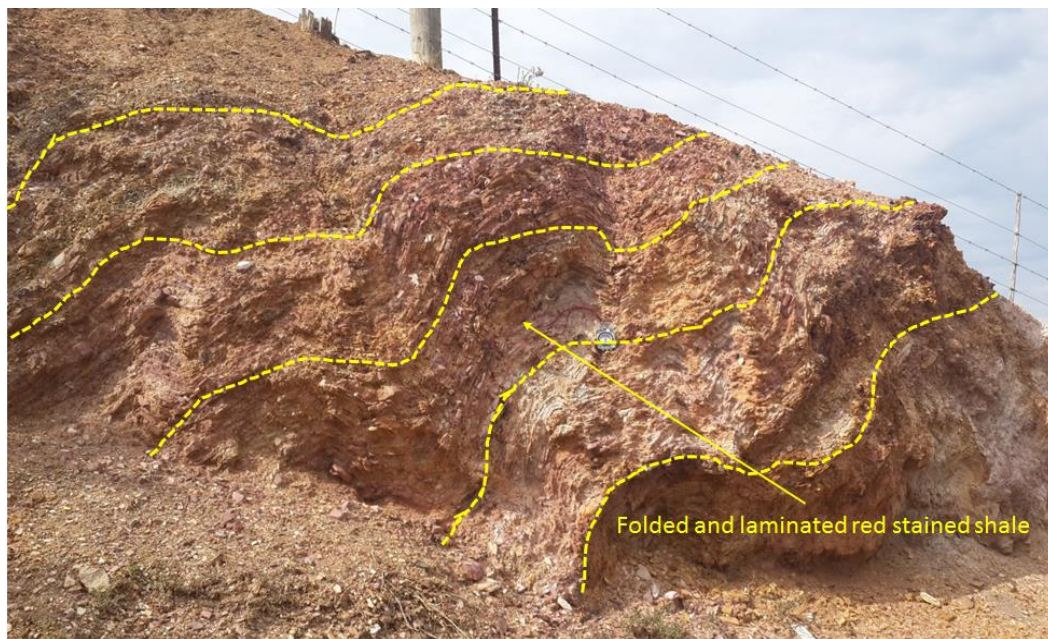
Figure 3.3: Photograph showing folded and well laminated red stained shale at the upper part of the Prince Albert Formation along the Ecca Pass (Elevation: 461 m; Longitude E 26º 37′ 38.4″; Latitude S 33º 12′ 59.5″). The reddish brown stained shales are weathered and folded due to structural deformation.

The Prince Albert Formation along Regional road R344 (Grahamstown-Adelaide) is relatively poorly exposed and there is no distinguishing features on the outcrop that differs from the earlier described exposures, thus they are not described here to avoid repetition. Based on the lithological features, the stratigraphy of the Prince Albert Formation can be subdivided into two members, namely; the Lower Grey Mudrock Member and Upper Khaki Mudrock Member. The Lower Grey Mudrock Member is made up of well-laminated to thin bedded grey shale, while the Upper Khaki Mudrock Member consists of khaki shale and mudstones with some silty layers. The stratigraphic subdivision of the Prince Albert Formation in the five locations is depicted in Figure 3.4.
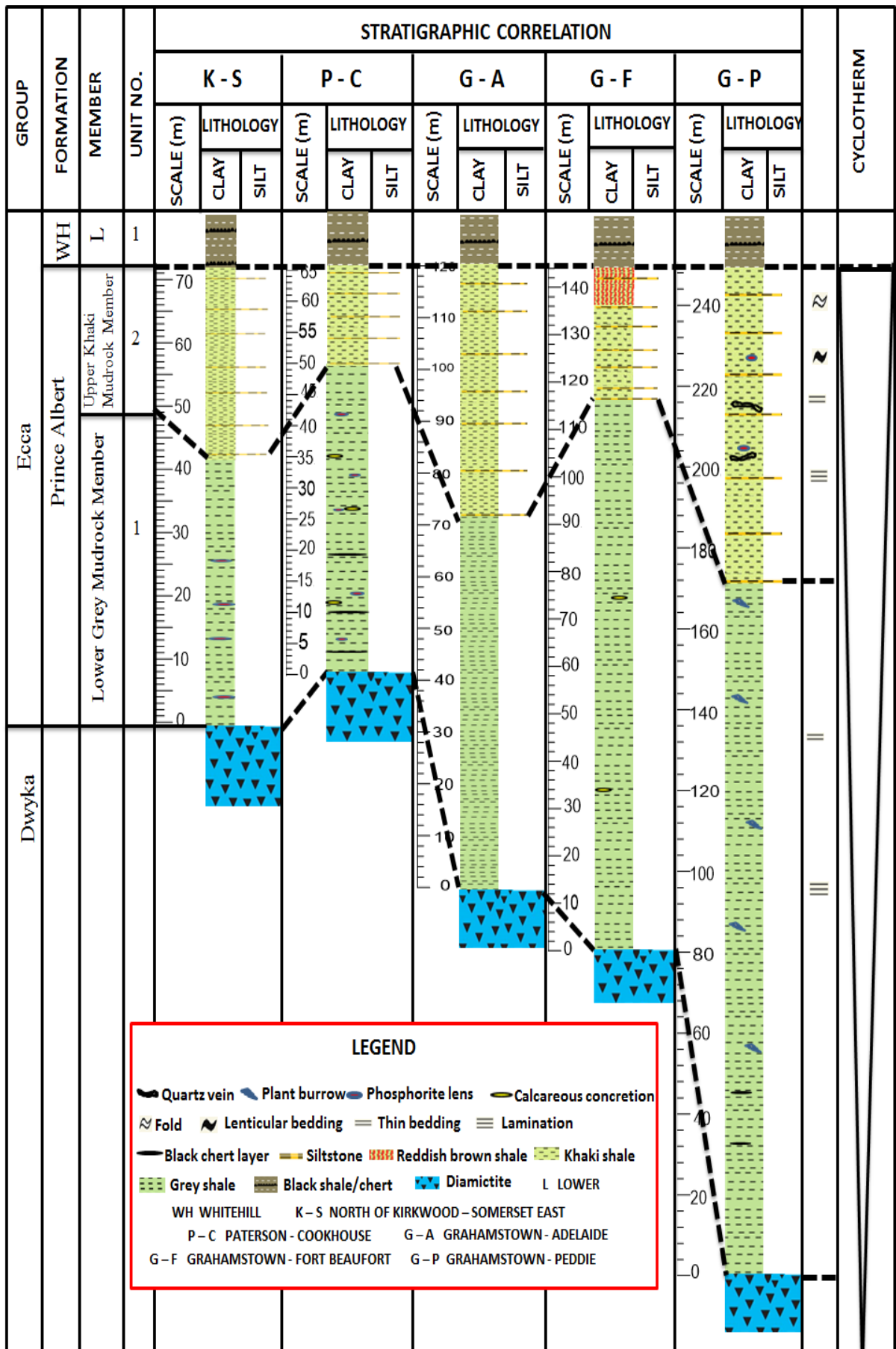
Figure 3.4: Stratigraphic correlation of the Prince Albert Formation in the study area.

3.3.2 Whitehill Formation

The Whitehill Formation disconformably overlain the Prince Albert Formation along Regional road R67 (Ecca Pass; Grahamstown-Fort Beaufort). There is a gradational-transitional zone between the Whitehill Formation and the underlying Upper Khaki Mudrock Member of the Prince Albert Formation. This zone was recognised by the slight or gradual changes in lithology and colour of the rock for approximately 1 m at the top of the underlying Prince Albert Formation (Figure 3.5).

Figure 3.5: Photograph showing disconformity contact between the Whitehill Formation and the underlying Prince Albert Formation along Regional road R67 between Grahamstown and Fort Beafort (Ecca Pass).

The Whitehill Formation is mainly made up of thin bedded, laminated, greyish-black carbonaceous shale with subordinate black chert lenses and mudstones. The black chert is more resistant to weathering and darker in colour than the black carbonaceous shale. The measured thickness of the formation along Regional road R67 (Ecca Pass) is about 41 m thick. The outcrop is generally extensive and ultra-tabular with a normal fault cutting through the formation, thereby dividing it into two lithological units. The strata generally have a dip angle of about 37°. The lower part of the formation (about 20.1 m from the base) consists of laminated, black carbonaceous shales interbedded with thin layers of black chert. The black colour shale is undergoing weathering to give grey-whitish shale (Figure 3.6).

Figure 3.6: Weathered thinly laminated carbonaceous shale with subordinate layers or lenses of black chert at the lower part of the Whitehill Formation along Regional road R67 between Grahamstown and Fort Beaufort (Ecca Pass). The black carbonaceous shale has been weathered to grey-whitish shale (Elevation: 499 m; Longitude E 26º 37′ 38.3″; Latitude S 33º 12′ 58.4″).

The chert layers in the basal part (0 to 13.6 m) are more dominant, thicker and longer in length (averaging about 2.1 m in length), while minor, shorter and thinner chert layers are present higher up the formation (13.6 m to 20.1 m). Some of the black carbonaceous shale has also been weathered to grey-whitish shale with patches of red and yellow shades (Figure 3.7) and are generally rich in iron sulphides (pyrite). The upper part of the formation is 20.9 m thick (20.1 m to 41 m), and consists of darkish-grey shales and thin bedded mudstones (Figure 3.8). The beds in the upper part of the formation are thicker than those of the lower part, ranging from about 1 cm to 15 cm thick for individual layers and point a much quicker deposition. The thicker beds have coarser grain size, while the thinner beds are finer grained.

Figure 3.7: Photograph showing weathered shale with patches of red and yellow shades at the lower part of the Whitehill Formation along the Ecca Pass (Elevation: 499 m; Longitude E 26º 37′ 38.3″; Latitude S 33º 12′ 58.4″).

Figure 3.8: Photograph showing darkish grey shales and thin bedded mudstones at the upper part of the Whitehill Formation along Regional road R67 between Grahamstown and Fort Beaufort (Ecca Pass).

The shale of the Whitehill Formation along National road N2 (Grahamstown-Peddie) easily split along bedding planes, and is bounded below by the Upper Khaki Mudstone Member of the Prince Albert Formation with a gradational contact. This formation is laterally extensive

and has lenses of hard cherts (about 4-6 cm thick), although not as prominent as the exposure along the Regional road R67 (Ecca Pass). Some faults developed within the formation but the shale beds below and above the faults are normally bedded and show no sign of any distortion. The measured thickness of this formation is approximately 22 m along the road cutting. The lowermost part of the formation is made of weathered grey to pale red contorted shale forming the base of the formation (0 to 15 m). Higher up the formation (15 m to 18 m), the colour of shale changes to light-grey colour and eventually becomes dark greyish shale with thin bedded mudstones at the upper part of the formation (18 m to 22 m), which is typical of the Whitehill Formation to the west of the section (Figure 3.9). Trace fossils, plant rootlets, nodules and ferruginous carbonate concretions are present on the weathered surface at the lower part of the formation (0 to 14 m).

Figure 3.9: Photograph showing the near vertical dark-grey shale of the Whitehill Formation along National road N2 between Grahamstown and Peddie.

The stratigraphy of the Whitehill Formation can be generally subdivided into two members, namely; the Lower Black Shale-Chert Member and Upper Grey Mudrock Member. The Lower Black Shale-Chert Member has laminated black shale intercalated with thin bedded black chert layers; the black shale is weathering off to give grey-whitish colour shale. The Upper Grey Mudrock Member consists of darkish-grey shale with minor chert and siltstone layers. The stratigraphic subdivision of the Whitehill Formation in the five locations is depicted in Figure 3.10.
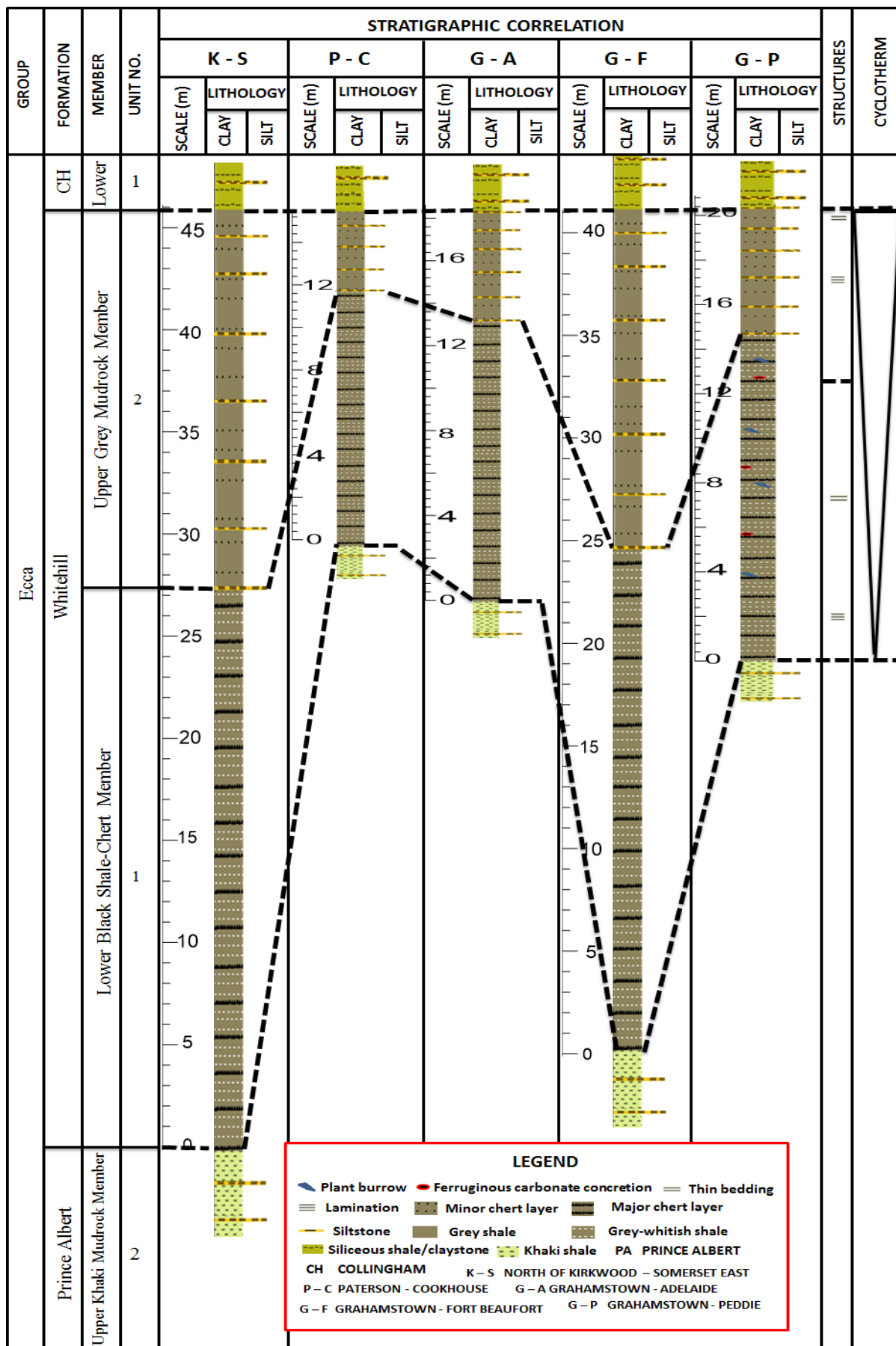
Figure 3.10: Stratigraphic correlation of the Whitehill Formation in the study area.

3.3.3 Collingham Formation

The Collingham Formation conformably overlies the Upper Grey Mudrock Member of the Whitehill Formation and has a transition zone of about 52 cm from the top of the Whitehill Member (Figure 3.11). The formation mainly consists of thin beds of dark greyish or dark greenish shales and very thin beds of weaker or softer yellowish claystones that are assumed to be ash-fall tuffs and had been altered to K-bentonite. The yellow layers have an average thickness of about 3 cm, while the interbedded mudstone has an average thickness of approximately 6.8 cm. The alternated layer structure depicts a classic rhythmite rock features which could be an indication that the deposits were possibly of turbidite sediments. The claystones and mudstones constitute multiple cyclotherms of repeated units or couplets which is referred to as rhythmite (Figure 3.12). This rhythmite is well jointed with both vertical and horizontal joints. The measured thickness of the Collingham Formation along Regional road R67 (Ecca Pass; Grahamstown-Fort Beaufort) is about 62.8 m thick. A fault runs through the formation, thus dividing the formation into two parts (lower and upper parts).

Figure 3.11: Photograph showing conformable contact between the Collingham Formation and the Upper Grey Mudrock Member of the Whitehill Formation along Regional road R67 (Ecca Pass).

The lower part of the formation along the road cutting at Ecca Pass is a rhythmite consisting of thin to medium bedded olive black or light grey shale layers (about 2.3 cm to 11.8 cm thick) alternating with thin and well laminated pale-yellowish claystones. The measured thickness of the lower part is 38.2 m thick, with beds that are mostly horizontal or flat

bedded. Originally, the colour of the shale and claystones are believed to be dark-grey, but due to weathering, the greyish colour of the claystones changed to the present pale-yellowish colour, as well as resulted in the purer clay content. Occasionally, convolute, flaser and wavy beddings are present at the contact between the shale and pale yellowish claystone (tuff), while convolute lamination occur at the basal part
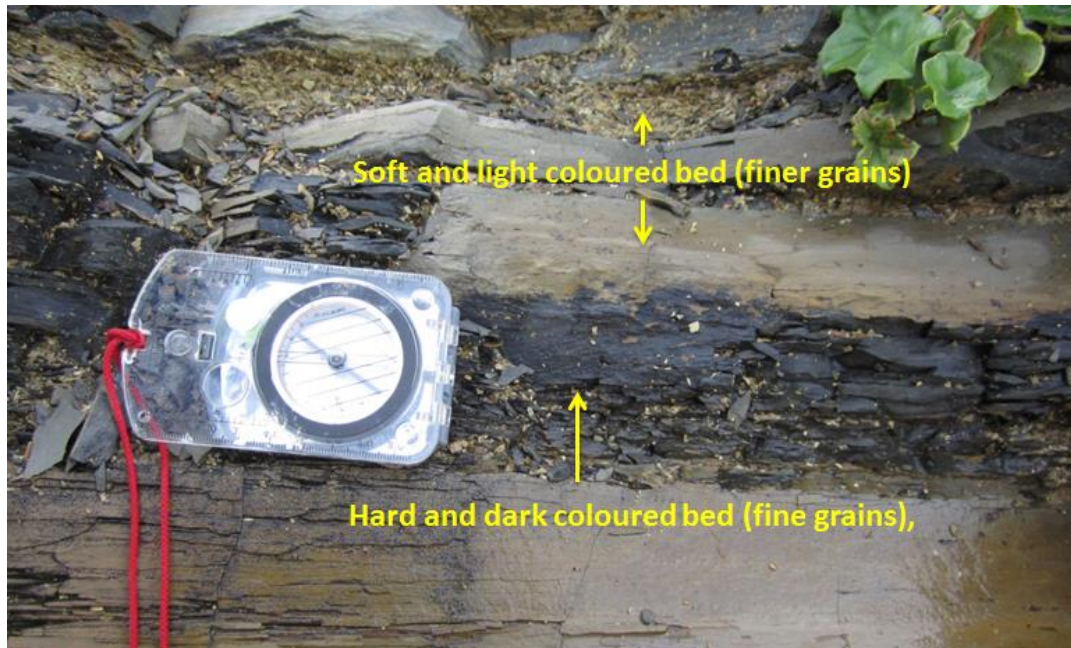
Figure 3.12: Well developed horizontal rhythmite of claystone (soft and light beds) interbedded with mudstones (hard and dark coloured beds) in the lower part of the Collingham Formation along Regional road R67 (Ecca Pass) (Elevation: 471 m; Longitude E 26º 37′ 35.7″; Latitude S 33º 12′ 56.0″).

The upper part of the formation has a thickness of about 24.6 m and most of the beds in this part are slightly inclined or tilted. It is made up of thin, well laminated dark grey shale which can be split along bedding planes and alternated with yellow claystone and silty layers that are weakly graded in some places. The thickness of the mudstone beds range from about 1.7 cm up to 11.9 cm thick. Fine grain size is usually associated with the thinner beds, while the thicker beds are mostly made up of the coarser grain sized. The mudstones are the hard and dark coloured layers with relatively coarser grain size, while the soft and light coloured layers with fine grained size are the claystones (Figure 3.13). The soft beds are well laminated with a pure clay mineral composition which resulted in their flakiness as well as crumble characteristics. The hardand dark coloured mudstones are believed to be deposited in a relatively disturbed water period, while the soft and light coloured claystones were deposited in a much quieter water period with lower energy. Trace fossils (burrows; about 2.4 mm wide and up to 6.9 mm in length) are relatively common from about 40.2 m above the base of the

formation, up to 56. 4 m. Also, there is presence of micro-ripple laminations in the mudstone layers, which are absent or not seen in the claystone layers.
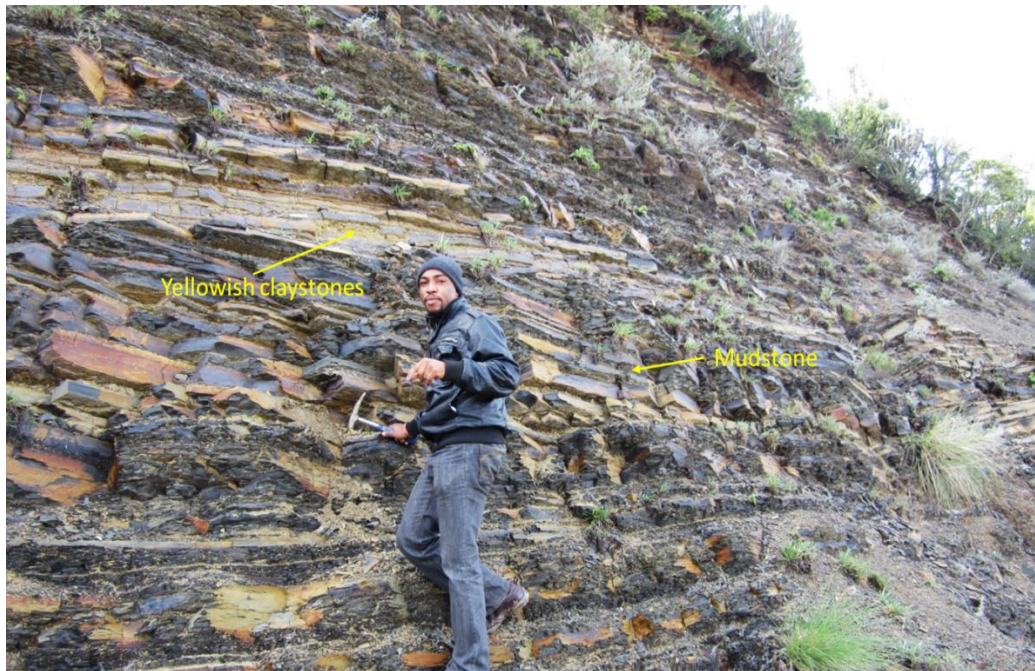
Figure 3.13: Photograph showing thinly bedded blackish mudstone of the Collingham Formation along Regional road R67 (Ecca Pass), interlayered with yellowish claystones that are assumed to be ash-fall tuffs and had been altered to K-bentonite.

Along National road N2 (Grahamstown-Peddie), the Collingham Formation is mainly made up of laminated shale, claystones and siltstones. The sequence has been intruded by dolerites and attained a measured thickness of about 100.4 m along the road cutting. Silty layers and scattered mica flakes is present throughout the formation. The silty layers are well laminated in the lower part of the formation (about 21.1 m from the base) and contain worm burrows (8.6 m above the base, up to 16 m). The most distinctive feature in this section is the presence of about 18 cm thick micaceous sandstones unit near the base of the formation (Figure 3.14).

Figure 3.14: Photograph showing the micaceous sandstones unit near the base of the Collingham Formation along National road N2 between Grahamstown and Peddie.

No distinctive feature is seen in the outcrop of the Collingham Formation along Regional roads R344 (Grahamstown-Adelaide), R350 (North of Kirkwood-Somerset East), and along National road N10 (Cookhouse-Paterson) that differs from the exposure along Regional road R67 (Ecca Pass) and National road N2 (Grahamstown-Peddie), so they are not describe here, to avoid repetition. Based on the lithological features, the stratigraphy of the Collingham Formation can be subdivided into two members, namely: the Lower Black Rhythmite Member and Upper Grey Mudrock Member. The Lower Black Rhythmite Member is made up of mudstone rhythmite, while the Upper Grey Mudrock Member consists of well laminated shale, claystone and minor siltstone. The stratigraphic subdivision of the Collingham Formation in the five locations is depicted in Figure 3.15.
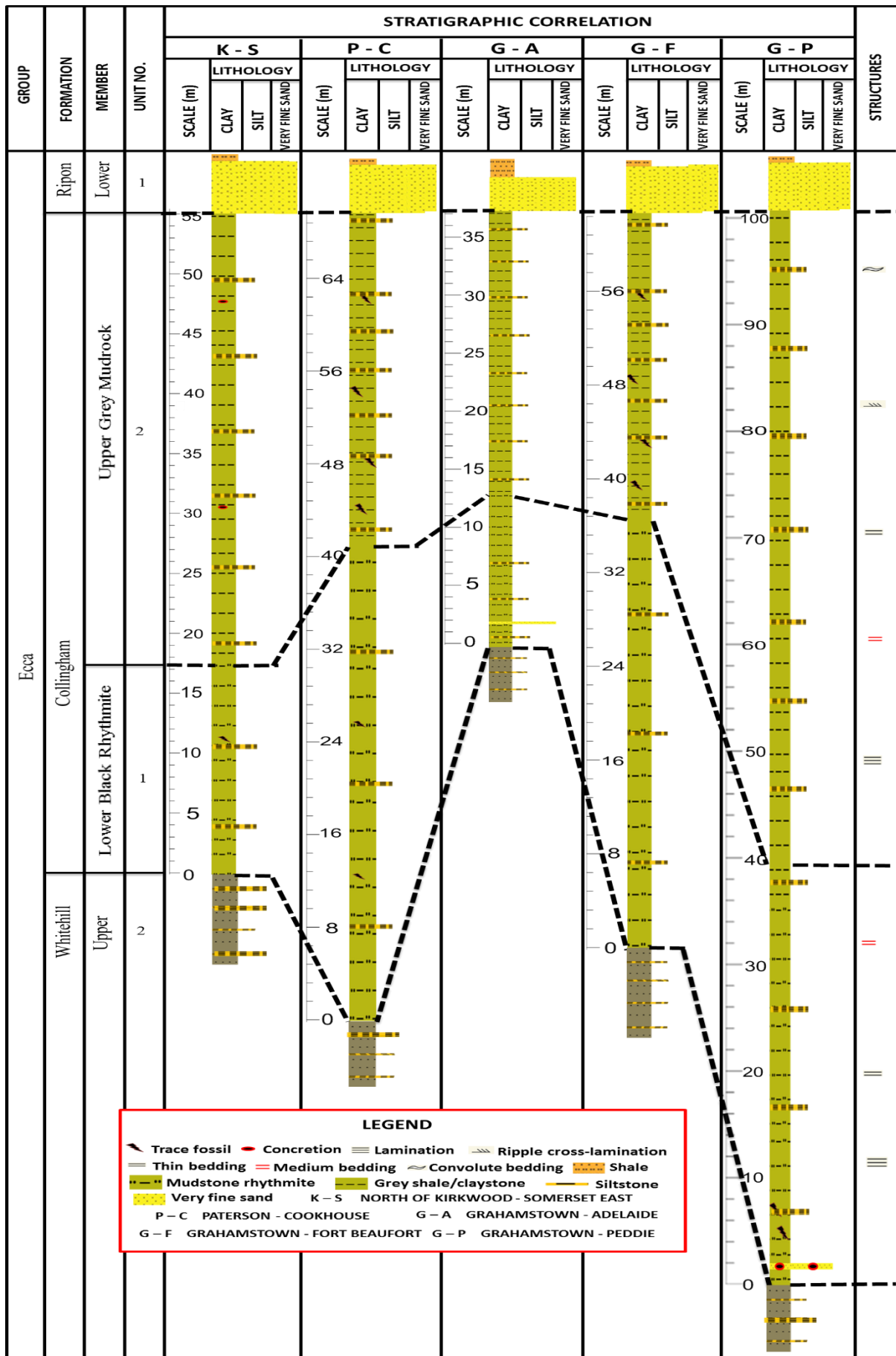
Figure 3.15: Stratigraphic correlation of the Collingham Formation in the study area.

3.3.4 Ripon Formation

The Ripon Formation conformably overlies the Upper Grey Mudrock Member of the Collingham Formation (Figure 3.16) and has a measured thickness of approximately 900 m along Regional road R67 between Grahamstown and Fort Beaufort (Ecca Pass). The formation consists of sandstones alternating with mudstones. Silicification is well-developed in the Ripon Formation than those of the Prince Albert, Whitehill and Collingham Formations.

Figure 3.16: Photograph showing the contact between the Ripon Formation and the underlying Upper Grey Mudrock Member of the Collingham Formation along Regional road R67 (Ecca Pass).

The whole sequence of the Ripon Formation along Regional road R67 (Ecca Pass; Grahamstown-Fort Beaufort) can be subdivided into three members (Lower, Middle and Upper Member). The Lower Member consists mainly of thick to massive bedded greywackes with subordinate mudstones (Figure 3.17). The measured thickness of Lower Member is about 319.6 m and is made up of three units (Units 1, 2 and 3). The first unit (Unit 1) is the basal unit; it is mainly made up of very fine grained greywacke, and has a measured thickness of about 80 m. The basal greywacke in this unit (Unit 1) is massive and has eight (8) alternating cycles of thin and thick bedded greywackes. The thickness of the thick bedded greywacke varies from about 2 m up to 12.8 m, while the thin beds vary between 0.4 m and 1.2 m thick.

Figure 3.17: Photograph showing thick to massive bedded greywackes with subordinate mudstones at the Lower Member of the Ripon Formation along Regional road R67 (Ecca Pass).

The first greywacke bed in Unit 1 is thick to massive bedded and conformably overlies the Upper Grey Mudrock Member of the Collingham Formation with a sharp disconformity contact. The massive greywacke beds probably developed in a river channel where sediments were deposited from a fast flowing or moving current environment carrying a large volume of suspended sediments. These currents then experienced a rapid decrease in velocity and the suspended sediments were suddenly dropped or deposited resulting in the massive beds. The flow rate of the current give no time for internal layering to develop, thus most of the greywacke shows massive bedding and faintly grade bedding in some places. Worm burrows are common in the greywacke beds (averaging 2.3 cm deep and 2 mm wide). These burrows are not confined to a particular environment; however the common rate at which they occur in the greywacke beds possibly suggests a prolific benthonic life at the time of deposition. Pre-depositional sedimentary structures (tool-produced markings) like groove casts, flute casts and striations are occasionally present in the basal part of the unit (10 m to 18 m above the base). Higher up the formation, the second unit (Unit 2) is recognised from about 80 m (top of the Unit 1) up to 210 m (about 130 m thick). This unit mainly consists of fine grained greywackes intercalated with shales and occasionally siltstones (Figure 3.18). The shale at the base of this unit is laminated and has sharp contact with the underlying very fine grained greywacke of the Unit 1.
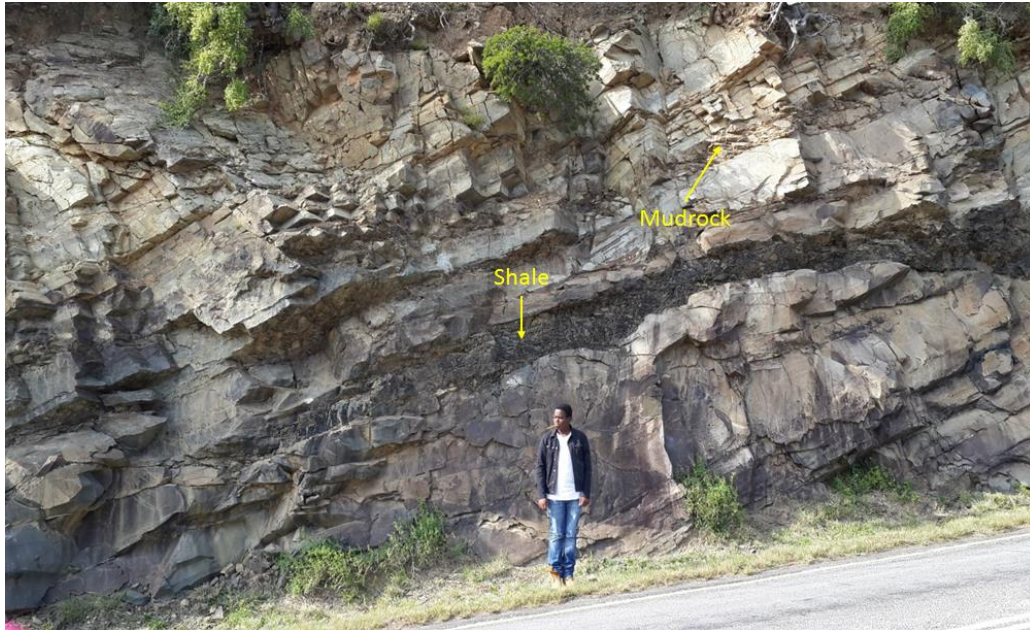
Figure 3.18: Photograph showing greywackes intercalated with shales and occasionally mudrock.

Generally, the contact between the greywackes and mudstones are sharp. In some places, the lower contact in the mudstones beds gradually grade from laminated siltstone to shale. Small scale syn-depositional structures (internal structures) like cross-bedding, micro-cross lamination, wavy bedding and graded bedding are present in the greywackes as well as in the coarse siltstones that occurs in the middle part of the unit (130.4 m to 159.1 m). Calcareous concretions of various shapes and sizes are present in this part of the unit. Some of the greywacke beds are mottled at the top of the unit (166.8 m to 198 m). Deformational or post-depositional structures like flame structures, load casts, convolute bedding and small-scale ball and pillow structures are common towards the top of the unit. Most of the bedding planes in the upper part of the unit have small worm trails with width varying from about 0.3 mm up to 1.7 mm. The upper unit (Unit 3) of the Lower Member is made up of alternating very fine grained greywackes and faintly laminated, thinly bedded shales. The measured thickness of this unit is 109.6 m (from 210 m to 319.6 m). The siltstone at the base of this unit has a sharp contact with the underlying fine grained sandstone layer. Calcareous concretions and trace fossils are relatively common throughout the unit. Some of the greywackes in this unit are mottled and are more vulnerable to weathering than the non-mottled greywackes. Generally, the mottled and non-mottled greywackes tend to alternate in the upper part of the unit. Small trace fossils (worm trails) and calcareous concretions are present in some of the mottled greywackes. Post-depositional structures like small scale load casts and ball and pillow structures are also occur in the non-mottled greywackes.

The Middle Member of the formation (319.6 m to 505 m) is mainly made up of greyish black shale and has a measured thickness of about 185.4 m (Figure 3.19). The base of this member is marked by faintly laminated dark-grey shale with measured thickness of 105.4 m. The shale is faintly laminated near the base of this member but become well laminated half-way up the succession. Higher up the member, there are two greywacke layers intercalating with the grey shales. The first greywacke layer is fine grained, thick bedded, mottled and has a measured thickness of about 7.6 m (388 m to 428.1 m). The second greywacke is very fine grained, thin bedded and has a thickness of about 0.6 m (420.5 m to 434.5 m). Most of the shales in the Middle Member of the formation are massive and faintly laminated but the laminations become conspicuous towards the top of the zone. Four large scale slumps of about 1.8 m, 6.2 m, 4.3 m and 2.4 m thick occur between 388.4 m to 390.2 m, 410.1m to 416.3 m, 440.3 m to 444.6 m and 461.8 m to 464.2 m, respectively. The shales in the slumping zones are mostly folded and occasionally faulted, although syndepositional structures (internal structures) like micro-cross lamination, wavy bedding are still visible in the shales.

Figure 3.19: Photograph showing greyish black shale in the Middle Member of the Ripon Formation along Regional road R67 (Ecca Pass).

The Upper Member of the formation mainly consists of alternating fine-very fine grained, dark grey greywacke and greyish-black shale (Figure 3.20). The alternated layer structure depicts a classic rhythmite appearance, with a measured thickness of about 395.4 m (504.6 m to 900 m). Three rhythms (Rhythm 1, 2 and 3) of approximately 155.8 m, 174.6 m and 65 m

thick were recognised in the sequence and they lies between 504.6 m to 660.4 m, 660.4 m to 835 m, and 835 m to 900 m, respectively.

Figure 3.20: Photograph showing dark grey greywacke and greyish-black carbonaceous shale in the Upper Member of the Ripon Formation along Regional road R67 (Ecca Pass).

The base of the first rhythm (Rhythm 1) disconformably overlies the non-mottled, well laminated shale of the Middle Member. The first rhythm has about five fine grained greywacke layers, five well to faintly-laminated shale layers and one well laminated, graded siltstone (about 6.8 m thick) occurring between the third greywacke bed and the third shale bed. The thickness of the greywacke beds varies between 10.5 m and 35.2 m, while the thickness of the laminated shale ranges between 4.5 m and 32.3 m. Deformational structures such as convolute bedding, and load casts are common towards the base of the rhythm (504.6 m to 580 m). Dish structures, flaser bedding and calcareous concretions occur in some of the horizons. The shale in the first rhythm shows pencil cleavage and has faint horizontal lamination. Sole cast structures (ranging from about 1.2 cm up to 9.8 cm long), wavy lamination with associated micro-cross-lamination (1.4 cm to 5 cm thick) are common towards the top of the first rhythm (Rhythm 1) where fining upward sequence is very distinct or and obvious.

The second rhythm (Rhythm 2) has eight very fine grained, olive-greyish greywacke layers alternating with the faintly-laminated shale layers and two well-laminated siltstone layers (between 660.4 m to 835 m). The first siltstone layer occurs between the second greywacke

bed and the second shale bed, while the second siltstone layer occurs between the sixth greywacke bed and the sixth shale bed. The thickness of the greywacke beds varies from about 4.2 m to 31.8 m, while the thickness of the laminated shale ranges between 0.8 m and 9.2 m. Just like the first rhythm, small scale wavy lamination, micro-cross-lamination, worm trail and calcareous concretions occur at several horizons. The sixth greywacke layer in the upper part of this rhythm grades into siltstone and shows small scale wavy lamination. The second siltstone layer grades upward into a greyish-black laminated shale. The third rhythm (Rhythm 3) lies between 835 m to 900 m, it mainly consists of fine grained, olive-greyish greywacke layers alternating with laminated shale layers. This rhythm is not complete along the Ecca Pass; however, it has three greywacke layers alternated with two shale layers. The first shale layer that overlies the basal greywacke layer is silty and shows wavy lamination. The second greywacke rests abruptly on the first silty shale layer. The second shale layer shows pencil cleavage. Generally, the greywacke beds vary from very thick bedded to thick bedded and finally thin bedded. Very thick bedded greywackes are encountered at the base of the rhythms, while thick bedded greywackes are often seen in the middle part of the rhythm but changes to thin bedded higher up the rhythm. Graded bedding commonly occurs in the greywacke beds, while faint or indistinct graded bedding is present in the mudstones.

The outcrop of the Ripon Formation along National road N2 (Grahamstown-Peddie) is also made up of thick bedded, dark-greyish greywacke alternating with thin bedded, faintly laminated silty shale. The whole sequence has a measured thickness of about 908.1 m along road cutting. This exposure can also be separated into three members (Lower, Middle and Upper Members) just like the exposure along the Regional road R67 (Ecca Pass). The Lower Member is predominantly of thick-very thick bedded greywacke and has a measured thickness of 174.3 m (Figure 3.21). Two thinly bedded, faintly laminated silty shale layers are seen at 97.6 m and 101.2 m, which alternate with the greywacke layers. The thickness of the first silty shale layer is about 0.8 m, while the second silty shale layer is approximately 1.4 m thick. Small scale wavy lamination, worm trail and calcareous concretions are seen in the shale layers. Higher up the succession, the Middle Member overlies the upper greywacke bed of the Lower Member at 174.3 m from the base of the formation. This zone has a measured thickness of 112.5 m (from 174.3 m to 286.8 m) and is mainly made up of shale layers. This shale is faintly laminated and exhibits pencil cleavage. Pre-depositional structures (tool-produced markings) like groove casts occur near the base of the middle zone (between 174.3 m to 208 m). The Upper Member is 621.3 m thick (from 286.8 m to 908.1 m) and consists of

dark-grey greywackes alternating with mudstones. The greywacke in the basal part of this member is thick bedded (about 30.9 m thick for the whole sequence) and mottled (between 352.3 m and 735 m). Just above the mottled greywackes, the overlying non-mottled greywackes are rhythmically intercalated with well laminated, thin bedded siltstones and shales (4 cycles, between 758 m and 830 m). Medium bedded greywackes occur in the middle part of this member (between 582 m and 730 m). Generally, the thickness of the greywacke ranges from 5.8 m up to 40 m thick. Small scale syndepositional structures like cross-bedding, flaser bedding, wavy bedding and graded bedding are common in the siltstone beds.

Figure 3.21: Photograph showing dark grey greywackes alternating with mudstones in the lower part of the Ripon Formation along the National road N2 between Grahamstown and Peddie.

Along National road N10 (Olifantskop Pass; Paterson-Cookhouse), the Ripon Formation disconformably overlies the Collingham Formation and attained a thickness of about 490 m along the road cutting. The sequence has been deformed (folded) and resulted in development of syncline and anticline (Figure 3.22). The basal part (Lower Member) mainly consists of massive, dark-grey greywacke alternated with thin bedded silty shale, and has a measured thickness of 135.7 m (0 to 135.7 m). The greywacke and the silty shale beds are generally arranged in cyclicity (regular alternating sequence). The greywackes are faintly laminated and mottled at some horizons. Higher up the formation (Middle Member), it is predominantly of laminated, yellowish-grey shale intercalated with three thin bedded greywacke layers. It is

about 134.3 m thick (from 135.7 m to 270 m) and the shale shows pencil cleavage. The upper part (Upper Member) of the formation is about 220 m thick (from 270 m to 490 m) and is made up of alternating sequence of dark grey greywacke and greyish black shale. Small scale syndepositional structures like cross-bedding, micro-cross lamination, wavy bedding and graded bedding similar to those observed in the outcrop of the Ripon Formation along the Ecca Pass are also seen in the siltstones and greywackes layers. No distinctive difference or change in character between this exposure and the exposure of the Ripon Formation along Regional road R67 (Ecca Pass) and National road N10 (Olifantskop Pass).
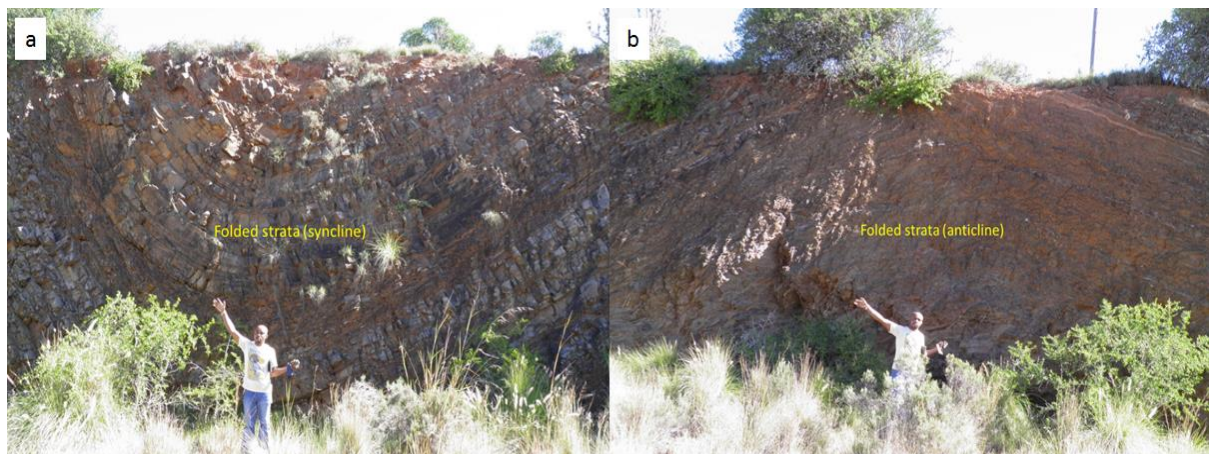
Figure 3.22: Photograph showing folded strata (syncline and anticline) of the Ripon Formation along National road N10 between Paterson and Cookhouse (Olifantskop Pass).

The outcrop of the Ripon Formation along Regional road R344 (Grahamstown-Adelaide) is about 660 m thick, and made up of greywacke alternating with mudstones (Figure 3.23a). There are a lot of quartz veins in the greywacke. Most of the strata on this exposure have been folded and they show geological structures like symmetrical folds, asymmetrical folds and chevron folds (Figure 3.23b-e). The Lower, Middle and Upper Members are 230 m (0 to 230 m), 170 m (from 230 m to 400 m) and 260 m (from 400 m to 660 m) thick, respectively. Almost all the characteristics seen on this exposure of the Ripon Formation are very similar or alike to those Ripon exposures along Regional roads R67 (Grahamstown-Fort Beaufort), and National roads N2 (Grahamstown-Peddie) and N10 (Cookhouse-Paterson), so they are not described here.
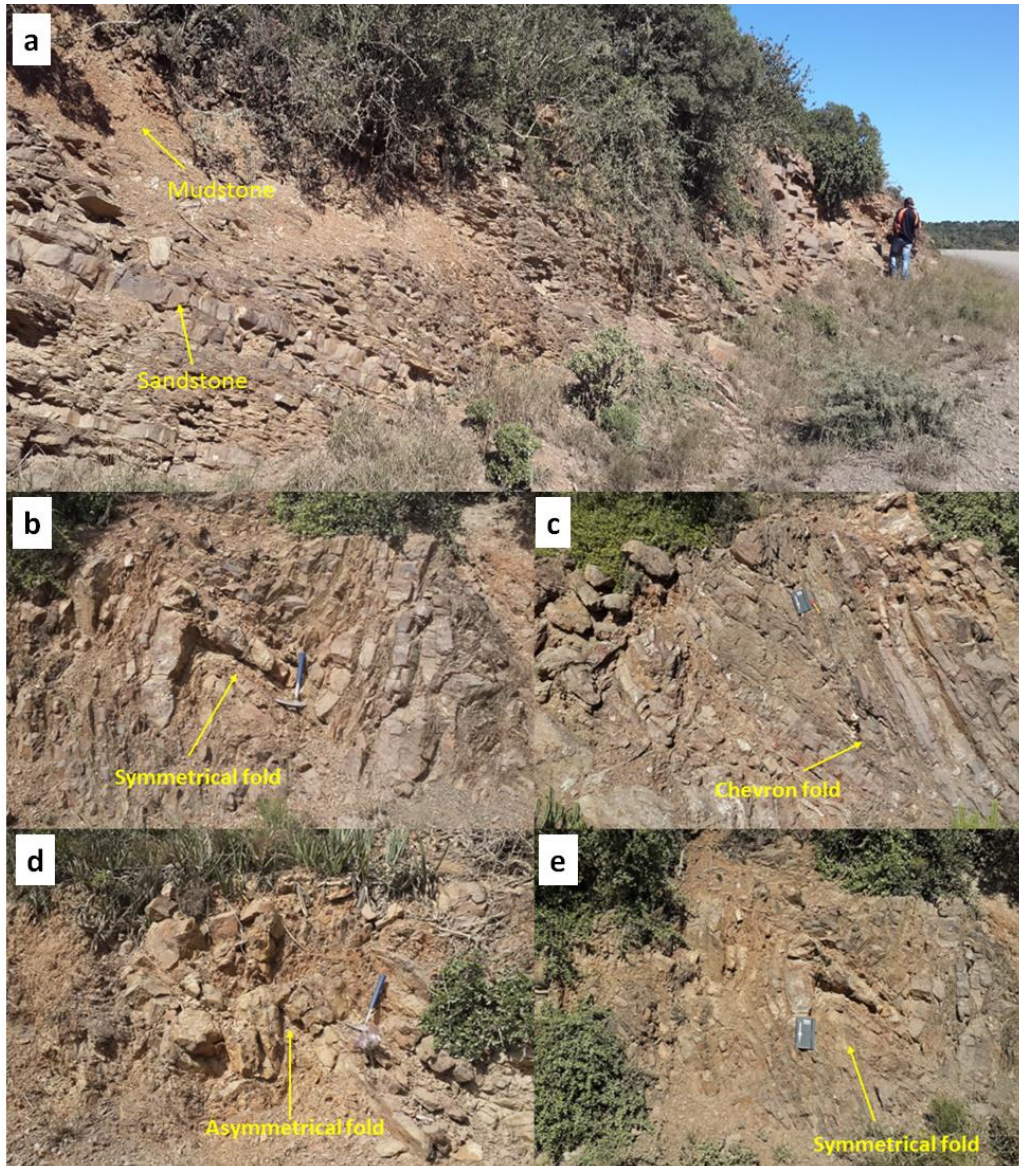
Figure 3.23: Photograph of theRipon Formation along Regional road R344 between Grahamstown and Adelaide showing: (a) Greywackes alternating with mudstones; (b) Symmetrical fold; (c) Chevron fold; (d) Asymmetrical fold; (e) Symmetrical fold.

Based on the lithological features, the stratigraphy of the Ripon Formation can be subdivided into three members, namely; the Lower Greywacke-Mudrock Member, the Middle Black Mudrock Member and the Upper Black Mudrock-Sandstone Member. The Lower Greywacke-Mudrock Member consists mainly of thick-massive bedded greywackes with subordinate mudstones. The Middle Black Mudrock Member is mainly made up of greyish-black shale with minor sandstone layers, while the Upper Grey Mudrock-Sandstone Member is made up of alternating dark-grey greywacke and greyish-black shale that depicts a classic rhythmite rock. The stratigraphic subdivisions of the Ripon Formation in the five locations are depicted in Figure 3.24.
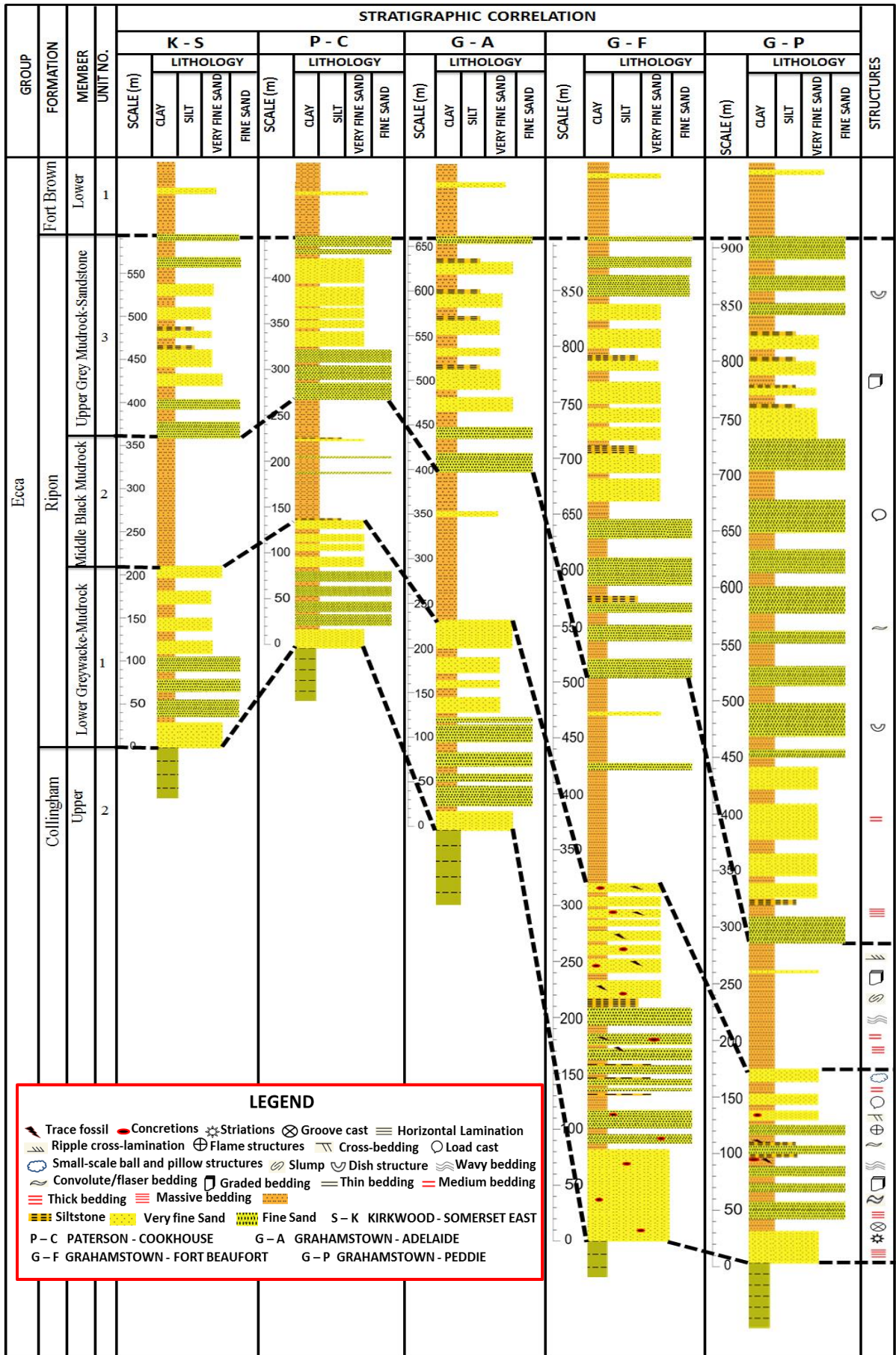
Figure 3.24: Stratigraphic correlation of the Ripon Formation in the study area.

3.3.5 Fort Brown Formation

The Fort Brown Formation conformably overlies the Upper Grey Mudrock-Sandstone Member of the Ripon Formation along Regional road R67 (Ecca Pass). It consists mainly of grey mudstones rhythmite intercalated with subordinate sandstones (Figure 3.25). The rhythmites are represented by regularly alternation of light and dark colour layers similar to varved laminations. The measured thickness of this formation along road cutting is about 910 m. Generally, the basal part of the formation (445 m from the base) is dominated by well laminated or varved rhythmites of dark grey mudstones, with minor lenticular siltstone or fine sandstone intercalation. The thickness of the light and dark colour layers (rhythmite) that regularly alternated are approximately the same, ranging from about 0.4 mm up to 1.8 mm.

Figure 3.25: Photograph showing greyish mudstones rhythmite intercalated with mudrock layers in the Fort Brown Formation along Regional road R67 between Grahamstown and Fort Beaufort (Ecca Pass).

Two thin bedded greywacke layers of about 0.6 m and 1.3 m thick are intercalated between 147.3 m and 147.9 m, and 162.2 m and 163.5 m, respectively. Syndepositional structures like micro-cross lamination and wavy lamination are seen but poorly developed in the greywacke beds. The contact between the shales and the greywackes are sharp. The upper part of the formation consists of silty, laminated, olive grey shale alternating with thin bedded sandstones. The silt content in the shale increases from lower succession upward; where the shales are silty they are often more graded. Higher up the formation (186.2 m to 407.4 m), the

olive grey shale becomes more silty and sometimes conspicuously grade into laminated, greenish grey siltstones in the beds. The contacts between the silty shale and siltstone are transitional. The thickness of the silty shale beds varies from about 4.2 m up to 12.6 m, and they crumble easily. There are more sandstones beds in the upper part of the formation compared to the basal or lower part. Wavy bedding, ripple cross-lamination and wave ripples are well-developed in the upper part of the formation, especially in the sandstone and coarse siltstone beds. Ripple-drift cross lamination is present in some of the thick silty beds. Burrows are common in the upper thick bedded sandstones layers. Along the National road N10 (Olifantskop Pass), the thickness of the Fort Brown Formation is about 1200 m. The base of the formation is placed where the greywacke of the underlying Upper Grey Mudrock-Sandstone Member of the Ripon Formation sharply change to silty shale bed (Figure 3.26).
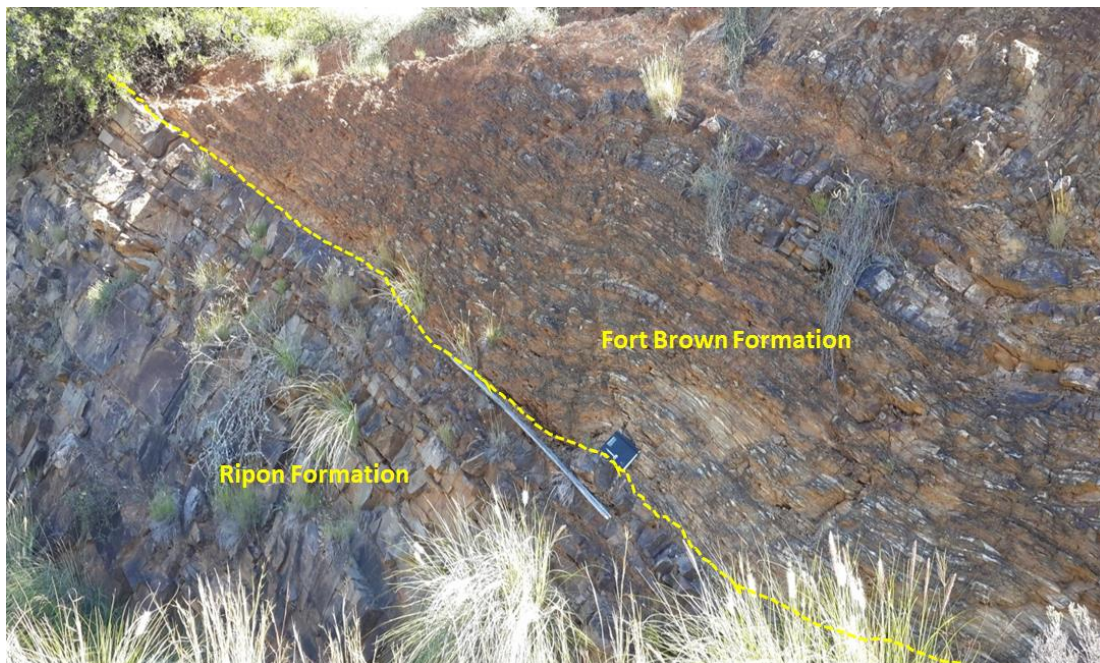
Figure 3.26: Photograph showing the sharp contact between the Fort Brown Formation and the underlying Upper Mudrock-Sandstone Member of the Ripon Formation along National road N10 between Paterson and Cookhouse (Olifantskop Pass).

The exposed part of this formation (from the base up to 36.9 m) consists of silty shale, siltstones intercalated with three thin bedded sandstones. The first, second and third sandstone beds are about 20 cm, 34.2 cm and 12.9 cm thick respectively. The silty shale crumbles easily and grades upward into siltstone (about 8 m thick). The siltstone beds have poorly developed wavy lamination and current ripple lamination. The upper part of the section is covered by soils, thus it affected the detailed description of the lithology and

sedimentary structure change. The outcrop of the Fort Brown Formation along National road N2 (Grahamstown-Peddie) consists of well laminated rhythmites of light grey mudstone, intercalated with lenticular sandstones, and generally shows upward coarsening tendency (Figure 3.27). The measured thickness of the whole formation is about 440.7 m thick along road cutting. The amount of silty materials in this section is greater or more than the silty content in the exposures of the Fort Brown Formation along the Regional roads R67 (Ecca Pass) and R344 (Grahamstown-Adelaide). The high content of silty materials as well as the low carbon content of the rocks in this section probably resulted in the lighter colour of the mudstones.

Figure 3.27: Photograph showing grey mudstones alternating with minor sandstones along National road N2 between Grahamstown and Peddie.

The lower part of the formation (0 to 80 m) consists of alternating layers of micaceous shale and sandstones. The contacts between the shale and the sandstones are often sharp but sometimes transitional. The shale shows pencil cleavage and split perfectly along bedding planes. Small scale wavy lamination, worm trail and calcareous concretions are seen in the silty shale layers. Higher up the formation, the strata are folded (Figure 3.28) and some of the siltstone grades into well laminated silty shale and shale. Wavy lamination, flaser and cross-lamination are present in some of the siltstone beds. The intercalated sandstone also shows horizontal lamination, wavy lamination and ripple lamination. Worm burrows and calcareous concretions of various sizes, ranging between 2.4 cm and 12.9 cm in diameters are

occasionally seen in the upper part of the formation (between 367.2 m and 440.7 m). Generally, the sequence (shale-silty shale-siltstone-sandstone) shows coarsening upward cycles. The sandstone becomes coarser and thicker in the upper part of the formation. There is more sandstone beds in the upper part of the formation compared to the lower part of the formation.
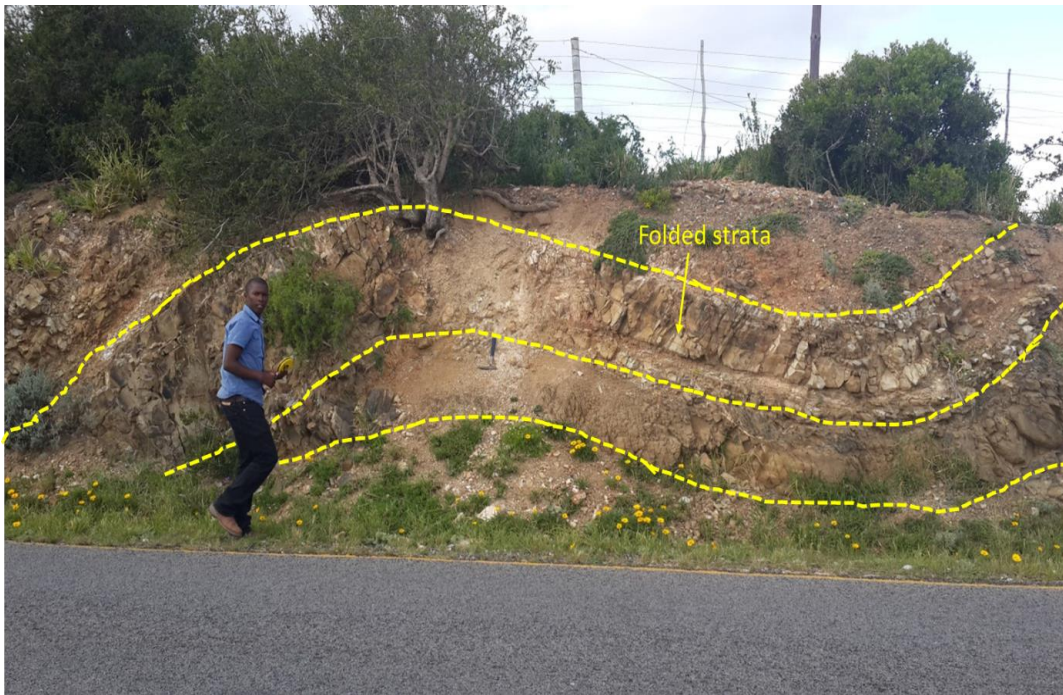
Figure 3.28: Photograph showing folded strata of the Fort Brown Formation along National road N2 between Grahamstown and Peddie.

Along Regional road R344 (Grahamstown-Adelaide), the Fort Brown Formation mainly consists of mudstones alternating with minor sandstones. The measured thickness of this section is approximately 790 m. The base of formation is made up of about 250 m thick, dark grey shale that directly overlies on the greywacke of the Upper Grey Mudrock-Sandstone Member of the Ripon Formation. The shale shows pencil cleavage and grades into silty laminated shale in some places. This silty shale is overlain by thin bedded greywacke in a thickness between 1.2 cm and 26 cm. Generally, the lower part of the formation (from the base up to 92.5 m) is characterized by thick bedded, very silty shale with minor thin bedded greywackes. These thin greywacke beds gradually increase in number and thickness upward. Higher up the formation (between 92.5 m and 250 m), the dark grey shale to silty shale dominates and grades into well laminated olive-grey siltstones. Thick bedded siltstone and very silty shale occupies most of the middle part of the formation. The contacts between the

mudstones and greywackes are transitional. A few calcareous concretions are seen at about 162 m. In the upper part of the formation (250 m to 790 m), the shale clearly grades into siltstone which later passes into sandstone unit. Wavy lamination and micro-cross lamination are occasionally seen in the sandstones beds. The uppermost part of the formation is characterized by an upward-coarsening sequence consisting of shale, silty shale, siltstone, very fine-grained greywacke and fine grained greywacke.

Based on the lithological features, the stratigraphy of the Fort Brown Formation can generally be subdivided into two members, namely; the Lower Grey Varved Rhythmite Member and the Upper Grey Mudrock-Sandstone Member. The Lower Grey Varved Rhythmite Member is made up of well laminated to thin bedded rhythmites of grey mudstone with minor lenticular siltstone and fine sandstone intercalation. The Upper Grey Mudrock-Sandstone Member consists of silty, well laminated greyish shale alternating with siltstone and sandstones. There are more sandstone beds in the Upper Grey Mudrock-Sandstone Member than the underlying Lower Grey Varved Rhythmite Member. The stratigraphic subdivision of the Fort Brown Formation in the five locations is depicted in Figure 3.29. Stratigraphic correlation of the Ecca Group within the study, from both borehole logs and outcrop sections are presented in Figures 4.30 and 4.31.
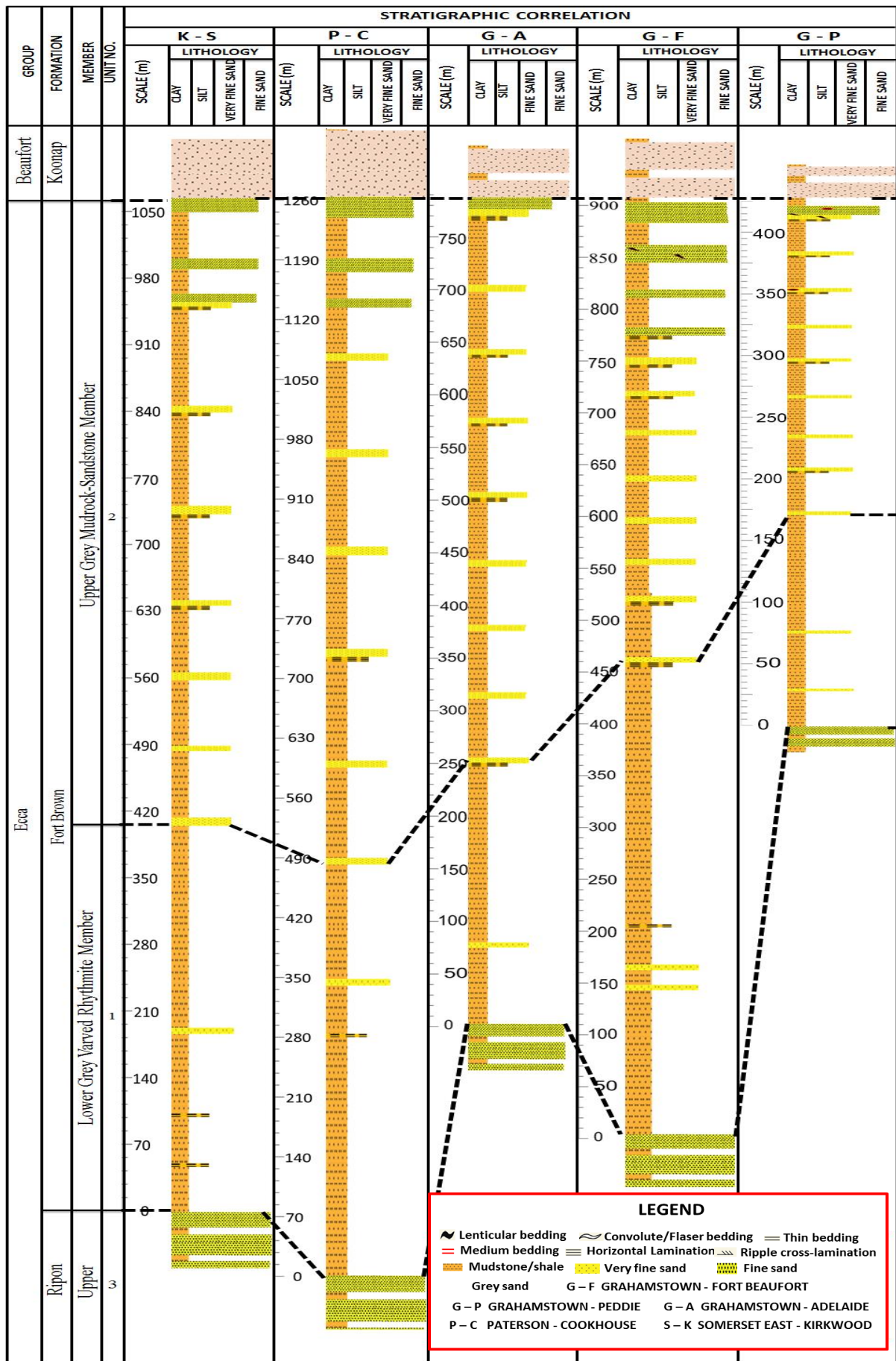
Figure 3.29: Stratigraphic correlation of the Fort Brown Formation in the study area.
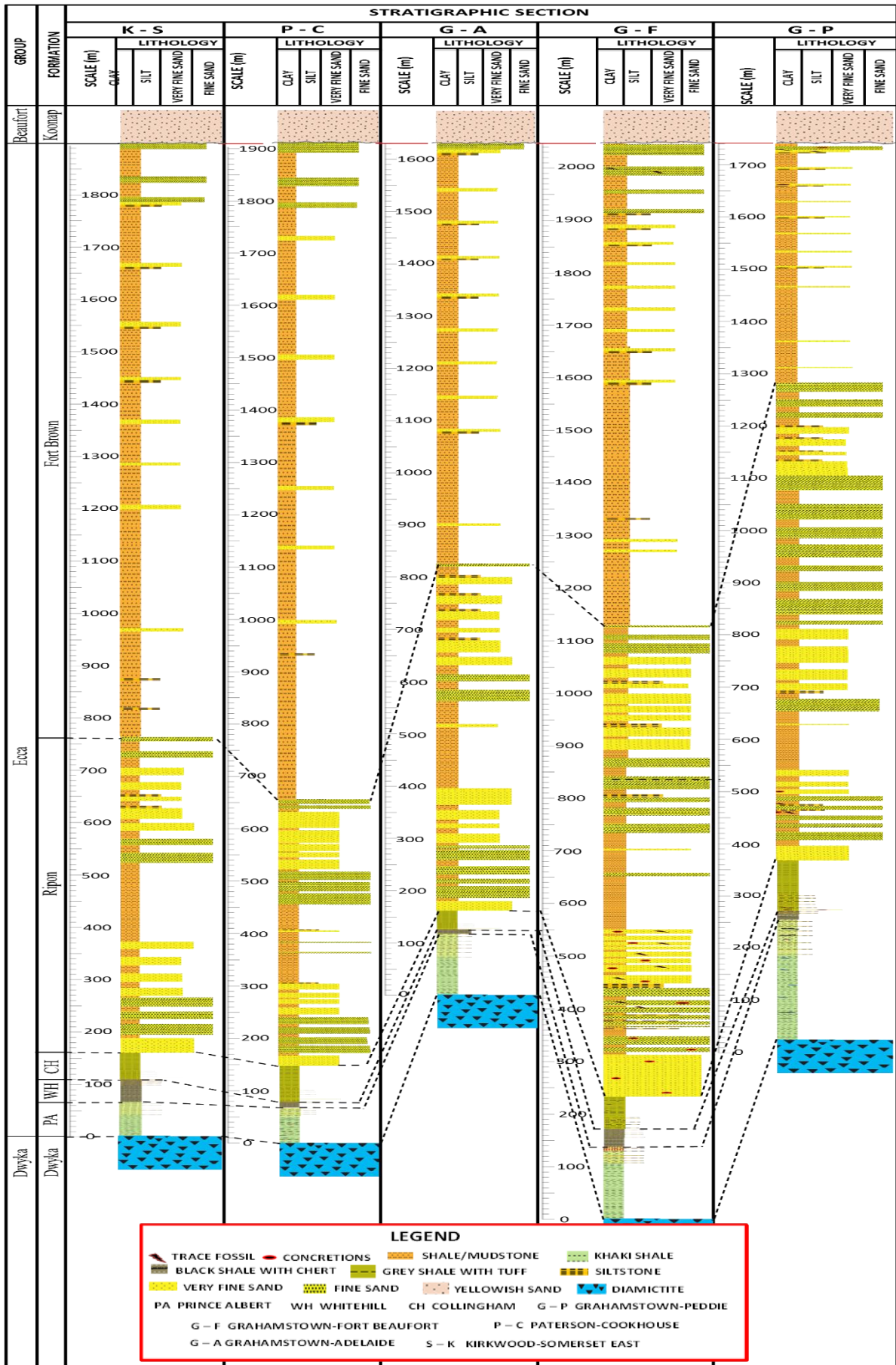
Figure 3.30: Stratigraphic correlation of the Ecca Group within the study area.
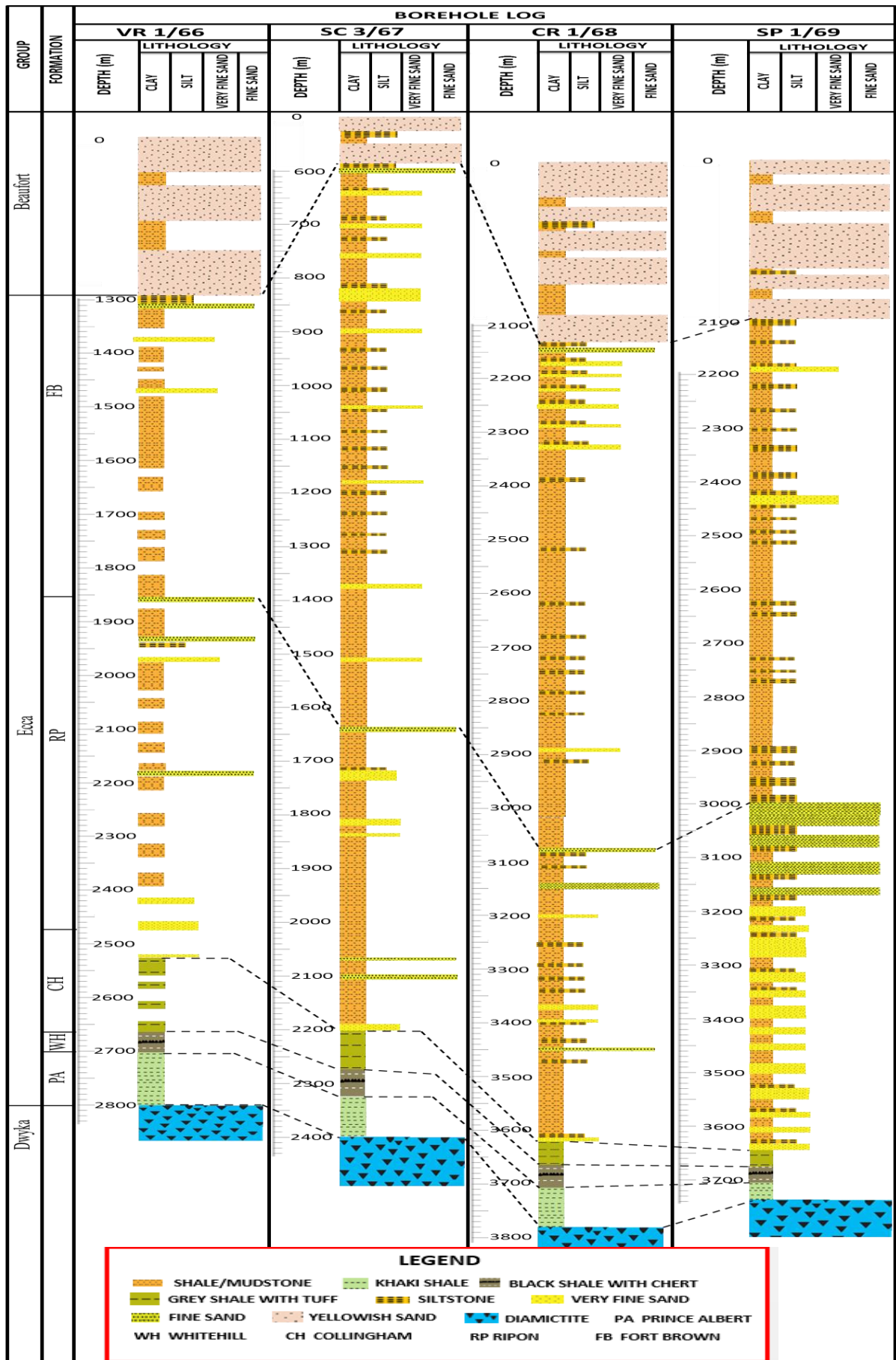
Figure 3.31: Stratigraphic correlation of the borehole logs within the study area.

3.4 Discussion and conclusions

The stratigraphy of the Ecca Group in the study area was previously divided into five formations, namely the Prince Albert, Whitehill, Collingham, Ripon and Fort Brown Formations (Rossouw, 1953; Johnson 1976; Kingsley, 1977; Johnson et al., 2006). These formations have now been further subdivided into several stratigraphic members based on their lithological features and sedimentary structures in order to give more detailed information about their lateral and vertical lithological changes along the stratigraphic sections of the different rock units of the Ecca Group.

The Prince Albert Formation is subdivided into the Lower Grey Mudrock Member and Upper Khaki Mudrock Member. The Lower Grey Mudrock Member is made up of well-laminated, thin bedded grey shale, whereas the Upper Khaki Mudrock Member consists of khaki shale and arenaceous mudstones with some graded silty layers.

The Whitehill Formation has an ultra-tubular nature and is laterally extensive just like the underlying Prince Albert Formation. The Whitehill Formation is subdivided into the Lower Black Shale-Chert Member and Upper Grey Mudrock Member. The Lower Black Shale-Chert Member has laminated black shale intercalated with thin bedded or lenticular black chert layers. The Upper Grey Mudrock Member consists of well laminated grey shale with thin bedded mudstones and siltstones.

The Collingham Formation is subdivided into the Lower Black Rhythmite Member and Upper Grey Mudrock Member. The Lower Black Rhythmite Member is made up of mudstone rhythmite, while the Upper Grey Mudrock Member consists of well laminated shale, claystone and minor siltstone. The main difference between the Lower Black Rhythmite Member and Upper Grey Mudrock Member is that the Lower Black Rhythmite Member has dark-black rhythmite showing multiple cyclotherm of repeated couplets of claystone and mudstone.

The stratigraphy of the Ripon Formation is subdivided into the Lower Greywacke-Mudrock Member, Middle Black Mudrock Member and Upper Grey Mudrock-Sandstone Member. The Lower Greywacke-Mudrock Member consists mainly of thick-massive bedded greywackes with subordinate mudstones. The Middle Black Mudrock Member is predominantly of laminated, grey shale intercalated with very minor thin bedded sandstone layers, while the Upper Grey Mudrock-Sandstone Member mainly consists of alternating dark grey greywacke and greyish-black shale and mudstones.

The Fort Brown Formation is subdivided into the Lower Grey Varved Rhythmite Member and the Upper Grey Mudrock-Sandstone Member. The Lower Grey Varved Rhythmite Member is made up of thin bedded, well laminated rhythmites of grey mudstone, with very minor lenticular sandstone intercalation. The Upper Grey Mudrock-Sandstone Member consists of silty, well laminated grey shale and mudstone, alternating with minor sandstones. The Lower Grey Varved Rhythmite Member is finely laminated and mostly argillaceous.

In this chapter, all the stratigraphic member names in each formation are the newly established members for the Ecca Group, and are proposed for the first time in the studies of the Ecca Group. From west to east, the measured thickness of the whole Ecca Group along the roads R350 (North of Kirkwood-Somerset East), N10 (Cookhouse-Paterson), R344 (Grahamstown-Adelaide), R67 (Ecca Pass) and N2 (Grahamstown-Peddie) are 1893 m, 1909.6 m, 1625.3 m, 2057 m, and 1738.2 m, respectively, while the borehole logs CR 1/68, SP 1/69, VR 1/66 and SC 3/67 are 1508.8 m, 1798.3 m, 1645.3 m, and 1673.4 m, respectively. The stratigraphic correlation of the measured sections and borehole core logs show that the Ecca Group generally undulate in thickness in the study area. The undulations in the thickness of the Ecca Group across the study area are inferred to be due to deformation.

CHAPTER 4

GRAIN SIZE STATISTICS AND DEPOSITIONAL PATTERN OF THE ECCA GROUP SANDSTONES

Abstract

Grain size analysis is a vital sedimentological tool used to unravel the hydrodynamic conditions, mode of transportation and deposition process of detrital sediments. The result of grain size analysis of thirty-five sandstone samples from the Ecca Group is presented in this chapter. Grain size statistical parameters, bivariate analysis, linear discriminate functions, Passega diagrams and log-probability curves were used to reveal the depositional processes, sedimentation mechanisms, hydrodynamic energy conditions and to discriminate different depositional environments. The grain size parameters show that most of the sandstones are very fine to fine grained, moderately well sorted, mostly near symmetrical and mesokurtic in grain-size distribution. The abundance of very fine to fine grained sandstones indicates the dominance of low energy deeper water environment. The bivariate plots show that the samples are mostly grouped together, except for the Prince Albert samples that show scattered trend, which is due to either mixture of two modes in equal proportion in bimodal sediments or good sorting in unimodal sediments. The linear discriminant function analysis is dominantly indicative of turbidity current deposits under shallow marine environments for samples from the Prince Albert, Collingham and Ripon Formations, while those samples from the Fort Brown Formation are lacustrine or deltaic deposits. The C-M plots indicated that the sediments were deposited mainly by suspension and saltation, and graded suspension. Visher diagrams show that saltation is the major process of transportation, followed by suspension.

Keywords: Grain size, hydrodynamic condition, depositional environment, Ecca Group

4.1 Introduction

Grain size is a fundamental feature of siliciclastic sediments and thus, it is one of the important descriptive properties of sedimentary rocks. Grain size characteristics are widely used by geologists to reveal depositional process, hydrodynamic condition and depositional environment (Boggs, 2009). As applied in a variety of sediments deposited in various environments, grain size analysis plays an important role in understanding and defining the hydrodynamic mechanisms and depositional environments of detrital sediments. Edwards

(2001) documented that grain size analysis is an important tool used to texturally characterise sediment properties, classify sedimentary rocks and define depositional environments. In addition, grain size parameters also provide valuable clues to the sediment provenance, transportation mechanism and depositional conditions (Blott and Pye, 2001). Several researchers (i.e. Folk and Ward, 1957; Passega, 1957, 1964; Sahu, 1964; Folk, 1966, 1974; Visher, 1969; Friedman, 1979; Pettijohn et al., 1987; Skaberne, 1996; Blott and Pye, 2001; Bhat et al., 2002; Selvaraj and Ram Mohan, 2003; Rao et al., 2005; Angusamy and Rajamanickam, 2006; Kovacs, 2008; Boggs, 2009; Srivastava and Mankar, 2009; Goswami and Ghosh, 2011; Srivastava et al., 2012; Rajganapathi et al., 2013; Kulkarni et al., 2015; Madukwe, 2016) have shown that indeed each sedimentary environment supposedly exhibits distinctively different grain size characteristics that distinguish them from sediments deposited in different environments. Furthermore, these studies documented that as soon as sediments from recent environments have been 'finger printed' by grain size properties, the information can be deduced and used in interpretation of the sediment depositional history. However, Boggs (1995) and Tucker (2001) highlighted the ambiguity of grain size analysis in respect of depositional environments.

According to Boggs (1995), there are three main aspects of particle size that sedimentologists focus on: (a) the method for measuring grain size and representing it in terms of grade scale, (b) techniques for quantifying grain size data and presenting them in a statistical or graphical form and (c) the genetic significance of the data. Graphical and mathematical methods are the two main ways for representing grain size data. The former often involves plotting the grain size data on bivariate diagrams in which either the cumulative weight percent or individual weight percent is plotted against the sieve size in phi units. The latter entails the use of mathematical expression or statistical parameters to represent grain size data. Grain size analysis produces statistical parameters like calculated mean (verbal grain size), standard deviation (verbal sorting), kurtosis and skewness. Two component variation diagrams and log-probability plots are the two main types of graphical plots that have been widely used in environmental studies when it comes to grain size analysis.

Friedman (1961, 1979) supported the use of the two component variation diagrams, in which one statistical parameter is plotted against another (i.e. mean grain size versus standard deviation and kurtosis versus skewness). This method allows the separation of various environments like river and beach from each other based on numerical parameters. On the other hand, several researchers have recommended the use of log-probability plots because of

the environmental significance that is associated with the shapes of grain size cumulative curves (Sagoe and Visher, 1977; Visher, 1969). Visher (1969) documented that such curves usually show two or three straight-line segments instead of the single straight line anticipated for a normally distributed population. These curve segments are interpreted by Visher (1969) and Sagoe and Visher (1977) to represent subpopulations of grains transported concurrently by different mechanism of transportation such as traction, saltation and suspension. The differences in shapes of the curve as well as the position of truncation points of the curve segments putatively allow discrimination of sediments from different environments. However, a number of researchers have reported success in using the two methods, while others have failed to identify the correct environment (Srivastava and Mankar, 2009; Goswami and Ghosh, 2011; Srivastava et al., 2012; Rajganapathi et al., 2013; Kulkarni et al., 2015).

The stratigraphic sequence of the Ecca Group in the study area consists of dark grey shale, sandstones and mudstones with subordinate chert, yellow claystones (tuff) and siltstones. So far, the Ecca Group in the area received a very casual attention for its sedimentological details, in spite of the excellent preservation of the stratigraphic sequence and variation in lithological characteristics (i.e. grain sizes and texture). Recently, the use of more sophisticated multivariate statistical methods like factor analysis and discriminant functions have yielded more successful results in identifying the correct depositional process and environments and this is supported by the works of Sutherland and Lee (1994), Martins (2003), Srivastava et al. (2009; 2010; 2012), Rajganapathi et al. (2013) and Kulkarni et al. (2015). This study provides the first relatively detailed grain size analysis of sandstones from part of the Ecca Group in the study area. The results presented in this chapter are based on the generation and integration of basic data on grain size parameters and multivariate statistical measures. Based on various basic statistical data, bivariate plots between different parameters, linear discriminant function, Passega diagram and log-probability curves, an attempt has been made to interpret the probable depositional environments and depositional process of the sediments in the area.

4.2 Materials and method

Thirty five representatives thin sections of different types of sandstone from the Ecca Group were selected systematically to cover textural variations (physical character such as grain size, shape and arrangement) were considered. The samples were analysed for their grain size

parameters and statistical relationships. Grain size measurements were conducted on the thin sections under petrographic microscope using an ocular with a millimetre scale. At least 500 grains per thin section were measured for each sample using the conventional method of grain's longest axis measurement (Adams, 1977; Johnson, 1994; Liu and Greyling, 1996). The frequencies of grain size ranges were calculated and the grain size classes were determined using the Udden-Wentworth grade scale (Udden, 1914; Wentworth, 1929). The dimension of grain sizes (millimetres) was converted to a phi scale which is a logarithmic scale to base 2.

$$\emptyset = -\log_2 D,$$

where $\emptyset$ is the phi size and D is the grain diameter in millimetres.

The results of the grain size analysis were graphical represented in the form of cumulative curves. On the other hand, the average grain size and sorting of the samples cannot be actually determined, thus mathematical techniques which allow statistical treatment of grain size data was derived from the cumulative curves (Figure 4.1) to describe grain size distribution mathematically.
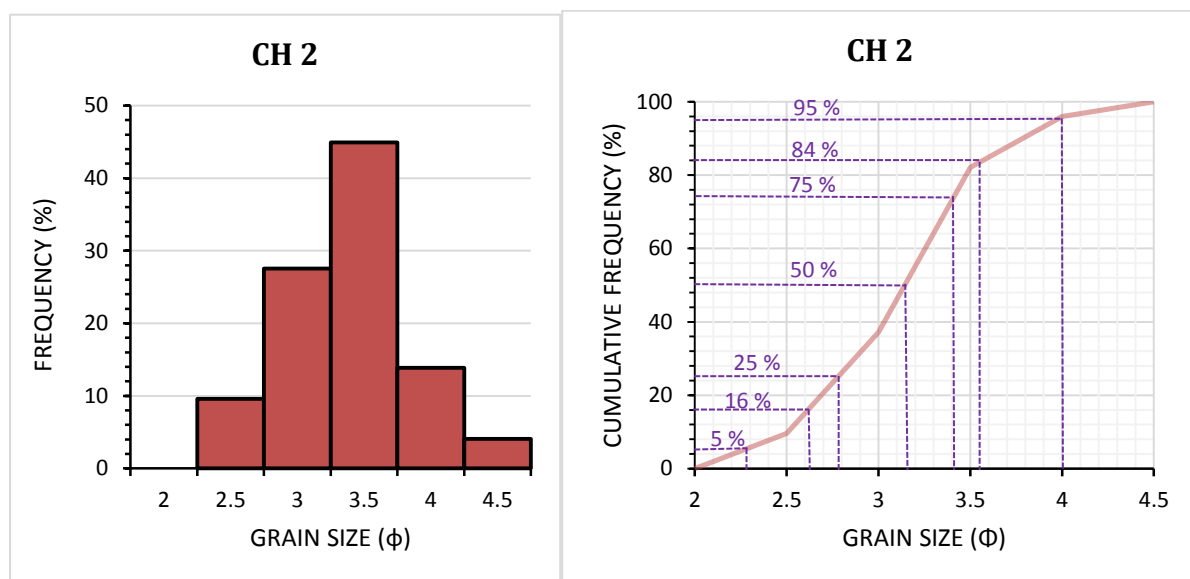
Figure 4.1: Illustration of histogram (left) and cumulative curve (right) plotted for one of the Collingham Formation sample. In addition, the cumulative curve shows the mathematical method for calculating percentile values.

The statistical parameters of grain size distribution were calculated using equation proposed by Folk and Ward (1957) (Table 4.1). Bivariate scatter plots were employed to discriminate between depositional settings based on the textural variations of sediment. The Sahu's (1962,

1964) linear discriminant function (LDF) was modified and used to determine and distinguish processes and environments of deposition. In addition, grain size statistical parameters, C-M plots and log-probability curves were used to reveal the different depositional processes, mechanism of sedimentation and energy condition of the transporting medium (Passega, 1964; Visher, 1969).

Table 4.1: Formulas for calculating grain size statistical parameters by graphical methods (After Folk and Ward, 1957).

Graphic mean(M_Z)	$M_Z = \dfrac{\emptyset_{16} + \emptyset_{50} + \emptyset_{84}}{3}$
Inclusive graphic standard deviation (σ_i)	$\sigma_i = \dfrac{\emptyset_{84} - \emptyset_{16}}{4} + \dfrac{\emptyset_{95} - \emptyset_5}{6.6}$
Inclusive graphic skewness (SK_i)	$SK_i = \dfrac{(\emptyset_{84} + \emptyset_{16} - 2\emptyset_{50})}{2(\emptyset_{84} - \emptyset_{16})} + \dfrac{(\emptyset_{95} + \emptyset_5 - 2\emptyset_{50})}{2(\emptyset_{95} - \emptyset_5)}$
Graphic kurtosis (K_G)	$K_G = \dfrac{(\emptyset_{95} - \emptyset_5)}{2.44(\emptyset_{75} - \emptyset_{25})}$

Where $\emptyset_5$, $\emptyset_{16}$, $\emptyset_{25}$, $\emptyset_{50}$, $\emptyset_{75}$, $\emptyset_{84}$ and $\emptyset_{95}$ represents 5th, 16th, 25th, 50th, 75th, 84th and 95th percentile, respectively, on the cumulative curve.

The parameters employed to describe the grain size distribution are categorised into four main groups that include, the mean, standard deviation, skewness, and kurtosis. The formula for calculating graphic mean, standard deviation, skewness and kurtosis is depicted in Table 4.1 above. The parameters are defined by Boggs (2009) as follows:

- Mean grain size (M_Z) is a descriptive parameter of grain size that measures the arithmetic average size of all the particles in a sample. It indicates the central tendency of a grain size distribution. An approximation of the arithmetic mean was determined by picking selected percentile values from the cumulative curve and averaging those values using the graphic mean formulae depicted in Table 4.1.

- Standard deviation or grain size sorting is a measure of a range of grain sizes present and the degree of spread or scatter of these sizes around the average or mean size. The inclusive graphic standard deviation is the mathematically expression for sorting (σ_i). The verbal term for sorting that corresponds to the values of the inclusive graphic phi standard deviation is depicted in Table 4.2.

Table 4.2: Verbal terms for sorting that correspond to the values of the inclusive graphic standard deviation (Folk, 1974).

Phi standard deviation	Verbal sorting
< 0.35	Very well sorted
0.35 to 0.50	Well sorted
0.50 to 0.70	Moderately well sorted
0.70 to 1.00	Moderately sorted
1.00 to 2.00	Poorly sorted
2.00 to 4.00	Very poorly sorted
> 4.00	Extremely poorly sorted

- Skewness is a measurement of the degree of symmetry of grain size distribution or it reflects sorting in the tails of the distribution. Also, it is a descriptive parameter that determines the majority of the grain size measurement inclusive graphic skewness. The more the calculated skewness values deviate from zero, the more the skewness.

Table 4.3: Verbal terms for skewness corresponding to the calculated skewness (Folk, 1974).

Calculated skewness	Verbal skewness
> +0.30	Strongly fine skewed
+0.30 to 0.10	Fine skewed
+0.10 to -0.10	Near symmetrical
-0.10 to -0.30	Coarse skewed
<-0.30	Strongly coarse skewed

- Kurtosisis a measure of the sharpness or peakedness of the grain size frequency curve. It is calculated by comparing the spread or the sorting of the tails in the central part of the distribution to the spread in the tails.

Table 4.4: Verbal terms for kurtosis that corresponds to the calculated kurtosis (Folk, 1974).

Calculated kurtosis	Verbal kurtosis
<0.67	Very platykurtic
0.67 to 0.90	Platykurtic
0.90 to 1.11	Mesokurtic
1.11 to 1.50	Leptokurtic
1.50 to 3.00	Very leptokurtic
> 3.00	Extremely leptokurtic

4.3 Results and discussion

4.3.1 Grain size statistics

The grain size frequency histograms and cumulative frequency curves for the analysed samples are presented in Appendix A. The cumulative volume percentage frequency curves show that most of the Ecca sandstones are unimodal in nature with peaks at 2.5Ø, 3.0Ø, and 3.5Ø (Figures 4.2, 4.3 and 4.4) and mostly display near asymmetrical distribution. Four samples from the Prince Albert Formation (PA 2-5) are bimodal in nature with peaks at 2.5Ø and 4.0Ø (Figure 4.2). However, one of the sample is positively (fine) skewed (PA 3), while others show near asymmetrical distribution. This bimodality is probably due to low energy of the marine setting. The unimodality of some of the Ecca sandstones indicates the consistent depositional process during which the sediments were settled. The positively skewed distribution in the Prince Albert sediment shows that the finer fraction is abundant in the depositional environment (Figure 4.2).
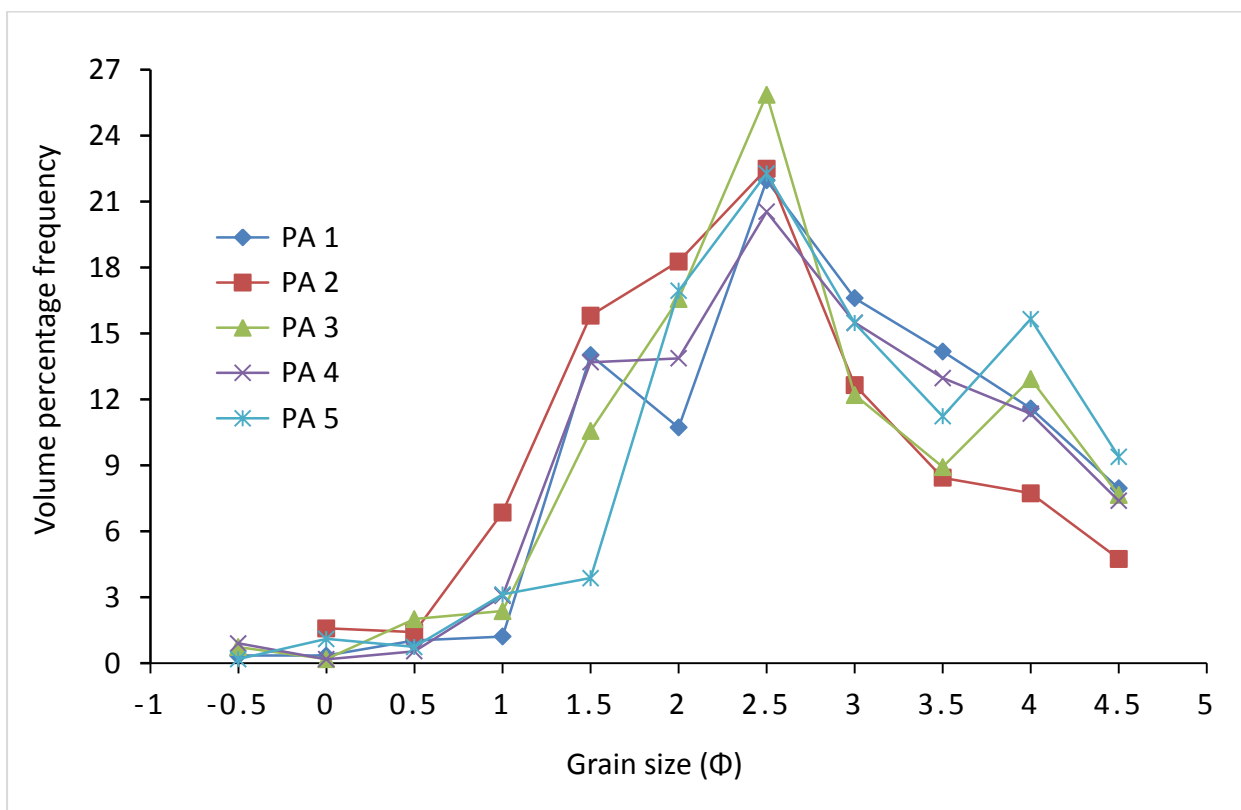
Figure 4.2: Volume percentage curves of samples from the Prince Albert Formation.

Most of the graphic curves for the samples of the Collingham, Ripon and Fort Brown Formations (Figures 4.3, 4.4 and 4.5) display almost similar trends, showing moderate well sorting to well sorting. The grain size diameters range from -0.5 to 4.5Ø classes on the

Udden-Wentworth grade scale. Most of the sandstones from the Collingham Formation are very fine grained (3-4∅), while sandstones from other formations are mostly fine grained (2-3∅). The presence and dominance of very fine-fine grained populations in the area, could be attributed to deposition of sediments mainly by low energy marine currents based on the grain size descriptive statistics. The bimodal nature as well as the absence of a particular trend in the Collingham Formation sandstones are probably due to mixing of particles supplied or brought in by different processes or transporting agents. Alternatively, it could also be due to the mineral composition differences.
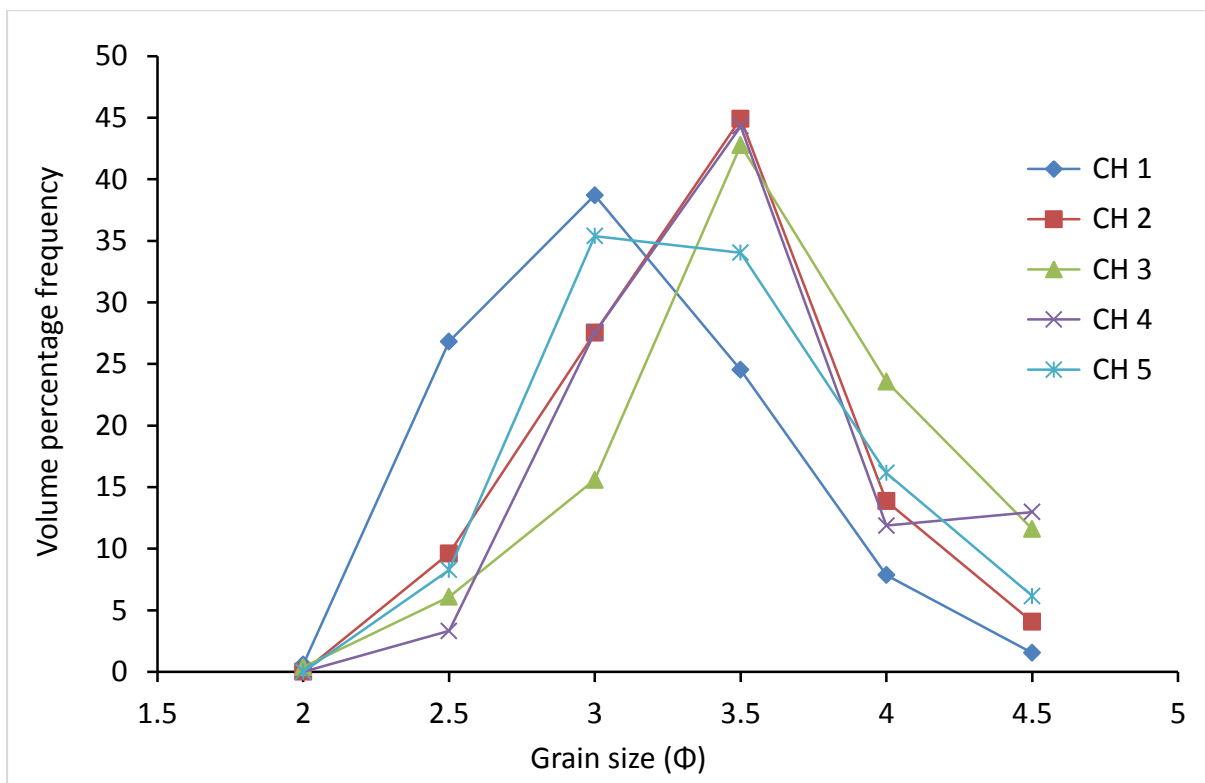
Figure 4.3: Volume percentage curves of samples from the Collingham Formation.
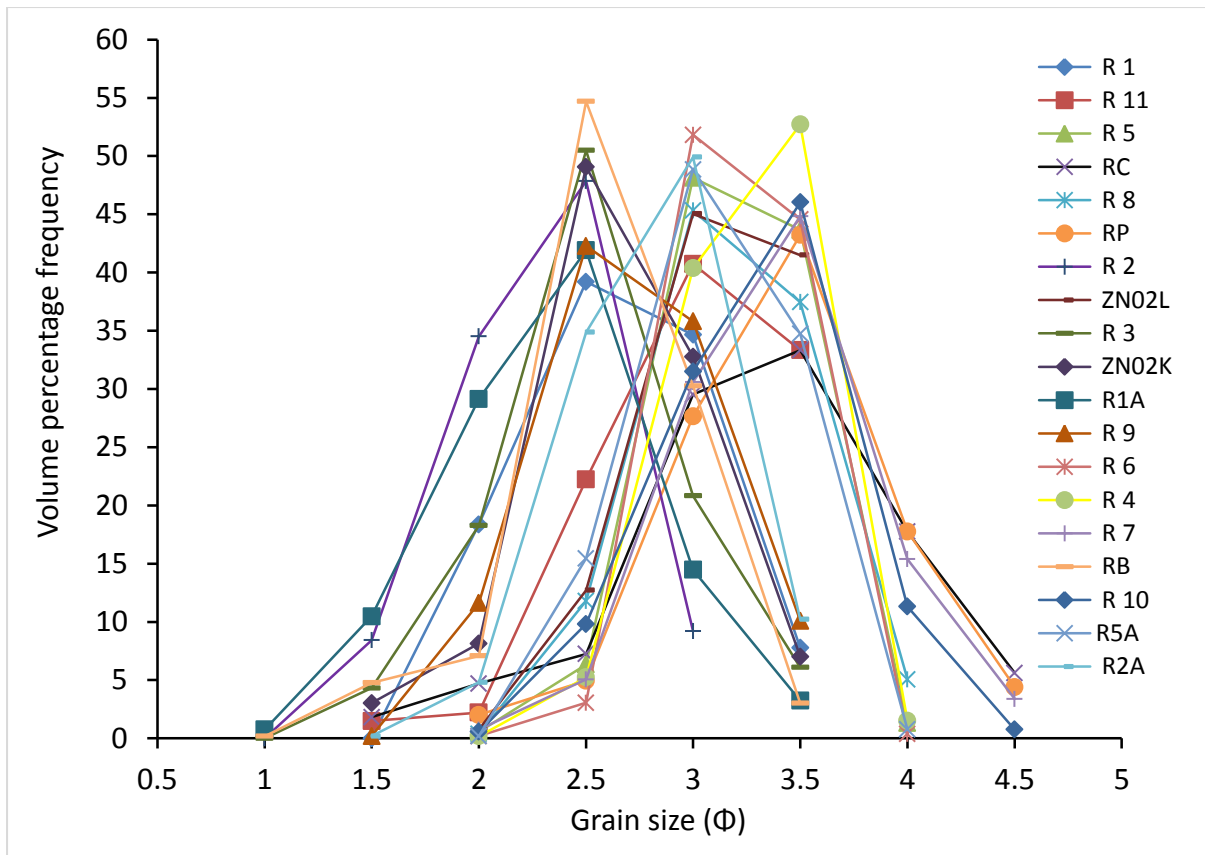
Figure 4.4: Volume percentage curves of samples from the Ripon Formation.
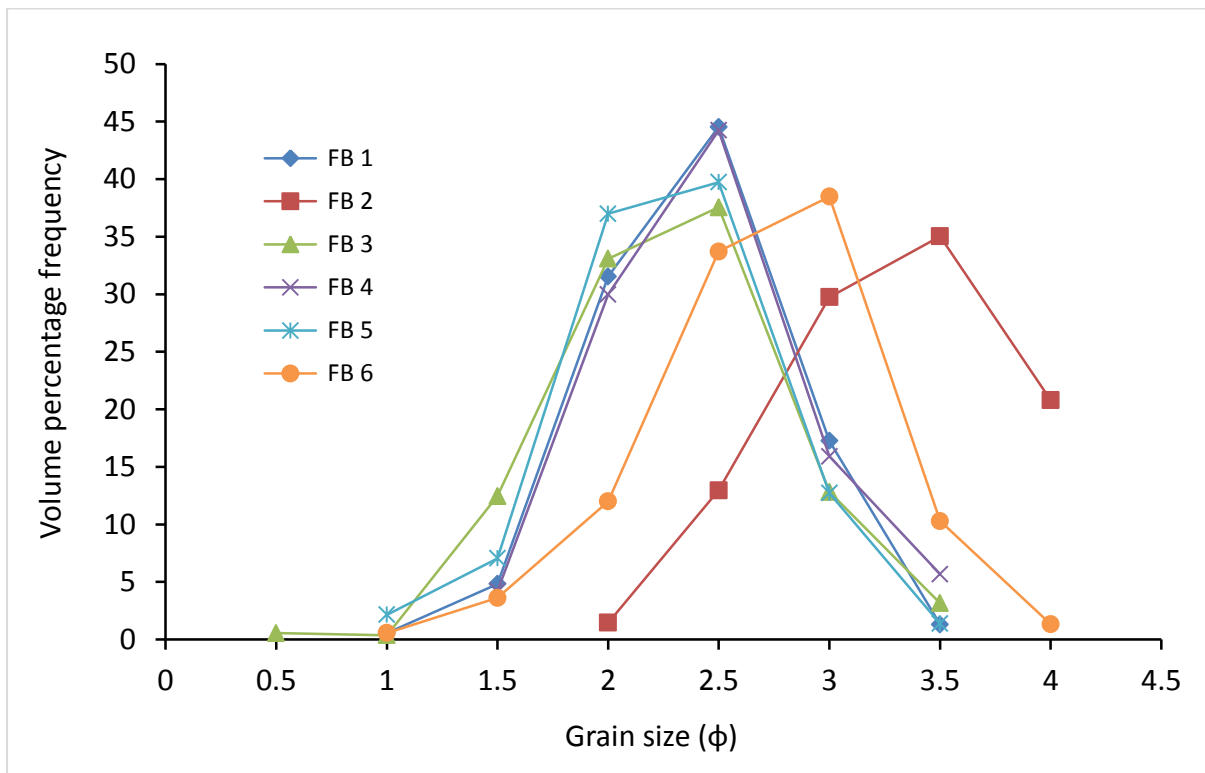
Figure 4.5: Volume percentage curves of samples from the Ripon Formation.

4.3.2 Grain size parameters

A series of grain size statistical parameters (i.e. mean, standard deviation, skewness and kurtosis) were calculated from the grain size distribution curves (After Folk and Ward, 1957). The parameters used to represent grain size characteristics of the Ecca sandstones (Table 4.5) are as follows:

4.3.2.1 Graphic mean (Mz)

The graphic mean size is a parameter that relates to the overall grain size. It is the average size of the sediment represented by phi (∅) mean size and connotes the index of energy conditions (Passega, 1964). The calculated mean values range from 2.03∅ to 3.34∅ with average values of 2.49∅, 3.13∅, 2.71∅ and 2.32∅ for the Prince Albert, Collingham, Ripon and Fort Brown sediments, respectively (Figure 4.6 and Table 4.6). The average mean grain size values of the Permian Ecca sediments in the area point to the predominance of fine sand (averaging 2.68∅). Likewise, it may show local variations within the formations, ranging from fine to very fine sands. The general variation in the mean size points to fluctuations in the energy condition during sediment deposition. Furthermore, the predominance of fine grained sediments and absence of coarse-grained sediments indicate a moderately low energy condition of deposition (Boggs, 2009).

4.3.2.2 Inclusive graphic standard deviations (σ_1)

The inclusive standard deviation measures the sorting or uniformity of the grain size distribution. It also indicates the fluctuations in the hydrodynamic energy conditions of depositional environment (Sahu, 1964). The inclusive graphic standard deviation values range from 0.32∅ to 1.03∅ and these values indicate that the Ecca sediments in the area are mainly well-sorted with some being poorly sorted in nature (Figure 4.6 and Table 4.6). The values range between 1.02-1.03∅ (poorly sorted), 0.50-0.56∅ (moderately well sorted), 0.32-0.63∅ (well sorted to moderately well sorted) and 0.44-0.53∅ (well sorted to moderately well sorted) for the Prince Albert, Collingham, Ripon and Fort Brown sediments, respectively. Generally, the moderately well sorted nature of the sediment could be due to partial winnowing action as well as the addition or influx of previously sorted sediments in marine environment (Angusamy et al., 2006; Rajesh et al., 2007; Ramanathan et al., 2009).

4.3.2.3 Inclusive graphic skewness (Sk$_1$)

The graphic skewness is a measure of grain size distribution that reflects the grain spread characteristics in the tails of the distribution. An asymmetrical curve with excess fine particles has a fine-size tail and displays a positive phi (∅) value, while one with excess coarse material shows negative phi (∅) value. A zero phi (∅) value is indicated by a symmetrical curve. The values of inclusive graphic skewness ranges from -0.09 to 0.16∅ (near symmetrical to fine skewed), with an average of 0.01∅ (near symmetrical). Most of the samples fall in the near symmetric field (Table 4.6). Only one sample (PA 3) from the Prince Albert Formation falls in the fine skewed field. Selvaraj and Vam Mohan (2003) documented that the near symmetrical nature of sediments perhaps indicate the absence of extreme conditions like tidal variations, wave breaking and seasonal supply of detrital materials.

4.3.2.4 Graphic kurtosis (KG)

The graphic kurtosis reflects the sharpness or peakedness of the grain size distribution. Sharp peaked curves point to better sorting in the central portion of the grain size distribution than in the tails, while the flat-peaked curves show otherwise (Folk, 1966; Boggs, 2009). The graphic kurtosis values for the Ecca sediments range from 0.76 to 1.21∅, which falls in the platykurtic to leptokurtic field (Figure 4.6). The average graphic kurtosis values for the sediments indicate the predominance of mesokurtic field (averaging 0.99∅). These values range from 0.85-1.01∅ (platykurtic to mesokurtic), 0.96-1.20∅ (mesokurtic to leptokurtic), 0.76-1.2∅ (platykurtic to leptokurtic) and 0.94-1.05∅ (mesokurtic) for the Prince Albert, Collingham, Ripon and Fort Brown sediments, respectively. The variations in kurtosis values are due to changes in the flow characteristics of the depositional medium (Hanamgond and Chavadi, 1998). The dominance of fine sand-size particles of platykurtic-mesokurtic nature and roundness of the particles reveal maturity of the sands. This could be attributed to the accumulation of fine sand-size particles in a dominant low-energy marine environment (Ramanathan et al., 2009). The well-sorted sediments with low kurtosis values in the Fort Brown Formation possibly imply that part of the sediments achieved their sorting in a relatively high energy environment.

Table 4.5: Graphic measures and grain size parameters of the samples from the Ecca Group.

SAMPLE	Ø1	Ø5	Ø16	Ø25	Ø50	Ø75	Ø84	Ø95	C (μm)	M (μm)
FB6	1.03	1.53	1.99	2.13	2.5	2.83	2.95	3.32	490	177
FB5	0.90	1.21	1.59	1.72	2.05	2.36	2.48	2.86	523	245
FB4	1.40	1.51	1.7	1.85	2.18	2.47	2.68	3.06	380	220
FB3	1.00	1.16	1.54	1.68	2.05	2.38	2.5	2.93	500	245
FB2	1.90	2.14	2.53	2.68	3.08	3.44	3.61	3.88	268	116
FB1	1.04	1.46	1.67	1.81	2.14	2.43	2.57	2.9	485	230
R 10	2.02	2.23	2.58	2.74	3.09	3.36	3.46	3.81	247	117
RB	1.10	1.50	2.04	2.12	2.35	2.64	2.79	2.97	470	198
R5A	2.02	2.16	2.51	2.60	2.86	3.15	3.30	3.44	246	140
R 7	2.00	2.42	2.67	2.82	3.15	3.43	3.59	3.945	250	110
R 4	2.10	2.46	2.63	2.74	3.04	3.28	3.37	3.47	238	123
R 6	2.10	2.52	2.62	2.71	2.95	3.22	3.34	3.46	235	131
R2A	1.58	2.00	2.16	2.29	2.6	2.85	2.94	3.25	343	165
R 9	1.54	1.71	2.05	2.16	2.45	2.79	2.92	3.25	347	187
R1A	1.00	1.20	1.58	1.74	2.12	2.41	2.56	2.94	500	230
ZN02K	1.35	1.62	2.05	2.14	2.40	2.73	2.86	3.14	400	187
R 3	1.10	1.52	1.79	2.02	2.27	2.55	2.76	3.08	470	208
ZN02L	2.01	2.17	2.53	2.63	2.91	3.20	3.32	3.44	249	136
R 2	1.04	1.29	1.61	1.74	2.07	2.33	2.43	2.73	485	240
RP	1.90	2.30	2.66	2.83	3.18	3.47	3.67	3.98	268	110
R 8	2.02	2.20	2.54	2.64	2.92	3.24	3.36	3.5	248	133
RC	1.40	1.83	2.54	2.69	3.10	3.48	3.71	4.06	380	117
R 5	2.02	2.35	2.60	2.69	2.95	3.23	3.33	3.46	247	131
R 11	1.45	2.03	2.28	2.48	2.80	3.12	3.26	3.43	372	143
R 1	1.52	1.64	1.94	2.08	2.41	2.75	2.88	3.18	348	187
CH5	2.06	2.3	2.61	2.74	3.09	3.46	3.7	4.09	240	117
CH4	2.12	2.53	2.73	2.89	3.22	3.50	3.87	4.31	230	107
CH3	2.04	2.38	2.81	3.04	3.32	3.71	3.9	4.28	245	101
CH2	2.04	2.26	2.61	2.78	3.14	3.42	3.57	3.96	243	113
CH1	2.01	2.08	2.29	2.46	2.79	3.18	3.36	3.772	250	145
PA5	-0.40	0.96	1.70	1.97	2.56	3.50	3.79	4.23	1355	170
PA4	-0.30	1.02	1.41	1.74	2.44	3.26	3.62	4.16	1245	186
PA3	0.00	0.94	1.51	1.79	2.34	3.26	3.68	4.18	1000	203
PA2	-0.10	0.65	1.20	1.48	2.13	2.83	3.29	3.98	1048	230
PA1	0.20	1.07	1.48	1.88	2.51	3.31	3.66	4.19	920	177

Where C is the coarser one- percentile value in micron and M is the median value in micron.
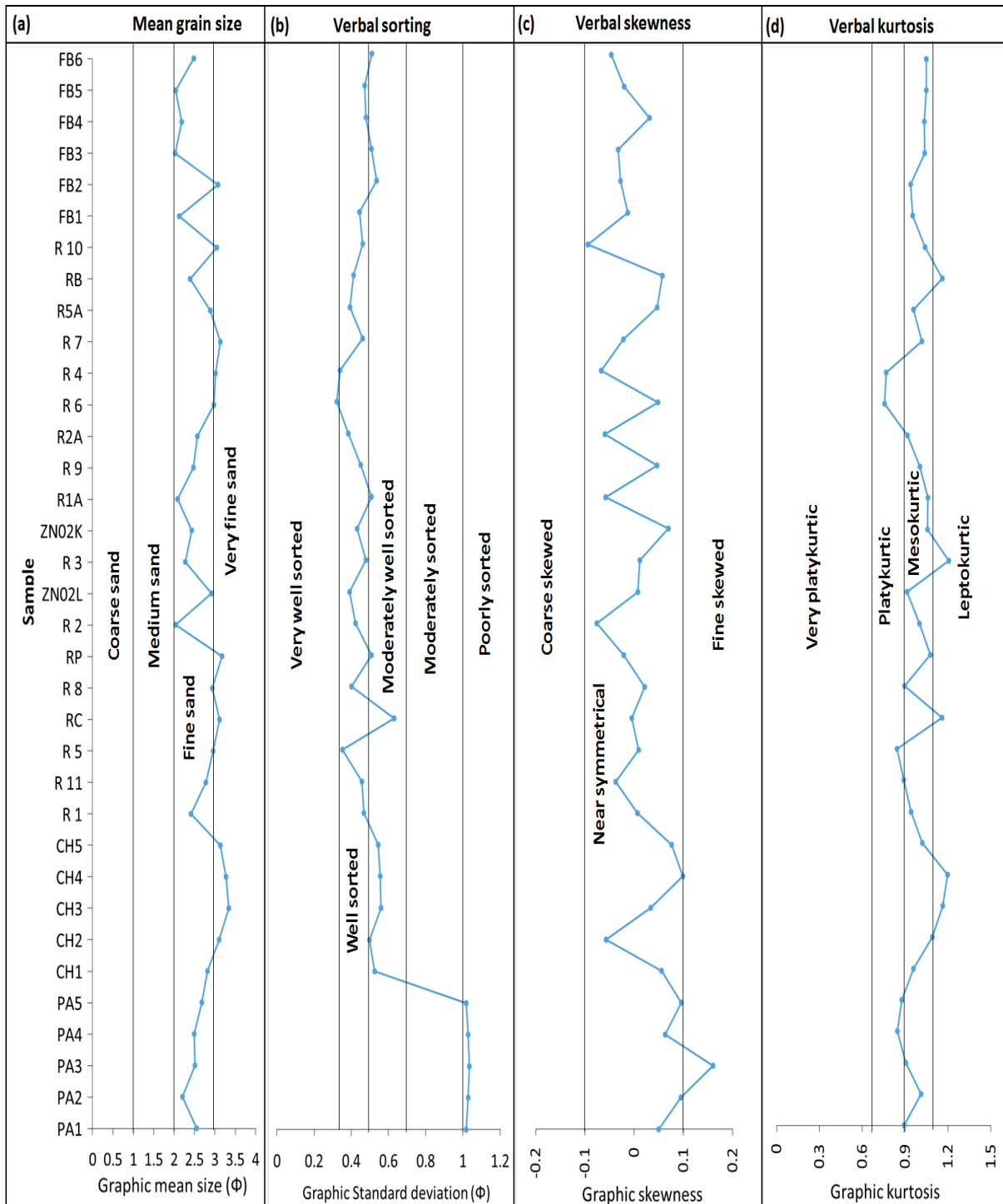
Figure 4.6: Variation of textural components of the Permian sandstone samples of the Ecca Group: (a) Graphic mean; (b) standard deviation; (c) skewness; and (d) kurtosis.

4.3.3 Bivariate plots of statistical parameters

The combination of several textural parameters in the form of bivariate plots has been used to identify depositional environment (Friedman, 1967). The bivariate plots are based on the assumption that statistical parameters reliably reflect differences in the fluid-flow

mechanisms of sediment transportation and deposition (Sutherland and Lee, 1994). Several researchers like Al-Ghadban (1990), Sutherland and Lee (1994), Martins (2003), and Srivastava et al. (2009, 2010, 2012) have proven and documented that bivariate plots serve as reliable tools for identifying mechanisms of different environments of sedimentation. Furthermore, they reported that bivariate plots of Folk and Ward (1957), Stewart (1958), Friedman (1967), and Moiola and Weiser (1968) are the most important and frequently used plots. These plots have also been attempted to differentiate between marine and fluvial sands. The bivariate plot of skewness against standard deviation, skewness versus mean, kurtosis against skewness, and standard deviation versus mean were used to distinguish between the different depositional settings.

4.3.3.1 Graphic standard deviation (sorting) versus mean size

The bivariate plot of graphic standard deviation (sorting) against graphic mean shows that the Ecca samples are poorly to well sorted and are very fine to fine sand (Figure 4.7). Sediments that are well sorted out during longer transportation have relatively the same grain sizes and if there are different sizes, the sediment were probably deposited close to its source or deposited quickly (Rajganapathi et al., 2013). Most of the Ecca sandstones are fine grained and well sorted meaning they had a reasonable time in the transporting medium and because of the grain to grain interaction, their sizes were perhaps reduced. The Prince Albert Formation is interpreted as deep marine sediment and sandstone has been found between the shales and mudstone. The dominance of poorly sorted sandstones in the Prince Albert Formation may point to a near source region. However, the considerable number of well sorted to moderately well sorted sediments in other formations indicate continuous reworking of the sediments by currents and waves (Srinivasa Rao et al., 1990). These fine grained and better sorted sandstones from the Prince Albert Formation are thought to have been previously reworked in the shallow-water environments and subsequently brought to the deep marine environment. The plot of standard deviation (sorting) against mean shows clustering of samples near the extreme end of right limb of the inverted V-shaped established trend of Folk and Ward (1957), signifying a smaller size range of the grains (Figure 4.8). Both mean grain size and sorting are hydraulically controlled, such that in all sedimentary environments, the well-sorted sediments have mean size in the fine sand size range (Griffths, 1967). The nature of the Ecca sediments is generally unimodal, of which the dominant constituent is fine sand. The very fine sediment (fine and silty sand) is subordinate making the admixture moderately-sorted.
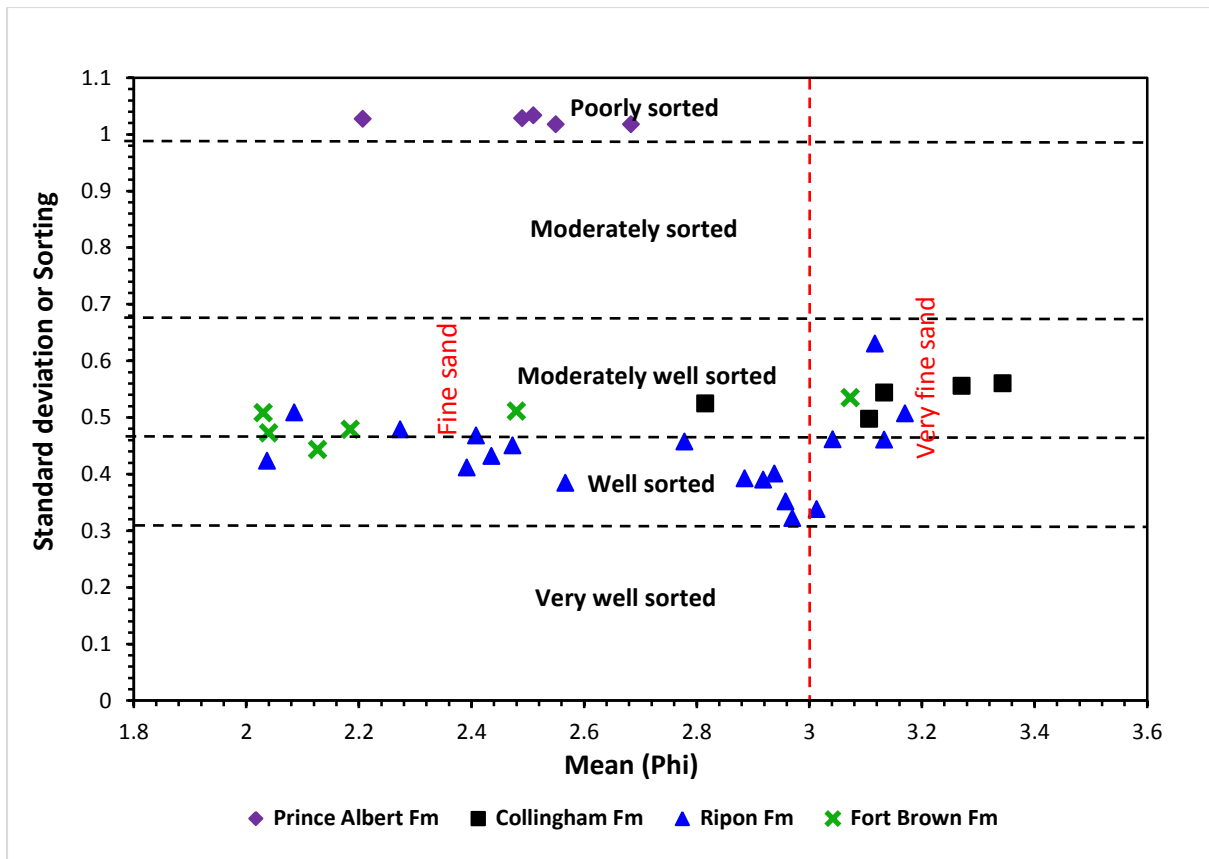
Figure 4.7: Bivariate plot of graphic standard deviation versus graphic mean skewness.
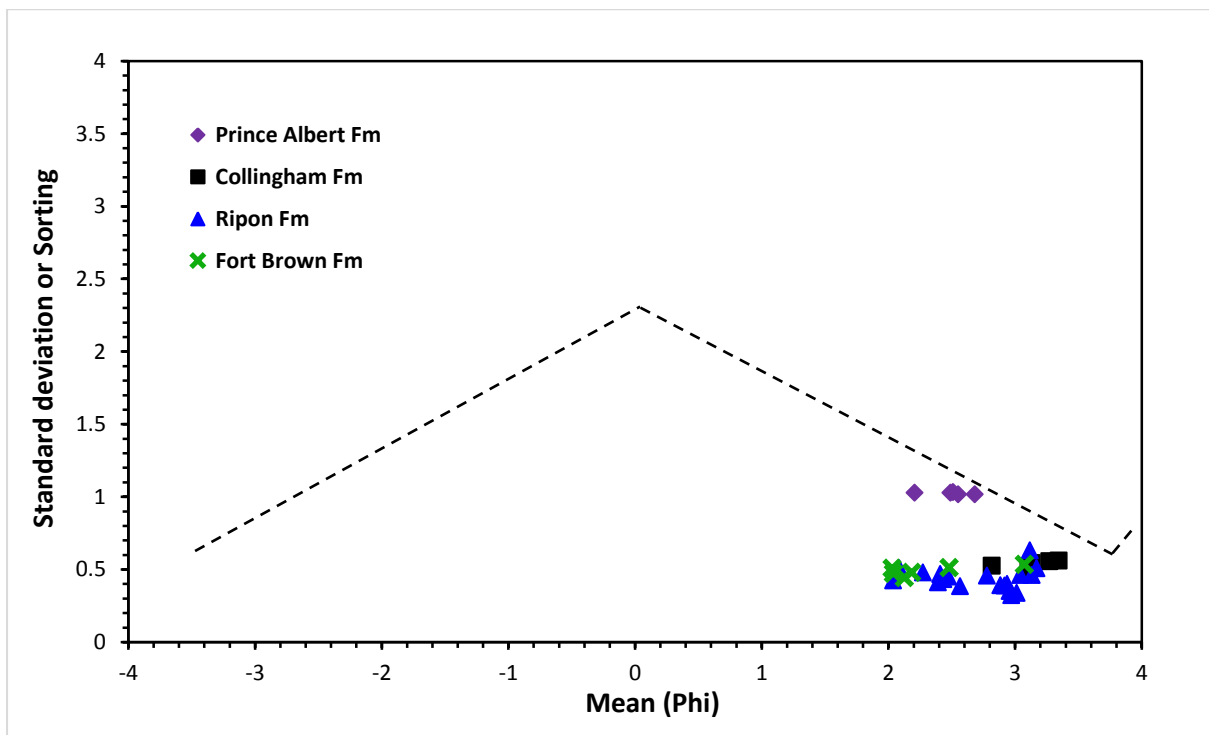
Figure 4.8: Bivariate plot of standard deviation versus mean showing the placement of Ecca samples in the model plot as proposed by Folk and Ward (1957).

4.3.3.2 Graphic skewness versus mean

The bivariate plot of graphic skewness versus mean grain size shows that most of Ecca samples are near symmetrical (Figure 4.9). Only one sample (PA 3) from the Prince Albert Formation is fine skewed. The plot of skewness against mean shows clustering of values near inside the sinusoidal curve of established trend of Folk and Ward (1957), which also point to a smaller size range of the grains (Figure 4.10). The sinusoidal nature of the studied sediments are due to the proportionate admixture of two size-classes of the sediments, i.e. fine sand and very fine silty sand. Again, this agrees with the inverted V-shaped curve of Figure 4.10 as proposed by Folk and Ward (1957). In general, the unimodal sediments are nearly symmetrical but the mixing produces either positive or negative skewness depending upon the proportions of size-classes in the admixture.
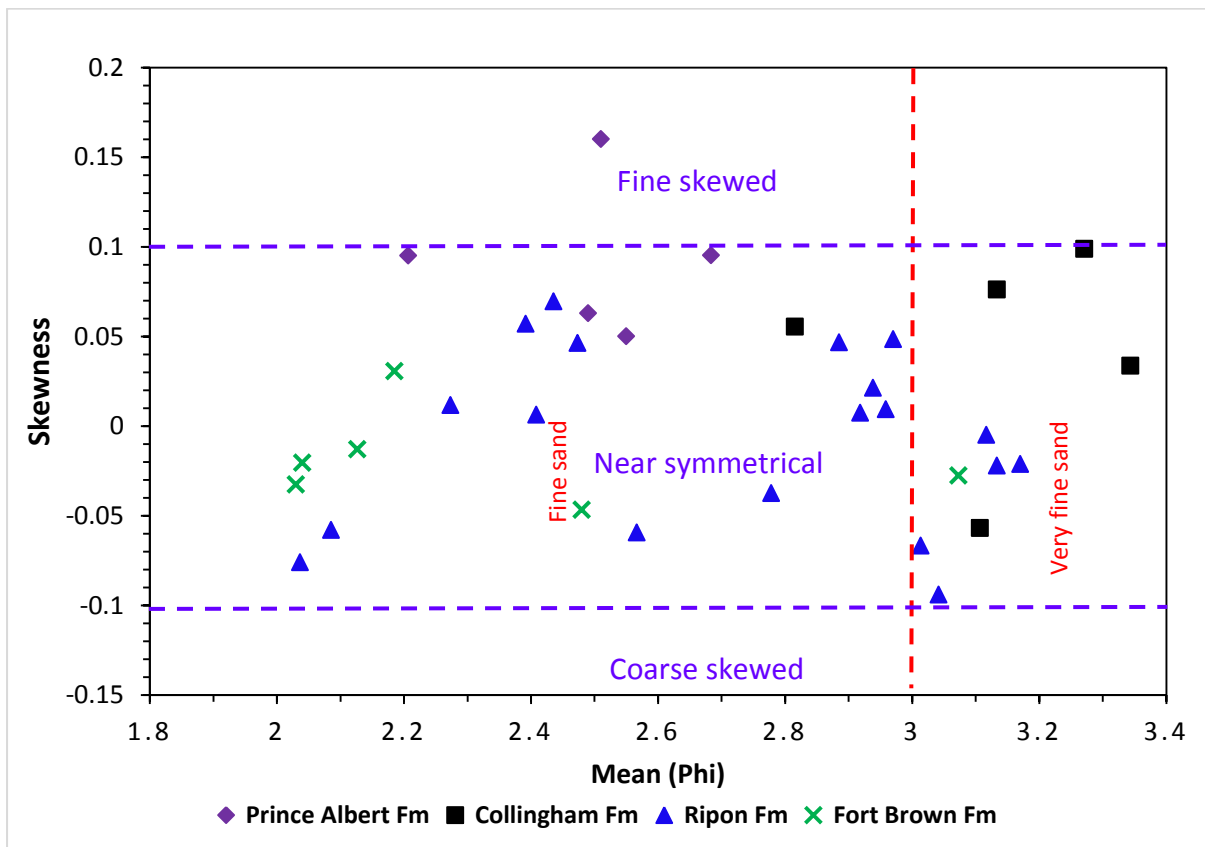
Figure 4.9: Bivariate plot of graphic skewness against mean.
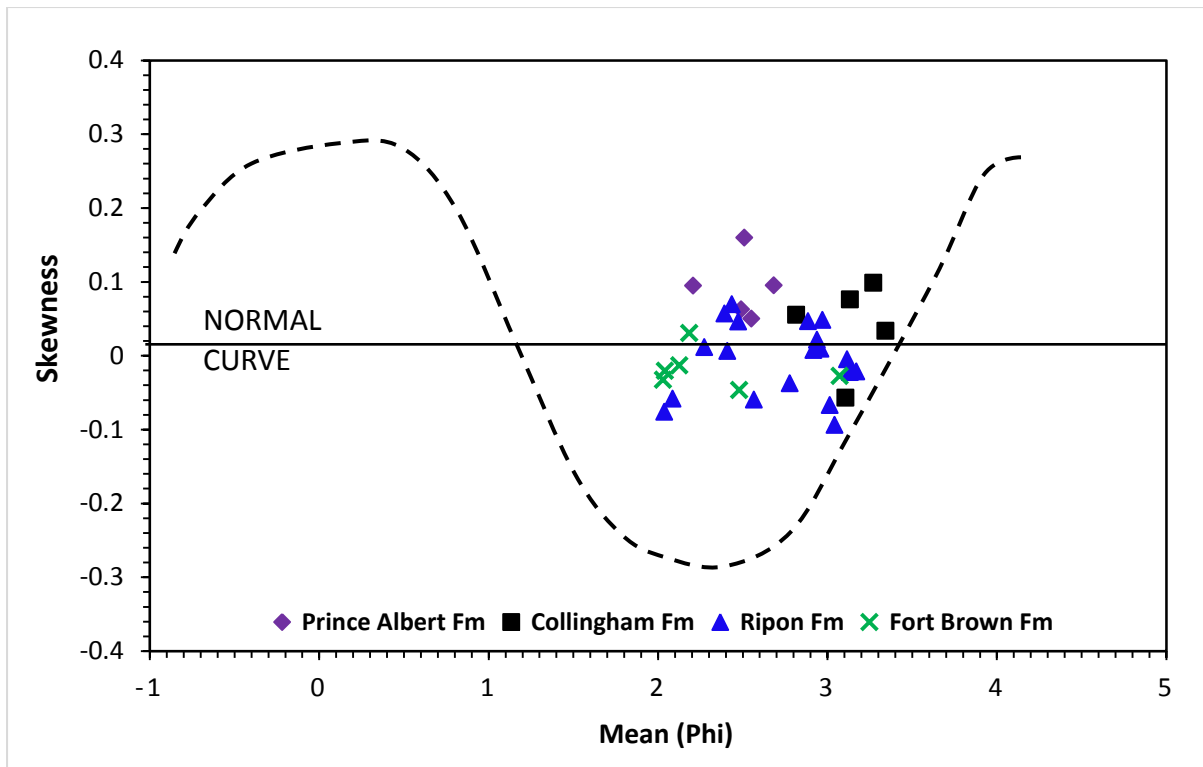
Figure 4.10: Bivariate plot of graphic skewness versus mean showing the placement of the Ecca samples in the model plot as proposed by Folk and Ward (1957).

4.3.3.3 Graphic kurtosis versus mean

The bivariate plot of graphic kurtosis versus graphic mean shows that the Ecca samples are platykurtic to leptokurtic (Figure 4.11). The mesokurtic (0.90-1.11) category dominates, followed by platykurtic (0.67-0.90) and leptokurtic (1.11-1.5), in the size-class range of approximately 2-3.4 Ø (fine to very fine sand). The relationship between kurtosis and mean-size is complex and theoretical (Folk and Ward, 1957). The plot of kurtosis against mean shows scattering of samples near the base, in the region of normal KG curve (mesokurtic category) established trend of Folk and Ward (1957) (Figure 4.12). Based on the model plot (Figure 4.12), it could be inferred that the scattering led to the mixing of two or more grain size-classes, which basically influenced the sorting in peak and tails (index of kurtosis) as well as the inverted 'V' trend. The grain mixture is dominantly fine-sand and subordinate very fine sand. The proportionate grain mixture makes the sorting good, with the exception of the Prince Albert Formation. The varying proportions of very fine sediments mixed with dominant fine sand mode reduced the degree of sorting, particularly in the tails; thus, platykurtic to leptokurtic conditions existed.
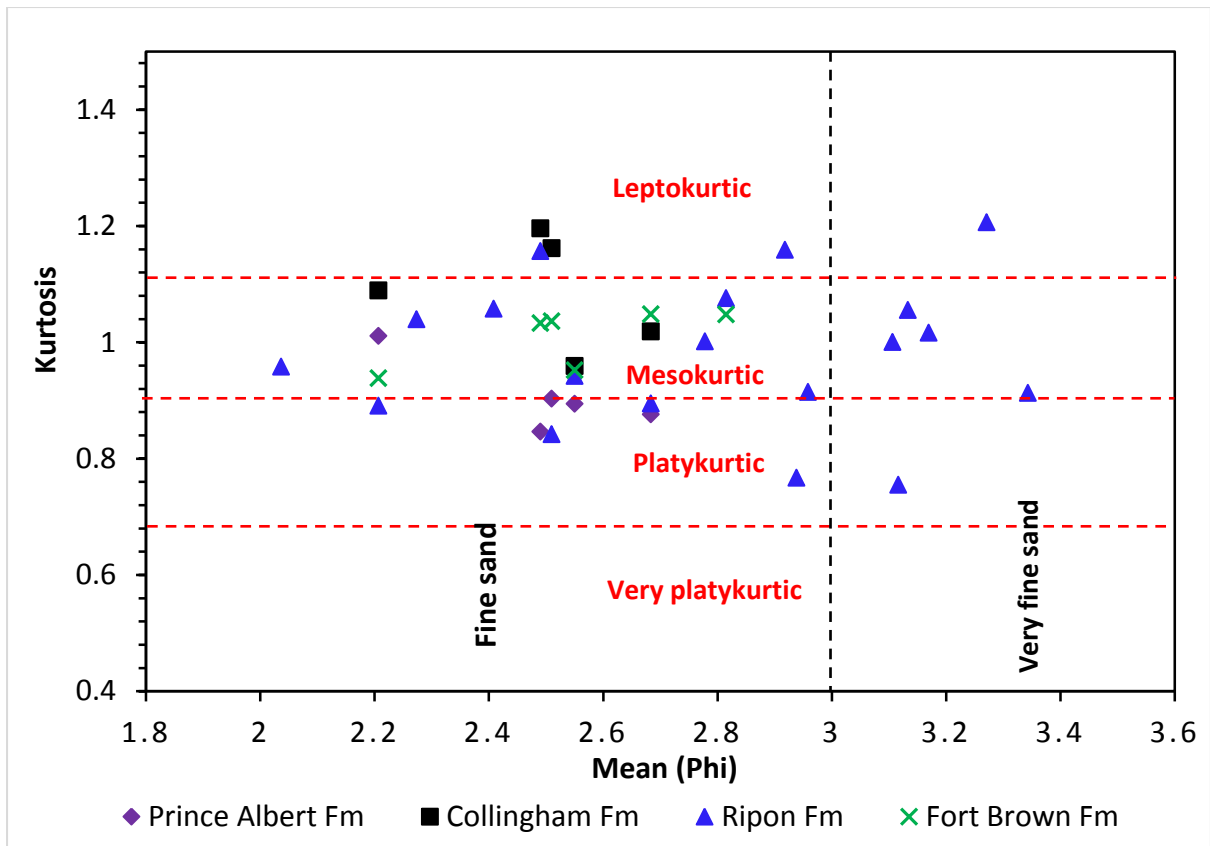
Figure 4.11: Bivariate plot of graphic kurtosis against mean.
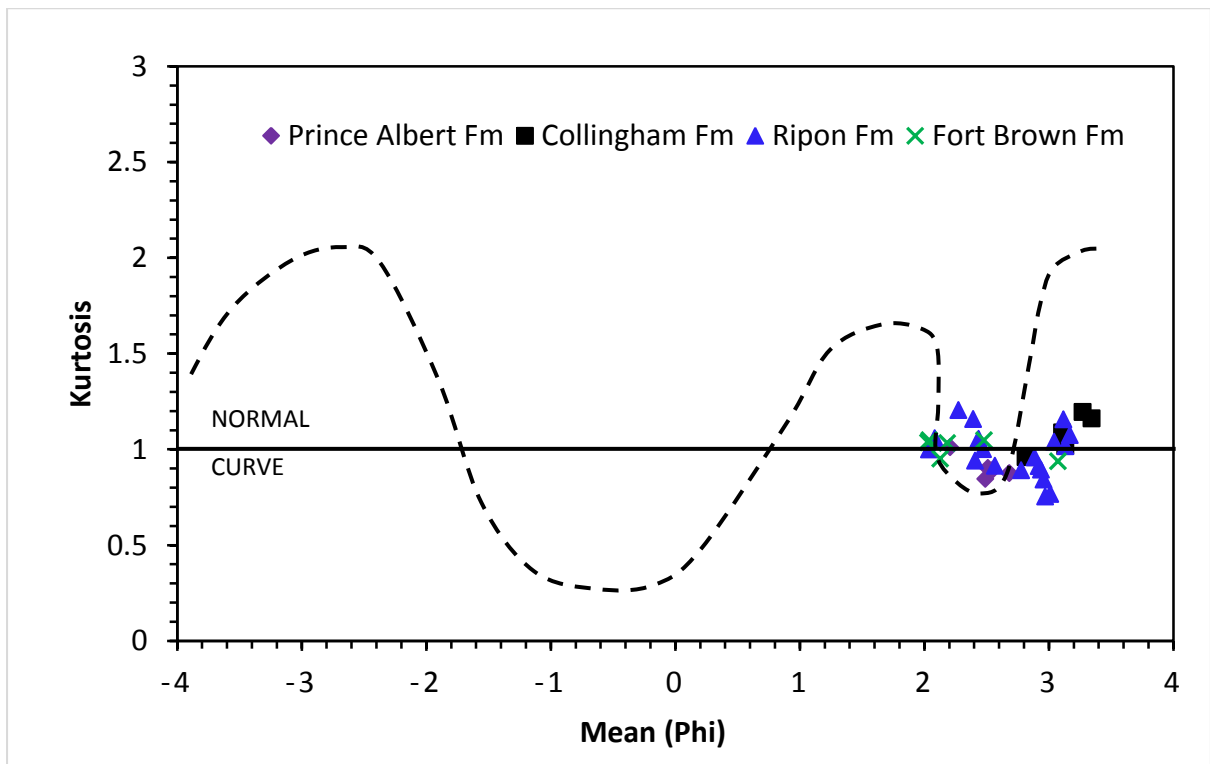
Figure 4.12: Bivariate plot of graphic kurtosis versus mean showing the placement of the Ecca samples in the model plot as proposed by Folk and Ward (1957).

4.3.3.4 Graphic standard deviation (sorting) versus skewness

The bivariate plot of graphic standard deviation (sorting) versus skewness shows that most of Ecca samples are well sorted and near symmetrical (Figure 4.13). However, one sample (PA 3) from the Prince Albert Formation is to very fine skewed and poorly sorted. The moderately well sorted to moderately sorted sediments are mainly clustered around the near symmetrical. The plot of standard deviation against skewness gives a scattered trend in the form of nearly circular ring (After Folk and Ward, 1957). This may be due to two conditions i.e. either mixture of two modes in equal proportion in bimodal sediments or good sorting in unimodal sediments. The scattering in Figure 4.13 shows clustering of grains in one sector, which denotes the dominance of fine sand mode having subordinate very fine sediments. The skewness values of sediments from the Ripon Formation are equally deviated around the normal curve (Sk = 0). Collingham samples are slightly positive skewed with higher proportion of fine grained sand except the CH 2, while samples from the Prince Albert Formation have the highest shift toward fine skewed values. In general, this bivariate plot (Figure 4.14) suggests, based on the position on the circle (well sorting and generally near symmetry; Sk around 0) that analysed sandstones are generally unimodal samples with good sorting. Samples from the Prince Albert Formation are an exception.
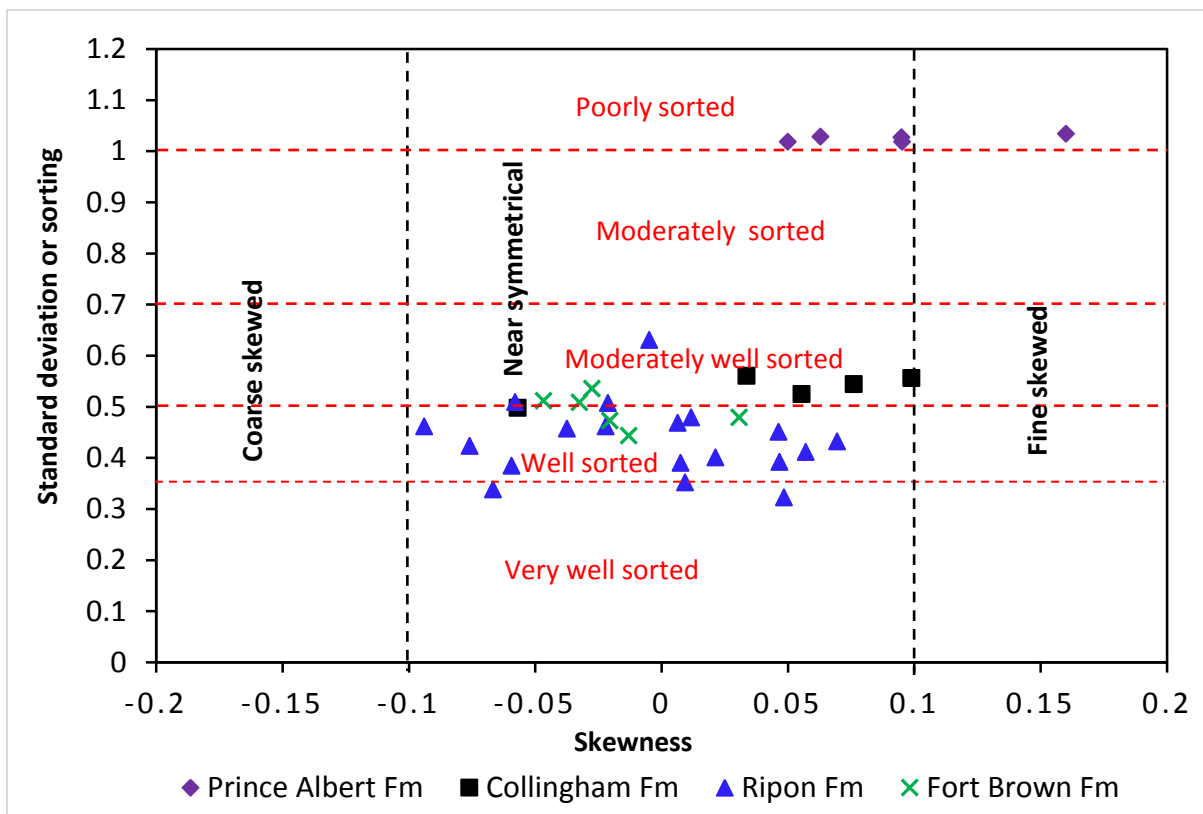
Figure 4.13: Bivariate plot of graphic standard deviation against skewness.
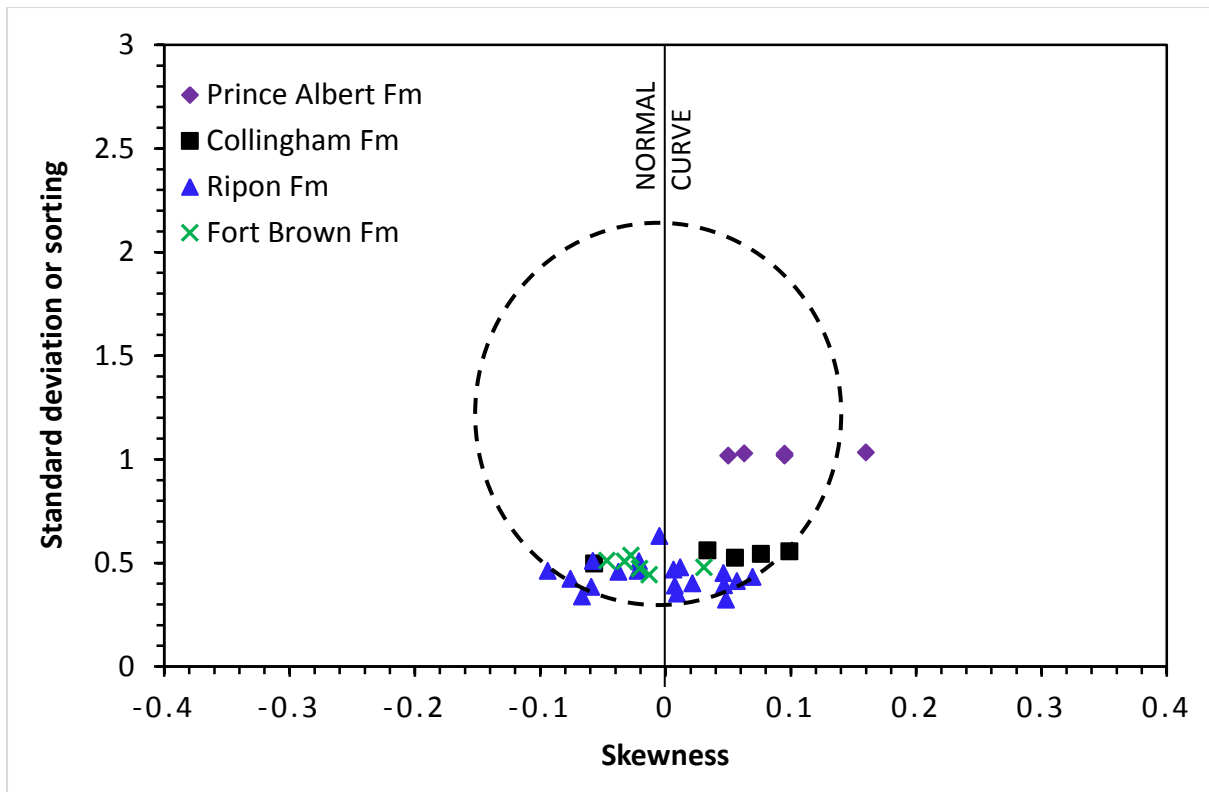
Figure 4.14: Bivariate plot of graphic skewness versus standard deviation showing the placement of Ecca samples in the model plot as proposed by Folk and Ward (1957).

4.3.3.5 Graphic kurtosis versus skewness

Friedman (1967) pointed out that the bivariate plot of kurtosis against skewness of a given sediment population is a powerful tool for distinguishing between depositional environments. The bivariate plot of graphic kurtosis versus skewness shows that the Ecca samples are platykurtic to leptokurtic (i.e. mesokurtic in average) and are mostly near symmetrical (Figure 4.15). According to Friedman (1961), extreme high or low values of kurtosis imply that part of the sediment achieved their sorting elsewhere in a high energy environment. The plot of kurtosis versus skewness (Figure 4.16) follows a regular path of sinusoidal pattern as the mean-size changes and is dependent on two modes (Folk and Ward, 1957). Generally, the Ecca samples plotted in the normal curve (shaded) area, which is represented by nearly pure sand and sand-silt mixture in the establish plot of Folk and Ward (1957) (Figure 4.16).
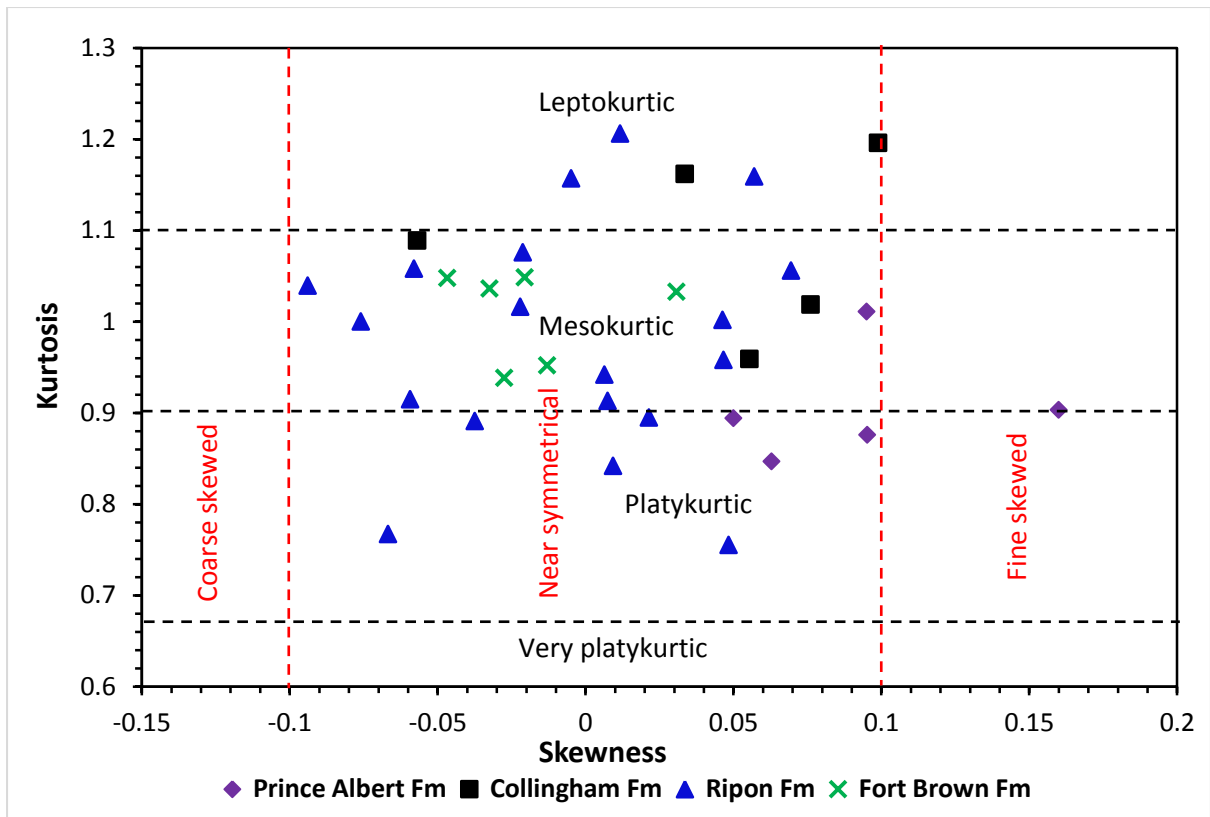
Figure 4.15: Bivariate plot of graphic kurtosis versus skewness.
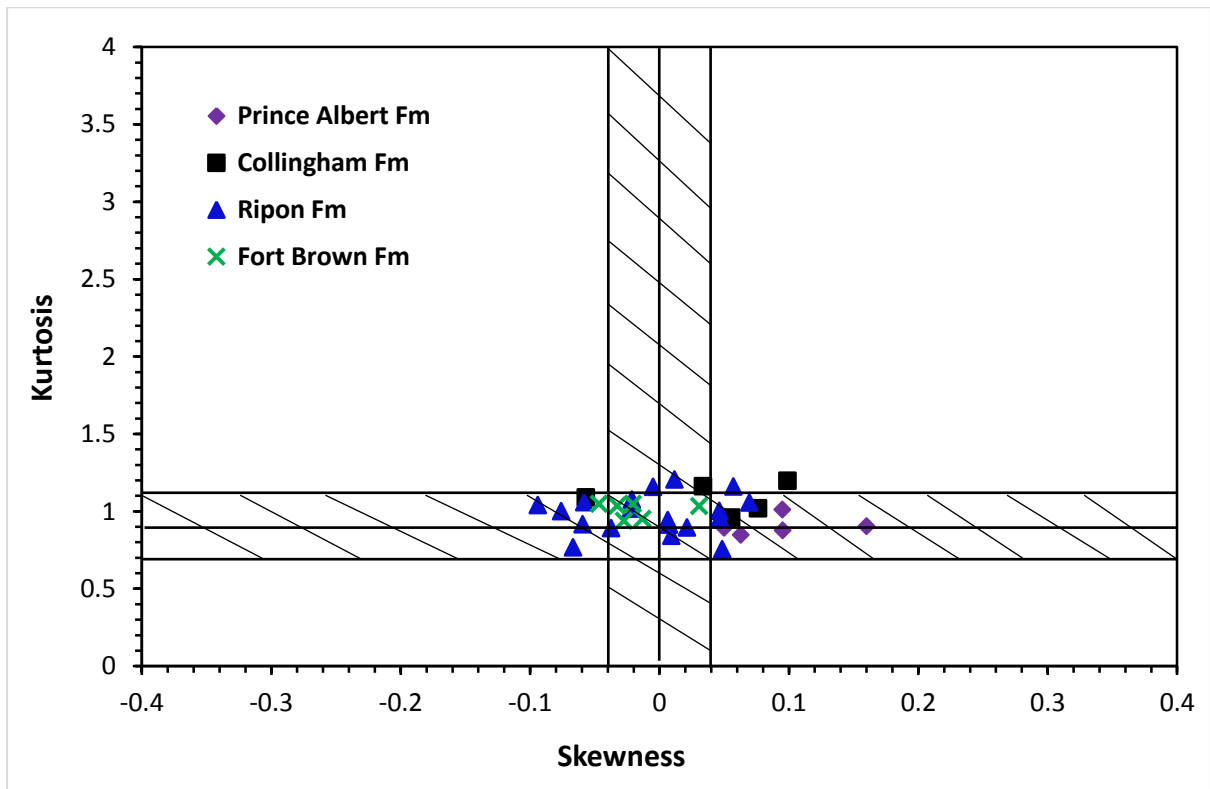
Figure 4.16: Bivariate plot of graphic kurtosis versus skewness showing the placement of Ecca samples in the model plot as proposed by Folk and Ward (1957).

4.3.4 Linear discriminate function (LDF)

The use of statistical analysis to interpret the variations in energy and fluidity factors during/prior to sediment deposition seems to have a very good correlation with the different processes and depositional environments (Sahu, 1964). The Sahu (1964) linear discriminant functions of Y_1 (shallow agitated water and beach), Y_2 (beach and shallow marine), Y_3 (shallow marine and deltaic or lacustrine) and Y_4 (turbidity and deltaic) were modified and used to discriminate between the different processes and depositional environments. To discriminate between shallow agitated water (SA) and beach (B), equation (i) below was applied:

$$Y_{1(SA:B)} = -3.5688M + 3.7016r^2 - 2.0766SK + 3.1135KG \qquad (i)$$

If Y_1 is < -2.7411, the environment is "shallow agitated water" and if Y_1 is > -2.7411, the environment is "beach".

Equation (ii) was used to distinguish between beach (B) and shallow marine (SM) environments.

$$Y_{2(B:SM)} = 15.6534M + 65.7091r^2 + 18.1071SK + 18.5043KG \qquad (ii)$$

If Y_2 is < -63.3650, the environment is "beach" and if Y_2 is > -63.3650, the environment is "shallow marine".

To distinguish environment of deposition between shallow marine (SM) and deltaic or lacustrine (L), equation (iii) was applied:

$$Y_{3(SM:F)} = 0.2852M - 8.7604r^2 - 4.8932SK + 0.0482KG \qquad (iii)$$

If Y_3 is > -7.4190, the environment is "shallow marine" and if Y_3 is < -7.4190, the environment is "deltaic or lacustrine".

To discriminate between deltaic (D) and turbidity current deposits, equation (iv) below was applied:

$$Y_{4(F:T)} = 0.7215M - 0.4030r^2 + 6.7322SK + 5.2927KG \qquad (iv)$$

If Y_4 is < 9.8433, it indicate turbidity current deposition and if Y_4 is > 9.8433, it indicate deltaic deposition. Where M, r, SK, and KG represents mean grain size, standard deviation, skewness and kurtosis, respectively.

After calculating the above mentioned linear discriminate functions (Y_1, Y_2, Y_3 and Y_4) for the Ecca Group samples, it was determined that the values for Y_1, Y_2, Y_3 and Y_4 range from -7.96 to -1.02, 60.79 to 133.58, -9.38 to -0.22 and 6.51 to 12.34, respectively (Table 4.6).

Table 4.6: Linear discriminate function (LDF) values and depositional environments for the Ecca sandstones (Modified from Sahu, 1964).

| Sample | Discriminate function | | | | Environment of deposition | | | |
No.	Y1	Y2	Y3	Y4	Y1	Y2	Y3	Y4
FB6	-3.21	128.02	-8.74	12.12	shallow agitated water	Shallow marine	Deltaic/Lacustrine	Deltaic
FB5	-2.47	125.26	-8.82	11.97	Beach	Shallow marine	Deltaic/Lacustrine	Deltaic
FB4	-2.52	129.07	-9.38	12.34	Beach	Shallow marine	Deltaic/Lacustrine	Deltaic
FB3	-1.02	124.27	-9.03	10.83	Beach	Shallow marine	Deltaic/Lacustrine	Deltaic
FB2	-3.59	125.42	-8.55	10.11	shallow agitated water	Shallow marine	Deltaic/Lacustrine	Deltaic
FB1	-3.87	133.58	-8.11	6.56	shallow agitated water	Shallow marine	Deltaic/Lacustrine	Turbidity
R 10	-6.64	79.13	-0.49	7.14	shallow agitated water	Shallow marine	Shallow marine	Turbidity
RB	-4.42	71.05	-1.02	8.31	shallow agitated water	Shallow marine	Shallow marine	Turbidity
R5A	-6.84	73.84	-0.71	7.53	shallow agitated water	Shallow marine	Shallow marine	Turbidity
R 7	-7.19	81.42	-0.81	7.58	shallow agitated water	Shallow marine	Shallow marine	Turbidity
R 4	-7.8	67.66	-0.22	5.83	shallow agitated water	Shallow marine	Shallow marine	Turbidity
R 6	-7.96	68.17	-0.26	6.51	shallow agitated water	Shallow marine	Shallow marine	Turbidity
R2A	-5.64	65.74	-0.23	6.35	shallow agitated water	Shallow marine	Shallow marine	Turbidity
R 9	-5.05	71.44	-1.25	7.48	shallow agitated water	Shallow marine	Shallow marine	Turbidity
R1A	-3.07	68.17	-1.34	6.82	shallow agitated water	Shallow marine	Shallow marine	Turbidity
ZN02K	-4.86	71.18	-1.23	7.89	shallow agitated water	Shallow marine	Shallow marine	Turbidity
R 3	-3.53	73.18	-1.36	8.2	shallow agitated water	Shallow marine	Shallow marine	Turbidity
ZN02L	-7.03	72.7	-0.49	7.04	shallow agitated water	Shallow marine	Shallow marine	Turbidity
R 2	-3.33	60.79	-0.57	6.32	shallow agitated water	Shallow marine	Shallow marine	Turbidity
RP	-6.97	86.03	-1.19	7.94	shallow agitated water	Shallow marine	Shallow marine	Turbidity
R 8	-7.15	73.49	-0.63	7.06	shallow agitated water	Shallow marine	Shallow marine	Turbidity
RC	-6.04	96.22	-2.51	8.4	shallow agitated water	Shallow marine	Shallow marine	Turbidity
R 5	-7.49	70.19	-0.25	6.7	shallow agitated water	Shallow marine	Shallow marine	Turbidity
R 11	-6.29	73.03	-0.81	6.55	shallow agitated water	Shallow marine	Shallow marine	Turbidity
R 1	-4.86	69.66	-1.22	6.85	shallow agitated water	Shallow marine	Shallow marine	Turbidity
CH5	-7.07	88.7	-2.02	8.28	shallow agitated water	Shallow marine	Shallow marine	Turbidity
CH4	-7.01	95.43	-2.2	9.4	shallow agitated water	Shallow marine	Shallow marine	Turbidity
CH3	-7.22	95.08	-1.91	8.92	shallow agitated water	Shallow marine	Shallow marine	Turbidity
CH2	-6.66	84.02	-0.95	7.72	shallow agitated water	Shallow marine	Shallow marine	Turbidity
CH1	-6.16	80.92	-1.83	7.59	shallow agitated water	Shallow marine	Shallow marine	Turbidity
PA5	-4.52	74.54	-1.3	7.63	shallow agitated water	Shallow marine	Shallow marine	Turbidity
PA4	-3.15	65.63	-1.22	7.13	shallow agitated water	Shallow marine	Shallow marine	Turbidity
PA3	-3.8	68.92	-1.48	8.1	shallow agitated water	Shallow marine	Shallow marine	Turbidity
PA2	-3	67.33	-1.47	8.01	shallow agitated water	Shallow marine	Shallow marine	Turbidity
PA1	-6.93	83.77	-1.45	7.33	shallow agitated water	Shallow marine	Shallow marine	Turbidity

Based on the Y_1 values, all the samples from the Prince Albert, Collingham and Ripon Formations falls in shallow agitated water process, while those from the Fort Brown Formation falls in both the shallow agitated water and beach processes. With reference to the Y_2 values, all the Ecca samples fall in the shallow marine environment. In addition, Prince Albert, Collingham and Ripon Formations fall in the (Y_3) shallow marine environment, while those from the Fort Brown Formation falls in the deltaic or lacustrine environment. With reference to the Y_4 values, samples from the Prince Albert, Collingham and Ripon Formations are turbidity current deposits, while those from the Fort Brown Formation are deltaic deposits. The binary plot of Y_2 versus Y_1 (Figure 4.17) showed that most of the Ecca samples fall in the shallow agitated waters/shallow marine, while few samples plotted into the beach/shallow marine environment. Furthermore, the plot of Y_3 against Y_2 (Figure 4.18) indicates that all the samples from Prince Albert, Collingham and Ripon Formations plotted in the shallow marine environments, while those samples from Fort Brown Formation falls in the deltaic or lacustrine environment. The plot of Y_4 against Y_3 (Figure 4.19) shows that all the samples from Prince Albert, Collingham and Ripon Formations are turbidity current deposits, while those samples from Fort Brown Formation are deltaic or lacustrine deposits.
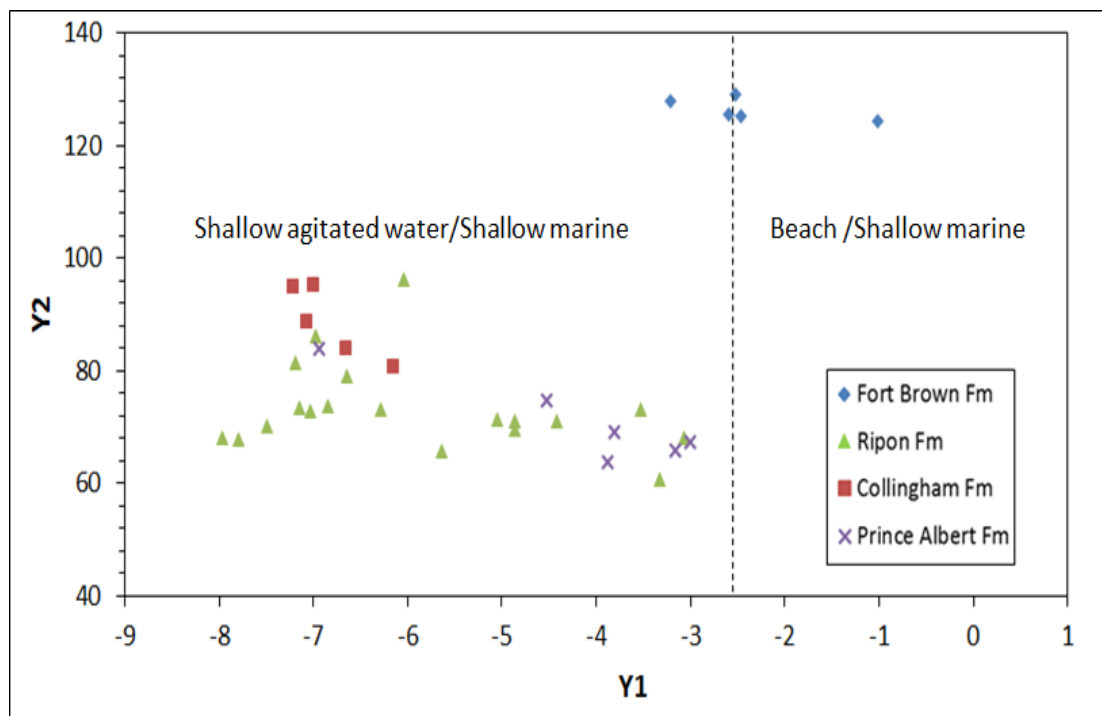
Figure 4.17: Discrimination of environments based on linear discrimination functions (LDF) plot of Y_2 against Y_1 (Modified from Sahu, 1964).
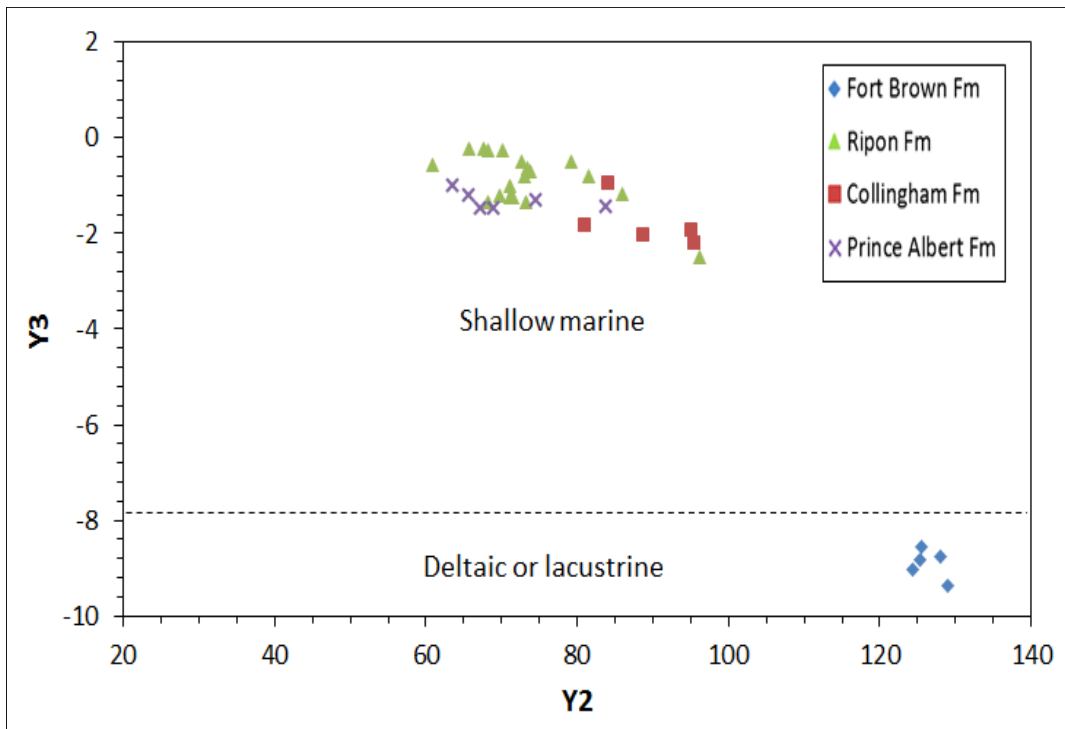
Figure 4.18: Discrimination of environments based on linear discrimination functions (LDF) plot of Y_3 against Y_2 (Modified from Sahu, 1964).
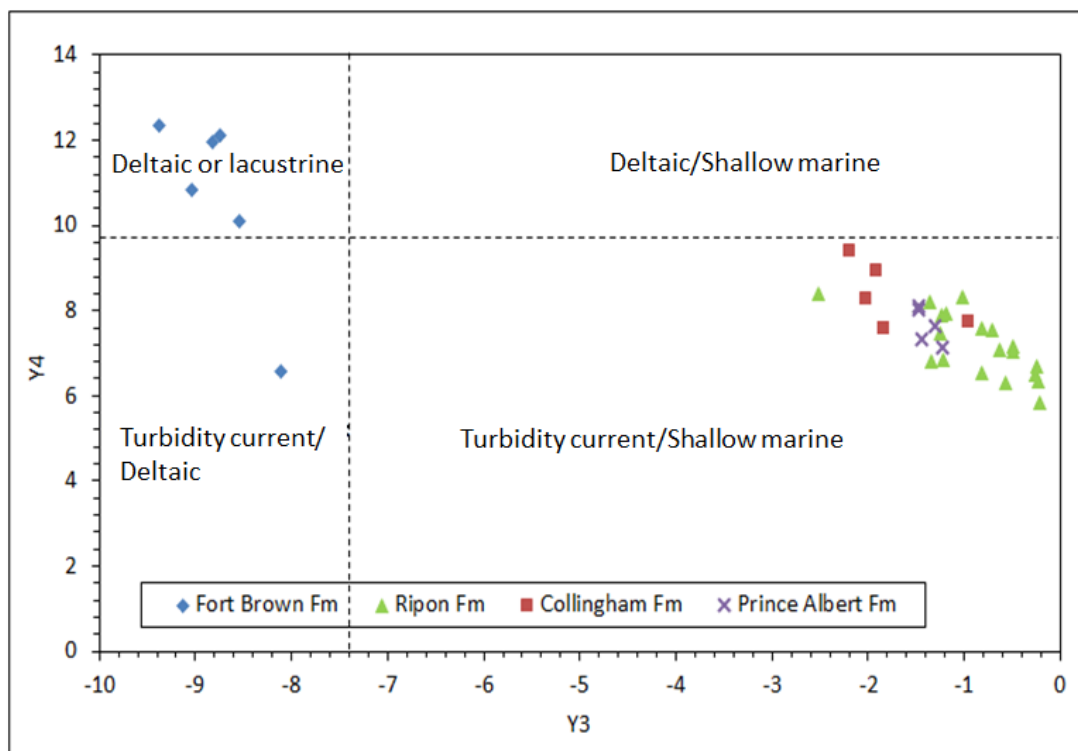
Figure 4.19: Discrimination of environments based on linear discrimination functions (LDF) plot of Y_4 against Y_3 (Modified from Sahu, 1964).

4.3.5 The Passega Diagram (CM pattern)

Passega (1957) introduced the use of C-M plot to decipher the hydrodynamic forces that works or prevails during sediment deposition. The C-Mplotis a binary plot of coarser one-percentile value (C) in micron against the median value (M) in micron on a log-probability scale (Table 4.5). The relationship between C and M is linked to the nature of the several sediment types and energy of the transportation medium (Passega, 1964; Visher, 1969). The Passega diagram depicted in Figure 4.20 shows several fields (rolling-NO, rolling and suspension-OP, suspension and rolling-PQ, graded suspension-QR, uniform suspension-RS, and pelagic suspension-T) that correspond to the various transport and sedimentation conditions in the marine and littoral/fluvial environments. The plot of C against M values (Table 4.5) on the Passega diagram (Figure 4.20) shows that all the samples from the Prince Albert Formation plotted in the rolling and suspension condition (OP), while those from the Collingham Formation falls in the graded suspension (QR) section. Samples from the Ripon and Fort Brown Formations are scattered in both the suspension and rolling (PQ) and graded suspension (QR) sections.
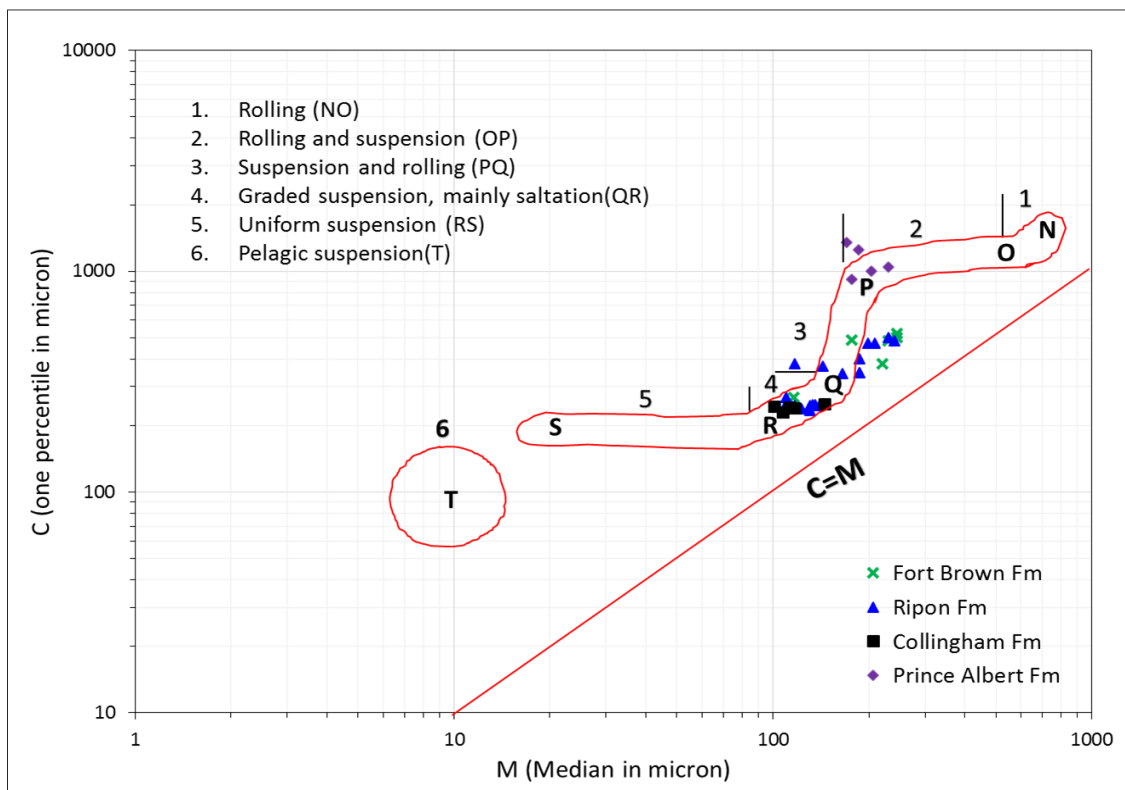
Figure 4.20: C-M plot showing the transporting mechanism of the Ecca sediments (After Passega, 1957).

The C-M plot showing depositional environment (Figure 4.21) indicate that the Ecca sediments were deposited by turbidity currents. Similar CM patterns are also documented for the Gondwana sandstone in the Godavari Basin (Ramanamurthy, 1985; Burhanuddin, 2007) as well as the Kamthi Sandstone (Murkute, 2001; 2002). Modern rivers like Gomti River (Kumar and Singh, 1978) and Gadilam River Basin (Rajamanickam and Muthukrishnan, 1995) also shows the same trend. Furthermore, this trend also agrees with the pattern determined by Rajesh et al. (2007) for the coastal sands of Kakapallam area, Marakkanam coast, Tamil Nadu.
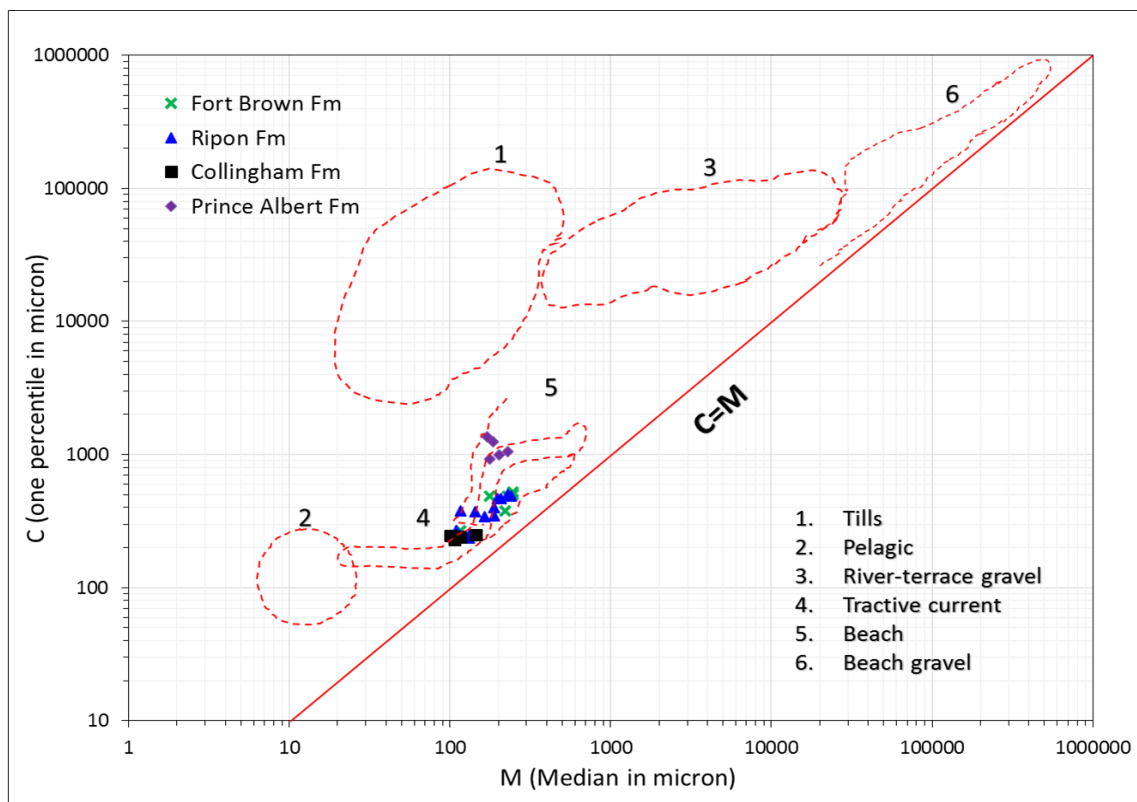
Figure 4.21: C-M plot showing depositional environment of the Ecca sediments (After Passega, 1957).

4.3.6 The Visher Diagram

The log-probability curves suggested by Visher (1969) were used to differentiate between the Ecca Group sediments based on their mechanism of transportation (i.e. traction, saltation and suspension). Visher plot for sediments from the Prince Albert Formation (Figure 4.22) clearly shows the dominance of double saltation populations (saltation I and II) with single suspension and traction population (maximum of about 3%). The suspension and saltation populations may range up to 30% and 75%, respectively. Figure 4.23 also indicates the

presence of a double saltation populations and a single suspension population for the Collingham Formation. Furthermore, the Visher plot for sediments from the Ripon Formation (Figure 4.24) shows the presence of a double saltation populations and single suspension characteristics. The saltation populations are comparatively better sorted than the suspension population. Figure 4.25 clearly shows the dominance of double saltation populations and single suspension for the Fort Brown samples. However, one of the samples shows very little traction population (about 1%) around 1∅ value. The suspension and saltation populations could be up to 25% and 85%, respectively. The traction represents minor quantity of poorly-sorted sediments, while the saltation populations are relatively better sorted than the fine-grained suspension population. The double saltation populations truncated mostly between 1.5∅ and 2.5∅, which could be attributed to internal forces that are causing sliding or rolling (Visher, 1969). The breaks in the log-probability curves for the Prince Albert Formation is not as sharp compared to other formations, which could be due to mixing of detritus carried by tractive currents with different energy (Sharda and Verma, 1977) or they may have been sourced from different provenances. The log probability curves presented in this study are comparable with well-known trends for modern and ancient fluvial deposits as suggested by Visher (1969), in which both saltation and suspension populations dominated.
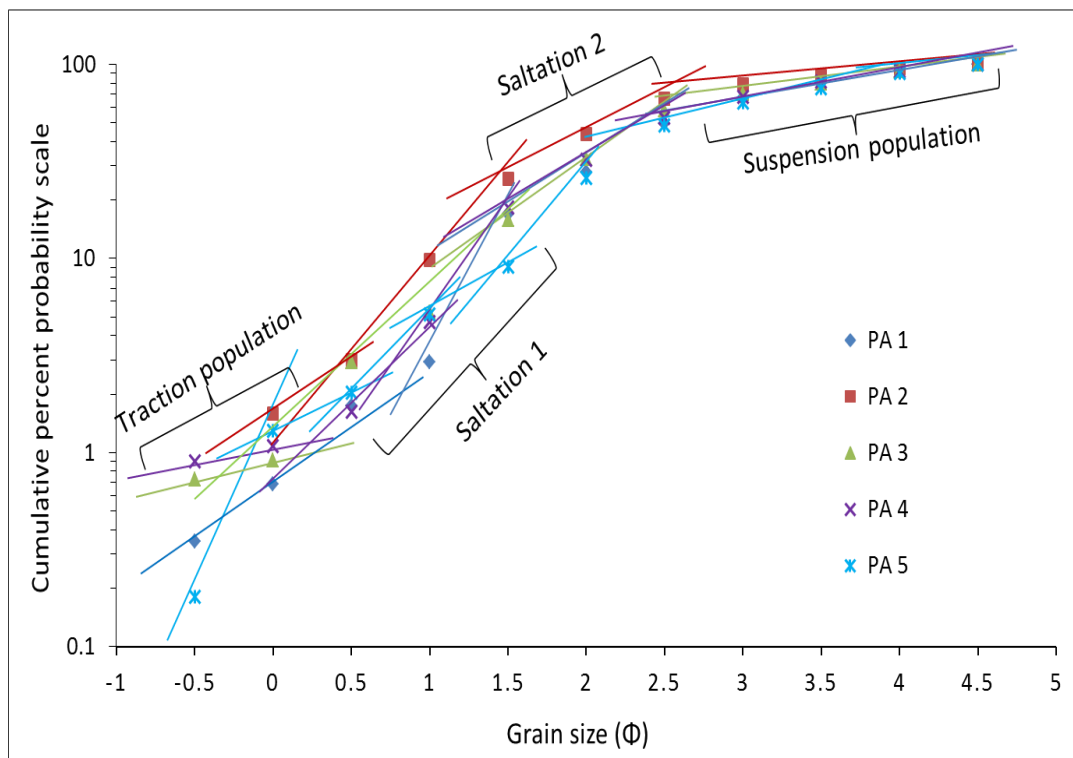
Figure 4.22: Arithmetic probability curves showing the trend of traction, saltation and suspension populations of the Prince Albert Formation samples.
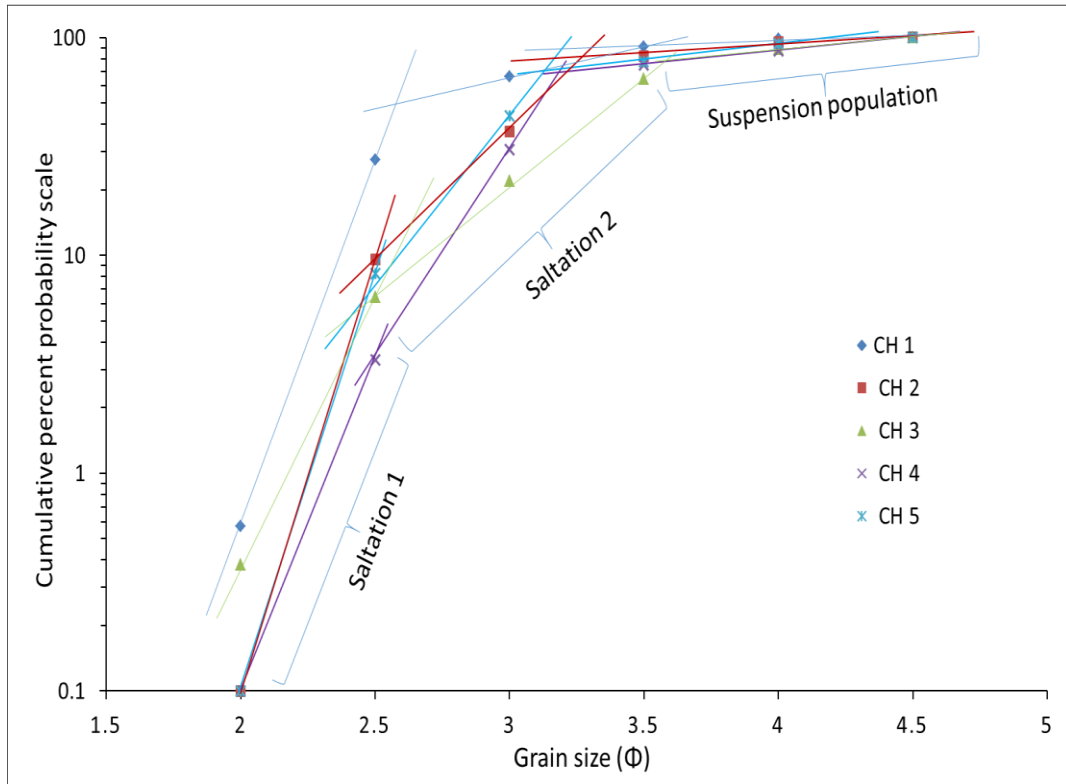
Figure 4.23: Arithmetic probability curves showing the trend of saltation and suspension populations of the Collingham Formation samples.
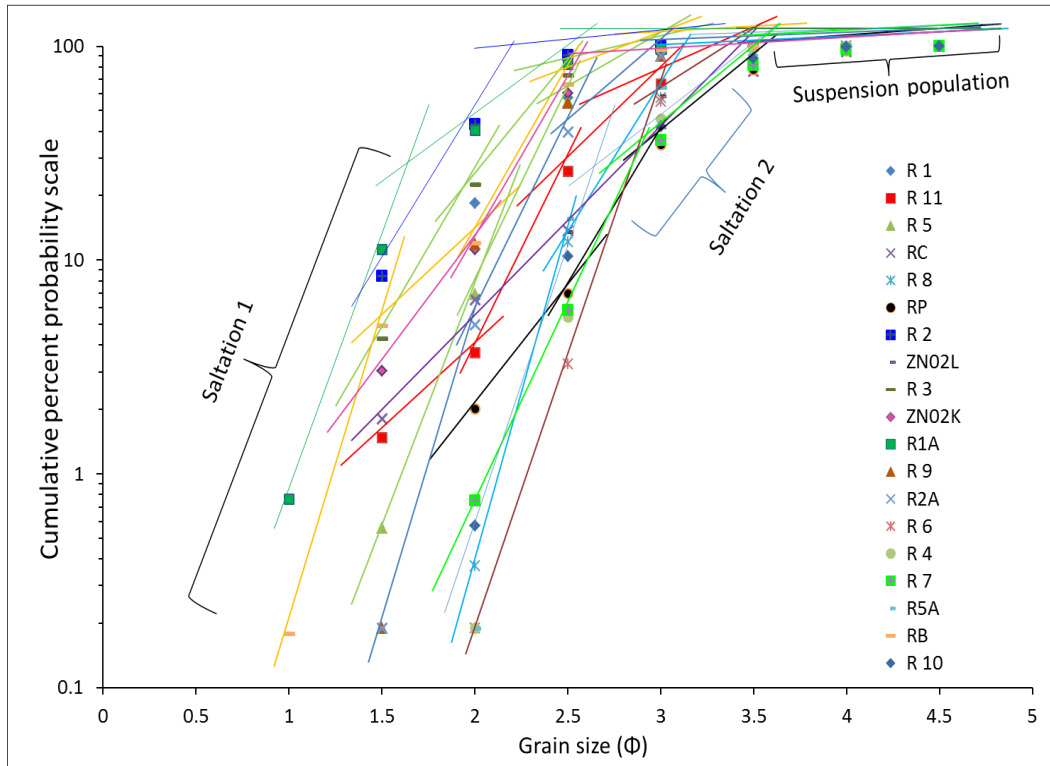
Figure 4.24: Arithmetic probability curves showing the trend of saltation and suspension populations of the Ripon Formation samples.
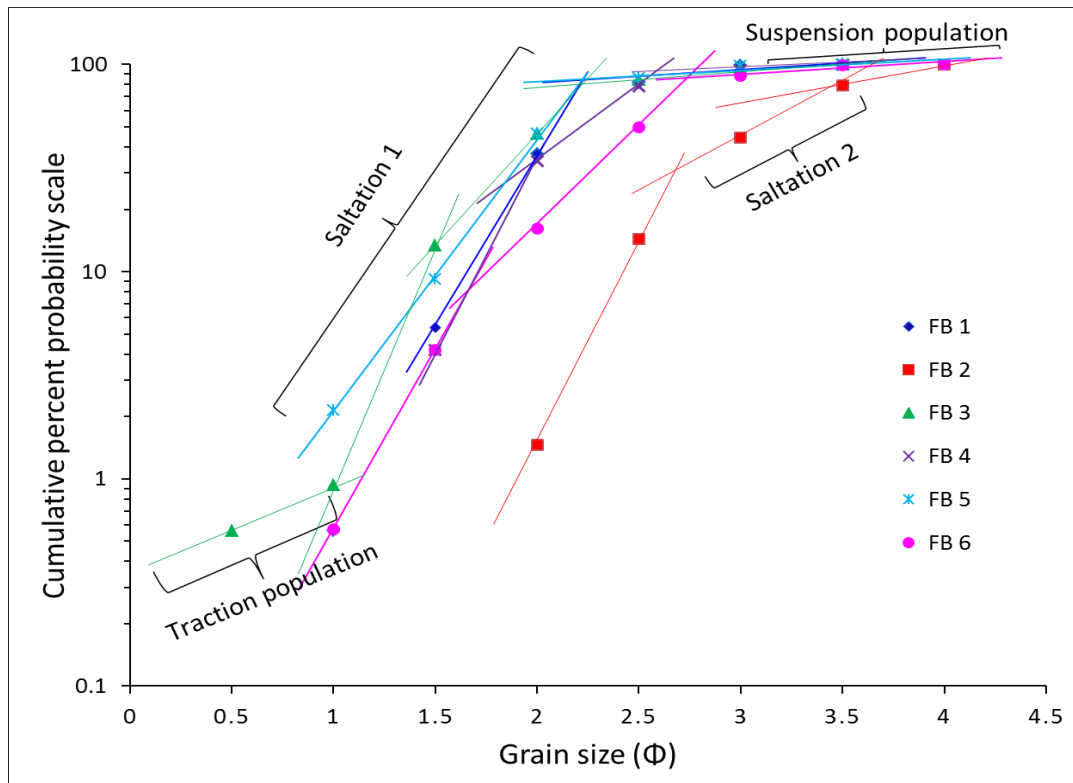
Figure 4.25: Arithmetic probability curves showing the trend of traction, saltation and suspension populations of the Fort Brown Formation samples.

4.4 Conclusions

Grain size analysis of thirty-five Permian Ecca sandstone samples was carried out. The important conclusions drawn are as follows:

- The cumulative weight percentage frequency curves and whole grain size statistics are mainly indicative of very fine to fine-grained nature of the sediments. Most of the sandstones in the Ecca Group show unimodal of grain-size distribution.

- The average sorting of all sandstones is 0.543 (moderately well sorting) and are mostly near-symmetrical in nature. Generally, the moderately well sorted nature of the sediment could be due to partial winnowing action as well as the addition or influx of previously sorted sediments in marine environment. In most cases, both peak and tails are equally sorted resulting in the mesokurtic in grain-size partten.

- The modified linear discriminant functions (LDF) analyses are dominantly indicative of turbidity current deposits under marine environments (deep and shallow marine) for samples from the Prince Albert, Collingham and Ripon Formations, while those samples from the Fort Brown Formation are lacustrine or deltaic deposits. The main weakness in the use of grain size analysis to decipher depositional environments is

that the approach does not distinguish between deep and shallow marine settings. The use of statistical methods may be helpful in characterizing depositional environment. However, there is need to use other approaches like facies associations, architecture of sediment bodies, bed thicknesses, sedimentary structures and fossils. In chapter 6, we will further carry out detailed facies analysis and cross-check the environments depicted from the grain size parameters with the facies characteristics.

- The graphic mean value shows the dominance of fine sand-size particles, which point to relatively low energy conditions of deposition. The linear discriminant functions (LDF) results point to low energy conditions during the deposition of the Prince Albert, Collingham and part of the Ripon Formation (Lower Greywacke-Mudrock Member and Middle Black Mudrock Member), whereas the Upper Grey Mudrock-Sandstone Member of the Ripon Formation and the Upper Grey Mudrock-Sandstone Member of Fort Brown Formation accumulated under high energy conditions.

- The CM pattern shows a clustered distribution of sediments in the PQ and QR segments, indicating that the sediments were deposited mostly by suspension and rolling/saltation, and graded suspension. Furthermore, the plots also show that the Ecca sediments are mainly deposited by turbidity currents.

- The log probability curves indicate the variability of hydraulic depositional conditions for the Permian Ecca Group sandstones. Saltation is the major process of transportation, although suspension and traction also played some role during deposition of the sediments. The sediments were mainly in saltation and suspension before being deposited.

CHAPTER 5

PETROGRAPHY, MODAL COMPOSITION AND SOURCE ROCK PROVENANCE

Abstract

Petrography of the sandstones of Ecca Group in the study area has been investigated in order to unravel the mineral types and abundance, and source rock provenance of the sandstones. Petrographic studies revealed that the detrital framework grains of the sandstones are quartz, feldspars and lithic fragments of igneous, metamorphic and sedimentary rocks. The matrix is made of clay minerals and fine silts. Kaolinite, smectite, illite, sericite and chlorite are the identified clay minerals and they exist in the sandstones either as detrital grains, cements or authigenetic minerals. The sandstones have an average framework composition of about 24.3% quartz, 19.3% feldspar, 26.1% rock fragments and 30.3% matrix plus accessory minerals. The absence of major petrographically distinctive compositional variations in the sandstones perhaps indicates homogeneity of their source. As a result of this, it is inferred that the transportation distance from the source area was quite short and relatively deeper and quiet water of depositional environment. The sandstones are generally very fine to fine grained, moderate to well sorted and subangular to subrounded in grain shapes. In addition, they are compositionally immature and can be classified as feldspathic wacke and lithic wacke. The detrital nature of the framework grains and the presence of lithic fragments, thus render the rocks to be siliciclastic sediments in origin. The provenance characteristics suggest the influence of plutonic and metamorphic terrains (meta-magmatic arc) as the main source rock with minor debris derived from recycled sediments. The detrital modal compositions of these sandstones are related to back arc to island and continental margin arc. These results therefore support previous studies that inferred foreland basin setting for the Karoo Basin.

Keywords: Petrography, provenance, tectonic setting, Ecca Group, Karoo Basin.

5.1 Introduction

Mineral modal composition analysis can be used to characterize and classify sedimentary rock types and to trace provenance of source materials. The purpose of sedimentary provenance study is to use measurements of compositional and textural properties of siliciclastic rocks as well as geological and geochemical data to reveal the provenance or source area of the sediments, tectonic setting of the sedimentary basins and the associated

geological processes responsible for the deposition of the sediments (Pettijohn et al., 1987; Johnson, 1991; Armstrong-Altrin et al., 2004; Bordy et al., 2004). The composition of clastic sedimentary rocks is a function of a complex interaction between several factors that include the nature and mineral composition of the source rocks, source area weathering, diagenesis and tectonism (McLennan et al., 1993). Tectonic setting of the sedimentary basin is thought to have general control on the composition of sedimentary rocks. This is due to the fact that different tectonic environments have distinctive mineral composition characteristics and they are characterized by distinctive sedimentary processes (Dickinson, 1985). Therefore, sedimentary rocks, especially sandstones, have been used to deduce provenance and to identify ancient tectonic settings since clastic detrital components preserve detailed information on the provenance, sediments transportation and the interaction of physical and chemical processes (Johnson, 1976; Dickinson et al., 1983; Bhatia, 1983; Dickinson, 1988; McLennan et al., 1993). The use of framework mineral composition (detrital modes) to determine the tectonic setting of sandstones was first proposed by Crook (1974) and has since undergone considerable modification and improvement such as the introduction of single-grain analysis (Dickinson and Suczek, 1979; Dickinson et al., 1983; Morton, 1985; Weltje, 2002; Basu, 2003).

The sandstones of the Ecca Group in the study area have not been studied previously in detail to classify the sandstones as well as determine their tectonic provenance. Previous studies carried out on the Ecca Group by several researchers mainly focused on the stratigraphy, lithofacies analysis, impact of dolerite intrusions and shale gas potential of the Ecca Group (Johnson, 1976; Kingsley, 1977; Cadle et al., 1993; Johnson et al., 1996; Catuneanu et al., 1998; Bamford, 2004; Catuneanu et al., 2005; Johnson et al., 2006; Geel et al., 2013; Scheiber-Enslin et al., 2014). However, the source(s) of Ecca sediments are still not well understood. This study was undertaken to interpret the sandstone petrography in order to characterize the detrital sediments of the Ecca Group and to deduce its provenance in the southeastern Karoo Basin of South Africa.

5.2 Materials and method

A total of one hundred and twenty four fresh sandstone samples were collected from the road-cut exposures of the Ecca Group (Figure 1.1). Thirty-five representative thin sections of different types of sandstone and mudrocks were prepared and studied under optical microscope and applied to modal composition analysis. Several petrologists have

documented that the Gazzi-Dickinson method is the most efficient and reliable point-counting method (Decker and Helmold, 1985; Blott and Pye, 2001; Bordy et al., 2004). In addition, previous researchers including Dickinson et al. (1983), Ingersoll et al. (1984), and Katemaunzanga and Gunter (2009) designated that at least three hundred grain count is sufficient to accurately determine the percentages of constituent grains. In this study, comparative abundance of the main mineral constituents were determined by counting at least 500 points per thin section using the methods of Dickinson and Suczek (1979) and Dickinson et al. (1983). Each thin section was analysed in accordance with the Gazzi-Dickinson's traditional point-counting method using an Olympus BX51 microscope equipped with an Olympus DP72 digital camera. An evenly spaced counting grid was employed to traverse the thin section, and mineral grains under the grid nodes were counted. The grids were equally spaced in such a way that each grid exceeds the average grain size in order to avoid counting an individual grain more than once.

Framework constituents were determined using the nomenclature advocated by Dickinson and Suczek (1979), Dickinson et al. (1983) and Dickinson (1985). Constituent minerals of the sandstones were classified into monocrystalline quartz, polycrystalline quartz, K-feldspar, plagioclase, lithic fragments (volcanic and sedimentary lithic fragments), accessory minerals and matrix. In order to classify the sandstones, framework detrital modes of the sandstones (Table 5.1) were normalized or recalculated to 100% and ternary diagrams of Q-F-L (quartz-feldspar-lithic fragments), Qm-F-Lt (monocrystalline quartz-feldspar-total lithic fragments) and Qt-F-L (total quartz-feldspar-lithic fragments) were plotted. Classifications of the sandstones were based on the methods adopted by Dott (1964), Pettijohn et al. (1973), Folk (1974) and Dickinson et al. (1983). Petrographic compositions of the Ecca sandstones are presented in Table 5.2. The Whitehill Formation of the Ecca Group is mainly made up of shale and chert. Therefore, the formation was not studied for modal compositional analysis. Clay minerals within the sandstone units and the whole rock analysis were determined by x-ray diffraction (XRD). The XRD result was used to confirm the petrographic framework. The X-ray diffraction measurements were performed on a Bruker XRD D8 Advance (Model: V22.0.28) at a room temperature of 25℃ and the samples were scanned at 2° 2θ per minute from 2° to 70° (wavelength of 1.5406).

5.3 Results

5.3.1 Petrography

The rocks in Ecca Group are both argillaceous and arenaceous rocks. The argillaceous rocks dominate the lower Ecca Group (Prince Albert, Whitehill and Collingham Formations), whereas arenaceous rocks are prevalent in the upper part (Ripon and Fort Brown Formations). The argillaceous rocks are primarily made up of detritus clay and silt size particles with some chemically precipitated cements and organic materials. Quartz and feldspar are the main minerals, although calcite, hematite and organic matter are also present. Detrital framework grains of the Ecca arenaceous rocks (sandstones) include quartz, feldspars, rock fragments, matrix and accessory minerals. This framework grains have been recalculated as 100% (Table 5.3) for QFL diagrams, allowing these to occupy one of the three poles in the ternary plot diagrams. The matrix is made of clay minerals and minor detrital silts. The amount of quartz, feldspar and rock fragments range from 18.4-31.8%, 10.6-34.4% and 14.8-32%, respectively (Table 5.4).

Table 5.1: Framework parameters of detrital modes (After Dickinson, 1985; Tucker, 2001).

Parameter	Explanation
Q	Quartz (Qm + Qp)
Qp	Polycrystalline quartz
Qm	Monocrystalline quartz
Qt	Total quartzose grains (Qm + Qp)
P	Plagioclase feldspar
K	Potassium feldspar
F	Total feldspar grains (P + K)
Lv	Volcanic-metavolcanic rock fragments
Ls	Sedimentary rock fragments
Lm	Metamorphic lithic fragments
Lsm	Metasedimentary lithic fragments
L	Unstable (Siliciclastic) lithic fragments (Lv + Ls + Lsm)
Lt	Total siliciclastic lithic fragments (L + Qp)

Table 5.2: Modal compositions of the sandstones from the Ecca Group.

SAMPLE	Qt (%)	Qm (%)	Qp (%)	F (%)	L (%)	Lt (%)	Mx (%)	Acc (%)	Normalized (100 %)					
									Qm-F-Lt (%)			Qt-F-L (%)		
									Qm	F	Lt	Qt	F	L
FB 6	27.4	21.6	5.8	32.0	17.6	23.4	18.6	4.4	28.05	41.6	30.4	35.6	41.6	22.9
FB 5	24.2	20.6	3.6	34.4	18.6	22.2	20.2	2.6	26.7	44.6	28.8	31.4	44.6	24.1
FB 4	31.8	27.8	4.0	26.4	20.4	24.4	17.2	4.2	35.4	33.6	31.0	40.5	33.6	26.0
FB 3	29.2	27.4	1.8	26.2	29.2	31.0	13.6	1.8	32.4	30.8	36.6	34.5	31.0	34.5
FB 2	30.6	26.2	4.4	26.2	16.8	21.2	21.4	5.0	35.6	35.6	28.8	41.6	35.6	22.8
FB 1	28.4	23.8	4.6	32.8	14.8	19.4	20.8	3.2	31.3	43.1	25.5	37.4	43.2	19.5
R 19	18.6	15.8	2.8	17.2	26.2	29.0	31.2	6.8	25.5	27.7	46.8	30	27.7	42.3
R 18	17.8	15.2	2.6	12.8	18.2	20.8	33.6	17.6	31.1	26.2	42.6	36.5	26.2	37.3
R 17	23.0	19	4.0	20.6	29.6	33.6	23.4	3.4	26.0	28.1	45.9	31.4	28.1	40.4
R 16	23.0	14.2	8.8	20.8	24.0	32.8	25.6	6.6	20.9	30.7	48.4	33.9	30.7	35.4
R 15	21.4	20.2	1.2	23.2	16.6	17.8	34.0	4.8	33.0	37.9	29.1	35.0	37.9	27.1
R 14	24.4	20.0	4.4	18.4	26.4	30.8	24.8	6.0	28.9	26.6	44.5	35.3	26.6	38.2
R 13	27.2	20.4	6.8	19.2	18.6	25.4	30.4	4.6	31.4	29.5	39.0	41.9	29.5	28.6
R 12	30.0	25.4	4.6	16.8	20.8	25.4	26.8	5.6	37.6	24.9	37.6	44.4	24.9	30.8
R 11	24.8	21.6	3.2	17.2	23.2	26.4	32.4	2.4	33.1	26.4	40.5	38.0	26.4	35.6
R 10	21.6	15.6	6.0	16.4	25.4	31.4	32.2	4.4	24.6	26.0	49.5	34.1	25.9	40.1
R 9	20.8	15.2	5.6	11.4	17.2	22.8	42.2	8.4	30.8	23.1	46.2	42.1	23.1	34.8
R 8	19.6	15.0	4.6	14.8	29.6	34.2	34.0	2.0	23.4	23.1	53.4	30.6	23.1	46.3
R 7	25.6	17.6	8.0	23.0	31.6	39.6	16.8	3.0	21.9	28.7	49.4	31.9	28.7	39.4
R 6	18.4	11.2	7.2	20.0	22.4	29.6	32.4	6.8	18.4	32.9	48.7	30.3	32.9	36.8
R 5	27.4	22.0	5.4	21.2	32.0	37.4	17.2	2.2	27.3	26.3	46.4	34	26.3	39.7
R 4	29.0	25.0	4.0	20.6	25.6	29.6	21.4	3.4	33.2	27.4	39.4	38.6	27.4	34.0
R 3	23.0	18.2	4.8	11.8	20	24.8	41.2	4.0	33.2	21.5	45.3	42.0	21.5	36.5
R 2	30.2	23.8	6.4	23.2	24.8	31.2	16.2	5.6	30.4	29.7	39.9	38.6	29.7	31.7
R 1	26.8	21.8	5.0	19	16.4	21.4	30.6	7.2	35.0	30.6	34.4	43.1	30.6	26.4
CH 5	31.6	26.4	5.2	16.8	19.6	24.8	25.6	6.4	38.8	24.7	36.5	46.5	24.7	28.8
CH 4	24.6	19.2	5.4	19	17.8	23.2	35.2	3.4	31.2	30.9	37.8	40.1	30.9	29.0
CH 3	28.6	26.2	2.4	20.4	18.0	20.4	28.4	4.6	39.1	30.5	30.5	42.7	30.5	269
CH 2	30.4	24.8	5.6	15.8	21.4	27.0	20.8	11.6	36.7	23.4	39.9	45.0	23.4	31.7
CH 1	27.8	21.2	6.6	12.8	20.6	27.2	32.0	6.8	34.6	20.9	44.4	45.4	20.9	33.7
PA 5	19.4	15.8	3.6	10.8	18	21.6	42.6	9.2	32.8	22.4	44.8	40.3	22.4	37.3
PA 4	23.2	20.4	2.8	13.8	18.6	21.4	34.0	10.4	36.7	24.8	38.5	41.7	24.8	33.5
PA 3	20.4	16.8	3.6	10.6	21.0	24.6	42.2	5.8	32.3	20.4	47.3	39.2	20.4	40.4
PA 2	23.8	19.2	4.6	12.8	16.0	20.6	35.0	12.4	36.5	24.3	39.2	45.3	24.3	30.4
PA 1	18.4	17.2	1.2	15.6	17.0	18.2	41.2	7.8	33.7	30.6	35.7	36.1	30.6	33.3

5.3.2 Texture

Thin sections were prepared from claystones to fine grained sandstone samples. The argillaceous rocks were classified based on their particle sizes and texture. The rocks have lamination or fissility texture, allowing the rocks to break along laminae planes (Figure 5.1).

The texture was mainly due to the deposition of suspended clay minerals, variations in compositional grain sizes of the sediments and fluctuations in sediment supply. In cases where lamination on the mudrocks did not occur, thin bedded and massive bedded mudstones were observed. The sandstone samples are generally very fine to fine grained and poor to very well sorted (Figures 5.2a-f). Grain morphology ranges from subangular to angular (Figures 5.2a-f). Most sandstone samples are cemented with mud matrix, whereas some are grain supported. The summary of the textural characteristics of the sandstones is depicted in Table 5.3.
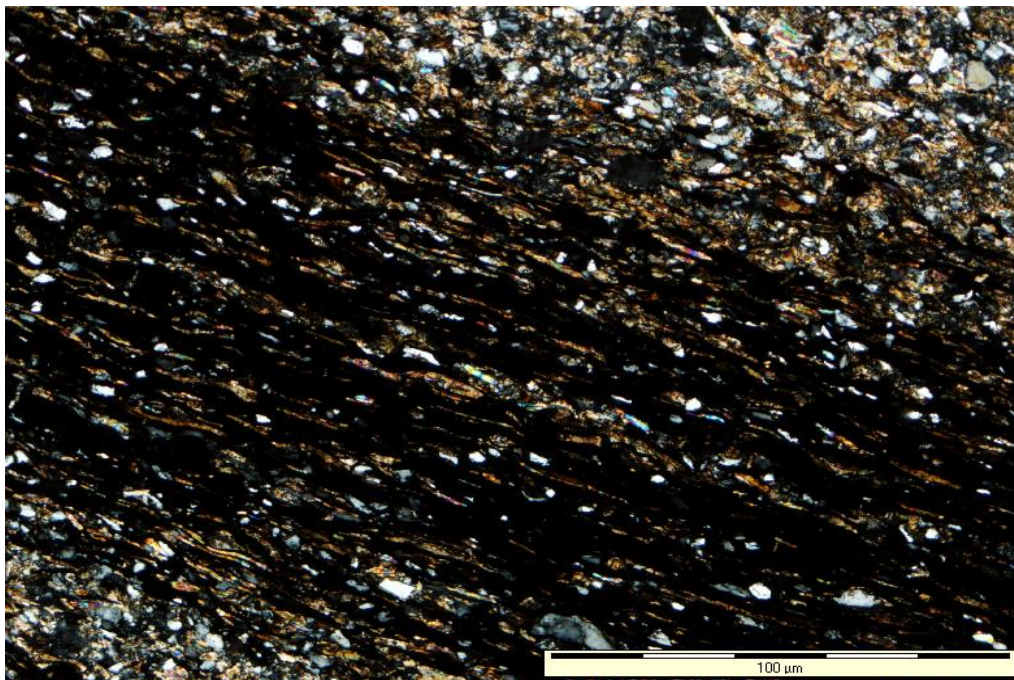
Figure 5.1: Thin section photomicrograph of mudrock depicting mineral grains lying parallel to the lamination planes.
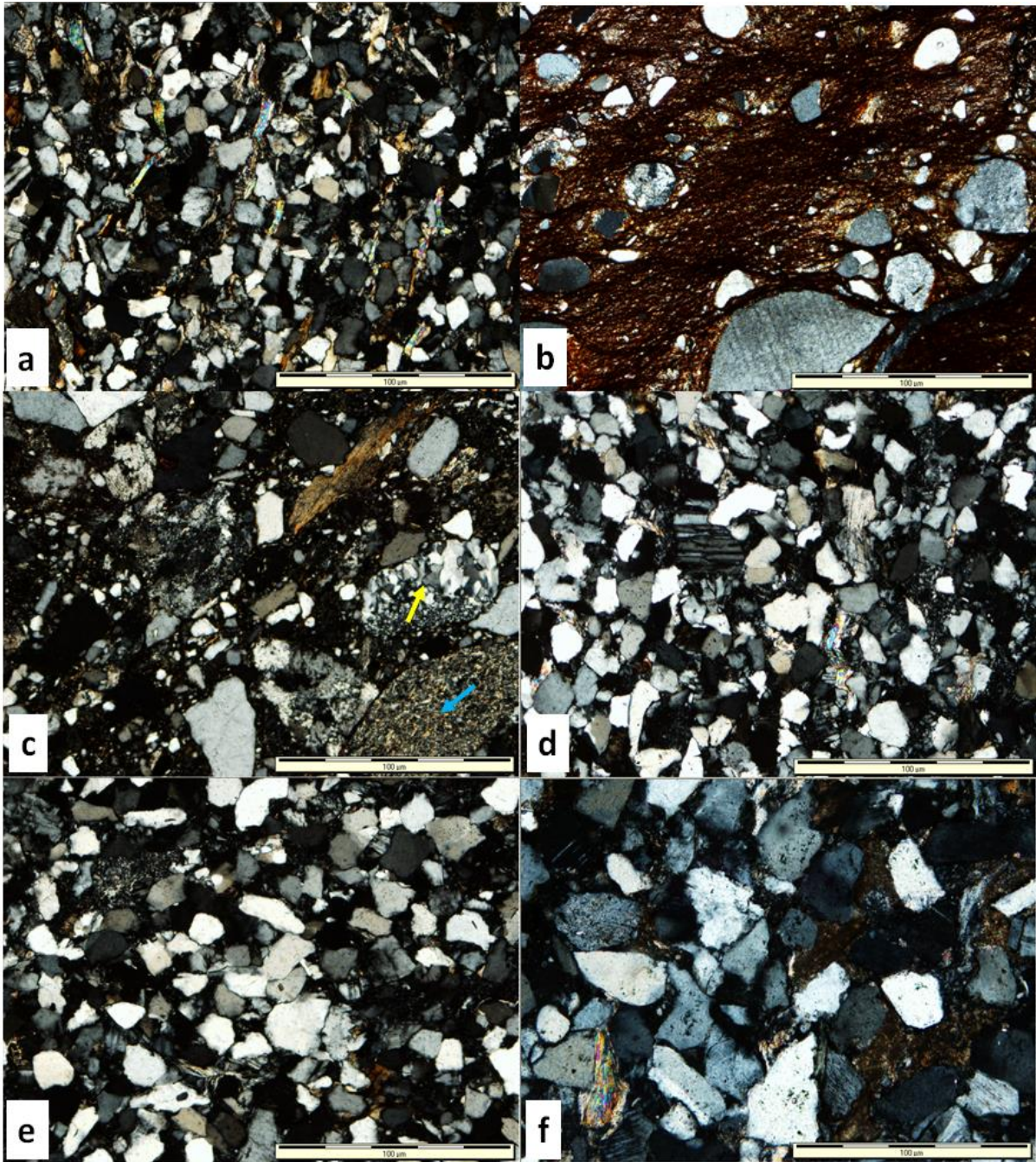
Figure 5.2: Photomicrograph showing: (a) Very fine grained sandstones from the Fort Brown Formation showing moderately well sorted and subangular to subrounded quartz grains; (b) Fine grained iron-stained greywacke from the Prince Albert Formation showing poorly sorted and angular to subrounded quartz grains, feldspar and lithic grains setting in clay matrix; (c) Poorly sorted sandstone (lithic greywacke) with mudstone (blue arrow) and metamorphic (yellow arrow) lithics; (d) Fine grained sandstones from the Ripon Formation showing moderately well sorted and subangular to subrounded quartz grains; (e) Fine grained sandstones from the Ripon Formation showing well sorted and subrounded quartz grains; (f) Moderately well sorted lithic greywacke with sub angular to subrounded detrital grains of feldspar, quartz and muscovite (lower left).

123

Table 5.3: Textural characteristics of the sandstones from the Ecca Group.

Formation	Sample	Mean grain size (φ)	Verbal grain size	Roundness	Sorting
Fort Brown	FB 6	2.48	Fine sand	Subrounded	Moderately well sorted
	FB 5	2.04	Fine sand	Rounded	Well sorted
	FB 4	2.19	Fine sand	Subrounded	Well sorted
	FB 3	2.03	Fine sand	Subangular	Moderately well sorted
	FB 2	3.07	Very fine sand	Subrounded	Moderately well sorted
	FB 1	2.13	Fine sand	Rounded	Well sorted
Ripon	RP 19	3.04	Very fine sand	Subrounded	Well sorted
	RP 18	2.39	Fine sand	Subrounded	Well sorted
	RP 17	2.89	Fine sand	Rounded	Well sorted
	RP 16	3.13	Very fine sand	Subrounded	Well sorted
	RP 15	3.01	Very fine sand	Rounded	Very well sorted
	RP 14	2.97	Fine sand	Subrounded	Very well sorted
	RP 13	2.57	Fine sand	Rounded	Well sorted
	RP 12	2.47	Fine sand	Rounded	Well sorted
	RP 11	2.09	Fine sand	Subangular	Moderately well sorted
	RP 10	2.44	Fine sand	Subangular	Well sorted
	RP 9	2.27	Fine sand	Subrounded	Well sorted
	RP 8	2.92	Fine sand	Subrounded	Well sorted
	RP 7	2.04	Fine sand	Rounded	Well sorted
	RP 6	3.17	Very fine sand	Subangular	Moderately well sorted
	RP 5	2.94	Fine sand	Rounded	Well sorted
	RP 4	3.12	Very fine sand	Subangular	Moderately well sorted
	RP 3	2.96	Fine sand	Subrounded	Well sorted
	RP 2	2.78	Fine sand	Subrounded	Well sorted
	RP 1	2.41	Fine sand	Subrounded	Well sorted
Collingham	CH 5	3.13	Very fine sand	Subrounded	Moderately well sorted
	CH 4	3.27	Very fine sand	Subrounded	Moderately well sorted
	CH 3	3.34	Very fine sand	Subangular	Moderately well sorted
	CH 2	3.11	Very fine sand	Rounded	Well sorted
	CH 1	2.82	Fine sand	Subrounded	Moderately well sorted
Prince Albert	PA 5	2.68	Fine sand	Subangular	Poorly sorted
	PA 4	2.49	Fine sand	Subangular	Poorly sorted
	PA 3	2.51	Fine sand	Angular	Poorly sorted
	PA 2	2.21	Fine sand	Subangular	Poorly sorted
	PA 1	2.55	Fine sand	Subangular	Poorly sorted

5.3.3 Mineral composition

5.3.3.1 Quartz

Quartz is the most dominant mineral within all sandstone samples, and it ranges from about 18.4-31.8%, averaging 25.1% of the overall composition. The shape of the quartz grains are mostly sub-angular to sub-rounded, with grain sizes ranging from 0.063 mm to 0.19 mm, which falls under very fine to fine grained. The quartz minerals exist as monocrystalline grains (Qm), polycrystalline grains (Qp) and quartz cement (i.e. quartz overgrowth; Figure 5.3a). The monocrystalline quartz consists of single crystalline quartz, whereas the polycrystalline quartz comprises of multiple crystalline grains. Some of the polycrystalline quartz grains have three or more crystals (Figure 5.3b) with straight to slightly curved intercrystalline boundaries. The monocrystalline quartz grains make up to 81.33% of the total quartz grains in the samples. Both the monocrystalline and polycrystalline quartz grains exhibit undulatory extinction and occasional intercrystalline suturing (Figure 5.4). However, the polycrystalline grains that show both properties are small compared to the monocrystalline grains In addition, some of the monocrystalline quartz grains have uniform extinction, unstrained and show overgrowth (Figure 5.3a). In few cases, the quartz grains contain muscovite, rutile needle and zircon inclusions within the grains.
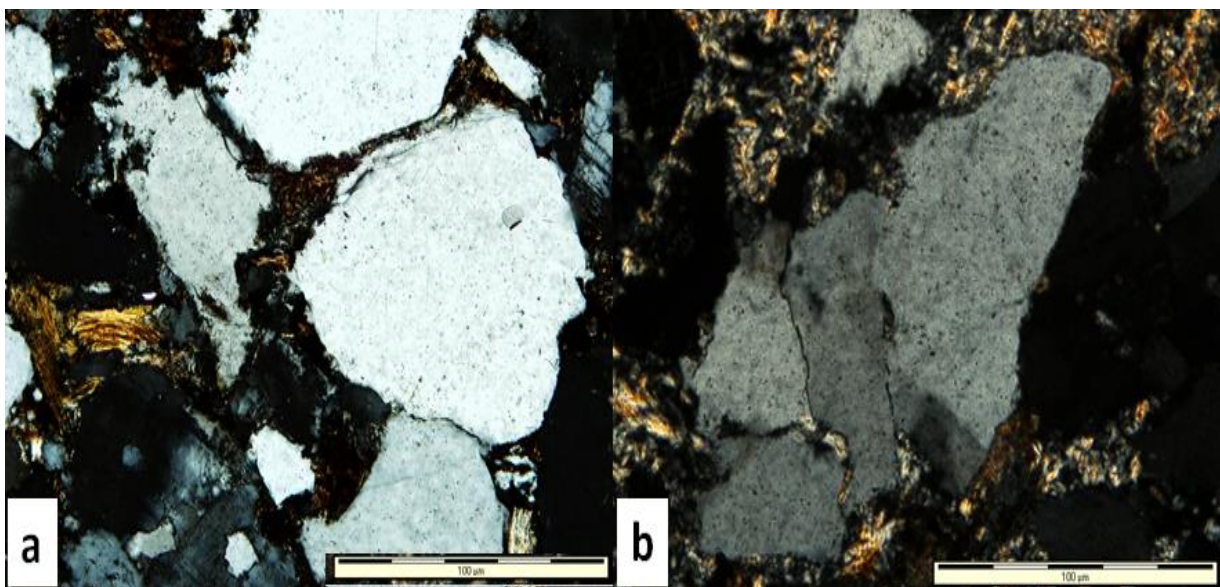
Figure 5.3: Thin section photomicrograph of sandstone showing: (a) Quartz grains and muscovite grains; (b) Polycrystalline quartz consisting of four quartz grains.
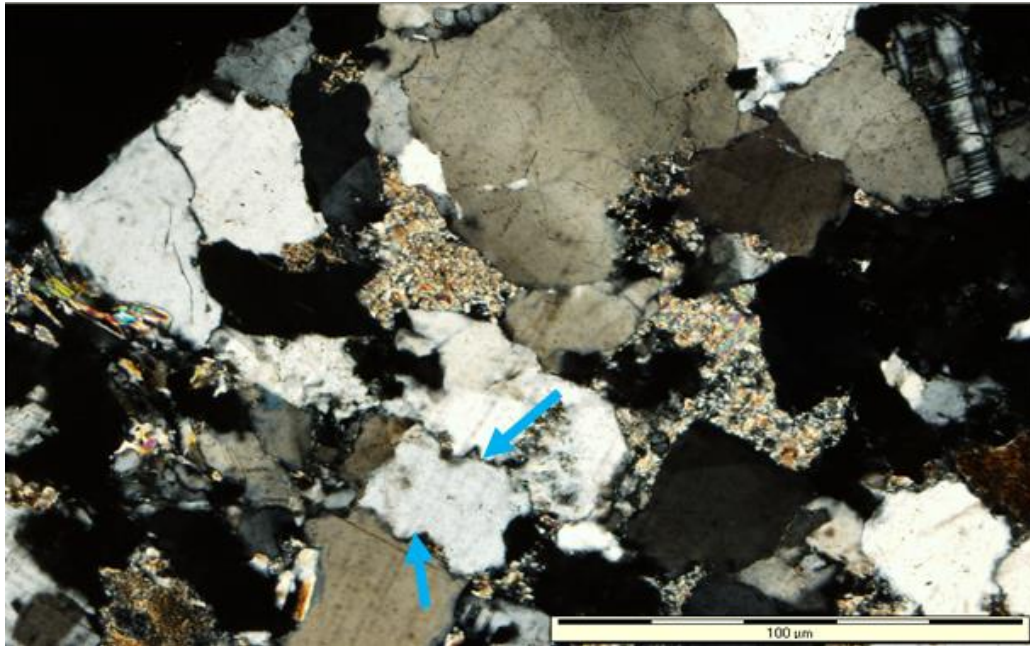
Figure 5.4: Thin section photomicrograph of sandstone showing K-feldspar twin crystals and sutured quartz grain (blue arrows).

5.3.3.2 Feldspar

Feldspar is the second most abundant detrital constituent of the samples with different grain sizes and types. Alkali feldspar (orthoclase and microcline) and plagioclase feldspar (albite) are the feldspar minerals present in the thin sections, with alkali feldspar and albite being the most dominant. The amount of feldspar grains range from 10.6-34.4%, averaging 19.41% of the total grains in the samples. Both monocrystalline and polycrystalline feldspar grains are present. The feldspar grains generally range from subangular to subrounded and some are partially replaced or altered to sericite. In few cases, they are altered to kaolinite, illite, muscovite or replaced by calcite. Albite and orthoclase are the dominant feldspar minerals occurring in both twinned and untwined forms. About 70% of the plagioclase shows twinning, while others appear to be untwined. Microcline only occurs in minor quantities, in few cases they are recrystallized to albite (Figure 5.5a). Microcline are completely absent in some samples. Albite grains are mostly elongated and show parallel twinning, while those of microcline shows cross-hatch twinning. The orthoclase grains are mostly cloudy in colour, but sometimes, they show simple twinning with perthite texture (Figure 5.5b).
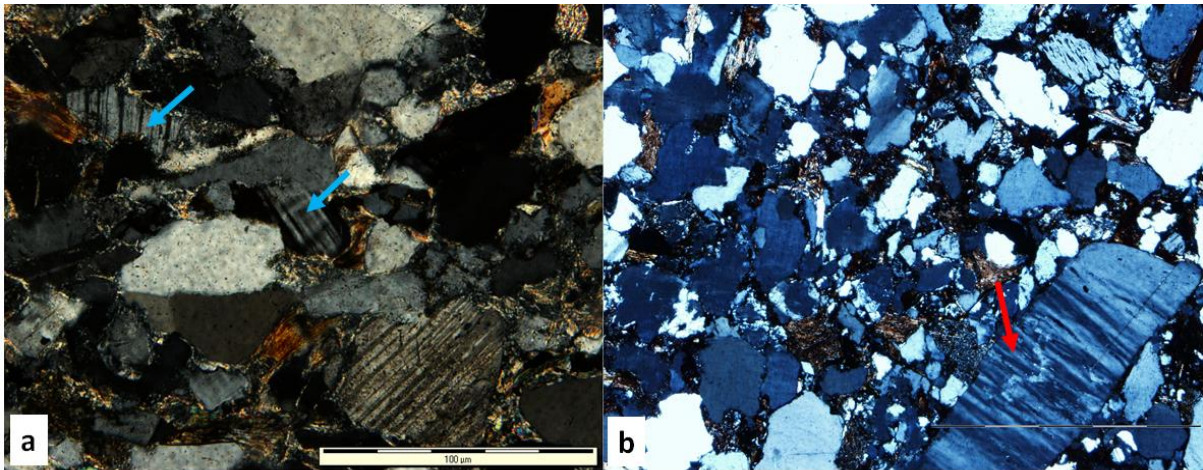
Figure 5.5: Thin section photomicrograph showing: (a) Microcline partially changed to albite (blue arrows); (b) Feldspar lithic with perthitic texture (red arrow).

5.3.3.3 Lithic fragments

Rock fragments that were identified are metamorphic, sedimentary and igneous or volcanic in nature (Figure 5.6a-c), and are mostly subangular to subrounded. It constitutes an average of about 19.51% of the total grains.
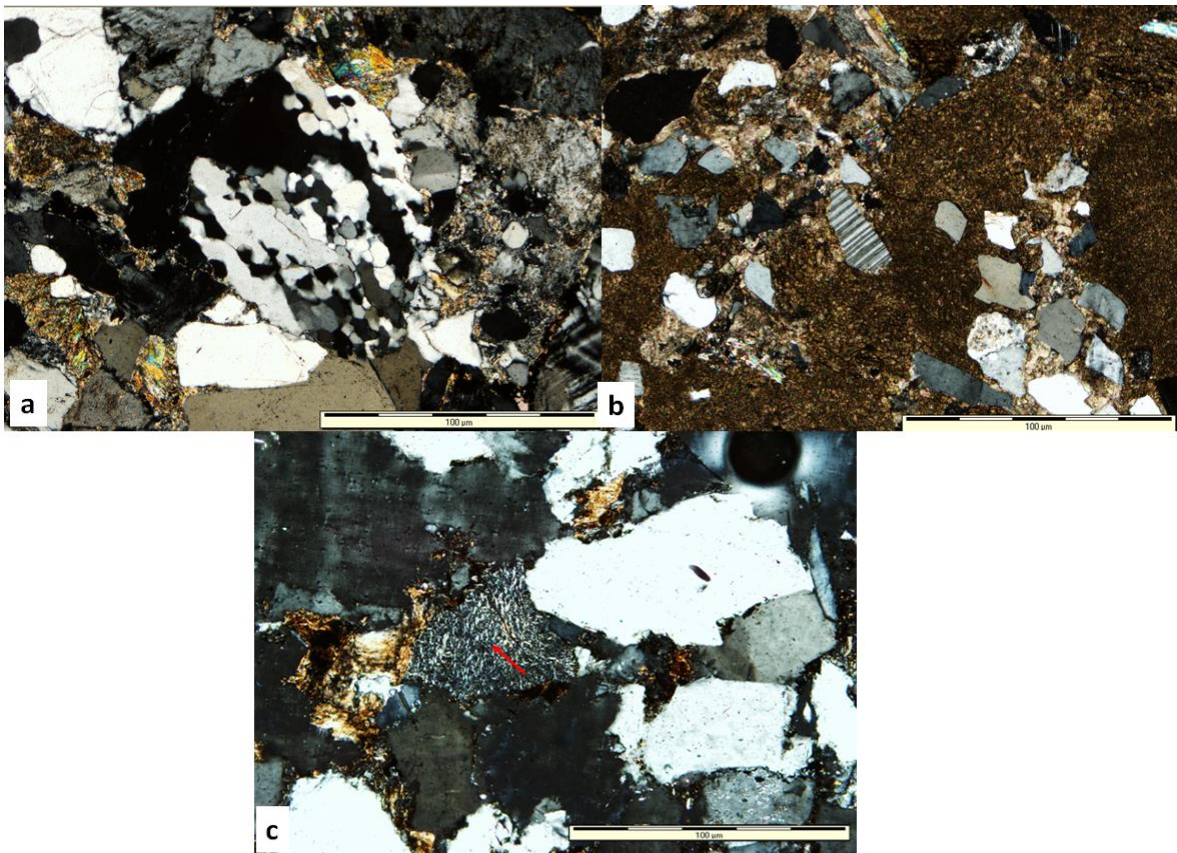
Figure 5.6: Thin section photomicrograph showing: (a) Metamorphic lithic (middle part); (b) Poorly sorted greywacke with subangular detrital grains of feldspar, quartz and sedimentary rock lithics; (c) Greywacke with volcanic lithic (red arrow).

Metamorphic and igneous clasts constitute a larger percentage than volcanic and sedimentary clasts. Metamorphic clasts are mainly shale schist, chert and quartzite, whereas igneous clasts include granitic and granodioritic rock types. Sedimentary rock fragments of sandstone, siltstone and shale constituting a small percentage of the total lithic fragments. These pieces of rocks have been eroded down to sand size and are now sand grains in the sedimentary rock.

5.3.3.4 Matrix and cement

The framework grains are bound together by both cement and matrix. The common cementing minerals are clay, quartz, feldspar and hematite. The matrix is mostly clay minerals (Figure 5.7) and they are either detrital or diagenetic in form.
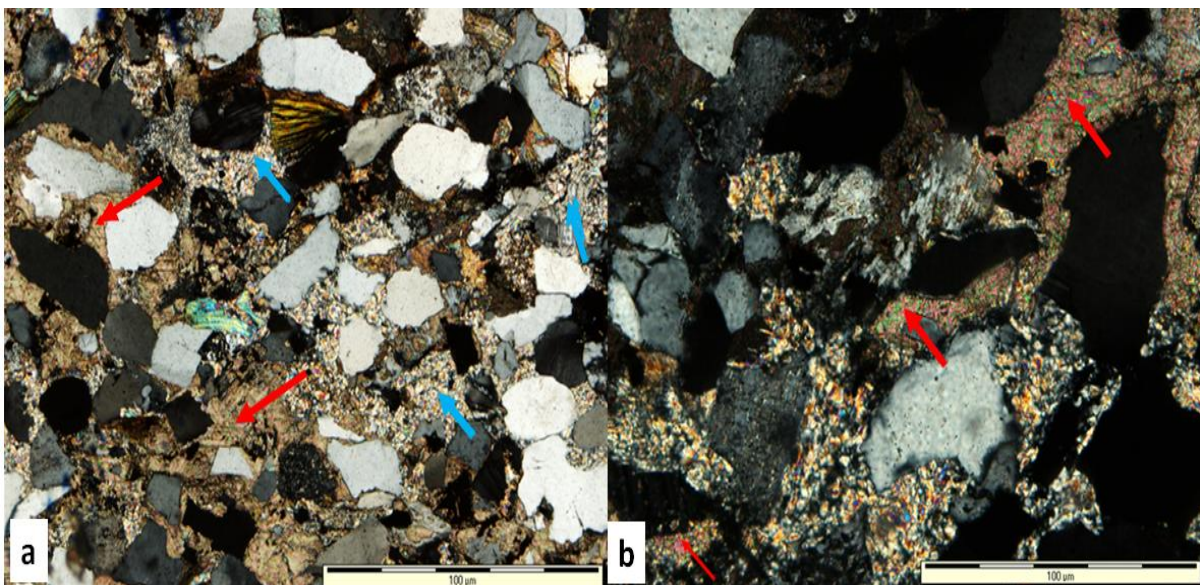
Figure 5.7: Thin section photomicrograph showing: (a) Calcite cement (red arrows) and clay matrix (blue arrows); (b) Calcite cement (red arrows) which also replaces matrix minerals and framework grains.

The diagenetic matrix minerals were formed as a result of framework grains alteration and precipitation, as well as recrystallization of other matrix minerals. The observed matrix minerals are sericite, kaolinite, smectite, illite, glauconite and mica (mostly muscovite). These minerals were best identified with the help of SEM and XRD. Glauconite is commonly associated with periods of hiatus and periods of sediment reworking. The mica minerals in the matrix are due to the recrystallization of clay minerals as well as the alteration of feldspars. Calcite (Figure 5.7), smectite and illite are the most abundant clay minerals with minor kaolinite and sericite clay minerals. Quartz cement is in the form of fine quartz and

quartz overgrowths that precipitated out in the pore-space between the original detrital grains. In thin sections, quartz overgrowths were distinguished from the detrital grains by rims of quartz cements around detrital grains. Hematite cement is present in few cases, and they fill the pore spaces within the sandstone grains. Quartz and calcite cements are the main types of cements in the sandstones.

5.3.3.5 Mica

Muscovite and biotite are the mica in the sandstones, with muscovite occurring more frequently than biotite. This could be due to the fact that muscovite is chemically more stable than biotite in the depositional environment. Noticeably, muscovite flakes appears parallel or squeezed flat amongst other grains and matrix (Figure 5.8). Sometimes, the muscovite grains are deformed and fractured. Most of muscovite grains have euhedral shape and they are authigenetically formed due to the recrystallization of clay matrix during diagenesis (Figure 5.8). Some of the muscovite grains are stained or invaded by chlorite. The detrital muscovite grains that are not altered or changed have an elongated flaky shape with clear or noticeable boundaries.
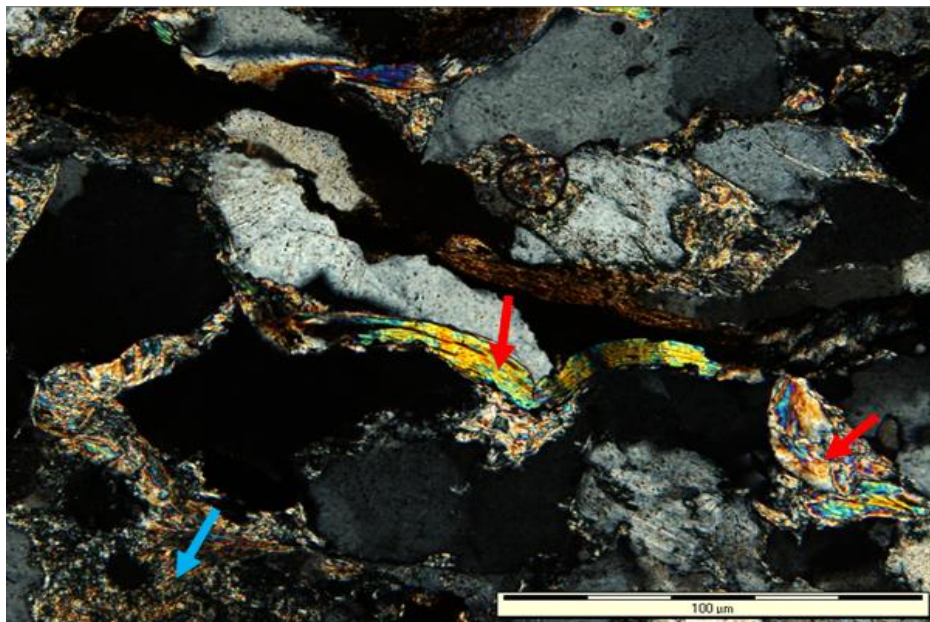
Figure 5.8: Thin section photomicrograph showing detrital muscovite flakes (red arrows) and recrystallized clay matrix to muscovite (blue arrow).

5.3.3.6 Heavy minerals

Heavy minerals in the rocks of the Ecca Group occur as accessory minerals of detrital hematite, garnet, rutile (Figure 5.9a) and zircon (Figure 5.9b). These minerals constitute less

than 1% of the total grains in the samples and their grains are mostly subrounded. Their presence in the rocks gives a firm confirmation to the fact that some of the Ecca Group sediments were derived from metamorphic and igneous sources.
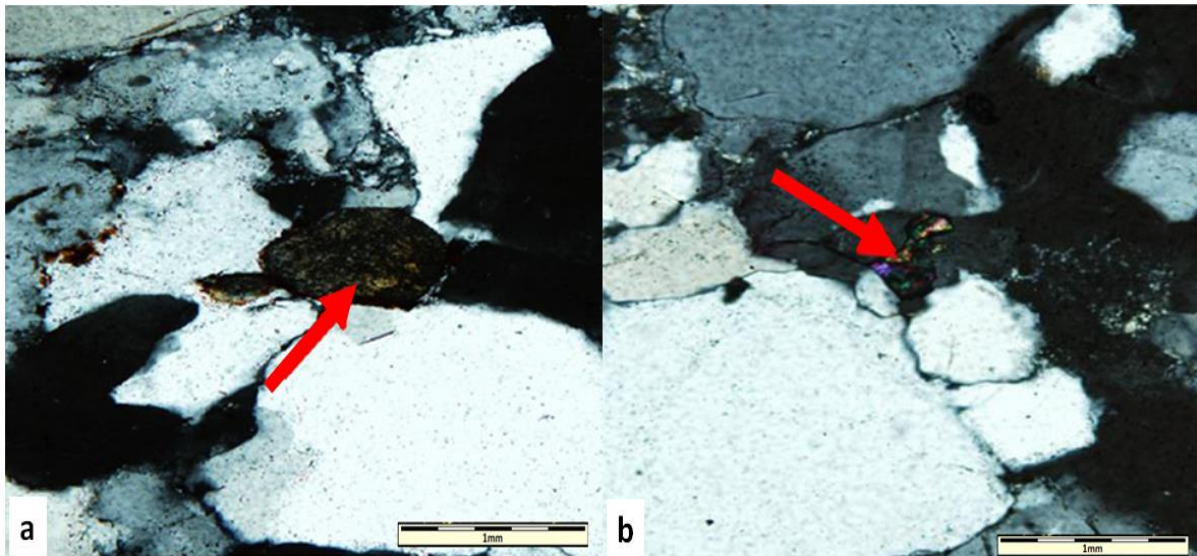
Figure 5.9: Photomicrograph of sandstone showing: (a) Rutile mineral grain (red arrow); (b) Zircon grain (red arrow).

5.3.4 Mineralogy and modal composition

The XRD analyses of some of the sandstones are presented in Apendix B (Table B1). The most abundant minerals include quartz (16-40%) and plagioclase (7-30%), while the dominant clay minerals are illite (5-30%), smectite (< 1-35%), and chlorite (1-14%). Quartz, feldspar, illite, sericite and muscovite were formed through recrystallization, whereas kaolinite was formed through the dissolution of K-feldspar. In addition, kaolinite was also observed as having replaced muscovite grains and in some cases, illite formed through the replacement of feldspar grains. The identified heavy minerals are hematite, garnet and zircon and they all exist in traces.

5.4 Interpretation and discussion

5.4.1 Petrography and mineralogy

The rock are dominantly feldspathic and lithic wackes, with textural data indicating very fine to fine grain sizes, poor to well sorted, subangular to subrounded shapes and sometimes rounded. The sandstones showed relatively high percentage of feldspar, lithic fragments and matrix (> 15%), indicating short transport distance and quick burial. The average contents and characteristics of different quartz and feldspar grains in these sandstones show igneous,

metamorphic and pre-existing sedimentary rock sources. These have been proven by overall variation in the relative abundance of different types of quartz and feldspar grains. Quartz and feldspar grains are both polycrystalline and monocrystalline, indicating that they were not fully separated by long transportation, which is consistent with the immature nature of the rocks. Based on the genetic and empirical classification of the quartz types (Folk, 1974), monocrystalline quartz grains are mainly plutonic, hydrothermal and recycled sedimentary sourced, whereas polycrystalline quartz grains are recrystallized and stretched metamorphic types. The dominance of monocrystalline quartz grains show that the sediments were mostly derived from a granitic source (Basu et al., 1975). On the other hand, Dabbagh and Rogers (1983) documented that such grains could have been formed due to disaggregation of the original polycrystalline quartz during high energy or long distance transport from the metamorphic source. Some of the polycrystalline quartz grains have three or more crystals with straight to slightly curved intercrystalline boundaries, which possibly suggest that they were derived from plutonic igneous rocks and metamorphic rocks (Folk, 1974; Blatt et al., 1980). Though, some monocrystalline and polycrystalline quartz grains exhibit undulatory extinction and occasional intercrystalline suturing, which indicate metamorphic source(s) for the rocks. In addition, other monocrystalline quartz grains have uniform extinction, unstrained and show overgrowth. In few cases, the quartz grains contain muscovite, rutile needle and zircon inclusions within the crystalline grains, which suggest an igneous or metamorphic rock source (Basu et al., 1975; Potter and Pettijohn, 1977).

The presence few pure fragments of feldspar grains in some of the sandstones probably indicate igneous source, whereas the altered feldspar grains point to a metamorphic source (Basu et al., 1975). The existence of microcline suggests that the source rock is of low grade metamorphic terrain and alkali-rich granites. The orthoclase and perthite in the sandstones possibly point to plutonic and metamorphic provenances. However, the percentage of alkali feldspar in the sandstones is small compared to other detrital components. Generally, mica is derived from metamorphic and igneous sources (Pettijohn et al., 1987). The relative abundance of muscovite and biotite in the sandstones suggest that the source rock is micaceous in nature, possibly of felsic igneous rocks or metamorphic rocks. The presence of heavy minerals (i.e. garnet, rutile and zircon) in the Ecca rocks suggests that the sediments were derived from metamorphic, sedimentary and igneous sources.

The identified clay minerals (kaolinite, smectite, illite, sericite and chlorite) possibly exist in the rock either as detrital grains or diagenetic minerals. The detrital nature of the framework

grains and the presence of lithic fragments, thus, render the rocks to be terrigenous in origin. From the observed lithics and heavy minerals and the nature of quartz and feldspar minerals, it can be inferred that the provenances of the sediments were derived mostly from igneous and metamorphic rock sources, rarely from sedimentary rock source. Furthermore, the relative abundance of monocrystalline quartz, zoned albite and tuffaceous material in the Collingham Formation also point to the existence of volcanic rocks in the sediment source area. Under the microscope, illite is more dominant in the Prince Albert and Collingham Formation where a deep marine environment existed, whereas kaolinite is dominant in the sandstones of Ripon and Fort Brown Formations that formed in a deltaic environment. Though, diagenetic processes may have played a role in the distribution of these minerals, the rate of sedimentation and the environmental conditions also contributed to nature of the sediments. Millot (1970) documented that weathered materials which are deposited slowly can migrate far out into the sea and be transformed through recrystallization into illite, while kaolinite was thought to have been deposited as large crystals along the coast where it would be able to grow by diagenetic processes. The distribution of these minerals puts further emphasis on the nature of the depositional environments, which is well represented in the model proposed by Smoot in Millot (1970). Based on the model depicted in Figure 5.10, it can be inferred that indeed the Prince Albert and Collingham Formations weredeposited in deep marine water environment, whereas Ripon and Fort Brown Formations were deposited in shallow marine waters under the influence of deltaic processes.
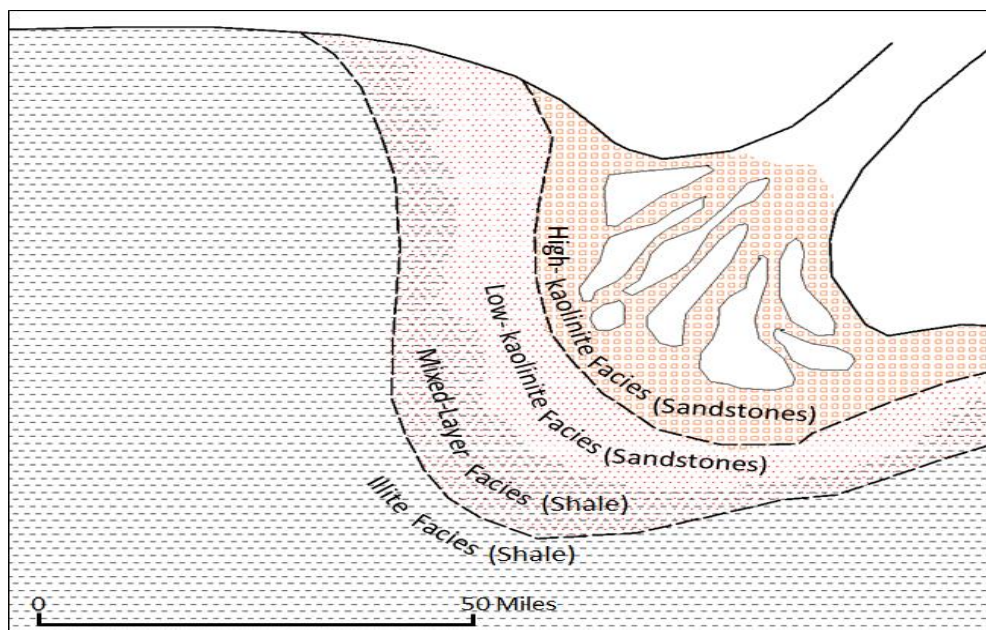
Figure 5.10: Idealised distributions of clay minerals as a function of facies, as proposed by Smoot in Millot (1970).

5.4.2 Sandstone classification

The most effective and commonly used methods for sandstone classification integrate both texture and mineralogy (McBride, 1963; Dott, 1964; Pettijohn et al., 1972; 1973; Folk, 1974; 1980; Dickinson et al., 1983; Herron, 1988; Johnson, 1991). Matrix minerals, which could have been introduced or diagenetically formed, are often taken into consideration. Folk's classification revealed vital information about provenance with the rock's name reflecting details of its composition as proven and documented by Raymond (1995). Based on the method of Pettijohn et al. (1973; 1987), the Ecca sandstones can be classified as wacke or greywacke. The characteristic feature of the greywacke is the dominance of matrix (> 15% matrix; Table 5.4). The Ecca greywacke can be further subdivided into feldspathic and lithic greywacke based on the framework grains (quartz, feldspar and lithic). This petrographic subdivision is supported by the QFL ternary classification scheme of Folk (1974) and Dickinson et al. (1983), in which the samples plotted as both feldspathic and lithofeldspathic sandstones (Figures 5.11-5.13). In the feldspathic grayweckes, feldspar grains were most dominant as compared to the lithics, whereas in the lithic greywacke, percentage of the rock fragments is higher than those of the feldspars. However, the lithic greywackes generally have a wide range of composition with respect to grain types.

Table 5.4: Classification of sandstones based on Pettijohn et al. (1987).

Matrix, i.e., terrigenously derived fine silts and clay minerals		Matrix prominent (>15%)		Matrix absent or minor (<15%)		
Sand fraction	Feldspar exceeds rock fragments	Greywacke	Feldspathic greywacke	Arkosic sandstone		Quartz arenite
				Arkose	Sub-arkose or feldspathic sandstone	
	Rock fragments exceed feldspar		Lithic greywacke	Lithic sandstones		
				Sub-greywacke	Proto-quartz arenite	
	Quartz content	Variable, generally < 75%		< 75%	> 75%	> 95%
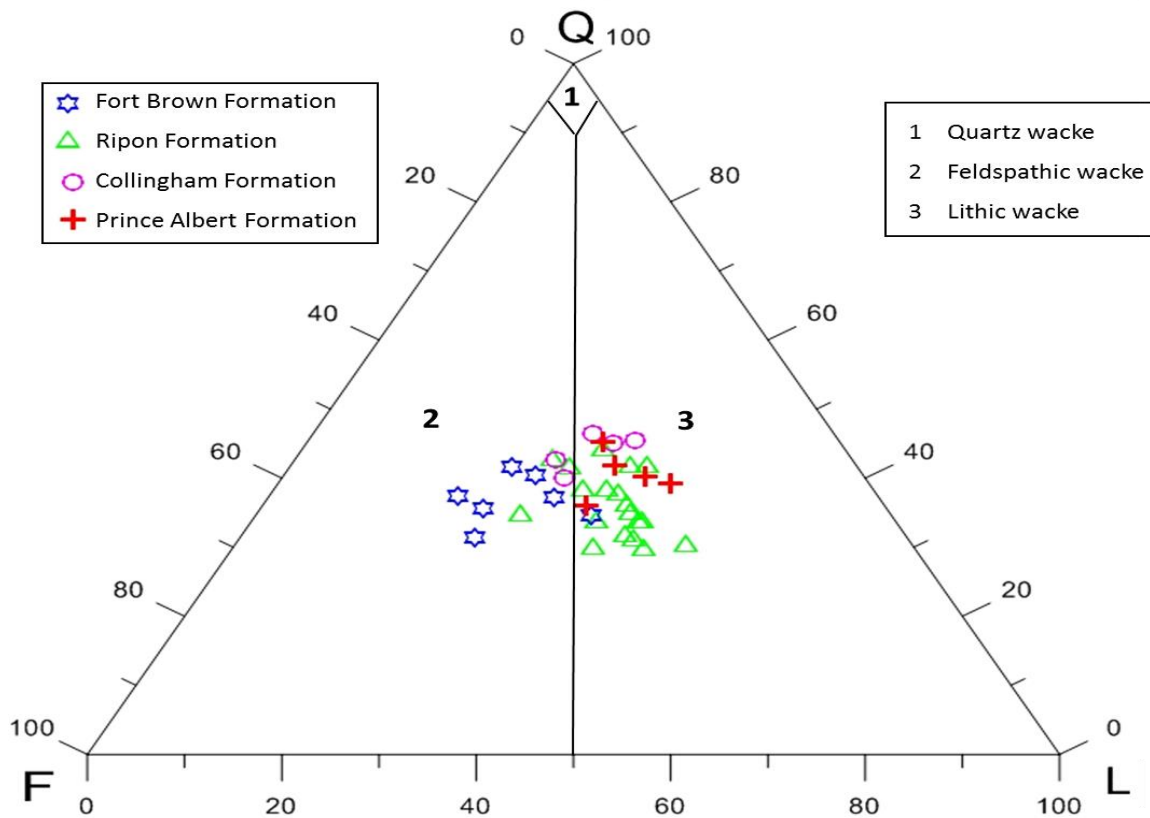
Figure 5.11: Q-F-L ternary plot of the data presented in Table 5.2, showing classification of the Ecca sandstones (After Dott, 1964; Pettijohn et al., 1973).
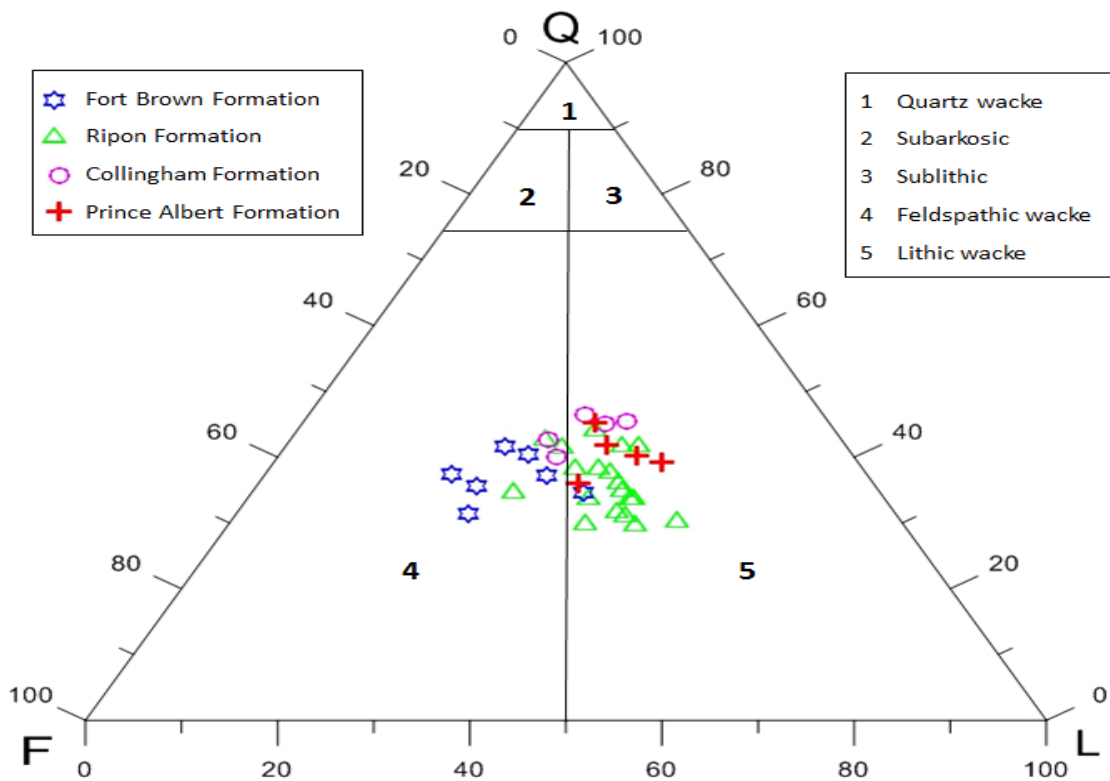
Figure 5.12: Q-F-L ternary plot of the data presented in Table 5.2, showing classification of sandstones from the Ecca Group (After Folk, 1974).
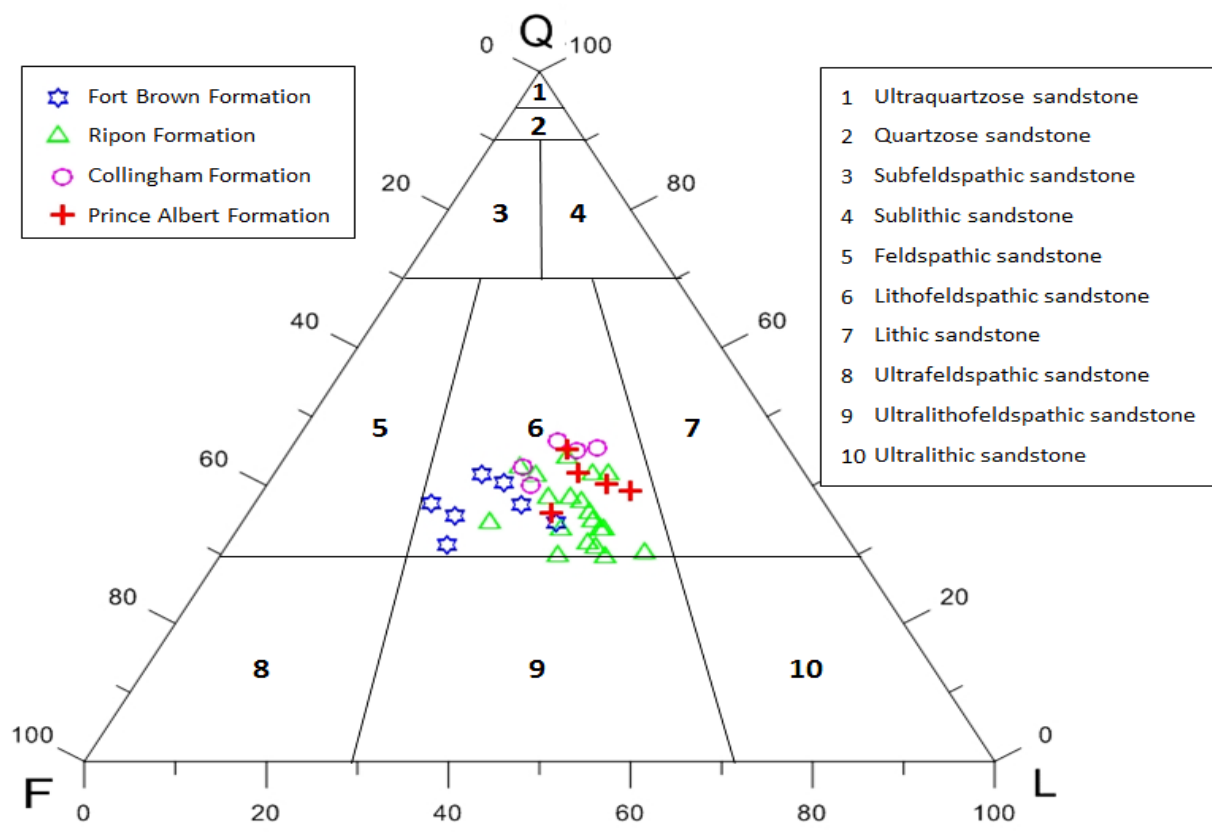
Figure 5.13: Q-F-L ternary plot of the data presented in Table 5.2, showing mineralogical classification of the Ecca sandstones (After Dickinson et al., 1983).

5.4.3 Tectonic setting

Provenance studies of sandstone are mainly based on the assumption that different tectonic environments contain distinctive characteristic rock types (Dickinson, 1985). Several researchers including Dickinson and Suczek (1979), Dickinson et al. (1983), Yerino and Maynard (1984) and Dickinson (1988) have linked detrital sandstone compositions to different provenance types (i.e. stable cratons, basement uplifts, magmatic arcs and recycled orogens) using the Qt-F-L and Qm-F-Lt ternary diagrams. The average compositions of sandstone suites sourced from different plate tectonic environments controlled provenance terranes tend to plot within discrete and separate fields on Qt-F-L and Qm-F-Lt diagrams (Dickinson and Suczek, 1979). These plots have also been attempted for the Ecca sandstones to discriminate between the different kinds of tectonic settings. In the Qt-F-L ternary diagram (After Dickinson and Suczek, 1979), the Ecca sandstones plotted in the dissected arc and recycled orogen field (Figure 5.14). This is an indication that the sediments' sources were derived from recycled orogeny and magmatic arc provenances. Within recycled orogens, sediment sources are mainly sedimentary with minor volcanic rocks, partly metamorphosed

and exposed to erosion by orogenic uplifted fold-belts (Dickinson et al., 1983; Dickinson and Suczek, 1979).

Ternary plot of Qm-F-Lt (After Dickinson, 1988) shows that the samples fall in the transitional arc, dissected arc and mixed fields (Figure 5.15). In contrast, this suggests that the primary or host rock where the sandstones were derived is solely of magmatic arc provenance. As documented by Dickinson et al. (1983), within active magmatic arcs, sediment sources are predominantly in the volcanic cover capping the fold belt and in granitic plutons of the arc roots. Minor debris is thought to have been derived from bounding envelopes of metamorphic rock and adjoining sediments cover. Sands that are derived from this environment tend to produce a spectrum of lithofeldspathic and feldspatholitic types of which the compositions are usually scattered across the central part of Q-F-L plot, as evidenced in Figure 5.14. The Qt-F-L ternary plot (After Kumon et al., 1992) indicates that the sandstones are of magmatic arc provenance, which comprises of dissected, renewed and matured magmatic arc provenances (Figure 5.16). Figure 5.17 shows that the sandstones plotted in the mixed and plutonic to volcanic sources of the Dickinson (1988) discrimination fields. Again, this is an indication that the sediments' sources were derived from plutonic and volcanic sources.

The detrital modal compositions of the Ecca sandstones are related to strike slip (SS), back arc to island (BA) and continental margin arc (CA) settings (Figure 5.18; After Yerino and Maynard, 1984). This also agrees with the work of Dickinson et al. (1983) in which they documented that arkosic sands (feldspathic wacke) predominantly derived from plutons of magmatic arcs are gradational. This sand has similar composition and characteristics with those sands derived from basement uplifts that expose granite and gneiss elsewhere within continental blocks. Generally, the Q-F-L provenance data indicate influence of plutonic, volcanic and metamorphic terrains as the main source rock with minor debris derived from recycled sedimentary rocks. The lithic wackes are characteristically volcano-plutonic sands derived from dissected arcs where erosion has exposed batholiths underneath volcanic cover. On the other hand, the feldspathic wackes with less lithic sands are thought to have been derived from the transitional arc.
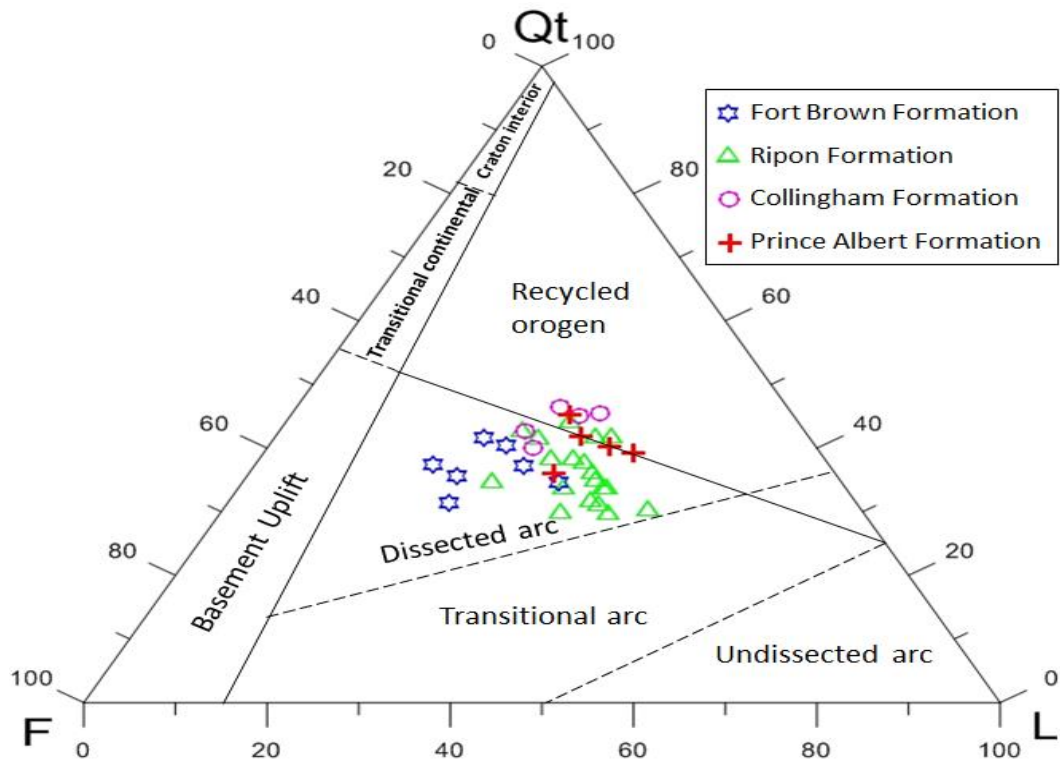
Figure 5.14: Qt-F-L plot for framework modes of the Ecca sandstones showing provisional subdivisions according to inferred provenance type (After Dickinson and Suczek, 1979).
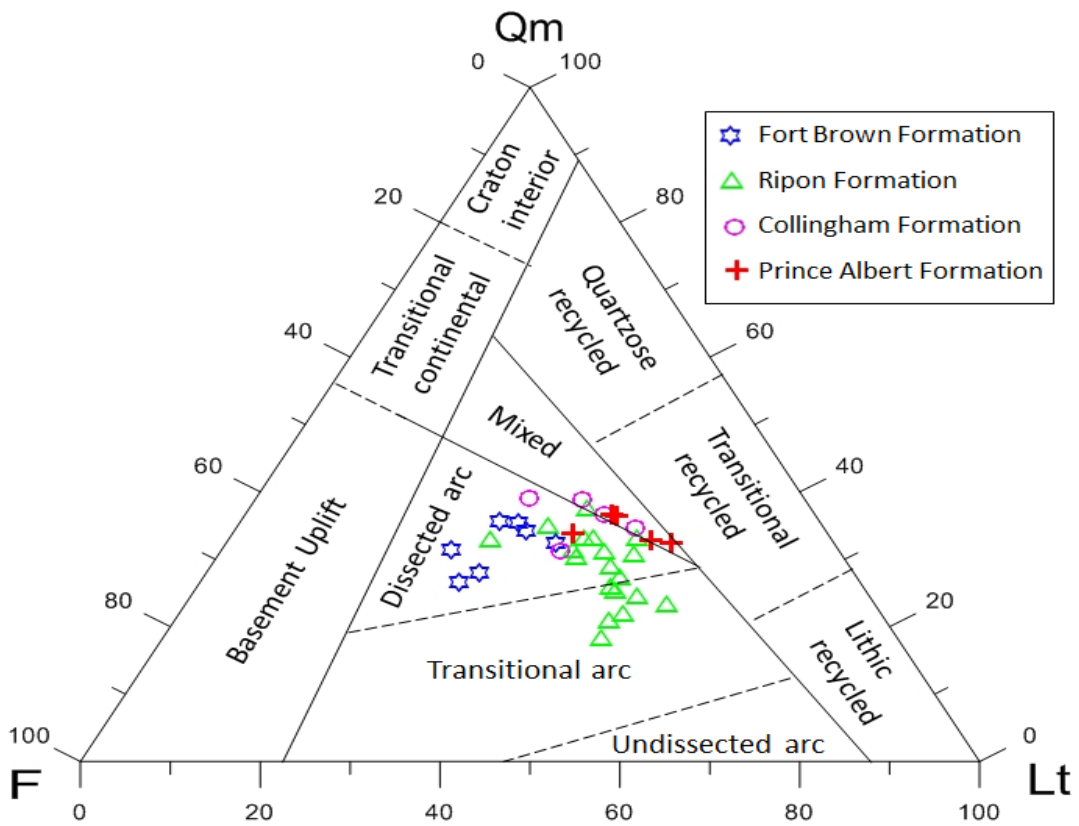
Figure 5.15: Qm-F-Lt ternary plot for framework modes of the Ecca sandstones showing provenance (After Dickinson, 1988).
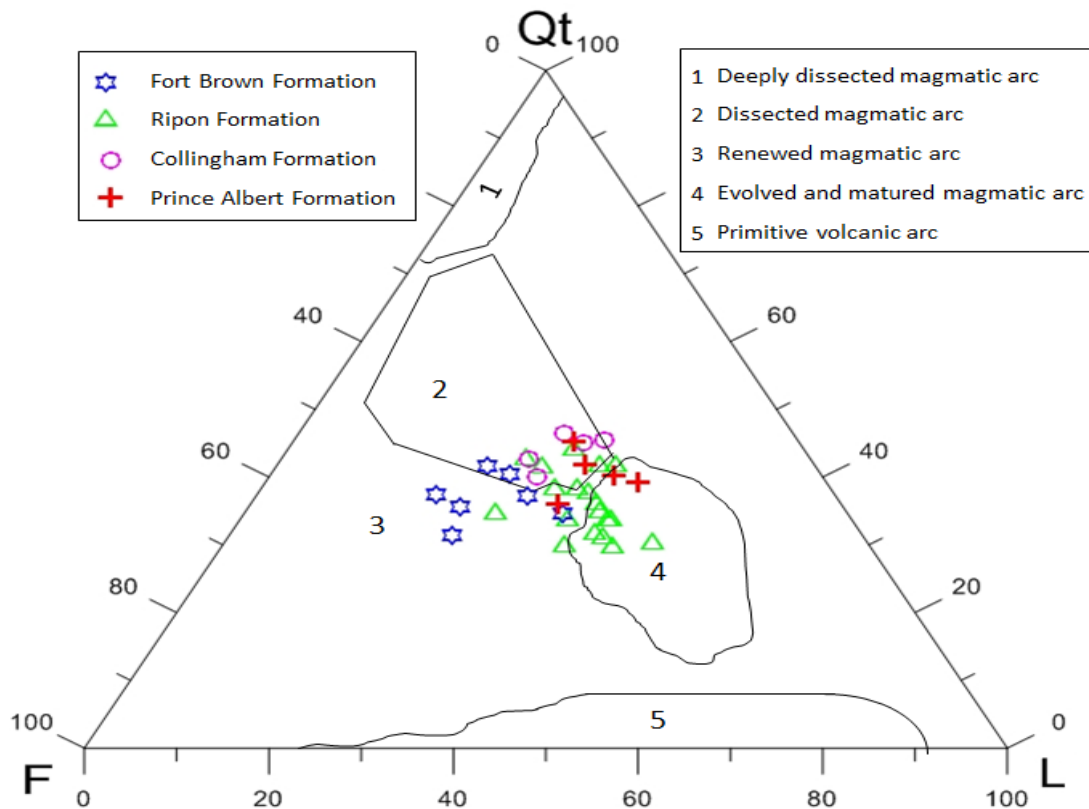
Figure 5.16: Ecca sandstone modal data plot on the Qt-F-L diagram used to discriminate between provenance types of magmatic arc, as proposed by Kumon et al. (1992).
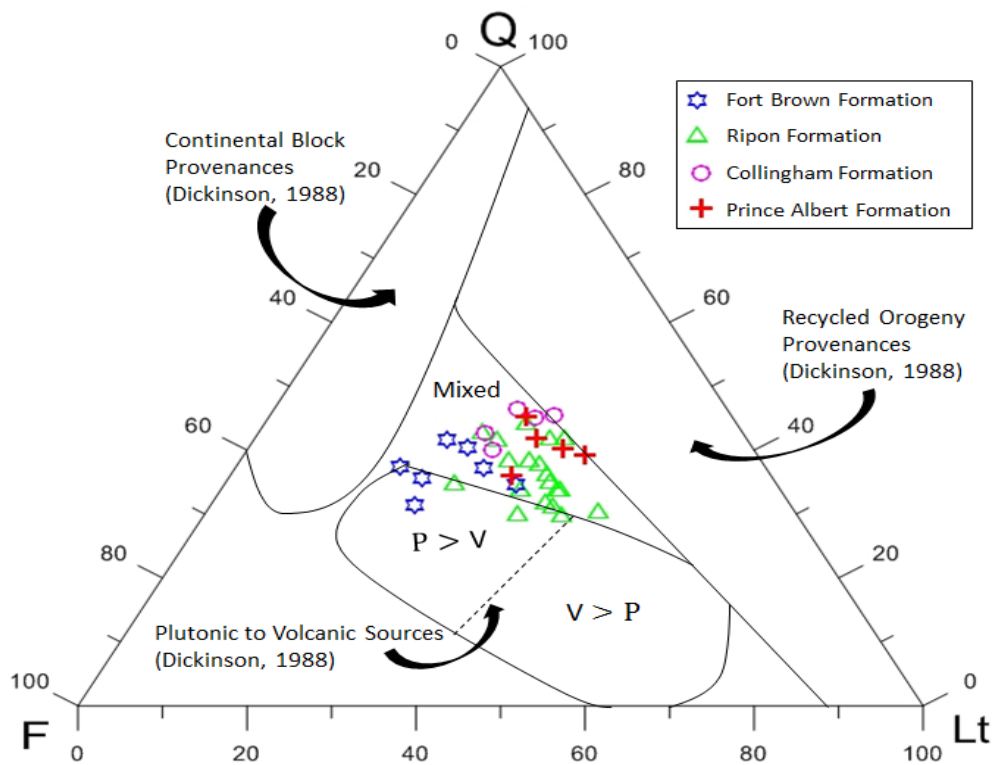
Figure 5.17: Ecca sandstone modal data plot on the Q-F-L diagram of Dickinson et al. (1983). Provenance field boundaries are taken from Dickinson (1988).
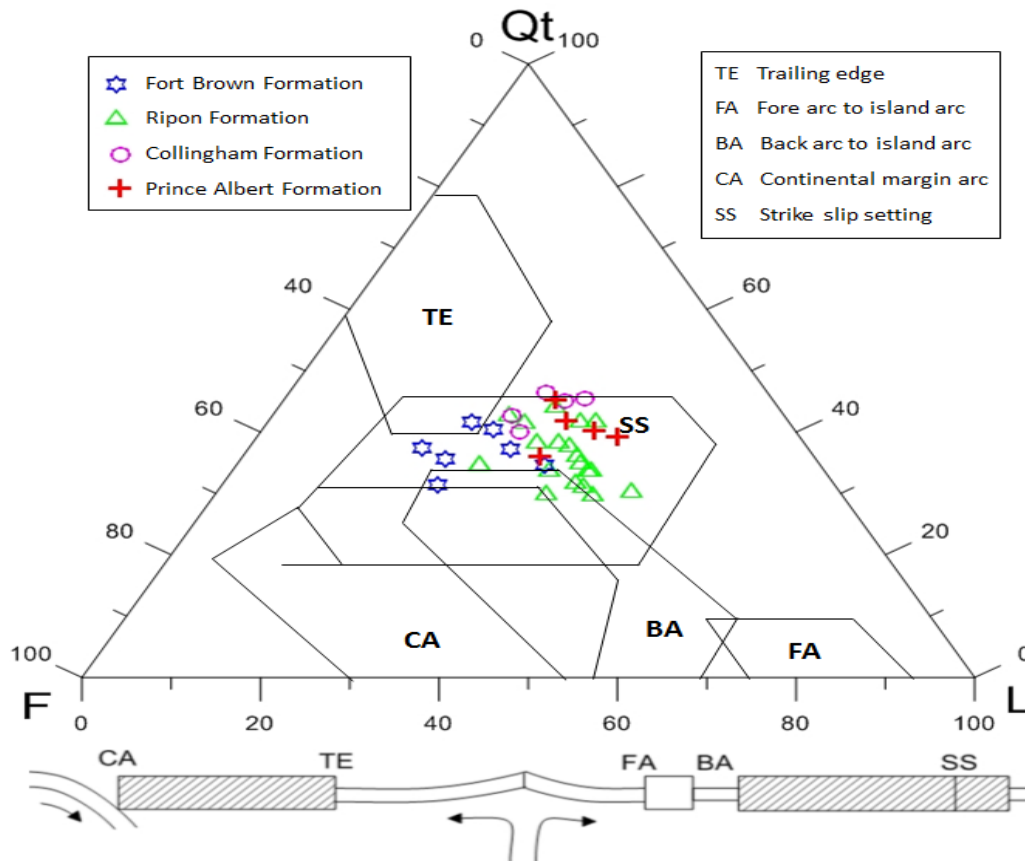
Figure 5.18: Qt-F-L ternary plot scheme proposed by Yerino and Maynard (1984) showing tectonic provenance of the Ecca sandstones.

5.5 Conclusions

The petrographic study of Ecca sandstones revealed that they are moderately to poorly sorted, texturally and compositionally immature and can be classified as feldspathic wacke and lithic wacke. The absence of major petrographically distinctive compositional variations in the sandstones perhaps indicates homogeneity of their source. As a result of this, it is inferred that the transportation distance from the source area was short and the main mechanism of transportation was by marine wave and current to the basin. Both Petrographic and XRD analyses revealed that the sandstones were derived from granitic, metamorphic and pre-existing sedimentary rock sources. The QFL ternary diagrams revealed dissected and transitional arc provenance pointing to a passive margin and uplifted basement preserving the signature of a recycled provenance. This is an indication that the sandstones were derived from a magmatic arc provenance. Since magmatic provenance includes transitional arc and dissected arc, it also shows that the source area of the Ecca sediments had a secondary sedimentary and metamorphic rock source from a marginal belt that developed as a result of rifting.

CHAPTER 6

SEDIMENTARY FACIES AND DEPOSTIONAL ENVIRONMENT

Abstract

Sedimentary facies analysis of the Ecca Group in the study area was performed in order to deduce their depositional environments. Fourteen lithofacies were identified and grouped into seven distinct facies associations (FAs), which are FA 1: Shale and mudstones intercalated with siltstones (Fls+Fss), FA 2: Carbonaceous shale, mudstone with chert beds (Fsc+Fsm), FA 3: Mudstone-claystone rhythmite with lenticular siltstone (Ftb+Fss), FA 4: Greyish medium bedded sandstone intercalated with laminated mudstone (Slt+SFt), FA 5: Dark-grey medium to thick bedded mudstone and siltstone (Fts+Fc), FA 6: Thin to medium bedded sandstone alternated with thin bedded carbonaceous mudstone (Fc+Fbm+Fms+SFm) and FA 7: Varved mudstone rhythmite intercalated with siltstone and sandstone (Frh+Srl). Based on the lithofacies analyses, it can be inferred that the Prince Albert (FA 1) and Whitehill Formations (FA 2) represents deep marine pelagic deposits. The overlying Collingham Formation (FA 3) represents suspension settling of mudstones intermixed with distal turbidites on the continental slope. The Ripon Formation that was subdivided into three facies associations: Lower Greywacke-Mudstone Association (FA 4), Middle Black Mudstone Association (FA 5) and the Upper Grey Mudstone-Sandstone Association (FA 6) represents alternated deep to shallow marine environment. FA 4, FA 5 and FA 6 represent mainly distal outer fan turbidites in the lower continental slope, pelagic sediments on the middle-upper continental slope, and continental shelf proximal turbidites, respectively. The overlying Fort Brown Formation (FA 7) represents lacustrine deposits. Sedimentological and sequence stratigraphic evidence revealed that the Ecca Group has progressively changed upwards from deep marine (FA 1, FA 2, FA 3, FA 4 and FA 5) to shallow marine environment (FA 6), and finally to lacustrine environment (FA 7). This implies that the Main Karoo Basin was gradually filling up with Ecca sediments resulting in the gradual shallowing up of the water depth of the depositional basin.

Keywords: Lithofacies, turbidites, depositional environment, facies model, Ecca Group

6.1 Introduction

The term "facies" was introduced into geology by Nicholaus Steno in 1669. The word "facies" is derived from a Latin word "facia" which means the external appearance or look of

something. Gressly (1838) used the word "facies" to describe the totality of the lithological and paleontological aspects of a stratigraphic unit. However, the term has been used by many geologists in different ways or context since then. The main argument about using the term is whether the term only applies to a particular set of characteristics as opposed to the stratigraphically unconfined rock bodies as used by Gressly (1838). On the other hand, whether the term only connotes "aerially restricted parts of a designated stratigraphic unit" as used by Moore (1949) or whether the term should be used purely for descriptive (i.e. mudstone facies) and interpretative purposes (i.e. fluvial facies) (Middleton and Hampton, 1976; Reading, 1978). Sedimentary facies is a body of sedimentary rock with specific petrological, compositional and sedimentary characteristics or features that reveal the conditions of the environment under which the rock was formed (Reading and Levell, 1996; Boggs, 2001).

The description of a sedimentary facies involve identifying and documenting all the characteristics that may be defined on the basis of lithology, colour, grain size, texture, fossil content and sedimentary structures or mineral compositions. Sedimentary facies are usually classified into two groups, i.e. lithofacies and biofacies. Lithofacies deals with the observable mineralogical or petrological characteristics like colour, grain size, sedimentary structures and mineral compositions; whereas biofacies points to biological characteristics like fossil contents. By identifying facies associations, it is possible to deduce the process or set of processes that prevail in the depositional environment. The processes that exist or present in the depositional environment resulted in the characteristics of a depositional environment, thus there is a connection between facies associations and depositional environment. However, several sub-environments may exist within a particular depositional environment, pointing to the fact that facies can vary within a particular depositional environment, which reflect the change from one sub-environment to the other within the same depositional environment. Hence, adjacent environments may be represented by the adjacent facies, and the ways in which these facies inter-relate with each other are always revealed in the characteristics of the facies change (Nyathi, 2014). This study provides new insight on detailed sedimentary facies analysis of the Ecca Group in the Eastern Cape Province of South Africa. The study is based on the integration of sedimentological data, including characteristics of lithology, sedimentary structures and vertical sequence patterns to refine the sedimentary processes and depositional paleoenvironments.

6.2 Materials and method

Road-cut exposures of the Ecca Group in the study area were examined in outcrops and boreholes. Lithologies and sedimentary structures were identified and investigated, and stratigraphic sections were measured using a measuring tape. Field data including lithology, colour, grain size, mineral composition, and sedimentary structures were obtained for each individual unit. Facies analysis of the stratigraphic formations was carried out using a modified version of lithofacies classification scheme by Miall's (1988a, 1988b, 1996). The scheme is based on bi-part or letter lithofacies coding system. The first part denotes lithology (G, gravel; S, sand; F, fine), whereas the second letter denotes distinctive sedimentary structure or texture of each lithofacies. In this study, a facies is a restricted lithofacies with specific sedimentary structures and constitutes a part of a stratigraphic unit with characteristics that significantly differs from other parts of the unit and is attributed to depositional features that point to a specific depositional process or combinations of processes. On a small scale, each of the stratigraphic member or formation is associated with a distinctive sedimentary facies based on their lithological characteristics and sedimentary structures. The description of the individual facies is in accordance with the work of Miall (1977), Miall (1995), Bordy and Catuneanu (2000), and Bordy et al. (2005). Facies association was deduced from the individual facies since individual facies cannot completely reconstruct or interpret the type of depositional environment and conditions that existed during the deposition of the sediments. The identified lithofacies types were grouped into facies associations (FAs) and used to interpret or deduce the possible depositional palaeoenvironments. Laboratory thin-section of microscope study was used to aid for the identification and distinguish different lithofacies, particularly the rock texture, grain size and mineral compositions.

6.3 Facies

The lithofacies in the different formations of the Ecca Group were identified based on different lithologies and sedimentary structures. Fourteen lithofacies were identified in the Ecca Group. The characteristics of these lithofacies are depicted in the Table 6.1.

Table 6.1: Lithofacies identified in the Ecca Group.

Facies Code	Facies	Sedimentary Structures
SFt	Thin to medium bedded sandstone interbedded with laminated shale	Thin to medium bedded, trough cross-bedding, and sometimes with deformational structures
SFm	Thin to medium bedded sandstone alternated with thin bedded mudstone	Thin to medium bedded, horizontal lamination, micro-cross lamination, current ripple cross-lamination, wavy lamination, graded bedding
Slt	Greyish lenticular and thin bedded sandstones	Fine grained, lenticular bedding
Srl	Ripple cross-laminated sandstone	Fine grained with ripple marks, or ripple lamination, sometimes with climbing ripple marks and low angle ($< 10°$) cross-lamination
Fc	Black thin to medium bedded carbonaceous mudstone	Thin to medium bedded, rich organic carbon or carbonized plant matter
Fbm	Dark thin bedded bioturbated mudstone	Thin bedded, roots, bioturbation and boring
Fls	Greyish laminated to thin bedded shale	Laminated to thin bedded, pencil cleavage
Fms	Greyish laminated to thin bedded mudstone and lenticular siltstone	Laminated, thin bedded, low angle cross bedding, deformational convolute bedding, slump structures
Frh	Greyish laminated mudstones rhythmite	Fine lamination to thin bedded, with laminae consisting of alternating light and dark coloured mudstone and claystone layers
Fsc	Greyish laminated shale intercalated with lenticular chert	Fine grained, thin laminated or lenticular bedded
Fsm	Laminated shale intercalated with mudstone and lenticular siltstone	Horizontally well-laminated, lenticular bedding, rich in organic carbon as well as iron sulphide (pyrite)
Fss	Black laminated to thin bedded shale with lenticular siltstone	Well laminated to thin bedded, lenticular bedding, sometimes with minor fine siltstone lenses and very small ripples
Ftb	Greyish mudstone and claystone turbidite	Varve bedded, fine lamination, micro-ripple laminations, climbing ripple lamination, convolute lamination and erosional wave mark structures
Fts	Dark-grey medium to thick bedded shale	Medium to thick bedded, massive beds sometimes faintly laminated and graded

6.3.1 Greyish laminated to thin bedded shale facies (Fls)

The rocks are predominantly well laminated and shows pencil cleavage (Figure 6.1). However, thin bedding (thickness of beds range from 3-9 cm) occurs at the base of the unit. At the exposure to the surface, the colour of the shale changes from greenish-grey to olive-grey half way up the unit and finally becomes khaki colour shale at the upper part of the unit. The khaki colour of the shale was the product of strong weathering that occurred as a result of tectonic uplift and exposure of the shale to atmospheric weathering. This resulted in the alteration of the original greenish-grey colour to khaki colour. The facies (Fls) is well developed in the basal part of Prince Albert Formation and is laterally extensive throughout the study area, covering several kilometers and lacks sandstone intercalation as well as current structures. The thickness of Fls is approximately 113 m in road-cut exposure of the Ecca Group along Regional road R67 (Ecca Pass). The topographic relief of Fls is presently very low because it crumbles easily and consists mostly of clay minerals.

Figure 6.1: Weathered laminated khaki shale with pencil cleavage in the lower part of Prince Albert Formation (Elevation: 461 m; Longitude E 26º 37′ 38.4″; Latitude S 33º 12′ 59.5″). The khaki colour is due to surface weathering and leaching.

6.3.2 Black laminated to thin bedded shale with lenticular siltstone facies (Fss)

Black laminated to thin bedded mudstone with lenticular siltstone facies (Fss) of about 30 m thick occurs just above the grey shale facies (Fls) along Regional road R67 (Ecca Pass; Figure 6.2). The shale is mostly thin bedded (at less than 8 cm for a single layer) with brownish soft materials that are rich in iron-bearing minerals like smectite, pyrite and

144

chlorite; thus they produce hematite after weathering. Due to the exposure of the black shale to surface, the original black colour of the shale changed to dark grey as a result of weathering. In few places, the mudstones are medium to thick bedded and faintly graded. Lenticular siltstone beds are intercalated within the mudstone. At the upper most part of the unit, reddish brown staining is present in the well laminated shales due to leaching/oxidation of iron-rich minerals (Figure 6.3).

Figure 6.2: Laminated to thin mudstone and lenticular siltstone (Fss) in the upper part of Prince Albert Formation.

Figure 6.3: Folded well laminated red stained shale and mudstone in the upper part of Prince Albert Formation (Elevation: 461 m; Longitude E 26º 37′ 38.4″; Latitude S 33º 12′ 59.5″).

In addition, weathered phosphatic lenses, and calcareous concretions of varying shapes and sizes (between 5cm and 13 cm thick) are scattered throughout in the unit. The red shales in Figure 6.3 are folded but still keep their lamination. Layers of iron rich minerals (pyrite and magnetite) are present at the topmost part of the unit. Underneath the microscope, the mudrocks are mainly made up of iron-rich clay minerals (mostly smectite and illite) with minor detrital grains of quartz, feldspar and muscovite. The detrital muscovites have been deformed. Apart from the iron-rich clay minerals, the dissolution and weathering of pyrite could also serve as alternative source of iron resulting in the red staining of the shales.

6.3.3 Greyish laminated shale intercalated with lenticular chert (Fsc)

The facies Fsc (Figure 6.4) is well developed in the Whitehill Formation. The shales of are generally extensive and well-laminated. The chert beds are greyish-black in colour and microcrystalline in nature, with no conspicuous organic carbon remains. The chert layers occur as lenticular beds incorporated into the shales. In addition, they are more resistant to weathering and darker in colour than the carbonaceous shale. The presence of chert points to the existence of silica (silicon dioxide or SiO_2) in the deep water prior to or during the deposition of the sediments. Besides the lenticular occurrence, the microcrystalline silicon dioxide occurs also as irregular nodules/concretions within the sediments; with time, these nodules/concretions may increase in size and merge with one another to form the nearly continuous chert layer within the sediment. The nearly continuous layers possibly indicate that the chert was chemically precipitated from the deep water. The organic materials within the clay sediments also serve as alternative source of silica from which the chert was formed. Some of the silicon dioxide in the chert is believed to have been formed through biological/biochemical process. A large number of diatoms and radiolarians that live in deep water tend to have a glassy silica skeleton, while some sponges produce "spicules" that are also made up of silica. When these organisms die, their silica skeletons are accumulated or settled to the bottom of the deep water, then dissolve and reprecipitate as chert lenses or nodules. The chert layers in the lower part of the unit are more dominant, thicker (3-8 cm thick layers) and longer (averaging about 2.1 m in length). Minor, thinner (less than 3 cm thick) and shorter chert layers (averaging about 0.45 m in length) are present in the upper part of the unit.

Figure 6.4: Laminated shale intercalated with chert layers (Fsc). Note: the carbon rich shale giving out a whitish colour after weathering.

6.3.4 Laminated shale intercalated with mudstone and lenticular siltstone facies (Fsm)

The shales are generally extensive, black-greyish in colour, well-laminated and rich in carbon as well as iron sulphide (pyrite). Fine to silt grained mudstones and minor lenticular sandstone layers are present in the basal part of the unit (Figure 6.5).

Figure 6.5: Laminated black-greyish shale with lenticular siltstone and minor sandstone (arrow) in the upper part of Whitehill Formation.

The carbon materials in the carbonaceous shales allowed for the dark grey colour to form. Some of the black-greyish carbonaceous shale has also been weathered to grey-whitish shale with patches of red and yellow shades. These shales are generally rich in iron sulphide (pyrite). Under the microscope, part of the black colour of the shale is weathering-off to give grey-whitish coloured shale due to subaerial oxidation of pyrite to gypsum.

6.3.5 Greyish mudstone and claystone turbidite facies (Ftb)

The facies (Ftb) forms the basal part of the Collingham Formation. It is a rhythmite consisting of alternation of regularly thin bedded mudstone and claystone (Figure 6.6). The claystone layers are yellowish and made up of purer clay mineral of bentonite that is assumed to be ash-fall tuffs (Figure 6.7). The claystones are soft, well laminated, crumbles easily, pale yellowish in colour and are relatively pure in clay mineral composition which resulted in their flakiness as well as crumble characteristics. The mudstone layers are hard, well laminated, greyish black in colour and finer grain sized. The original colour of the shales and claystones are assumed to be dark-grey. However, the greyish colour of the claystones has now changed to pale-yellowish colour due to weathering. Average thickness of the soft claystone and hard mudstone layers are 2.8 cm and 4.2 cm thick, respectively.
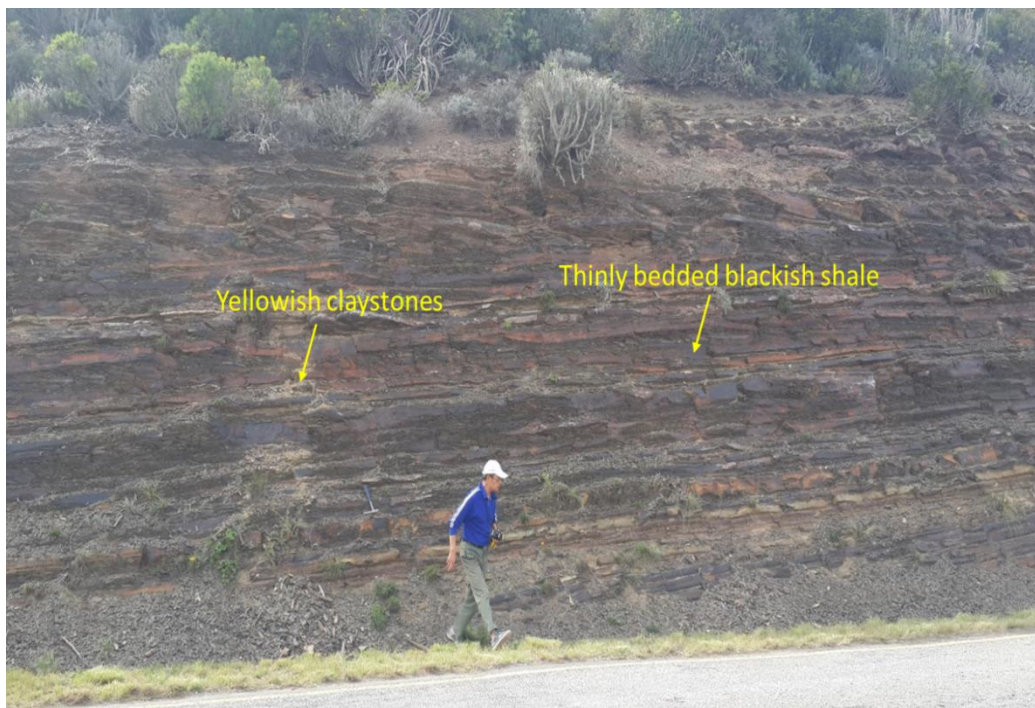
Figure 6.6: Greyish mudstone and claystone turbidite (Ftb) showing laminated to thin bedded greyish black mudstone layers and softer yellowish bentonite claystone layers which are thought to be ash-fall tuffs.
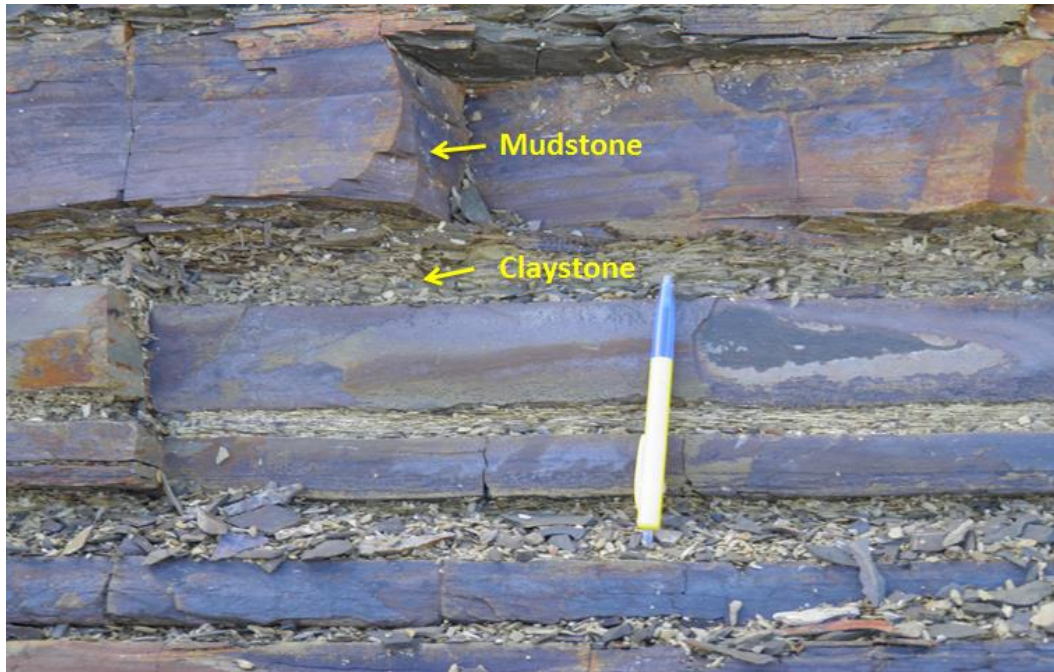
Figure 6.7: Well developed horizontal rhythmite of mudstone (hard and dark layers) alternated with claystone (soft and yellowish layers) in the basal part of Collingham Formation.

The claystones and mudstones constitute multiple cyclotherms of repeated units or couplets which is referred to as rhythmite. The rhythmite is well jointed with both horizontal and vertical joints. Very thin beds of softer, fine grained yellowish bentonite that is assumed to be volcanic ash fall tuffs. The shales are weakly graded in some places and split along bedding planes. Some of the shale contains brownish weathered calcareous concretions and small worm burrows. Generally, the mudstone beds exhibits horizontally lamination. In addition, micro-ripple laminations, climbing ripple lamination and ripple marks (Figure 6.8) have been found in the dark hard mudstone but are absent in the soft claystone layers. In some places, the claystones alternated with minor silty layers that are weakly graded.

Figure 6.8: Ripple marks in the mudstone and fine siltstone of the Collingham Formation along Regional road R67 between Grahamstown and Fort Beaufort (Ecca Pass).

6.3.6 Greyish lenticular and thin bedded sandstones facies (Slt)

The facies (Slt) occupies the basal part of the Lower Greywacke-Mudrock Member in the Ripon Formation and overlies the Ftb facies. It is mainly made up of very fine to fine grained lenticular bedded sandstones and sometimes horizontally laminated with low angle cross bedding. Furthermore, the original dark-grey colour of the sandstone has changed to light grey colour as a result of weathering (Figure 6.9). These sandstones are light-grey in colour, thin to thick bedded, poorly sorted and immature with sub-angular to sub-rounded grain shapes. Generally, the sandstones have irregular jointing pattern with the sub-horizontal joints being the most common and related to the bedding planes. In addition, steeper, straight and curved joints are present within the beds as well as cutting across the bedding planes. The thickness of the sandstone beds usually increases from the bottom to the top of the unit, with thickness ranging between 1.8 m and 13 m. Low angle cross bedding (averaging about 6°), joints and calcareous nodules are present in the light-grey coloured, medium to thick bedded sandstones.
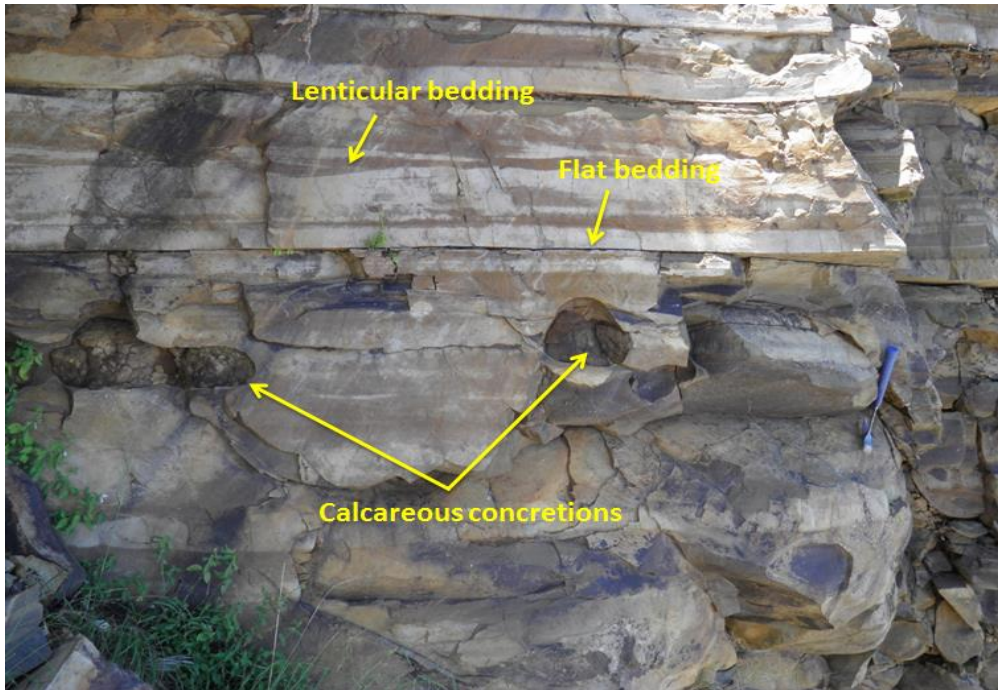
Figure 6.9: Greyish lenticular and thin bedded sandstones (Slt) with diagenetic nodules.

Under the microscope, the grains consist of quartz, potash feldspar and plagioclase and metamorphic, volcanic and igneous lithic fragments. The matrix is composed of kaolinite, sericite, illite and smectite. Calcium cement is the dominant cement in the rock. The nodules are thought to have been formed due to precipitation of calcium carbonate as well as the alteration or mineral replacement of feldspars to calcium carbonate. The presence of calcite cement also supports the earlier statement that calcium carbonates precipitated to form the nodules. Calcite concretions are mostly seen in the thick bedded and structureless sandstones and occasionally present in the thin bedded sandstones. The nodules are mostly spherical in shape although a few of them are elongated. Originally, the sandstones are dark-grey in colour, but have been weathered to greyish-white due to the alteration of feldspars to kaolinite. Apart from the calcitization of feldspar, diagenetic changes that are observed in the rocks are sericitization of feldspars, alteration of feldspar to illite as well as the recrystallisation of matrix materials.

6.3.7 Thin to medium bedded sandstone interbedded with laminated shale facies (SFt)

SFt occupies the upper part of the Lower Greywacke-Mudrock Member and overlies the Slt facies in the Ripon Formation. It consists of greyish thin to medium bedded sandstone alternating with laminated shale beds (Figure 6.10). The thickness of the sandstone beds vary between approximately 0.4 m and 35 m. The sandstone beds usually grade from fine grained

sandstone at the base to well-laminated siltstone and silty shale at the top. Generally, the contact between the sandstones and mudstones are sharp. In some places, the lower contact in the mudstones beds gradually grade from laminated siltstone to shale. Occassionally, some of the sandstone beds lack sedimentary structures with the shales only displaying lamination. The lack of lamination in the sandstones was probably due to sudden deposition. In most cases, small scale syn-depositional structures like horizontal and cross lamination (Figure 6.11), trough cross bedding (Figure 6.12), climbing ripple lamination (Figure 6.13), convolute bedding, plane parallel lamination, wavy bedding, and calcareous concretions are present in the medium bedded sandstones as well as in the coarse siltstones. Some of the sandstones in the upper part of the unit are mottled and are more vulnerable to weathering than the non-mottled sandstones. Mostly, the mottled sandstones tend to alternate with the non-mottled sandstones. Small trace fossils (worm trails) and calcareous concretions are occasionally present in the mottled sandstones. Deformational structures like flame structures, load casts, convolute bedding and small-scale ball and pillow structures are scattered throughout the unit.

Figure 6.10: Photograph showing sandstone intercalated with shale of SFt facies.

Figure 6.11: Horizontal and faint cross lamination in the sandstone of SFt facies.
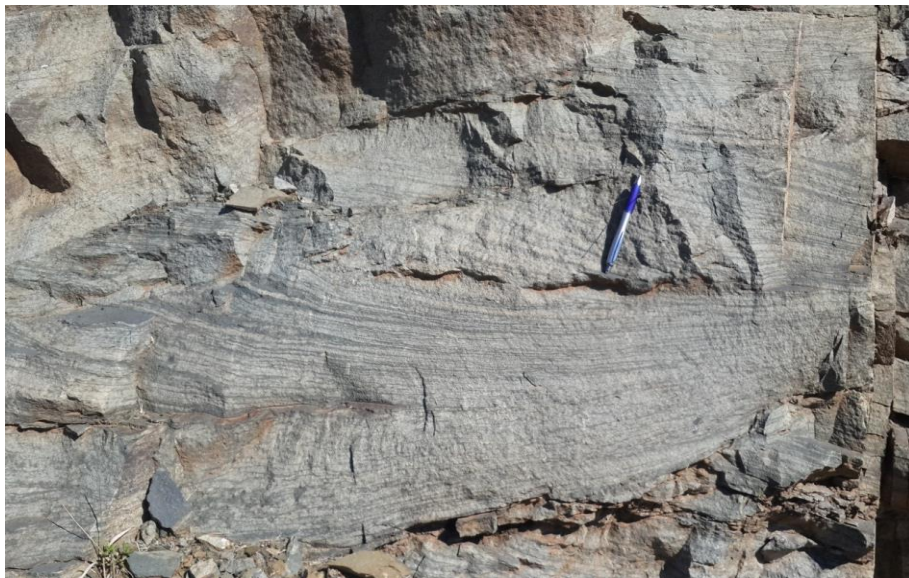
Figure 6.12: Trough cross bedded sandstone of SFt facies.

Figure 6.13: Climbing ripple lamination sandstone of SFt facies.

6.3.8 Dark-grey medium to thick bedded mudrock facies (Fts)

The Middle Black Mudrock Member of the Ripon Formation largely consists of medium to thick bedded dark-grey shale (Fts) (see Figure 3.29). The shale split perfectly along well-defined bedding planes. The thickness of the homogenous shale generally increases from east to west side of the study area (Figure 1.1). The westward increase in the thickness can be attributed to the large-scale slumping that occurred in the middle part of the member. Occasionally, the shale is massive with very faint lamination. Well-laminated, medium bedded shales are interbedded with four small-scale sandy beds at the upper part of unit. The massive shale beds probably developed in a river channel where sediments were deposited from a fast flowing current carrying a large volume of suspended sediments. These currents then experienced a rapid decrease in velocity and the suspended sediments were suddenly deposited resulting in the massive beds. The rate at which the current flows give no time for internal layering to developed, thus most of the shale shows massive bedding and faintly graded in some places.

6.3.9 Black thin to medium bedded carbonaceous mudrock facies (Fc)

The Upper Black Mudrock-Sandstone Member of the Ripon Formation is made up of thin to medium bedded sandstones alternating with mudrocks (see Figure 3.30). The basal part of the member (thickness of about 12 m from the top of Fts facies) is made up of tabular laminated, organic-rich black shale with greyish mudstone (Fc). The basal shale layer is dark-grey in colour, homogenous, and faintly laminated. The dark-grey colour of the shale becomes greyish-black (5-7 m) and eventually changes to black in the upper part of the basal shale layer (9-12 m). The change in the colour of the shale signifies that the organic carbon content increases from bottom to the top of the basal shale layer. It is thought that the persistence of the reducing conditions/environment resulted in the increase of organic carbon content. Very small micro cross-lamination of about 2 mm thick occurs in some of the thin bedded mudstones. Mostly, the black shales are well-laminated and crumble easily as compared to the dark grey and greyish-black shale. The crumble or flaky nature of the black shale can be attributed to their high organic carbon content, as well as the alignment of clay particles and presence of laminae.

6.3.10 Dark thin bedded bioturbated mudstone facies (Fbm)

Dark thin bedded bioturbated mudstone (Fbm) occurs in the Upper Black Mudrock-Sandstone Member of the Ripon Formation, just above the Fc facies. The mudstones have

traces of plant fossils (Figure 6.14). The presence of these trace fossils perhaps point to shallow waters in the depositional basin, which allows plants to flourish in the presence of sunlight. The original dark or black colour of the mudstone changed to the present light grey colour due to weathering.

Figure 6.14: Trace fossils (burrows) in the mudstone of the Ripon Formation.

6.3.11 Greyish laminated to thin bedded mudstone and lenticular siltstone facies (Fms)

The Fms facies occur in the Upper Black Mudrock-Sandstone Member of the Ripon Formation and it is made up of greyish laminated to thin bedded mudstone and lenticular siltstone facies (Figure 6.15). The laminations on the siltstone are thin, perhaps indicating that the supply of silt materials into the depositional basin was deficient. The siltstones show low angle cross bedding (Figure 6.16) and unidirectional scouring surfaces. In some places, especially near the top of the unit, these structures have been truncated and their amplitude considerably decreased. It is believed that the siltstone surfaces were probably reworked by erosional processes. The sedimentary structures that were observed on the mudstones include deformational convolute bedding and folding structures (Figure 6.17).

Figure 6.15: Greyish laminated to thin bedded mudstone (dark colour) intercalated with lenticular siltstone (light colour).

Figure 6.16: Micro low angle cross bedding on the lenticular siltstone (arrow) of Fms facies.

Figure 6.17: Recumbent deformation structures in the greyish mudstone of the Ripon Formation.

6.3.12 Thin to medium bedded sandstone alternated with mudstone facies (SFm)

The SFm facies cover the largest extent of the Upper Black Mudrock-Sandstone Member in the Ripon Formation. It consists of thin to medium bedded sandstones alternating with thin bedded mudstones. The basal part of the unit is made up of greyish-black organic-rich shale with light-grey mudstone and sandstone (Figure 6.18). In the middle to upper part of the unit, the sandstones are dark grey in colour and very fine to fine grained. Micro-cross lamination and current ripple cross-lamination are present in the sandstone beds. In some places, micro-cross lamination is associated with wavy lamination (Figure 6.19), ball and pillow load cast structures.

Figure 6.18: Thin to medium bedded sandstone alternated with thin bedded mudstone.
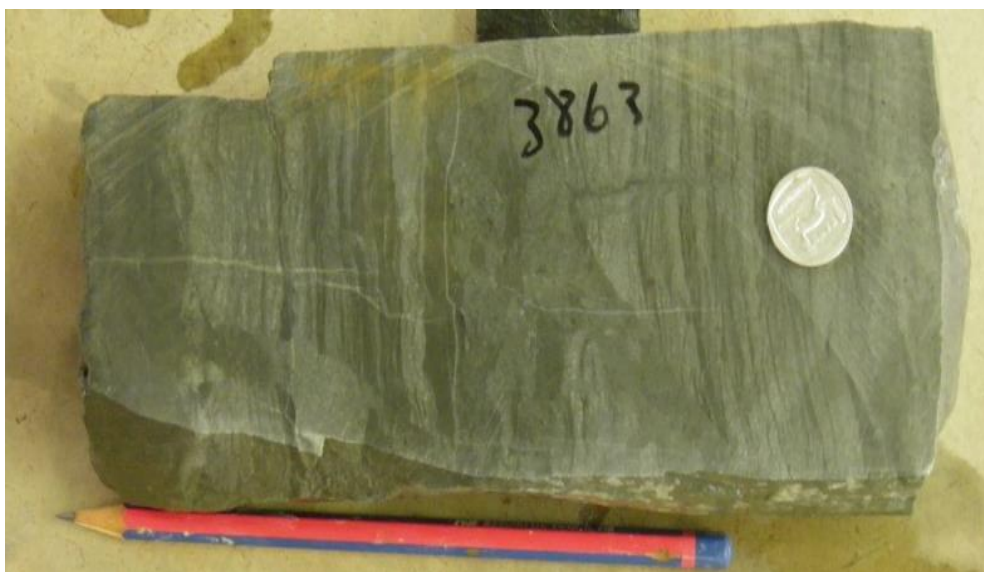
Figure 6.19: Wavy laminated sandstones of SFm facies (core sample).

The sandstone beds in the upper part of the unit often shows continuous trend of A (graded bedding), B (horizontal lamination), and C (micro-cross lamination) of the Bouma sequences (Bouma, 1962). The upper mudstone units are faintly laminated and thin bedded. The thickness of mudstone beds increases from about 0.4 m in the basal part to roughly 4.3 m in the upper part of the unit. The mudstones have higher amount of carbon materials compared to the sandstones and this is evidence in the greyish-black colour of the mudstones. In some places, the laminated sandstone grades upwards into poorly defined wavy laminated silty shale. Some of the slightly silty shale bed shows indistinct graded bedding. In most cases, the upper and lower boundaries between the shale and sandstone are sharp. However, some of the upper contacts are irregular and this irregularity can be attributed to load casting of the overlying sandstone bed. Erosional surface and worm burrows (Figure 6.20), few calcareous concretions, small-scale ball and pillow structures, disc structures and load casts are present in some of the sandstone bed. The sandstones are originally greyish in colour but they have been weathered to reddish-brown in the exposure along Grahamstown-Adelaide road (Figure 6.21).
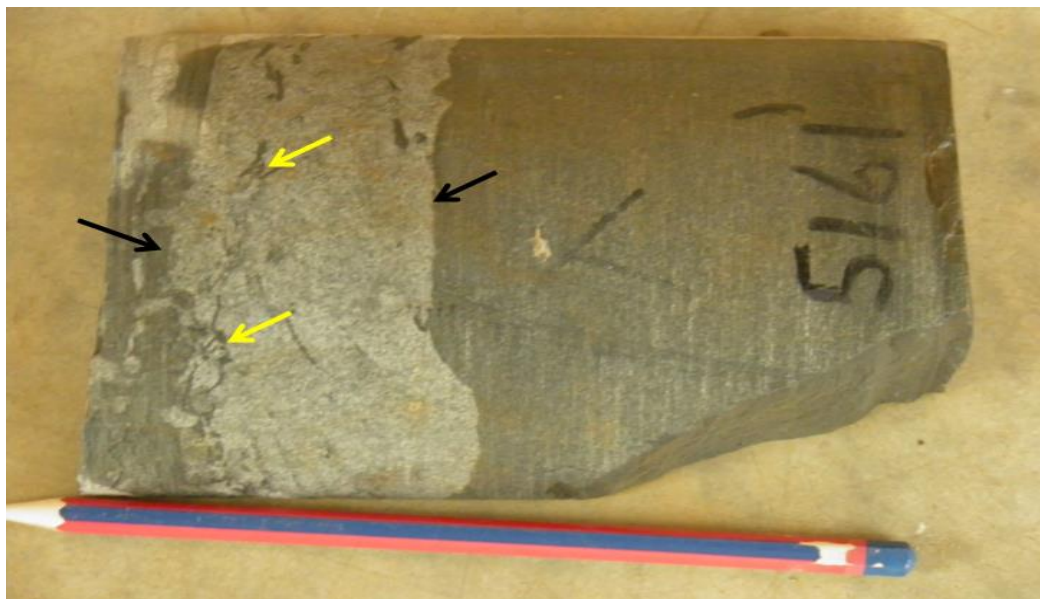
Figure 6.20: Photograph showing erosional surface (black arrows) and mudrock intraclast (dark colour part; yellow arrows) in the bottom of sandstone (whitish).

Figure 6.21: Greyish thin to medium bedded sandstone intercalated with thin bedded shale. The red-brownish colour is due to weathering after exposed to surface.

6.3.13 Greyish laminated mudstones rhythmite facies (Frh)

The basal part of Fort Brown Formation is entirely made up of Frh facies. It consists of greenish-grey, well laminated to thin bedded mudstone varved rhythmite. The varved rhythmites are represented by the regular alternation of claystone and siltstones (Figure 6.22).

Figure 6.22: Greyish laminated mudstones rhythmite facies (Frh). The alternated light and dark coloured mudstone depict seasonal changes.

The light coloured varve layers are siltstones, whereas the dark coloured varve layers mainly consist of clay minerals. The thickness of the regularly alternated light and dark coloured layers are approximately the same, ranging from about 0.3 mm up to 2.0 mm. The alternation is perhaps as a result of compositional changes as well as changes in grain sizes of the sediments. The light coloured (coarser) sediments were transported into the basin when the flow of water energy was high, whereas the dark coloured (finer) sediments were deposited from suspension settling when the flow of the water was slow. The rhythmites are lacustrine facies. The alternated light and dark coloured mudstones reflect deposition of summer and winter seasonal changes.

6.3.14 Ripple cross-laminated sandstone facies (Srl)

The Srl facies occur in the upper part of Fort Brown Formation and is interbedded with the Frh facies. The sandstones are very fine to fine grained, thin bedded and often shows ripple-cross lamination (Figure 6.23). The thickness of the sandstone layers increase upwards. Several finely laminated siltstones, shale and a few medium bedded sandstones are present in the upper part of the unit. The contact between the shale and sandstone are mostly sharp, and some of the sandstone beds grade into shale. In addition, the shale is occasionally silty with faint to well-developed lamination.
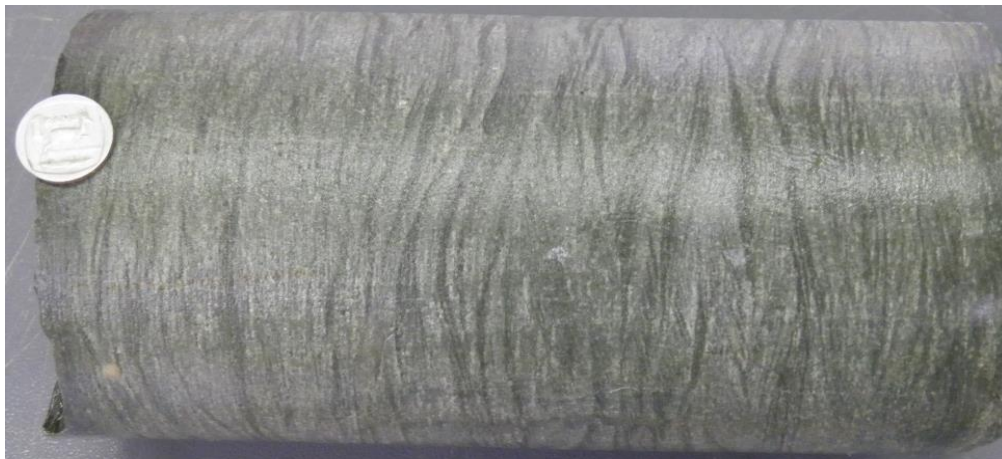
Figure 6.23: Wavy ripple-lamination in the sandstone beds of the Upper Member of Fort Brown Formation (core sample).

Generally, where the shale is very silty, it tends to be olive-grey in colour, well laminated, graded and displays a blocky type of weathering. But where the silty content is low or small, the shale usually has a dark-grey to black colour and exhibit pencil cleavage. A few of the current rippled sandstone beds are very calcareous with laminae that are characterized by

brownish weathered surfaces. Cross-beds with average length of about 25 cm are well defined in the upper part of unit (Figure 6.24). Trace fossils (trails, horizontal and vertical worm burrows) are fairly abundant in the sandstone beds.

Figure 6.24: Weathered greyish cross-bedded sandstones with multiple reactivation surfaces.

6.4 Facies association

Seven distinct facies associations were recognized and interpreted based on the identified lithofacies type, internal and external geometry in the formations. The characteristics of the facies associations (FA) are summarized in the Table 6.2.

Table 6.2: Facies associations identified in the Ecca Group.

Facies association	Facies code	Interpretation of depositional environments
FA 1: Shale and mudstones intercalated with siltstones	Fls, Fss	Deep marine deposits, mainly deep pelagic sediments
FA 2: Carbonaceous shale, mudstone with chert beds	Fsc, Fsm	Deep marine deposits, deep basin pelagic sediments
FA 3: Mudstone-claystone rhythmite with lenticular siltstone	Ftb, Fss	Deep marine deposits, suspension settling of mud intermixed with distal turbidites on the continental slope

FA 4: Greyish medium bedded sandstone intercalated with laminated mudstone	Slt, SFt	Deep marine deposits, distal outer fan turbidites on the continental slope
FA 5: Dark-grey medium to thick bedded mudstone and siltstone	Fts, Fc	Deep marine deposits, pelagic sediments on the middle - upper continental slope (upper to midfan sediments)
FA 6: Thin to medium bedded sandstone alternated with thin bedded carbonaceous mudstone	Fc, Fbm, Fms, SFm	Shallow marine deposits, mainly proximal turbidites on the upper continental shelf
FA 7: Varved mudstone rhythmite intercalated with siltstone and minor sandstones	Frh, Srl	Lacustrine deposits, distal turbidites

6.4.1 Shale and mudstones intercalated with siltstones (FA 1)

FA 1 is made up of Fls and Fss facies, and it covers the Prince Albert Formation. It is greyish in colour and shows coarsening upward sequence with the basal part comprising of the Fls facies, whereas the upper part is made up of the Fss facies. The contact between Fls and Fss is sharp but in few cases, it is gradational. FA 1 reaches a maximum thickness of about 145 m along Regional road R67 (Ecca Pass), with an average thickness of 131 m in the Eastern Cape Province.

6.4.1.1 Interpretation

FA 1 is interpreted as deep-sea (pelagic) sediments. The lateral extensive, well-developed lamination, fine-grained homogenous nature, as well as the absent of current structures and sandstone intercalation in the FA 1 point to deposition in a relatively deep, undisturbed large body of water environment, possibly a deep sea basin or abyssal plain. Kingsley (1977) documented that the homogeneity of the dark colour and appearance of the mudrock (FA 1) over a relatively large area perhaps indicate uniform environmental condition during the deposition of the pelagic sediments. The dominant of smectite-illite clay minerals in FA 1 with relatively high pyrite content possibly indicate suspension settling of mud in a relatively deep water reducing environment. The slightly graded siltstones near the top of FA 1 were deposited as a result of suspension settling or tractional fall-out from low-density turbidity

currents. Furthermore, the well-developed lamination and the pyrite-rich sediments may also indicate a slower depositional rate and possibly a scarce source of sediment supply when considering the lamination which is usually less than 3 mm in thickness. The weathered phosphatic lenses/concretions were probably formed as a result of biological or chemical precipitation under anoxic conditions in areas where cold water upwelling occurred. This upwelling current could have enhanced the rich marine life, which supplied the organic matters that were trapped in the bottom mud. The aforementioned characteristics tend to favour a deep-sea marine environment. The organic matters accumulated under reducing or anoxic condition in a deep marine environment, probably were the main source for shale gas hosted in the Ecca Group.

6.4.2 Carbonaceous shale, mudstone with chert beds (FA 2)

FA 2 correspond to the Whitehill Formation and it is approximately 42 m thick in the road-cut exposure of the Ecca Group along Regional road R67 (Ecca Pass), averaging 28.6 m thick in road-cut exposures in the Eastern Cape Province. The basal, middle and upper parts of FA 2 are made up of Fc, Fsc and Fsm facies, respectively. Thus, they show coarsening upward sequence. Fsc and Fsm facies dominates FA 2. Occassionally, water escape or deformation structure is present in the Fsm facies. The contact between Fc and Fsc is gradational, whereas the contact between Fsc and Fsm is sharp.

6.4.2.1 Interpretation

The presence of organic carbon in FA 2 suggests that the deep-sea basin was anoxic (or under reducing condition). The chert layers point to a chemical or biochemical precipitation in a deep marine environment. The shales are generally extensive, black in colour, thin bedded, well-laminated, rich in carbon as well as iron sulphide (pyrite), and has subordinate black chert layers. The aforementioned characteristics are almost the same with the characteristics that was envisaged by Pettijohn (1957) for the true euxinic (black shale) facies which are exclusively of marine environment. The black colour, fine-grain size, and laminated structure in FA 2 indicate deposition by suspension sedimentation in a low-energy, deep marine environment, presumably a deep sea floor or deep sea plain environment. Thus, FA 2 represents deep marine or pelagic basin deposits.

6.4.3 Mudstones-claystone rhythmite with lenticular siltstone (FA 3)

FA 3 comprises of the Ftb and Fss facies, making up the Collingham Formation. The contact between Ftb and Fss facies is gradational. FA 3 shows finning upward sequence with Ftb facies making up the basal part, while the upper part comprises of the Fss facies. FA 3 (Collingham Formation) reaches a maximum thickness of about 60 m in road-cut exposure along the Ecca Pass, with an average thickness of about 64 m in the Eastern Cape Province.

6.4.3.1 Interpretation

The laterally extensive individual bed, fine grained characteristics as well as the absence of current structures in the FA 3 point to deposition in relatively deep water, probably a deep-sea basin. The regularly alternation of thin bedded mudstones and claystones (Ftb) depicts a classic rhythmite facies, which possibly signify that the deposits were probably turbidite sediments in origin. The laminated mud point to pelagic sedimentation or fine grained low-density turbidity deposition. The combination of climbing ripple cross lamination, parallel lamination and ripple cross lamination within the hard mudstone beds (Fss) also support the assumption that low-density distal turbidity currents existed during the time deposition of the pelagic sediments. Turbidites in ancient and modern basins are mostly reported from deep-sea marine basins near continental slope, thus deformation bedding could have occurred as a result of slope instability. However, Bartolini et al. (1975) documented that turbidity currents could also exist in shallow and non-marine environments. The presence of the wave mark structures point to the fact that the water energy was not always quiet during the deposition of the thin bedded sediments. The hard mudstones layers with horizontal lamination and graded bedding, ripple lamination are alleged to have been deposited in a relatively disturbed water period, showing that the energy of the turbidity current rises and fall or varied irregularly when the sediments were deposited. FA 3 is interpreted as suspension settling of mudstones intermixed with distal turbidites on the continental slope. The turbidity current that transported the sediments into the deep basin is thought to be non-channelized or have spread across a wide front from a depositionally active prograding slope as envisaged by Kingsley (1977) rather than turbidity current that moved along the channels.

6.4.4 Greyish medium bedded sandstone intercalated with laminated mudstone (FA 4)

FA 4 is made up of Slt and SFt facies. It is greyish in colour and covers the Lower Greywacke-Mudrock Member of the Ripon Formation. The basal part of FA 4 comprises of the greyish lenticular and thin bedded sandstones facies (Slt) whereas the upper part is made

up of thin to medium bedded sandstone interbedded with laminated mudstone facies (SFt). The contact between Slt and SFt facies is sharp.

6.4.4.1 Interpretation

The co-existence of depositional and deformational structures like current ripple lamination, convolute bedding and graded bedding in FA 4 shows that the sandstone beds are of turbidity current origin. The presence of thick convolute bedding in the basal sandstone bed signifies fast rate of deposition, just above the bed where convolute bedding occurred, the thickness of the overlying sandstone beds increases which also support fast rate of sediments supply from the source area. The pelagic sediments are believed to have been eroded/transported down the slope by turbidity current or by a large river system. The ideal conditions for the development of lenticular bedding is usually a shallow sea and intertidal flats where tidal currents are active. However, the well-developed lenticular beddings and numerous perfect joints in the basal sandstones of FA 4 point to existence of tides in the depositional environment. It is believed that the turbidites could have been possibly reworked by tidal currents. The multiple cyclicity of alternating sandstone and mudstone layers point to the fact that the turbidites are essentially related to autocyclic processes like fan progradation or recession and lobe-switching among others (Walker, 1978). Kingsley (1977) documented that the turbidity current that transported the Ecca sediments down the slope must have spread across a wide front from a depositionally active prograding slope instead of turbidity current that moved along the channels. The transportation of the turbidites down the slope in the turbidite fan complexes is possibly associated with the major regression that occurred during the Ecca time. The general thickening upward sequence of FA 4 also point to the fact that the depositional lobe progrades since marginal facies in depositional lobes are expected or thought to be thinner bedded than those near the apex of the lobe. FA 4 is interpreted as distal outer fan turbidites in the lower continental slope environment (lobe region).

6.4.5 Dark-grey medium to thick bedded mudstone and siltstone (FA 5)

The Middle Black Mudrock Member of the Ripon Formation largely consists of dark-grey medium to thick bedded mudstone and siltstone (FA 5). FA 5 is made up of Fts and Fc facies and dark-grey colour is due to their enrichment in organic carbon. The homogenous shale in FA 5 split perfectly along well-defined bedding planes.

6.4.5.1 Interpretation

FA 5 represents pelagic sedimentation or low energy periodic sedimentation, low-density turbidity current deposition (moderate depth setting) in the middle - upper continental slope environment. Kingsley (1977) reported that FA 5 marks a recession in the supply of sediments possibly during a period of small transgression of the southern basin edge. The parallel horizontal laminated shale suggests turbulent suspension in a relatively deep water environment with frequent variation of hydrodynamic energy. Decreased organic-carbon content in FA 5 point to increased clastic dilution, as well as increased rate of consumption by benthic organisms.

6.4.6 Thin to medium bedded sandstone alternated with thin bedded carbonaceous mudstone (FA 6)

The Upper Black Mudrock-Sandstone Member of the Ripon Formation is made up of FA 6 that consists of Fc, Fbm, Fms and SFm facies. FA 6 is generally greyish-black in colour with the basal, middle and upper parts consisting of Fc and Fbm, Fms, and SFm facies, respectively. SFm facies cover the largest part of the Upper Black Mudrock-Sandstone Member in the Ripon Formation (FA 6). Most of the mudstones are thin bedded and have traces of plant fossils. The thickness of mudstone beds increases from about 0.4 m in the basal part to roughly 4.3 m in the upper part of FA 6. In most cases, the upper and lower boundaries between the mudstone and sandstone are sharp and occasionally irregular.

6.4.6.1 Interpretation

The alternation of sandstone and mudstone beds point to deposition under fluctuating energy conditions. The laminations and flat beds in the mudstones are indicative of quiet waters and slow settling of the sediments, whereas the thin to medium beds of the sandstone layers are indicative of rapid deposition and high water energy during the deposition. The presence of parallel laminated shale in FA 6 possibly shows that the sediments were deposited in floodplain environments with frequent variation of hydrodynamic energy. The presence of carbonaceous mudstone points a moderate growth of vegetation in the depositional environment. The trace fossils/burrows possibly point to shallow waters in the depositional basin, thus letting or permitting plants (vegetation) to flourish in the presence of sunlight. The organic carbon-rich shale and mudstone were able to accumulate in the swamps that form on the flood plains. The medium bedded mudstone in FA 6 was due to the aggrading of the

braided streams, resulting in the deposition of the thick fine grained sandstone in the river channel. FA 6 is interpreted as proximal turbidites in the continental shelf.

6.4.7 Varved mudstone rhythmite intercalated with siltstone and sandstones (FA 7)

The Fort Brown Formation is entirely made up of FA 7. It consists of varved, well laminated to thin bedded greenish-grey mudstone rhythmite (Frh) with minor sandstones intercalation (Srl). The basal part of FA 7 is made up of the Frh facies whereas mudstones are intercalated with Srl facies in the upper part of FA7. Thus they show coarsening upward sequence. In addition, thickness of the sandstone layers increases upward. Several finely laminated siltstones and a few medium bedded sandstones are present in the upper part of FA 7.

6.4.7.1 Interpretation

The regular alternation of layers of light (coarser) and dark (finer) sediments (varved rhythmite) possibly signify a fluctuating sedimentary supply and that the lake freezes seasonally. The FA 7 is believed to have been deposited in lacustrine environment due to the existence of well-developed varved rhythmite structure and seat-earth layers. The abundance of finely laminated siltstone in the upper part of FA 7 point to sedimentation from suspension settling took place continuously. Consequently, the intercalated sandstone beds were deposited during periods of high energy floods when there was influx of fluvial sediments. It is believed that, in places where there was sufficient sand, ripple marks were formed and these rippled sandstone lenses points to periodic influxes and deposition of current-borne sediment which was later affected by wave action. The deposition of the sediments must have taken place below the wave base because wave formed rippled marks are only present in the upper part of FA 7. The increase in the sandstone interbeds upwards as well as the occurrence of wave ripples in the upper part of FA 7 and the general coarsening upward sequence of FA 7 point to a slightly more proximal turbidites in the prodelta setting and shallowing up of the basin as a result of continued accumulation or deposition of sediments. FA 7 perhaps represents lake (lacustrine) deposits. FA 7 is more argillaceous and Kingsley (1977) proposed that it represent deposition in a pro-delta setting.

6.5 Depositional environments

Detailed analysis of the fourteen lithofacies types and seven identified facies association in the Ecca Group clearly point to three main depositional environments, namely, deep marine, shallow marine and lacustrine depositional environments. The deep marine environment

consist of deep plain sediments (FA 1: Shale and mudstones intercalated with siltstones, Prince Albert Formation), restricted deep-basin with hydrothermal silica (chert) sediments (FA 2: Carbonaceous shale, mudstone with chert beds, Whitehill Formation), continental slope turbidite deposits (FA 3: Mudstones-claystone rhythmite with lenticular siltstone, Collingham Formation), distal outer fan turbidites on the lower continental slope (FA 4: Greyish medium bedded sandstone intercalated with laminated mudstone, Lower Member of the Ripon Formation) and pelagic sediments on the middle - upper continental slope (FA 5: Dark-grey medium to thick bedded mudstone and siltstone, Middle Member of the Ripon Formation). The shallow marine environment is made up of continental shelf proximal turbidites (FA 6: Thin to medium bedded sandstone alternated with thin bedded carbonaceous mudstone, Upper Member of the Ripon Formation). The lacustrine environment consists of more proximal turbidites in the prodelta setting or distal turbidites (FA 7: Varved mudstone rhythmite intercalated with siltstone and minor sandstones). The Ecca sequence shows a progressive change upwards from deep-water marine environment (basin plain-continental slope) to shallow marine environment (continental shelf), and finally to lacustrine environment.

From bottom towards the top of the Ecca succession, it is believed that the Prince Albert (FA 1) and Whitehill Formations (FA 2) were deposited in a deep-water marine environment. The latter was deposited in more restricted part of the deep marine water, thus allowing the chert layers in the carbonaceous shale of FA 2 to develop. The source of the silica for chert formation probably came from underwater hydrothermal or volcanic silica. The overlying Collingham Formation (FA 3) is interpreted as suspension settling of mud intermixed with distal turbidites on the continental slope. The classic rhythmite facies in FA 3 signify that the deposits are of turbidite sediments in origin and formed in a reducing environment, presumably a marine continental slope environment. This Ecca turbidite sequence is thought to have experienced a major volcanic event thus the mudstone and bentonite claystone turbidite was accumulated on the basin floor. The presence of volcanic materials in FA 3 points to volcanic activity at near the source area and lead the formation of bentonitic claystone. These volcanic materials are thought to ash-fall in the sea due to the fact that the thin layers of the volcanic materials can be traced over relatively long distance. If the materials were deposited by turbidity current, they would have intermixed with other detrital materials. But since the yellowish material retained their pure volcanic nature (not intermixed), they are believed to be of ash-fall origin. The distal turbidites and volcanic ash

layers in FA 3 is the only layer of the Ecca Group that can be directly linked to the volcanism with evidence of active volcanic ash. There is possibility that these tuff beds are products of the Permian silicic-andesitic and volcanoes (Veevers et al., 1994; Wickens, 1994). Palaeocurrent, thickness and provenance studies by Kingsley (1977) also indicate that the Ecca sequence was sourced from the south-southeast and deposited in an east-west trending Karoo Basin.

The sandstone of the Lower Greywacke-Mudstone Member (Pluto Vale Member) of the Ripon Formation (FA 4) is interpreted as distal turbidites on the lower continental slope. Most part of the member is occupied by FA 4 due to slumping of sediments over a wide area. The multiple cyclicity of alternating sandstone and mudstone layers in FA 4 point to the fact that the turbidites are essentially related to autocyclic processes like fan progradation or recession and lobe-switching among others (Walker, 1978). The overlying shale unit (Middle Black Mudstone Member) of the Ripon Formation (FA 5) represents low energy sedimentation in a continental slope environment. This marks a recession in the supply of sediments possibly at a period of small transgression occurred in the southern edge of the Karoo Basin. The shallow marine environment is mainly made up of proximal turbidites on the continental shelf (FA 6, Upper Member of the Ripon Formation), while the lacustrine environment consist of lacustrine deposits (FA 7, Fort Brown Formation). The varved rhythmite in the lower part of FA 7 is believed to represent lake (lacustrine) deposits that was formed as a result of vertical aggradation and possibly some progradation during successive floods. The regular alternation of varve layers of light and dark sediments which show typically varve rhythmite of layer structure, signifying a fluctuation of seasonal sediment supply and deposition of the well-developed varves.

Kingsley (1977) documented that this flooding period is noted by the gradual increase in the rate of sedimentation as well as the shallowing of the environment when a fast or rapid regressions or regressive episode occurred which is characterized by the presence of relatively shallow-water muds, silts and sands. The abundance of finely laminated siltstone intercalated in mudstone in the upper part of FA 7 point to sedimentation from suspension settling shifted to traction settling, and the intercalated sandstone beds were deposited during periods of high energy floods when there was influx of fluvial sediments. The increase in the sandstone interbeds upwards as well as the occurrence of wave ripples and the general coarsening upward sequence point to a more proximal sedimentation and shallowing up of the basin as a result of continued accumulation or deposition of sediments. The Beaufort

Group that overlies the Ecca Group comprises mainly of sandstones and minor shale. It is believed that the group was deposited in a fluvial environment and could be linked to the continuous dropping or retreating of the water as a result of sea-level dropping of the Karoo Basin. Thus the depositional environment subsequently changed from a marine setting to deltaic and then continental inland fluvial environments. This also agrees with the findings of Catuneanu and Elango (2001) that the deeper marine facies of the early Ecca Group were accumulated during the under-filled phase of the foreland system, whereas the shallow marine facies of the late Ecca Group correspond to the filled phase of the basin, which was followed by an overfilled phase dominated by fluvial sedimentation of the Beaufort Group.

6.6 Facies model

Facies model is thought to be a general summary of a particular sedimentary process and depositional environment. Internal sedimentary structures, boundary conditions lithofacies, their inter-relationship, sequence and facies associations are taken into consideration for the interpretation of depositional environments. Likewise, in the studied portion of the southeastern Karoo deposits (Ecca sediments), sedimentation commenced with the deposition of mudstones intercalated with siltstones and carbonaceous shale, with subordinate chert and sandstone layers (deep marine environment). This sequence is overlain by mudstones rhythmite with thin bedded mudstone and lenticular siltstone on the lower continental slope. In addition, the overlying medium bedded sandstone intercalated with laminated mudstone and medium to thick bedded mudstone and siltstone are both deposited on the middle to upper continental slope. This sequence is overlain by thin to medium bedded sandstone alternated with thin bedded carbonaceous mudstone deposited on the continental shelf (shallow marine environment). Subsequently, the varved mudstone rhythmite intercalated with sandstone (Fort Brown Formation) accumulated in a lacustrine environment. In here, facies model for the depositional environment of the Ecca sediments is expressed as a geographical and depositional process restoration which shows deep marine basin and turbidity dynamics as well as their deposits by using a simplified depositional model for the Ecca sediments in the southeastern Karoo Basin. Most of the Ecca turbidites occurred at the base of the continental slope, resulting in the formation of a turbidite fan complex. The fan was differentiated into an outer fan (distal fan), midfan and proximal fan consisting of hemipelagic sediments that encloses large sandstone bodies resulting from the filling of fan valleys (Figur 6.25). This was done in accordance to Walker (1978) who attempted to

combine the model of Normark (1970) and Mutti and Ricci Lucchi (1972) on a research of facies, facies models and modern stratigraphic concepts. The graphic map and proposed depositional model for the Ecca sediments in the southeastern Karoo Basin in South Africa is depicted in Figures 6.26 and 6.27.
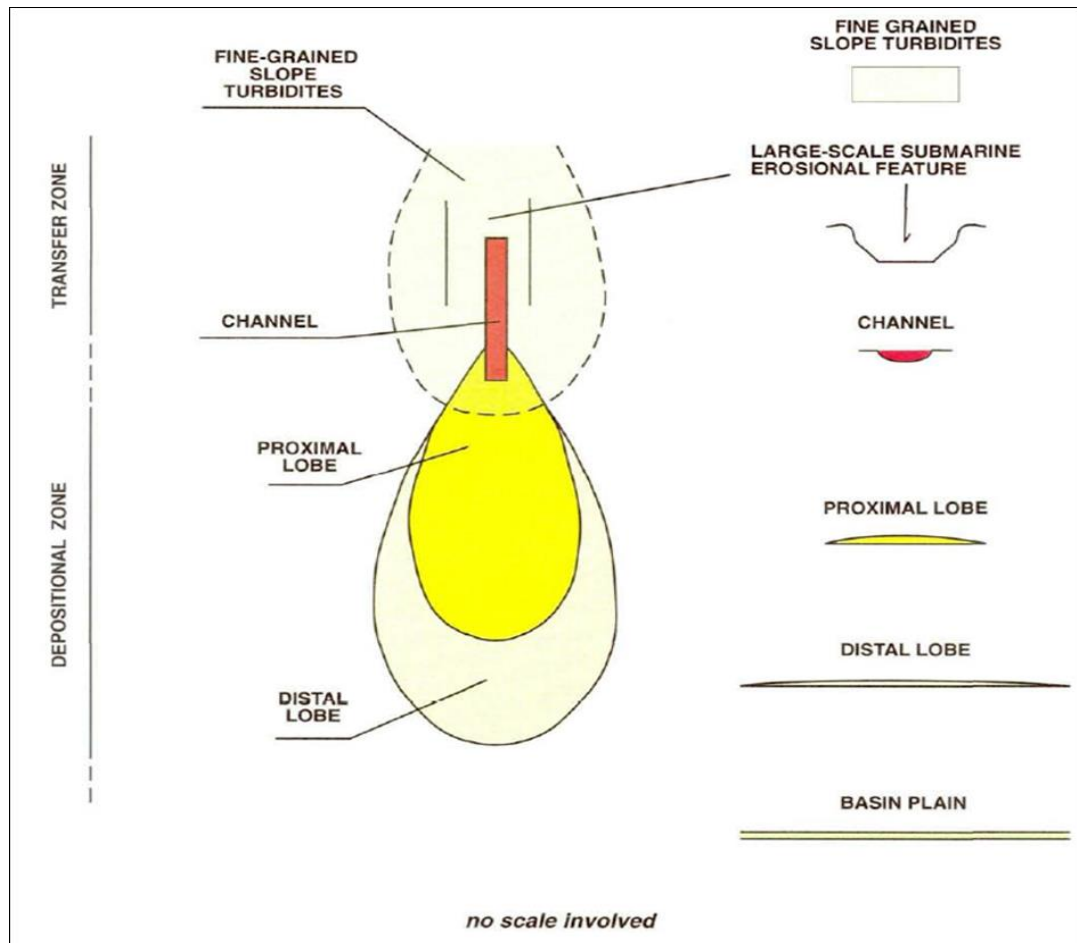
Figure 6.25: Simplified fan model showing the basics of all ancient and modern fans (After Mutti et al., 1999).

GRP.	FORMATION	FACIES ASSO.	LITHOLOGY	DESCRIPTION	INTERPRETATION	DEPOSITIONAL ENVIRONMENT	CLIMATE CHANGE
ECCA GROUP	FORT BROWN	FA 7		Varved mudstone rhythmite intercalated with sandstone	Lake deposits	Lacustrine	Warm temperature
	RIPON	FA 6		Alternated thin to medium bedded sandstone and shale	Mainly proximal turbidites on the continental shelf	Shallow marine	Relatively warm temperature (warm up)
		FA 5		Medium bedded dark-grey mudstone	Mainly pelagic sediments in the continental slope	Deep marine (Relatively deep water)	
		FA 4		Greyish sandstone and mudstone intercalation	Distal outer fan turbidites on the continental slope	Deep marine	
	COLLINGHAM	FA 3		Mudstone rhythmite and thin beds of yellowish tuff alternation	Suspension settling of mud intermixed with turbidites on the continental slope	Deep marine	Normal temperature
	WHITEHILL	FA 2		Laminated black-greyish shale and interbedded chert	Deep marine or pelagic basin deposits	Deep marine (Deep sea floor)	Cool temperature
	PRINCE ALBERT	FA 1		Laminated to thin bedded black-greyish shale and mudstones	Deep-sea pelagic sediments	Deep sea basin or abyssal plain	Cool temperature
	DWYKA GROUP						

Tuff/claystone ▮ Shale ▮ Mudstone ▮ Chert ▮ Sandstone ▮ Mudstone rhythmite ▮ Organic shale ▮ Siltstone ▮ Diamictite

Figure 6.26: Graphic map and interpretation of the facies association in the Ecca Group.

Depositional Environments

Lacustrine | Shallow Marine | Deep Marine

Sea Level

FA 7

Lake

Lacustrine

FA 6

Slump

Debris flow

Volcano

FA 4

FA 3

INLAND

FA 1

CONTINENTAL SHELF

Fault

Turbidity current

FA 5

Slide

SLOPE

Fault

CONTINENTAL RISE

FA 2

ABYSSAL PLAIN
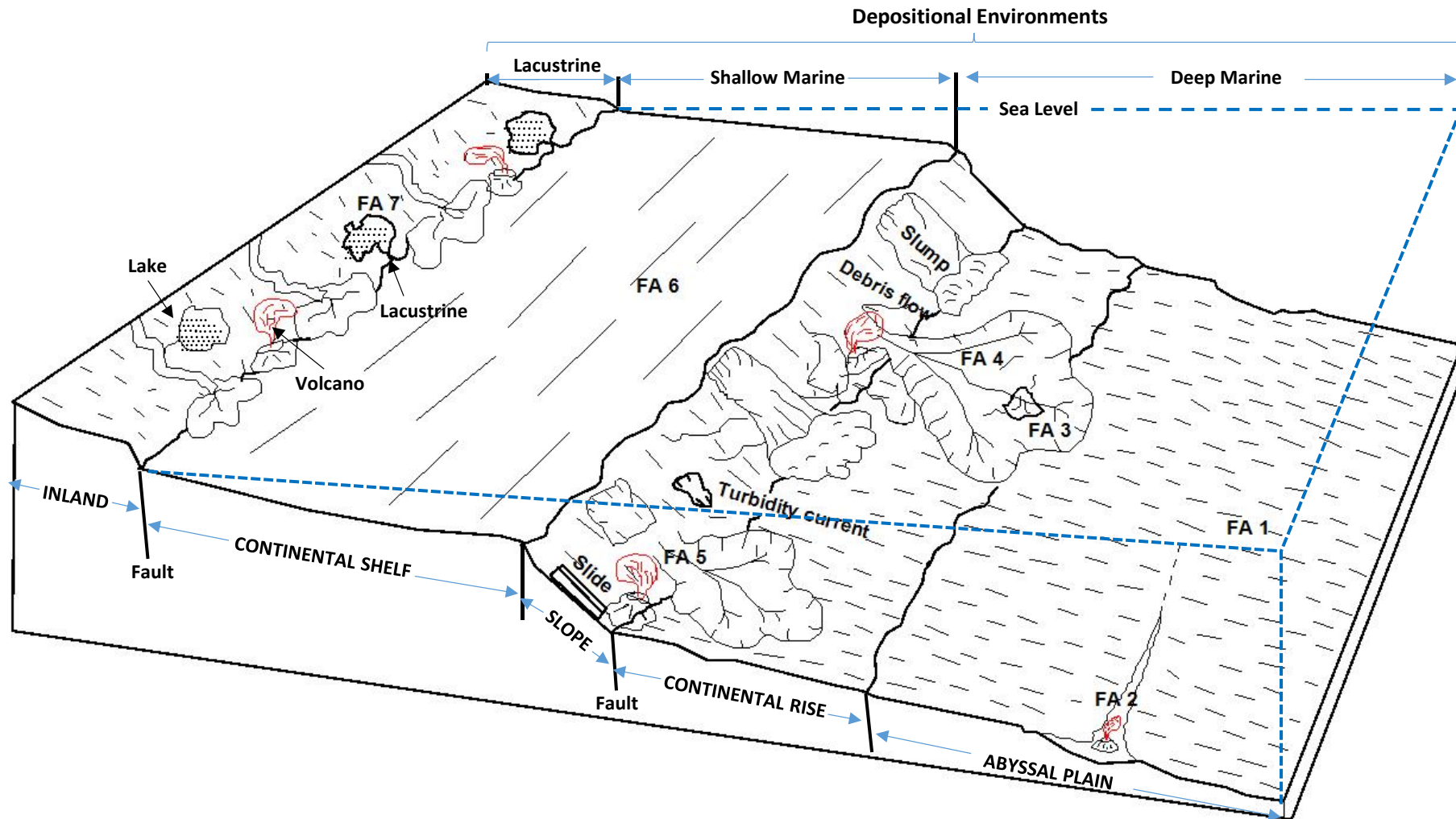
Figure 6.27: Proposed depositional model for the Ecca sediments in the southeastern Karoo Basin of South Africa. The model shows that FA 1 and FA 2 are deposited in deep water, FA 2, FA 4 and FA 5 are deposited on the continental rise and slope and FA 6 is deposited on the continental shelf whereas FA 7 is deposited on coastaline (possibly lake).

Sedimentological and sequence stratigraphic evidence revealed that the Ecca Group has progressively changed upward from deep marine environment to shallow marine environment, and finally to lacustrine environment, which implies that the Main Karoo Basin was gradually filling up with Ecca sediments resulting in the gradual shallowing up of the water depth of the depositional basin. It is observed that the depostional environments deduced from grain size parameters agrees to an extent with those from sedimentary facies analysis. The weakness in the grain size analysis is that the samples from the Prince Albert and Whitehill Formations plotted in the shallow marine environment, whereas these formations are purely deep marine sediments based on the facies architecture. On the other hand, the Collingham and Ripon Formations are turbidites (turbidity current deposits) while the overlying Fort Brown Formation is fluvial deposit as indicated by both facies architecture and grain size approaches. This also agrees with the findings of Catuneanu and Elango (2001) that the deeper marine facies of the early Ecca Group were accumulated during the under-filled phase of the foreland system, whereas the shallow marine facies of the late Ecca Group correspond to the filled phase of the basin, which was followed by an overfilled phase dominated by fluvial sedimentation of the Beaufort Group.

6.7 Conclusions

The study on the sedimentary facies of the Ecca Group in the study area was performed to give new insight to enhance the understanding of the sediment characteristics and the depositional environments of the Ecca sequence. A total of fourteen lithofacies were identified in the Ecca Group, and were further grouped into seven distinct facies associations (FAs): Shale and mudstones intercalated with siltstones (FA 1); Carbonaceous shale, mudstone with chert (FA 2); Mudstones-claystone rhythmite with lenticular siltstone (FA 3); Greyish medium bedded sandstone intercalated with laminated mudstone (FA 4); Dark-grey medium to thick bedded mudstone and siltstone (FA 5); Thin to medium bedded sandstone alternated with thin bedded carbonaceous mudstone (FA 6); and varved mudstone rhythmite intercalated with siltstone and minor sandstones (FA 7). The Ecca Group is interpreted to have progressively changed upwards from deep marine environment (FA 1, FA 2, FA 3, FA 4 and FA 5) to shallow marine environment (FA 6), and finally to lacustrine environment (FA 7). This is also consistent with the evidence that the overlying strata of the Beaufort Group was deposited in a fluvial environment, which was the result of basin water and sea-level continuously retreating or dropping; a marine environment then shifted to a continental inland environment at last.

CHAPTER 7

GEOCHEMISTRY OF THE ECCA GROUP SANDSTONES AND MUDROCKS: IMPLICATIONS FOR PROVENANCE, WEATHERING AND TECTONIC SETTING

Abstract

Geochemical compositions of twenty-four sandstone and mudrock samples from the Ecca Group were analysed to decipher their provenance, paleoweathering conditions and tectonic setting. The result shows that the shales have high Fe_2O_3, K_2O, TiO_2, Ce, Cu, Ga, La, Nb, Nd, Rb, Sc, Sr, Th and Y content more than the sandstones, whereas, sandstones are higher in SiO_2, Hf and Zr than the shales. The positive correlations of Al_2O_3 with other elements as well as the abundance of Ba, Ce, Th, Rb, Zn and Zr revealed that these elements are primarily controlled by the dominant clay minerals. Tectonic discrimination diagrams revealed that the sandstones and shales are mostly of quartzose provenance in the source, suggesting that they were derived from a cratonic interior or recycled orogen. The entire samples plotted in the post-Archaean field, indicating that felsic component was dominant in the source area. The binary plots of TiO_2 versus Ni, TiO_2 against Zr and La/Th versus Hf as well as the ternary diagrams of V-Ni-Th*10 indicated that the shales and sandstones were derived from felsic igneous source-rocks. A-CN-K (Al_2O_3-CaO-K_2O) ternary diagram and indices of weathering (CIA, CIW and PIS) suggest that the granitic source rocks underwent moderate to high degree of chemical weathering. The CIA values range between 24.41% and 83.76%, indicating low to high weathering conditions. The CIW values for the studied sandstones and shales range from 25.90 to 96.25%, suggesting moderate to high intensive chemical weathering. ICV values for the sandstones and shales vary from 0.71 to 3.6 (averaging 1.20) and 0.41 to 1.05 (averaging 0.82), respectively. The K_2O/Na_2O ratios for the samples vary from 0.71 to 8.29, pointing to a moderate-high maturity. The plot of CIA against ICV shows that most of the shales are geochemically mature and were derived from both weak and intensively weathered source rocks. The tectonic setting discrimination diagrams support passive continental margin setting of the provenance.

Keywords: Geochemistry, provenance, weathering, tectonic setting, Ecca Group.

7.1 Introduction

Clastic sedimentary rocks have vital information about the composition, tectonic setting and evolution of continental crust, mainly when the traditional petrographic methods are unclear. Nonetheless, their chemical and mineralogical composition can be influenced by factors like source rock characteristics, weathering, sorting processes during transportation, sedimentation and diagenetic processes to an extent (Nesbitt and Young, 1996; Nesbitt et al., 1997; Armstrong-Altrin, 2009). Trace elements such as La, Y, Sc, Cr, Th, Zr, Hf, Nb and rare earth elements (REE) are thought to be useful indicators of provenance, geological processes and tectonic setting due to their relatively low mobility and insolubility during sedimentary processes (Taylor and McLennan, 1985; Bhatia and Crook, 1986; Cullers et al., 1987, 1988; McLennan et al., 1993). Hence, the geochemistry of clastic sediments (i.e. sandstone and shale) reflects a combination of provenance, chemical weathering, hydraulic sorting, and abrasion (Taylor and McLennan, 1985; Wronkiewicz and Condie, 1987; McLennan et al., 1993; Condie, 1993; Nesbitt et al., 1997; Yan et al., 2007).

In geochemical provenance studies, fine grained sedimentary rocks like shales are considered to be the most useful rock because of their homogeneity before deposition, post-depositional impermeability and higher abundance of trace elements (Taylor and McLennan, 1985; Condie, 1993; McLennan et al., 2000; Bracciali et al., 2007). Taylor and McLennan (1985) and Condie (1991) documented that some relatively immobile elements like Sc, Th, Zr, Hf and rare earth elements (REE) show very low concentrations in natural waters and are transported almost quantitatively throughout the sedimentary process from parent rocks to clastic sediments. The relative distribution or enrichment of these immobile elements in felsic and basic rocks have been used to infer the relative contribution of felsic and basic sources in shales from different tectonic environments (Wronkiewicz and Condie, 1990). For example, La and Th are enriched in felsic rocks, whereas Sc, Cr, and Co are more concentrated in basic rocks relative to felsic rocks. These elements are relatively immobile during weathering (Cullers et al., 1987; Condie and Wronkiewicz, 1990; Cullers, 1994a; 1994b). Hence, the ratios of La or Th to Co, Sc, or Cr are sensitive indicators of source rock compositions. Similarly, felsic igneous rocks contain negative Eu anomalies (Eu/Eu* from chondrite-normalized plots of the REE), whereas basic igneous rocks have little or no Eu anomalies, and the size of the negative anomalies in the provenance seems to be preserved in fine-grained sediment (Cullers, 1994b). Furthermore, some major elements such as alkali and alkali earth elements, which are water mobile elements and very sensitive to climatic change,

can be used as a proxy of paleoclimate evolution (Nesbitt and Young, 1984; Wei et al., 2004). Geochemical data on sandstones of unmetamorphosed sedimentary sequences deposited in epicratonic or intracratonic basins also give important clues on paleoweathering conditions, variations in provenance composition and tectonic settings (Condie et al., 2001; Armstrong-Altrin et al., 2004; Araújo et al., 2010).

Several researchers such as Bhatia (1983) and Roser and Korsch (1986) have proposed K_2O/Na_2O versus SiO_2 tectonic setting discrimination diagrams for sedimentary rocks in order to identify tectonic setting of unknown basins. These diagrams are still commonly used to deduce the tectonic setting of ancient basins. However, more detailed results can be obtained using the calc-alkaline oxide ternary diagram ($CaO-Na_2O-K_2O$) of Bhatia (1983) and modified by Toulkeridis et al. (1999). Weaver (1989) as well as Nesbitt and Young (1984) also documented that the index of compositional variability (ICV), K_2O/Al_2O_3 ratio, chemical index of alteration (CIA) and $Al_2O_3-(CaO+Na_2O)-K_2O$ (A-CN-K) ternary plots are useful geochemical parameters for the study of provenance and maturity of the rocks. In addition, Crook (1974), Roser and Korsch (1986) and McCann (1991) used alkali metal oxides to reveal information about the provenance of clastic sediments. Recent geochemical investigations on sandstones and shales have focused on deciphering the provenance and tectonic evolution of sedimentary basins (Armstrong-Altrin et al., 2004; Lee et al., 2005; Wanas and Abdel-Maguid, 2006). However, little attention has been paid to the study of provenance in this region, despite the fact that the targeted carbonaceous shales for shale gas exploration in the region is hosted in the Ecca Group. Furthermore, it is also important in understanding the tectonic evolution of the southeastern Karoo basin. To date, the geochemistry of fine-grained sediments of the Ecca Group in the Eastern Cape Province of South Africa has not been studied in detail to determine their source rock characteristics, provenance and tectonic setting. This study was therefore aimed at evaluating the geochemistry of the Ecca shales and sandstones in the study area in order to provide information on the source rock characteristics, provenance, paleoweathering and tectonic setting using their major, trace and rare earth elements geochemistry.

7.2 Materials and method

Twenty-four rock samples of the shale and sandstone representing various formations of the Ecca Group were analysed for the major and trace element (including rare earth element) concentrations. X-ray Fluorescence (XRF) analysis was performed at the Council for

Geoscience, Pretoria, South Africa. XRF analysis of the major and trace elements geochemistry of the samples was performed using MagiX Fast, XRF spectrometer. Bulk sample preparation consists of drying where necessary, crushing to 10 mm, splitting and milling in a tungsten carbide milling pot to less than 75 μm. Major element analyses were analysed on fused beads, while trace elements were executed on pressed powder pellets. Major elements were analysed following the procedure documented by Ahmedali (1989), while the concentration of trace and rare earth elements were determined by ICP-MS (Inductively Coupled Plasma Mass Spectrometry) following the procedure described by Jenner et al. (1990). Accuracy and precision was estimated and monitored from the control samples and duplicates. The analytical precision is better than 5% for major and trace elements. Samples were dried at 100 ℃ (Weight A) and heated at 1000 ℃ (Weight B), to determine the percentage loss on ignition (LOI) using the following equation:

$$\% \, \text{LOI} = \frac{\text{Weight}_A - \text{Weight}_B}{\text{Weight}_A - \text{Weight}_{\text{crucible}}} \times 100$$

Several discriminatory plots of the major and trace elements were used to determine the provenance and tectonic setting. The ternary plot of Al_2O_3-$(CaO+Na_2O)$-K_2O (represented as A-CN-K) as well as the formulas for chemical index of alteration (CIA), chemical index of weathering (CIW) and plagioclase index of alteration (PIA) were used to quantify the degree of weathering. In the formulas, CaO* is the amount of CaO incorporated in the silicate fraction of the rock. In this study, correction for CaO from carbonate contribution was not performed due to the absence of CO_2 value. Thus, to compute for CaO* from the silicate fraction, the assumption proposed by Bock et al. (1998) was employed. Based on this, CaO values were accepted only if CaO < Na_2O. Thus, when CaO > Na_2O, it was presumed that the concentration of CaO is the same with that of Na_2O. This procedure provides measure for the ratio of the secondary aluminous mineral to feldspar, and forms a basis for the measure of intensity of weathering. Index compositional variation (ICV) proposed by Cox et al. (1995) was used to determine maturity of the sediments. Graphs and ternary diagrams were drawn and interpreted for compositional analysis of samples (sandstone and shale), provenance, weathering and tectonic setting.

7.3 Element compositions

7.3.1 Major elements

The major element concentrations in the Ecca sandstones and shales are depicted in Table B2 (Appendix B). The major element compositions are quite variable but still comparable with

the average compositions documented by Pettijohn (1957), Gromet et al. (1984) and Turekan and Wedephol (1961) (Table 7.1). All the samples show high concentrations of SiO_2, ranging from 55.94 to 87.99%. The Al_2O_3, CaO and Fe_2O_3 contents are moderately high, ranging from 5.91 to 16.10%, 0.06 to 16.67% and 0.47 to 6.88%, respectively. The concentrations of TiO_2, MnO, MgO, Na_2O, K_2O and P_2O_5 are generally low, ranging from 0.13 to 0.80%, 0.004 to 0.197%, 0.25 to 1.58%, 0.17 to 3.27%, 0.95 to 4.42% and 0.053 to 0.219%, respectively. Sandstones are higher in SiO_2 content than shales. On the other hand, shales are higher in Fe_2O_3, K_2O and TiO_2 contents than sandstones, which reflect their association with clay-sized phases (Madhavaraju and Lee, 2010).

Table 7.1: Comparing average chemical composition of the sandstones and shales from the Ecca Group with published average shales.

Oxides	This study		Average shale (Pettijohn, 1957)	Turekan and Wedephol (1961)	UCC	PAAS	NASC (Gromet et al., 1984)
	shale	Sandstone					
SiO_2 (%)	68.72	76.43	58.10	58.50	66.60	62.40	64.82
TiO_2 (%)	0.58	0.46	0.60	0.77	0.64	0.99	0.80
Al_2O_3 (%)	14.26	9.02	15.40	15.00	15.40	18.78	17.05
Fe_2O_3 (%)	4.30	3.61	6.90	4.72	5.04	7.18	5.70
MnO (%)	0.06	0.07	Trace	-	0.10	0.11	-
MgO (%)	1.28	0.59	2.40	2.50	2.48	2.19	2.83
CaO (%)	1.57	2.65	3.10	3.10	3.59	1.29	3.51
Na_2O (%)	1.63	1.40	1.30	1.30	3.27	1.19	1.13
K_2O (%)	3.08	1.57	3.20	3.10	2.80	3.68	3.97
P_2O_5 (%)	0.17	0.09	0.20	0.16	0.12	0.16	0.15

The abundance of Al_2O_3 were used as a normalization factor to make comparisons among the different lithologies because of their immobile nature during weathering, diagenesis and metamorphism (Bauluz et al., 2000). Major oxides of the studied shales and sandstones were plotted against Al_2O_3 as depicted in Figures 7.1 and 7.2. In addition, average UCC (Upper Continental Crust) and PAAS (Post-Archaean Australian Shale) values were extracted from Rudnick and Gao (2003) andTaylor and McLennan (1985), respectively and included in the plots for comparison purposes. In shale samples, major elements like TiO_2, Fe_2O_3, MgO and K_2O shows positive correlation with Al_2O_3, whereas MnO, CaO, Na_2O and P_2O_5 shows no particular trend (Figures 7.1). Similarly, in the sandstone samples, TiO_2, Fe_2O_3, MgO, K_2O and P_2O_5 shows positive correlations with Al_2O_3, while TiO_2, MnO, CaO and Na_2O shows no particular trend (Figure 7.2). The strong positive correlations of these major oxides with Al_2O_3 indicate that they are associated with micaceous/clay minerals.
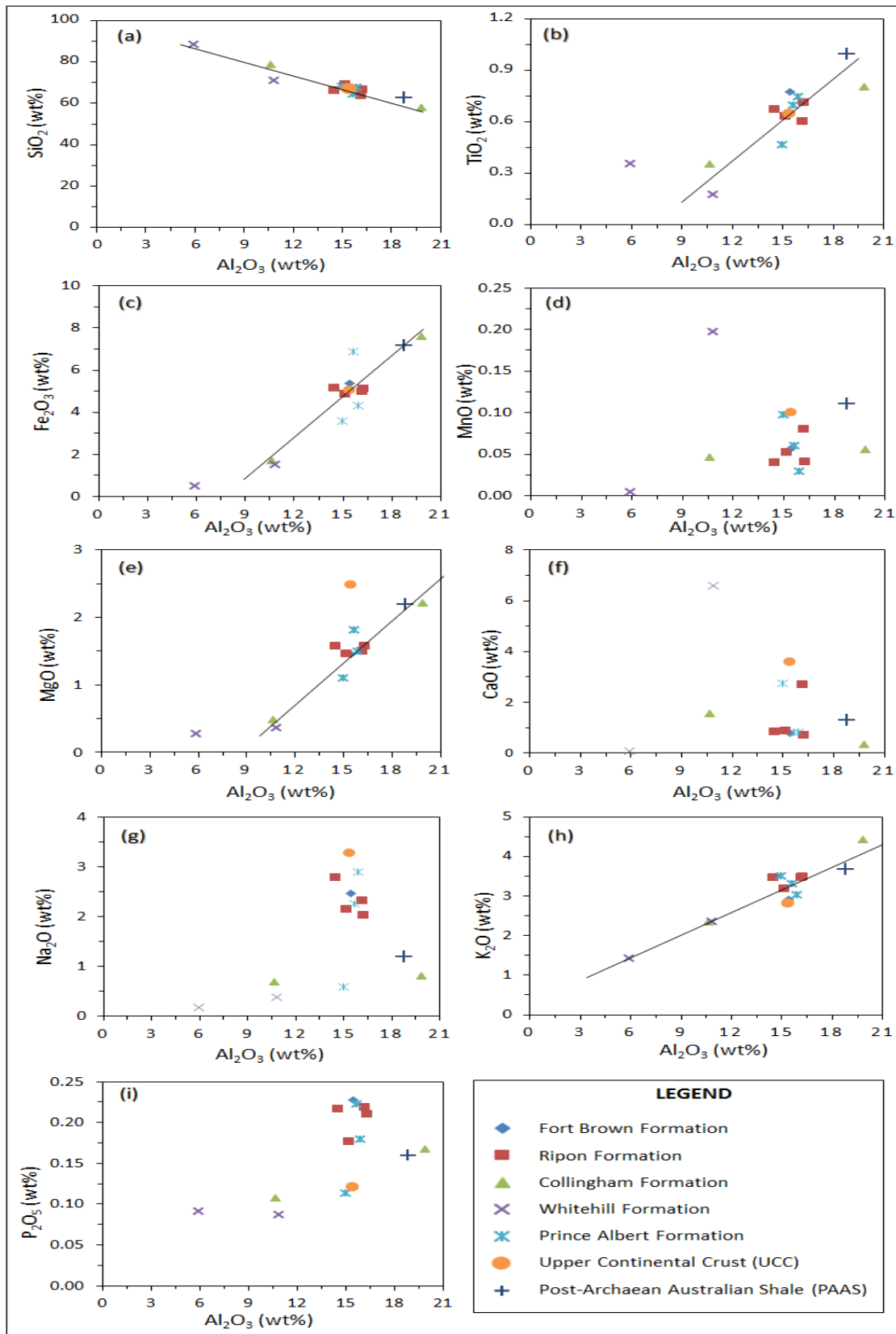
Figure 7.1: Major elements versus Al₂O₃ graph showing the distribution of shale samples from the Ecca Group. Average data of UCC and PAAS from Rudnick and Gao (2003) and Taylor and McLennan (1985) respectively, were also plotted for comparison.
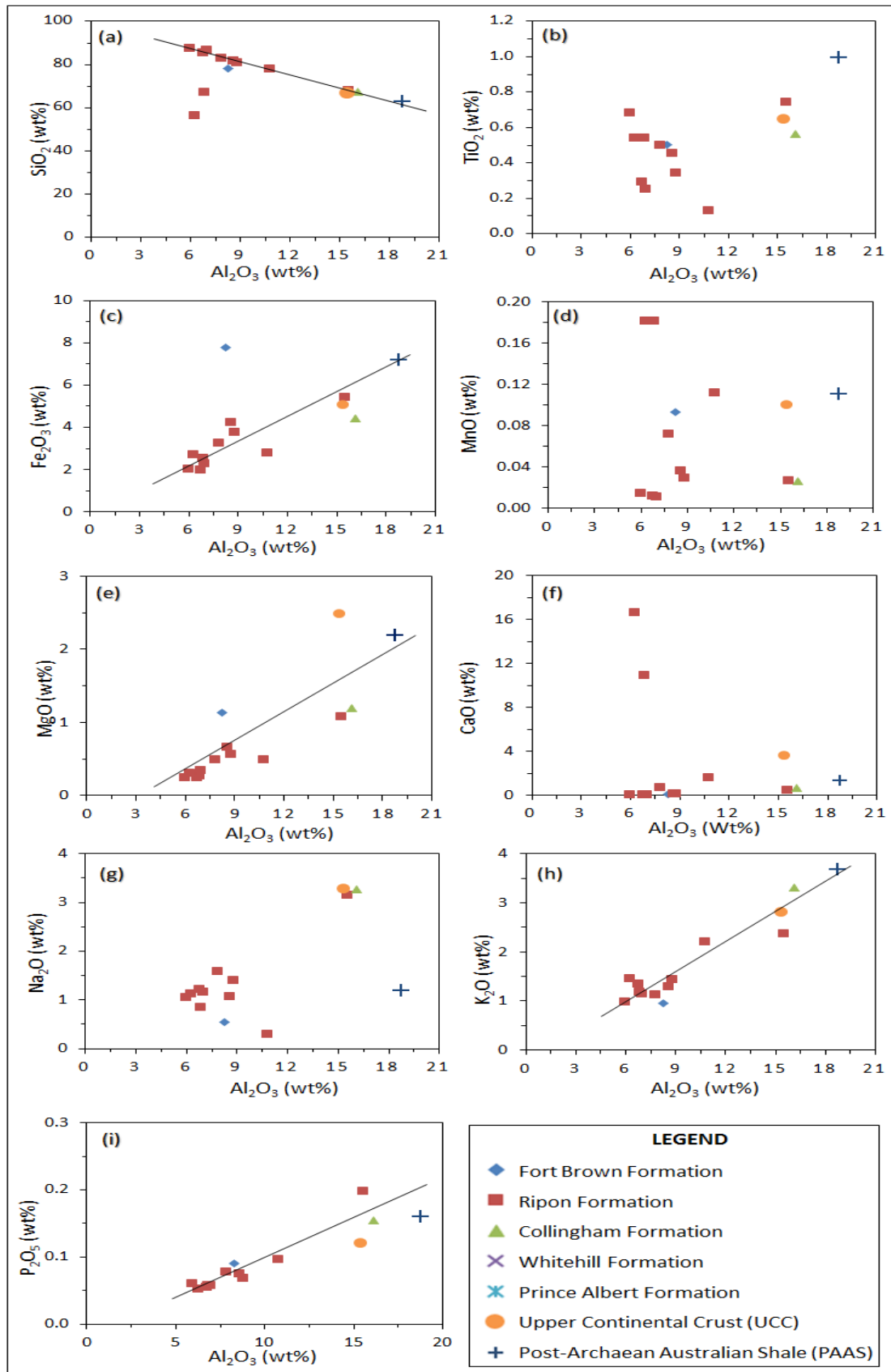
Figure 7.2: Major elements versus Al_2O_3 graph showing the distribution of sandstone samples from the Ecca Group. Average data of UCC and PAAS from Rudnick and Gao (2003) and Taylor and McLennan (1985) respectively, were also plotted for comparison.

The shale and sandstone samples were normalized to UCC (Rudnick and Gao, 2003) and PAAS (Taylor and McLennan, 1985) as depicted in Figures 7.3, 7.4, 7.5 and 7.6.
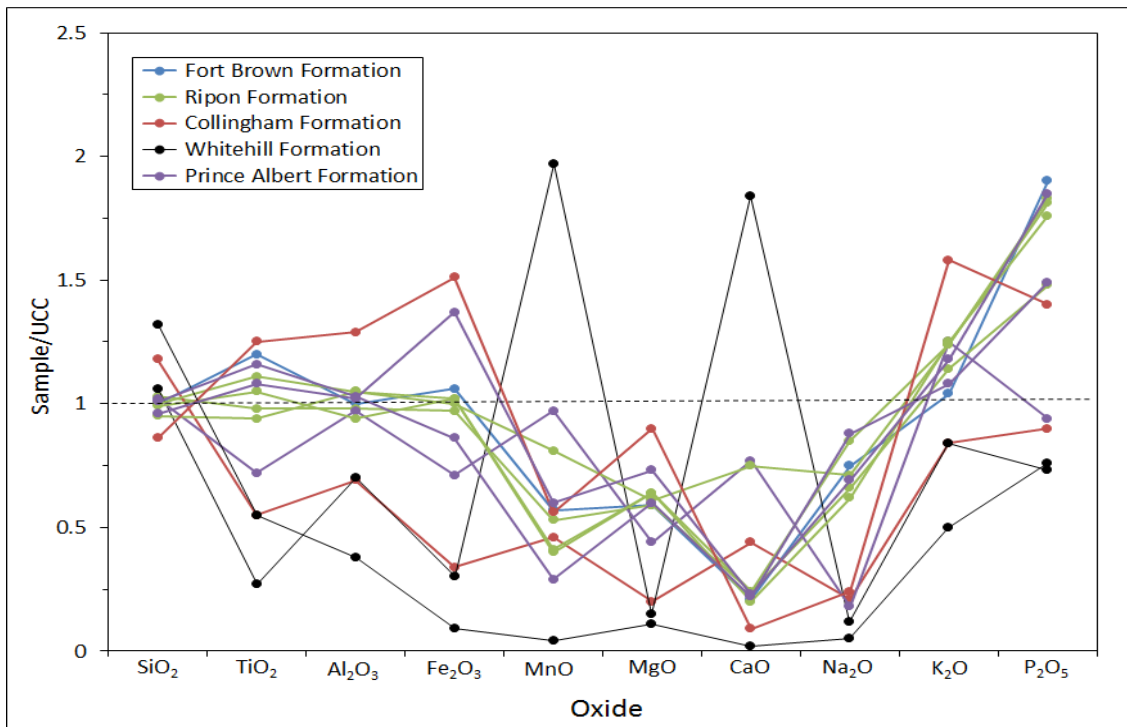
Figure 7.3: Spider plot of major elements composition for the Ecca shales, normalized against UCC (After Rudnick and Gao, 2003).
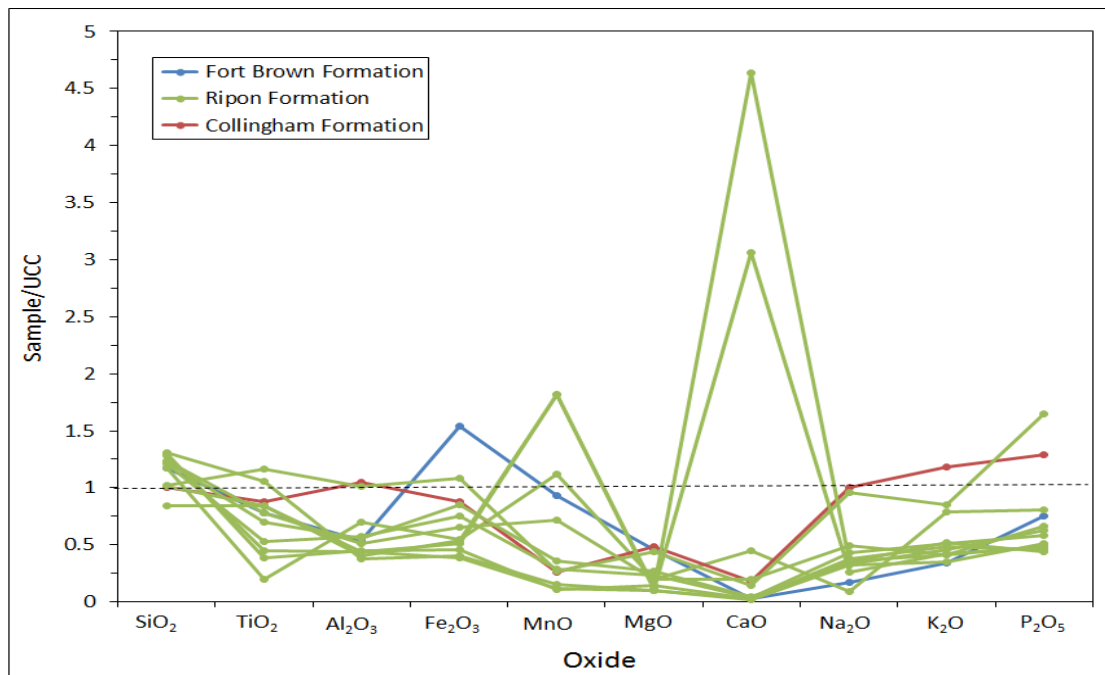
Figure 7.4: Spider plot of major elements composition for the Ecca sandstones, normalized against UCC (After Rudnick and Gao, 2003).
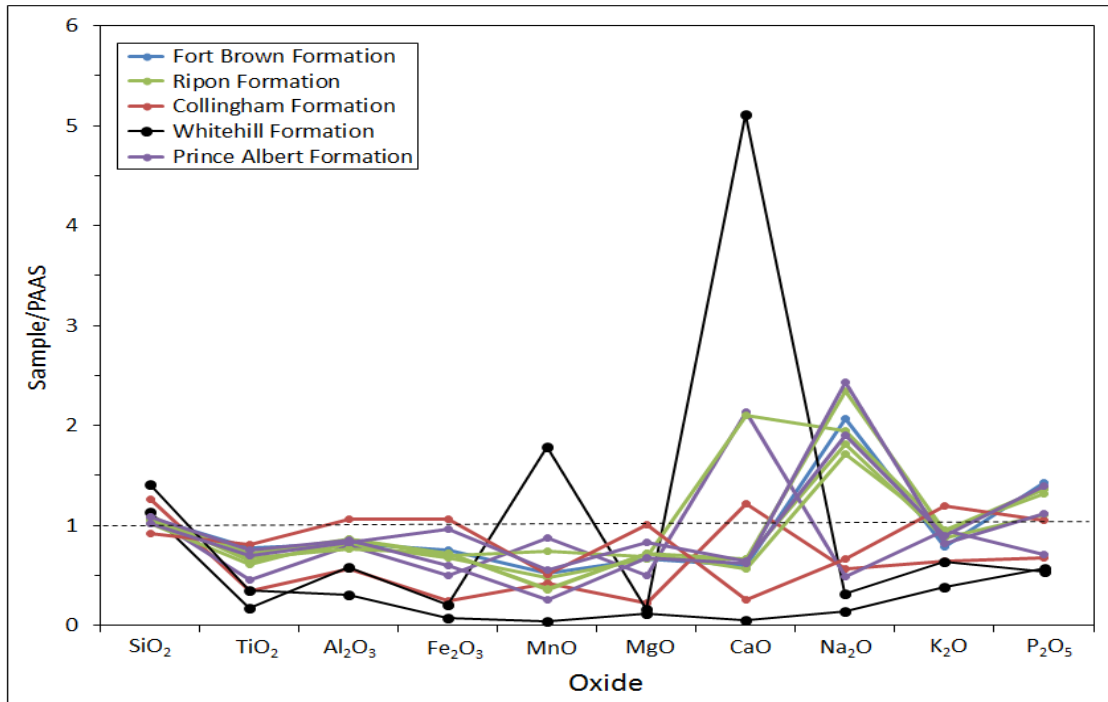
Figure 7.5: Spider plot of major elements composition for the Ecca shales, normalized against PAAS (After Taylor and McLennan, 1985).
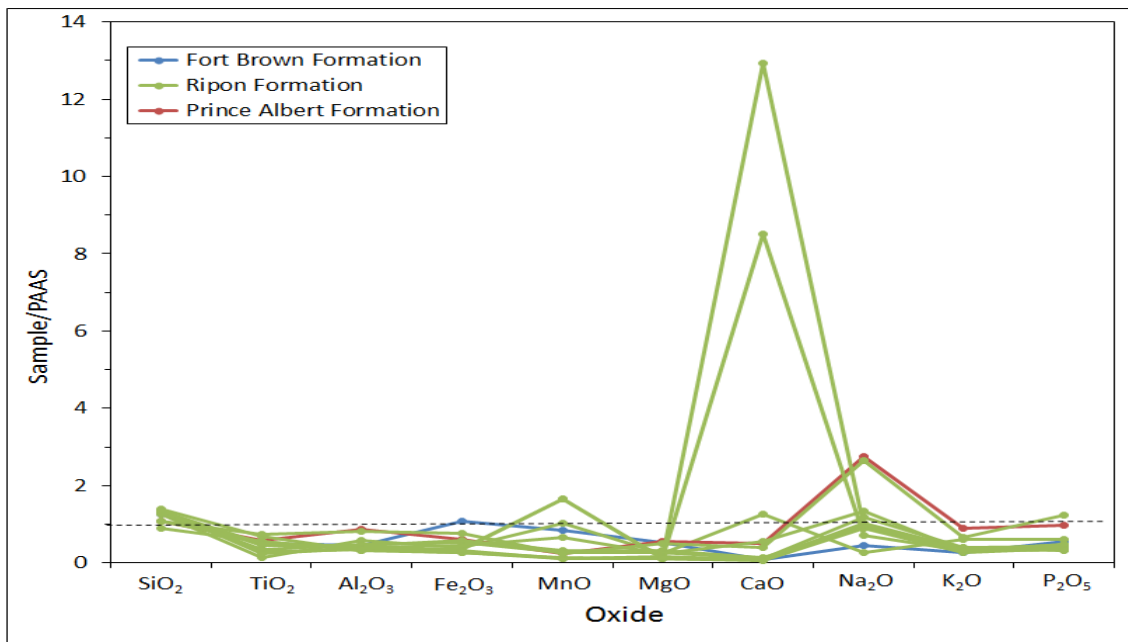
Figure 7.6: Spider plot of major elements composition for the Ecca sandstones, normalized against PAAS (After Taylor and McLennan, 1985).

Relative to UCC, the average concentrations of SiO_2, TiO_2, Al_2O_3, Fe_2O_3, MnO, CaO, K_2O and P_2O_5 in the sandstones are 1.09, 0.79, 0.73, 0.71, 0.65, 0.59, 0.83 and 1.07 respectively, which are generally comparable to UCC. On the other hand, the average concentration of

Na$_2$O and MgO relative to UCC are 0.36 and 0.37 respectively, which are generally low as compared to UCC. The depletion of Na$_2$O ($< 1\%$) in the Ecca sandstones can be attributed to a relatively smaller amount of Na-rich plagioclase in them, which is consistent with the petrographic results (Chapter 5). K$_2$O and Na$_2$O contents and their ratios (K$_2$O/Na$_2$O > 1) are also consistent with the petrographic observations, which revealed that K-feldspar dominates over plagioclase (albite) feldspar. K$_2$O enrichment relates to presence of illite as common clay mineral in the shales and sandstones. In addition, the enrichment of CaO (averaging 0.59 relative to UCC) can be attributed to the presence of diagenetic calcite cement, which is also consistent with the petrographic results. Relative to UCC, the shales are low in MgO, CaO, Na$_2$O, MnO and high in SiO$_2$, TiO$_2$ and Al$_2$O$_3$. Al and Ti are easily absorbed on clays and concentrate in the finer, more weathered materials (Das et al., 2006). In support of this, XRD analysis (Table 5.4 and Table B1 in Appendix B) of the shales revealed that they are dominated by kaolinite (Al$_2$Si$_2$O$_5$(OH)$_4$). In comparison with PAAS, the average concentrations of SiO$_2$, TiO$_2$, Al$_2$O$_3$, Fe$_2$O$_3$, MnO, CaO, Na$_2$O, K$_2$O and P$_2$O$_5$ are 1.16, 0.52, 0.62, 0.55, 0.59, 1.64, 1.27, 0.63 and 0.80, respectively, which are generally comparable to PAAS. Conversely, the average concentration of MgO relative to PAAS is low, averaging 0.43.

7.3.2 Trace elements

The trace element concentrations in the sandstones and shales are presented in Tables B3 and B4 (Appendix B). The trace element compositions are quite variable but still comparable with the average compositions documented by Levinson (1974), Vine and Tourtelot (1970), Turekan and Wedephol (1961) and Gromet et al. (1984) (Table 7.2). In the sandstones and shales, the contents of large ion lithophile elements (LILE) like Rb, Ba, Sr and Th vary from 39 to 197 ppm, 208 to 909 ppm, 23 to 340 ppm and 2.8 to 23 ppm, respectively. The content of high field strength elements (HFSE) like Zr, Y and Nb range from 108 to 652 ppm, 9.1 to 35 ppm and 5 to 17 ppm, respectively. Similarly, transition trace elements (TTE) like Sc, V, Cr, Ni and Zn range from 3 to 16 ppm, 6.4 to 96 ppm, 4.8 to 85 ppm, 2.1 to 31 ppm and 1.5 to 121 ppm, respectively. Generally, shales have high Ce, Cu, Ga, La, Nb, Nd, Rb, Sc, Sr, Th and Y content than the sandstones. On the other hand, sandstones are higher in Hf and Zr than the shales. The high Sr content in shales indicate that Sr may be associated with calcite minerals.

Table 7.2: Average trace element composition in the Ecca sandstones and shales compared to shales from other sedimentary basins.

Trace element	This study		Levinson (1974)	Vine and Tourtelot (1970)	Turekan and Wedephol (1961)	UCC	PAAS	NASC (Gromet et al., 1984)
	Shale	Sandstone						
Ba (ppm)	560.10	382.3	300.00	700.00	580.00	628.00	650.00	636.00
Co (ppm)	5.11	5.40	10.00	20.00	-	17.30	23.00	n.a.
Cr (ppm)	43.37	30.73	-	-	-	92.00	110.00	-
Cu (ppm)	28.06	5.10	70.00	50.00	45.00	28.00	50.00	n.a.
Ga (ppm)	18.25	10.92	-	-	-	17.50	20.00	n.a.
Hf (ppm)	6.08	8.91	-	-	-	5.30	5.00	n.a.
Nb (ppm)	13.32	9.50	20.00	20.00	n.a.	12.00	19.00	-
Ni (ppm)	17.00	13.00	50.00	70.00	-	47.00	55.00	58.00
Pb (ppm)	21.00	17.00	20.00	n.a.	n.a.	17.00	20.00	
Rb (ppm)	132.00	60.70	140.00	n.a.	n.a.	84.00	160.00	n.a.
Sc (ppm)	11.90	7.94	-	-	-	14.00	16.00	n.a.
Sr (ppm)	145.90	89.17	200.00	300.00	300.00	320.00	200.00	142.00
Th (ppm)	17.80	10.20	12.00	n.a.	n.a.	10.50	14.60	n.a.
U (ppm)	4.27	2.20	4.00	n.a.	n.a.	2.70	3.10	n.a.
V (ppm)	70.00	39.80	150.00	150.00	130.00	97.00	150.00	130.00
Y (ppm)	30.40	19.70	30.00	25.00	-	21.00	27.00	n.a.
Zn (ppm)	70.98	37.08	300.00	100.00	95.00	67.00	85.00	n.a.
Zr (ppm)	166.00	267.00	70.00	160.00	160.00	193.00	210.00	200.00

NB. UCC- Upper Continental Crust; PAAS- Post Archean Australian Shale; NASC- North-American Shale Composite; n.a. not analysed.

7.3.2.1 Large ion lithophile elements (LILE): Rb, Ba, Sr, Th and U

Based on the LILE average values, except for Sr and Ba, almost all the shale samples exhibit similar LILE abundances relative to UCC and PAAS (Figures 7.7 and 7.8). In contrast, the sandstones exhibit similar Th and U contents relative to UCC and PAAS, but are depleted in Rb, Ba and Sr (Figures 7.9 and 7.10). Th has very strong positive correlations with Nb in the shales and sandstones. This possibly implies that it may have been controlled by clays and/or other phases (i.e., Ti- and Nb-bearing phases) associated with clay minerals. Rb and Ba are positively correlated in the sandstone and shales, perhaps indicating a similar geochemical behaviour. These correlations indicate that their distributions are mainly controlled by illites and other minor clays.

7.3.2.2 High field strength elements (HFSE): Zr, Hf, Y and Nb

As documented by Bauluz et al. (2000) and Bauluz et al. (2005), HFSE elements are enriched in felsic rocks rather than mafic rocks. The concentrations of Zr, Hf and Y in the shales and sandstones are comparable to UCC contents (Figures 7.7 and 7.9), whereas Nb is depleted. Relative to PAAS contents, the concentrations of Y and Nb in the shales and sandstones are depleted, while Zr and Hf concentrations are relatively similar to PAAS contents (Figures 7.8 and 7.10). Generally, Zr and Hf have high positive correlations and the ratio of Zr to Hf in the analysed samples range from approximately 21-43. This suggests that the elements are controlled by zircons, since the values are similar or nearly the same with those documented by Murali et al. (1983) for zircon crystals. The average contents of Zr in the shales are lower than those in the sandstones, which perhaps indicate that the mineral zircon tends to be preferentially concentrated in fine-grained sands.

7.3.2.3 Transition trace elements (TTE): Sc, V, Cr, Co, Cu, Ni and Zn

TTE in the Ecca sandstones and shales are depleted in comparison with UCC and PAAS (Figures 7.7, 7.8, 7.9 and 7.10), except for Cu and Zn which is relatively comparable with UCC and PAAS in the shales. The TTE in the studied sandstones do not behave uniformly. Among TTE, Sc correlated positively with Ni which indicates that it is mainly concentrated in the phyllosilicates.
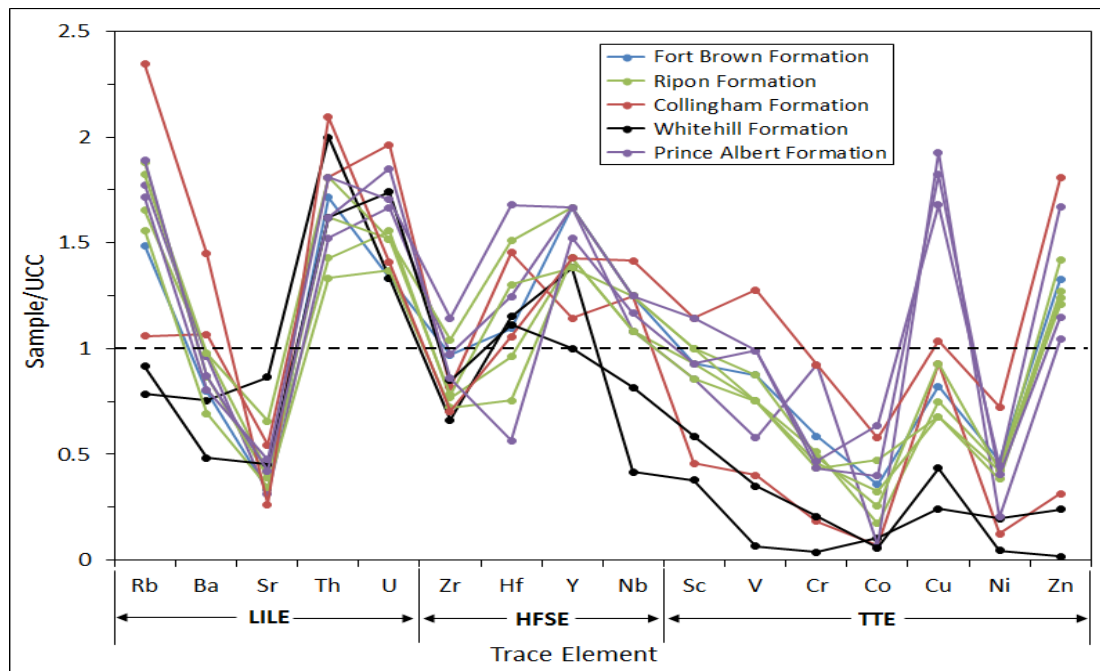
Figure 7.7: UCC normalized trace elements distribution of shale samples from the Ecca Group. The UCC values are cited from Rudnick and Gao (2003).
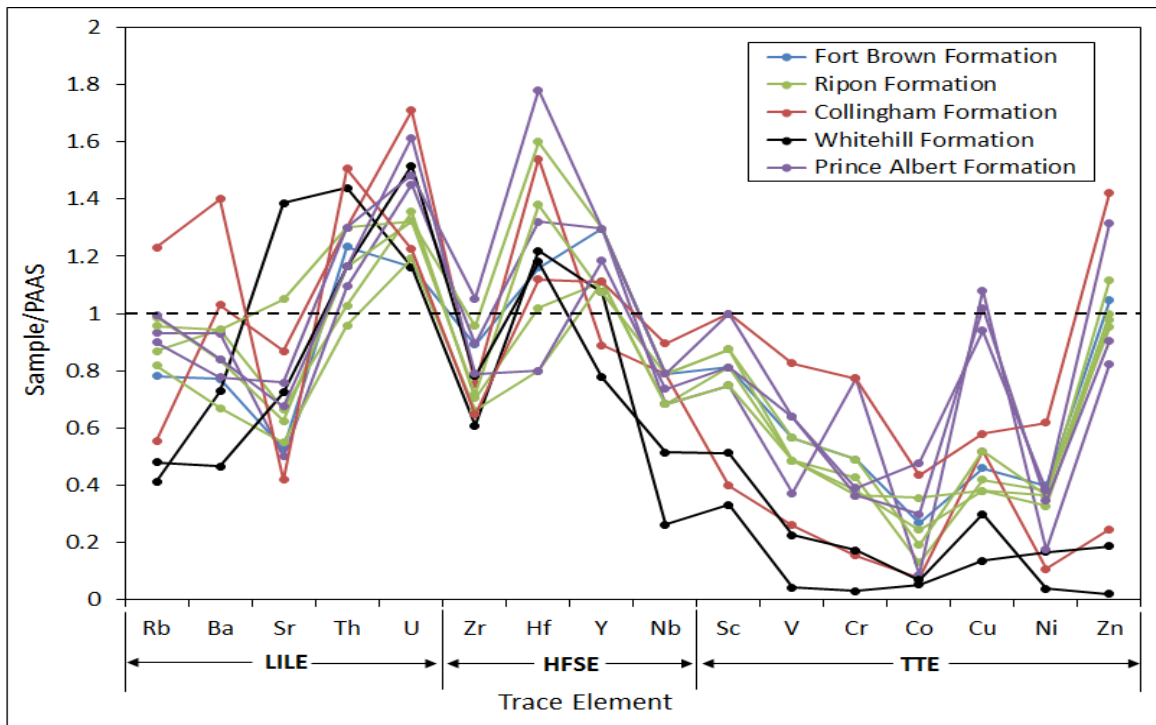
Figure 7.8: PAAS normalized trace elements distribution of shale samples from the Ecca Group. The PAAS values are cited from Taylor and McLennan (1985).
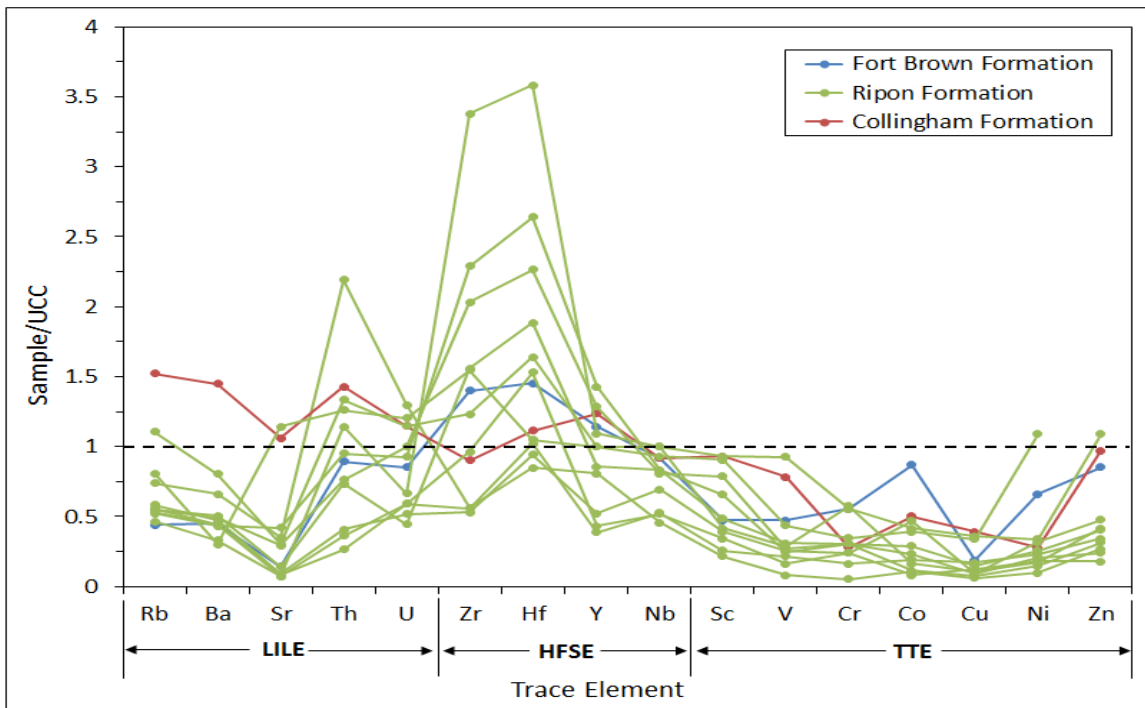
Figure 7.9: UCC normalized trace elements distribution of sandstone samples from the Ecca Group. The UCC values are cited from Rudnick and Gao (2003).
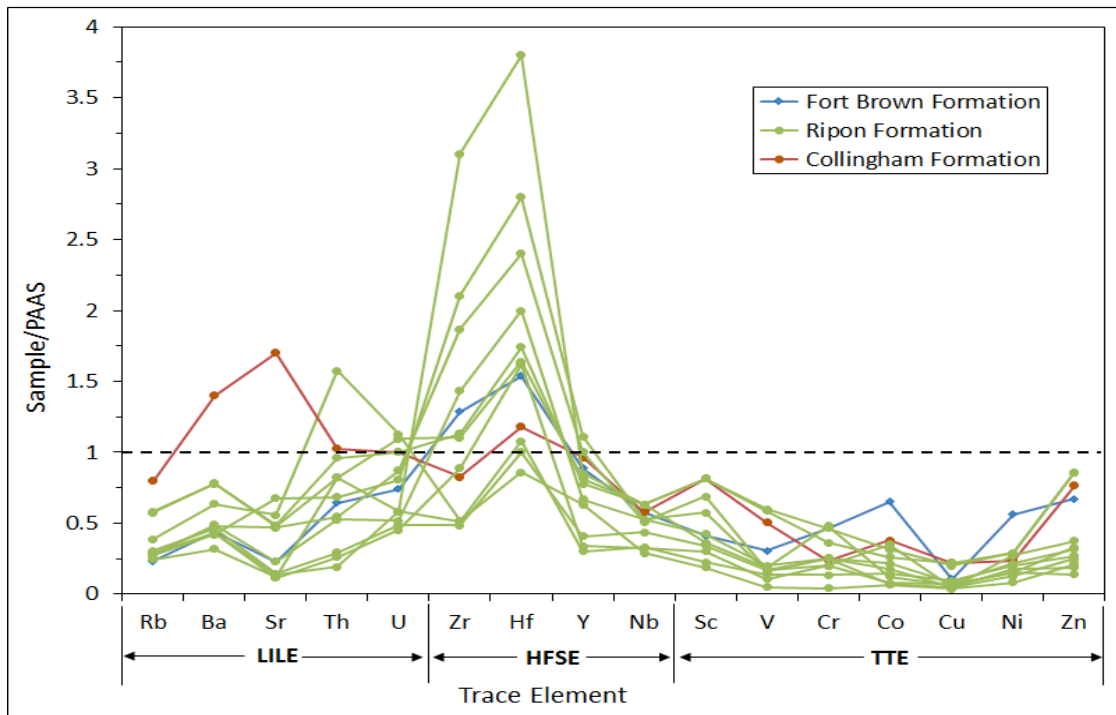
Figure 7.10: PAAS normalized trace elements distribution of sandstone samples from the Ecca Group. The PAAS values are cited from Taylor and McLennan (1985).

7.4 Source rock provenance

The compositions of major element or oxides in sandstones and shales have also been used to determine sedimentary provenance by the application of discriminant function analysis (Roser and Korsch, 1988). This discriminant function analysis distinguishes between four major provenance fields, namely, mafic igneous, intermediate igneous, felsic igneous and quartzose sedimentary or recycled. In Figure 7.11, the sandstone samples plot in the quartzose sedimentary provenance field. In contrast, the shale samples are scattered in both quartzose sedimentary provenance and intermediate igneous provenance field, but they are mostly within the quartzose sedimentary provenance field (Figure 7.12).
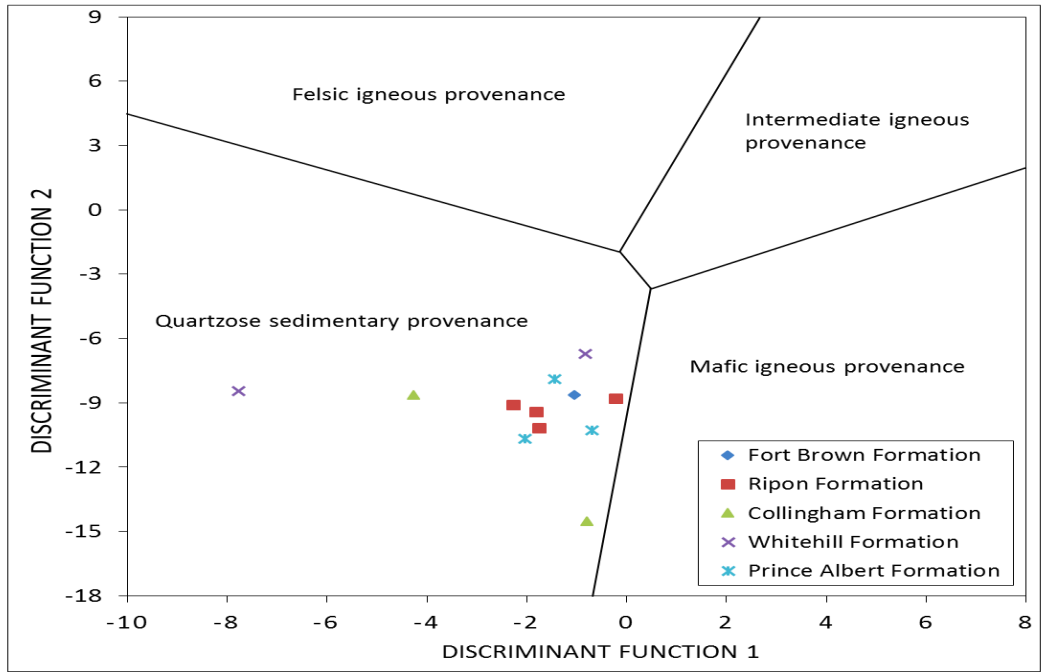
Figure 7.11: Major element Discriminant Function diagram for provenance of source rocks (shale) (After Roser and Korsch, 1988). The discriminant functions are: Discriminant Function 1 = (-1.773 TiO_2) + (0.607 Al_2O_3) + (0.760 Fe_2O_3) + (-1.500 MgO) + (0.616 CaO) + (0.509 Na_2O) + (-1.224 K_2O) + (-9.090); Discriminant Function 2 = (0.445 TiO_2) + (0.070 Al_2O_3) + (-0.250 Fe_2O_3) + (-1.142 MgO) + (0.438 CaO) + (1.475 Na_2O) + (-1.426 K_2O) + (-6.861).
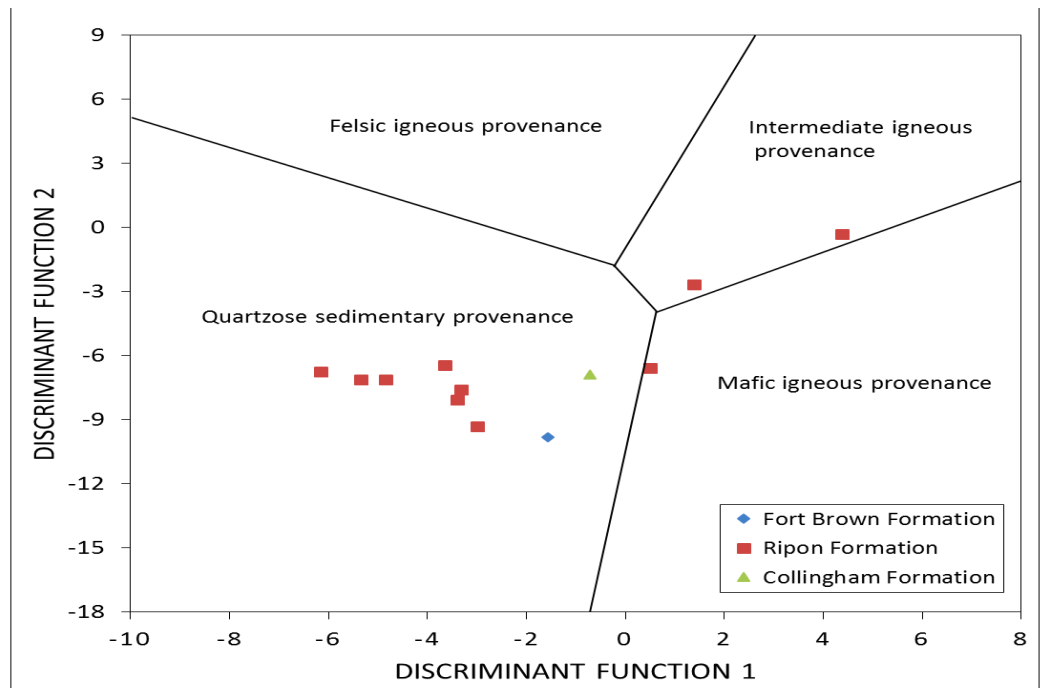
Figure 7.12: Major element Discriminant Function diagram for provenance of source rocks (sandstone) (After Roser and Korsch, 1988). The discriminant functions are: Discriminant Function 1 = (-1.773 TiO_2) + (0.607 Al_2O_3) + (0.760 Fe_2O_3) + (-1.500 MgO) + (0.616 CaO) + (0.509 Na_2O) + (-1.224 K_2O) + (-9.090); Discriminant Function 2 = (0.445 TiO_2) + (0.070 Al_2O_3) + (-0.250 Fe_2O_3) + (-1.142 MgO) + (0.438 CaO) + (1.475 Na_2O) + (-1.426 K_2O) + (-6.861).

The binary plot of TiO_2 versus Zr shows that all the shales and sandstones samples are from felsic igneous rocks (Figure 7.13; After Hayashi et al., 1977). Again, the TiO_2-Ni diagram of Floyd et al. (1989) revealed that the source area for most of the Ecca sandstones and shales were predominantly of acidic magmatic nature (Figures 7.14 and 7.15), despite the fact that a few samples plot outside the field assigned for felsic source. The plot Th/Co against La/Sc revealed that the Ecca shales and sandstones were both derived from felsic source rocks (Figures 7.16 and 7.17; After Cullers, 2002). The bivariate plot of La/Th against Hf (Figures 7.18 and 7.19; After Floyd and Leveridge, 1987) and ternary diagrams of V-Ni-Th*10 (Figures 7.20 and 7.21; After Bracciali et al., 2007) also indicate that the studied sandstones and shales were derived from felsic source rocks.
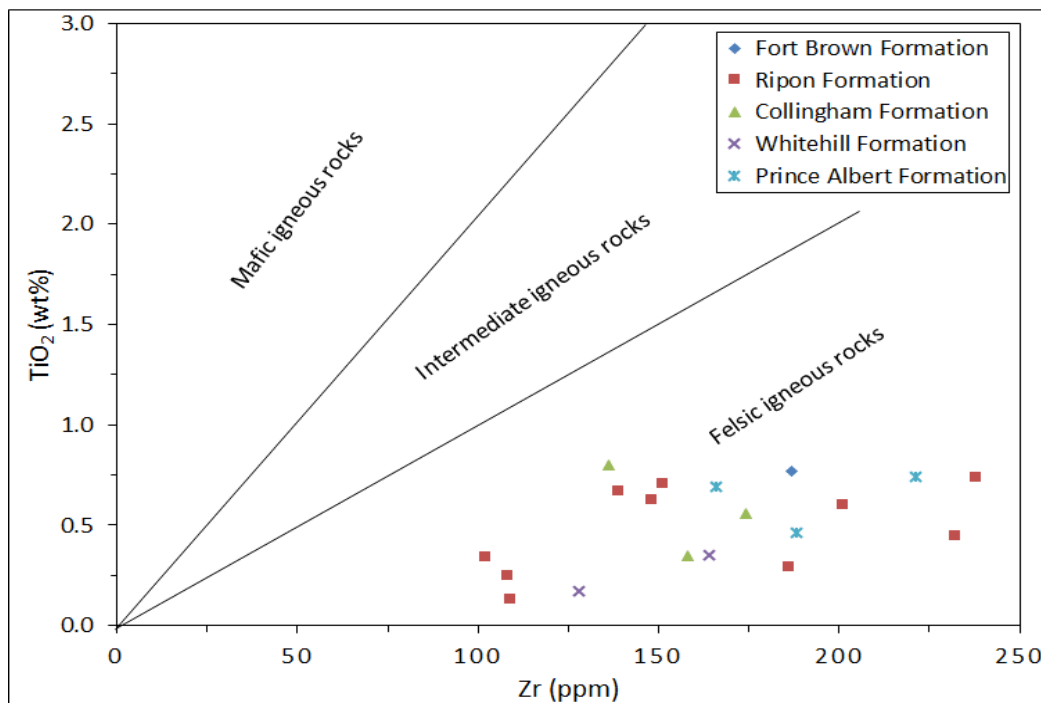
Figure 7.13: TiO_2–Zr plot of shales and sandstones samples from the Ecca Group (After Hayashi et al., 1977).
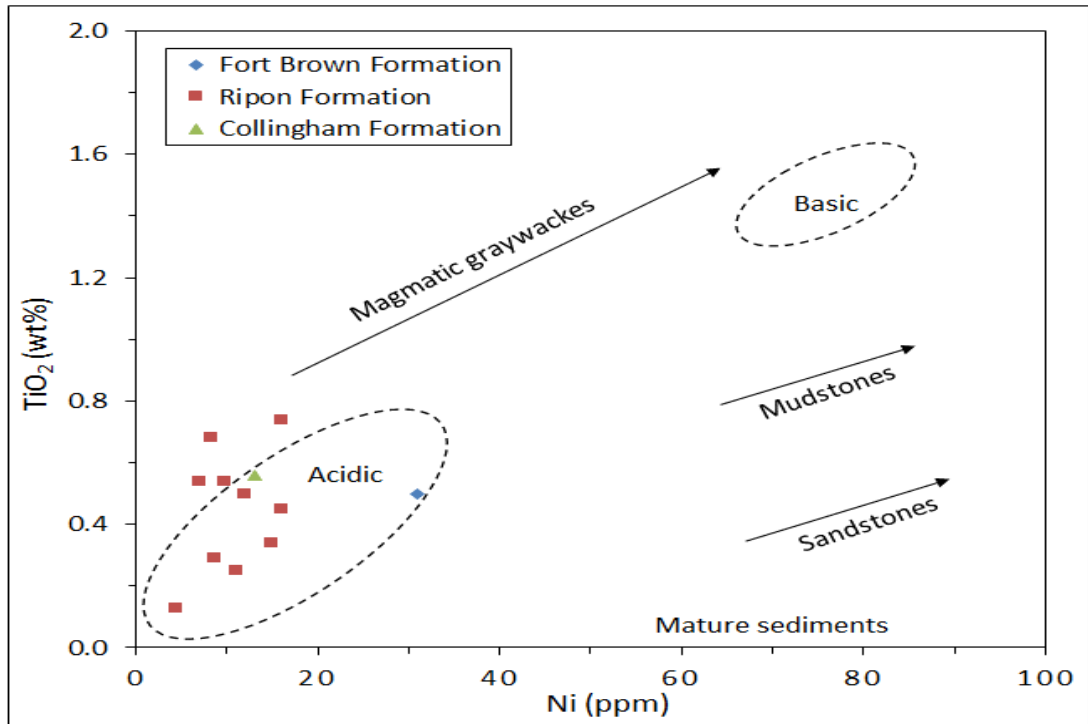
Figure 7.14: TiO₂ versus Ni bivariate plot for the sandstones from the Ecca Group (After Floyd et al., 1989). Most of the samples plotted near the acidic source field.
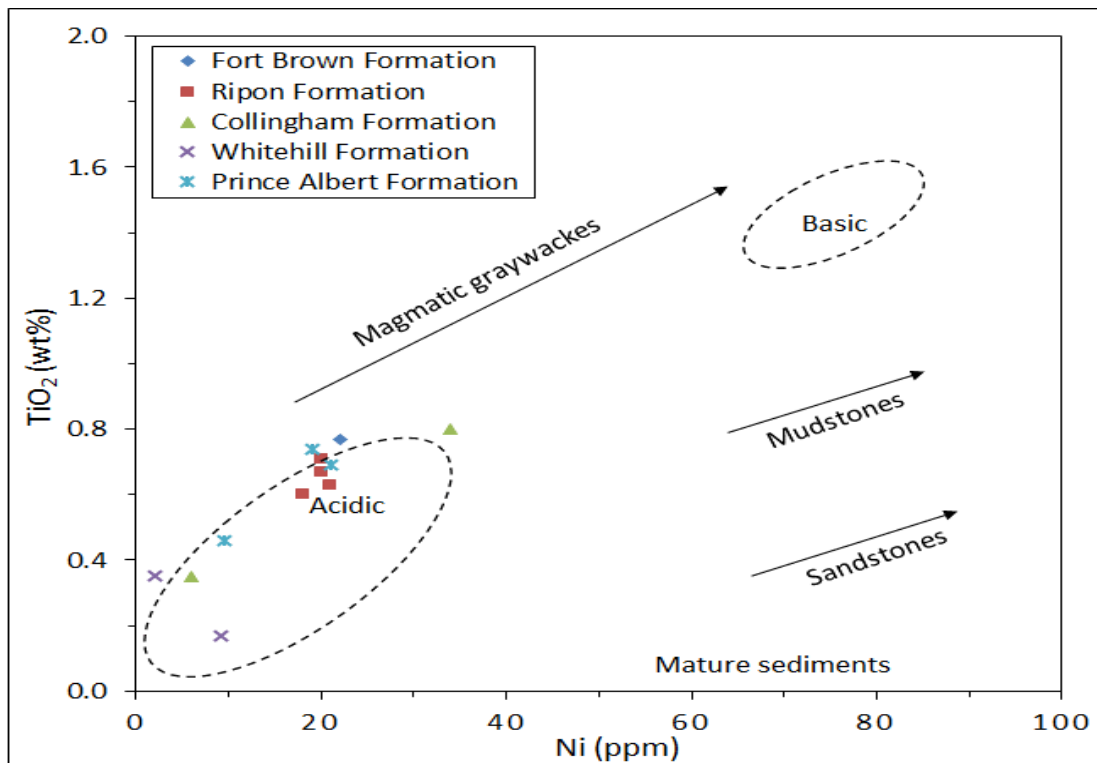
Figure 7.15: TiO₂ versus Ni bivariate plot for the shales from the Ecca Group (After Floyd et al., 1989). Majority of the samples plotted near the acidic source field.
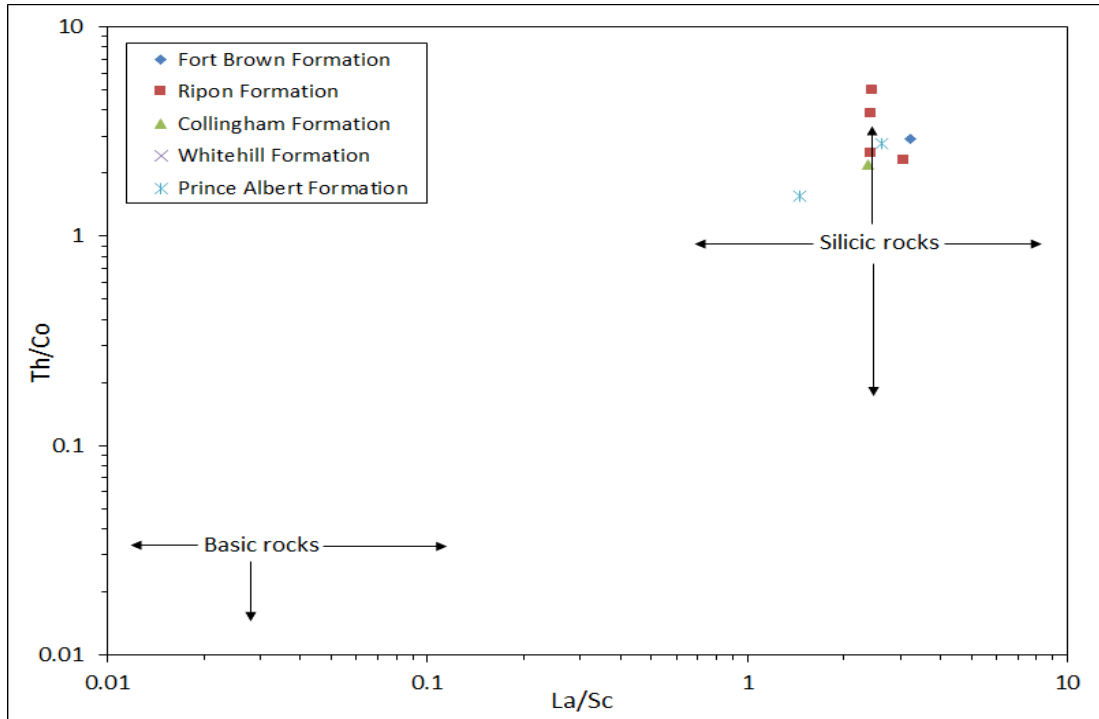
Figure 7.16: Th/Co versus La/Sc plot showing source rock composition for the Ecca shales (After Cullers, 2002).
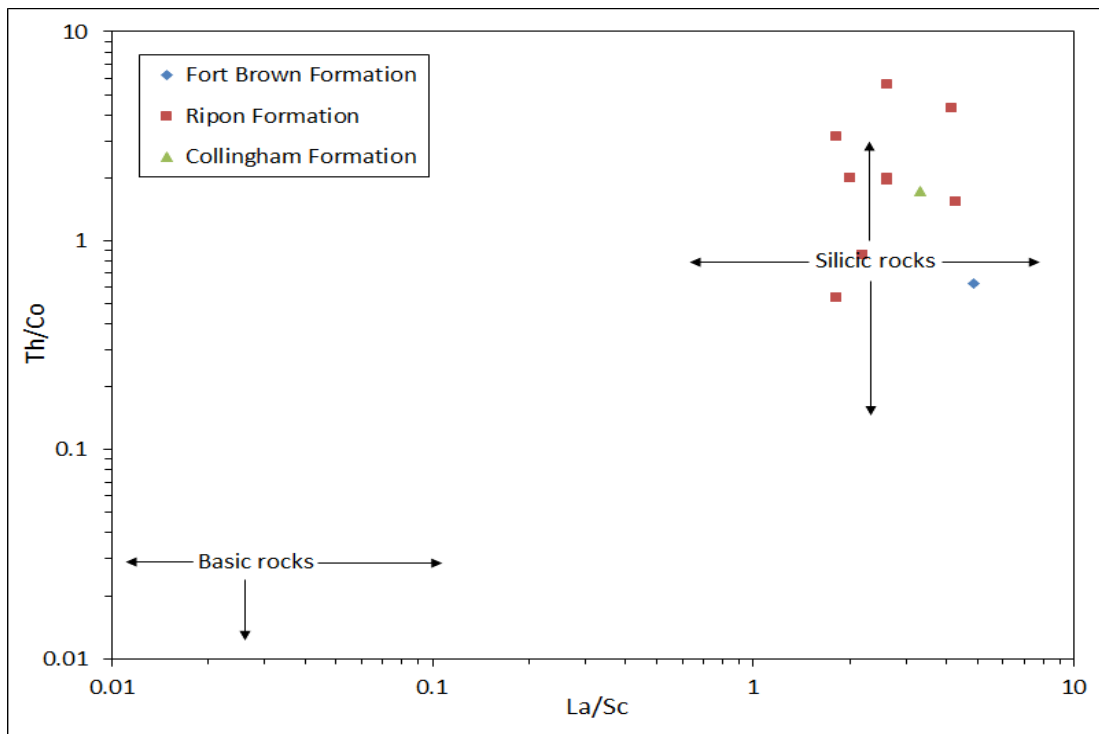
Figure 7.17: Th/Co versus La/Sc plot showing source rock composition for the Ecca shales (After Cullers, 2002).
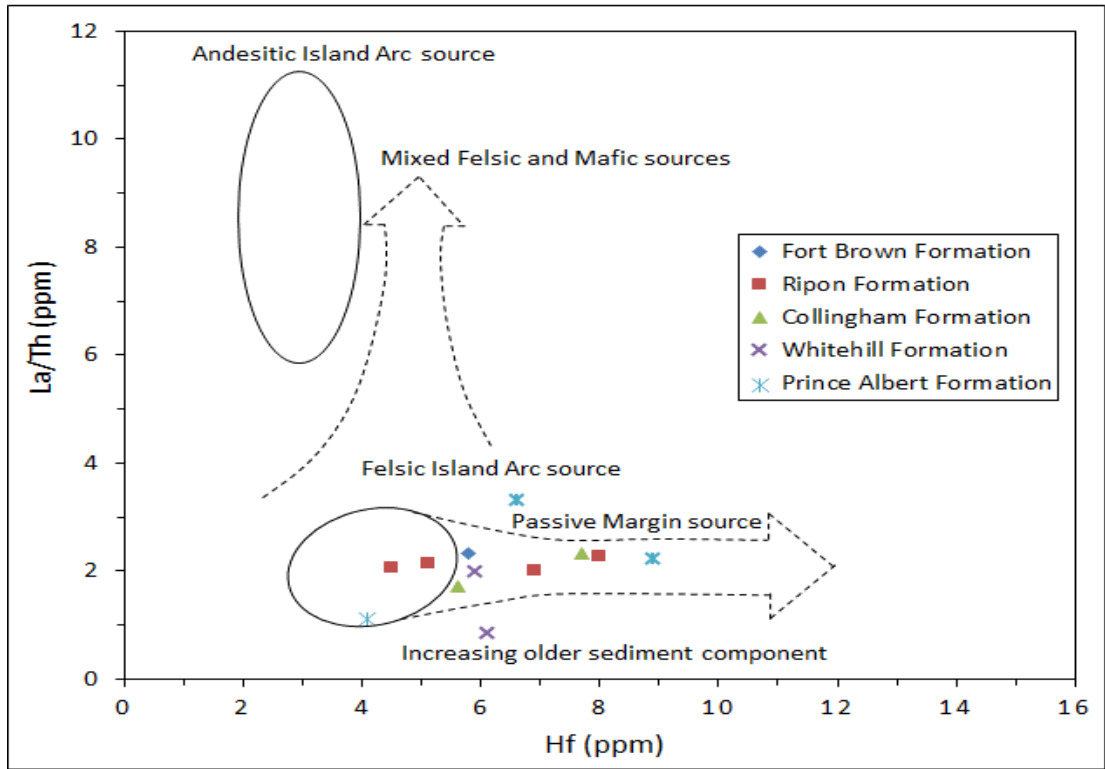
Figure 7.18: Plot of Hf versus La/Th for the Ecca shales (After Floyd and Leveridge, 1987).
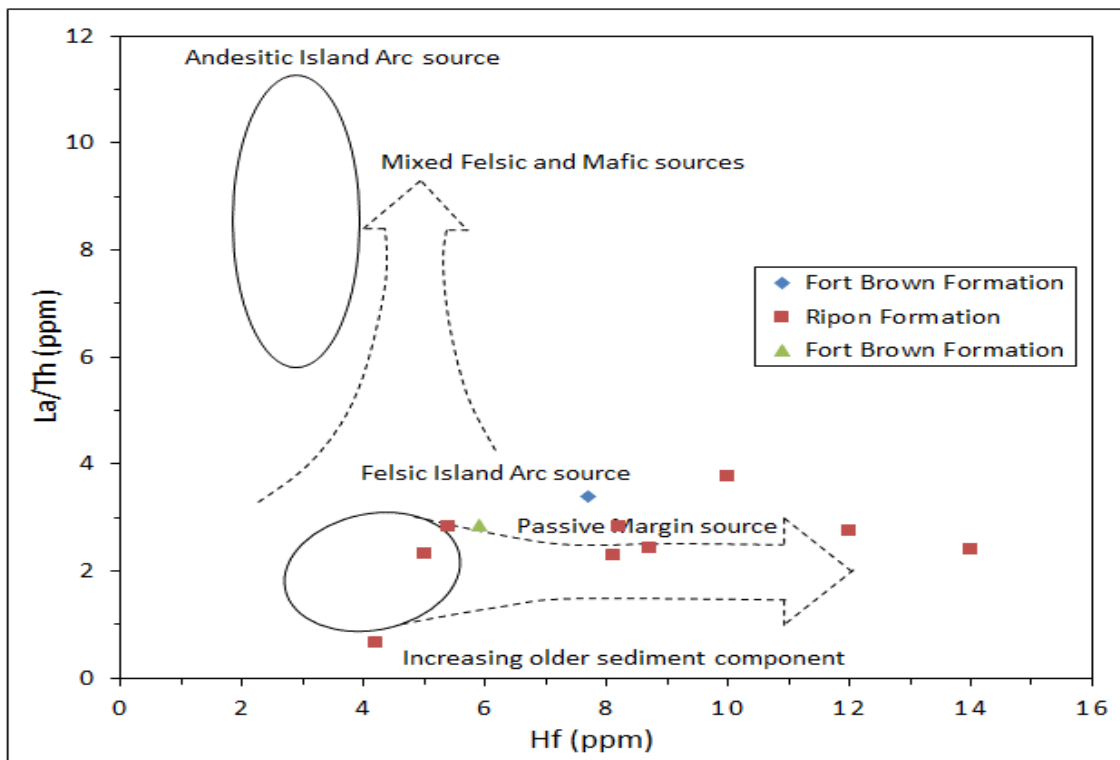
Figure 7.19: Plot of Hf versus La/Th for the Ecca sandstones (After Floyd and Leveridge, 1987).
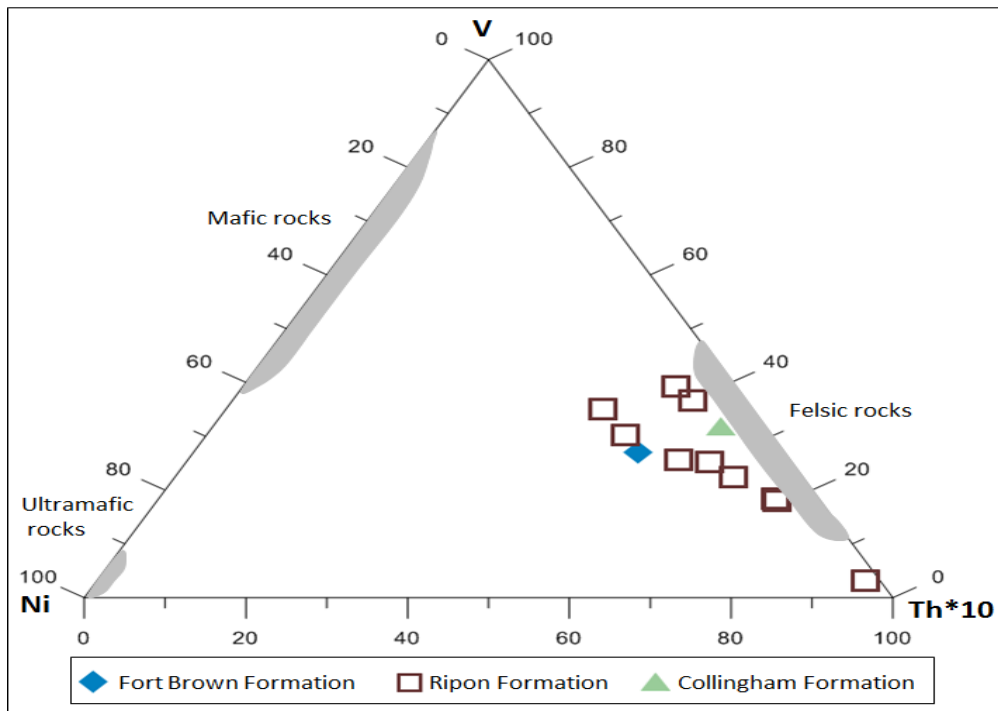
Figure 7.20: V-Ni-Th*10 triangle diagram for the Ecca sandstones (After Bracciali et al., 2007). Shaded area represents composition of the felsic, mafic and ultramafic rocks.
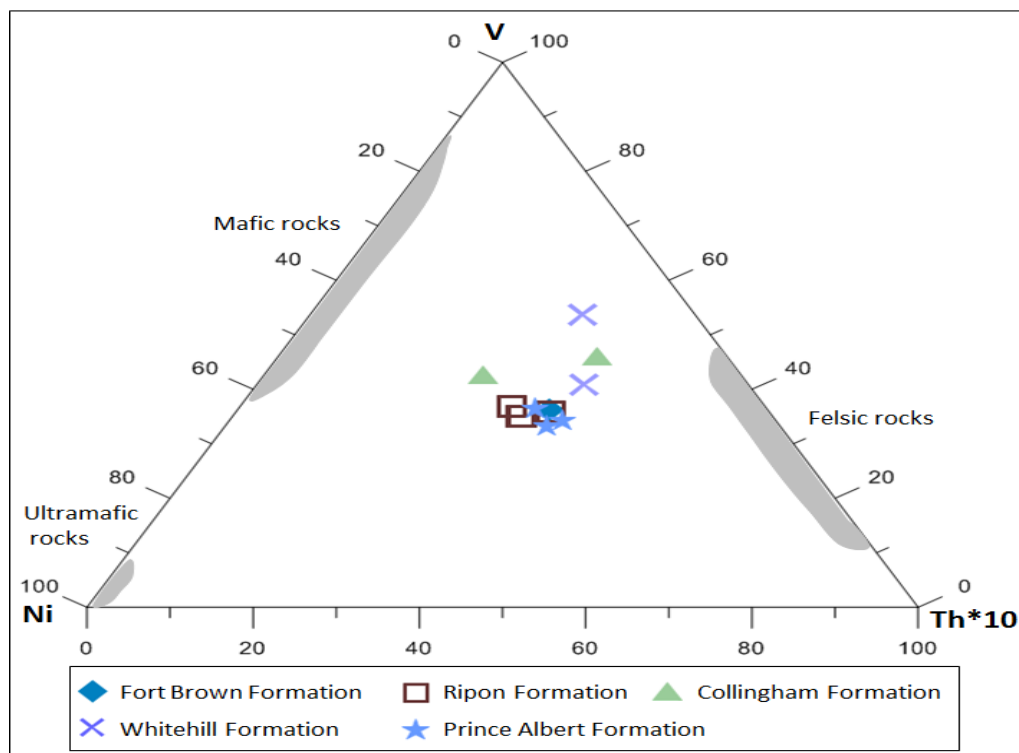
Figure 7.21: V-Ni-Th*10 triangle diagram for the Ecca shales (After Bracciali et al., 2007). Shaded area represents composition of the felsic, mafic and ultramafic rocks.

Post-Archaean pelites have low concentrations of mafic elements particularly Ni and Cr, when compared to Archaean pelites (McLennan et al., 1993). The reason for the high

concentrations of Ni and Cr in the Archaean pelites is due to the deficiency of ultra-mafic rocks in the post-Archaean Period (Taylor and McLennan, 1985). The Ecca sandstones and shales plot in the post-Archaean field (Figures 7.22 and 7.23) and this suggest that felsic component was dominant in the source area.
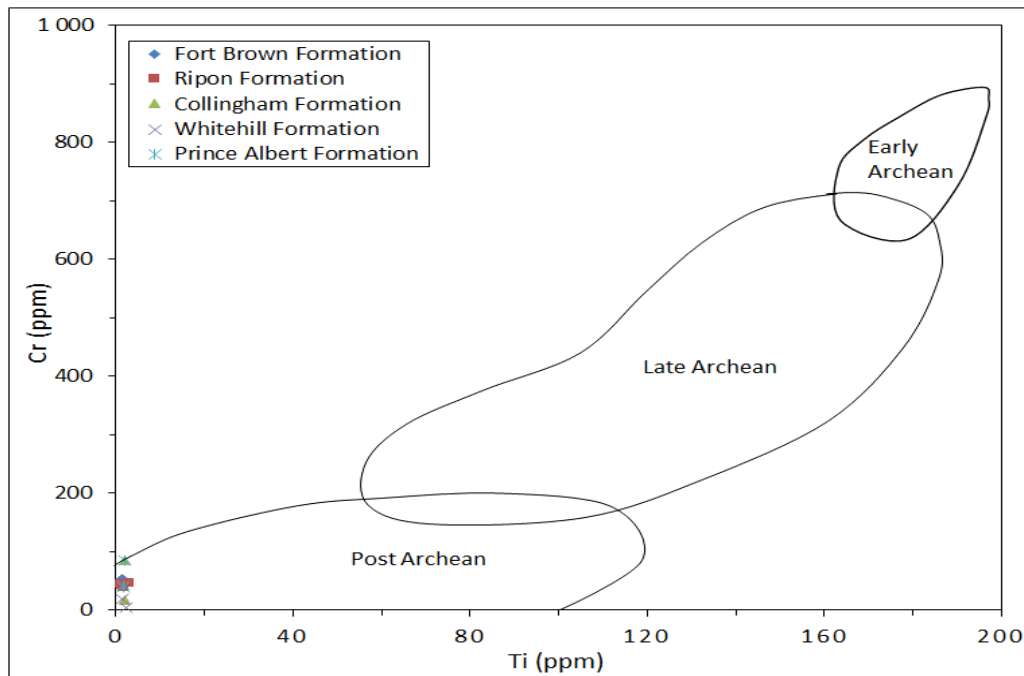
Figure 7.22: Plot of Cr against Ti for the shale samples from the Ecca Group (After McLennan et al., 1993). The samples plotted close to the boundary (bottom left) of the post Archean field.
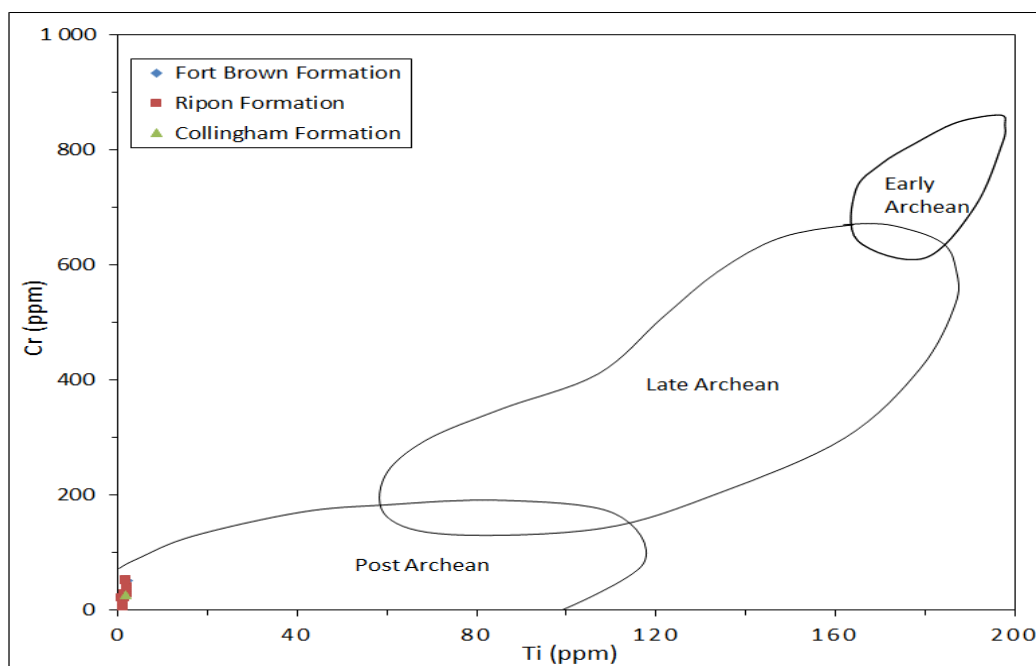
Figure 7.23: Plot of Cr versus Ti for the sandstone samples from the Ecca Group (After McLennan et al., 1993). The samples plotted close to the boundary (bottom left) of the post Archean field.

7.5 Source area weathering

7.5.1 Paleoweathering conditions

Intensity of chemical weathering of source rocks are mainly controlled by the composition of the source rock, duration of weathering, climatic conditions and rates of tectonic uplift of source region (Wronkiewicz and Codie, 1987). Several researchers like Nesbitt and Young (1984; 1989), Taylor and McLennan (1985) and Fedo et al. (1995) have documented that about 75% of labile materials in the uppercrust are composed of feldspars and volcanic glass. Chemical weathering of these materials finally results in the formation of clay minerals. During chemical weathering, Ca, Na and K are largely removed from source rocks and the amount of these elements surviving in sediments derived from the rocks serve as indicator of the intensity of chemical weathering (Nesbitt et al., 1997). According to Lindsey (1999), if siliciclastic sedimentary rocks are free from alkali related post-depositional modifications, then their alkali contents ($K_2O + Na_2O$) and K_2O/Na_2O ratios should be considered as reliable indicators of the intensity of source material weathering. In order to determine the degree of source rock weathering, a few indices of weathering have been proposed based on the molecular proportions of mobile and immobile element oxides (Na_2O, CaO, K_2O and Al_2O_3). Thus the chemical composition of weathering products in a sedimentary basin is expected to reveal the mobility of various elements during weathering (Singh et al., 2005). The indices of weathering/alteration includechemical index of alteration (CIA), chemical index of weathering (CIW) and plagioclase index of alteration (PIA). Chemical index of alteration (CIA) proposed by Nesbitt and Young (1982) is the most widely used chemical index to determine the degree of source area weathering. Nesbitt and Young (1982) defined the CIA formula to evaluate the degree of chemical weathering as:

$$CIA = [Al_2O_3 / (Al_2O_3 + CaO^* + Na_2O + K_2O)] \times 100, \qquad [7.1]$$

where CaO^* is the content of CaO incorporated in silicate fraction.

Indices of weathering (CIA, CIW and PIS) calculated from the major elements are tabulated in Table 7.3. The value of CIA gives a measure of the ratio of original/primary minerals and secondary products such as clay minerals. CIA values range from almost 50 in case of fresh rocks to 100 for completely weathered rocks. Thus, CIA values increase with increasing weathering intensity, reaching 100 when all the Ca, Na and K have been leached from weathering residue. The CIA values in the studied Ecca sandstone and shale samples range from 24.41 to 83.76 (averaging 66.30), and 53.77 to 78.28 (averaging 69.74), respectively. These CIA average values revealed relatively moderate to high degree of chemical

weathering in the source area. In addition to CIA, chemical index of weathering (CIW) also provides information on the intensity of chemical weathering the sediments have undergone. In comparison to other weathering indices, the CIW is a superior method involving a restricted number of components that are well-known with consistent geochemical behaviour during weathering. Harnois (1988) expressed the CIW formula as shown below:

$$CIW = [Al_2O_3 / (Al_2O_3 + CaO^* + Na_2O)] \times 100 \qquad [7.2]$$

The CIW values of the studied sandstone and shale samples range from 25.90 to 92.70 (averaging 75.20), and 76.23 to 96.25 (averaging 82.36) respectively. These CIW values point to moderate-high intensive chemical weathering. As documented by Fedo et al. (1995), source area weathering and elemental redistribution during diagenesis also can be assessed using the plagioclase index of alteration (PIA). PIA monitors and quantifies progressive weathering of feldspars to clay minerals (Fedo et al., 1995; Armstrong-Altrin et al., 2004). The maximum value of PIA is 100 for completely altered materials (i.e. kaolinite and gibbsite) and weathered plagioclase has a PIA value of 50. Fedo et al. (1995) defined the PIA formula to evaluate the amount of chemical weathering as:

$$PIA = [(Al_2O_3 - K_2O)/(Al_2O_3 + CaO^* + Na_2O - K_2O)] \times 100 \qquad [7.3]$$

The PIA values of the studied sandstone and shale samples range from 21.910 to 91.82 (averaging 72.23) and 54.92 to 95.14 (averaging 78.76), respectively. Again, The PIA values suggest moderate-high or intense destruction of feldspars during source weathering, transport, sedimentation, and diagenesis. During the initial stages of weathering, Ca is quickly leached than Na and K. With increasing weathering, the total alkali content ($K_2O + Na_2O$) decreases with increase in K-Na ratio (K_2O/Na_2O). This is due to destruction of feldspars among which plagioclase is more favourably removed than K-feldspars (Nesbitt and Young, 1984). Feldspathic materials in the studied sandstone and shale samples were subjected to variable intensities of weathering during the different evolution stages. The individual bivariate plots of K_2O/Na_2O, $K_2O + Na_2O$, Na_2O, K_2O and CaO against PIA can be used to unravel the mobility of elements during the final stages of chemical weathering of previously altered feldspars. In the bivariate plot of K_2O/Na_2O against PIA (Figure 7.24a), the values of K_2O/Na_2O in the sandstone commonly increases with increasing values of PIA. On the contrary, the total content of alkalis in the most of the sample decreases with increasing values of PIA in the plot of $K_2O + Na_2O$ versus PIA (Figure 7.24b). Figures 7.24 and 7.25

(c-e) shows the behaviour of Na, Ca and K during progressing weathering of feldspars in the sandstones and shales.

Table 7.3: Indices of weathering (CIA, CIW and PIS) calculated from the major elements.

Sample ID	Formation	Lithology	CIA	CIW	PIA	ICV
FB	Fort Brown	Shale	71.53	82.69	79.49	0.84
FB2	Fort Brown	Sandstone	83.76	92.70	91.82	1.29
RP*	Ripon	Sandstone	72.11	84.76	81.51	0.70
R 11	Ripon	Sandstone	24.41	25.90	21.10	3.61
R 9	Ripon	Sandstone	77.03	87.24	85.29	0.88
R 8	Ripon	Sandstone	71.46	83.46	80.12	0.74
R 6	Ripon	Sandstone	34.34	36.51	32.23	2.35
R 5	Ripon	Sandstone	73.78	84.07	81.49	0.75
R 4	Ripon	Sandstone	71.93	80.88	78.16	0.81
R 3	Ripon	Sandstone	74.51	84.94	82.49	0.84
R 2	Ripon	Sandstone	69.34	77.18	74.27	0.94
R 1	Ripon	Sandstone	73.88	84.31	81.73	0.74
RPP	Ripon	Shale	70.89	83.35	79.80	0.83
RC	Ripon	Shale	72.15	85.46	82.17	0.80
R 10	Ripon	Shale	67.01	79.87	75.09	0.96
R 7	Ripon	Shale	65.46	76.23	71.55	0.94
CH1	Collingham	Shale	69.75	82.53	78.61	0.64
CA	Collingham	Shale	78.10	94.56	93.11	0.78
CH	Collingham	Sandstone	69.04	80.42	76.56	0.80
WH1	Whitehill	Shale	53.77	60.86	54.92	1.05
WH	Whitehill	Shale	78.28	96.25	95.14	0.40
PA2	Prince Albert	Shale	68.65	81.77	77.46	0.78
PA1	Prince Albert	Shale	70.32	81.16	77.73	0.79
PA	Prince Albert	Shale	71.01	83.56	80.03	0.97
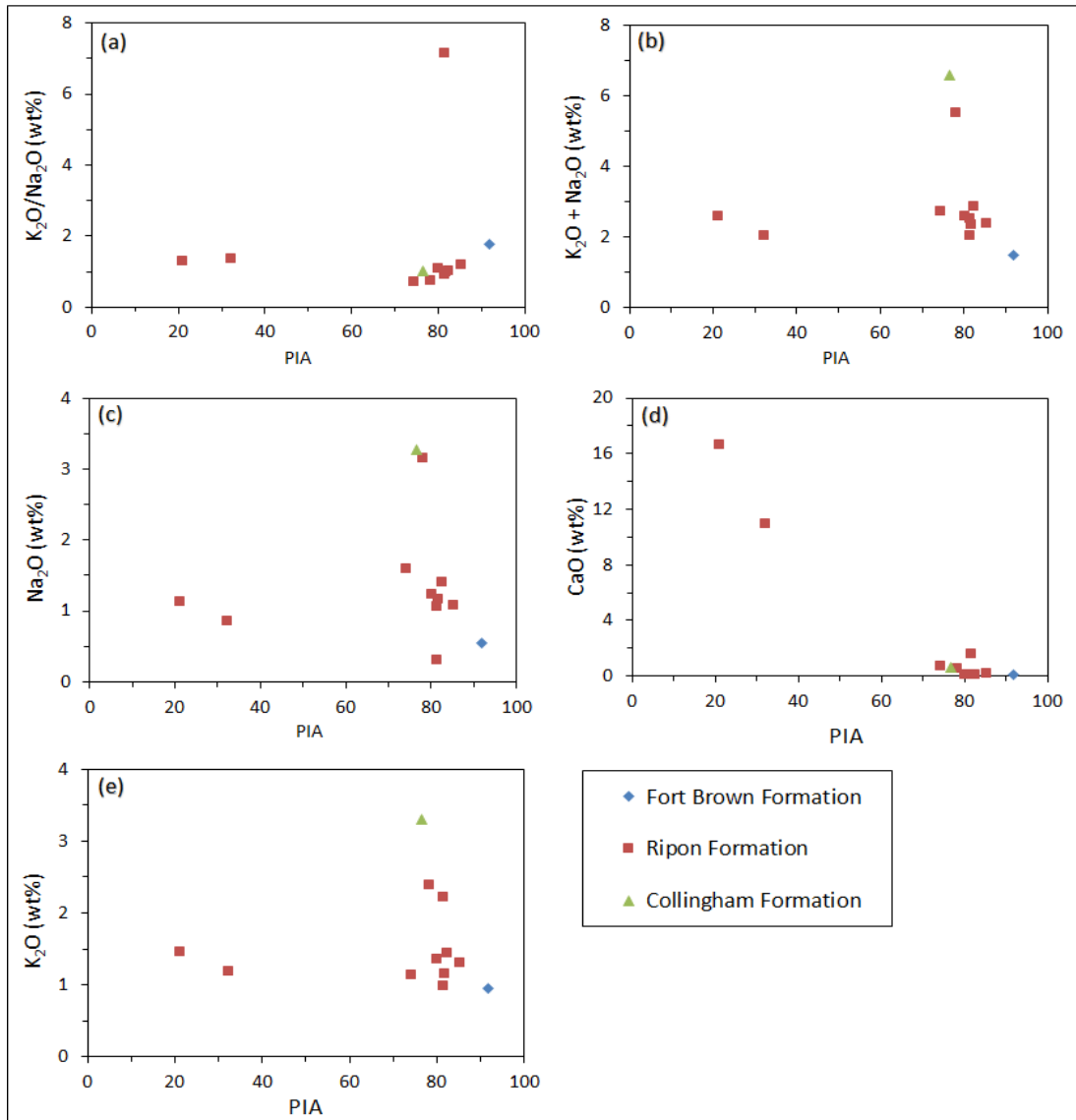
Figure 7.24: Bivariate diagrams depicting mobility of elements during weathering of feldspars in the sandstone samples from the Ecca Group. (a) (K_2O/Na_2O) wt.% versus PIA. (b) ($K_2O + Na_2O$) wt.% versus PIA. (c) Na_2O wt.% versus PIA. (d) CaO wt.% versus PIA. (e) K_2O wt.% versus PIA.
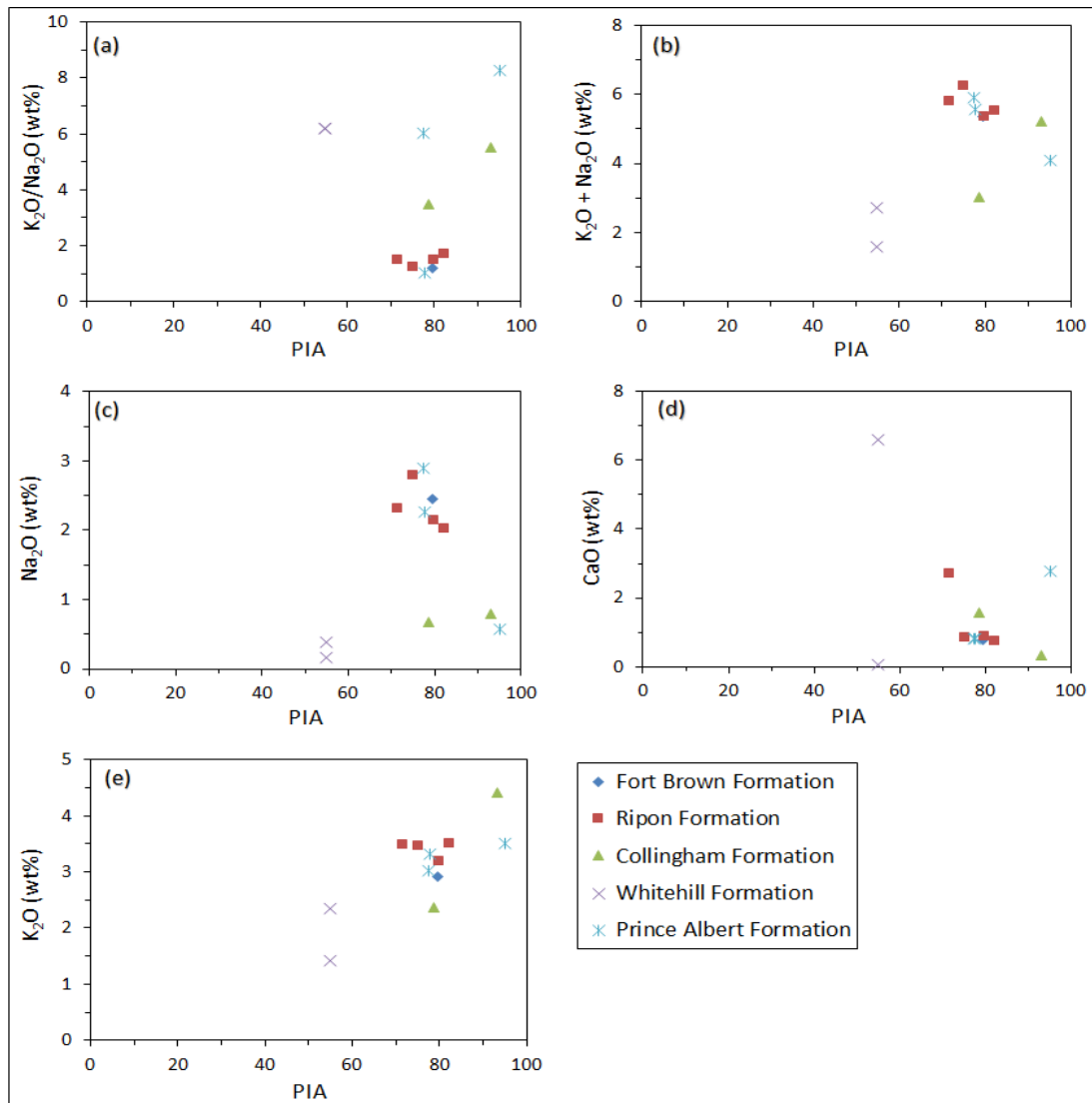
Figure 7.25: Bivariate diagrams depicting mobility of elements during weathering of feldspars in the shales from the Ecca Group. (a) (K_2O/Na_2O) wt.% versus PIA. (b) ($K_2O + Na_2O$) wt.% versus PIA. (c) Na_2O wt.% versus PIA. (d) CaO wt.% versus PIA. (e) K_2O wt.% versus PIA.

Ternary plot of A-CN-K proposed by Nesbitt and Young (1984) is another method used to assess the composition of original source rock as well as the mobility of elements during the process of chemical weathering of source material and post-depositional chemical modifications. The ternary plot of Al_2O_3-(CaO + Na_2O)-K_2O (represented as A-CN-K) is useful for identifying compositional changes of shales and sandstones that are related to chemical weathering, diagenesis and source rock composition. Geochemical data of the sandstones and shales from the Ecca Group are plotted in an A-CN-K diagram (Figures 7.26 and 7.27; After Nesbitt and Young, 1984). The arrows 1 to 5 in Figures 7.26 and 7.27 represent the weathering trends of gabbro, tonalite, granodiorite, adamellite and granite, respectively (Fedo et al., 1997).
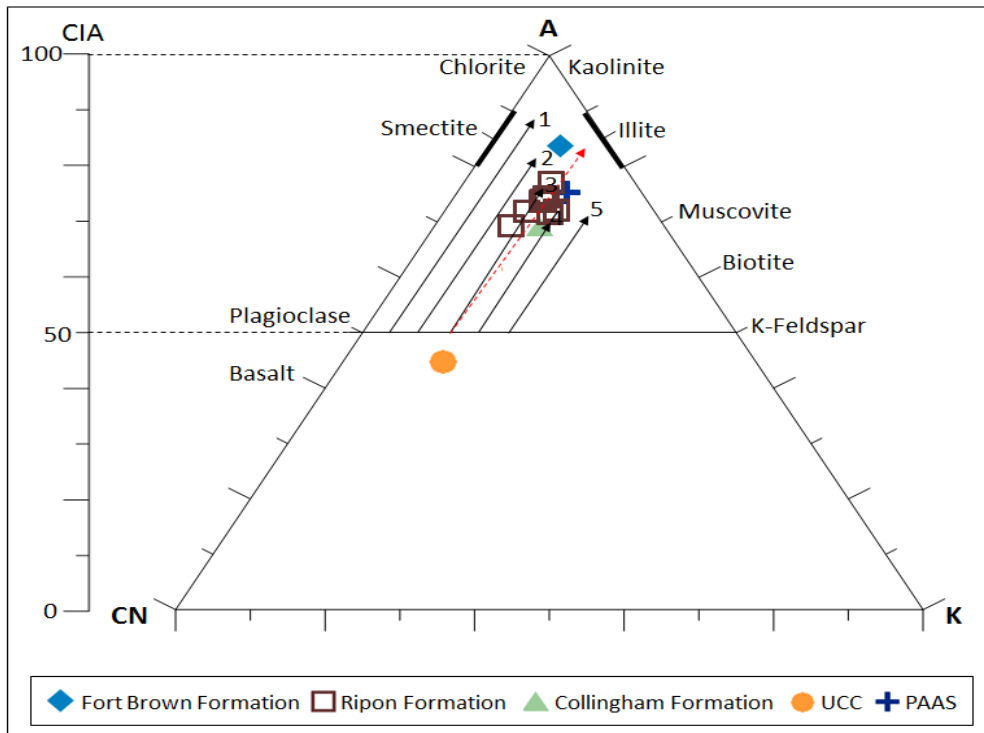
Figure 7.26: A-CN-K ternary diagram of molecular proportions of Al$_2$O$_3$-(CaO+Na$_2$O)-K$_2$O for sandstones from the Ecca Group (After Nesbitt and Young, 1984). The dotted arrow shows the actual weathering trend for the samples. The CIA scale shown at the left side is for comparison.
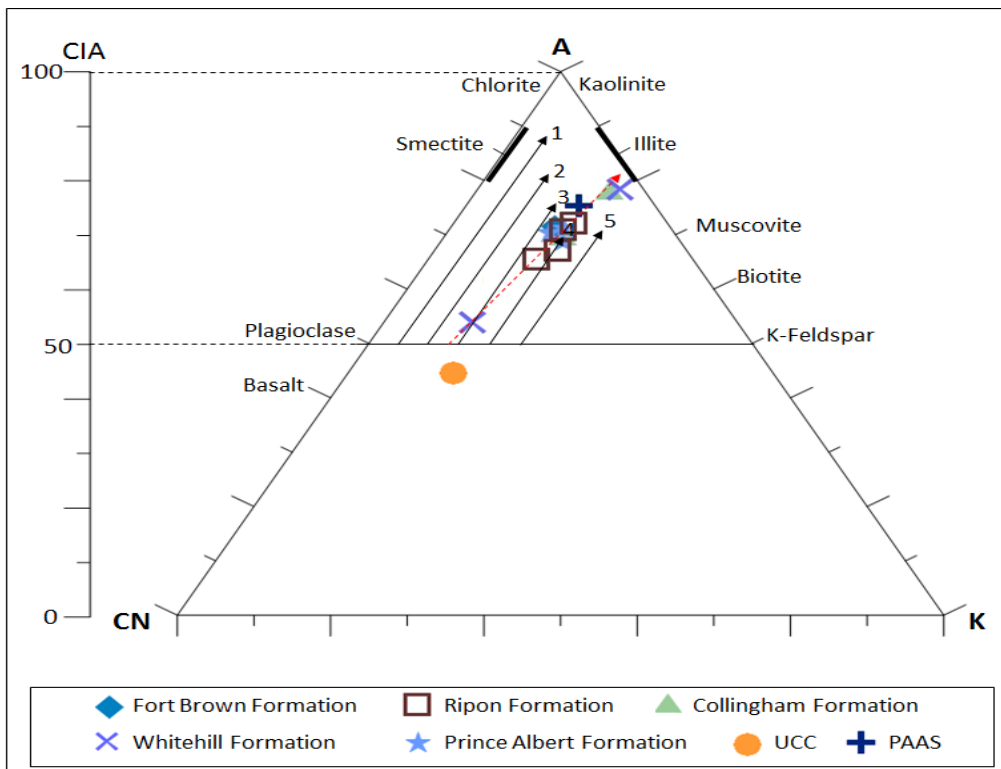
Figure 7.27: A-CN-K ternary diagram of molecular proportions of Al$_2$O$_3$-(CaO+Na$_2$O)-K$_2$O for shale samples from the Ecca Group (After Nesbitt and Young, 1984). The dotted arrow shows the actual weathering trend for the samples.

In the A-CN-K diagram (Figures 7.26 and 7.27), the sandstones and shales plot above the line joining plagioclase and potash feldspar. The plots define a narrow linear trend which runs slightly at an angle parallel to the A-CN edge. This is possibly due to the fact that the removal rate of Na and Ca from plagioclase is generally greater than the removal rate of K from microcline (Nesbitt and Young, 1984). The plots trend towards illite on the A-K edge and do not show any inclination towards the K apex, thus indicating that the sandstones and shales are free from potash metasomatism during diagenesis. The trend line when extended backward intersects the plagioclase-potash feldspar join near arrow 3, which is the field of granodiorite (potential ultimate source). Linear weathering trend point to steady state of weathering conditions where material removal matches with production of weathering material (Nesbitt et al., 1997).

7.5.2 Climatic conditions and sediment maturity

The original character and maturity of sediments as well as the prevailed climatic conditions can be determined by calculating the index of compositional variability (ICV) proposed by Cox et al. (1995). The ICV tends to be highest in minerals that are high in weathering intensity and decreases in more stable minerals (less weathered minerals). The ICV decreases further in the montmorillonite group clay minerals and is lowest in the kaolinite group minerals (Cox et al., 1995). In addition, more mature shale tends to have low ICV values ($<$ 1.0).

$$ICV = (Fe_2O_3 + K_2O + Na_2O + CaO + MgO + MnO)/Al_2O_3 \quad [7.4]$$

As documented by Cox et al. (1995), sandstones or shales with ICV $>$ 1 are compositionally immature with the first cycle of sediments deposited in tectonically active settings. On the other hand, those with ICV $<$ 1 are compositionally mature and are deposited in the tectonically quiescent or cratonic environment where sediment recycling is active. For the studied sandstones and shales, the ICV values range from 0.71 to 3.6 (averaging 1.20) and 0.41 to 1.05 (averaging 0.82). Based on the average ICV values, it can be inferred that the sandstones are compositionally immature whereas the shales are compositionally mature and deposited in the tectonically quiescent or cratonic environment. The K_2O/Na_2O ratios for the sandstones vary from 0.71 to 7.16 (averaging 1.61) and 1.04 to 8.29 (averaging 3.26) for the shale samples. These ratios revealed moderate to high maturity of the shales and it agrees with the ICV values (Wronkiewicz and Codie, 1987). The K_2O/Na_2O ratios are comparable to those of sediments from passive margins, which increase with maturity of rocks (Bhatia,

1983). The binary plot of CIA against ICV for the studied samples (Figure 7.28) shows that most of the shales are geochemically mature and were derived from both weak and intensively weathered source rocks.
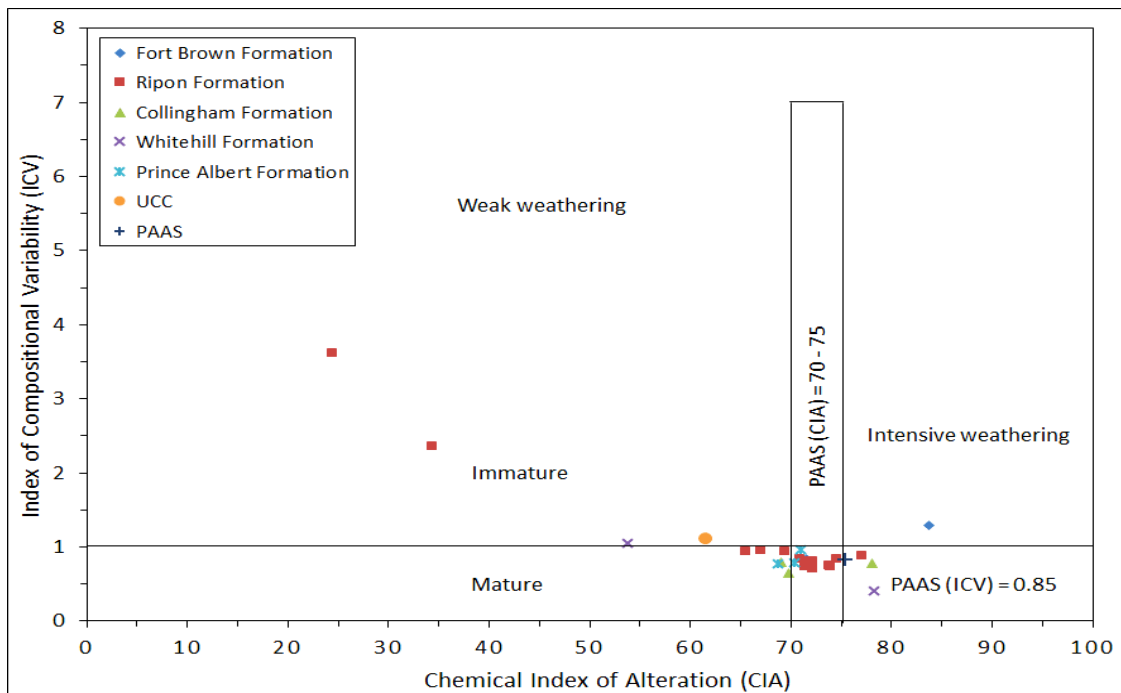
Figure 7.28: Binary plot of CIA against ICV for the Ecca shale and sandstone samples.

Alternatively, SiO_2/Al_2O_3 ratios of siliciclastic rocks are sensitive to sediment recycling and weathering process and can serve as an indicator of sediment maturity. Roser and Korsch (1986) and Roser et al. (1996) documented that, with increasing sediment maturity, quartz survives preferentially to feldspars, mafic minerals and lithics. The average SiO_2/Al_2O_3 ratios in unaltered igneous rocks range from ∼ 3.0 (basic rocks) to ∼ 5.0 (acidic rocks). Values of SiO_2/Al_2O_3 ratio > 5.0 in sandstones and shales point to progressive maturity (Roser et al., 1996). The SiO_2/Al_2O_3 ratios of the sandstones vary from 4.16 to 14.77 (averaging 9.45), while those of the shales range from 3.94 to 14.89 (averaging 5.50). The K_2O/Na_2O ratios of the sandstones range from 0.76 to 7.16 (averaging 1.61), while those of the shales vary from 1.04 to 8.29 (averaging 3.26). The low values of K_2O/Na_2O ratios as well as the high values of SiO_2/Al_2O_3 indicate low to moderate sediment maturity. To constrain the climatic condition during sedimentation of siliciclastic sedimentary rocks, the Suttner and Dutta (1986) proposed plot of SiO_2 against $(Al_2O_3 + K_2O + Na_2O)$ was used to classify the maturity of Ecca sandstones and shales as a function of climate. Figure 7.29 shows that the sandstones and shales mostly plot in the field of arid climate with few samples plotting in the humid climate field with varied maturity.
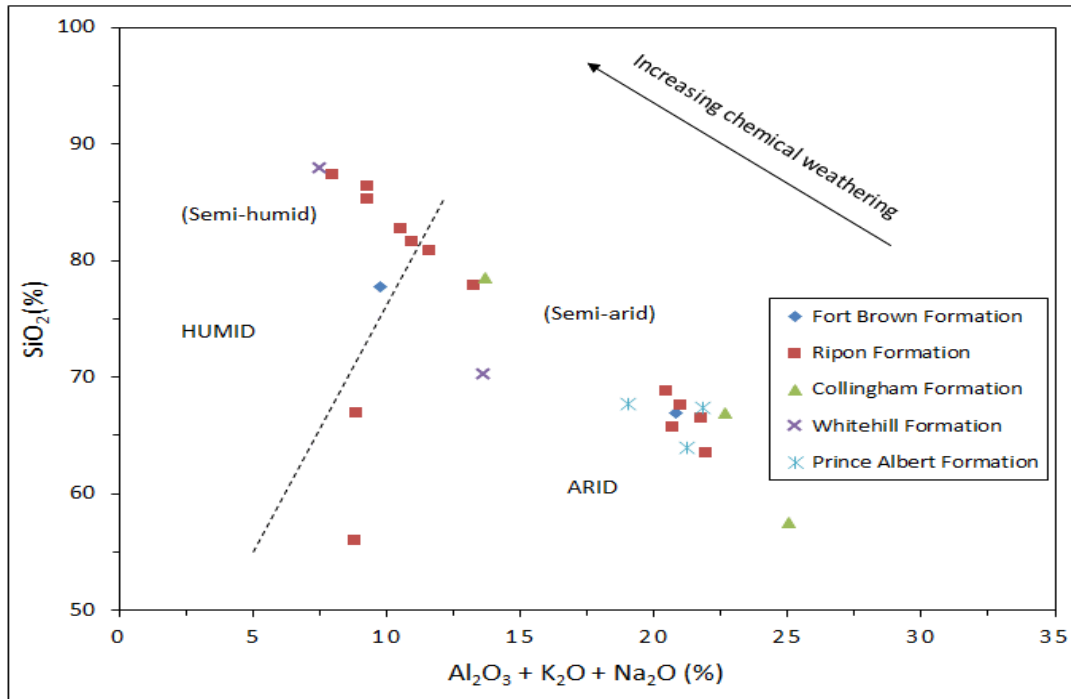
Figure 7.29: Chemical maturity of the Ecca sandstones and shales (After Suttner and Dutta, 1986).

7.6 Tectonic setting of the source area

Several researchers like Bhatia (1983), Bhatia and crook (1986) and Roser and Korsch (1986) documented that the chemical compositions of siliciclastic sedimentary rocks are considerably controlled by plate tectonic settings of their provenances and depositional basins. Thus, siliciclastic rocks from different tectonic settings possess terrain-specific geochemical signatures. McLennan et al. (1993) documented that the tectonic setting discrimination diagrams give reliable results for siliciclastic rocks that have not been strongly affected by post-depositional weathering and metamorphism. Bivariate plots of major and trace element geochemistry have been used by several researchers to determine the tectonic setting of sandstones and shales (i.e. Bhatia, 1983; Roser and Korsch, 1986; McCann, 1991; Toulkeridis et al., 1999; Murphy, 2000). Among the various tectonic setting discrimination diagrams, the major element-based discrimination diagrams of Bhatia (1983) and Roser and Korsch (1986) are widely used. Bhatia (1983) divided a series of plots to differentiate between four main tectonic settings, namely, oceanic island arc (OIA), continental island arc (CIA), active continental margin (ACM) and passive continental margin (PM). Chemical analyses data of the sandstones and shales have been plotted on 4 tectonic setting discrimination diagrams of Bhatia (1983), Roser and Korsch (1986), Bhatia and Crook (1986) and Toulkeridis et al. (1999). Bivariate plots of TiO_2 versus ($Fe_2O_3 + MgO$) and Al_2O_3/SiO_2

against $Fe_2O_3 + MgO$ shows that most of the studied samples plot in the passive margin, active continental margin and continental island arc fields (Figures 7.30 and 7.31; After Bhatia, 1983). In Figure 7.31, only one sample plot in the oceanic island arc field. The Bivariate plot of K_2O/Na_2O versus $(Fe_2O_3 + MgO)$ and $Al_2O_3/(CaO + Na_2O)$ versus $(Fe_2O_3 + MgO)$ reveal that the sandstones and shales are related to continental margin (Figures 7.32 and 7.33; After Bhatia, 1983).
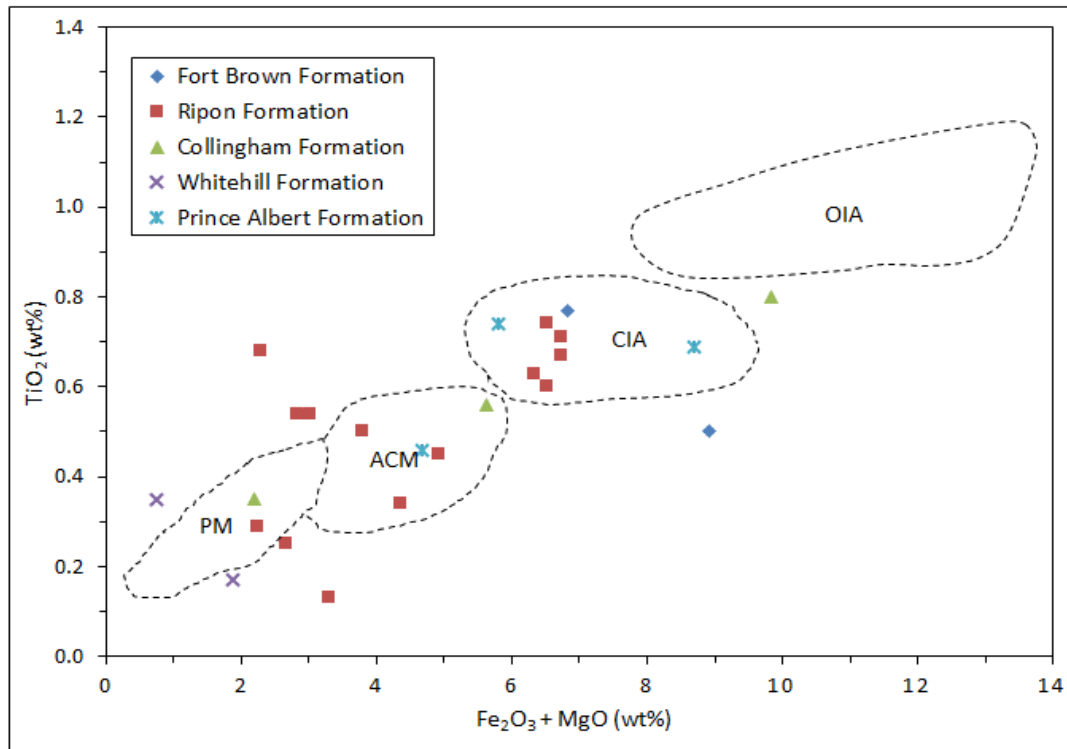
Figure 7.30: Bivariate plot of TiO_2 (wt.%) versus $(Fe_2O_3 + MgO)$ (wt.%) of the Ecca rocks on the tectonic setting discrimination diagram of Bhatia (1983). PM: Passive Margin, ACM: Active Continental Margin, CIA: Continental Island Arc, OIA: Oceanic Island Arc.
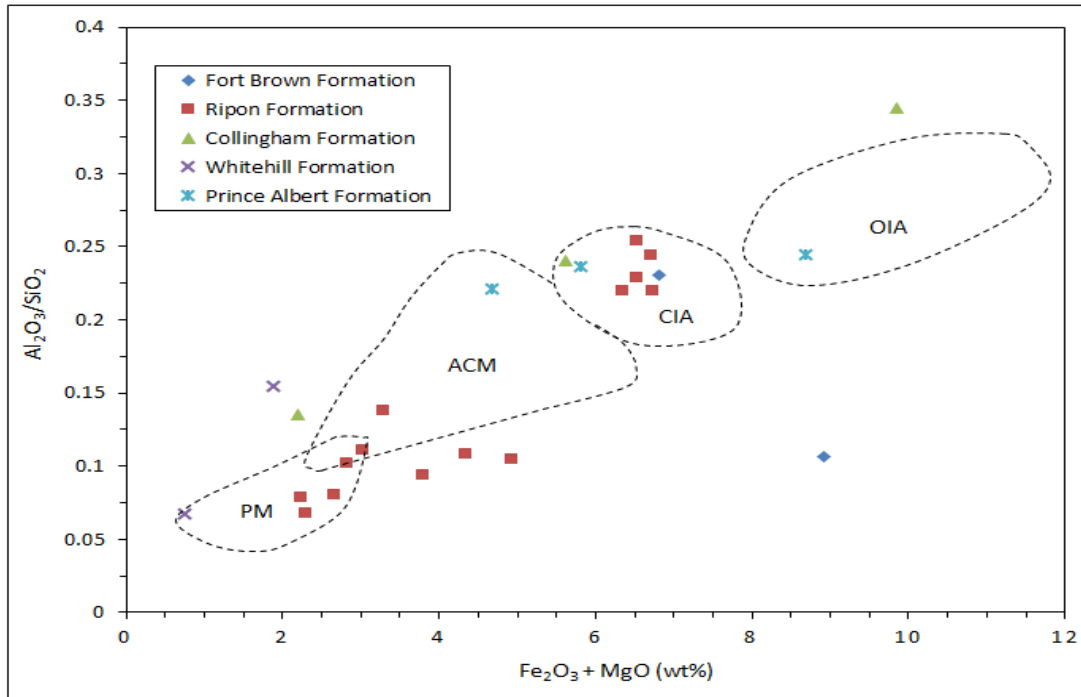
Figure 7.31: Plot of Al_2O_3/SiO_2 versus Fe_2O_3 + MgO (wt.%) of the Ecca sandstones and shales on the tectonic setting discrimination diagram of Bhatia (1983). PM: Passive Margin, ACM: Active Continental Margin, CIA: Continental Island Arc, OIA: Oceanic Island Arc.
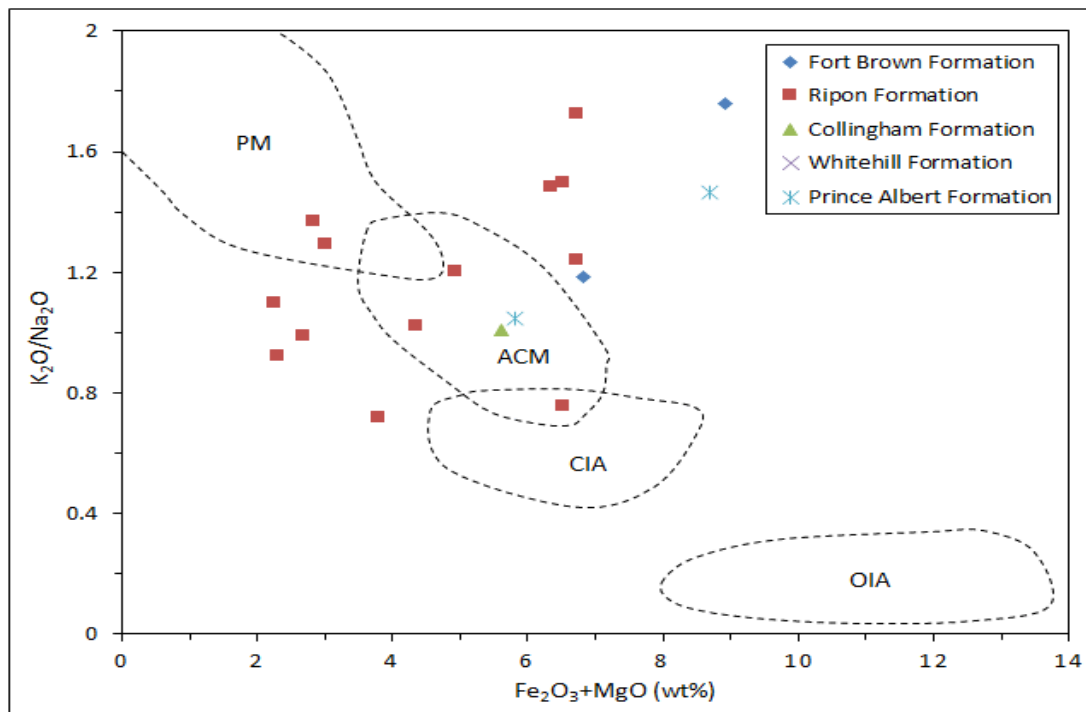
Figure 7.32: Plot of K_2O/Na_2O versus (Fe_2O_3 + MgO) (wt.%) of the Ecca sandstones and shales on the tectonic setting discrimination diagram of Bhatia (1983). PM: Passive Margin, ACM: Active Continental Margin, CIA: Continental Island Arc, OIA: Oceanic Island Arc.
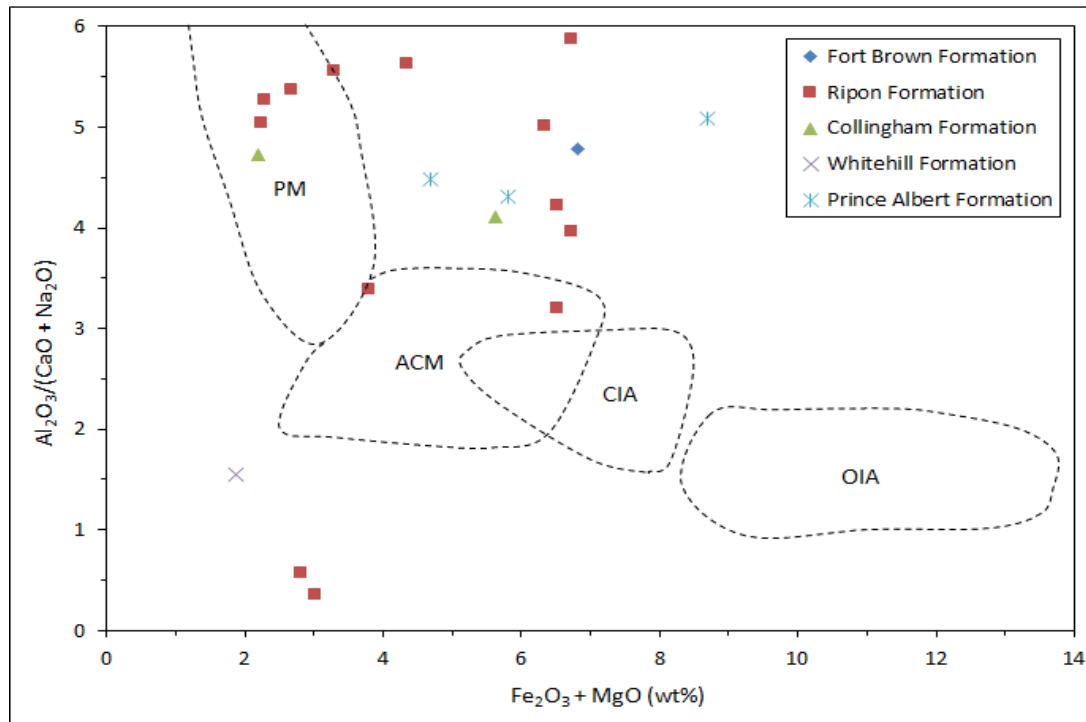
Figure 7.33: Bivariate plot of $Al_2O_3/(CaO + Na_2O)$ versus $(Fe_2O_3 + MgO)$ (wt.%) of the Ecca sandstones and shales on the tectonic setting discrimination diagram of Bhatia (1983). PM: Passive Margin, ACM: Active Continental Margin, CIA: Continental Island Arc, OIA: Oceanic Island Arc.

Most of the shale samples represent the active continental margin and few samples fall in the passive continental margin field (Figure 7.34). In addition, only one sample from the Prince Albert Formation plotted in the island arc field. Active continental margins are subduction related basins, continental basins and pull-apart basins associated with strike-slip fault zones. On the other hand, passive continental margins are basins on continental crust and basins associated with ocean floor spreading, failed rifts and Atlantic-type continental margins. Most of the sandstone samples plotted in the passive continental margins and two samples each fall in the island arc and active continental margin fields (Figure 7.35). Similarly, more detailed results can be obtained using the calc-alkaline ternary diagram $(CaO-Na_2O-K_2O)$. The calc-alkaline ternary diagram depicted in Figure 7.36 shows that most sandstone samples are related to passive continental margin. Shale samples are also represented in both active continental margin and passive continental margin (Figure 7.37).
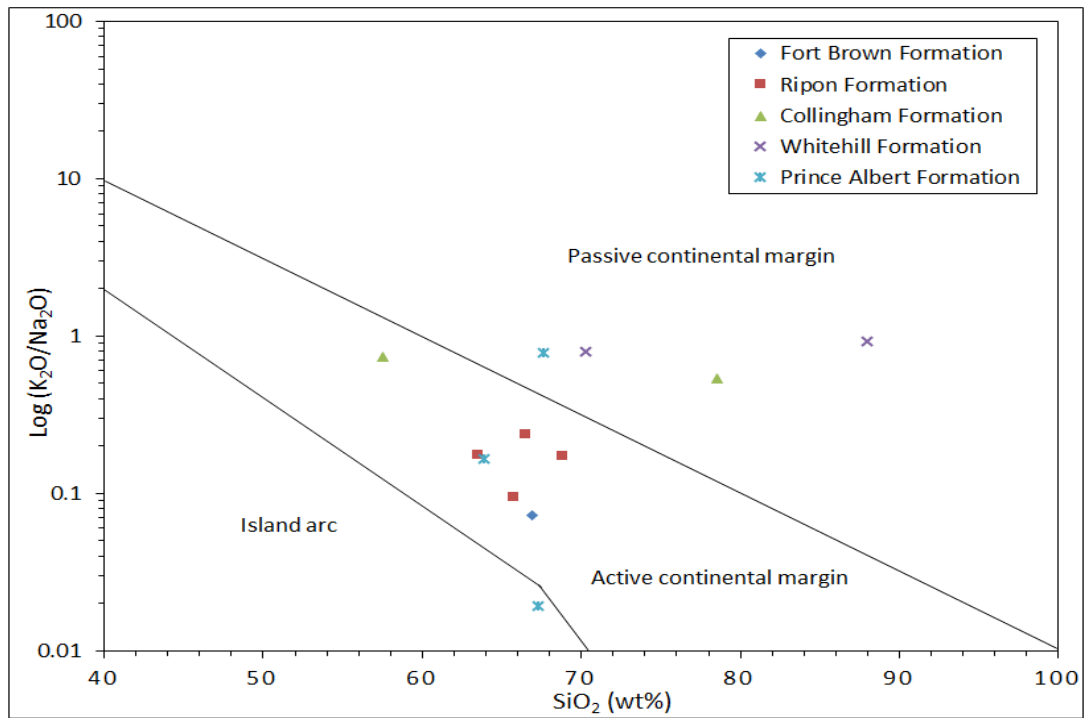
Figure 7.34: K_2O/Na_2O versus SiO_2 tectonic-setting discrimination diagram for Ecca shales (Background field after Roser and Korsch, 1986).
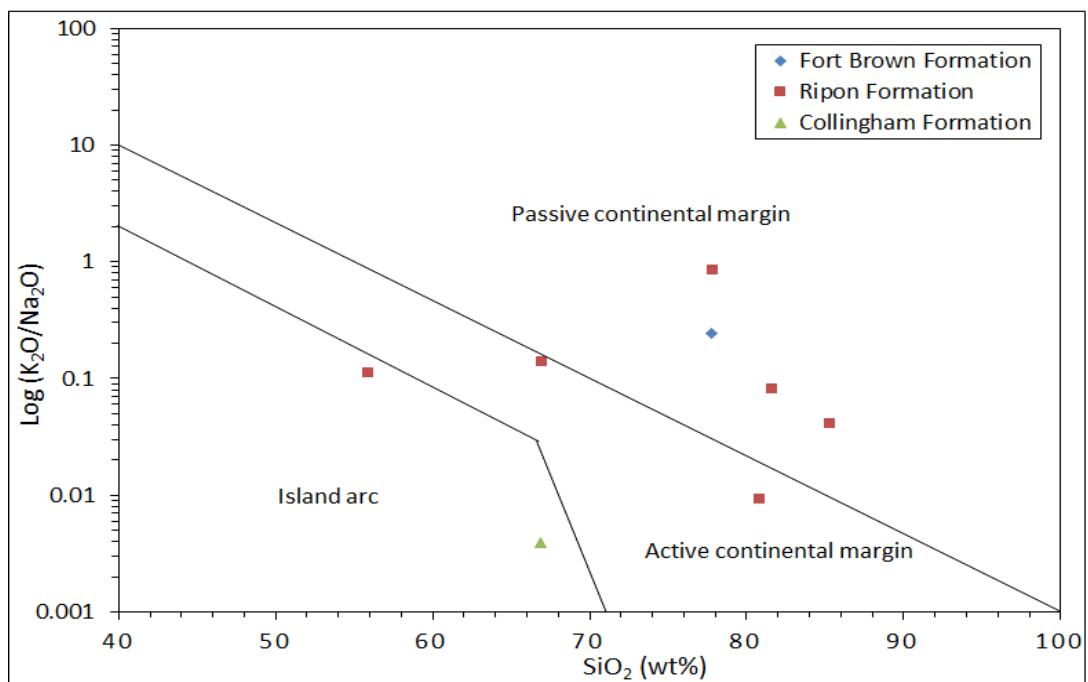
Figure 7.35: K_2O/Na_2O versus SiO_2 tectonic-setting discrimination diagram for Ecca sandstones (Background field after Roser and Korsch, 1986).
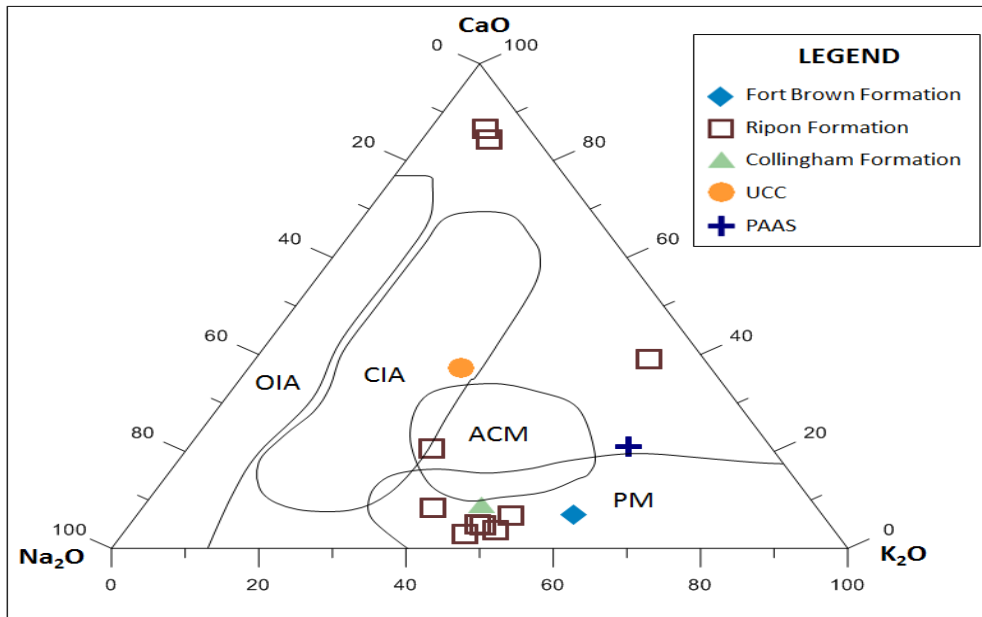
Figure 7.36: Na$_2$O-CaO-K$_2$O ternary plot for sandstone samples from the Ecca Group (Background field after Toulkeridis et al., 1999). OIA = Oceanic Island Arc, CIA = Continental Island Arc, ACM = Active Continental Margin, PM = Passive Continental Margin.
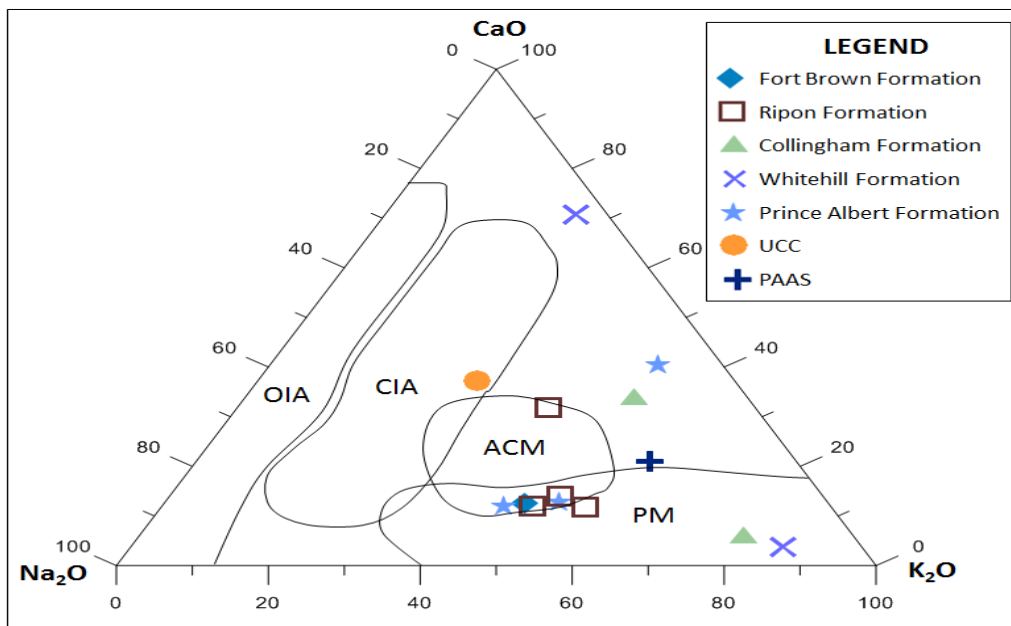
Figure 7.37: Na$_2$O-CaO-K$_2$O ternary plot for shale samples from the Ecca Group (Background field after Toulkeridis et al., 1999). OIA = Oceanic Island Arc, CIA = Continental Island Arc, ACM = Active Continental Margin, PM = Passive Continental Margin.

Th-Sc-Zr/10 tectonic discrimination diagram of Bhatia and Crook (1986) revealed that the source area for most of the Ecca samples is predominantly of passive continental margin (Figures 7.38 and 7.39). Several researchers (i.e. Bhatia, 1983) have documented that immobile elements like La, Zr and Hf are enriched in the passive margin setting. La-Th-Sc

tectonic discrimination diagram demonstrates the passive margin setting of the depositional basin for the Ecca sandstones and shales (Figures 7.40 and 7.41).
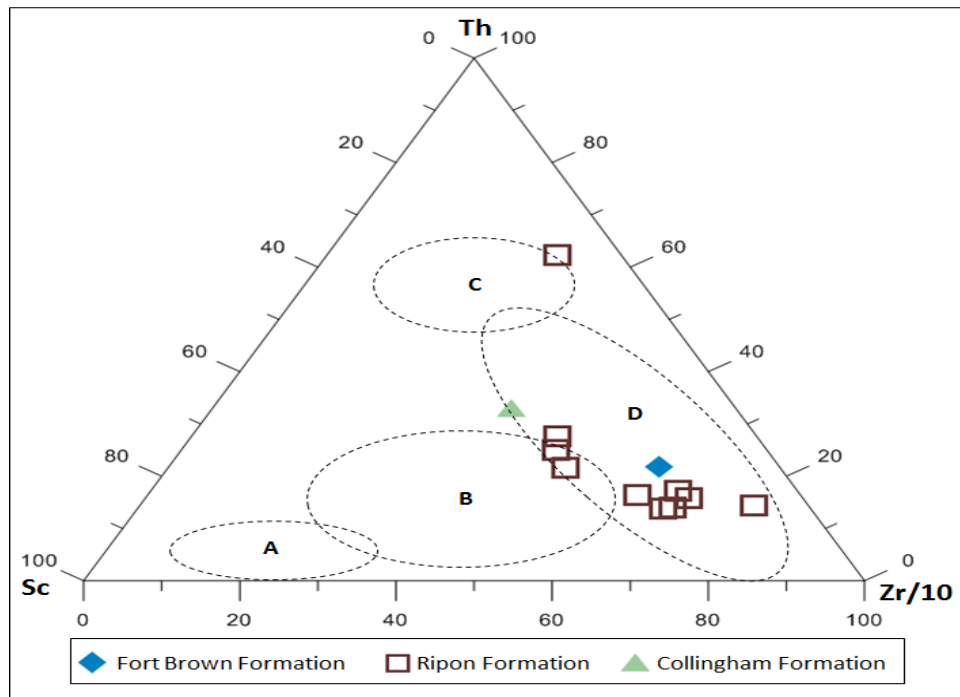
Figure 7.38: Th-Sc-Zr/10 tectonic discrimination diagram for the Ecca sandstones (Background field after Bhatia and Crook, 1986). A = Oceanic Island Arc, B = Continental Island Arc, C = Active Continental Margin, D = Passive Continental Margin.
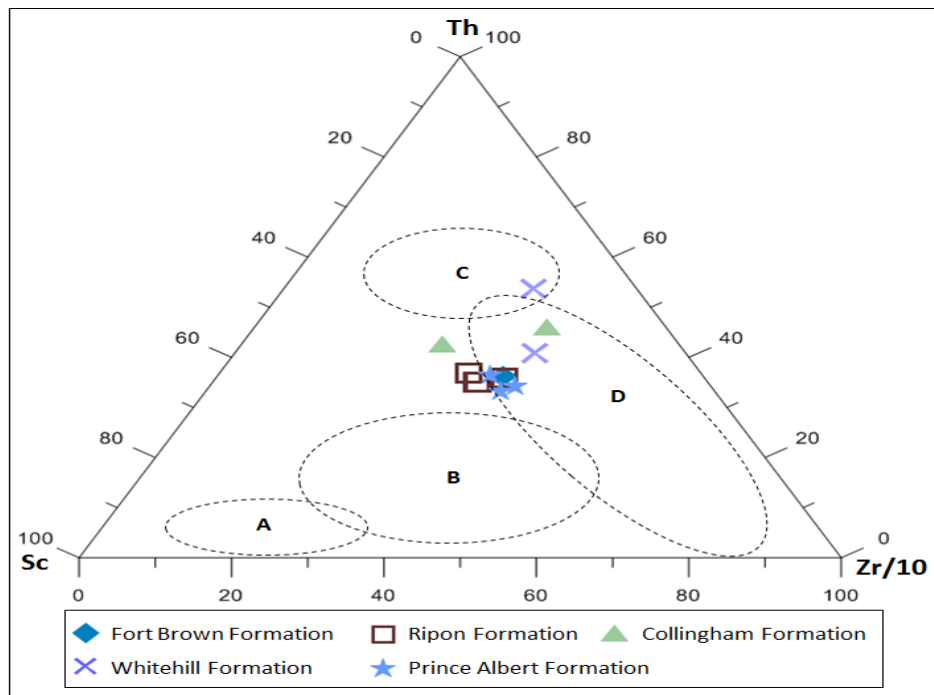
Figure 7.39: Th-Sc-Zr/10 tectonic discrimination diagram for the Ecca shales (After Bhatia and Crook, 1986). A = Oceanic Island Arc B = Continental Island Arc, C = Active Continental Margin, D = Passive Continental Margin.
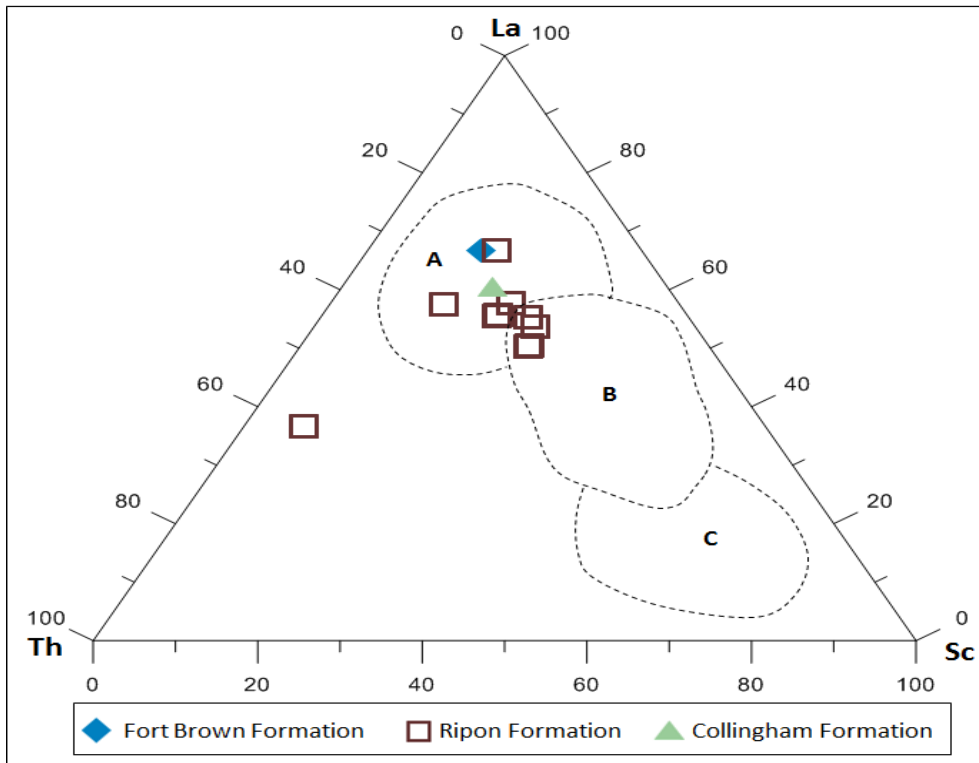
Figure 7.40: La-Th-Sc tectonic discrimination diagram for the Ecca sandstones (After Bhatia and Crook, 1986). A = Passive and Active Continental Margin, B = Continental Island Arc, C = Oceanic Island Arc.
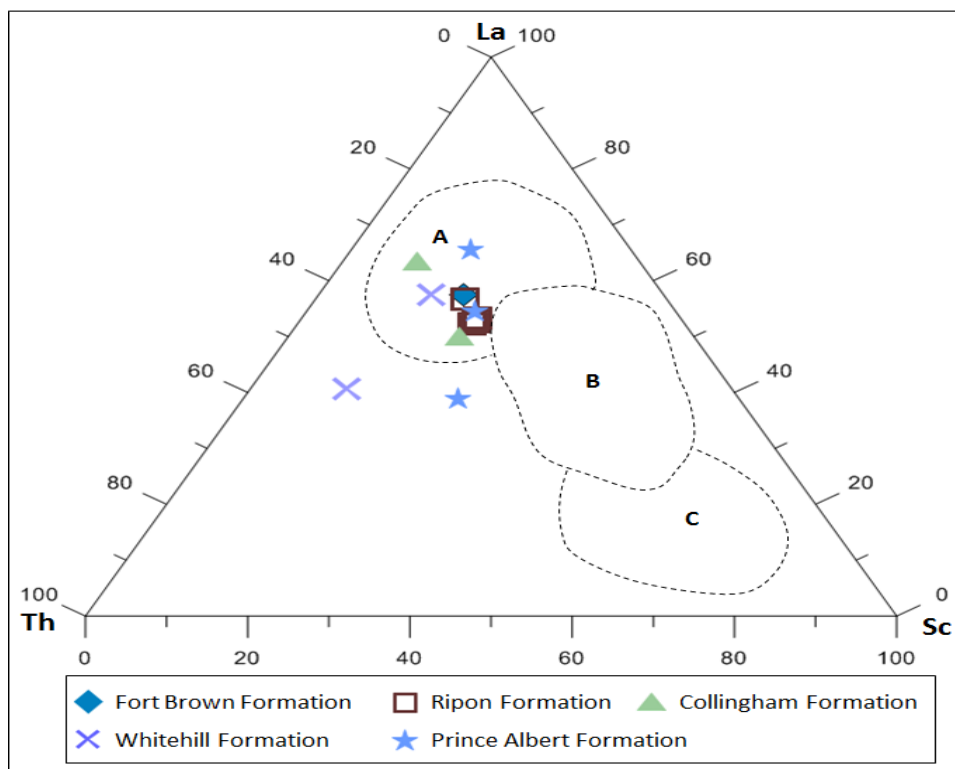
Figure 7.41: La-Th-Sc tectonic discrimination diagram for the Ecca shales (After Bhatia and Crook, 1986). A = Passive and Active Continental Margin, B = Continental Island Arc, C = Oceanic Island Arc.

7.7 Discussion and conclusions

Selected trace elements such as La, Ce, Nd, Y, Th, Zr, Hf, Nb, Sc, Co and Ti are useful in discriminating provenance and tectonic setting of sedimentary basins because of their relative immobility during sedimentary processes (Bhatia and Crook, 1986; Rollinson, 1993). These elements are present in very low concentrations in sea and river water, chiefly transported as particulate matter and reflect the signature of the parent material (Bhatia, 1983; Bhatia and Crook, 1986; Rollinson, 1993). The trace element data of sandstones and shales from the Ecca Group are generally comparable with the trace element data of UCC and PAAS. In the studied samples, the concentrations of high field strength elements like Hf and Zr are higher in the sandstones than the shale samples. The low content of these elements and elemental ratios like La/Sc and Th/Sc points to the presence of fractionated source rocks with lower compatible element contents and recycled sediments in the source area. The variation in chemical composition depicts change in the supply of material and a variation in physic-chemical environment of deposition. The pattern of geochemical behaviour of individual element shows that most of the trace elements that found their way into the ancient sedimentsseem to have invaded the lattices of the silicates and clay minerals and structurally combined with them.

The geochemical data of major and trace elements show that the studied sandstone and shales have the same source. Based on the discriminant function plots, it can be inferred that the sandstones and shales are mostly of quartzose sedimentary provenance, suggesting that they were derived from a cratonic interior or recycled orogen. The binary plots of TiO_2 versus Ni suggest that most of the Ecca samples are sourced from an acidic magmatic nature (Figures 7.14 and 7.15). Furthermore, the binary plots of TiO_2 versus Zr (Figure 7.13), La/Th against Hf (Figures 7.18 and 7.19) and the ternary diagrams of V-Ni-Th*10 (Figures 7.20 and 7.21) shows that the shale and sandstone samples were derived from felsic igneous rocks. The results of the trace elements correlate well with that of the major elements. The result of the provenance study also agrees with the work of Bowden (2014). The study conducted by Bowden (2014) on detrital zircon population in Karoo Supergroup shows that the Karoo succession spans a supercontinent cycle with deposition having taken place in various plate tectonic environments, from passive margins, basins formed due to collisional tectonics and environments present during rifting and ocean basin formation. As documented by Bowden (2014), the upper part of the Karoo Supergroup was deposited much later than previously thought and even during times of breakup of the Gondwanaland. In addition, deposition of

different units comprising the stratigraphy of the Karoo Supergroup occurred at the same time in different parts of the basin, which was controlled by the presence of different depositional environments and climatic conditions in the basin at the same in different places. The stratigraphic units in the Karoo Supergroup do not always represent a timeline in the Karoo Basin bit is often time-transgressive, typical of stratigraphic units.

The CIA values (24.41 to 83.76%) in the Ecca rocks indicate low to high weathering degree of the source rocks. The relatively high CIA values (53.77 to 78.28%) in the shales probably reflect the presence of clay minerals and low percentage of detrital feldspars. Alternatively, the low CIA values in few shales (< 40%) point to a low weathering condition in the source area and perhaps reflect cool conditions. The variations in CIA reflect changes in the properties of feldspar versus aluminous clay minerals. The observed changes in the CIA values indicate that the sediments are moderately to highly weathered, which possibly suggests that the sediments were derived from source rocks that have been subjected to both chemical and physical weathering. The CIW values for the studied sandstones and shales range from 25.90 to 96.25%, suggesting moderate to high intensive chemical weathering. In the analysed samples, the CIW values are higher than those of CIA due to exclusion of K_2O from the index. Based on the CIW values, the Ecca sandstones and shales are inferred to have undergone moderate to high chemical weathering. The PIA values of the studied samples range from 21.91 to 95.14%. Again, the PIA values suggest moderate to high or intense destruction of feldspars during source weathering, transport, sedimentation and diagenesis. During the initial stages of weathering, Ca is quickly leached than Na and K. With increasing weathering, the total alkali content ($K_2O + Na_2O$) decreases with increase in K-Na ratio (K_2O/Na_2O). This is due to destruction of feldspars among which plagioclase is more favourably removed than K-feldspars (Nesbitt and Young, 1984; Nesbitt et al., 1997).

The bivariate plots of Na_2O versus PIA, K_2O against PIA, and CaO versus PIA show weak correlation which could be attributed to the presence K-bearing minerals (i.e. muscovite and biotite) as well as the retention of most of the mobilized K by aluminous material resulting in the formation of illite. The above described and documented imprints of progressing chemical weathering of detrital feldspars perhaps give an impression (may be misleading) that major event of chemical weathering of detrital feldspars has taken place essentially in the terminal basin prior to the lithification of the detritus and during diagenesis. The observed systematic depletion of Na_2O content with increasing degree of chemical weathering of the feldspars (Figures 7.24c and 7.25c) tend to support above assumption. However, it is known

that detrital feldspar grains can survive more than one sedimentary cycle. The A-CN-K diagram of the sandstone and shale samples show that paleoclimate of the source area was relatively warm, which caused chemical weathering of source rocks reducing some initial feldspar in source rocks. Fairly long distance of transport (i.e., perhaps hundreds of kilometres) is also an important process responsible for further reduction of feldspars. Diagenetic alteration of feldspar was the most important factor reducing feldspar in the sandstone.

The ICV values for the Ecca sandstones and shales range from 0.41 to 3.6, while K_2O/Na_2O ratios vary from 0.71 to 8.29. The K_2O/Na_2O ratios are comparable to those of sediments from passive margins, which increase with maturity of rocks (Bhatia, 1983). The binary plot of CIA against ICV (Figure 7.28) shows that most of the shales are geochemically mature and were derived from both weak and intensively weathered source rocks. The bivariate plot of K_2O/Na_2O versus $(Fe_2O_3 + MgO)$, $Al_2O_3/(CaO + Na_2O)$ against $(Fe_2O + MgO)$ and log (K_2O/Na_2O) versus SiO_2 revealed that the sandstones and shales are generally related to continental margin. The Na_2O-CaO-K_2O ternary plot after Toulkeridis et al. (1999) suggests continental margin provenance for the Ecca shales and sandstones. Triangular Th-Sc-Zr/10 tectonic discrimination diagram of Bhatia and Crook (1986) revealed that the source area for most of the Ecca samples are predominantly of passive continental margin with a minor contribution from continental island arc and active continental margin sources (Figures 7.38 and 7.39).

The La-Th-Sc ternary plot also suggests passive and active margin settings for the Ecca samples. The similarity of the La/Th versus Hf diagram (Figures 7.18 and 7.19) and the La-Th-Sc tectonic discrimination diagram (Figures 7.40 and 7.41) is a clear indication of a passive-active margin depositional basin. The data from these immobile trace elements correlate well with Figures 7.34 and 7.35 (K_2O/Na_2O versus SiO_2) as well as Figures 7.36 and 7.37 (Na_2O-CaO-K_2O). The study of paleoweathering conditions based on chemical index of alteration (CIA), plagioclase index of alteration (PIA) and A-CN-K (Al_2O_3-$CaO+Na_2O$-K_2O) indicate that perhaps chemical weathering in the source area and recycling processes have been more significant in the shales and sandstones. The CIA values indicate low to high weathering conditions of the samples and the paleoclimate of the source area was probably warm. The tectonic setting discrimination diagrams support continental margin setting of the provenance.

CHAPTER 8

ORGANIC GEOCHEMICAL EVALUATION OF THE ECCA GROUP SHALE: IMPLICATIONS FOR HYDROCARBON POTENTIAL

Abstract

Shale gas has recently been the exploration focus for future energy resource in South Africa. Specifically, the black shales of the lower Ecca Group in the study area are considered to be one of the most prospective targets for shale gas exploration. Evaluation of this potential resource has been restricted due to the lack of exploration and scarcity of existing drill core data. Thus, only limited previous geochemical data exist for these formations. In this study, outcrop and core samples of the Ecca Group were analysed to assess their total organic carbon (TOC), organic matter type, thermal maturity and hydrocarbon generation potential (SP). The results show that these rocks have TOC ranging from 0.11 to 7.35 wt.%. The SP values vary from 0.09 to 0.53 mg HC/g, suggesting poor hydrocarbon generative potential. The plot of S1 versus TOC shows that the source rocks were characterized by autochthonous hydrocarbons. S2/S3 values range between 0.40 and 7.5, indicating Type- II/III, III, and IV kerogen. With the exception of one sample from the Collingham Formation which has HI value of 53 mg HC/g TOC, all other samples have HI values of less than 50 mg HC/g TOC, thus suggesting Type-IV kerogen, which is mostly derived from reworked organic matter (mainly dead carbon) with little or no potential for hydrocarbon generation. Tmax values range from 318 to 601℃, indicating immature to over-maturity of hydrocarbon. The vitrinite reflectance values range from 2.22 to 3.93%, indicating over-maturity of the kerogen. Binary plots of HI against OI, and HI versus Tmax show that the shales are of Type II and mixed Type II-III kerogen, which are capable of generating both natural gas and minor oil at suitable burial depth. Based on the geochemical data, it can be inferred that the source rocks are immature to over-matured variable from localities and have potential of producing wet to dry gas at present-stage. Generally, the Whitehill Formation of the Ecca Group is comparable to the Marcellus and Barnett Shales. This further supports the assumption that the Whitehill Formation has a high probability of being a profitable shale gas play, but only when explored in dolerite-free area and away from the Cape Fold Belt.

Keywords: Source rock, organic matter type, thermal maturity, hydrocarbon generation potential, Ecca Group.

8.1 Introduction

Shales are widely distributed in the world and until recently (almost two decades ago); they were only regarded as a potential source rock and/or seal/cap rock for conventional petroleum reservoirs. The last decade has marked an increase in the interest in natural gas, particularly unconventional natural gas, as a "cleaner" alternative or/and additional source of energy generation. The depletion in conventional petroleum sources and commercial production of shale gas in the United States have led to the realisation that organic-rich shale or fine grained rocks can also serve as potential unconventional reservoirs for hydrocarbons (Curtis, 2002; Montgomery et al., 2005; Jarvie et al., 2007). Presently, global petroleum exploration is undergoing a strategic shift from conventional to unconventional hydrocarbon resources. This development led to a change in the way exploration companies (geoscientist) consider resource plays. Shale-gas formations are now regarded as both source and reservoir rocks. The term "shale" does not limit the host of the gas to only to the rock type shale; shale gas plays with variable facies (i.e. the Lewis Shale of the San Juan Basin) are common and are well documented (Bustin et al., 2009). Natural gas produced and trapped within sedimentary facies such as mudrocks, carbonates and siltstones of extremely low permeability is also termed shale gas.

According to Horsfield and Schulz (2010), shale gas is self-sourced, an unconventional resource that is hosted in fine-grained and organic carbon-rich siliclastic sediments. The gas can either be generated in shale, or contributions from deeper subsurface can also contribute to the gas that is stored in the shale (Bustin et al., 2009). The source rock is one of the primary components of a hydrocarbon system, and thermal maturity is the main factor that determines whether a source rock can either produce oil, gas, or condensate (Lecompte et al., 2010). Organic matter preserved in shales may change to oil and gas as temperature and pressure increases. The duration and degree of post-depositional burial are the two main parameters controlling the conversion of organic matter to natural gas. This gas may be trapped in the shale as free gas in natural fractures and intergranular porosity, as gas sorbed into kerogen and clay-particle surfaces, or as gas dissolved in kerogen and bitumen (Curtis, 2002). Shale gas can be thermogenic or biogenic in origin as well as a combination of both (Curtis, 2002; Martini et al., 2008; Suarez-Ruiz et al., 2012). Chemically, the gas can either be dry (i.e. consisting over 90% methane) or wet (i.e. predominantly composed of longer chained hydrocarbons such as ethane and propane etc.), however, combinations of the two are common.

As the world moves toward a more sustainable energy future, unconventional hydrocarbon resources are becoming increasingly important in global onshore petroleum exploration and development. Recently, shale gas has been the exploration focus for energy in many countries and regions (i.e. Canada, Europe, South Africa, and Australia) and its extraction has improved considerably with recent advances in horizontal well-drilling, reservoir stimulation and hydraulic fracturing (fracking) of rocks (Cook et al., 2013; Zoback and Arent, 2014; Ratner and Tierman, 2015). Like many other countries in the world, South Africa is faced with the challenge of generating enough energy to meet the current and increasing future demands for energy as a result of the growing economy and better living standards. About 90 % of energy generated in South Africa is from coal (Macmullin, 2013), but according to the South African Energy Department in Mbendi Information Services (2014), about 12.5 million people in South Africa had no access to electricity. The demand for power is projected to increase at an estimated rate of 1,000 Megawatt per year with a shortfall of 9 Terawatt per hour in subsequent years. This indicates that South Africa will need over 40,000 Megawatt by 2025. BP Statistical Review of Energy (2012) reported that the shortfall in electricity generation is equal to the quantity of electricity that is being consumed annually by a large city (i.e. Cape Town).

To boost national energy security, the South African government is trying to explore the potential unconventional shale gas reservoir in the southern Main Karoo Basin. The Ecca Group in the basin is considered to be the most prospective area for shale gas in South Africa, due to the presence of deeply buried, thermally mature black shales. The targeted gas is methane (dry gas), which represents the final stage of hydrocarbon thermal maturation and can be used as a power source for electricity generation and production of fuels. In 1968, exploration well CR 1/68 in this basin yielded a gas flow rate of about 1.83 mmscf/day for 23 hours from the fractured Fort Brown shale. This shale formation was thought to be self-sourcing (i.e. a gas shale), but may also have been charged by the underlying Whitehill and Prince Albert Formations. Shale gas was explored from these formations in the 1960s, but exploration stopped in the late 1970s due to poor technical know-how (Cole, 1992; Branch et al., 2007). Presently, there is a renewed interest in the hydrocarbon-bearing potential of the lower Ecca Group shales in the Main Karoo Basin of South Africa (Geel et al., 2015). Recent analysis by Decker and Marot (2012) and Advanced Resources International (2013) revealed that the basin has potential gas reserves that range from 32-485 trillion cubic feet (Tcf) of

technically recoverable shale gas resources and that most conservative prediction or likelihood is still an important gas resource.

Kuuskraa et al. (2011) initially suggested an optimistic prospective area of about 183,000 km^2 with potential gas reserves of about 485 Tcf, making it the fifth largest shale gas prospect in the world (Vermeulen, 2012). However, an area with smaller extent of approximately 155,000 km^2 is now considered in relation to thinning of Karoo formations to the north and folding effects associated with the Cape Fold Belt (CFB), as well as the intrusion of dolerites (Geel et al., 2013; 2015). The more recent resource assessments indicate gas reserves ranging between 14 and 172 Tcf, with an average of approximately 40 Tcf (Business Day Live, 2014). Although there was a substantial drop in the estimated recoverable reserves of shale gas, the reserve is still considered to be feasible, especially when taking into account that the Moss-gas project (which is currently the only gas exploration project in South Africa) was planned on a reserve of merely 3 Tcf (Vermeulen, 2012). Exploration of the gas reserve has raised serious environmental concerns leading to arguments and series of on-going debate. Supporters of shale gas exploration argue that it can help to meet the current and increasing future demands for energy, reduce dependency on coal-generated electricity, create jobs, and contribute to the mitigation of climate change or reduce environmental pollution (Cook et al., 2013; Council of Canadian Academies, 2014). However, those against shale gas exploration argue that hydraulic fracturing of the Karoo for shale gas will contaminate the already scarce surface and groundwater resources, as well as induce seismicity (Bipartisan Policy Center, 2012; Cook et al., 2013; Council of Canadian Academies, 2014; du Toit and O'Connor, 2014; Vengosh et al., 2014). Presently, many states in the US have started to investigate the effects of hydraulic fracturing, while developing rules that will help to regulate the industry (Hackett et al., 2012). Nevertheless, the negative effects of fracking are highly contested by the extraction industries, and are still open to debate or research (Zoback and Arent, 2014). South Africa plans on having rules and regulations in place prior to shale gas production, should it be viable.

Unlike the basins in US, the geology of the Main Karoo Basin is quite complex considering the fact that the basin was intruded by multiple dolerite sills and dykes at about 183 Ma (Chevallier and Woodford, 1999; Chevalier et al., 2001; Steyl and van Tonder, 2013). These dolerite intrusions could impact the quality of the shale resources and increase the risks of shale gas exploration. Nonetheless, the Ecca Group formations in the study area are thought to have a considerable carbon content and suitable thickness to make it an ideal target for

shale gas development. According to Geel et al. (2015), the two main factors that affect the shale gas content and the distribution of gas are: (i) proximity of the host rocks to the south, near the Cape Fold Belt (CFB), and (ii) proximity of the host rocks to the north, where multiple dolerite intrusions existed, especially in the north of the southern African escarpment. They further documented that, in the first scenario, deformation and metamorphism of strata within the tectonic front of the CFB perhaps might have expelled most of the gas during the Cape Orogeny at about 276 Ma to 248 Ma (Hälbich, 1993; Hansma et al., 2015). In the second instance, contact metamorphism of gas bearing strata adjacent or close to dolerite intrusions that are related to the Karoo Large Igneous Province (Duncan at al., 1997) may have resulted in substantial gas loss due to thermal devolatization (Svensen et al., 2007; 2008). However, the loss of shale gas as a result of the aforementioned cases is not reported here. To date, only sparse data exists on the geochemical characteristics of this Karoo Ecca aged formations. In this chapter, the lower Ecca black shales in the Eastern Cape Province were geochemically evaluated to identify characteristics that would classify the shales as a potential unconventional gas reservoir.

8.2 Materials and method

A total of eighty two outcrop samples of shale rock presumed to be rich in organic matter were collected from road-cut exposures of the Ecca Group along Regional roads R67 (Ecca Pass; Grahamstown-Fort Beaufort), R344 (Grahamstown-Adelaide), R350 (North of Kirkwood-Somerset East), and National roads N2 (Grahamstown-Peddie), and N10 (Paterson-Cookhouse) for source rock analysis (Figure 1.1). In addition, 38 core samples of Ecca shale from boreholes CR 1/68, SC 3/67, SP 1/69 and KWV 1 (Figure 1.1) were collected from the Council for Geosciences core library in Pretoria, making a total of 120 shale samples that were tested for TOC content. Twenty eight shale samples from boreholes SP 1/69 and KWV 1 were further analysed, while samples from boreholes CR 1/68 and SC 3/67 were not analysed in detail because some of the Ecca shale cores were missing and the available shales were weathered. Intrinsically, TOC is a good indicator of organic matter enrichment at the time of deposition, with high TOC values perhaps pointing to good source rocks. The use of outcrop samples for TOC analysis is not entirely without merit. The TOC values obtained from outcrop samples represent the absolute minimum TOC value as a result of oxidation and weathering. These values are useful because fresh core samples are expected to have higher TOC values than outcrop samples. Thus, determination of TOC on outcrop samples could serve as a preliminary tool or test for delineating or identifying potential areas

before drilling is carried out or performed. Dembicki (2009) caution against the overreliance on TOC content, as the hydrogen content in the organic matter is equally, if not more important, for hydrocarbon generation. Hence, TOC was determined first to screen the samples before they were sent to different laboratories for vitrinite reflectance and rock-eval analyses. The rock-eval analysis yielded several parameters (i.e. S1, S2, S3, Tmax, HI, OI, and PI) that were used to assess organic matter in terms of its geochemical properties, thermal maturation, and abundance. Petrophysical properties (i.e. porosity, permeability and density) of the Ecca shales in boreholes KWV 1 and SP 1/69 were extracted from the borehole log sheets and used for comparison.

8.2.1 Total organic carbon content (TOC)

Samples for TOC determination were cleaned, crushed and milled to fine powder form, passing through a 60-mesh (250 μm) sieve. 20 g of each sample was accurately weighed into clean LECO crucibles. The shale samples were then de-mineralized by adding hot 10 % hydrochloric acid and afterwards distilled water was added to halt the reaction. The acid was removed from the sample using a filtration apparatus fitted to a glass microfiber filter. Thereafter, the samples were dried in an oven at 60 ℃ for 24 hours. The dried samples were weighed and then introduced into a muffle furnace at 650 ℃ for combustion. After combustion, the samples were allowed to cool down and re-weighed to determine the TOC content. Samples that have TOC value above 0.5 wt.% are considered to be source rocks and termed adequate, whereas those with TOC value below 0.5 wt.% are termed inadequate because they are not reflected to be source rocks (Tissot and Welte, 1978). The shale samples that have TOC value above 0.5 wt.% were further analysed for vitrinite reflectance and rock-eval pyrolysis.

8.2.2 Rock-eval pyrolysis

Twenty eight organic-rich shale samples were analysed using Rock-eval-6 pyrolyser at GeoMark Research Laboratory in the United States to determine the hydrocarbon generation potential, maturity, kerogen type and hydrogen richness. The samples were cleaned, crushed, weighed accurately in a sample holder and heated in an inert atmosphere to 600 ℃ using a special temperature programme.The samples were initially heated at 300 ℃ for 3 min to generate the first peak (S_1) which represents free and adsorptive hydrocarbon in the sample. This was followed immediately by programmed pyrolysis as the oven temperature was ramped up rapidly to 600 °C at the rate of 25 °C/min to give the S_2 peak. The second peak (S_2)

represents hydrocarbon generated during thermal cracking of kerogen. Simultaneously, the CO_2 produced during the temperature interval was recorded as the S_3 peak. Both the S_1 and S_2 hydrocarbon peaks were measured by the flame ionization detector (FID). The splitting arrangement allows measurement of S_3 peak (carbon dioxide) by means of a thermal conductivity detector (TCD). T_{max} which is the temperature that corresponds to the maximum S_2 peak was obtained from the instrument (Figure 3). Other parameters like hydrocarbon potential (SP), production index (PI), hydrogen index (HI) and oxygen index (OI) were calculated. In this study, rock-eval data were interpreted based on guidelines documented by Tissot and Welte (1984), Peters (1986), and Nuñez-Betelu and Baceta (1994) which utilizes graphs of various parameters in addition to evaluating the appropriate parameters individually.
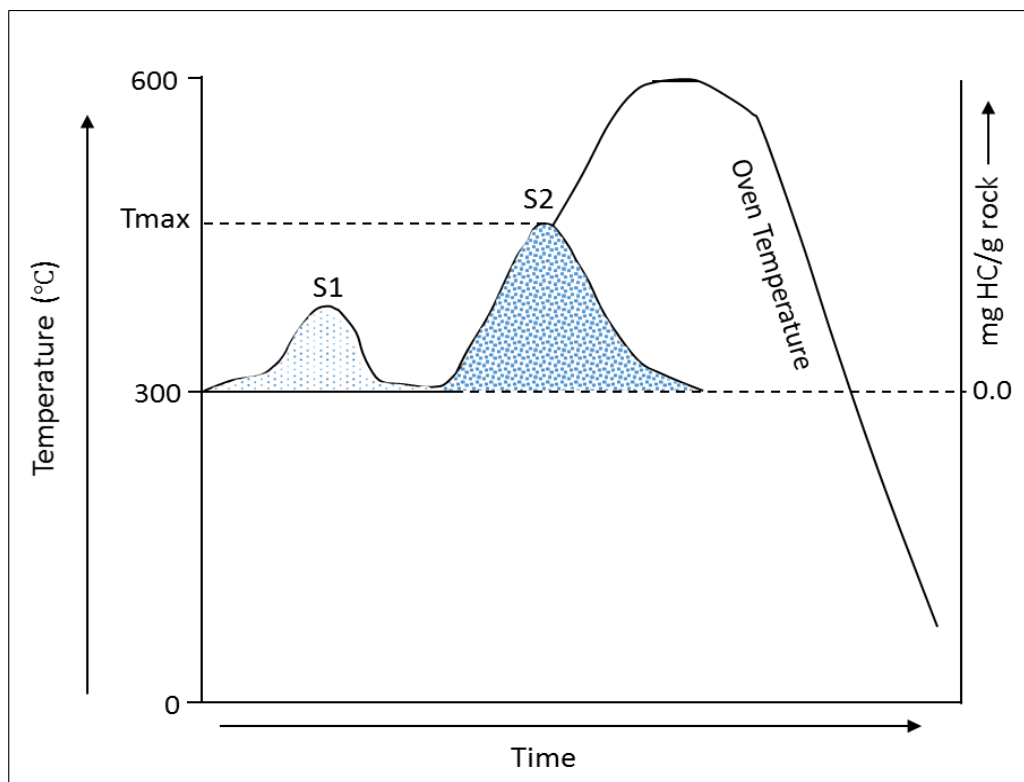
Figure 8.1: Response of organic matter to controlled heating during pyrolysis. S1 corresponds to hydrocarbons formed in the subsurface and already present in the rock, whereas S2 represents hydrocarbons generated during the pyrolysis process. Tmax corresponds to the maximum generation of hydrocarbons during pyrolysis and is much higher that the temperature governing the formation of hydrocarbons in nature (Barker, 1996).

Table 8.1: Measured and calculated parameters derived from rock-eval pyrolysis.

Measured parameters
S_1 = hydrocarbons thermally distilled from the whole rock at temperature < 300 ℃. Units: mg of hydrocarbon/gram of rock
S_2 = hydrocarbons generated by pyrolytic degradation of kerogen between 300 and 650 ℃. Units: mg of hydrocarbon/gram of rock
S_3 = a measure of organic CO_2 generated between temperature of 300 and 390 ℃. Units: mg of CO_2/gram of rock
Calculated parameters
SP (hydrocarbon potential) $= S_1 + S_2$ SP indicates the total amount of hydrocarbons that the source rock, at matured level, can generate. Thus accounts for free hydrocarbons in the source rock (S1) and these hydrocarbons can still produce with increased maturation (S2) (McCarthy et al., 2011). $$PI \text{ (production index)} = \frac{S_1}{(S_1 + S_2)}$$ PI is used to characterise the evolution of the organic matter as PI increases with depth in very fine grained rocks, also with source rock maturation before hydrocarbon are expelled (McCarthy et al., 2011). $$HI \text{ (hydrogen index)} = \left(\frac{S_2}{TOC}\right) \times 100$$ HI is proportional to the amount of hydrogen contained within the kerogen, with higher HI indicating a potential for oil production (McCarthy et al., 2011). $$OI \text{ (oxygen index)} = \left(\frac{S_3}{TOC}\right) \times 100$$ OI is related to the amount of oxygen in the kerogen and useful to in tracking the maturation path of the kerogen (McCarthy et al., 2011). It is generally higher in kerogen derived from terrestrial sources.

8.2.3 Vitrinite reflectance (R_O)

Nineteen samples out of the twenty eight organic-rich shale samples were analysed for vitrinite reflectance. Three samples originate from borehole SP 1/69 (small chips) and 16

samples are from borehole KWV 1. Samples were taken from different horizons: Ripon, Collingham, Whitehill, and Prince Albert. The chips or portions of core samples were prepared perpendicular to the bedding plane. The samples were mounted in epoxy resin, ground and polished in accordance with SANS ISO 7404-2:2009. Random reflectance at 546 nm using immersion oil and total magnification of ×500 in non-polarised light was conducted following ASTM D7708-14:2014. The analysis was conducted on a Zeiss AxioImager reflected light microscope fitted with Hilgers Diskus software for vitrinite reflectance determination. The equipment was calibrated following SANS ISO 7404-5:2009 and ASTM D7708-14:2014, using calibration standards YAG 0.90, and CZ 3.24. Twenty to fifty readings were taken on each sample across the surface at a magnification of ×500. In order to accurately determine the organic matter, the samples were viewed under white light (monochromatic and colour cameras), fluorescent mode (to determine degree of fluorescence), and under x-polars (to determine degree of anisotropy).

8.3 Results and discussion

8.3.1 Total organic carbon (TOC) content

The Ecca shales have TOC values ranging from 0.11 to 7.35 wt.% (Table 8.2; Figures 8.2 and 8.3). The obtained data for the outcrop and core samples show that the TOC values are between 0.17 and 7.35 wt.%, 0.11 and 7.30 wt.%, 0.22 and 0.93 wt.%, 0.17 and 2.62 wt.%, and 0.31 and 0.45 wt.% for the Prince Albert, Whitehill, Collingham, Ripon and Fort Brown Formations, respectively. Along the Ecca Pass, the calculated average TOC value (i.e. 1.5 wt.%) for the Whitehill Formation is higher than those of the underlying Prince Albert Formation and overlying Collingham and Ripon Formations. Thus, it can be inferred that the Whitehill Formation is more organically rich than the underlying and overlying formations at this location. Along Grahamstown-Peddie, where the lower Ecca formations are intruded by dolerites, the TOC values range from 0.17 to 0.62 wt.%, with an average of 0.35 wt.%. The TOC values are significantly lower than those obtained along the Ecca Pass (without dolerite intrusions on the surface). In borehole SP 1/69 (located near East London), the average (TOC) content in the shale of Prince Albert, Whitehill, Collingham and Ripon Formations are 6.6 wt.%, 5.7 wt.%, 0.7 wt.%, and 2.2 wt.%, respectively. These TOC values are generally higher than 2.0 wt.%, and such levels of organic enrichment are considered as good source rocks for hydrocarbon generation (Hedberg and Moody, 1979; Hunt, 1979; Peters and Cassa, 1994).

On the other hand, at borehole KWV 1 (located near Transkei), the average TOC values of the Prince Albert, Whitehill and Ripon shales are 0.77 wt.%, 2.14 wt.%, and 0.85 wt.%, respectively, indicating a fair-to-good source rock. Generally, the average TOC values of the Ecca shales in borehole SP 1/69 are higher than those in KWV 1, suggesting that the hydrocarbon potential for the Ecca lithofacies in East London area is better than in the Transkei area. In both outcrop and boreholes samples, the TOC values tend to be smaller in samples that are within areas intruded by dolerites or close to dolerite intrusions. The impact of dolerite intrusions could have possibly reduced the TOC content in the host rock and thus areas that are intruded by dolerites are unlikely to be good shale gas reservoirs. Summary of the petrophysical properties of the Ecca Group rocks is presented in Table 8.3.

Table 8.2: Results of TOC analyses of shale samples from the Ecca Group.

S. ID	Sample type	Formation	TOC (wt.%)	S. ID	Sample type	Formation	TOC (wt.%)
FB5	Outcrop (G-F)	Fort Brown	0.45	WK8	Core (KWV 1)	Whitehill	2.36
FB4	Outcrop (G-F)	Fort Brown	0.34	WK7	Core (KWV 1)	Whitehill	2.07
FB3	Outcrop (G-F)	Fort Brown	0.37	WK6	Core (KWV 1)	Whitehill	2.28
FB2	Outcrop (G-F)	Fort Brown	0.31	WK5	Core (KWV 1)	Whitehill	2.06
FB1	Outcrop (G-F)	Fort Brown	0.39	WK4	Core (KWV 1)	Whitehill	1.72
RK6	Core (KWV 1)	Ripon	0.68	WK3	Core (KWV 1)	Whitehill	1.25
RK5	Core (KWV 1)	Ripon	0.52	WK2	Core (KWV 1)	Whitehill	2.42
RK4	Core (KWV 1)	Ripon	0.51	WK1	Core (KWV 1)	Whitehill	3.02
RK3	Core (KWV 1)	Ripon	0.70	WS3	Core (SP 1/69)	Whitehill	4.30
RK2	Core (KWV 1)	Ripon	1.18	WS2	Core (SP 1/69)	Whitehill	5.60
RK1	Core (KWV 1)	Ripon	0.68	WS1	Core (SP 1/69)	Whitehill	7.30
RS2	Core (SP 1/69)	Ripon	1.72	WC3	Core (CR 1/68)	Whitehill	0.37
RS1	Core (SP 1/69)	Ripon	2.62	WC2	Core (CR 1/68)	Whitehill	0.52
RC3	Core (CR 1/68)	Ripon	0.32	WC1	Core (CR 1/68)	Whitehill	0.48
RC2	Core (CR 1/68)	Ripon	0.31	WSC4	Core (SC 3/67)	Whitehill	0.44
RC1	Core (CR 1/68)	Ripon	0.48	WSC3	Core (SC 3/67)	Whitehill	0.45
RSC3	Core (SC 3/67)	Ripon	0.46	WSC2	Core (SC 3/67)	Whitehill	0.22
RSC2	Core (SC 3/67)	Ripon	0.27	WSC1	Core (SC 3/67)	Whitehill	0.31
RSC1	Core (SC 3/67)	Ripon	0.41	WH19	Outcrop (G-F)	Whitehill	0.36
RP24	Outcrop (G-F)	Ripon	0.28	WH18	Outcrop (G-F)	Whitehill	0.43
RP23	Outcrop (G-F)	Ripon	0.48	WH17	Outcrop (G-F)	Whitehill	0.51
RP22	Outcrop (G-F)	Ripon	0.39	WH16	Outcrop (G-F)	Whitehill	0.62
RP21	Outcrop (G-F)	Ripon	0.47	WH15	Outcrop (G-F)	Whitehill	0.40
RP20	Outcrop (G-F)	Ripon	0.46	WH14	Outcrop (G-F)	Whitehill	0.36

RP19	Outcrop (G-F)	Ripon	0.40	WH13	Outcrop (G-P)	Whitehill	0.20
RP18	Outcrop (G-F)	Ripon	0.37	WH12	Outcrop (G-P)	Whitehill	0.24
RP17	Outcrop (G-F)	Ripon	0.50	WH11	Outcrop (G-P)	Whitehill	0.37
RP16	Outcrop (G-F)	Ripon	0.38	WH10	Outcrop (G-P)	Whitehill	0.11
RP15	Outcrop (G-P)	Ripon	0.29	WH9	Outcrop (G-P)	Whitehill	0.42
RP14	Outcrop (G-P)	Ripon	0.43	WH8	Outcrop (C-P)	Whitehill	0.35
RP13	Outcrop (G-P)	Ripon	0.34	WH7	Outcrop (C-P)	Whitehill	0.38
RP12	Outcrop (G-P)	Ripon	0.44	WH6	Outcrop (C-P)	Whitehill	0.29
RP11	Outcrop (C-P)	Ripon	0.39	WH5	Outcrop (C-P)	Whitehill	0.24
RP10	Outcrop (C-P)	Ripon	0.49	WH4	Outcrop (G-A)	Whitehill	0.38
RP9	Outcrop (C-P)	Ripon	0.47	WH3	Outcrop (G-A)	Whitehill	0.46
RP8	Outcrop (C-P)	Ripon	0.40	WH2	Outcrop (G-A)	Whitehill	0.43
RP7	Outcrop (C-P)	Ripon	0.28	WH1	Outcrop (G-A)	Whitehill	0.39
RP6	Outcrop (G-A)	Ripon	0.31	PK4	Core (KWV 1)	Prince Albert	0.53
RP5	Outcrop (G-A)	Ripon	0.45	PK3	Core (KWV 1)	Prince Albert	1.04
RP4	Outcrop (G-A)	Ripon	0.44	PK2	Core (KWV 1)	Prince Albert	0.98
RP3	Outcrop (G-A)	Ripon	0.35	PK1	Core (KWV 1)	Prince Albert	0.50
RP2	Outcrop (G-A)	Ripon	0.42	PS3	Core (SP 1/69)	Prince Albert	6.73
RP	Outcrop (G-A)	Ripon	0.33	PS2	Core (SP 1/69)	Prince Albert	5.71
RP1	Outcrop (G-A)	Ripon	0.37	PS1	Core (SP 1/69)	Prince Albert	7.35
CS2	Core (SP 1/69)	Collingham	0.52	PC2	Core (CR 1/68)	Prince Albert	0.52
CS1	Core (SP 1/69)	Collingham	0.93	PC1	Core (CR 1/68)	Prince Albert	0.49
CC2	Core (CR 1/68)	Collingham	0.44	PSC2	Core (SC 3/67)	Prince Albert	0.53
CC1	Core (CR 1/68)	Collingham	0.30	PSC1	Core (SC 3/67)	Prince Albert	0.17
CSC2	Core (SC 3/67)	Collingham	0.40	PA12	Outcrop (G-F)	Prince Albert	0.42
CSC1	Core (SC 3/67)	Collingham	0.34	PA11	Outcrop (G-F)	Prince Albert	0.44
CH10	Outcrop (G-F)	Collingham	0.27	PA10	Outcrop (G-F)	Prince Albert	0.31
CH9	Outcrop (G-F)	Collingham	0.36	PA9	Outcrop (G-F)	Prince Albert	0.42
CH8	Outcrop (G-F)	Collingham	0.49	PA8	Outcrop (G-P)	Prince Albert	0.46
CH7	Outcrop (G-P)	Collingham	0.50	PA7	Outcrop (G-P)	Prince Albert	0.49
CH6	Outcrop (G-P)	Collingham	0.39	PA6	Outcrop (G-P)	Prince Albert	0.28
CH5	Outcrop (G-P)	Collingham	0.37	PA5	Outcrop (C-P)	Prince Albert	0.37
CH4	Outcrop (G-A)	Collingham	0.30	PA4	Outcrop (C-P)	Prince Albert	0.33
CH3	Outcrop (G-A)	Collingham	0.22	PA3	Outcrop (G-A)	Prince Albert	0.45
CH2	Outcrop (G-A)	Collingham	0.28	PA2	Outcrop (G-A)	Prince Albert	0.38
CH1	Outcrop (G-A)	Collingham	0.24	PA1	Outcrop (G-A)	Prince Albert	0.47

Note: S. ID represents sample identification. G-F, G-A, G-P and C-P represent the Ecca sections along Regional roads R67 (Grahamstown-Fort Beaufort; Ecca Pass), R344 (Grahamstown-Adelaide), and National roads N2 (Grahamstown-Peddie section), N10 (Cookhouse-Paterson), respectively.

Table 8.3: Petrophysical properties of the Ecca Group rocks in the study area.

Formation	Lithology	Average Thickness (m)	Average Density (kg/m³)	Average Porosity (%)	Average Permeability (mD)
Fort Brown	Sandstone	892	2.774	0.444	0.042
	Shale		2.656	0.574	0.032
Ripon	Sandstone	700	2.721	1.241	0.024
	Shale		2.662	0.595	0.046
Collingham	Shale	65	2.598	0.388	0.018
Whitehill	Shale	21	2.526	2.310	0.892
Prince Albert	Shale	87	2.641	0.560	0.014
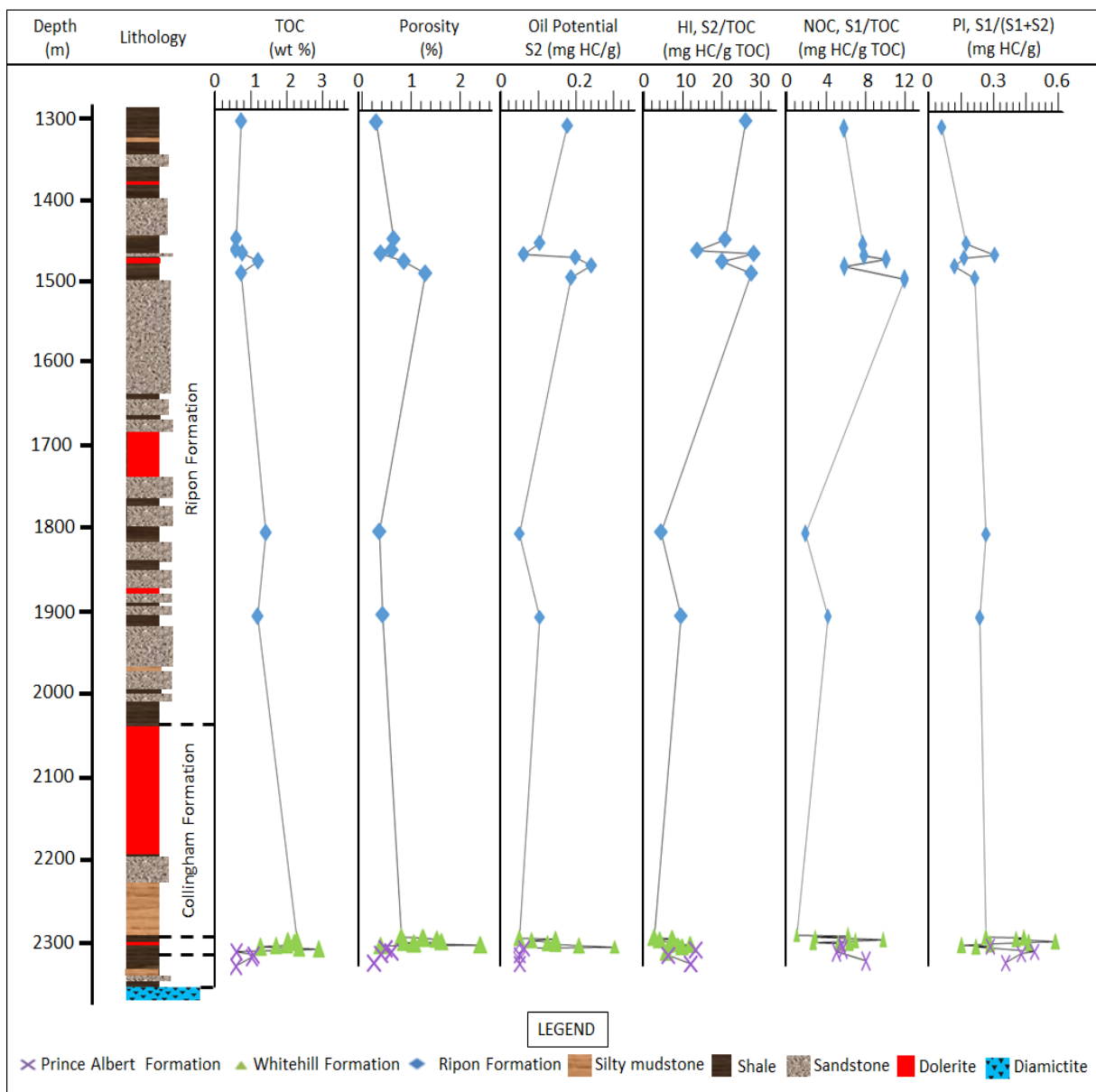
Figure 8.2: Downhole TOC, porosity, oil potential, hydrogen index, normal oil content, and production index for borehole KWV 1.
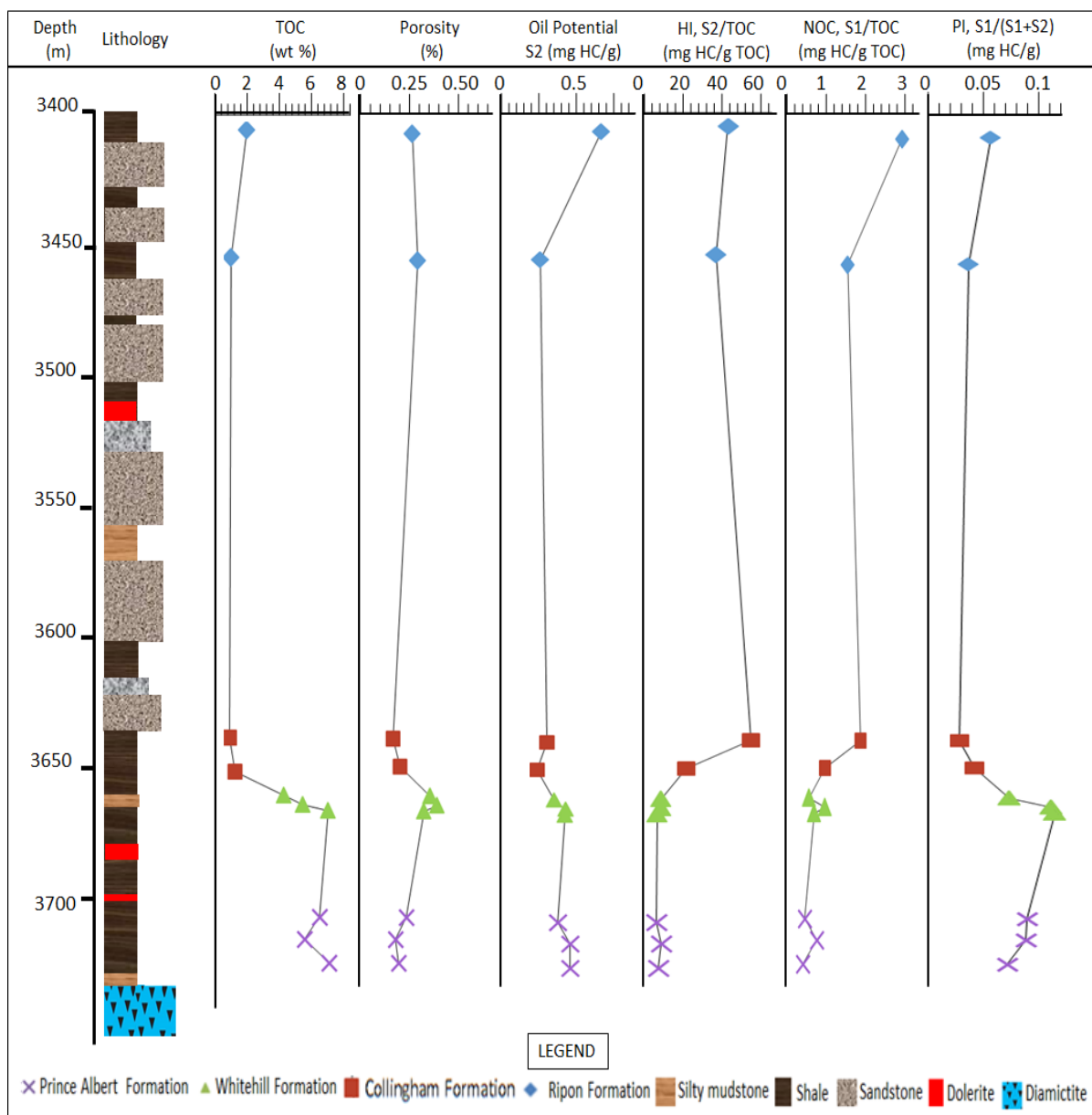
Figure 8.3: Downhole TOC, porosity, oil potential, hydrogen index, normal oil content, and production index for borehole SP 1/69.

8.3.2 Quality and type of organic matter

The organic matter type is a vital parameter to be considered when evaluating source rock potential because it significantly influences the nature of hydrocarbon products (Hunt, 1979; Tissot and Welte, 1984; Barker, 1996). The type of organic matter gives insight to the depositional environment of the source rock and aids in predicting the generative potential of oil and gas. Organic matter types can be categorized into Type I, II, III and IV kerogen using bivariate plots of HI versus Tmax, S2 versus TOC, and HI against OI. In the HI versus OI classification diagram (known as Van Krevelen diagram), the source rocks are analysed for

kerogen using known evolution paths for different kerogen types (Peters, 1986). Generally, HI value of more than 600 mg HC/g TOC indicates the predominance of Type I kerogen and has potential to produce oil (Peters and Cassa, 1994). Type I kerogen is derived mainly from algae and associated with lacustrine depositional settings (McCarthy et al., 2011). Type II kerogen is associated with the production of oil, with HI values ranging between 300 mg HC/g TOC and 600 mg HC/g TOC (Peters and Cassa, 1994). The Type II kerogen is primarily derived from plankton, with some contribution from algal material, thus point to a marine depositional setting (McCarthy et al., 2011). HI values varying from 200 mg HC/g TOC to 300 mg HC/g TOC suggest a mix of Type II and III kerogens; expected to produce a mix of oil and gas (Peters and Cassa, 1994). Marine environments with significant terrestrial input, and vice versa, are the likely depositional environments for this type of organic matter. A shallow marine environment receives terrestrial input, especially in sea level regression, and is a suitable example for the deposition of mixed kerogen type. HI values between 50 mg HC/g TOC and 200 mg HC/g TOC are usually associated with Type III kerogen which are mainly derived from higher plants and produces gas when matured. Type IV kerogen have HI values of less than 50 mg HC/g TOC and McCarthy et al. (2011) documented that such kerogen type are mostly derived from reworked organic matter with little or no potential for hydrocarbon generation.

The result of rock-eval analysis of shale samples from borehole KWV 1 and SP 1/69 is presented in Table 8.4. The Rock Eval-6 pyrograms for some of the samples are shown in Appendix C (ii). Based on the classification schemes of Peters and Cassa (1994) and McCarthy et al. (2011), with the exception of one sample from the Collingham Formation (sample CS2), all other samples have HI values of less than 50 mg HC/g TOC, thus suggesting Type-IV kerogen and are mostly derived from reworked organic matter with little or no potential for hydrocarbon (dry gas) generation. On the other hand, S2/S3 values for the shales range between 0.4 and 7.5, indicating mixed Type II/III, III, and IV kerogen and are expected to produce mixed oil and gas, and gas (Table 8.5; after Peters and Cassa, 1994). In addition, most of the samples have S1 and S2 values below 0.5 and 2.5 respectively, indicating poor quality of the organic matter (Table 8.6; After Peters, 1986). The plot of HI against OI (modified Van Krevelen diagram) and HI versus Tmax shows that the samples are of Type II and mixed Type II-III kerogen, which are capable of generating both oil and gas at suitable burial depth (Figures 8.4 and 8.5). The cross plots of S2 versus TOC, and HI against OI (Figures 8.6-8.9) shows that the samples are mostly type III kerogen (mainly derived from

higher plants) and are expected to produce gas when matured. Generally, these results are comparable with the findings from Faure and Cole (1999) and Geel et al. (2013; 2015), where the lower Ecca Group formations were found to have Type-II/III, III and IV kerogen.

Table 8.4: Results of rock-eval analysis of Ecca shales from boreholes KWV 1 and SP 1/69.

S. ID	Sample type	Formation	TOC	S1	S2	S3	S2/S3	HI	OI	Tmax	Ro_c	Ro_m
RK6	Core (KWV 1)	Ripon	0.68	0.04	0.18	0.04	4.50	26	6	456	3.32	-
RK5	Core (KWV 1)	Ripon	0.52	0.04	0.11	0.03	3.67	21	6	447	3.20	-
RK4	Core (KWV 1)	Ripon	0.51	0.04	0.07	0.03	2.33	14	6	430	3.18	-
RK3	Core (KWV 1)	Ripon	0.70	0.07	0.2	0.08	2.50	29	11	488	3.49	*
RK2	Core (KWV 1)	Ripon	1.18	0.07	0.24	0.16	1.50	20	14	481	3.48	-
RK1	Core (KWV 1)	Ripon	0.68	0.08	0.19	0.09	2.11	28	13	483	3.42	-
RS2	Core (SP 1/69)	Ripon	1.72	0.05	0.75	0.34	2.21	44	20	460	3.26	-
RS1	Core (SP 1/69)	Ripon	2.62	0.01	0.23	0.14	1.64	37	22	492	3.56	*
CS2	Core (SP 1/69)	Collingham	0.52	0.01	0.29	0.20	1.45	53	36	513	3.67	*
CS1	Core (SP 1/69)	Collingham	0.93	0.01	0.20	0.79	0.25	21	83	599	3.89	-
WK8	Core (KWV 1)	Whitehill	2.36	0.03	0.06	0.04	1.5	3	2	405	3.05	3.44
WK7	Core (KWV 1)	Whitehill	2.07	0.13	0.15	0.04	3.75	7	2	334	2.82	3.55
WK6	Core (KWV 1)	Whitehill	2.28	0.07	0.09	0.06	1.50	4	3	333	2.79	3.49
WK5	Core (KWV 1)	Whitehill	2.06	0.2	0.15	0.1	1.50	7	5	320	2.70	3.69
WK4	Core (KWV 1)	Whitehill	1.72	0.12	0.13	0.06	2.17	8	3	318	2.61	2.22
WK3	Core (KWV 1)	Whitehill	1.25	0.08	0.15	0.02	7.50	12	2	385	3.24	*
WK2	Core (KWV 1)	Whitehill	2.42	0.07	0.21	0.1	2.10	9	4	408	3.07	3.24
WK1	Core (KWV 1)	Whitehill	3.02	0.16	0.3	0.18	1.67	10	6	411	3.10	3.53
WS3	Core (SP 1/69)	Whitehill	4.30	0.03	0.35	0.25	1.40	8	6	524	3.61	*
WS2	Core (SP 1/69)	Whitehill	5.60	0.06	0.45	0.66	0.68	8	12	568	3.75	-
WS1	Core (SP 1/69)	Whitehill	7.30	0.06	0.44	0.79	0.56	6	11	601	3.93	-
PK4	Core (KWV 1)	Prince Albert	0.53	0.03	0.07	0.03	2.33	13	6	421	3.13	*
PK3	Core (KWV 1)	Prince Albert	1.04	0.06	0.06	0.14	0.43	6	13	429	3.17	-
PK2	Core (KWV 1)	Prince Albert	0.98	0.05	0.06	0.15	0.40	6	15	425	3.15	-
PK1	Core (KWV 1)	Prince Albert	0.50	0.04	0.06	0.02	3.00	12	4	415	3.12	*
PS3	Core (SP 1/69)	Prince Albert	6.73	0.04	0.38	0.34	1.12	6	5	590	3.83	*
PS2	Core (SP 1/69)	Prince Albert	5.71	0.05	0.48	0.81	0.59	8	14	555	3.62	*
PS1	Core (SP 1/69)	Prince Albert	7.35	0.04	0.48	0.46	1.04	7	6	579	3.84	*

Ro_c and Ro_m represents the calculated and measured vitrinite reflectance respectively, * indicates not analysed, and – depicts not determined.

Table 8.5: Geochemical parameters for describing kerogen type and hydrocarbon type generated (After Peters and Cassa, 1994).

Kerogen type	HI (mg HC/g TOC)	S2/S3 (mg)	Atomic H/C	Main expelled at peak maturity
I	> 600	> 15	> 1.5	Oil
II	300-600	10-15	1.2-1.5	Oil
II/III	200-300	5-10	1-1.2	Mixed oil and gas
III	50-200	1-5	0.7-1.0	Gas
IV	<50	<1.0	<0.7	Dry Gas

Table 8.6: Organic carbon richness based on TOC data (After Peters, 1986).

Quality	TOC (wt.%)	S1 (mg)	S2 (mg)
Poor	0.0-0.5	0.0-0.5	0.0-2.5
Fair	0.5-1.0	0.5-1.0	2.5-5
Good	1.0-2.0	1.0-2.0	5-10
Very good	> 2.0	> 2.0	> 10
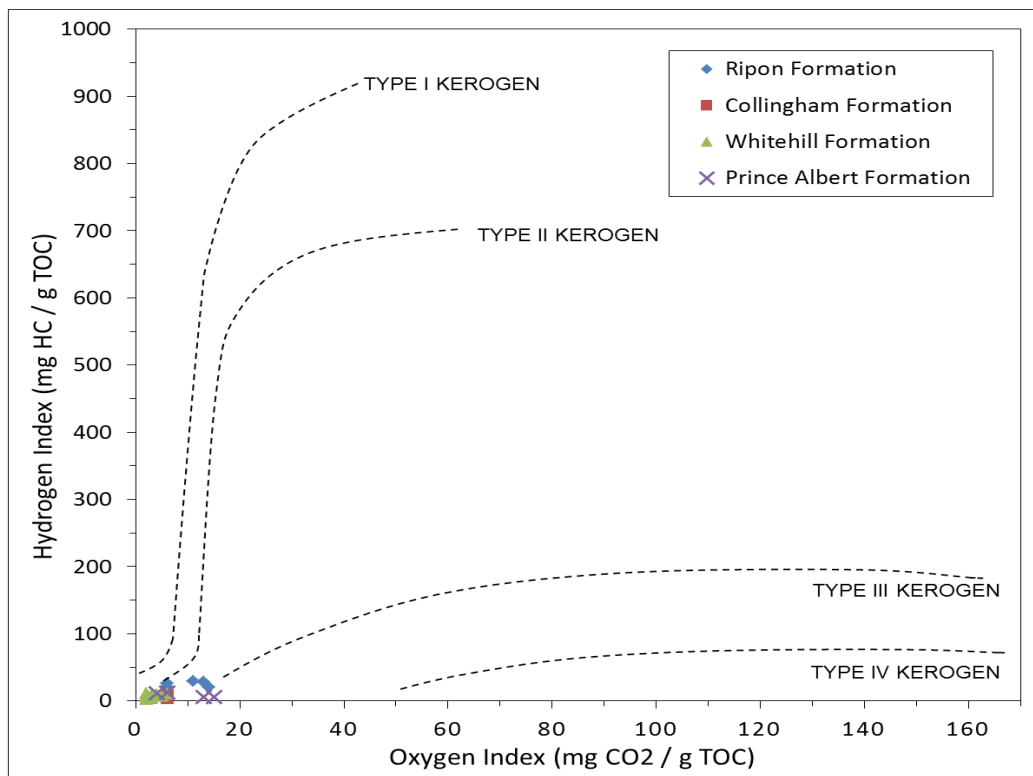
Figure 8.4: Modified van Krevelen diagram of hydrogen index (HI) versus oxygen index (OI) for the Ecca Group in borehole KWV 1, showing kerogen types. Organic matter in the Ecca Group is most consistent with Type II and III Kerogen.
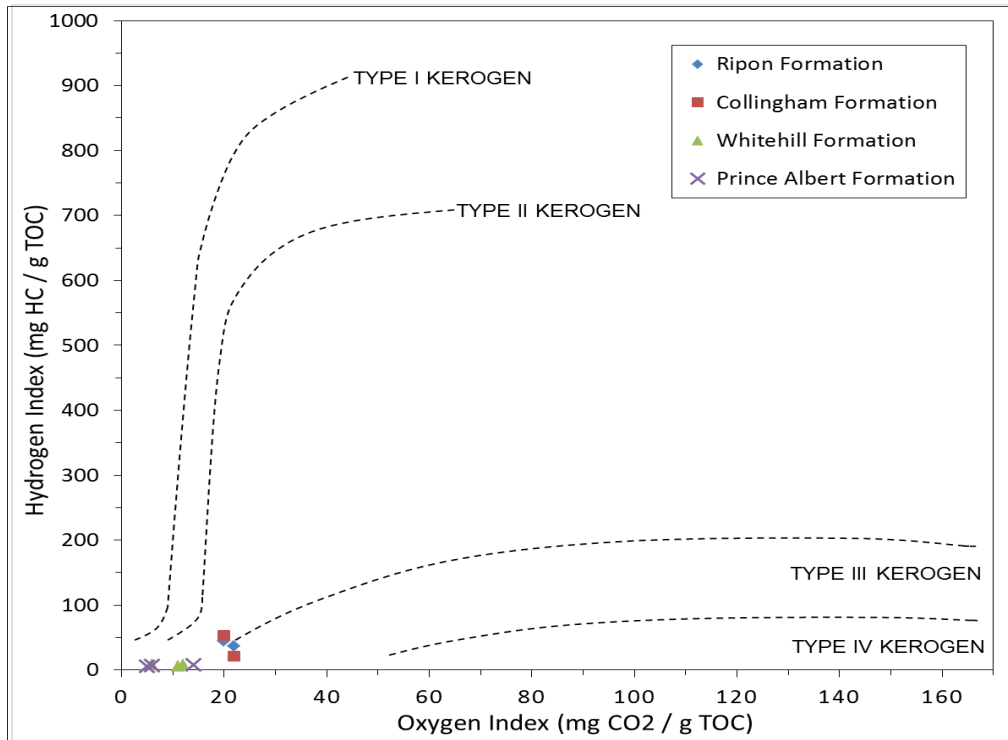
Figure 8.5: Modified van Krevelen diagram of hydrogen index (HI) versus oxygen index (OI) for the Ecca Group in borehole SP 1/69, showing kerogen types. Organic matter in the Ecca Group is most consistent with Type II and III Kerogen.
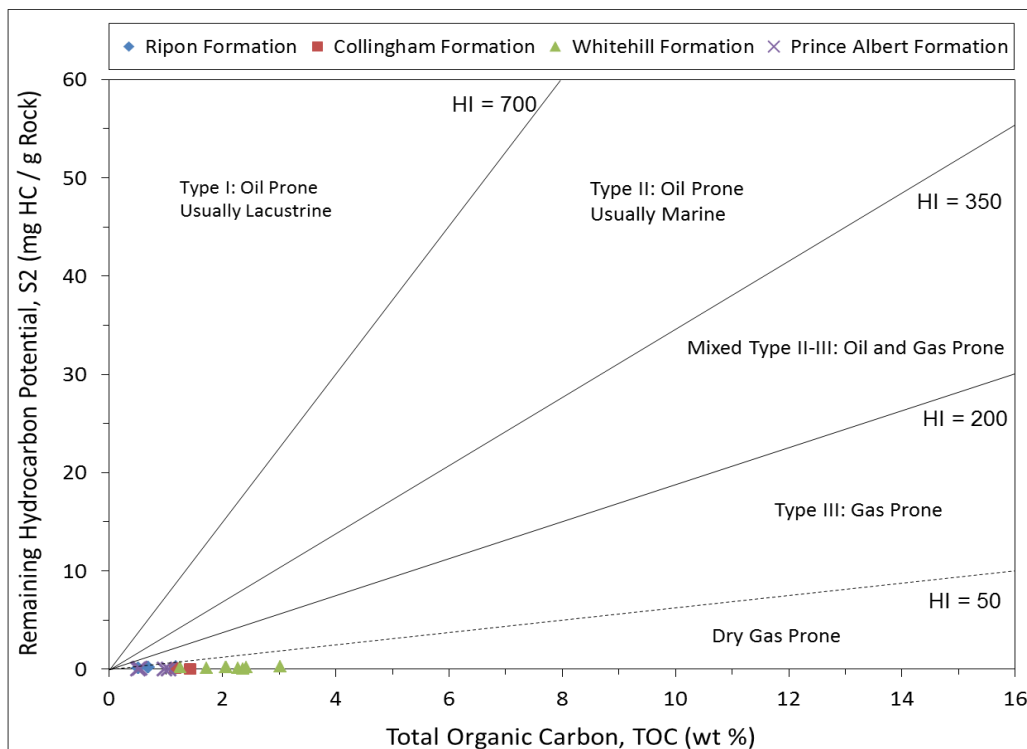
Figure 8.6: Distribution of the analysed samples into pyrolysis S2 versus total organic carbon (TOC) plot, showing kerogen quality of the Ecca shales in borehole KWV 1.
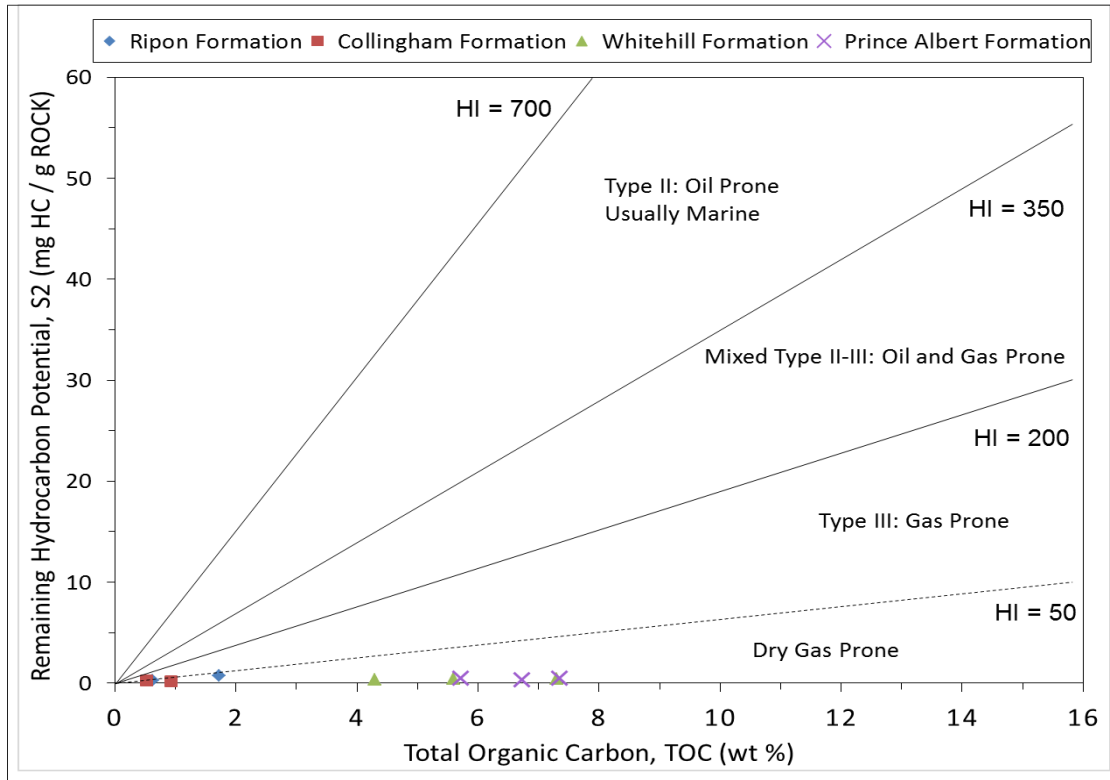
Figure 8.7: Distribution of the analysed samples into pyrolysis S2 versus total organic carbon (TOC) plot, showing kerogen quality of the Ecca shales in borehole SP 1/69.
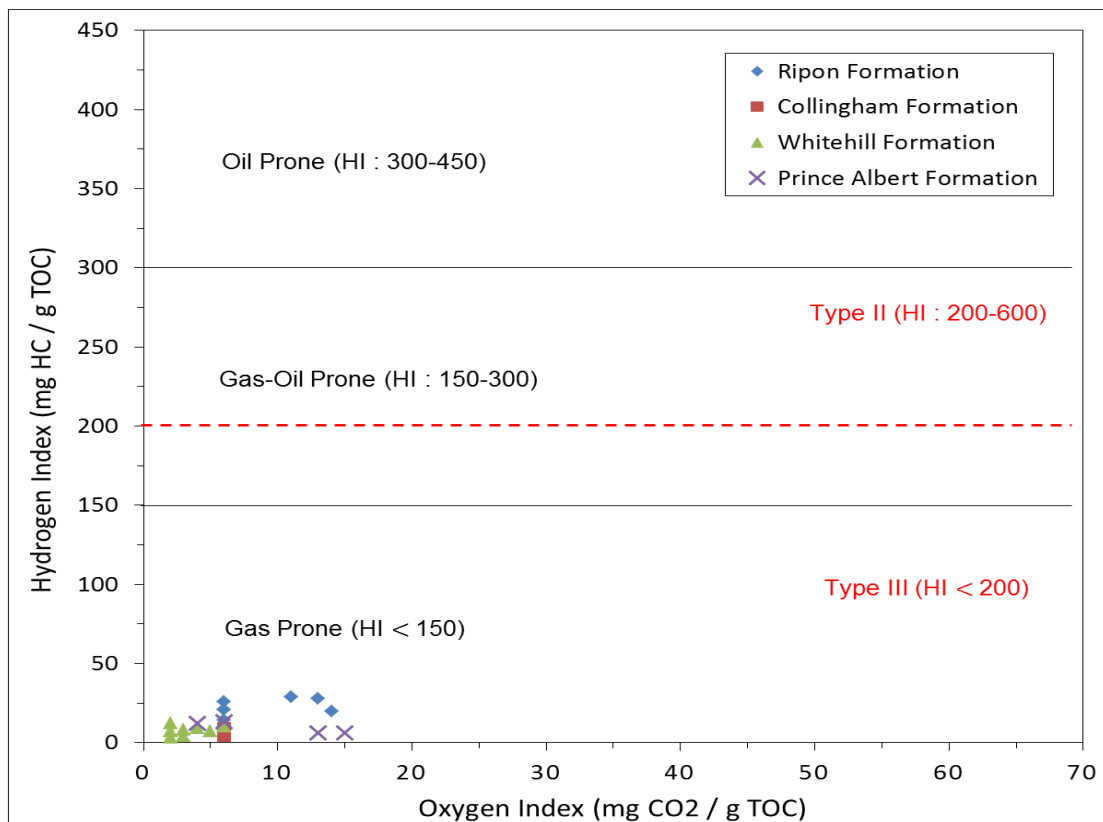
Figure 8.8: Modified Van Krevelen diagram showing the organic matter types of the studied samples in borehole KWV 1. The plot indicates gas prone for the Ecca Group rocks.
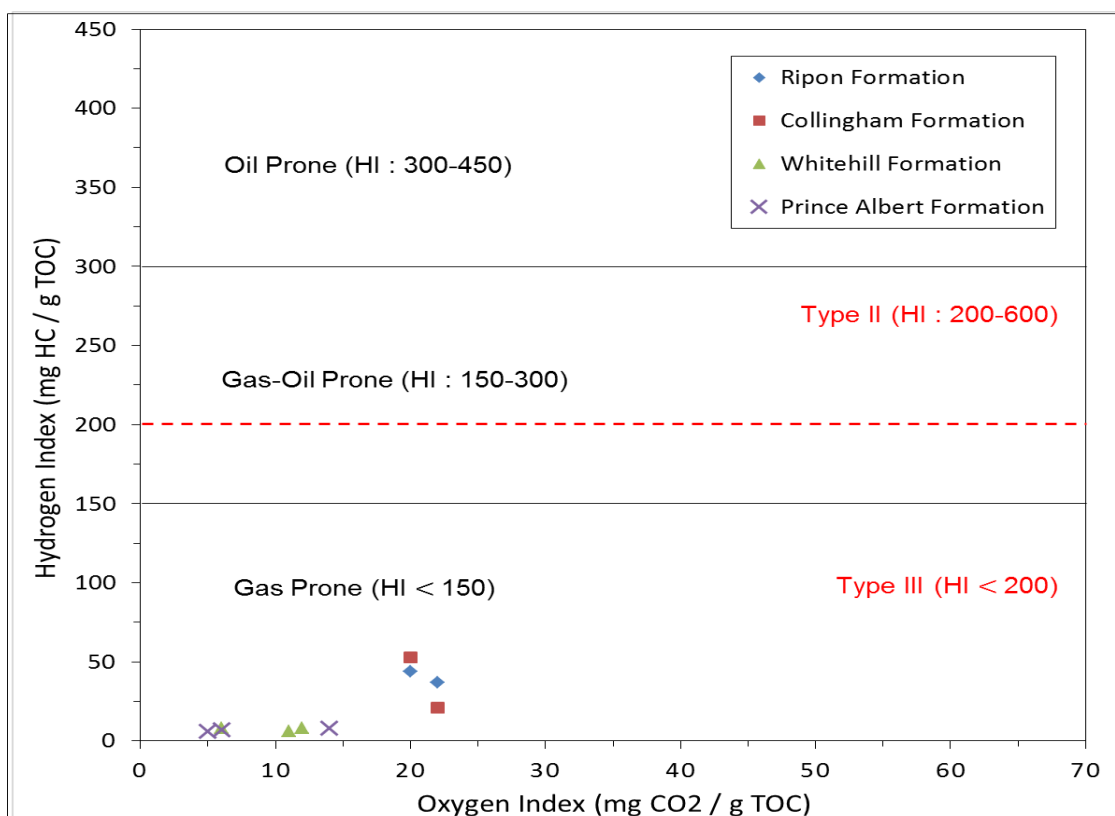
Figure 8.9: Modified Van Krevelen diagram showing the organic matter types of the studied samples in borehole SP 1/69. The plot indicates gas prone for the Ecca Group rocks.

8.3.3 Thermal maturity level

The effects of deep burial on organic matter are irreversible and highest P-T conditions preserved after sedimentary sequences are exhumed. Thus, maturity indicators in organic matter are essential in assessing the level of thermal maturity. During pyrolysis, the obtained maximum temperature (Tmax) signifies the thermal energy required to break the most abundant chemical bonds in kerogen that are associated with generation of hydrocarbons (Mahlsterdt and Horsfield, 2012). The production of these hydrocarbons are related to the amount of hydrogen that is present in the rock and consequently, to its level of maturation (Nuñez- Betelu and Baceta, 1994). This is due to the fact that, the more mature the rock is, the lower the amount of hydrogen it contains and the higher amount of energy is required to liberate the hydrocarbons. Peters and Cassa (1994) documented that Tmax values of less than 435℃ indicates immaturity of samples, Tmax values between 435℃ and 470℃ reflects maturity, and Tmax values above 470℃ represents over-maturity of the source rock. In this study, the thermal maturation level was estimated from the Tmax, vitrinite reflectanceand production index (PI), at least where the TOC reached the minimum threshold of 0.5 wt.% expected for clastic source rocks (Hunt, 1979; Hedberg and Moody, 1979). In addition,

thermally mature sediments are thought to have Tmax values of ≥ 430℃, with vitrinite reflectance (Ro) values ranging between 0.6% and 1.3% (Peters and Cassa, 1994). Based on the aforementioned parameters, contrasting levels of maturity were attained in the shales of the Ecca Group. In borehole KWV 1 (Table 8.4; Figure 8.10), the Tmax values vary between 415℃ and 429℃, 318℃ and 411℃ in the Prince Albert and Whitehill Formations respectively, indicating that the shales are immature. In contrast, the measured vitrinite reflectance (Ro_m) values for the Whitehill shales range between 2.22% and 3.69%, indicating over maturity. The overlying Ripon shales are over matured, with Tmax values varying from 430℃ to 488℃.
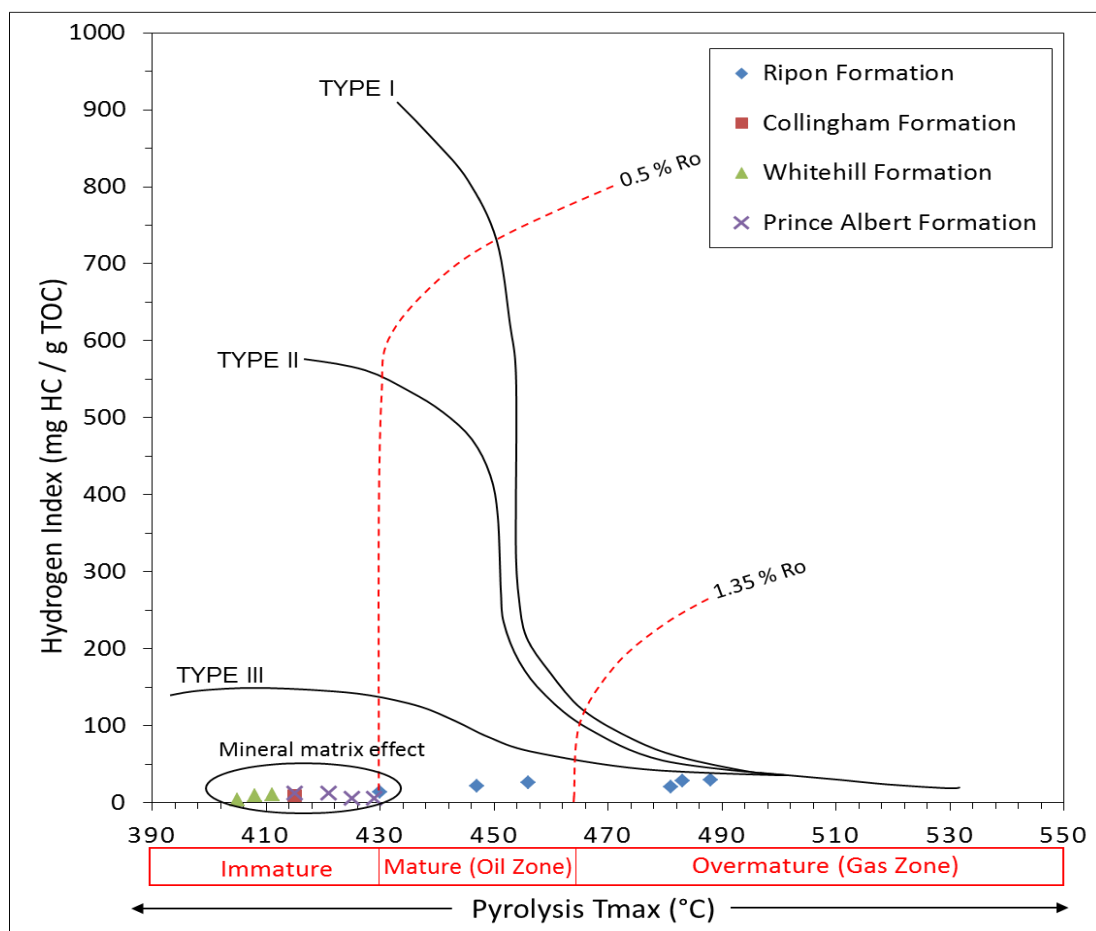
Figure 8.10: Modified van Krevelen diagram of hydrogen index (HI) against Tmax of shale samples from the Prince Albert, Whitehill, Collingham and Ripon Formations in borehole KWV 1, showing kerogen type and maturity.

At borehole SP 1/69 (Table 8.4; Figure 8.11), Tmax values range between 555-590 ℃, 524-601 ℃, 513-599 ℃, and 460-492 ℃ for the Prince Albert, Whitehill, Collingham and Ripon

Formations, respectively. These values show that the shales are thermally over-mature, except for one sample from the Ripon Formation which is marginally mature.
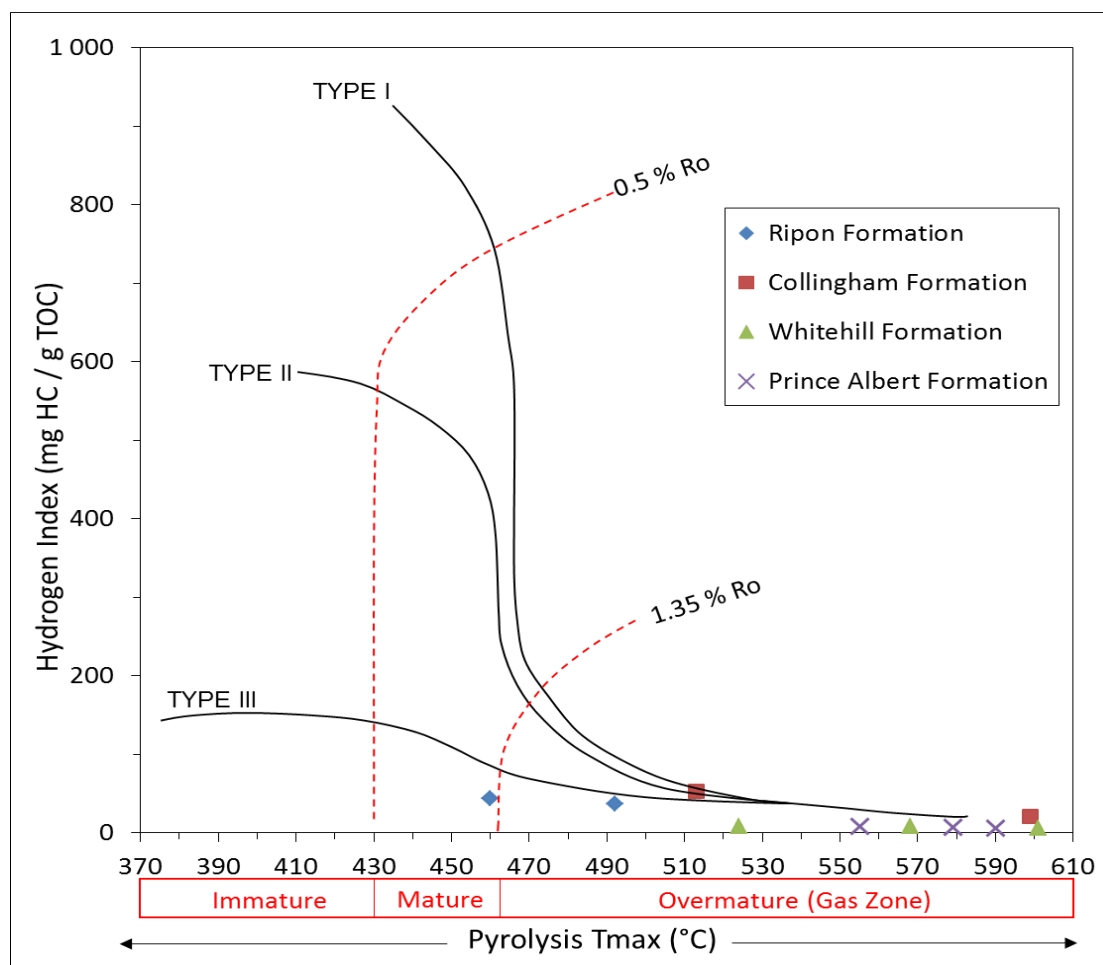
Figure 8.11: Modified van Krevelen diagram of hydrogen index (HI) against Tmax of shale samples from the Prince Albert, Whitehill, Collingham and Ripon Formations in borehole SP 1/69, showing kerogen type and maturity.

In both boreholes, the Ecca shales are consistent with low HI values and relatively high Tmax values. The low HI values may reveal a high level of thermal maturity and/or higher proportions of reworked vitrinites in the shales. Generally, HI decreases at higher maturation levels as a result of the generated hydrocarbons and this could also explain the low values of HI recorded at boreholes SP 1/69 and KWV 1. Perhaps, the organofacies of the lower Ecca formations show substantial contribution from terrestrial sources as indicated on the HI/Tmax plots where most of the samples plot in the Type III kerogen field (Figures 8.10 and 8.11).

In terms of vitrinite reflectance, the samples are generally vitrinite-lean; in fact most samples do not appear to contain vitrinite (See Appendix C). Vitrinite particles were only determined

in the Whitehill samples from borehole KWV 1. A variety of solid bitumen and inertinite fragments, and possibly bituminite were observed in most samples (Figure 8.12). Inertinite includes fusinite and inertodetrinite particles. Bituminite is an amorphous primary liptinite (ASTM D7708-14:2014). Solid bitumen is a secondary maceral generated from kerogen, and can be difficult to distinguish from vitrinite. By definition, solid hydrocarbons indicate hydrocarbon generation and migration in petroleum systems as a result of thermal conversion of kerogen, detected in shales and siltstones/sandstones that are mature and post-mature. Its absence would indicate thermal immaturity or lack of generative potential in the host rocks, or extreme maturity (average Ro of > 5%). Figure 8.12 show images taken from four samples, providing an idea of changes in organic matter through the stratigraphy. It is obvious from the images that not all horizons actually contained organic matter beyond a few inertinite fragments. The TOC value possibly includes substantial carbonates rather than organic matter in most of the samples. Only samples from the Whitehill Formation contained appropriate organic matter on which to obtain reflectance data. The mean reflectance readings (%) indicate that the samples are over mature, with readings ranging between 2% and 4%. Furthermore, with the exception of one sample from the Ripon Formation, all other samples have calculated vitrinite reflectance (Ro_c) values which are greater than 1.35%, indicating over maturity of the samples.
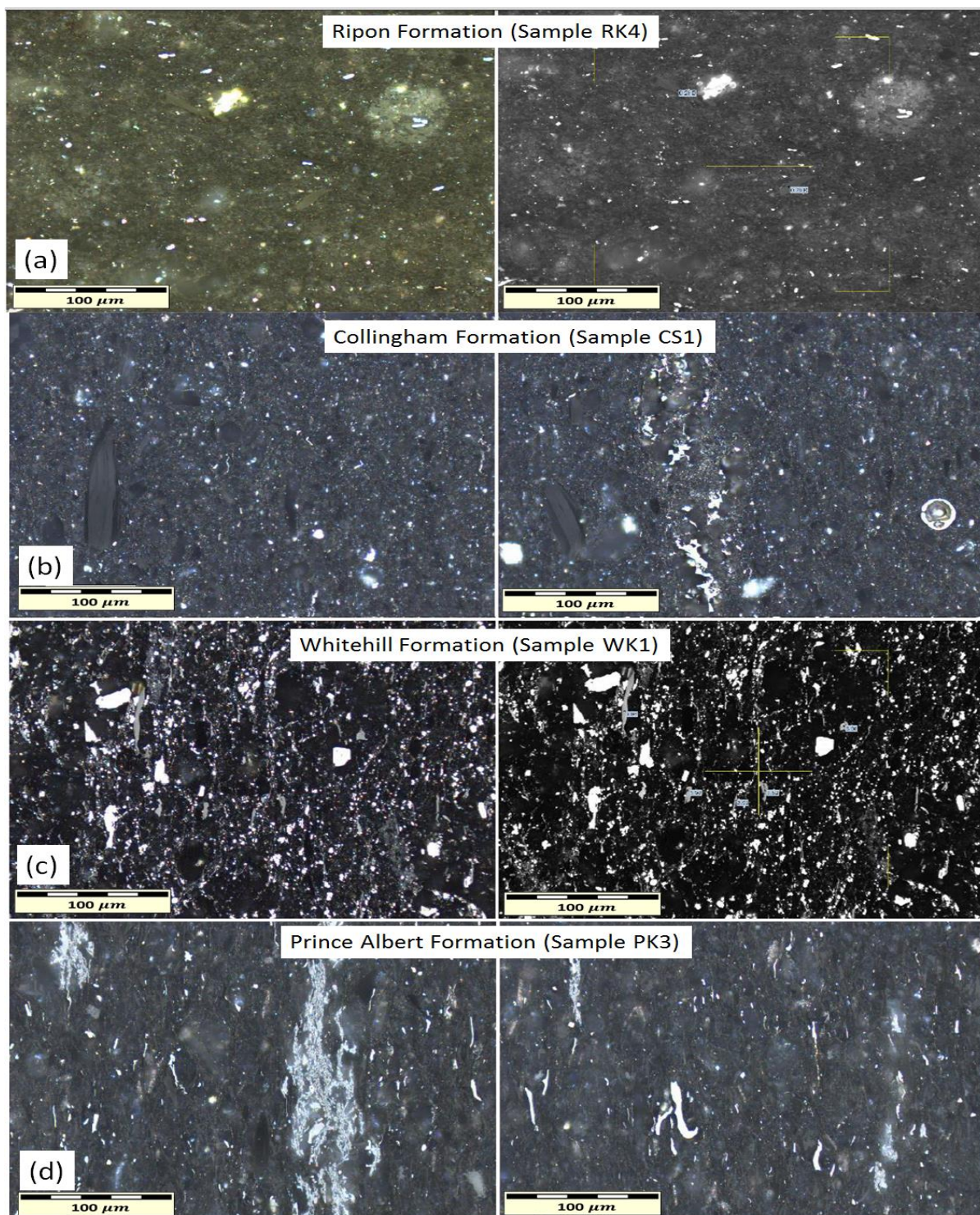
Figure 8.12: Dispersed organic matter assessment of the Ecca shales, with colour images on the left and monochromatic images on the right: (a) Very fine grained mudstone with carbon inclusions, no vitrinite and fluorescence determined and very rare inertinite fragments; (b) Very fine mudstone with quartz fragments. No vitrinite determined, fluorescing component possibly carbon, rare inertinite particle, possible solid bitumen occurrence; (c) Very fine grained mudstone, more organic matter than samples from other formations, also confirmed by higher TOC. Many fine disseminated pyrite, blobs of solid bitumen, clear differentiation between organic matter-inertinite and vitrinite, rare evidence of possible devolatilisation in vitrinite-like particles; (d) Fine mudstone, rare inertinite fragments with unusual white mineral inclusions, but no vitrinite.

The binary plot of Tmax versus production index (PI) can be also used as thermal maturity indicators (Figures 8.13 and 8.14).
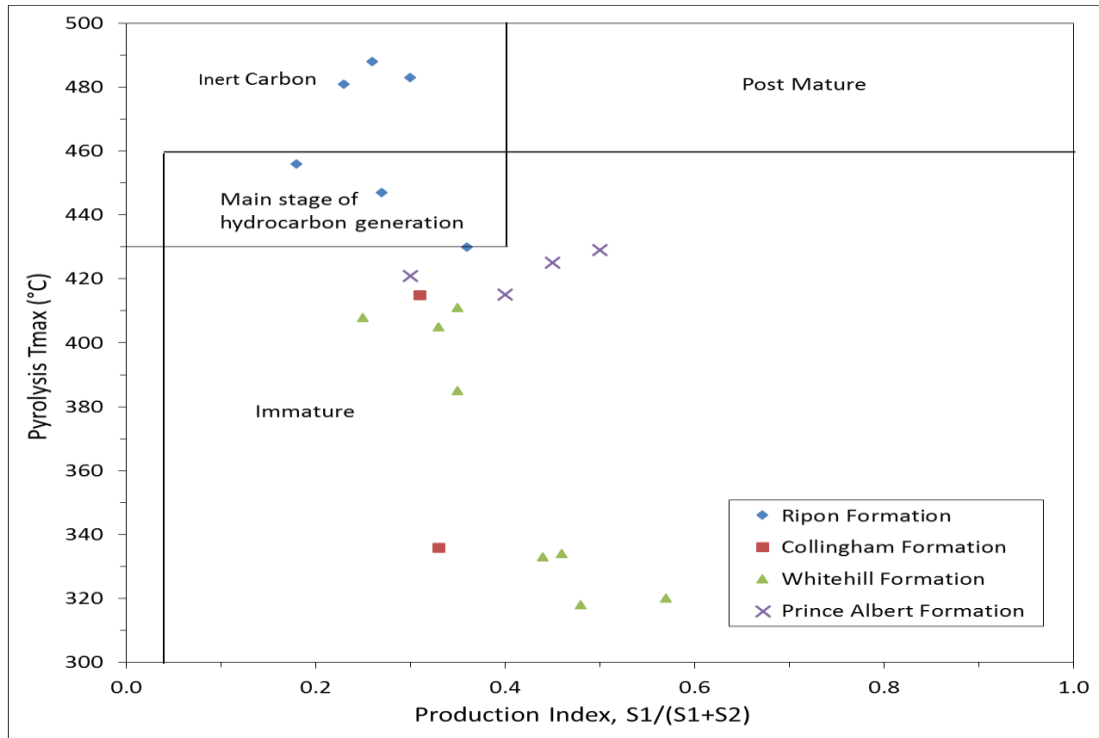
Figure 8.13: Plot of pyrolysis Tmax versus production index (PI), showing the maturation and nature of the hydrocarbon products of the Ecca Group rocks in borehole KWV 1.
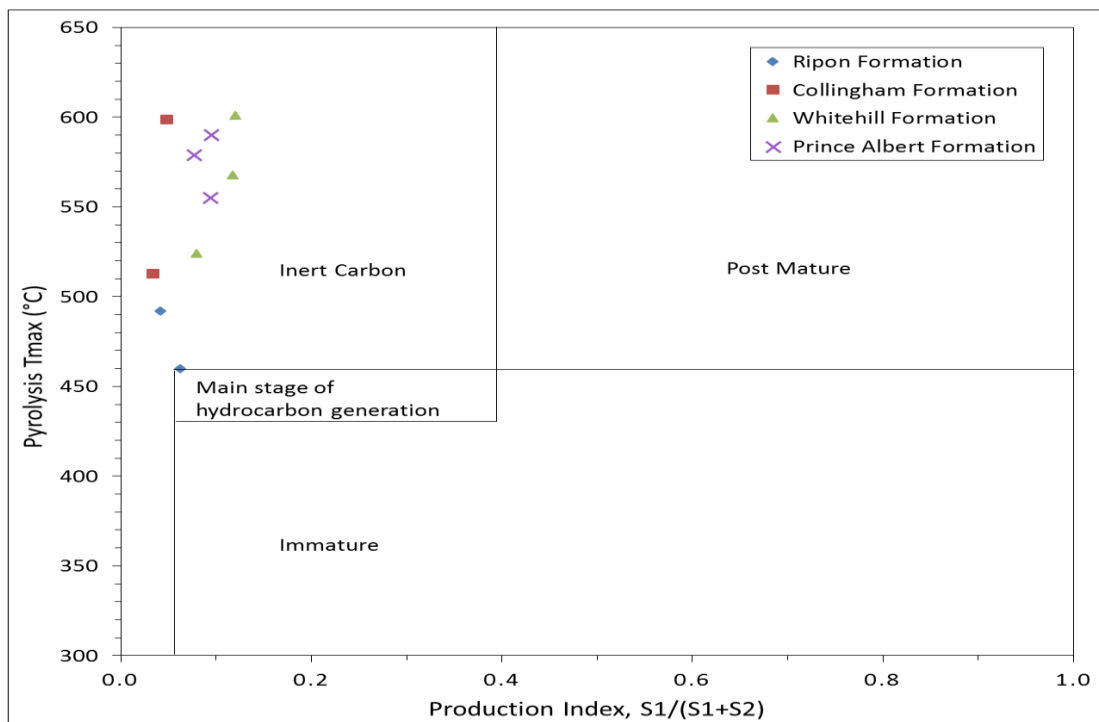
Figure 8.14: Plot of pyrolysis Tmax versus production index (PI), showing the maturation and nature of the hydrocarbon products of the Ecca Group rocks in borehole SP 1/69.

In borehole KWV 1, the Ecca source rocks have pyrolysis Tmax and PI in the range of 318-488 ℃ and 0.16-0.57, respectively, indicating that most of the rocks are thermally immature (Figure 8.13). Conversely, in borehole SP 1/69, the source rocks have pyrolysis Tmax and PI values varying between 460-599 ℃ and 0.04-0.13 respectively, signifying that most of the shales are thermally over-matured and can only generate little or no hydrocarbon generation (inert carbon) (Figure 8.14). The Tmax and PI values are partially in agreement with the vitrinite reflectance (Ro %) values, indicating that the Ecca source rocks have entered mature to late-mature gas window and are considered as an effective source rocks in the Main Karoo Basin of South Africa.

8.3.4 Hydrocarbon generation potential

TOC content alone cannot be used to satisfactorily establish the presence of potential and/or effective petroleum source rocks. This is due to the fact that different types of organic matter have different hydrocarbon yields for the same organic carbon content (Katz, 2006). Hence, a more direct measure of source rock hydrocarbongenerative potential is required for detailed assessment. Tissot and Welte (1984) proposed a genetic potential (SP=S1+S2) for the classification of source rocks. According to their classification scheme, rocks having SP of less than 2 mg HC/g rock are gas-prone, rocks with SP between 2 and 6 mg HC/g rock are oil-gas prone, and those with SP greater than 6 mg HC/g rock are good source rocks for oil. In borehole KWV 1 (Figure 8.15), SP values vary between 0.10-0.12 mg HC/g rock, 0.09-0.46 mg HC/g rock and 0.11-0.31 mg HC/g rock in the Prince Albert, Whitehill and Ripon shales, respectively. On the other hand, in borehole SP 1/69 (Figure 8.16) where TOC are relatively high (0.33-7.42 wt.%), SP values vary between 0.42-0.53 mg HC/g rock in the Prince Albert Formation, 0.38-0.51 mg HC/g rock in the Whitehill Formation, 0.21-0.30 mg HC/g rock in the Collingham Formation and 0.24-0.8 mg HC/g rock in the Ripon Formation. These values in both boreholes are less than 2 mg HC/g rock, indicating gas-prone rocks.
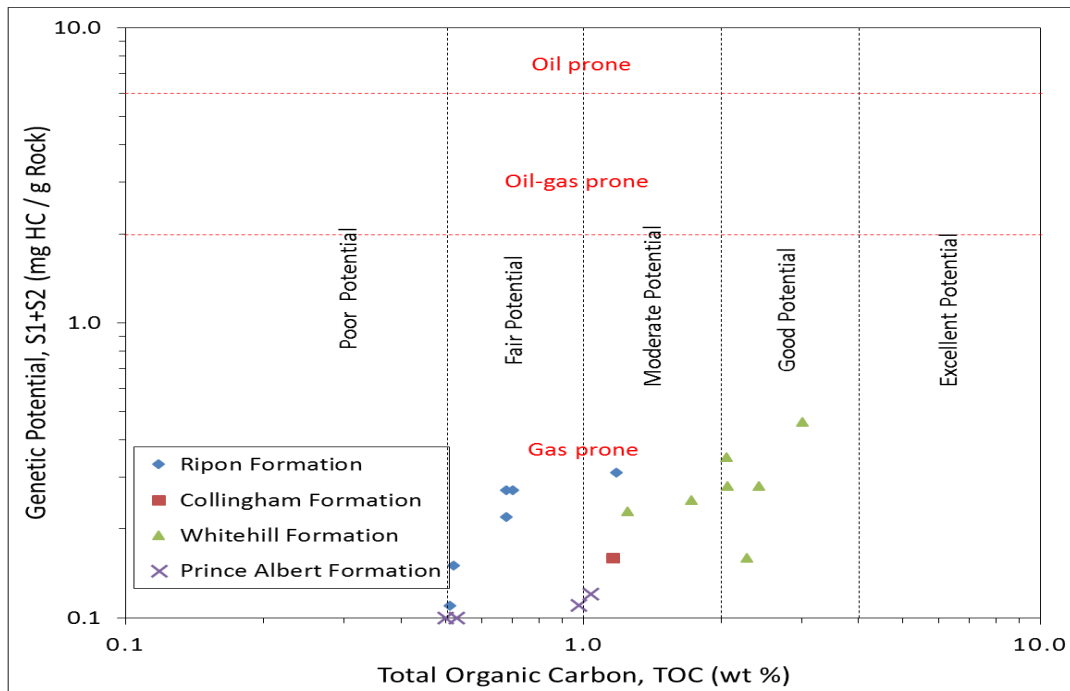
Figure 8.15: Binary plot of genetic potential versus TOC for the Ecca shales in borehole KWV 1 showing source rock generative potential (After Maravelis and Zelilidis, 2010).
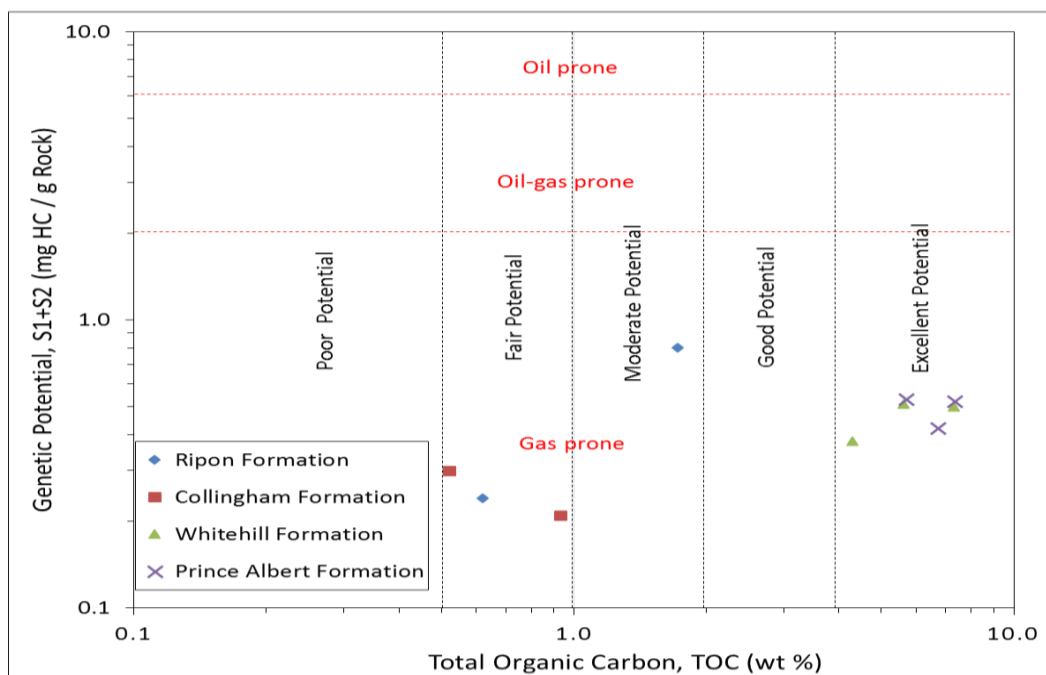
Figure 8.16: Binary plot of genetic potential versus TOC for the Ecca shales in borehole KWV 1 showing generative source rock potential (After Maravelis and Zelilidis, 2010).

In borehole KWV 1, the binary plots of PI versus Tmax (Figure 8.17) and S2/S3 against TOC (Figure 8.19) indicate that the Ecca rocks have potential to generate oil and gas. However, in borehole SP 1/69, the plots of PI against Tmax (Figure 8.18) and S2/S3 versus TOC (Figure 8.20) shows that the rocks are mostly of Type III kerogen with fair to good potential of

generating dry gas and minor condensate (wet gas). Likewise, the plot of HI against TOC revealed that the Ecca rocks are fair to excellent gas-oil source rocks (Figures 8.21-8.24). A comparison of the similarities in the yield of hydrocarbons in the data set indicates that the carbonaceous shales of the Whitehill Formation have the highest yield in both boreholes. Burwood et al. (1995) reported that effective primary source rocks have S2 value of greater than 5 mg HC/g rock and effective non-source rocks (ENS) have S2 value of less than 1 mg HC/g rock. The S2 values for the analysed samples are less than 1 mg HC/g rock, indicating both secondary source field and ENS (Figures 8.25 and 8.26). The plot of S1 versus TOC can be used to discriminate between non-indigenous (allochthonous) and indigenous hydrocarbons (autochthonous). This relation (Figures 8.27 and 8.28) shows that the studied Ecca rocks are characterized by autochthonous hydrocarbons.
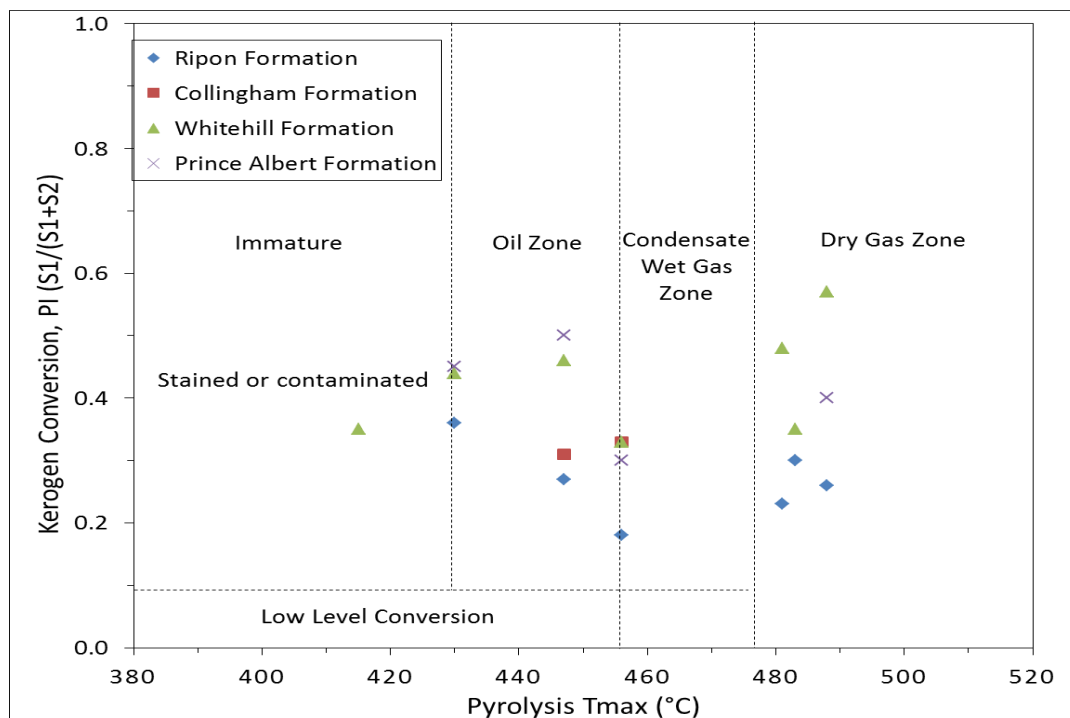
Figure 8.17: Plot of production index (PI) versus Tmax showing hydrocarbon production for the Ecca Group rocks in borehole KWV 1.
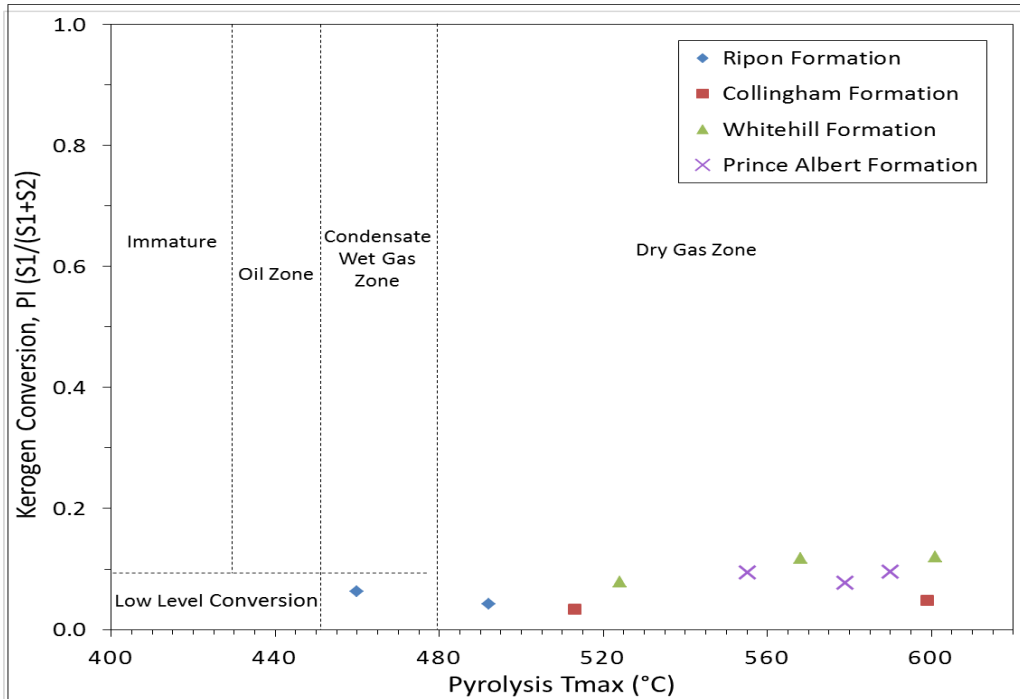
Figure 8.18: Plot of production index (PI) versus Tmax showing hydrocarbon production for the Ecca Group rocks in borehole SP 1/69.
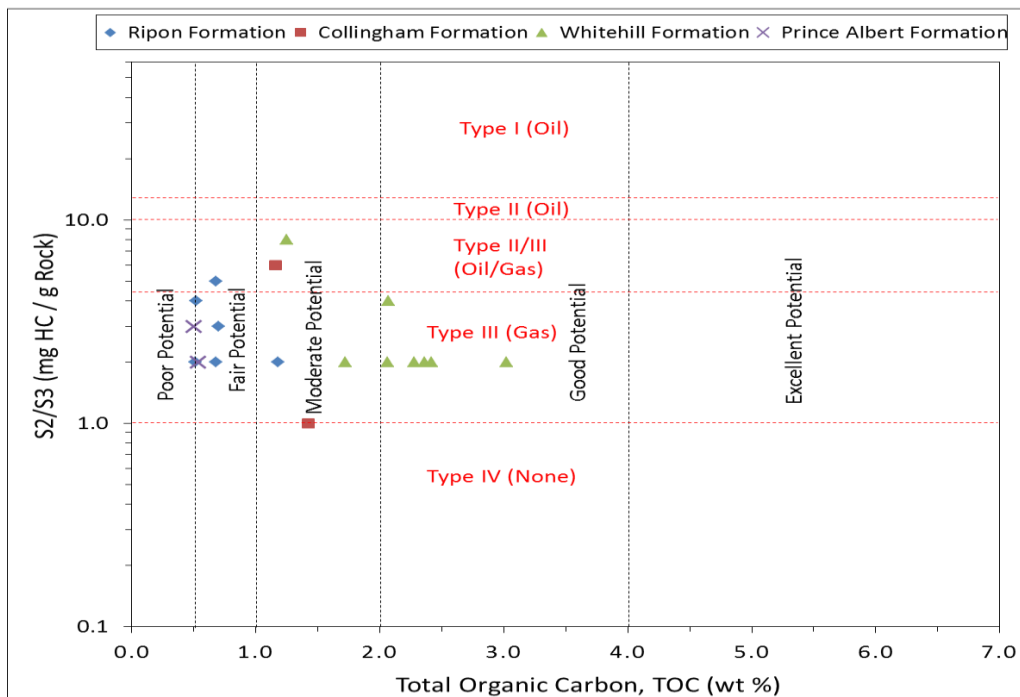
Figure 8.19: Binary plot of S2/S3 versus total organic carbon (TOC) showing generative source rock potential for the Ecca Group in borehole KWV 1.
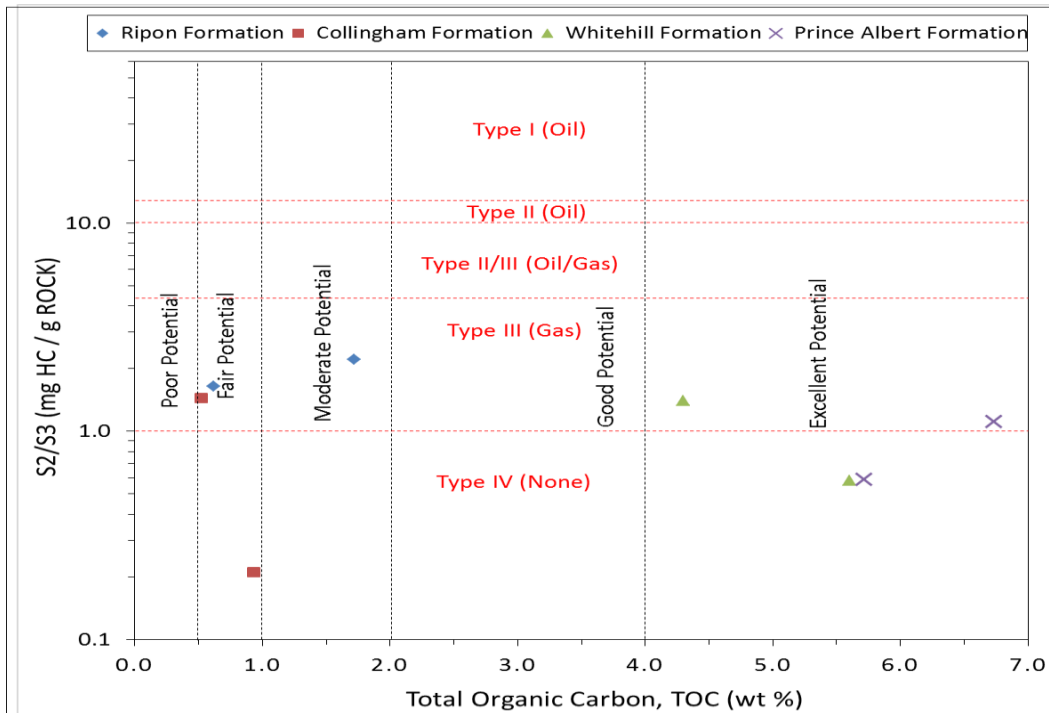
Figure 8.20: Binary plot of S2/S3 versus total organic carbon (TOC) showing generative source rock potential for the Ecca Group in borehole SP 1/69.
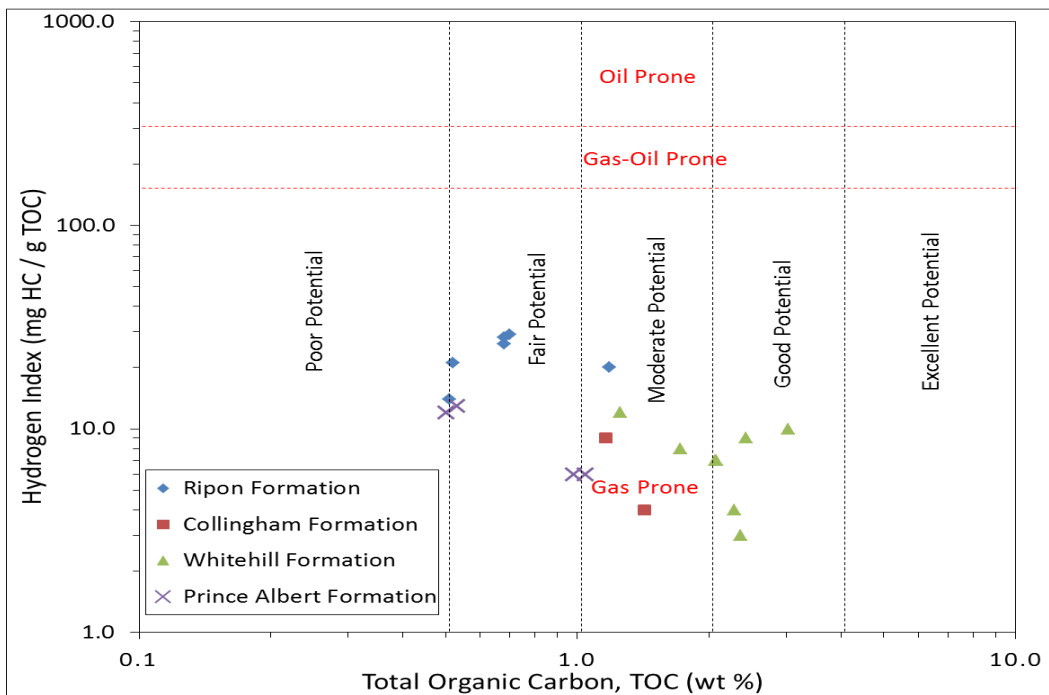
Figure 8.21: Binary plot of hydrogen index (HI) against TOC for the Ecca Group shales in borehole KWV 1 showing generative source rock potential (Plot from Maravelis and Zelilidis, 2010).
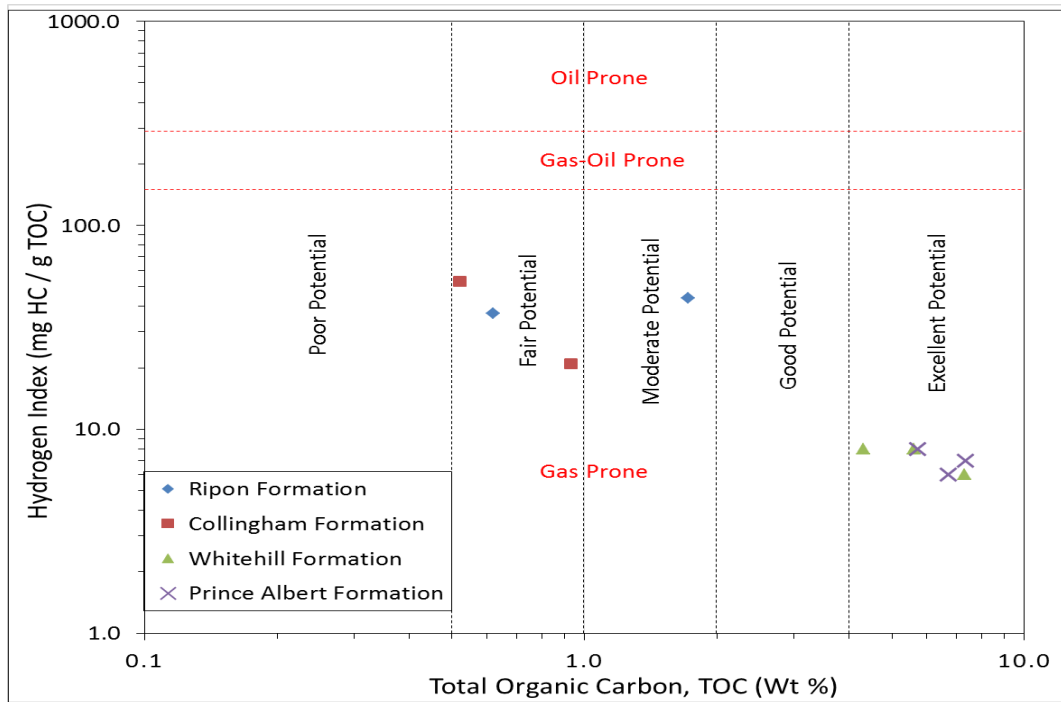
Figure 8.22: Binary plot of hydrogen index (HI) against TOC for the Ecca Group shales in borehole SP 1/69 showing generative source rock potential (Plot from Maravelis and Zelilidis, 2010).
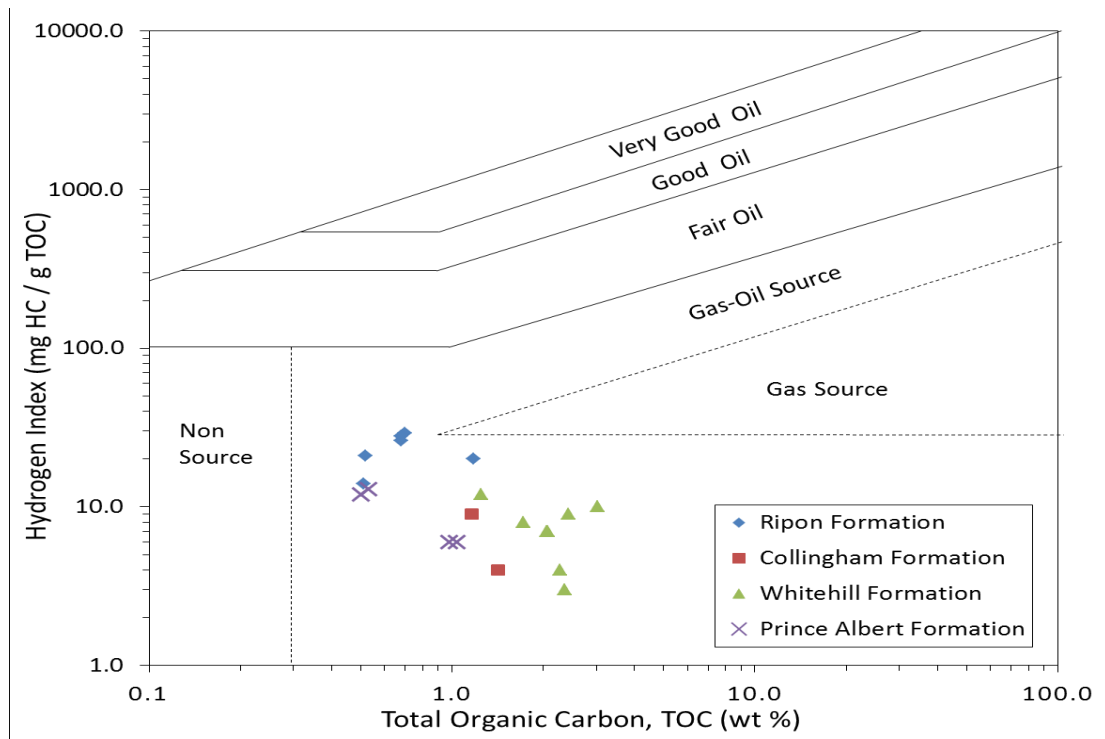
Figure 8.23: Binary plot of HI versus total organic carbon (TOC) showing source rock richness for the Ecca Group in borehole KWV 1.
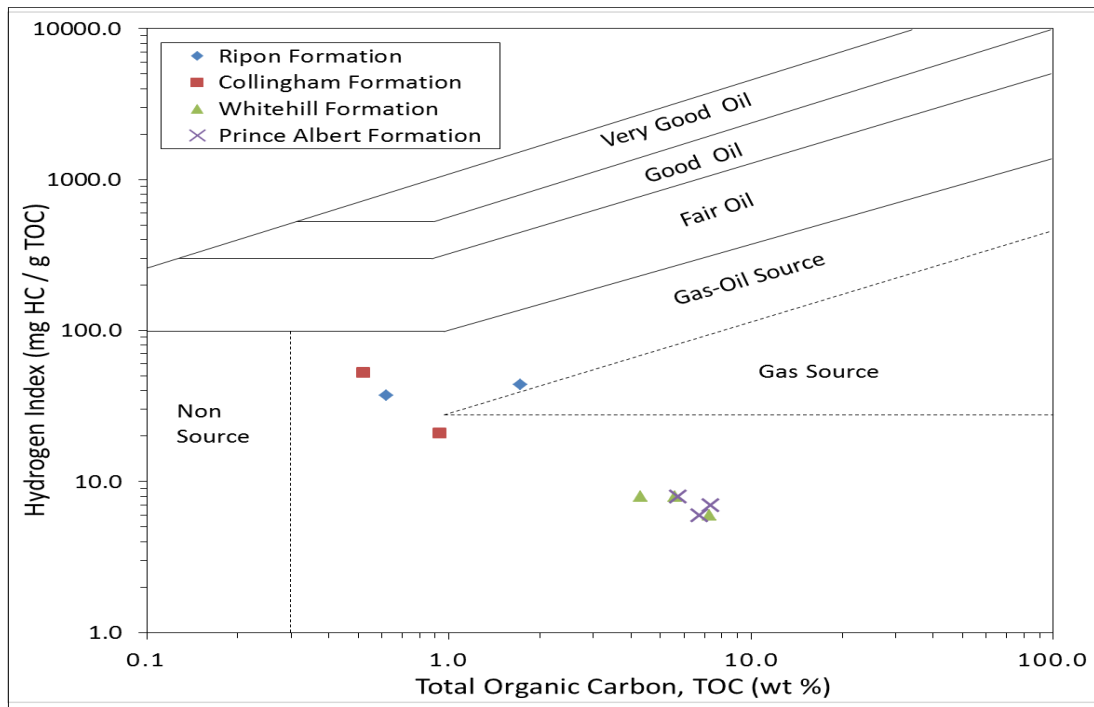
Figure 8.24: Binary plot of HI versus total organic carbon (TOC) showing source rock richness for the Ecca Group in borehole SP 1/69.
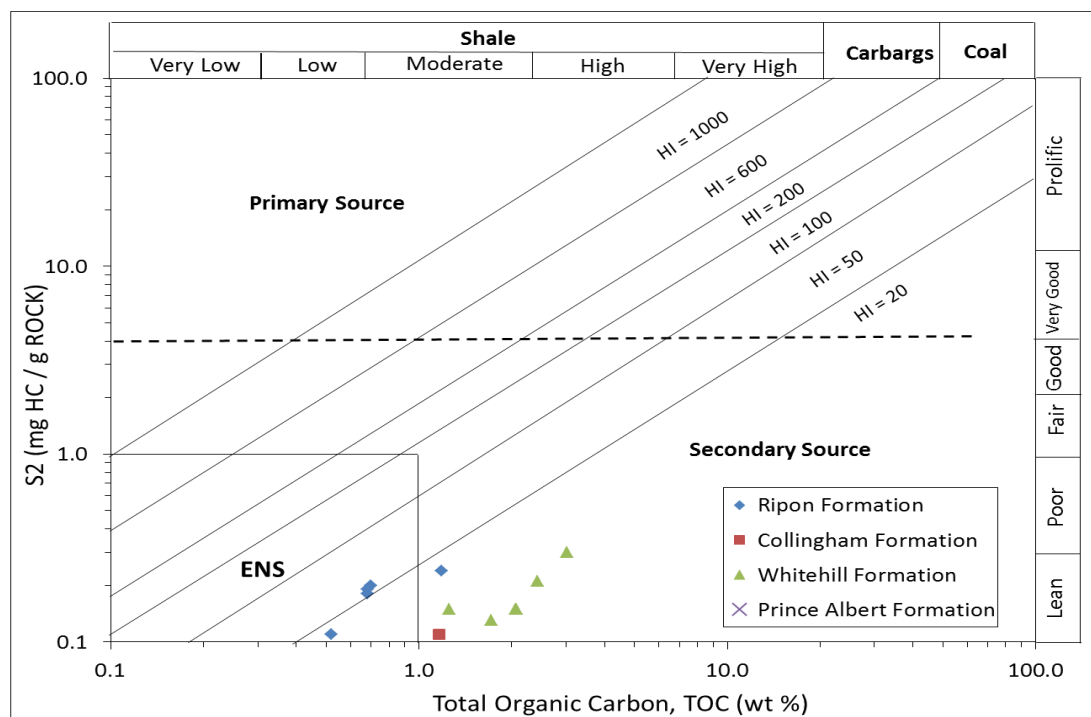
Figure 8.25: S2 versus TOC plot for source rock quality of the Ecca shales in borehole KWV 1. Note: Primary source field is ascribed to sediments with S2 greater than 5 kg/ton rock; ENS refers to effective non-source field (Plot from Burwood et al., 1995).
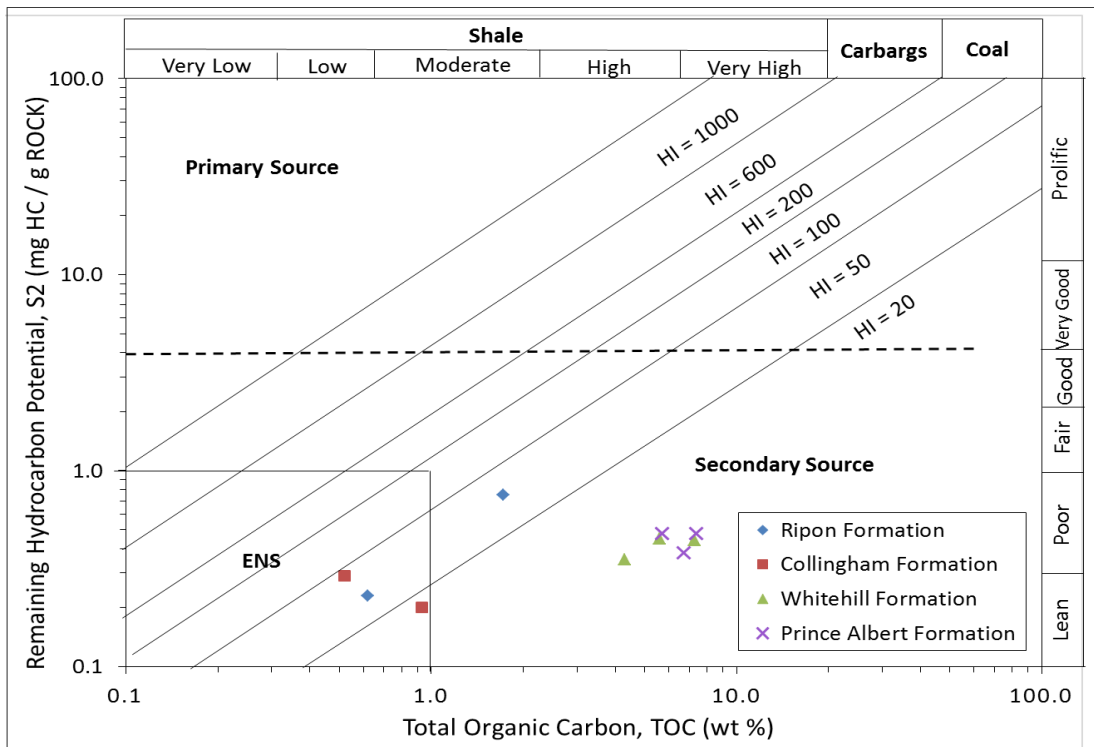
Figure 8.26: S2 versus TOC plot for source rock quality of the Ecca shales in borehole SP 1/69. Note: Primary source field is ascribed to rocks with S2 greater than 5 kg/ton rock; ENS refers to effective non-source field (Plot from Burwood et al., 1995).
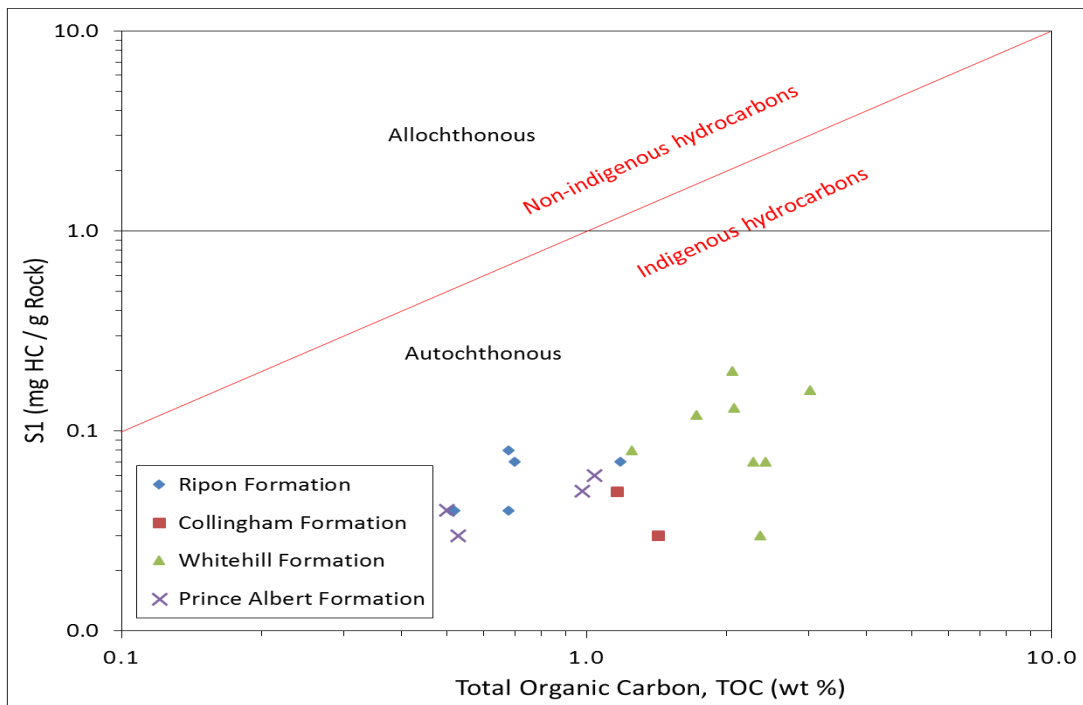
Figure 8.27: Plot of S1 against TOC for the Ecca shales showing generated indigenous-non indigenous hydrocarbon from borehole KWV 1 (Plot from Maravelis and Zelilidis, 2010).
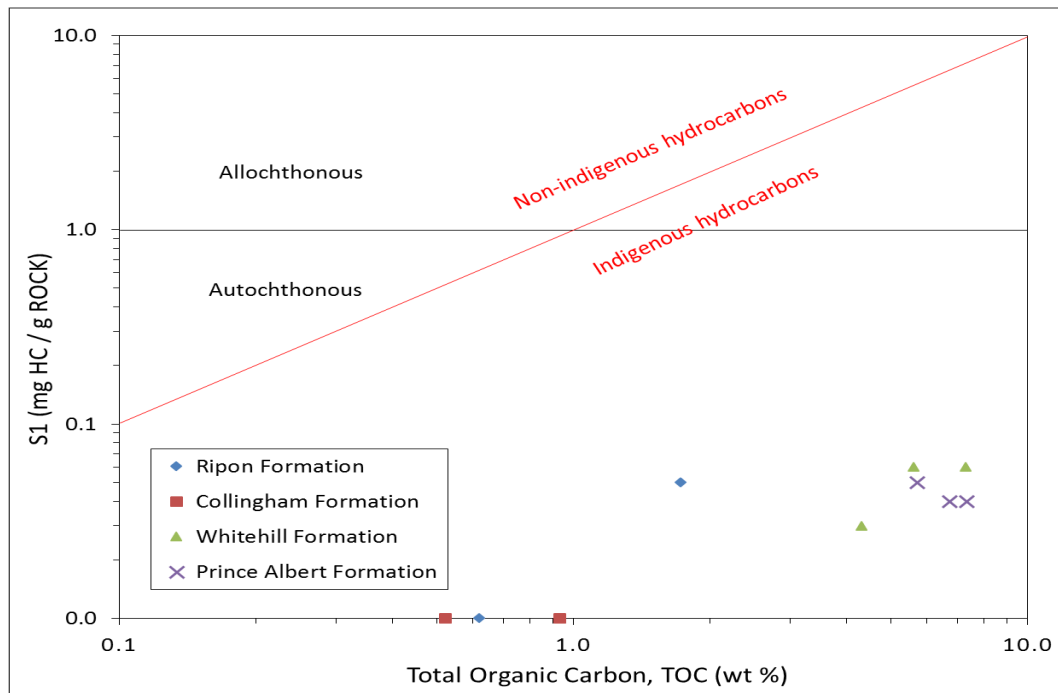
Figure 8.28: Plot of S1 against TOC for the Ecca shales showing generated indigenous-non indigenous hydrocarbon from borehole SP 1/69 (Plot from Maravelis and Zelilidis, 2010).

8.4 Comparison of reservoir characteristics

The potential of shale gas in a sedimentary basin is largely dependent on the structural and thermal history. Basins that have undergone significant folding and faulting are less likely to retain hydrocarbons due to thermo-tectonic driven migration. Hydrocarbons within deeply buried basins are subjected to high temperatures and pressures, and may only have potential for dry gas. Reservoir characteristics of the Ecca shales in the study area are compared to Marcellus and Barnett Shales in the United States. The area investigated is located close to the Cape Fold Belt (CFB) and intruded by dolerites, whereas the Marcellus and Barnett Shales are structurally variable. Exploitable gas-bearing shales generally have reservoir characteristics that include high organic richness, thermally mature, high porosity resulting from decomposition of organic matter, and mineral induced brittleness. Mineralogy of shale from the Whitehill Formation suggests suitable brittleness due to high quartz, calcite and dolomite content. Several studies including those of Kuuskraa et al. (2011) and Geel et al. (2013, 2015) shows that the Whitehill Formation complies with most of the aforementioned characteristics and therefore is the main target for unconventional shale gas explorationin the southern Main Karoo Basin. Reservoir characteristics (i.e. carbon content, lateral extent, thickness, porosity and permeability) of the Whitehill Formation as a suitable shale gas host compare favourably with the Marcellus and Barnett shales, which are currently exploited for

gas in the United States. For instance, on an average, the measured TOC value for the carbonaceous black shale of the Whitehill Formation is slightly higher than the average TOC value for the Barnett Shale (Table 8.7).

Table 8.7: Comparison of reservoir characteristics of the Whitehill Shales to those of the Marcellus and Barnett Shales.

Property		Whitehill (Permian Ecca shale, Karoo Basin, RSA) (This study)	Marcellus (Devonian Shale, Appalachian Basin USA) (Bruner and Smosna, 2011)	Barnett (Mississippian shale Fort Worth Basin, USA) (Bruner and Smosna, 2011; Hoelke, 2011)
Lithology		Organic rich black shale	Organic rich black shale	Organic rich black shale
Mineralogy (%)	Quartz	20-42	10-60	35-50
	Clays (illite)	4-26	10-35	10-50
	Calcite, sericite, dolomite	2-38	3-50	0-30
	Feldspars	0-28	0-4	7
	Pyrite	2-12	5-13	5
	Phosphate, gypsum	trace	trace	trace
	Mica	0-3	5-30	0
TOC (wt.%)		0.5-7.3	1-10	2-6
Tmax (℃)		318-601	≥ 475	≥ 455
Vitrinite reflectance (%Ro$_m$)		2.2-3.5	0.7-3.5	0.6-1.9
Kerogen Type		Mixture of Type II/III, III,	Type II and III	Mostly Type II
Porosity (%)		1-5.5	3-6	3-6
Average permeability (mD)		0.89	-	-
Thickness (m)		18-46	15	Max. 304; average 31
Estimated potential yield		-	50-900	2.5bcf-40tcf

Furthermore, the measured vitrinite reflectance values reach maximum values of about 3.5 % Ro, which is the same with those measured in the Barnett Shale. This perhaps indicate that the Whitehill Formation has a potential of being a profitable shale gas resource, especially in areas or locations where the shales are not intruded by dolerites and are far away from the CFB. Because dolerite intrusions as well as proximity to CFB in combination with depth of burial may have destroyed or over-cooked the organic matter that is present in the rock. Across the study area, the thickness of the Whitehill Formation ranges between 18 m and 45 m, which falls within the lower range of the Barnett Shale of 31 m. However, with respect to the Whitehill Formation, the Barnett Shale is unique due to the co-existence of the dry gas

with shale oil, condensates and wet gas; making it highly profitable for extraction of shale gas. Generally, it can be said that the Whitehill Formation is comparable to the Barnett and Marcellus Shales. The characteristics of shales from the Whitehill Formation (Table 8.7) shows that they have the potential for holding significant amounts of gas and are frackable.

Decker (2013) documented that the Collingham Formation should also be considered for shale gas exploration, if TOC values are consistently found to be above 3% over large areas of the basin. In this study, the measured TOC values for the Collingham Formation range from 0.22 to 0.93%. In addition, the shales have an average porosity and permeability values of 0.39% and 0.02 mD respectively, which is very much lower than that measured in the Whitehill Formation as well as those determined for active shale gas plays in the United States (Table 8.7). The combination of low carbon content, very low porosity and permeability values as well as the laminate nature of the strata shows that the Collingham Formation would be a poor source rock for gas, and an effective seal to the underlying potentially gas-bearing Whitehill Formation. The overlying carbonaceous shale of the Ripon Formation has an average TOC, porosity and permeability of 2.62%, 0.60% and 0.05 mD, respectively. This unit could also be a good hydrocarbon reservoir due to their proximity to the organic-rich Whitehill Formation. Furthermore, the formation contains laterally extensive thick sandstone units intercalating or capping the impermeable shales. These features are usually associated with an ideal hydrocarbon reservoir as long as the poroperm values are conducive to hydrocarbon storage. In terms of porosity and permeability, the Ripon Formation is not comparable with globally productive sandstones of the Marnoso Arenacea Formation and Foinaven Field (Table 8.8).

Table 8.8: The reservoir potential of the carbonaceous shale and sandstones of the Ripon Formation compared to those of Marnoso Arenacea Formation and Foinaven Field.

Property	Ripon (Permian Ecca sandstone) (This Study)	Marnoso Arenacea Formation, (Northern Italy) (Amy et al., 2009)	Foinaven Field (Palaeocene sandstone, Off-shore, Scotland) (Huggins, 2007)
Lithology	Fine grained sandstones intercalated with shale	Sandstone and mudstone	Fine to medium grained sandstone
Porosity (%)	0.380-0.840	0.150	23.000-30.000
Permeability	0.001-0.992	< 100.000	500.000-2000.000

For instance, the currently producing Foinaven Field has porosity values that are about 30 times higher than that of the Ripon Formation, allowing for the effective storage of

hydrocarbons. The potential pore spaces in the sandstone of the Ripon Formation are filled by smaller particles (i.e. clay minerals) and organic matter, thus reducing the potential hydrocarbon storage volume of the sandstone. Again, the permeability of the Ripon Formation is very low as compared to the Foinaven Field, thus preventing the migration of potential hydrocarbons.

8.5 Conclusions

The organic geochemical investigation of shale samples from the Ecca Group indicates the presence of gas-prone potential source rocks with fair to excellent source generative potential. Specifically, the shale of Prince Albert Formation are fair-good, while the carbonaceous shales of the Whitehill Formation are good to excellent. The Ecca source rocks have TOC values ranging from 0.11 to 7.35 wt.%. Generally, the average TOC values of the shales in borehole SP 1/69 are higher than those in KWV 1, suggesting that the hydrocarbon potential for the Ecca lithofacies in East London area is better than in the Transkei area. The Ecca shales are consistent with low HI values and relatively high Tmax values. The low HI values possibly indicate high level of thermal maturity and/or higher proportions of reworked vitrinites in the shales. The over-maturity of the shale may be due to the proximity of the study area to CFB. Also, excessive burial might have resulted in the loss of potential hydrocarbons. Compartmentalisation of reservoirs and burning off of hydrocarbons due to the intrusion of numerous dolerite dykes and sills may have contributed to additional loss of potential hydrocarbons. The binary plots of HI against OI, and HI versus Tmax shows that the Ecca shales are of Type II and mixed Type II-III kerogen, which are capable of generating both gas and minor oil at suitable burial depth. The bulk of the organic matter appeared to be either Type II or mixed Type II/III. There is a possibility that during deposition, the southeastern Karoo region was closer to a shelf, enabling terrestrial input, whereas the marine signature is potentially derived from short lived marine transgressions. The S2 values for the analysed samples are less than 1 mg HC/g rock, indicating secondary source field. The plot of S1 versus TOC shows that the source rocks were characterized by autochthonous hydrocarbons. Based on the geochemical data, it can be inferred that source rocks are in immature to over-mature and have potential of producing gas in present-day. Generally, the Whitehill Formation of the Karoo is comparable to the Marcellus and Barnett Shales. This further supports the assumption that the Whitehill Formation has a high probability of being a profitable shale gas play, but only when explored in dolerite-free area and away from the CFB.

CHAPTER 9

DIAGENESIS AND RESERVOIR PROPERTIES OF THE SANDSTONES AND MUDROCKS

Abstract

Diagenesis is one of the most important factors that affect reservoir rock property. Despite there are many previous studies on the stratigraphy, sedimentology and general geology of the Ecca Group in the Main Karoo Basin of South Africa, there is still lack of knowledge on the diagenesis of the potentially feasible or economically viable sandstones and mudrocks of the Ecca Group. This chapter aims to provide an account of the diagenesis of sandstones and mudstones from the Ecca Group. Twenty-five diagenetic textures and structures are identified and grouped into three stages that include early diagenesis, burial diagenesis and uplift-related diagenesis. Clay minerals are the most common cementing materials in the sandstones. Smectite, kaolinite and illite are the major clay minerals that act as pore-filling matrix and pore lining rim-cement. Calcite precipitates locally in the pore spaces and partially or completely replaced clay matrix, feldspar and quartz grains at or around their margins. Precipitation of cements and formation of pyrite and authigenic minerals occurred during the early diagenetic stage. This process was followed by lithification and compaction which brought about an increase in tightness of grain packing, loss of pore spaces and thinning of bedding thickness due to sediment overloading and selective dissolution of framework grains. Mineral overgrowths, mineral replacement, clay-mineral transformation, dissolution, deformation and pressure solution occurred during burial diagenetic stage. After rocks were uplifted, weathered and unroofed by erosion, this resulted in decementation and oxidation of iron-rich minerals, and saussuritization of feldspar minerals. The rocks were subjected to moderate-intense mechanical and chemical compaction during its progressive burial. Intergranular pores, secondary dissolution and fractured pores are well developed in the rocks. The presence of fractured and dissolution pores tend to enhance reservoir quality. However, the isolated nature of the pore linkage makes them unfavourable producers of hydrocarbons, which at best would require stimulation. The understanding of the space and time distribution of diagenetic processes in these rocks will allow the development of predictive models of their reservoir quality, which may contribute to the reduction of risks involved in the hydrocarbon exploration.

Keywords: Diagenesis, reservoir properties, diagenetic textures and stages, Ecca Group

9.1 Introduction

The early search for oil and gas reservoirs focused on acquiring or knowing the regional tectonics, stratigraphy and sedimentology of the reservoir rocks, followed by a more detailed assessment of diagenetic features, porosity and permeability changes. During petroleum exploration, reservoir quality is one of the main controlling factors on prospectivity. Therefore, it is important to have a detailed understanding of the factors that controls reservoir quality in order to assist with the appraisal of the economic feasibility of hydrocarbon discoveries. As documented by Selley (1997), once petroleum has been discovered in a basin, it is very important to have detailed understanding of reservoir quality to help focus further exploration and appraisal efforts. Reservoir quality in clastic and fine grained rocks is controlled by several interconnected factors such as mineral composition, pore water chemistry, diagenetic events, temperature, fluid flow, depositional environment, tectonic setting, time, burial depth, uplift process, geothermal gradient and subsurface pressure (Bjorlykke, 1988; Noh and Lee, 1999; Zou et al., 2012). Diagenesis is the most crucial factor impacting reservoir property (Salem et al., 2005; Honarmand and Amini, 2012). Hence, reconstruction of the diagenetic history is important in understanding reservoir porosity and permeability to predict the reservoir characteristics of clastic rocks.

In general term, diagenesis encompasses all of the changes that sediments undergo between the time of deposition and before the transition to metamorphism. These changes (i.e. physical, chemical and mineralogical) occurred as a result of several factors including compaction, deformation, dissolution, cementation, authigenesis, replacement, recrystallization, hydration and bacterial actions (Boggs, 2009). The economic importance of certain shale and/or sandstone units as a source or reservoir rock for petroleum may ultimately depend on the diagenetic history of the units as well as their original depositional characteristics (Boggs, 2009). Diagenetic processes are continually active as the ambient environment changes in terms of temperature, pressure and chemistry during deposition, burial and uplift cycle of the basin history (Burley and Worden, 2003). These processes are thought to occur above the zone of metamorphism with temperatures below about 195℃-220℃ and at pressures ≤ 5 kb (Boggs, 2009). The lower and upper limits of diagenesis can be determined using certain minerals, for instance, Tucker (2001) reported that the stable limit temperatures of limonite (195℃-220 ℃) can be used as the highest temperature of diagenesis, whereas the stable limit temperatures of chlorastrolite and zonochlorite (≥ 250 ℃) are used as the lowest limiting temperature of metamorphism.

Several researchers including Curtis (1977), Giles and Marshall (1986), Wright (1993), Bloch et al. (2002), Mackenzie (2005) and Milliken (2006) have documented that diagenetic alterations in siliciclastic rocks have a significant influence on reservoir quality by modifying the rock's primary porosity, permeability and consequently, on reservoir quality. Petrographic studies are of key importance for characterizing the types, timing and rate at which the diagenetic processes are affecting porosity and permeability of the sandstones and mudrocks (Ajdukiewicz and Lander, 2010). The relationship between diagenesis and reservoir quality is investigated and documented by several researchers (i.e. Roswell and De Swart, 1976; Reed et al., 2005; Geel et al., 2013; Macquaker et al., 2014). However, the major factors influencing diagenesis are not well understood and diagenetic alterations in reservoir properties remain largely unpredictable (Molenaar, 1998). Since variety of diagenetic processes and products are very high in clastic sediments, particularly sandstones.

In recent years, shale gas exploration has gained huge economic success in many countries, particularly in United State of America, Canada and China, which stimulate other countries to follow these examples. Thus, the study of diagenesis on Ecca Group sandstones and mudrocks has not only theoretical significance, but also has potential economic importance. Presently, the lower Ecca Group formations of the Main Karoo Basin attract a great interest for hydrocarbon exploration in South Africa. The efficient exploitation of the Ecca Group reservoirs depend on several factors, including better understanding of the impact of diagenetic alterations on reservoir quality (porosity and permeability). However, there are very few published studies on the diagenesis of the clastic rocks from the Ecca Group within the study area. Despite the fact that such rocks may themselves constitute prospectable reservoirs, apart from providing vital palaeoenvironmental information for the understanding of the detrital marine clastic reservoirs. The purpose of this research work is to examine if diagenesis has significantly altered the original petrologic characteristics of the Ecca sandstones and mudrocks after deposition. The study is also to add new information on the cement types, pore types, diagenetic sequence (as well as the impact of diagenesis on their quality as potential clastic reservoirs. The diagenetic study on the Ecca Group sandstones and mudrocks will contribute to reduce the exploration risks in this extensive area.

9.2 Materials and method

Thin sections of 152 rock and core samples (104 sandstones and 48 mudrocks) were prepared and studied under optical microscope in order to determine mineral compositions, rock

textures, shape and size of grains and cements. The core samples were taken from borehole KWV 1, SC 3/67 and SP 1/69 (Figure 1.1). In addition, a total of 30 samples (20 sandstones and 10 mudrocks) were properly cleaned and glued on a glass microscope slide using Struers specifix resin mixed with Struers specifix-40 curing agent in the ratio 5:2 by weight (the mounted samples were left for 24 hours). After the samples had been stuck to the microscope slide, they were carbon coated using Cressington Carbon Coater 108 Carbon/A machine combined with a pumping system and thickness monitor into a space of approximately 42 cm x 60 cm. The coated samples were analysed using a scanning electron microscopy (SEM) instrument (Model: JEOL JSM-6390LV) in the working condition of 15KV, and equipped with a link system Energy Dispersive X-Ray microanalyser (EDX). The diagenetic study reported in this chapter focuses more on the sandstones, with minor emphasis on the mudrocks. The studied samples were examined in secondary electron imaging (SEI) and backscattered electron (BSE) modes of imaging. The description of cementation textures, primary and authigenic mineralogy of the shales and sandstones were described based on petrographic study of thin sections, SEM and EDX analyses. In addition, clay minerals, dissolution effect, quartz overgrowth, diagenetic textures, pore geometry and other related diagenetic textures were investigated using SEM. Both SEM and petrographic microscopy were carried out at the University of Fort Hare, South Africa. Mineral compositions of the shales, mudstones and sandstones were determined by XRD at the Council for Geoscience laboratory in Pretoria. The X-Ray diffraction measurements were performed on a Bruker XRD D8 Advance (Model: V22.0.28) at a room temperature of 25℃ and the samples were scanned at 2° 2θ per minute from 2° to 70° (wavelength of 1.5406).

9.3 Result

9.3.1 Diagenesis of sandstones

The main diagenetic processes that have strongly affected the sandstones of the Ecca Group are cementation, mechanical compaction, dissolution, grain replacement and recrystallization.

9.3.1.1 Cementation

Cementation is one of the most important processes leading to the loose sediments to form a consolidated rock, thus resulting in porosity reduction. Four types of cements were identified in the sandstones of the Ecca Group, which are quartz cement, calcite cement, feldspar cement and authigenic clay mineral cements.

9.3.1.1.1 Quartz cementation

Quartz cement exists in the rocks as a result of precipitation of silica into the pore spaces between grains. Quartz cement occurs as both pore-filling and overgrowths in the rocks. This type of cement was formed early in the shallow marine diagenetic environment and in the early diagenetic stage. Quartz overgrowths occur as syntaxial overgrowth, growing outwardly from detrital quartz grain surface. The overgrowths have the same optical properties as the original detrital quartz grains. In some cases, the boundaries between the detrital quartz and overgrowths are marked by clay coatings and dust lines. The result of overgrowths commonly gives the grain more euhedral crystal faces. The dissolution of feldspars and micas led to the release of silica, thus providing silica source for the formation of quartz cement and authigenic quartz. Quartz cement exists in the rocks as fine granular quartz (Figure 9.1) as well as quartz overgrowths (Figure 9.2). Quartz cements were formed due to silica precipitation in pore spaces.
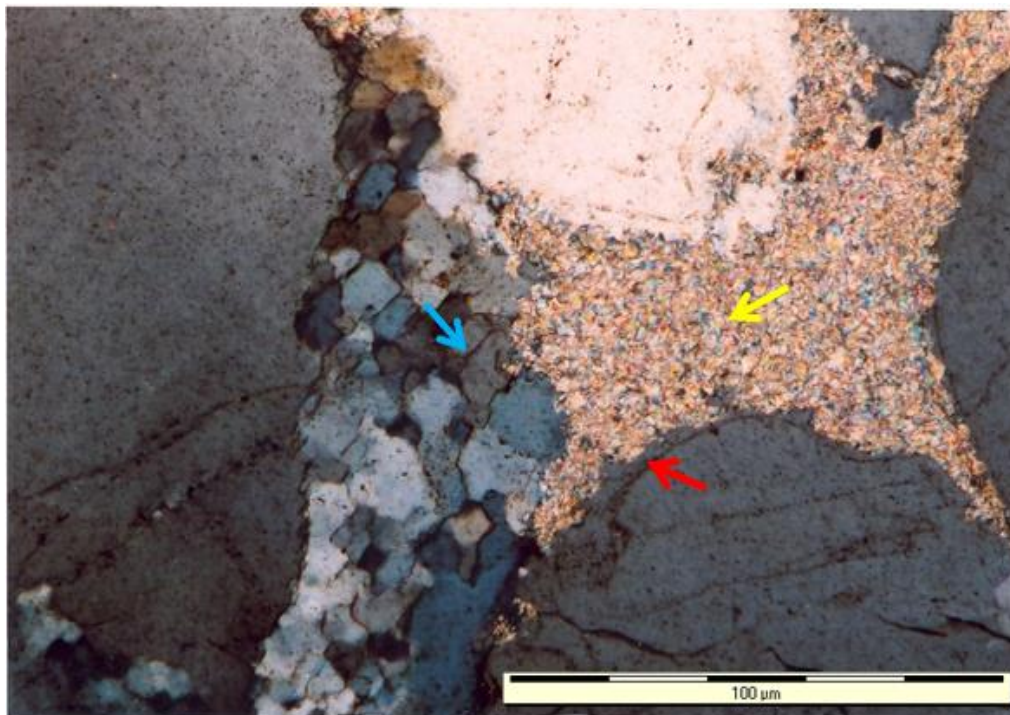
Figure 9.1: Thin section photomicrograph of fine sandstone showing fine granular quartz cement (blue arrow), clay matrix (red-brownish area; yellow arrow) and quartz overgrowth (red arrow)
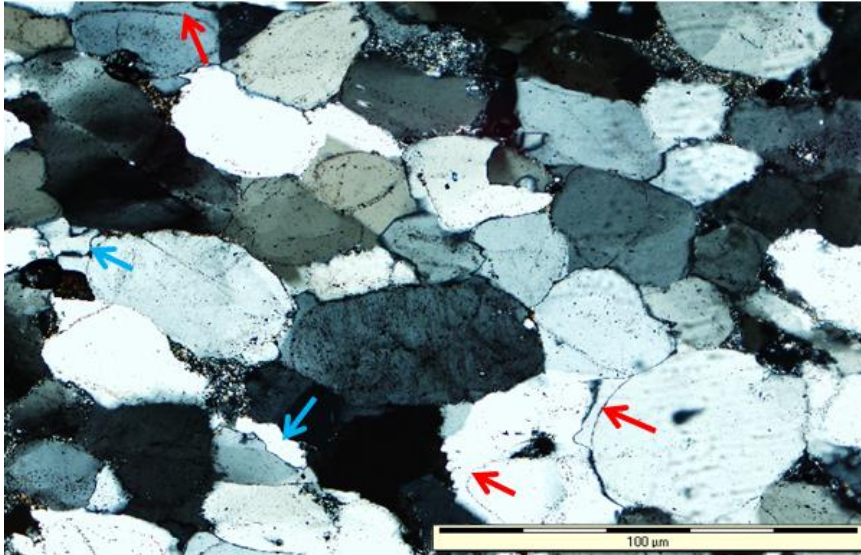
Figure 9.2: Thin section photomicrograph of sandstone showing quartz overgrowths (red arrows) and quartz cement (blue arrows). The overgrowth part has optically continuity with the original detrital quartz grain.

9.3.1.1.2 Calcite cementation

Calcite cementation is another type of cement in the Ecca Group. It occurs mainly as a pore-filling and replacement mineral of clay matrix and detrital grains. This possibly point to precipitation in different diagenetic stages. Calcite precipitates locally in pore spaces and partly or completely replaced feldspar and quartz grains, commonly at their margins. Most of the clay minerals (matrix) and detrital grains were seriously attacked and replaced by calcite (Figure 9.3).
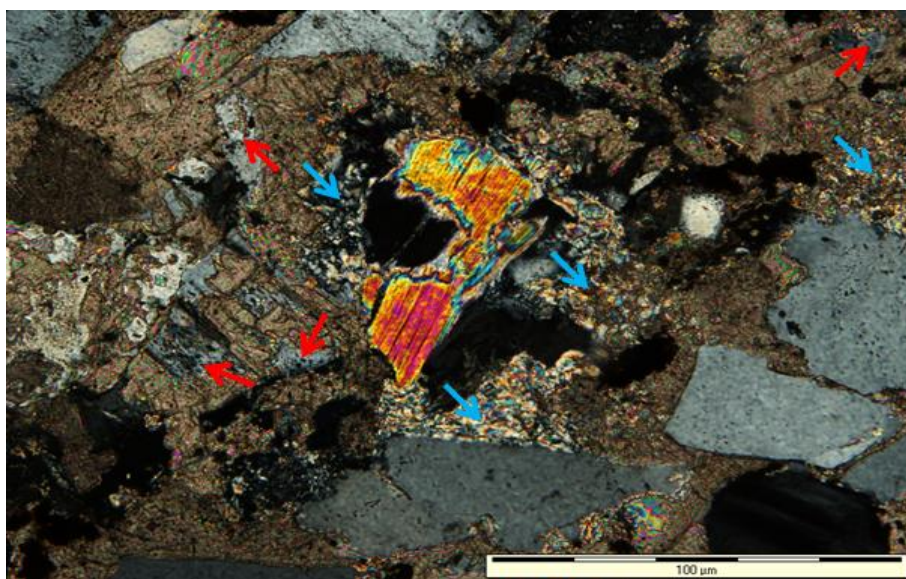
Figure 9.3: Thin section photomicrograph of sandstone showing calcite replacement of feldspar grains (red arrows) and clay matrix (illite and sericite, blue arrows). The middle is a detrital muscovite.

256

In some cases, the replacement even penetrated into the cores of grains. Calcite cementation replaces (post-dates) quartz overgrowths. Calcite filled most of the secondary pores after dissolution of feldspar.

9.3.1.1.3 Feldspar cementation

Feldspar cement is a minor cement type in the sandstones and siltstones. It occurs as pore-filling feldspar and as overgrowths around detrital K-feldspar grains (Figure 9.4). In few cases, the feldspar overgrowth shows hematite rims (dust rim) around the original detrital grain. Feldspar overgrowths behave as an authigenic feldspar pore-filling cement and represents early diagenetic mineral. Most of feldspar syntaxial overgrowths are associated with quartz overgrowths. This cement was formed after quartz cementation.
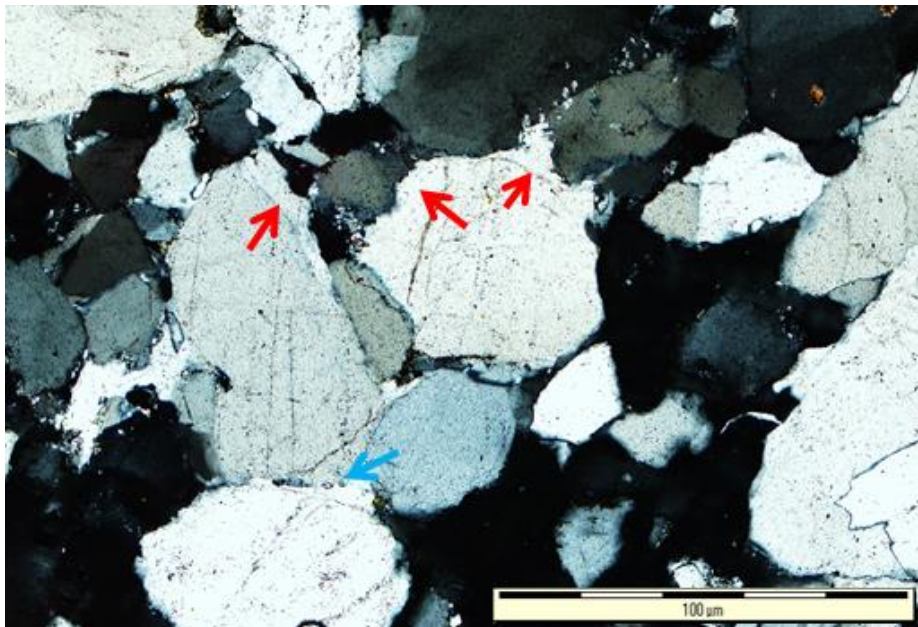
Figure 9.4: Thin section photomicrograph of sandstone depicting feldspar overgrowths (red arrows) and feldspar cement (blue arrow).

9.3.1.1.4 Clay mineral cementation

Clay minerals are the most common cementing materials in the Ecca sandstones. These minerals act as pore lining rim cement and pore-filling matrix. Smectite, kaolinite and illite are the major clay minerals that act as cementing agent in the rocks. These authigenic clay minerals are formed through recrystallization of fine matrix and dissolution of K-feldspars. In addition, they may also have been formed due to modification or alteration of one kind of clay mineral to another, for instance, both smectite and kaolinite were transformed into illite. Other clay minerals that occurred as minor constituent in the rocks are sericite and chlorite.

Smectite recrystallized into illite and chlorite, kaolinite recrystallized into illite. Illite also further changed to sericite, which later recrystallized to muscovite.

9.3.1.1.4.1 Kaolinite clay

Kaolinite occurs as both pore filling and lining clay matrix or cement. In addition, kaolinite clay also occurs as common replacement mineral, replacing weak detrital K-feldspar after weathering (Figure 9.5) and muscovite grains. Kaolinite can either be detrital or authigenic in origin.
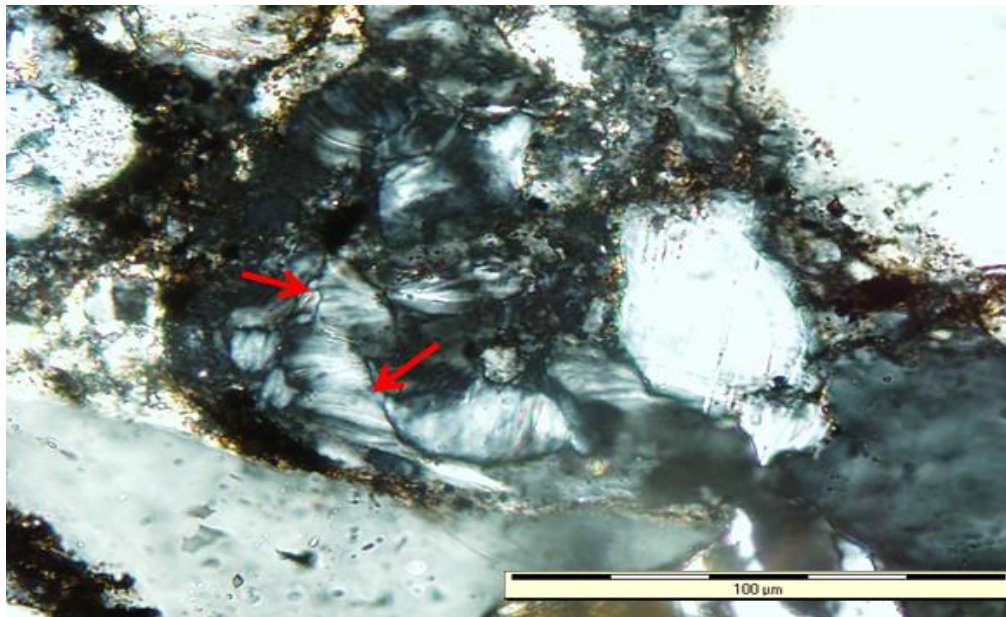
Figure 9.5: Thin section photomicrograph of sandstone showing feldspar grains undergoing alteration to kaolinite vermicules (red arrows).

Detrital kaolinite is deposited in the depositional basin by erosion and transportation, whereas authigenic kaolinite is formed in situ in the depositional basin. The former shows erosion and transportation effects such as angular and broken grain shapes, while the latter shows fibrous or euhedral crystalline shape, or booklet crystalline shape under SEM. SEM studies revealed that accordion-shaped clay flakes occur as euhedral crystals in the intergranular pores (Figure 9.6). Kaolinitized intraclasts occur as relatively large, irregular, scattered patches of kaolinite. On the other hand, partially kaolinitized mica sometimes has thin, thread-like remnants of the muscovite. Thus some kaolinite resembles fragments of detrital mud or silt-size lithic grains. In some cases, kaolinite patches, which are squeezed and deformed between the grains, fill nearby intergranular pores. This possibly point to kaolinitized pseudomatrix. Completely kaolinitized feldspars occur as patches of kaolinite with well-defined relic outlines, similar in

size to the original detrital feldspar grains. But partially kaolinitized feldspars have detrital feldspar remnants. In some cases, the kaolinite is engulfed by quartz overgrowth, and thus pre-dates the quartz overgrowths. The kaolinite was formed in the early diagenetic stage and uplift stage. Hence, the presence of altered K-feldspar and muscovite serves as sources of silica and aluminium resulting in the formation of kaolinite.
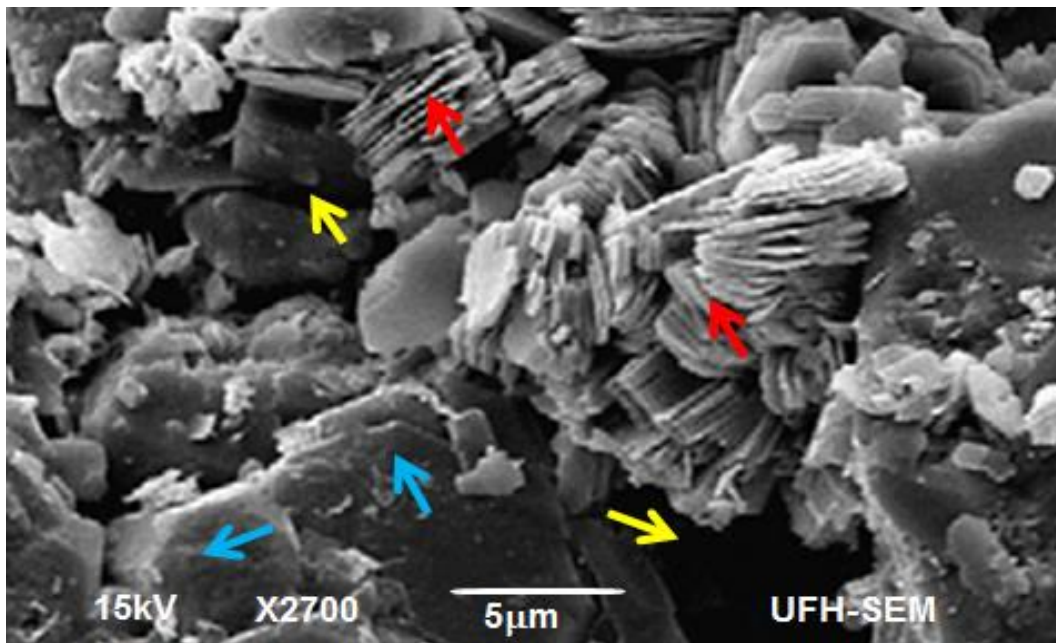
Figure 9.6: SEM (BSE) photomicrograph showing accordion or book-page shaped kaolinite (red arrows) and quartz cements (blue arrows) partly filling the intergranular pores (yellow arrows).

9.3.1.1.4.2 Illite clay

Illite clay occurs as pore filling and lining clay minerals. They also occur as booklets and vermicular stacked platelets that resemble kaolinite, and thus were likely formed as a result of partial to complete alteration or recrystallization of kaolinite and smectite (Figure 9.7). Illitization usually occurred after the precipitation of kaolinite and smectite, and requires influx of potassium under a higher temperature. Despite the fact that illitic clays are often associated with the decomposition of kaolinite, kaolinite decomposition is not always accompanied by illitization nor does kaolinite always decompose when illitic cements form (Hurst and Irwin, 1982). Illite commonly retained the shape of its predecessors especially when it is formed due to dissolution of kaolinite. Authigenesis of illite clay depends on the presentation and alteration of smectite/kaolinite and other labile detrital minerals that are easily to be altered and require alkaline (illite) and acidic (kaolinite) pore fluid.
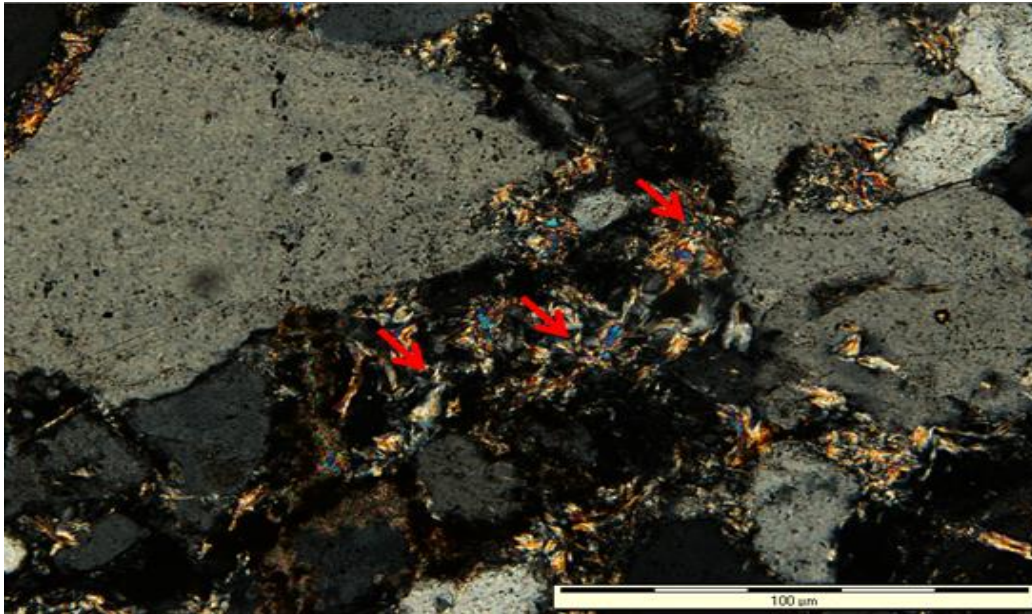
Figure 9.7: Thin section photomicrograph of sandstone showing recrystallization of smectite/kaolinite to illite (red arrows).

Illite is usually formed in shallow burial diagenesis under increased temperature. Smectite changed to illite at temperatures ranging from 55-200 ℃ (Hurst and Irwin, 1982). As temperature increases, smectite change to illite, starting with the growth of single illite pellets on smectite to their nucleation (Figure 9.8). The observed smectite generally have honey-comb shape (Figure 9.11a) and curved flake or platy box-work shapes with illite growing from its surfaces, resulting in the formation of a mixed illite-smectite layers. As temperatures continued to increase, illite is transformed into sericite. Afterwards, the sericite are altered to muscovite. The formation of illite requires a growth medium (pore fluid and space) with high potassium (K), silica (Si) and aluminium (Al) compositions. The EDX graph (Figure 9.9) shows that the mineral is mainly composed of silica and aluminium, whereas potassium, iron and magnesium elements only occur in small quantity. This agrees with the chemical formula or composition of illite $((K,H_3O)(Al,Mg,Fe)_2(Si,Al)_4O_{10}[(OH)_2,(H_2O)])$. Therefore, the occurrence of illite or illite-smectite mixed layers lies merely on the transformation/conversion of smectite clay mineral during shallow burial diagenetic process at increased temperature between 90 ℃ and 130 ℃ (Pollastro, 1985).
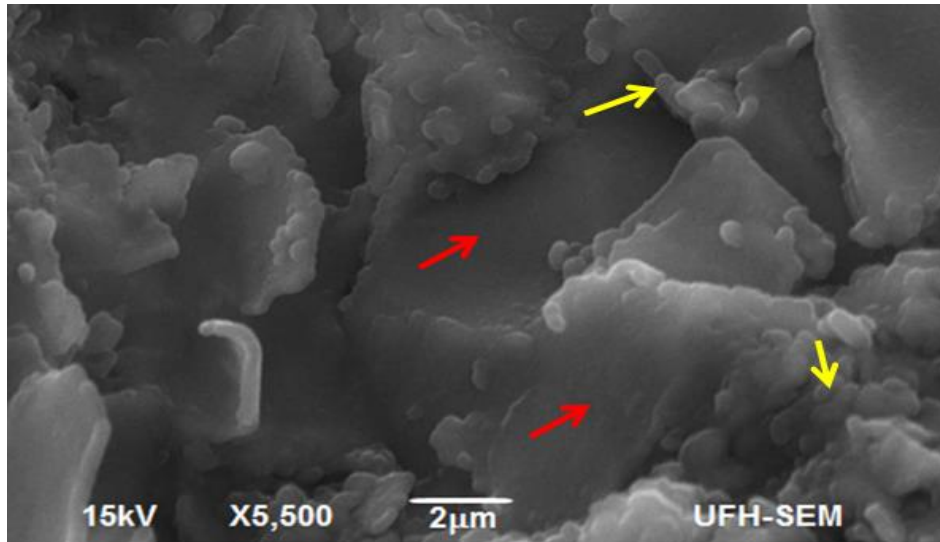
Figure 9.8: SEM (BSE) photomicrograph showing illite growth (yellow arrows) on smectite flakes (red arrows).
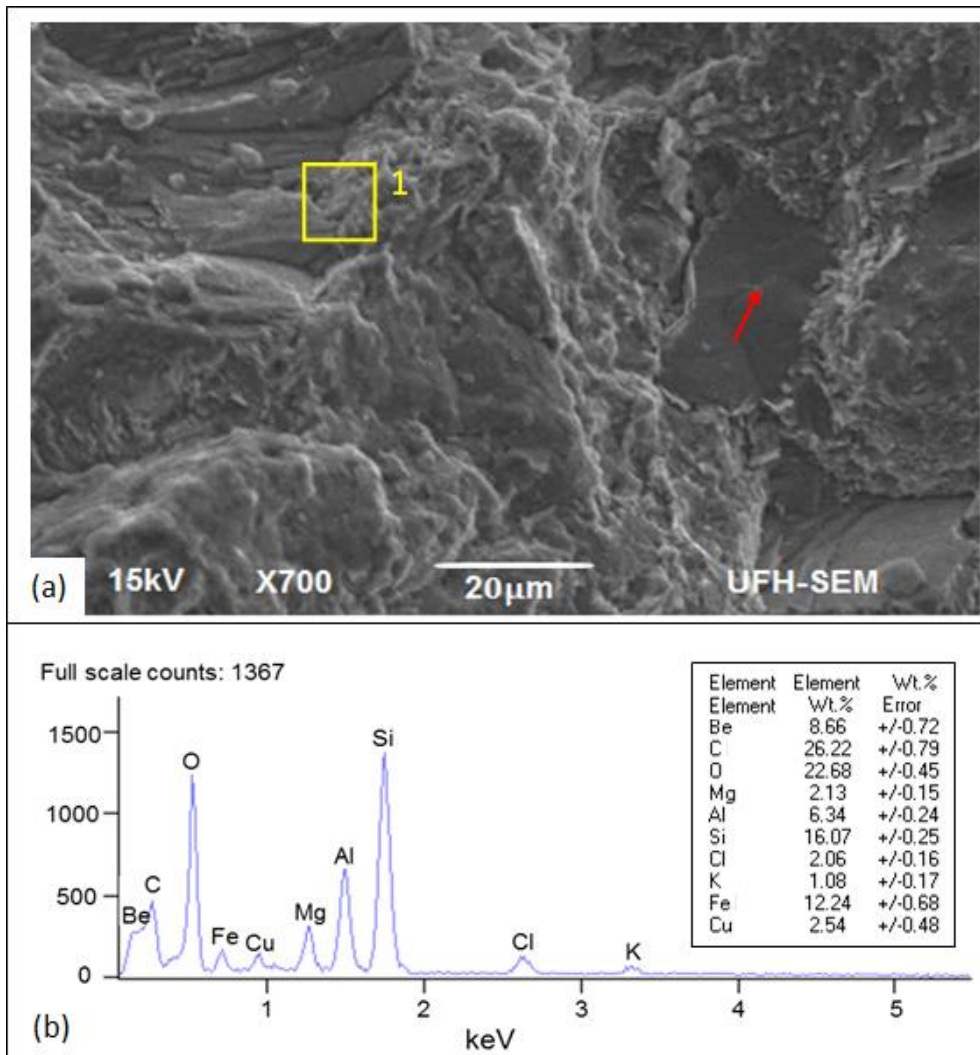
Figure 9.9: (a) SEM (BSE) photomicrograph showing fabric shaped illite and detrital quartz (red arrow); (b) EDX graph showing elemental composition of illite at point 1 (yellow area).

9.3.1.1.4.3 Smectite clay

Smectite occurs as grain coatings and microcrystalline matrix aggregates (Figure 9.10). SEM examinations revealed that smectite clay seems to have a cornflake-shaped texture and sometimes appear to have honey-comb morphology (Figure 9.11a). In some cases, illite grows from the surface of the cornflake-shaped smectite or forms mixed illite-smectite interlayers. The smectite flakes also recrystallized to pelletic and fibrous illite (Figure 9.12). Smectite can be transformed to illite through the process of illitization.
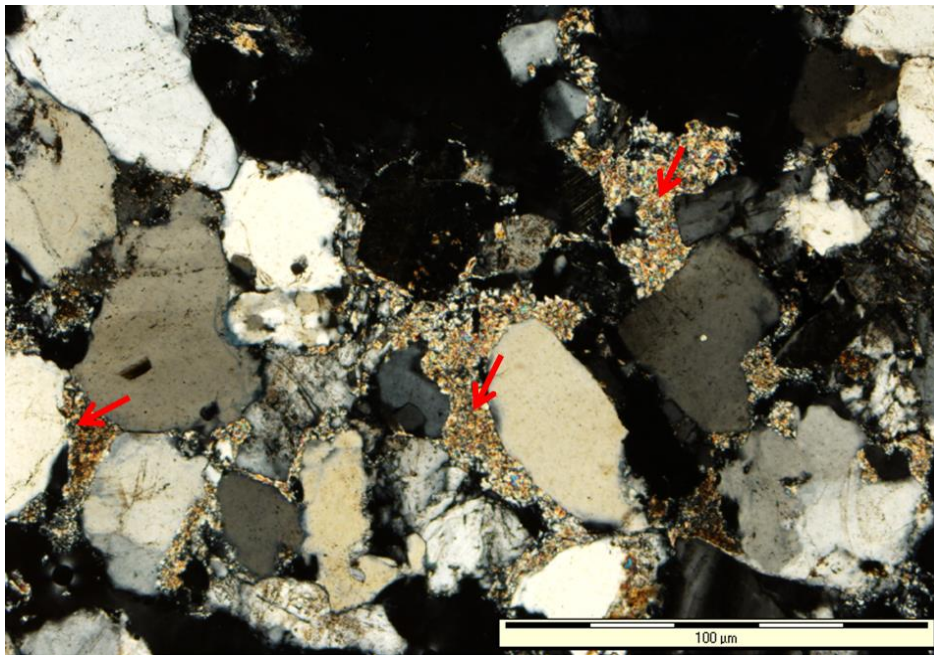
Figure 9.10: Thin section photomicrograph of sandstone showing clay (illitized smectite) matrix around feldspar and quartz grains (red arrows).

Smectite can contain substantial amounts of Fe and Mg. Thus, destruction of smectite layers during illitization can release significant amounts of these elements, depending on the initial composition of the rock. Pollastro (1985) documented that, for smectite to be converted to illite, it is essential that K^+ must be added in the interlayer space and the amount of tetrahedral Al^{3+} must be increased. The mathematical expression is shown below:

$$Smectite + Al^{3+} + K^+ = Illite + Si^{4+}$$
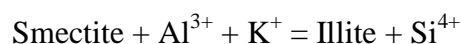
The released silica (Si^{4+}) is believed to form or add to the quartz cement in rocks, whereas the Fe and Mg (Figure 9.11 (b and c)) are believed to form as part of reaction products that are more stable under the increased burial temperature conditions. Smectite in the studied samples does not uniformly change to illite. Al-rich layers are more susceptible to illitization than

those containing Fe and Mg. Alteration of smectite to illite also led to the increase of sodium (Na) in the Ecca sediments. At uplift-related diagenesis, weathering, dissolution and oxidation may result in the alteration of smectite to chlorite. In addition, it may also cause the rocks and minerals to break down, decompose and get weathered.
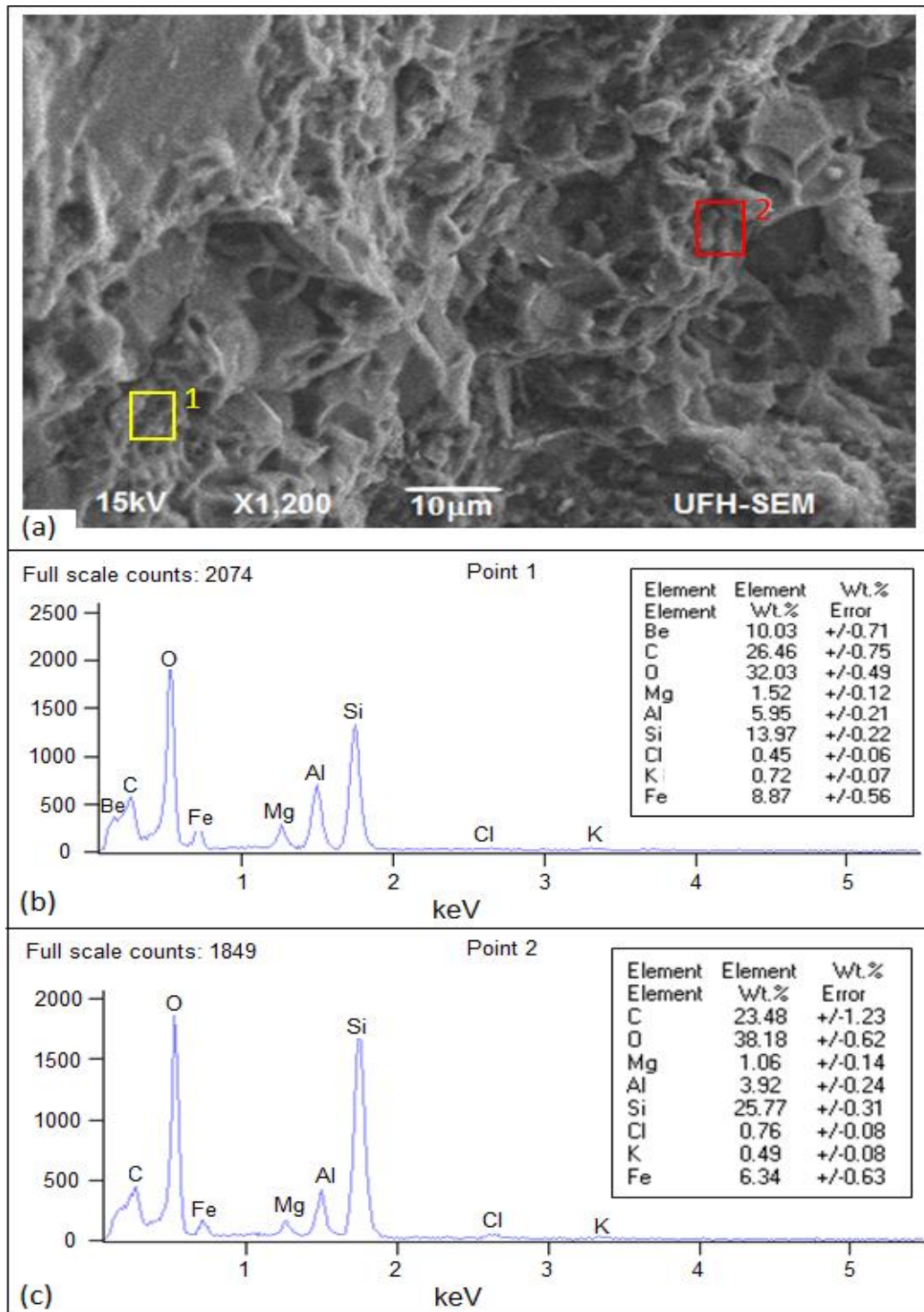
Figure 9.11: (a) SEM (BSE) photomicrograph of sandstone showing honey-comb shaped smectite; (b) EDX graph showing elemental composition of smectite at point 1 (yellow area); (c) EDX graph showing elemental composition of smectite at point 2 (red area).
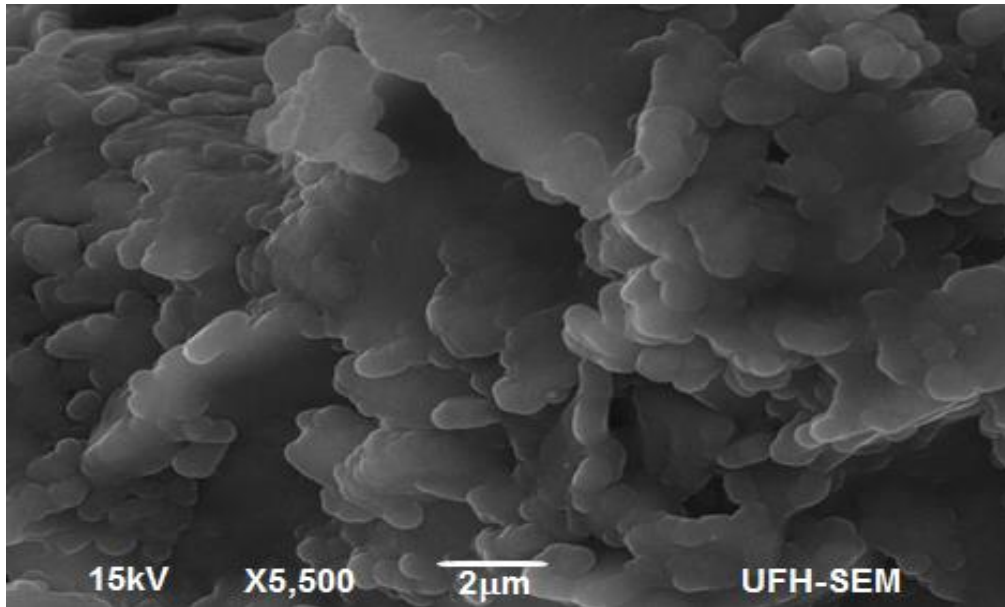
Figure 9.12: SEM (BSE) photomicrograph showing recrystallisation of smectite flakes to pelletic and fibrous illite.

9.3.1.2 Compaction

During the initial stages where diagenesis took place under oxidizing pore waters, mechanical compaction start to influence the soft sediments when it was buried by overloading deposits. The higher the overburden, the more intense is the compaction. The overburden pressure results in bed thinning in sedimentary rocks, expelling intergranular fluids (dewatering), closer packing of the grains and porosity reduction (Figure 9.13).
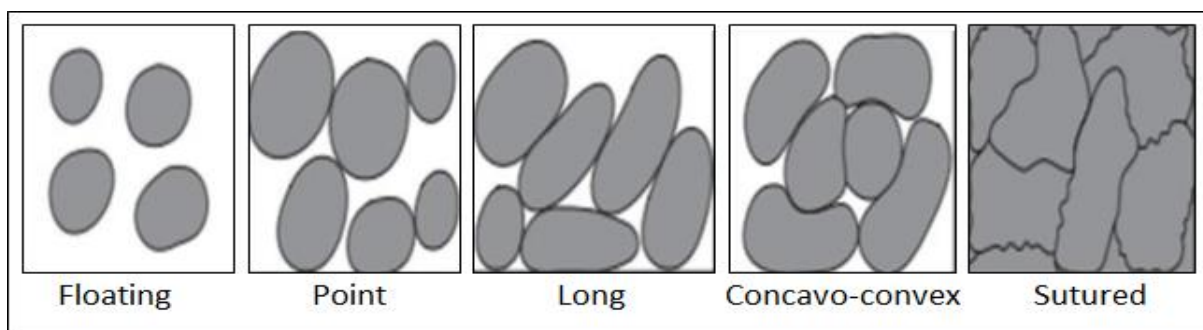
Figure 9.13: Variables of grain to grain contact patterns due to increasing burial depth (Boggs, 2009).

The sandstones of Ecca Group were subjected to moderate-intense mechanical and chemical compaction during its progressive burial. This is revealed by the change in grain contacts, with long (Figure 9.14), concavo-convex and sutured contacts of neighbouring framework grains (Figures 9.15).
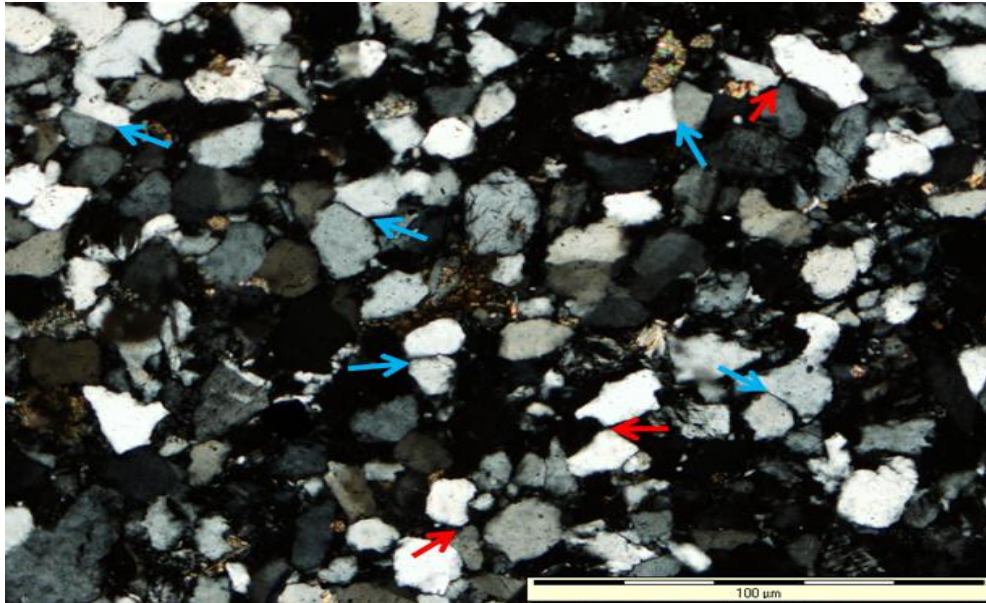
Figure 9.14: Photomicrograph of fine sandstone showing point (red arrows) and long (blue arrows) contacts between detrital grains.
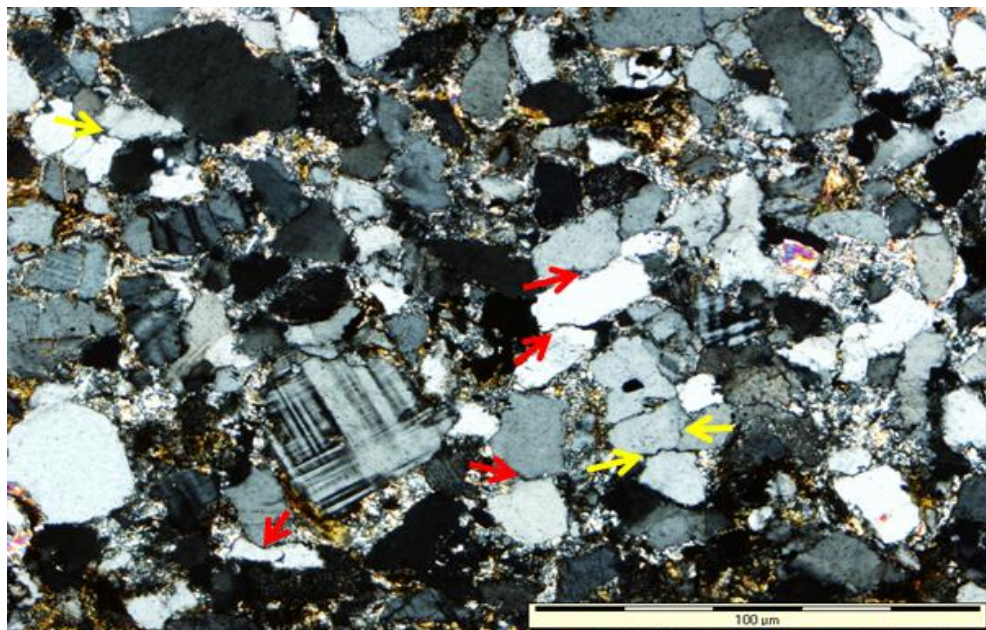
Figure 9.15: Thin section photomicrograph of fine sandstone showing concavo-convex grain contacts (red arrows) and sutured grain contacts (yellow arrows).

The grain contact patterns progressively changed from non-contact to point contacts, to long contact, then to concavo-convex contact. In a more advanced stage, the concavo-convex contacts become sutured. The overburden that compact the sediments also resulted in the fracturing of some of the grains, particularly the feldspar and muscovite grains (Figure 9.16). Some muscovite grains were completely deformed in shape. In few cases, mica flakes and mudstone intraclasts are cracked or bent. Long contacts are common in the examined samples

and their existence point to moderate degree of compaction. Concavo-convex and sutured contacts are also common and they can be attributed to deep burial diagenesis. Progressive burial resulted in increasing compaction and porosity loss either by grain rotation or slippage, leading to eventual fracturing of resistant minerals. This resulted in pressure dissolution, which is a deformation mechanism that involves the dissolution of minerals at grain to grain contacts (boundaries) into an aqueous pore fluid in areas of relatively high stress. Quartz and muscovite grains are occasionally deformed due to pressure dissolution. Stylolites structures are present in some of the siliciclastic sandstones. The occurrence of stylolite points to the effect of deep-burial diagenesis. Fracturing is generally uncommon, but when present they are mostly observed as minor fractures on detrital quartz grains. Grain fracturing in the sandstones also point to burial compaction.
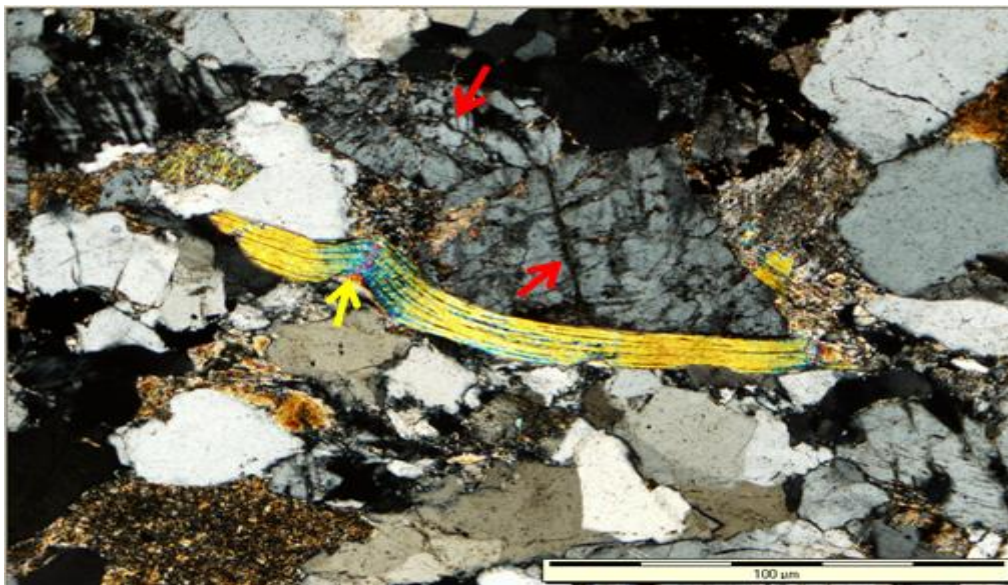
Figure 9.16: Thin section photomicrograph of sandstone showing fractured feldspar grains (red arrows) and deformed mica (yellow arrow).

9.3.1.3 Dissolution

Dissolution generally involves the removal in solution of all or part of previously existing minerals, leaving pore spaces in the rocks (Boggs, 2009). It provides silica source for quartz cement and quartz overgrowths. High temperature under deep burial depth led to the dissolution of some mineral grains at their boundaries (Figure 9.17). SEM observation revealed that some kaolinite and albite grains were formed due to dissolution of weak detrital K-feldspars. In addition, the dissolution of feldspars and micas resulted in the release of silica, thus providing silica source for the formation of authigenic quartz. The dissolution and replacement of feldspar to illite also favoured the formation of authigenic quartz.
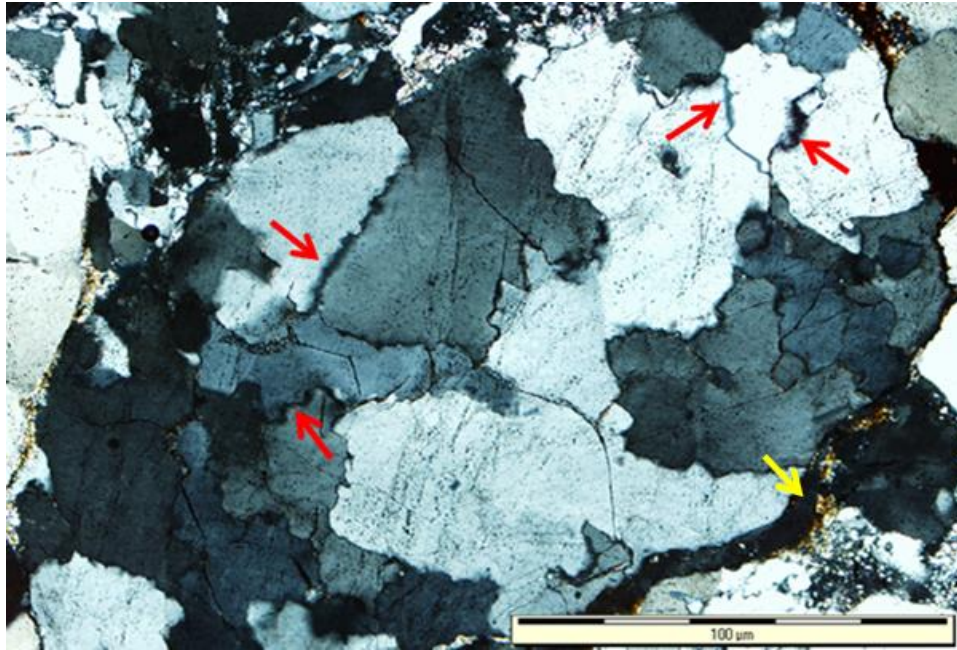
Figure 9.17: Thin section photomicrograph of sandstone showing dissolution crack (yellow arrow) and sutured grain contacts formed by pressure solution along grain boundaries (red arrows).

9.3.1.4 Mineral replacement

Mineral replacement encompasses dissolution of one mineral and simultaneous precipitation of another mineral in situ. This dissolution and re-precipitation may take place over a period of time, with new minerals progressively replacing the host or existing minerals. Replacement is a relatively common diagenetic process in the rocks of Ecca Group and is possibly due to the fact that K-feldspars are liable to alteration in burial diagenesis. When temperature increases as a result of increase in burial depth, some minerals become weak and unstable, subsequently, these minerals are replaced by more stable minerals in a new diagenetic environment. The observed mineral replacements in the studied rocks are calcite replacing quartz, feldspar and clay matrix, as well as albitization and kaolinitization/illitization.

9.3.1.4.1 Replacement with calcite

Calcite is the most abundant replacement mineral in the sandstones. Calcite replaced both the clay matrix and framework grains (Figure 9.18), i.e. the detrital feldspars, quartz and volcanic fragments are replaced by calcite. The most affected feldspars were the K-feldspar (microcline) and minor plagioclase. Mineral replacement of the feldspars by calcite also resulted in the formation of pores in sediments.
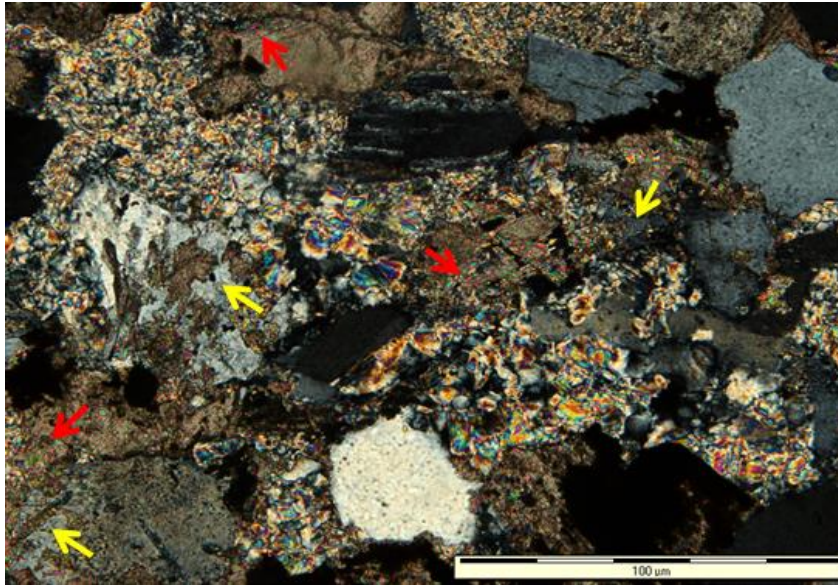
Figure 9.18: Thin section photomicrograph of very fine sandstone showing calcite replacement of clay matrix (red arrows) and detrital feldspar grains (yellow arrows).

9.3.1.4.2 Replacement with albite

Feldspars are easily susceptible to alteration whenever their diagenetic environmental conditions are changed. The K- or Ca-feldspar framework grains were either partially or completely replaced by albite. In the rocks of Ecca Group, albitization of K- and Ca-feldspar is one of the major diagenetic changes during burial diagenesis. Albite replaced particularly the K-feldspar mineral grains. In some cases, albite grain precipitated out after partial dissolution of weak detrital feldspar grain (i.e. calcite first replace K-feldspar, and it was later replaced by albite). Albite formed through replacement was revealed by the blocky to tabular sector extinction patterns where incomplete replacement occurred (Figure 9.19). Albitization occurred preferentially along microfractures, cleavages and grain contact margins.
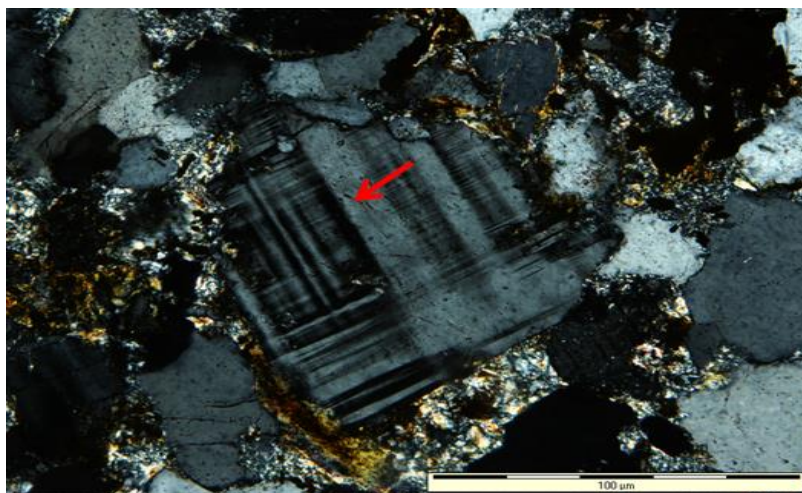
Figure 9.19: Thin section photomicrograph of sandstone showing partial recrystallization of microcline to albite (red arrows).

9.3.1.4.3 Authigenic clay minerals

K-feldspar grains are also commonly altered to kaolinite and sericite (Figure 9.20). The sericite grains appear as scattered fine flakes along cleavage planes or on the entire feldspar grain. SEM observation shows that fibrous kaolinite partially to completely replace both the matrix and framework grains of K-feldspar and muscovite. In few instances, illite and sericite replaced some of the feldspar grains.
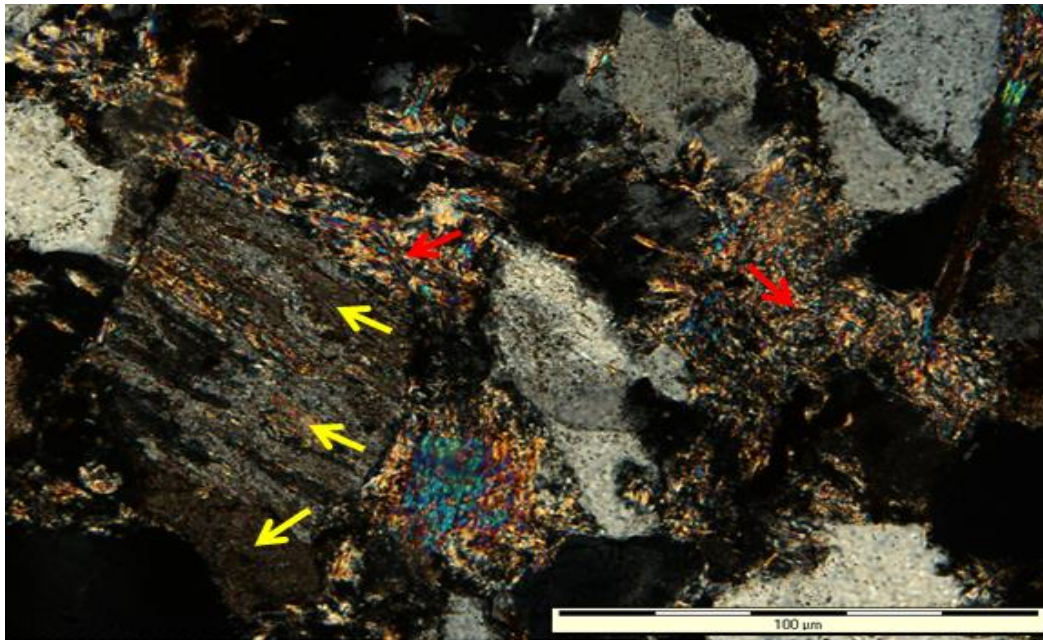
Figure 9.20: Thin section photomicrograph of sandstone showing feldspar grains replaced by clay mineral (saussuritization) along the cleavage (yellow arrows) and clay matrix (red arrows).

9.3.1.5 Recrystallization

Mineral recrystallization is a common phenomenon in the rocks of Ecca Group. Recrystallization involves the change in shape or size of crystals of a given mineral, without subsequent change in the mineralogy or chemical composition. As temperature and pressure increases with burial depth, micro-granular and fine minerals can transform into coarse textures. Existing minerals can also retain their chemical composition, while only changing in size. On the other hand, some existing mineral may be completely transformed or changed into a new mineral. Petrographic and SEM observations revealed that authigenic quartz, muscovite, chlorite, illite, sericite and feldspars are the transformed silica or silicate minerals in the rocks. With regard to clay minerals, smectite transformed into illite and chlorite, kaolinite transformed into illite. As temperature increases, illite further changed to sericite (Figure 9.21) and muscovite. The mica was further altered to clay mineral (kaolinite), usually around the edges or along the boundary as depicted in Figure 9.22.
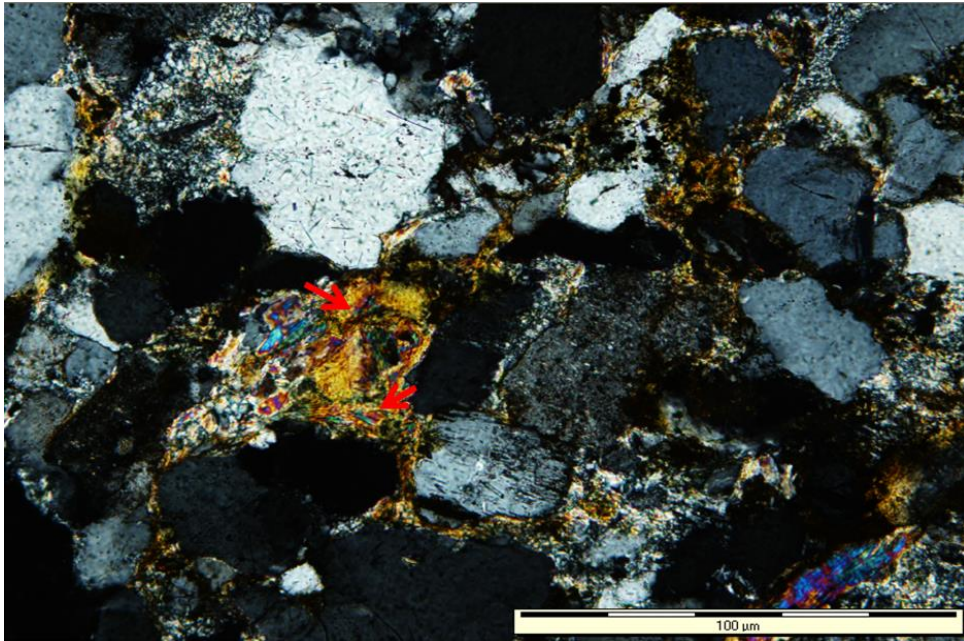
Figure 9.21: Thin section photomicrograph of fine sandstone showing transformation of clay matrix to sericite (red arrows).
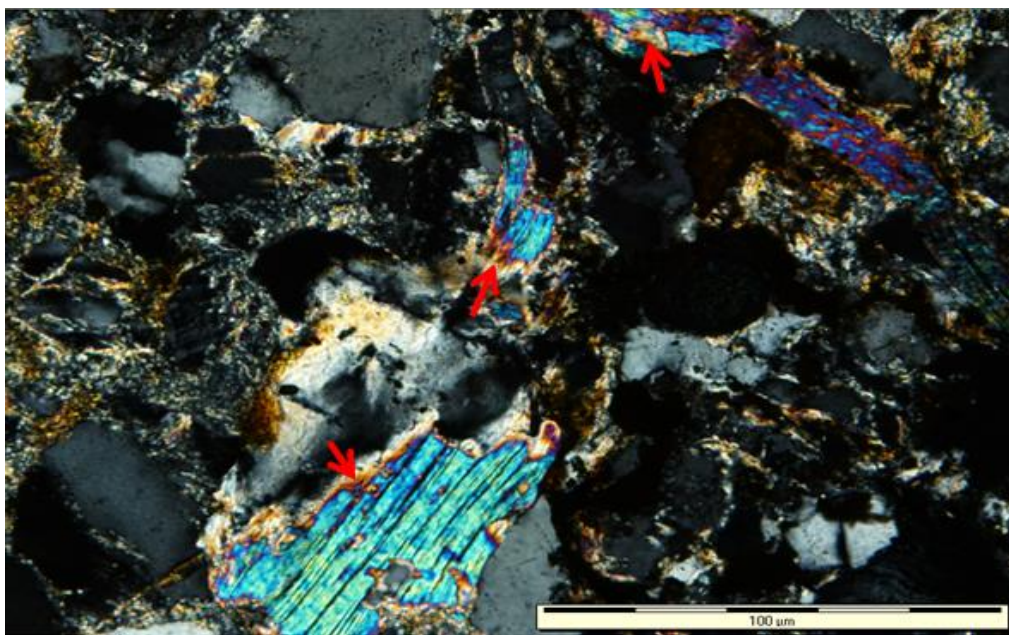
Figure 9.22: Thin section photomicrograph of sandstone showing alteration of mica to clay mineral (kaolinite) along its boundary (red arrows).

Some quartz cements were formed through transformation of fine matrix minerals. Furthermore, detrital grains, such as quartz and feldspar were observed to gradually transformed and increase their crystalline size. Through progressive recrystallization, the crystalline grain size is increased, which tend to reduce the pore space between the grains as well as the pore interconnectivity.

9.3.2 Diagenesis of mudrocks

The main diagenetic processes that have affected the mudrocks are mechanical compaction, authigenic minerals and replacement by calcite. The mudrocks are mostly composed of detritus clay, mudstones (Figure 9.23) and silt-sized nodules with some chemically precipitated and authigenic minerals, and carbonaceous or organic materials.
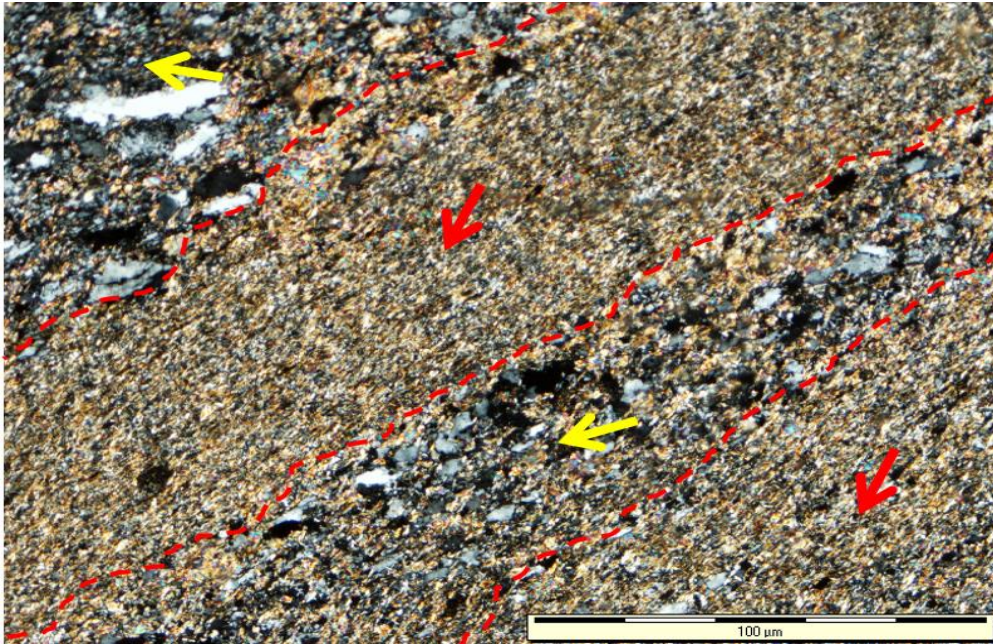
Figure 9.23: Thin section photomicrograph of mudrock showing claystone (red arrows) and siltstone (yellow arrows, more than half are clays) layers.

Manganese iron rich nodules, dark micrite and chalcedony nodules are present in some of the mudrock (Figures 9.24 and 9.25). Dolomite concretions and lenses ocassionally occurred near the base of the Whitehill Formation and are often laminated and have a physical texture that look-like microbial mats and/or stromatolite-like features. SEM observation shows spherical 'holes' that are enclosed within the dolomite crystals which may possibly enhance porosity in the mudrock. The micrite consists of chemically precipitated calcite mud, whose crystals are generally 1-4 micrometers in diameter. Chalcedony is a cryptocrystalline form of silica, composed of very fine intergrowths of quartz and observe to have whitish-gray colour. Most marine micrites started as soft carbonate mud on the sea floor. Carbonate mud is much like regular mud. The mud particles are generally thought to have originated with coralline algae. Coralline algae are little green crunchy plant-like organisms that using microscopic grains of calcium carbonate to give their tissues some support. When these plants die, the tissues rot and the tiny grains add to the local mud. In addition, some of the micrites may have

271

originated when calcium carbonate precipitated as tiny grains in the water column and settled to the sea floor. Quartz, feldspar and few micromicas (muscovite) are surrounded by abundant clay minerals (kaolinite, smectite), organic matters, and glauconite pellets. The observed detrital and authigenic minerals include smectite, kaolinite, illite, sericite, feldspar and quartz silts and chlorite.
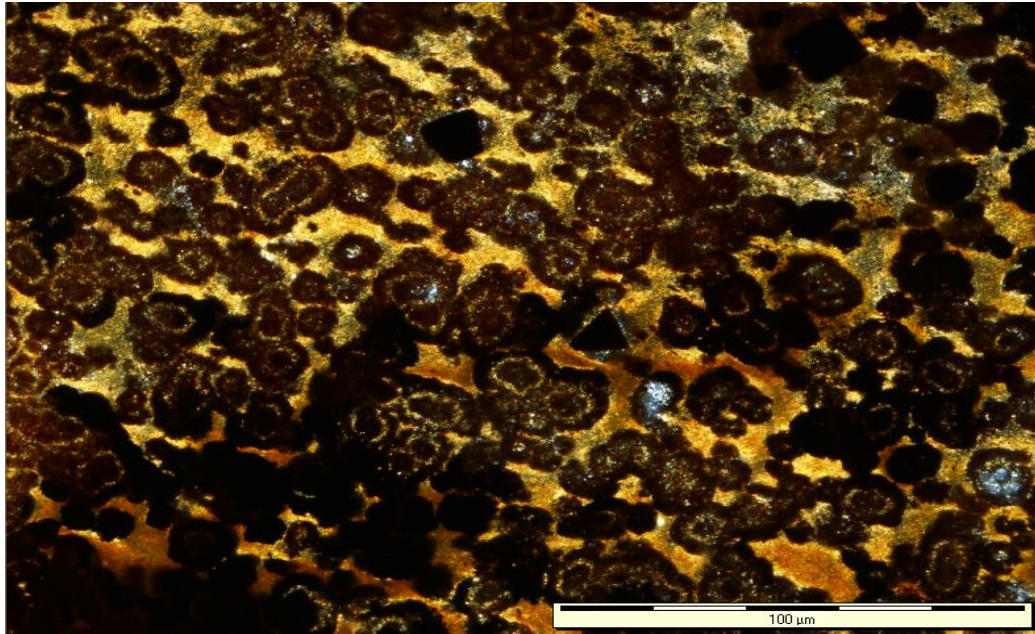
Figure 9.24: Thin section photomicrograph of mudrock showing manganese-iron rich nodules in mudrock of the Collingham Formation.
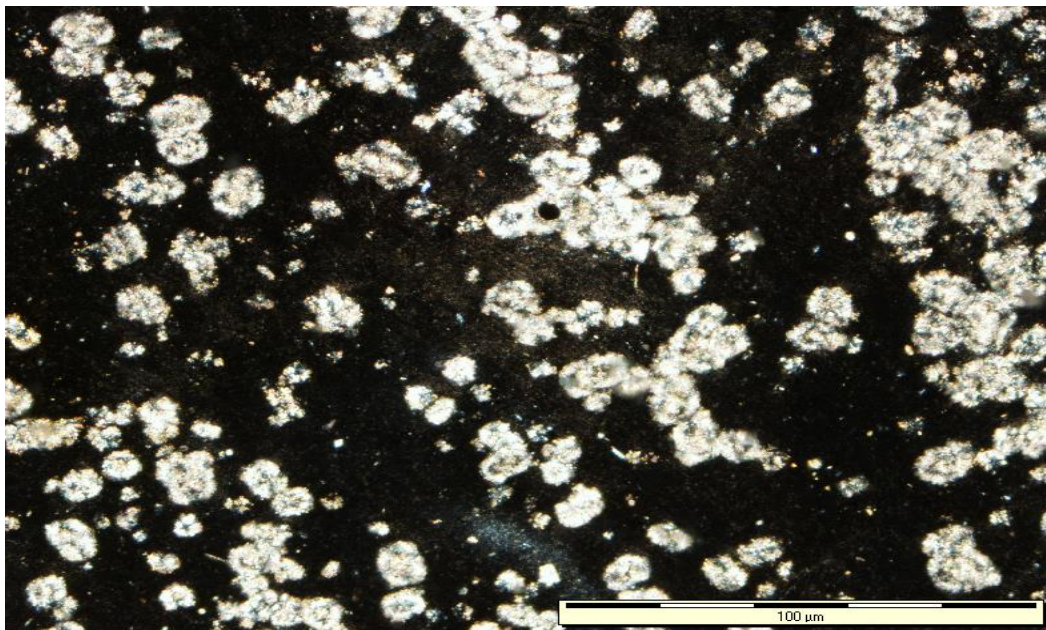
Figure 9.25: Thin section photomicrograph of mudrock showing dark micrite and white chalcedony nodules in the Whitehill Formation.

9.3.2.1 Physical compaction

Some of the mudrocks of the Ecca Group have the fissility texture allowing the rocks to break along laminae planes. The fissility of the shale is as a result of the high organic content, the alignment of clay particles and presence of laminae. The texture was affected by compaction allowing the clay and silt grains to lie parallel to the lamination of the rocks as shown in Figure 9.26.
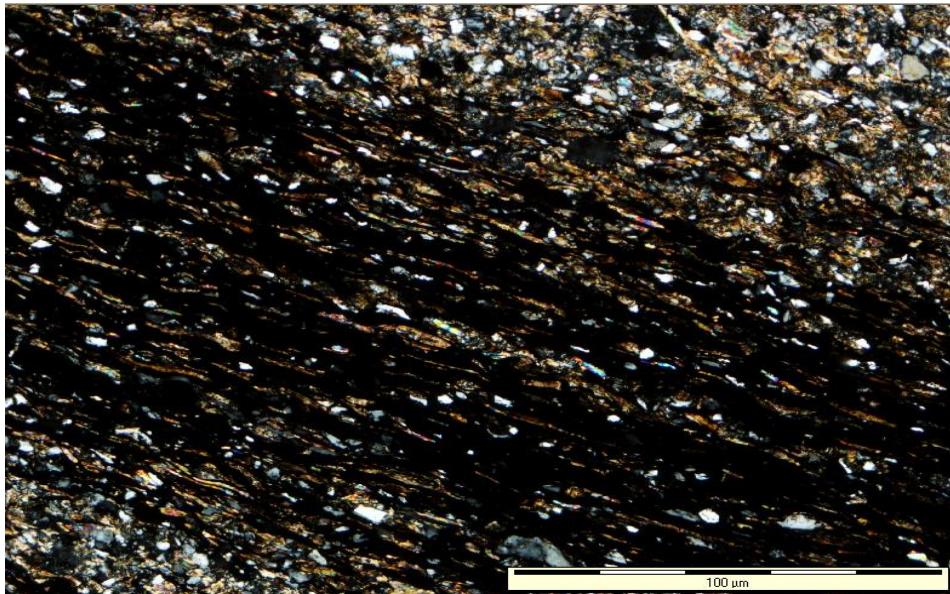
Figure 9.26: Thin section photomicrograph of carbonaceous siltstone of the Whitehill Formation showing mineral grains lying parallel to the lamination planes.

The detrital muscovite has been deformed and the deformation is possibly due to compaction of the sediments by the overburden. The occurrence of stylolite in the mudrocks points to deep-burial diagenesis. The mudrocks of Ecca Group are subjected to moderate-intense physical compaction during its progressive burial. This is revealed by the cracks or fractures in the rock (Figures 9.27 and 9.28).
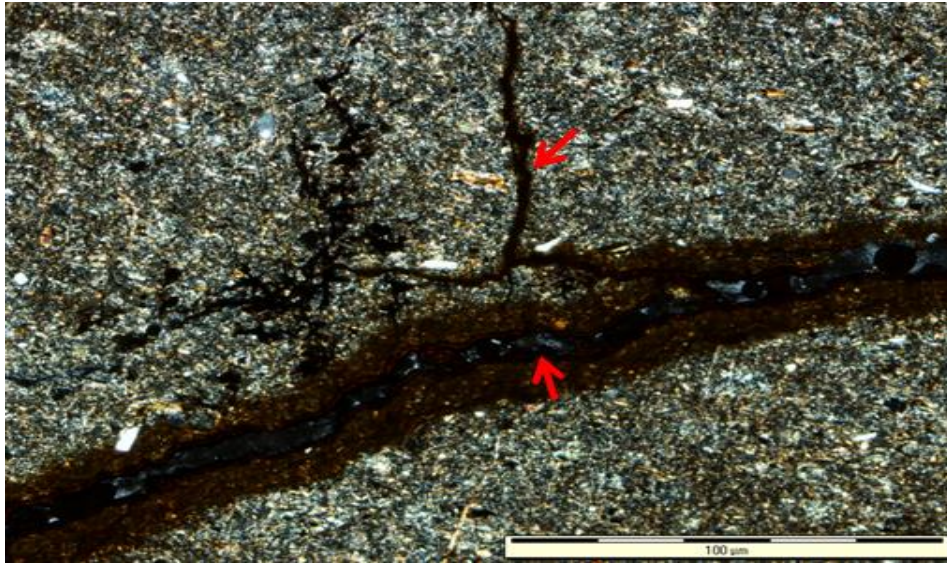
Figure 9.27: Thin section photomicrograph of mudrock from the Prince Albert Formation showing iron-oxide stained/filled secondary cracks (red arrows).
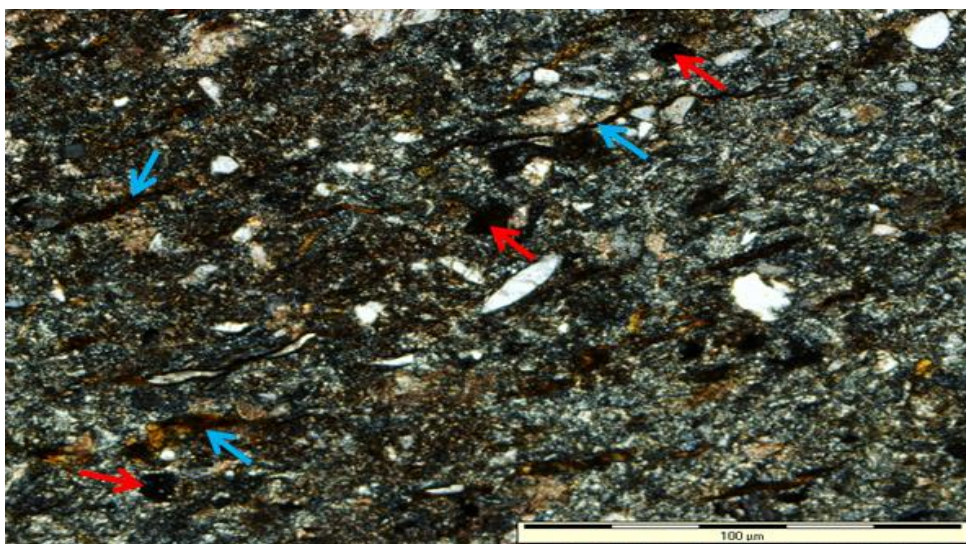
Figure 9.28: Thin section photomicrograph of mudrock from the Prince Albert Formation showing siltstone with pyrite (dark area, red arrows) and hematite staining (blue arrow).

9.3.2.2 Mineral replacement

Calcite is the most abundant replacement mineral in the mudrocks. Calcite replaced both the clay matrix and silt-grains (Figure 9.29), i.e. the detrital feldspars, quartz and volcanic fragments are replaced by calcite. The most affected feldspars were the K-feldspar (microcline) and minor plagioclase. Mineral replacement of the feldspars by calcite also resulted in the formation of micropores in sediments. In few cases, the detrital muscovite have been recrystallized and chloritized. The recrystallization of the minerals is due to high temperature as burial depth increases.
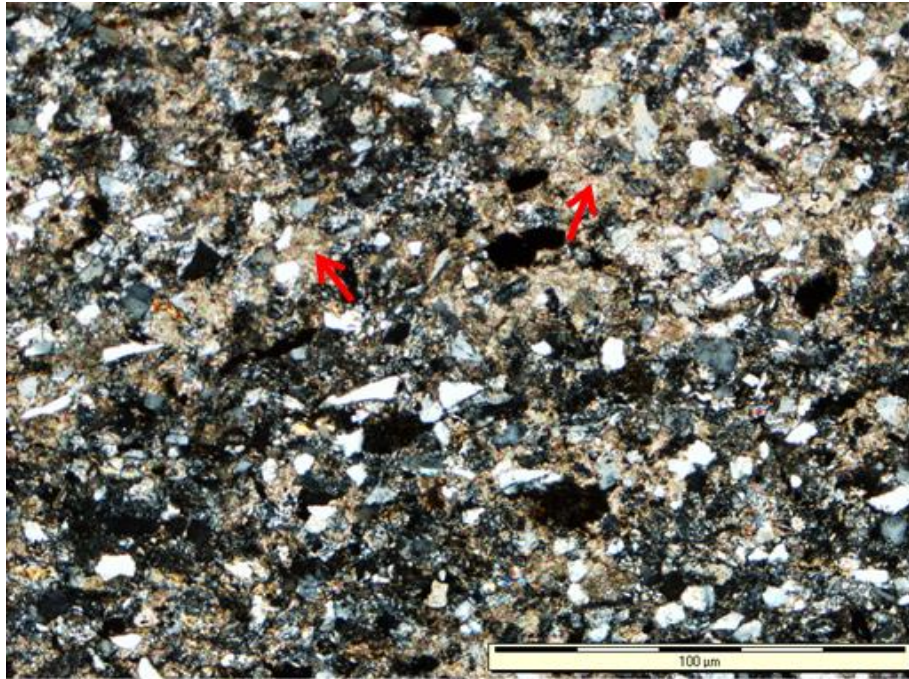
Figure 9.29: Thin section photomicrograph of mudrock showing calcite replacement of clay matrix and framework grains (brownish area, red arrows).

9.3.2.3 Mineral compositions

Kaolinite, illite, smectite clay minerals and hematite are present in the mudrocks. Parallel lines were also seen which could possibly represent laminations that were observed in the field. These minerals formed from both the dissolution of potassium feldspars and through the recrystallization of fine sediments. The minerals also formed through the modification of one clay mineral to another; for instance, both kaolinite and smectite were transformed into illite. In addition, illite and sericite recrystallized from both smectite and kaolinite. Hematite is a common type of authigenic mineral in the mudrocks of the Prince Albert Formation. It is recognized for its red-brownish staining colour, and it stains the detrital grains and clay minerals with a red brownish colour (Figure 9.30). This iron oxide in the form of reddish-brown crypto-to microcrystalline mineral occurs as thin coatings around detrital grains and within mica flakes and along cracks boundary. This suggests that the formation of these iron-oxide mineral occurred in early diagenesis under oxidizing condition. In this stage, chemistry of the interstitial waters was mainly controlled by the depositional environment. The abundant of biotite and other iron-bearing minerals in the mudstones could possibly be the source of iron for the formation of hematite mineral. The SEM-EDX results for mudstone sample shows that the dominant minerals in rock are clay minerals (Figure 9.31).
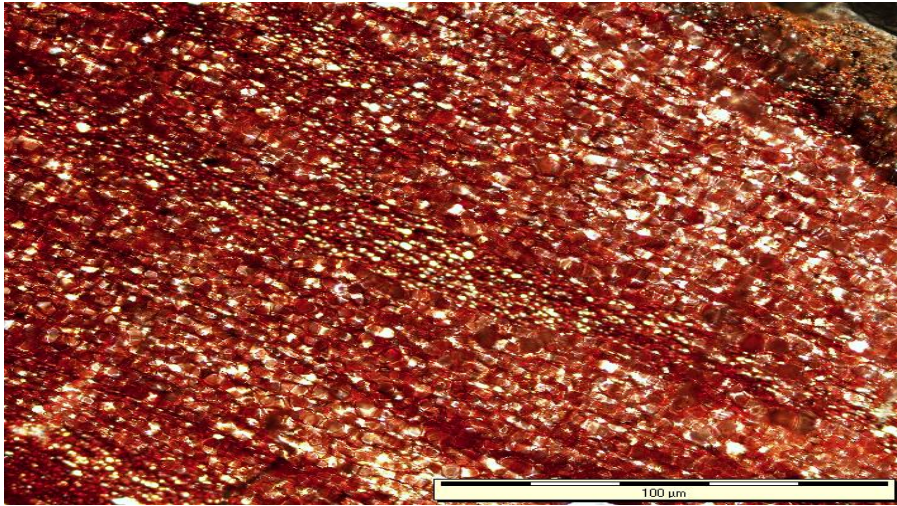
Figure 9.30: Thin section photomicrograph of mudrock from the Prince Albert Formation showing mud-siltstone with (iron-oxide) hematite staining.
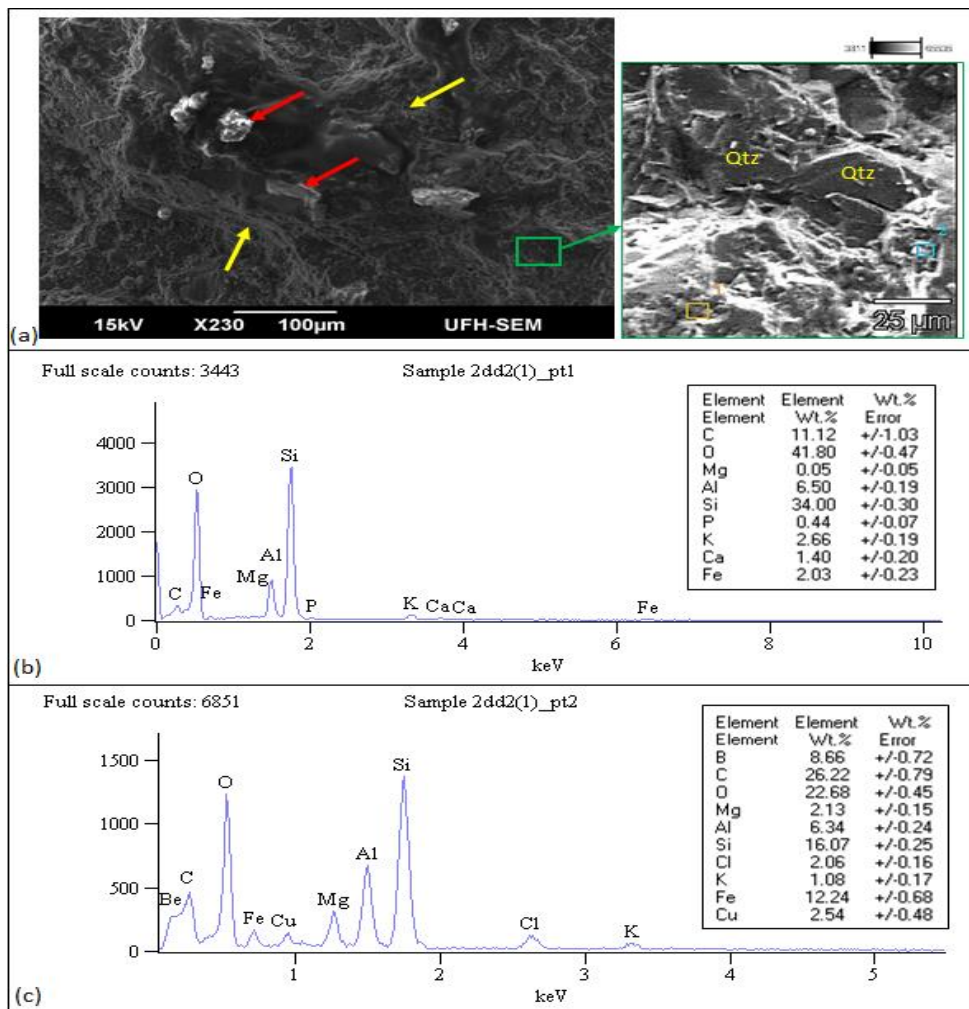
Figure 9.31: (a) SEM (BSE) photomicrograph of mudrocks showing silt-sized calcareous nodules (red arrow) amongst clayey matrix (yellow arrow); (b) SEM-EDX graph showing elemental composition of clay matrix at point 1 (yellow area); (c) SEM-EDX graphs showing elemental composition of clay matrix at point 2 (blue area). The SEM-EDX results for mudstone sample shows clay minerals (Al, Si, Mg, Fe, and K) as the dominant minerals in the rock.

276

9.4 Discussion of the sandstones and mudrocks diagenesis

Thin section and SEM-EDX studies revealed that the minerals in the Ecca Group include detrital minerals of quartz, plagioclase (i.e. albite), mica and clay minerals (kaolinite, illite, smectite, sericite and chlorite). These minerals constitute the rock framework grains, and some occurring as cements. Whereas the authigenic minerals of pyrite, hematite, glauconite, calcite, and vitrinite (organic maceral) were formed during diagenesis. The XRD result for the analysed sandstones and mudrocks is presented in Apendix B (Table B1). The most abundant framework minerals are quartz (16-40%) and plagioclase (7-30%), while the dominant clay minerals are illite (5-30%), smectite (< 1-35%), and chlorite (1-14%). The identified heavy minerals are hematite, garnet and zircon and they all exist in traces. It is observed that the percentages of quartz and feldspar for some of the mudstone/shales are relatively high or over estimated. This could be an over estimation caused as a result of authigenic silicification which was recorded as quartz. Actually, most of mudstone/shale contains more clay minerals than detrital minerals like quartz and feldspar (cf. Table B1 in Apendix B), only a part of the studied samples contain near a half of detrital mineral. Furthermore, some of the quartz and feldspar are authigenic minerals, other than detrital minerals; therefore the total percentage of quartz and feldspar is basically still normal or okay. Talc/pyrophyllite was identified in most of the samples indicating low grade metamorphism. Low-grade metamorphism takes place at temperatures between about 200 to 320 °C, and relatively low pressure. Low-grade metamorphism explores processes and transformations in rocks during the early stages of metamorphic recrystallization. The low grade metamorphic rocks are generally characterized by an abundance of hydrous minerals. With increasing grade of metamorphism, the hydrous minerals begin to react with other minerals and/or break down to less hydrous minerals.

9.4.1 Diagenetic stages

Diagenetic features in the rocks of Ecca Group are divided into three stages that include early diagenesis, burial diagenesis and uplift-related diagenesis. The time is relative, with the earliest diagenetic event occurring shortly after deposition and the latest occurring up to present time.

9.4.1.1 Early diagenetic stage

Early diagenesis covers all the changes that the Ecca sediments changed from soft loose state until it becomes a consolidated hard rock. The main factors that affect early diagenesis are

time–temperature history, primary mineralogy and fabric, geochemistry of the pore water, and presence of petroleum-related fluids (i.e. oil and shale gas). The observed processes in the early diagenetic stage include precipitation of and authigenic clay minerals, development of minor quartz and hematite coatings, pyrite formation and lithification. Minor quartz cementation due to remobilization of biogenic silica as well as compaction starts forming at early diagenetic stage. But, quartz syntaxial overgrowths occur at about 70℃ to 80℃, at several kilometres depth, well beyond the realms of early diagenesis and after most compaction. Grain compaction and dissolution possibly supplies much of the quartz and feldspar cements. Lewin (1971) documented that the early occurrence of quartz cements in marine sandstones and mudstones possibly point to the decomposition of biogenic siliceous organisms just after the sediments were deposited. Cementation almost began immediately and precipitation of different cement types was initiated. The first minerals that precipitated out of pore-spaces between framework detrital grains are the clay matrix. Authigenic smectite and kaolinite cements are the second group of cement that were formed in the Ecca Group. Quartz, feldspar and hematite cements are the third group of cement. Illite, kaolinite and smectite are the most common clays in the Ecca sandstones and mudstones. They occur as pore-filling and pore-lining cements and clay rims around grains. Alkaline pore fluids with sufficient K, Si and Al are required for illite formation whereas kaolinite requires more acid pore waters. The ions for kaolinite and illite precipitation are largely derived from the alteration of detrital minerals, in particular clay minerals and feldspars. Hematite directly precipitates on some quartz and feldspar grain surfaces, visible as reddish-brown rims on grain surfaces. This revealed that the formation of these grain coatings occurred during early diagenesis through iron oxide rich pore-water. At this stage, the oxidizing conditions in the interstitial waters must have existed to allow for the formation of iron cement since chemistry of the interstitial waters was primarily controlled by the depositional environment as documented by Schmidt and McDonald (1979a and b).

Despite the fact that iron oxide (hematite cement) is not a common cement type in the sandstones and siltstones, the presence of iron oxide allowed the red staining of the Prince Albert siltstone and mudstone. The iron was released during the breakdown of unstable iron-rich clay minerals in the mudstones under surface temperature and pressure conditions. Also, iron may have been transported into the basin by meteoric waters from weathering of the adjacent hinterland and precipitated under favourable oxic conditions. Walker (1967) reported that the interstitial dissolution of hornblende, magnetite, biotite and pyroxene grains

is usually the most probable source of iron. As the depth gradually increases, the fine organic matter preserved in the mudstones becomes involved in diagenetic reactions, contributing reaction products to the pore waters. With time, the oxic condition becomes reducing as oxygen is been used up in bacterial processes (due to the reaction of hydrogen sulphide with iron bearing minerals), thus pyrite is precipitated. Glauconite is another clay mineral that precipitates at early diagenetic stage. The process of glauconite precipitation must have occurred at interface between reducing and oxidizing zones in muddy sediments and in the presence of Si, Fe, Al and K containing pore fluids (Harder, 1980). Silica content is one of the controlling factors in the precipitation of glauconite. With regard to this, the organic materials content in the mudstones is more than those of the sandstones. This possibly led to the higher amounts of glauconite in the clayey sediments than in the sandy sediments. Lithification of the soft sediments occurred due to cementation and mechanical compaction. The compaction which involves dewatering and a closer packing of grains is the result of increased burial depth as well as the overburden pressure. In summary, the early diagenetic processes were characterised by matrix and cement precipitation, authigenic mineral formation, compaction and minor cementation.

9.4.1.2 Burial diagenetic stage

Burial diagenesis covers all the changes that may happen to the rocks after consolidation and before metamorphism. The main factors that affect diagenesis in burial diagenetic stage are increased temperature and pressure, as well as change in pore-water compositions (Boggs, 2006). These factors resulted in both physical (i.e. compaction and porosity loss) and chemical/mineralogical changes (i.e. mineral replacement, dissolution of minerals and precipitation of new cements) that tend to get the sediments into equilibrium with the diagenetic environment. During deeper burial, pore waters were further modified or changed by reactions with clay minerals. In addition, dissolution of unstable grains occurred. Diagenesis in the burial diagenetic environment is not complete without considering the influence of organic matter (Boggs, 2009). During burial, organic matter is originally changed chiefly by microbial activity, but as burial depth increases, it further undergoes chemical changes due to chemical processes like polymerization, polycondenzation and insolublization. These processes convert the organic matter into a highly complex geopolymer (kerogen) which may be a predecessor to petroleum generation (Clayton, 1994). Kerogen has carboxylic and phenolic functional groups that undergo thermal cracking at high temperature (about 80 ℃) to form soluble organic acids in associated shales and mudstones

(Boggs, 2009). These organic acids are forced out of the shales during clay-minerals dewatering into the related sandstones. As burial depth increases with further increase in temperature into a range of 120-200 ℃, the carboxylic acid anions are destroyed by thermal decarboxylation (Boggs, 2009). In addition, dissolution of both carbonates (i.e. calcite cements) and some silicate minerals (i.e. feldspar) may occur in reaction to the organic-inorganic interactions.

The diagenetic processes that occurred in burial diagenetic stage are physical and chemical compaction, dissolution, recrystallization, precipitation and replacement of minerals (i.e. albitization, sericitisation and chloritisation), pressure-solution, grain-deformation and fracturing. Compaction of the Ecca Group sediments continues during burial diagenesis due to increase in overburden pressure. This brought about an increase in tightness of grain packing and partial loss of pore spaces. Likewise, the increase in temperature and pressure as a result of compaction also led to partial dissolution of silicate grains and recrystallization of fine minerals. Subsequently, quartz and feldspar overgrowths, as well as mineral replacement and clay minerals alteration (i.e. alteration of smectite to illite, sericite or chlorite, kaolinite to illite or sericite) dominate the burial diagenetic changes. Albite and illite are formed through replacement of K- and Ca-feldspars, particularly the K-feldspars. Some K-feldspars are replaced by calcite, with authigenic quartz being released as a by-product. Unstable detrital grains released cations to pore-waters, allowing the calcite cements to precipitate in the pore-space or replace detrital grains and matrix. Some of the calcium carbonate ions move towards a centre in pore-solution within the sandstones and mudstones, which resulted in the formation of calcareous concretions or nodules that commonly found in the sandstones of Ripon Formation and mudrock of the Collingham and Whitehill Formations (Figures 9.24 and 9.25). These calcareous concretions are usually related to the original depositional environment such as marine sediments, and also could be linked with later diagenesis due to leaching and evaporation of pore-water (caliche). Solutions rich in Ca^{2+} and CO_3^{2-} ions are capable of destroying the potash feldspar lattice, possibly by causing the silica tetrahedral units to go into solution under high pH burial environment (Dapples, 1967).

In the rocks of Ecca Group, mineral replacement was not only confined to the K-feldspars. Clay matrix and quartz grains also undergo partial replacement. Precipitation of calcite inside clay minerals can be linked to the crystalline structures of minerals consisting of Ca^{2+} ions, which occupy less interstitial space. Thus, allowing the remainder to be filled by the precipitated carbonate (Dapples, 1967). Some of the calcite precipitation could have been due

to clay mineral replacement in burial environment with pH of > 8 in addition to a high concentration of Ca^{2+} ions, a condition that rendered clay minerals unstable. Furthermore, the CO_2 released when organic materials decayed during diagenetic processes, may also be an additional source of carbonate ion for the precipitation of calcite cements. High temperatures and pressure resulted in the dissolution of silicate materials from which some of the silicate minerals recrystallized. For example, smectite recrystallized into illite and chlorite, whereas kaolinite changed into illite. Illite also further recrystallized to sericite, which later changed into muscovite. Partial to complete replacement of some detrital grains and clay matrix by new minerals is a common phenomenon in this stage. Albitization of feldspar possibly occurred during fracturing of the detrital K-feldspar grains. As a result of progressive increase in burial depth, detrital grains started to pack more tightly resulting in thinning of the beds as well as porosity reduction.

The effects of compaction are evidenced in both the sandstones and mudrocks. In the sandstones, point and line contacts are formed between the grains, whereas in the mudrocks, the grains developed an alignment parallel to lamination and show signs of bed thinning. Due to further compaction, the initial point and line contacts changed to convex-concave grain contacts and finally to suture contacts. Furthermore, muscovite flakes became bent and deformed due to over compaction. Secondary porosity was created when the detrital feldspar, rock fragments and muscovite grains were also fractured. As a result of high temperatures, organic materials in the sediments were altered to vitrinite. Thin section examination of the argillaceous rocks also revealed the existence of plant fossils in the rocks. The vitrinite is thought to have formed from the lignin and cellulose of the plant materials (Appendix C).

9.4.1.3 Uplift-related diagenetic stage

Uplift and exposure of marine Ecca Group rocks to influx of surface water takes the rock into uplift-related diagenetic environment. Hurst and Irwin (1982) reported that marine deposited materials are never invaded by large quantities of meteoric or surface waters unless they are uplifted and subjected to weathering. In general, oxidizing and meteoric pore waters as well as lowered temperatures and pressures characterises the uplift-related diagenetic stage. Mineral assemblages that were initially formed under high temperature and pressure in the burial diagenetic stage become unstable in the uplift-related diagenetic stage. This could result in alteration or dissolution of unstable minerals. Furthermore, the original detrital mineral assemblages may undergo additional diagenesis. Diagenetic alteration in the Ecca

Group rocks take place at some depth below the Earth's surface, but still within the region of meteoric water circulation. It continued at the surface as a result of uplift and weathering processes. At uplift, the rocks were exposed to acidic rain water, which led to dissolution of previously formed carbonate cements (decementation), thus resulting in porosity increase.

Mudstones of the Prince Albert Formation also underwent changes after being exposed on the surface. The changes may include in situ alteration of framework grains to clay minerals (weathering), which will tend to occlude or block porosity. Most of the clay minerals have been stained by iron oxide thus resulting in the red or brownish colour. The red pigmentation in the mudstones of the Prince Albert Formation can be related to the change that took place when the rocks were exposed to surface or meteoric waters. The leaching/oxidation of iron-rich minerals (i.e. illite and pyrite) resulted in red colouration or stained in the mudstones. Apart from the clay minerals, the dissolution of hornblende and weathering of pyrite could be another source of iron that stained the Prince Albert Formation shales to red brownish. The red colour is secondary in nature because it was not the original colour of the sediment. Parts of detrital feldspars are altered to illite and chlorite. Also, some of the observed kaolinites are formed due to weathering and alteration of feldspar. This type of kaolinite is found in minor quantities possibly due to the fact that argillaceous rocks which are mainly made up of smectite clay rather than kaolinite in the Ecca Group. The kaolinization of feldspars was due to the presence of fresh surface-water at uplift. Flushing of sediments by fresh water is generally thought to be a vital process in kaolinization, especially in the kaolinization of sandstones (Bjorlykke et al., 1979). Calcite and kaolinite were also partially dissolved and leached, which created pore-space. In summary, the uplifted related diagenetic processes were characterised by chloritisation, grain fracturing and dissolution.

9.4.2 Diagenetic sequence

A series of diagenetic changes in the Ecca Group are associated with each other and can constitute a diagenetic pathway and sequence. The diagenetic processes and pathway for the development of different minerals in rocks of the Ecca Group is tabulated in Table 9.1.

Table 9.1: Diagenetic events and pathway of the Ecca Group in the study area.

Diagenetic events	Time		
	Early diagenesis	Burial diagenesis	Uplift-related diagenesis
Clay matrix	━━━━		
Smectite	━━		
Kaolinite	━━		
Point contact	━━		
Physical compaction	━━━━━		
Planar contact	━━━━━		
Feldspar cementation	━━━━━		
Quartz cementation	━━━━━		
Authigenic pyrite	━━━		
Authigenic quartz	━━━		
Authigenic feldspar	━━━		
Hematite cement	━━━		
Quartz overgrowth	━━━━━━		
Feldspar overgrowth	━━━━━━		
Illitization	━━━━━━		
Sericite	━━━━━━		
Calcite replacement		━━━━	
Albitization		━━━━	
Muscovite alteration		━━━	
Concave-convex contact		━━━	
Suture contact		━━━	
Chemical compaction		━━━	
Stylolite structure		━━━━━━	
Chlorite		━━━	━━━
Grain fracturing		━━━━━━━━━━	
Dissolution		━━━━━━━━━━	
Saussuritization			━━━━━
Weathering			━━━━━

9.5 Implications of diagenesis for reservoir quality

Reservoir quality mainly depends on the relationship between porosity and permeability, which may be of different types. Porosity and permeability are two vital properties of sedimentary rocks that are partially influenced by the textural characteristics of grain size, shape, packing and arrangement. In addition, they play a very crucial role in the diagenesis of sediments by controlling the flow of fluids through rocks. The fluid that flows in the rock causes dissolution, cementation and authigenesis of minerals. Petrographic and SEM examination of the Ecca Group rocks revealed both primary and secondary porosity. Primary porosity is the pore space that existed in the sediment just after deposition before diagenetic modification. It comprises of intergranular (pore space between grains) and micro porosity (matrix micro pores). Diagenesis may cause a change of porosity types, for instance, precipitation of authigenic clay minerals in pores causing the pore throats to decrease.

Reservoir quality of Ecca sandstones and mudrocks is largely determined by diagenetic processes that either reduce or enhance porosity and permeability. The most important diagenetic processes in the rocks of the Ecca Group are compaction, cementation by calcite, quartz, feldspar, clays, and iron oxide. The observed primary porosities are primary intergranular and matrix micro pores. As sediments get compacted due to overburden, point and line contacts are formed. The progressive burial was responsible for primary porosity reduction due to compaction as indicated by long and sutured contact between neighboring clastic grains. Primary intergranular porosity and pore radii are reduced due to changes in grain contacts. In some samples, the carbonate cement reduced or prevented further compaction and the resulting close packing of clastic grains. Authigenic kaolinite and iron oxide also played an important role in the preservation of porosity. Kaolinite and mixed layer clays caused reduction in primary porosity, but can form and preserve porosity between kaolinite crystals (Figure 9.32). Generally, the pores in the matrix are very small in size, possibly due to the high percentage of smectite-illite minerals. However, a few, relatively big and elongated pores were observed in the rocks (Figure 9.33). Since quartz cements are known to be destructive on primary porosity, the existence of quartz cements could have possibly limit the preservation of primary porosity in the rocks. In some samples, quartz overgrowth coats the detrital quartz grains resulting in the decrease of pore radii and consequently reducing porosity and permeability. In few cases, chlorite rims surround the overgrowths and thus preserving the ineffective matrix micro pores. Calcite cement in the samples appears as patches and partially occupied the intergranular pores (Figure 9.34).
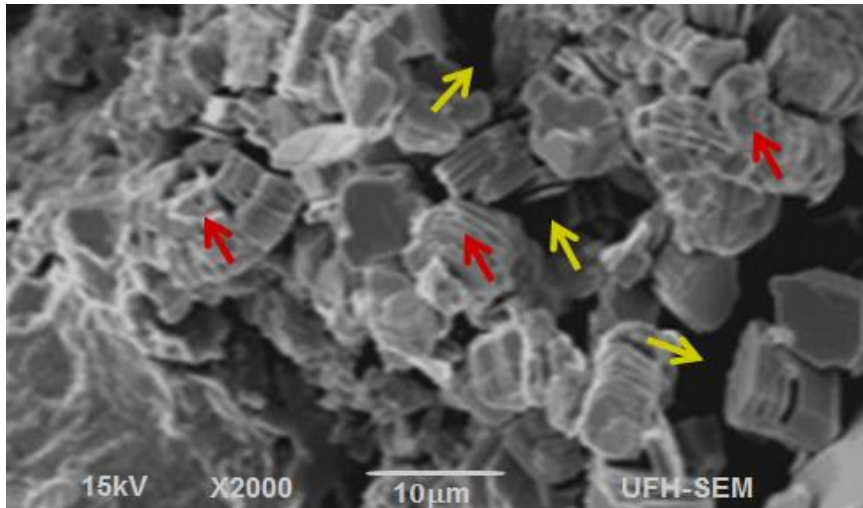
Figure 9.32: SEM photomicrograph showing intercrystalline pores (yellow arrows) occuring between vermicular kaolinite crystals (red arrows).
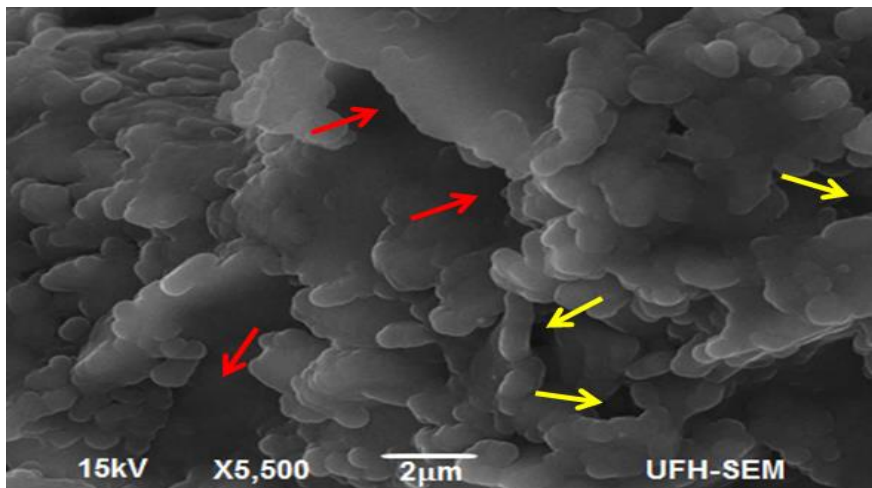
Figure 9.33: SEM photomicrograph showing elongated (red arrows) and rounded pores (yellow arrows) within the matrix of smectite and illite.
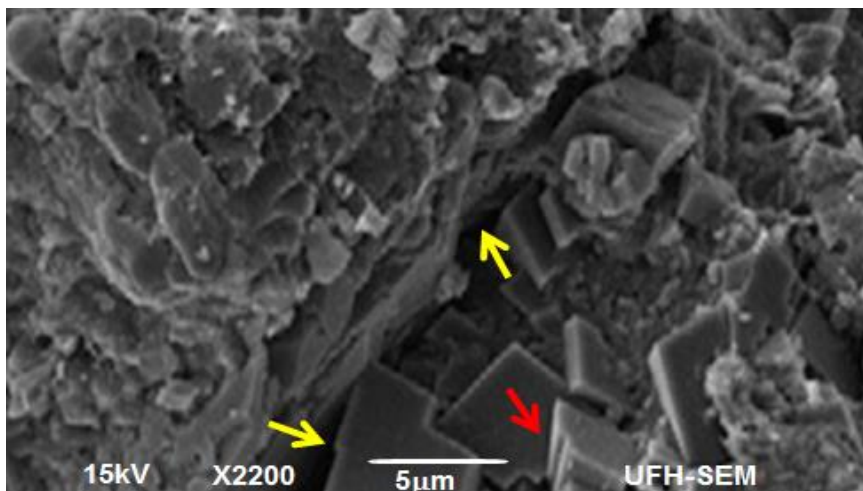
Figure 9.34: SEM photomicrograph showing calcite cement (red arrows) blocking pore spaces (yellow arrows).

Primary intergranular pores are reduced as a result of intense compaction and cementation. Most of the primary pores have been destroyed by the same process that resulted in generation of the pseudomatrix of wackes. However, Small amount of secondary porosity occurred in the rocks. During burial diagenesis, preferential destruction of less stable minerals or clastic grains by pore fluids produced pore spaces for secondary cementation. Another episode of dissolution which occurred during uplift-related diagenesis and involves partial removal or dissolution of earlier formed carbonate cements also creates secondary porosity. The observed secondary porosities in the rocks are secondary intragranular, dissolution and fractured pores. Secondary intragranular and dissolution pores resulted from the dissolution of unstable feldspar grains, from dissolution of clay minerals formed by alteration of pseudomatrix and from the dissolution of carbonate materials (i.e. calcite cement). Conversely, the fractured pores are due to structural forces and differential compaction. Some of the detrital feldspar and muscovite grains are cracked probably due to compaction as burial depth increases. Fracturing also point to over-compaction which in some case resulted in porosity reduction.

With regard to reservoir quality, the initial porosity was decreased by compaction and cementation and then increased by dissolution of unstable minerals and calcite cement (decementation). Most of the secondary pores are very small and isolated, resulting in very low porosity and permeability, resulting in poor-medium potential reservoir quality (Figure 9.35). The low porosity and permeability of most of the Ecca rocks make them unfavorable producers of hydrocarbons, which at best would require stimulation or fracking. The measured thin section porosity values for the outcrop samples (shale and sandstones) from the Prince Albert, Whitehill, Collingham, Ripon and Fort Brown Formations vary between 0.2-2.6%, 1-3.2, 0.4-2.0%, 1-5.1%, and 0.3-3.5% (Table 9.2), respectively. Due to the development of cracks, joints and faults in the outcrops of the Ecca Group, the actual or real porosity of the rocks in the field could be much higher than the observed or measured thin section porosity. The size of pores in the mudrocks are predominantly < 1 μm (nanopores), thus providing evidence that the formations as a whole is characterised by low permeability values. The shales (core samples) of the lower Ecca Group formations (Prince Albert, Whitehill and Collingham Formations) have average porosities that are lower than those determined for active shale gas plays (Marcellus shale in Appalachian Basin and Barnett shale in Fort Worth Basin) in the United States. Productive, organic rich units of the Marcellus and Barnett Shale play have average porosities of ranging between 3% and 6%

(Bruner and Smosna, 2011) and permeabilities of ≤ 0.1 mD (Montgomery et al., 2005), which are slightly higher than those measured in the potentially gas bearing shales of the Whitehill Formation.

Table 9.2: Measured petrophysical properties of the Ecca Group rocks in the study area.

Formation	Lithology	Av. Thickness (m)	Av. Density (kg/m^3)	Av. Porosity (%)
Fort Brown	Sandstone	892	2.774	2.444
	Shale		2.656	1.574
Ripon	Sandstone	700	2.721	3.241
	Shale		2.662	1.595
Collingham	Shale	65	2.598	1.188
Whitehill	Shale	21	2.526	2.710
Prince Albert	Shale	87	2.641	1.260

Note: Av. represents average

DEPOSITION

MUDROCK

Clay matrix

Physical compaction

Calcite replacement

SANDSTONE

Clay matrix

Smectite cementation

Kaolinite cementation

Point contact

Physical compaction

Planar contact

Feld spar cementation

Quartz cementation

Authigenic pyrite

Authigenic quartz

Authigenic Feldspar

Quartz overgrowth

Feldspar overgrowth

Illitization

Sericitization

Calcite replacement

Albitization

Muscovite alteration

Concave-convex contact

Suture contact

Chemical compaction

Chloritization

Pore water expulsion, tighter grain packing, reduction in pore space, thinning of bed and mineral/grain alignment

EARLY DIAGENESIS

BURIAL DIAGENESIS

UPLIFT-RELATED DIAGENESIS

Poor reservoir quality

Poor reservoir quality

Calcite dissolution (decementation)

Weathering and de-compaction; mineral deformation

Oxidation of iron-rich minerals

Poor-medium reservoir quality

Figure 9.35: Flow chart of the main diagenetic processes in mudrocks and sandstones of the Ecca Group as well as their impact on the potential reservoir quality.

9.6 Conclusions

This study revealed that the rocks of Ecca Group were subjected to moderate-intense mechanical and chemical compaction during its progressive burial, and diagenetic process had passed through early, burial and uplift diagenetic stages. The main diagenetic processes that have affected the rocks are cementation, mechanical compaction, crystallization,

replacement, and dissolution of framework grains and cements. During early diagenesis, sediments mainly undergo cementation and light lithification. Mechanical compaction, pressure solution, dissolution by pore fluids, mineral replacement, clay-minerals authigenesis and mineral deformation are the major diagenetic processes during burial diagenesis. Uplift-related diagenesis comprises of decementation, dissolution, mineral replacement, oxidation of ferromagnesian minerals and destruction of feldspar minerals by saussuritization and weathering. The identified cements are quartz cement, calcite cement, hematite cement, feldspar cement and authigenic clay minerals. Quartz and feldspar cements occur as both pore-filling and overgrowths in the rocks. The authigenic clays are mostly smectite, kaolinite, illite, and illite/smectite. Calcite cements occurring as replacement mineral of clay matrix in the rock.

The primary porosities (inter- and intra-granular pores, intercrystalline pores, and sheltered pores) are reduced due to intense mechanical compaction and filling of early authigenic cements such as carbonate, quartz, clay minerals and iron oxides. The dissolution of carbonates, Fe-Mg rich minerals and feldspars after diagenetic modification as well as the effects of tectonic forces and differential compaction led to the formation of secondary pores. These diagenetic processes that resulted in secondary porosities (solution pores, secondary intragranular pores, tectonic fracture pores, and joints) occurred during both burial diagenesis and uplift-relat diagenetic stage when meteoric water influx was significant. Conversely, the diagenetic process also resulted in production of some diagenetic products, for example, clay cements (i.e. smectite filling and lining) which reduces porosity. Mechanical compaction and authigenic cements also reduce porosity and permeability. Grain-coating rims of iron oxide in some cases prevented the formation of quartz overgrowths and thus preserved porosity. Generally, there is no single diagenetic process that is mainly or solely controlling the pattern of porosity evolution in the rocks. Instead, it appears that the main types of cements (carbonates, clay minerals and quartz) as well as compaction have collectively controlled the porosity and the reservoir quality of the rocks. Petrophysically, potential reservoir quality of the Ecca Group is poor to medium. Porosity types are dominated by primary intergranular pores and secondary solution and fracture pores. However, both inter- and intragranular porosity decreases systematically with increasing burial depth. The presence of fractured and dissolution pores tend to enhance reservoir quality. However, the low porosity as well as the isolated nature of the pores (low permeability) makes them unfavourable producers of hydrocarbons, which at best would require stimulation and fracking.

CHAPTER 10

GEOPHYSICAL CHARACTERIZATION OF THE ECCA GROUP USING ELECTRICAL RESISTIVITY METHOD

Abstract

A geoelectrical resistivity survey using horizontal resistivity profiling (HRP) and vertical electrical sounding (VES) were carried out on road-cut exposures of the Ecca Group in the study area. The survey was undertaken in order to reveal the lateral and vertical variation in resistivity of the subsurface as well as determine the number of geoelectric layers, layer thickness and depth to the top of each of the layers of the Ecca Group. A total of 32 resistivity profiles of various lengths using Wenner array and 37 VES using Schlumberger array were carried out to investigate the area. Current electrode spacing, AB of 27 m (a = 9 m) was chosen for the HRP survey such that the lower Ecca Group rocks were covered. On the other hand, the VES current electrode spacing was chosen such that there were 6 logarithmically spaced intervals in a decade resulting in AB spacing ranging from 3-200 m. The field data were collected using a Geotron resistivity meter and processed using Geosoft Oasis Montaj, IPI2WIN and RES2DINV software. The HRP result revealed that, at a depth of about 9 m, the apparent resistivity of the subsurface varies laterally between 2 Ωm and 500 Ωm. The VES curves are predominantly combination of HA, HK, KH, QH, AAK, HAA, HAK, HKH, HKQ, KHA and QHA curve-types indicating four to five geoelectric layers. The first layer (topsoil) is composed of dry sandy clay with resistivity and thickness ranging between 34-844 Ωm and 0.27-2.19 m, respectively. The resistivity and thickness of the second layer varies between 8-7009 Ωm and 0.62-5.42 m, respectively. This layer is mostly inferred to be mudstone, although in some places, it has been replaced by weathered sandstone and dolerites. The resistivity and thickness of the third layer ranges between 1 Ωm and 31601 Ωm, and 2.31 m to 19 m, respectively. This layer is inferred to be sandstone (occasionally weathered). However, in some of the VES points, this layer is also inferred to be dolerite intrusion, mudstone, consolidated shale and clay/tuff. The fourth and fifth layers have resistivity values ranging from 35-556996 Ωm and 3-240000 Ωm, respectively. The thickness of the fourth layer mostly varies between 1.01-44.5 m, while the thickness of the fifth layer is not defined since it is the last layer that the current could not fully penetrate. The 2-D resistivity pseudosections revealed that the lower Ecca Group rocks are generally characterised by low resistivity compared to the upper Ecca Group rocks. These low

resistivities (high conductivities) are thought to be a result of the high organic matter and pyrite contents in the lower Ecca shales. With the exception of the Cookhouse section, all the measured sections have been intruded by dolerites. These dolerite intrusions could possibly act as barriers for fluid migration as well as introduce technical difficulty in the drilling stage of the hydraulic fracturing process.

Keywords: Vertical electrical sounding, horizontal resistivity profiling, geoelectric layers, pseudosections, Ecca Group

10.1 Introduction

Geophysics is the application of the principles of physics to the study of the Earth. It involves the measurement of responses due to contrasts in the physical properties of materials beneath the Earth surface as well as attempting to deduce the nature and distribution of the materials responsible for these signals at the surface. Geophysical methods used for investigating shallow and/or deep features of the Earth's crust include electrical, gravity, and magnetic methods. These aforementioned methods vary based on the physical properties of rocks such as resistivity/conductivity, rock density and susceptibility, respectively. The use of geophysics for hydrological, mineral prospecting and mining, engineering and environmental studies has increased over the last few years due to the rapid advances in computer software and associated numerical modelling solutions. Electrical methods are generally classified into natural and artificial methods, based on the energy source involved. The self-potential (SP) and telluric currents fall under the natural source method, while electrical resistivity, electromagnetic (EM) and induced polarization (IP) methods are artificial source methods. The method used in this study is the electrical resistivity method.

The electrical resistivity method is by far the oldest established geophysical tool in Africa and is mostly used for hydrological and environmental investigations. It utilizes direct currents or low frequency alternating currents to investigate the electrical properties (resistivity) of the subsurface. The idea of measuring subsurface variations using electrical resistivity within the Earth was first successfully conducted by Schlumberger in the field of Normandy in 1912 by injecting electrical currents into the ground and mapping the resulting potential field distribution. Thereafter, the same idea was also developed by Frank Wenner in the USA (Kunetz, 1966). Geo-electrical resistivity method has developed greatly and has become an important instrument in hydrological studies, mineral prospecting and mining as well as in environmental and engineering applications (Griffiths et al., 1990; Griffiths and Barker,

1993). Resistivity measurements are associated with varying depths depending on the separation of the current and potential electrodes in the survey and can be interpreted in terms of a lithologic or geohydrologic model of the subsurface.

The Karoo Supergroup comprises one of the rare instances of a sedimentary basin where dolerite intrusions occur interbedded with sediments. The very high resistivity contrast between the resistive dolerite and the conductive sediment results in an extraordinarily high degree of electrical anisotropy (van Zijl, 2006a). This feature has provided a unique opportunity to study the configuration of the network of dolerite intrusions in the sedimentary succession. But on the other hand, it has seriously restricted the depth of investigation in many situations. As documented by van Zijl (2006b), the main Karoo Basin is underlain by highly resistive rocks of the Kaapvaal Craton in the north and the Namaqua-Natal Metamorphic Belt further south and is bounded by the Cape Supergroup in the extreme south. Its thickness gradually increases towards the south until the Karoo Trough is reached in the extreme southern portion of the basin, where total thicknesses of the Karoo sequence is about 12 km (Smith, 1995). Sedimentation began with the deposition of glacial related rocks of the Dwyka Group followed by the mudrock dominated lower Ecca Subgroup under conditions of offshore suspension settling. Shallowing of the basin and termination of oceanic circulation led to stratification of the water and reducing conditions, resulting in the deposition of the carbonaceous Whitehill Formation. This highly conductive rock with resistivities varying from 0.01 to 10 Ωm and attaining thicknesses of up to 30 m forms a very effective electrical basement in the areas where it is well developed (van Zijl, 2006a). After the deposition of the Whitehill Formation, there was a sudden influx of coarser material from a provenance south of the present basin, accompanied by rapid down warping of the Karoo Trough, together with a build-up of sandy and silty submarine fans and basin plain turbidites of the upper Ecca Subgroup in the south, wedging out rapidly to the north (Kingsley, 1981).

Previous studies carried out on the Ecca Group by several researchers mainly focused on the stratigraphy, lithofacies analysis, depositional environment, electrical resistivity and conductivity, impact of dolerite intrusions and shale gas potential of the Ecca Group (i.e. Kingsley, 1981; Smith, 1990; de Wit, 1992; 2011; Smith et al., 1993; Johnson et al., 1996, 2006; Catuneanu et al., 1998; 2005; Chevalier et al., 2001; van Zijl, 2006a; 2006b; Geel et al., 2013; 2015). A review of the resistivity structure of the Karoo Supergroup in South Africa, with emphasis on the dolerites (a study in anisotropy) was carried out by van Zijl (2006b). van Zijl (2006a) documented that several deep structural studies in the Karoo basin

were carried out by the Council for Scientific and Industrial Research (CSIR) by means of direct current resistivity sounding and profiling using the Schlumberger array (Kunetz, 1966) between the period of 1966 and 1980. These surveys were said to have been carried out at the request of the Southern Oil Exploration Corporation (SOEKOR) and the Water Research Commission (WRC), respectively. In the SOEKOR investigation, the deep electrical sounding (ES) method was used as a complement to the seismic reflection method, especially in areas where results were seriously affected by the presence of the extensive network of dolerite intrusions. In the WRC studies, ES was used as one of the geophysical methods to study the groundwater potential and deep structure along the Doornberg Fault Zone, marking the boundary between the Kaapvaal Craton in the north and the Namaqua-Natal Mobile Belt in the south (de Beer and Meyer, 1984; Hartnady et al., 1985). The latter project was prompted by the sudden large inflow of groundwater along steep fractures into the Orange-Fish River Tunnel during its construction near Venterstad (Olivier, 1972). The results from both studies show that thevery conductive carbonaceous Whitehill Formation acts as an electrical basement to deep soundings where it is well developed. Beyond its limit in the east and south, the electrical basement is highly resistive consisting of igneous and metamorphic rocks of the Kaapvaal Craton and the Namaqua-Natal Metamorphic Belt, respectively. The average sediment resistivity above the Whitehill Formation in their study area was documented to have increased with depth in the absence of dolerites, perhaps due to weathering effects.

The Ecca Group formations outcrop in the study area, and are part of the targeted area for shale gas exploration in South Africa. Despite the vast amount of available information on the Ecca Group, to date, the lateral and vertical variation in resistivity of the Ecca Group is still not well documented or understood. The exposure quality of the Ecca sequence is considerably better along road cuttings and easily accessible when compared to outcrops in private farms and game reserves. Thus, in this study, we carried out electrical resistivity survey on the road-cut exposures of the Ecca Group along Regional roads R67 (Grahamstown-Fort Beaufort), R344 (Grahamstown-Adelaide), R335 (North of Kirkwood-Somerset East), R350 (Grahamstown-Bedford) and National roads N2 (Grahamstown-Peddie), and N10 (Paterson-Cookhouse) (Figure 10.1) in order to investigate lateral and vertical variations in resistivity of the subsurface layer(s) and also to detect bodies of anomalous electrical conductivity (inverse of resistivities). The main advantage of using this method is that the result can be quantitatively interpreted using computer software and

accurate estimates of depth, thickness and resistivity of subsurface layers could be deduced from the resulting models. Furthermore, the method is cheap, time efficient and reliable.
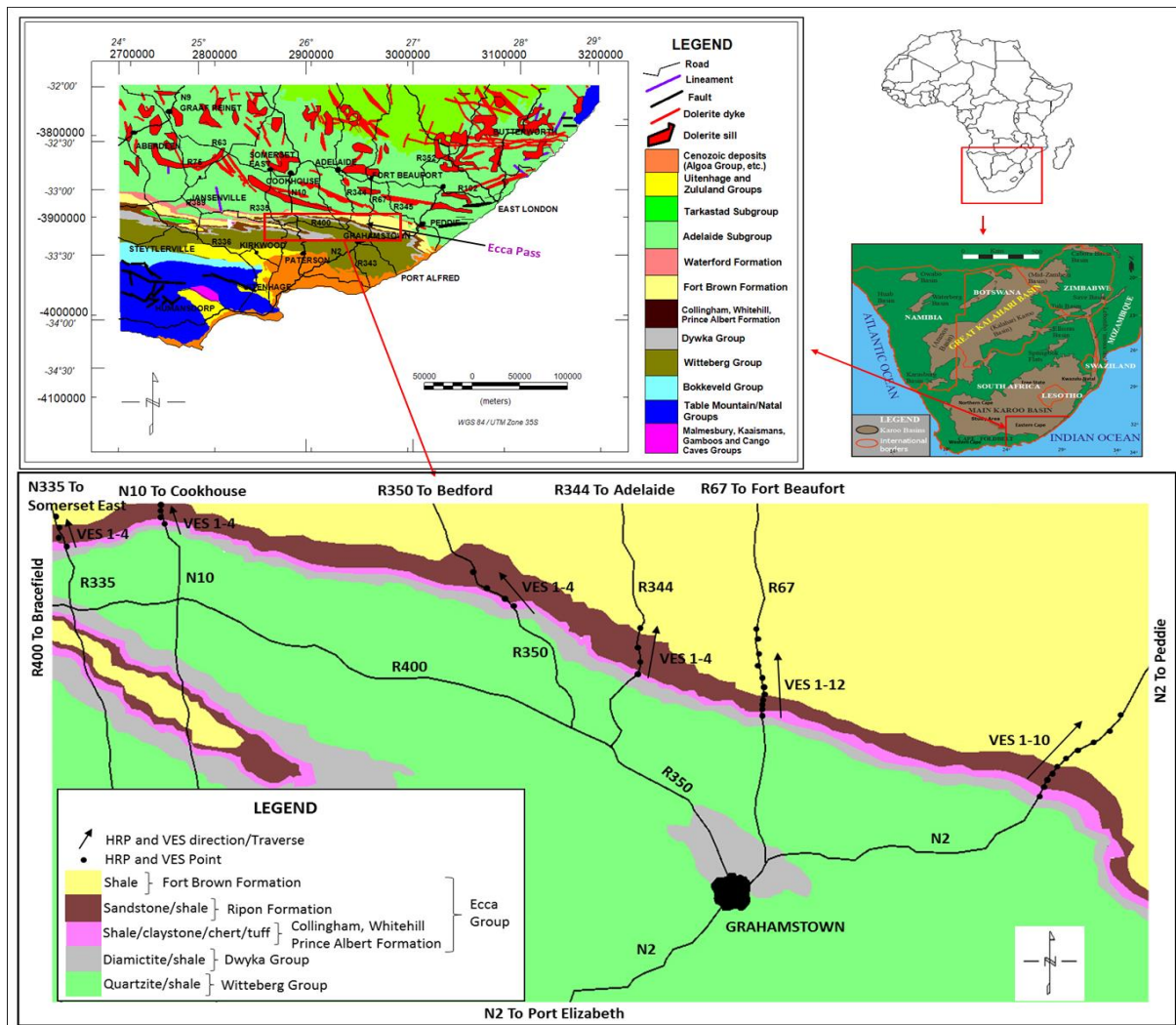
Figure 10.1: Geological map of the study area showing HRP and VES points, and direction. Note that the HRP is horizontal resistivity profiling and VES is vertical electrical sounding.

10.2 Electrical resistivity method

The electrical resistivity involves injecting direct current or low frequency alternating current into the ground through a pair of current electrodes and the measurement of the resulting potential (Pd) through another pair of electrode called potential electrodes. Since the current is known and the potential difference can be measured, an apparent resistivity can be calculated. The three main ways of passage of electric current in rocks and minerals are by electronic, electrolytic and dielectric conductions. Electronic conduction is the normal type of current conduction in metallic materials which contain free electrons. In electrolytic conduction, current is carried by ions at comparatively slow rate. Dielectric conduction takes

place in poor conductors or in insulators which have very few or no free charge carriers (Telford et al., 1990; Lowrie, 1997). Generally, most substances tend to retard the flow of electric current so that energy must be expended to move charged particles. The extent to which a substance resists this movement is described by its "electrical resistivity". Therefore, the main aim of electrical resistivity surveying is to measure this property (resistivity) as a basis for distinguishing layering and structure of the Earth. Resistivity values vary in different geological materials (Singh, 2005). Most rocks and minerals are not connective or are resistive in their dry state. However, in nature, they usually contain some water with varying quantity of dissolved salts within their pores, fractures and cracks (primary and secondary porosity). The presence of water and dissolved salts in the subsurface material substantially reduces the resistivity or increases the conductivity of the rocks.

10.2.1 Electrical resistivities of geological materials

The ground resistivity is related to various geological parameters such as mineral and fluid content, porosity and degree of water saturation in the rock (Loke, 1999). In general, most rock resistivities are roughly equal to that of pore fluids divided by the fractional porosity. Resistivity of rocks depends on porosity, saturation, content of clay and resistivity of pore water (Archie's formula). Archie's law provides a closer approximation for electrical resistivity ρ_r of a porous rock containing water and cement to the fraction of the pore space that is filled with water as shown in equation 10.1:

$$\rho_r = a\emptyset^{-m}S^{-n}\rho_w, \qquad\qquad [10.1]$$

where $\emptyset$ is the fractional pore volume (porosity), S is the fraction of pores containing water, ρ_w is the resistivity of water, a, m, and n are empirically determined constants, i.e. $0.5 < a < 2.5$, $1.3 < m < 2.5$ and $n \sim 2$.

Variation in the properties of different rocks and the fluids within them give rise to different resistivity or conductivity signatures. Most rock forming minerals are insulators; however, this does not imply that rocks have no conductivity. Rocks are usually porous and the pores are filled with fluids (mostly water), making them to act as electrolytic conductors, allowing the passage of currents (in the form of ions) through the pores. In most cases, rock or soil with high clay and/or moisture and water content would have low resistivity (or high conductivity) and vice versa. This is due to the presence of mineral particles that potentially carry electrical charges, and the presence of moisture/water that aids electrolytic conduction. Fractured consolidated rocks would measure lower resistivity (or higher conductivity) than

similar rocks with no fractures because fractures are potential paths for groundwater flow, and they usually harbour fluids. Contaminated water and saline water will show higher conductivity (or lower resistivity) compared to fresh water because they contain dissolved ions that aid electrical conductivity. Therefore, porosity plays a major role in the control of resistivity, with resistivity generally increasing as porosity decreases. Generally, rocks and minerals are considered good, intermediate, and poor conductors within the following range:

i.   Minerals of resistivity 10^{-8} to about 1 Ωm (metals, graphite, sulphides, arsenides, oxides such as magnetite) are good conductors;

ii. Minerals and rocks of resistivity 1 to 10^7 Ωm (most oxides, ores, porous rocks containing water) are intermediate conductors;

iii. Minerals and rocks of resistivity above 10^7 Ωm (common rock forming minerals, silicates, phosphates, nitrates, etc.) are poor conductors.

Resistivity values of common geological materials are depicted in Table 10.1. Kearey and Brooks (2002) argued that it is apparent that there is a considerable overlap between the different rock types and therefore, the identification of a rock cannot be solely done on the basis of resistivity data.

Table 10.1: Resistivity values for some common geological units (After Telford et al., 1990).

Geologic materials	Nominal resistivity (Ωm)
Quartz	3×10^2 - 10^6
Granite	3×10^2 - 10^6
Granite (weathered)	30 - 500
Consolidated shale	20 - 2×10^3
Sandstones	200 - 5000
Sandstones (weathered)	50 - 200
Clays	1 - 10^2
Boulder clay	15 - 35
Clay (very dry)	50 - 150
Gravel (dry)	1400
Gravel (saturated)	100
Lateritic soil	120 - 750
Dry sandy soil	80 - 1050
Sand clay/clayed sand	30 - 215
Sand and gravel (saturated)	30 - 225
Mudstone	20 - 120
Siltstone	20 - 150

10.2.2 Basic principles of the electrical resistivity method

Ground resistivity is measured by passing an electric current through the ground using two electrodes (C_1 and C_2) and measuring the resultant potential difference using two or more potential electrodes (P_1 and P_2). The schematic diagram depicted in Figure 10.2 shows the basic concept of electrical resistivity measurement. The depth of investigation is often given as a function of the electrode spacing, implying that the greater the current electrodes spacing, the deeper the electrical currents will flow in the Earth, thus the greater the depth of penetration.
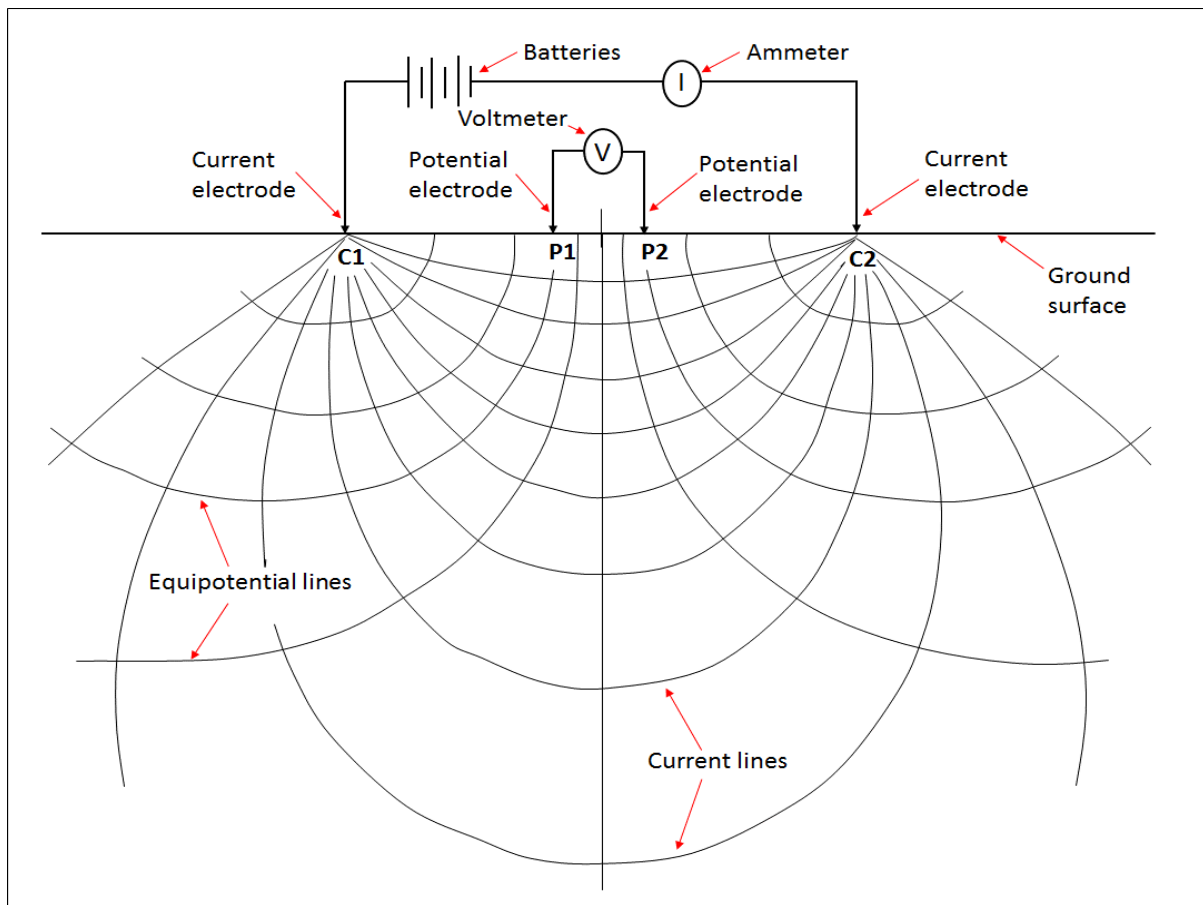
Figure 10.2: Schematic diagram illustrating basic concept of electrical resistivity (ER) measurement.

The principle of the ER method is based on Ohm's law, which gives the relationship between the electrical current, potential difference and the resistance. The application of this relationship is that as electrical current is injected into the ground, it encounters both Earth materials that are good conductors and bad conductors (more resistive). It is on the basis of this conductivity or resistivity contrast that the ER method is used to identify different underground features. Assuming an electrically conductive body lends itself to the description of a one-dimensional body (like a wire), the relationship between the electrical

current, potential difference and resistance could be described by Ohm's law as shown in equation (10.2).

$$R = \frac{V}{I},$$ [10.2]

where V is the potential difference (in volts), I is the current (in Amperes) and R is the resistance (in ohms).

The electrical resistance (R) of a material is related to its physical dimensions (i.e. cross sectional area, A, length, L) and the resistivity ρ or conductivity (σ) is given as follows:

$$\rho = \frac{1}{\sigma} = \frac{RA}{L}$$ [10.3]

The resistance is therefore given by:

$$R = \frac{V}{I} = \rho\left(\frac{L}{A}\right)$$ [10.4]

For an area, $A = 2\pi r^2$, equation (10.5) can be rewritten in terms of voltage, V as:

$$V = \frac{\rho I}{2\pi r},$$ [10.5]

Considering an electrode pair with current I at electrode C_1, and $-I$ at electrode C_2 as shown in Figure 10.2, the potential V at any point is given by the algebraic sum of the individual contributions. Hence,

$$V = V_{C_1} + V_{C_2} = \rho I\left(\frac{1}{2\pi r_{C_1}} - \frac{1}{2\pi r_{C_2}}\right) = \frac{\rho I}{2\pi}\left(\frac{1}{r_{C_1}} - \frac{1}{r_{C_2}}\right),$$ [10.6]

where r_{C_1} and r_{C_2} are distances from the point to the current electrodes C_1 and C_2, respectively.

For the potential electrodes P_1 and P_2, the potential difference is given as:

$$V = V_{P_1} - V_{P_2} = \frac{\rho I}{2\pi}\left(\frac{1}{C_1 P_1} - \frac{1}{C_2 P_1} + \frac{1}{C_2 P_2} - \frac{1}{C_1 P_2}\right),$$ [10.7]

where V_{P_1} and V_{P_2} are potentials at P_1 and P_2, $C_1 P_1$ is the distance between C_1 and P_1, $C_1 P_2$ is the distance between C_1 and P_2, $C_2 P_1$ is the distance between C_2 and P_1, $C_2 P_2$ is the distance between C_2 and P_2.

Equation (10.8) can be rewritten as:

$$V = V_{P_1} - V_{P_2} = \frac{\rho I}{2\pi}\left(\frac{1}{C_1 P_1} - \frac{1}{C_2 P_1} + \frac{1}{C_2 P_2} - \frac{1}{C_1 P_2}\right)$$ [10.8]

Let $\frac{1}{k} = \frac{1}{2\pi}\left(\frac{1}{C_1 P_1} - \frac{1}{C_2 P_1} + \frac{1}{C_2 P_2} - \frac{1}{C_1 P_2}\right)$, then equation (10.7) becomes:

$$V = \frac{\rho I}{k},$$ [10.9]

substituting for ρ in equation (10.8):

$$\rho = \frac{kV}{I} = kR_{app}, \qquad\qquad [10.10]$$

where ρ is theresistivity (in ohm m), k is the geometric factor (in m) and R_{app} is theapparent resistance (in ohm). The geometric factor (k) varies for different electrode configurations.

Resistivity meters normally give the resistance value (R_{app}), so in practice, the apparent resistivity value is calculated as:

$$\rho_a = kR_{app} \qquad\qquad [10.11]$$

The calculated resistivity value is not the true resistivity of the subsurface, but an "apparent" value which is the resistivity of a homogeneous ground. In general, all field data are termed apparent resistivity because the resistivity values measured are actually averages over the total current path length but are plotted at one depth point for each potential electrode pair. The apparent resistivities are subject to interpretation techniques including the curve matching and/or computer interpretation. Resistivity measurements are associated with varying depths depending on the separation of the current and potential electrodes, and can be interpreted in terms of a lithologic and/or geohydrologic model of the subsurface. Depending on the survey geometry, the apparent resistivity data are plotted as 1-D soundings, 1-D profiles, or in 2-D cross-sections in order to reveal anomalous regions. The 2-D images of the subsurface apparent resistivity variation are called pseudosection.

10.2.3 Electrode configurations

There are various electrode configurations which can be used in a resistivity surveyand each has its own advantages and disadvantages. The electrical resistivity method is conducted fundamentally using four collinear electrodes. The apparent resistivity measurement determined is a function of the configuration of these four electrodes. The configuration of electrodes enables the computation of the geometric factor, which depends on the arrangement of the potential and current electrodes. The Wenner, Lee-Partitioning and Schlumberger arrays were the most commonly used electrode arrays for resistivity surveys in the 1960s. However, in recent years, more electrode arrays including the dipole-dipole, pole-dipole, square and gradient arrays have been used for several electrical resistivity explorations. To date, the most widely used array types are the Wenner and Schlumberger arrays. Likewise, these two electrode configurations were adopted in this study and are discussed below.

10.2.3.1 Wenner array

The Wenner array has the simplest geometry, consisting of four collinear equally spaced electrodes. The outer two electrodes are typically the current (source) electrodes and the inner two electrodes are the potential (receiver) electrodes. The array spacing is expanded about the array midpoint while maintaining an equivalent spacing between each electrode (Figure 10.3). The Wenner array has five variations, three referred to as the tri-potential method with $\alpha, \beta,$ and γ configurations, one as the Lee partitioning method (which has a fifth electrode at the array centre acting as a third potential electrode), and one as the Offset Wenner electrode array, which reduces the effects of lateral inhomogeneities. The advantages of the Wenner array are that the apparent resistivity is easily calculated in the field and the instrument sensitivity is not as crucial as with other array geometries. In addition, relatively small current magnitudes are needed to produce measurable potential differences.
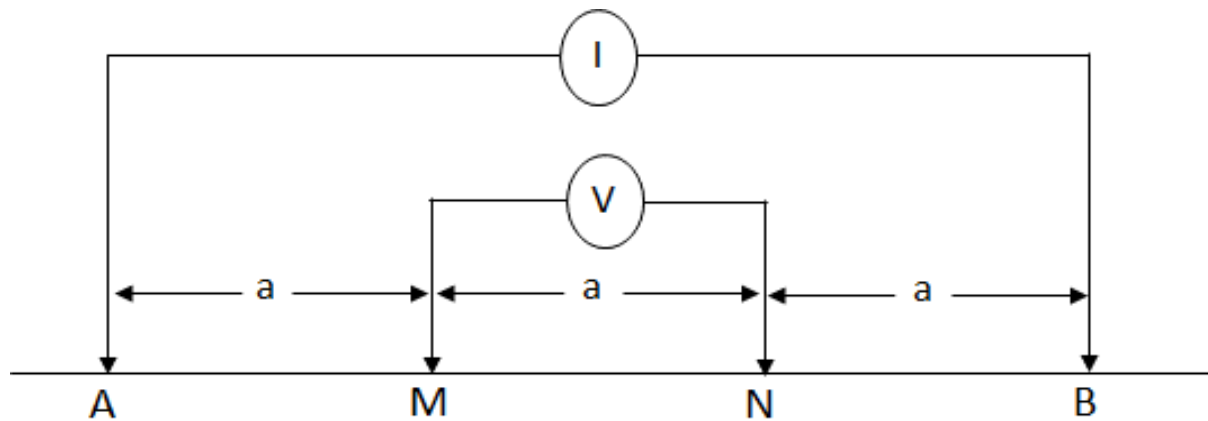
Figure 10.3: Configuration of the Wenner array electrodes. Note that 'a' is the electrode spacing, A and B are current electrodes, and M and N are potential electrodes.

The geometric factor (k) for the Wenner array is expressed as:

$$k = 2\pi a, \qquad\qquad [10.12]$$

Therefore:

$$\rho_a = 2\pi a \left(\frac{V}{I}\right), \qquad\qquad [10.13]$$

where a is the electrode spacing.

10.2.3.2 Schlumberger array

The Schlumberger array consists of four collinear electrodes with spacing not equal. The outer two electrodes A and B are current (source) electrodes and the inner two electrodes M and N are the potential (receiver) electrodes (Figure 10.4). The potential electrodes are

installed at the centre of the electrode array with a small separation, typically less than one fifth of the spacing between the current electrodes. The current electrodes spacing is increased to a greater separation distance during the survey while the potential electrodes remain in the same position until the observed voltage becomes too small to measure. The advantages of the Schlumberger array are that fewer electrodes need to be moved for each sounding and the cable length for the potential electrodes is shorter. Schlumberger soundings generally have better resolution, greater probing depth, and are less time-consuming in the field deployment than the Wenner array.
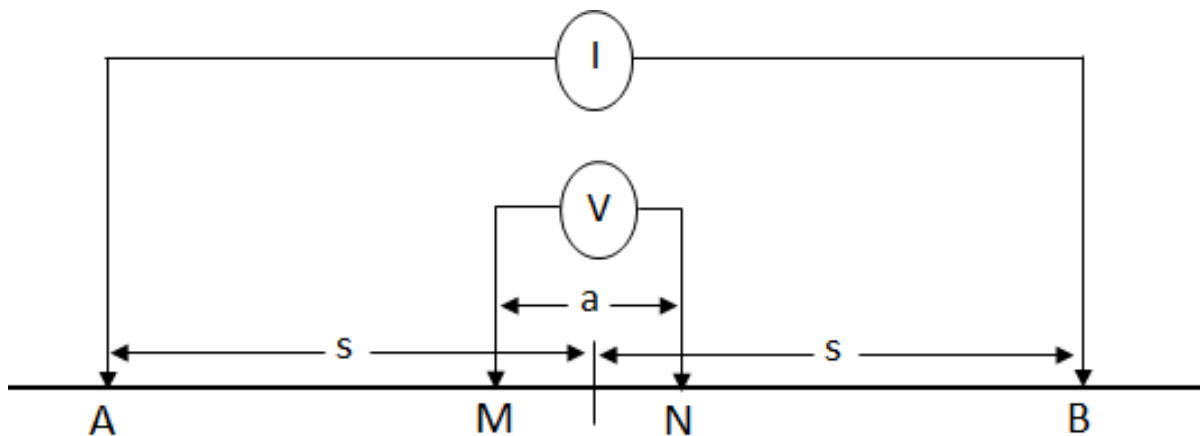
Figure 10.4: Configuration of the Schlumberger array electrodes.

A measurable amount of current is transmitted into the ground through A and B and the value of the current I is measured with an ammeter and recorded. The resultant potential difference ΔV across M and N is determined by means of a voltmeter and recorded. The geometric factor (k) for the Schlumberger arrayis given as:

$$k = \frac{\pi}{a}\left[\left(\frac{s}{a}\right)^2 - \left(\frac{a}{2}\right)^2\right],$$
[10.14]

where a and s are as shown in Figure 10.4.

Using the variables ΔV and I, and the geometric factor (k) for the Schlumberger array, the apparent resistivity value can be calculated as shown in equation (10.15).

$$\rho_a = \frac{\pi\left(s^2 + a^2/4\right)}{a}\frac{\Delta V}{I}$$
[10.15]

10.2.4 Electrical resistivity surveys

Each of the aforementioned electrode configurations is suitable for a particular geological situation. It is possible for apparent resistivity values observed by the different array types

over the same structure to differ since the array types have different penetration depths. Therefore, the choice of a particular array depends on a number of factors that include the geological structures to be delineated, heterogeneities of the subsurface, sensitivity of the resistivity meter, and the background noise level. Other factors which are worth considering include the sensitivity of the array to vertical and lateral variations in the resistivity of the subsurface, its depth of investigation and the horizontal data coverage and signal strength of the array (Ahzegbobor, 2010). The horizontal resistivity profiling (HRP) and vertical electrical sounding (VES) were carried out in this study. The HRP with Wenner array was used to determine lateral variations in the Earth resistivity along the traverses and within a limited depth range of up 9 m. The VES method with Schlumberger array was used to investigate vertical variation in electrical resistivity to a depth of about 134 m.

10.3 Materials and method

10.3.1 Instrumentation and data acquisition

The instrument used for the electrical resistivity survey was a Geotron resistivity meter (Model G41) together with connecting cables, four steel electrodes, hammers, measuring tape and compass clinometers. The period for the fieldwork was between March and May, 2016 when the ground was considerably moist. This ensured good current conduction between the Earth and the electrodes. Sites for surveys were selected in areas where the Ecca Group formations are exposed to the surface (mostly road-cut exposures). Both the HRP and VES measurements were performed along approximately straight roads to determine the lateral and vertical variations in subsurface resistivity that might exist in the survey area along the selected profiles. The survey was performed by a four-man crew, including the author who operated the instrument and recorded measurements (Figure 10.5). The resistivity meter usually displays an error or negative resistance when the injected current is insufficient and when this happened, the current was increased to a higher value.
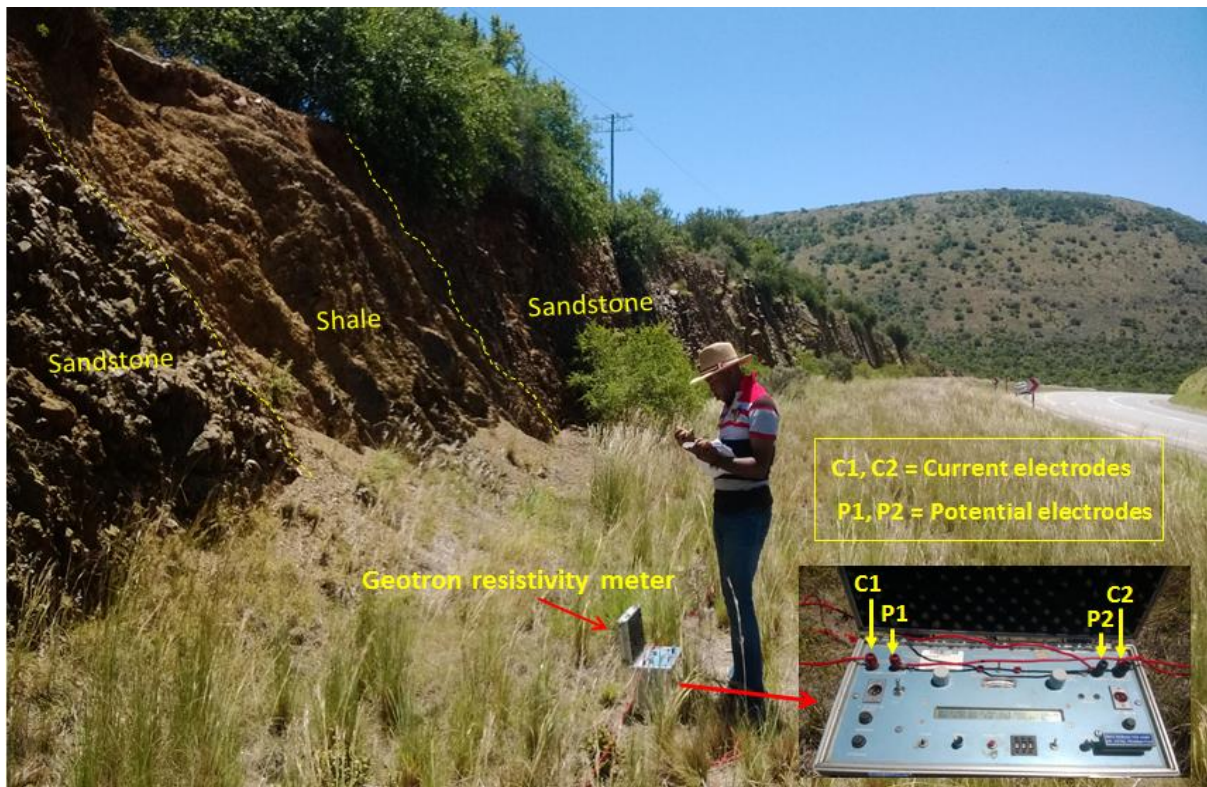
Figure 10.5: Electrical resistivity survey (Schlumberger array) on road-cut exposures of the Ecca Group along National road N10 to Cookhouse using a Geotron resistivity meter (Model G41). Note the author recording measurements in a field notebook.

The survey began with HRP using the Wenner array configuration. A current electrode spacing of AB = 27 m (a = 9 m) was chosen for the HRP survey such that the lower Ecca Group formations with a small outcrop thickness of about 28 m would be sampled i.e. at least one measurement with AB fully within the outcrop. 32 resistivity profiles of various lengths (varying between 54 m and 225 m) were carried out along side the roads.

In addition, a total of 37 VES sites were carried out in the area. The VES current electrode spacing were chosen such that there were 6 logarithmically spaced intervals in a decade resulting in AB spacing ranging from 3 m to 200 m (i.e. AB/2 = 1.5 m to 100 m). The potential electrode spacing (MN) was 1 m throughout the soundings (i.e. MN/2 = 0.5 m). For the VES, in order to increase the depth of investigation, the potential electrodes remain fixed at a point whereas the current electrodes were expanded symmetrically about the centre of the spread up to 100 m.

10.3.2 Data processing

An appropriate geometric factor (see equations 12-15) was applied to the recorded measurements of the potential difference ΔV and current I to calculate the apparent resistivity (ρ_a) of the subsurface for the HRP and VES data. Profiles of the HRP data were generated in Geosoft Oasis Montaj software (version 8.2.0.4) to display the lateral resistivity variations of the geologic formations. On the other hand, the VES data were initially inverted using the software IPI2WIN (version 2.1) developed by Alexey Bobachev, Moscow State University, Russia. This software iteratively generates a model that has a least root-mean square (RMS) error between the calculated resistivity of the model and the actual field data (observed curve). When this was achieved, the observed geoelectric properties are considered to represent the subsurface geology, and the iterated results were accepted and saved as RES2DINV file format that can be read in RES2DINV inversion software. Several single site modelled data exported from the IPI2WIN, were combined into a pseudosection and further modelled in RES2DINV to generate a 2-D model for the subsurface. The 2-D model used by this program divides the subsurface into a number of rectangular blocks and determines the resistivity of the rectangular blocks that will produce an apparent resistivity pseudosection that agrees with the actual field measurements through an iteration process. The program uses a forward modelling subroutine to calculate apparent resistivity values from field data which are then inverted using a non-linear least-squares optimization technique (Loke and Barker, 1996). The inversion routine in RES2DINV software is based on the smoothness-constrained least-squares method (DeGroot-Hedlin and Constable, 1990; Loke and Barker, 1996), which can be mathematically expressed as:

$$(J^T J + \mu F)d = J^T g - \mu F r, \qquad [10.16]$$

where F is a smoothing matrix, J is the Jacobian matrix of partial derivatives, r is a vector containing the logarithm of the model resistivity values, μ is the damping factor, d is the model perturbation vector, and g is the discrepancy vector.

The discrepancy vector (g) contains the difference between the calculated and measured apparent resistivity values. The magnitude of g is usually given as a root-mean squared (RMS) value, which is the quantity that the inversion method tends to reduce in an attempt to find a better model after each iteration. The model perturbation vector (d) is the change in the model resistivity values calculated using equation (10.16), which normally results in an "improved" model. The expression in equation (10.16) is minimised by a combination of two quantities: the difference between the calculated and measured apparent resistivity values as

well as minimise the roughness (i.e. inverse of the model smoothness) of the model resistivity values. The weight given to the model smoothness during inversion is known as the damping factor (μ). The damping factor in the model range from 0.05 to 0.3, and the larger the noise, the higher the required damping factor and vice versa (the larger the damping factor, the smoother will be the model). Generally, after each iteration, the inversion subroutine will reduce the damping factor in equation (10.16). Due to the differential level of noise in the data, a minimum limit of 0.1 was set for the damping factor in order to stabilise the inversion process. The iterative process proceeds as follows: (1) the inversion routine produces an initial model of subsurface resistivity using the calculated apparent resistivity values and generates a response resistivity field based on the initial model, and (2) it calculates a RMS value that describes the level of agreement between the synthetic and observed resistivity fields. A large RMS value usually > 5% indicates a poor fit. In this study, the initial model is adjusted iteratively until the RMS became acceptable or falls below the desired threshold (< 5%), after which the iterative process is terminated and the results saved as the final model.

10.3.3 Presentation and interpretation of data

The HRP data is displayed as either a single profile or several profiles are used to generate profiling contour map (isoapparent resistivity map), then interpreted quantitatively. The VES single site data are presented as sounding curves, obtained by plotting graphs of log apparent resistivity (ρ_a) versus log of half electrode spacing (AB/2). Furthermore, the apparent resistivity data for several sites are plotted as pseudosections in order to give an approximate picture of the true subsurface resistivity distribution. Thus qualitative interpretation is done in the case of VES data to determine the thickness, nature and lateral variations of the geological formations. A number of VES curves are published for comparison. These curves include simple curves for 2, 3, 4 and 5 layer cases and this aid the interpretation of the geoelectric models. These shapes are known as Q-type (or DA. descending Hummel), H-type (Hummel type with minimum), A-type (ascending) and the K-type (or DA, displaced anisotropic) (see Figure 10.6).

The K-type curve (Figure 10.6a) rises to a maximum level, and then falls, indicating that the middle layer has the highest resistivity compared to the top and bottom layers. The type-H curve shows the opposite effect; it falls to the minimum then increases again due to an intermediate layer that is a better conductor than the top and bottom layers. The A-type curve

may show some changes but the apparent resistivity generally increases continuously along with increased electrode spacing, indicating that the resistivity increases with depth from layer to layer. The Q-type curve exhibits the opposite effect; it decreases continuously along with a progressive increase of resistivity with depth.

The basis Q, H, A, and K curves can be combined to yield curves for four or more layers. The four (Figure 10.6 (a-b)) and five layer case models are observed in the surveyed sites and typical curves for such models are shown in Figure 10.6 (c-d) and Table 10.2.
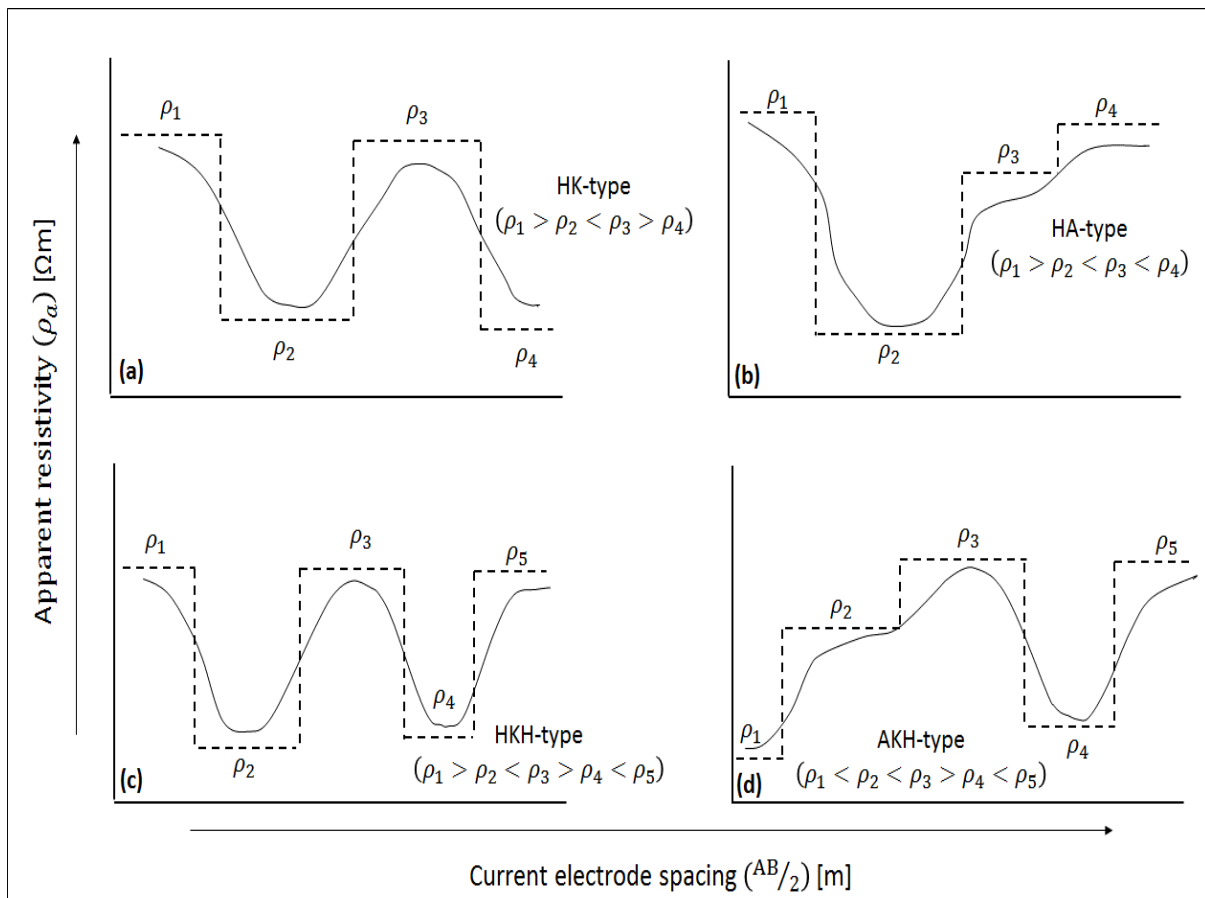
Figure 10.6: Typical four (a-b) and five (c-d) layer case models of electrical resistivity (VES).

Table 10.2: Typical examples of four and five layer resistivity curves.

Number of layers	Specifications	Curve type
4	$\rho_1 > \rho_2 < \rho_3 < \rho_4$	HA
	$\rho_1 > \rho_2 < \rho_3 > \rho_4$	HK
	$\rho_1 < \rho_2 < \rho_3 < \rho_4$	AA
	$\rho_1 < \rho_2 < \rho_3 > \rho_4$	AK
	$\rho_1 < \rho_2 > \rho_3 < \rho_4$	KH
	$\rho_1 < \rho_2 > \rho_3 > \rho_4$	KQ
	$\rho_1 > \rho_2 > \rho_3 < \rho_4$	QH
	$\rho_1 > \rho_2 > \rho_3 > \rho_4$	QQ
5	$\rho_1 > \rho_2 < \rho_3 > \rho_4 < \rho_5$	HKH
	$\rho_1 > \rho_2 < \rho_3 > \rho_4 < \rho_5$	HKQ
	$\rho_1 < \rho_2 > \rho_3 > \rho_4 < \rho_5$	KQH

10.4 Presentation and discussion of results

10.4.1 Horizontal resistivity profiling (HRP)

The HRP single profiles are presented in Figure 10.7(a-f). The maximum depth of penetration of the HRP using Wenner array is 1/3 of the maximum distance of current electrodes (Frohlich et al., 1996). The current electrode spacing in the HRP survey is 27 m (a = 9), thus the depth of penetration is 9 m. The measured apparent resistivities along Regional roads R335 to Somerset East and R344 to Adelaide are generally low, ranging between 9.1 Ωm and 135 Ωm (Figure 10.7 (a and e)). The result of HRP along Regional road R350 to Bedford is shown in Figure 10.7(f). Along this profile (A-B), the resistivity value increases from about 70 Ωm at the start of the line to ~ 500 Ωm at a distance of about 240 m. Thereafter, the resistivity value decreases to ~ 80 Ωm at a distance of about 300 m and slightly increases to ~ 130 Ωm at the end of the line. The resistivity values measured along Regional road R67 between Grahamstown and Fort Beaufort (Ecca Pass) is characterized by heterogeneous resistivity or generally undulate, with minimum and maximum resistivity values of about 10 Ωm and 275 Ωm, respectively (Figure 10.7c). The resistivity values along National roads N10 to Cookhouse and N2 to Peddie are fairly high, ranging from about 100 Ωm to ~ 200 Ωm (Figure 10.7d). The isoapparent resistivity map (combined profiles map) is depicted in Figure 10.7(g). The map shows that apparent resistivity of the subsurface varies laterally between 2 Ωm and 500 Ωm in the study area. Since current is conducted electrolytically by groundwater (in saturated layers) and dielectrically by effective surface of minerals (in dry layers), it is inferred that areas with low apparent resistivity values are possibly due to buried rock or soil with high clay and/or moisture and water content and vice versa.
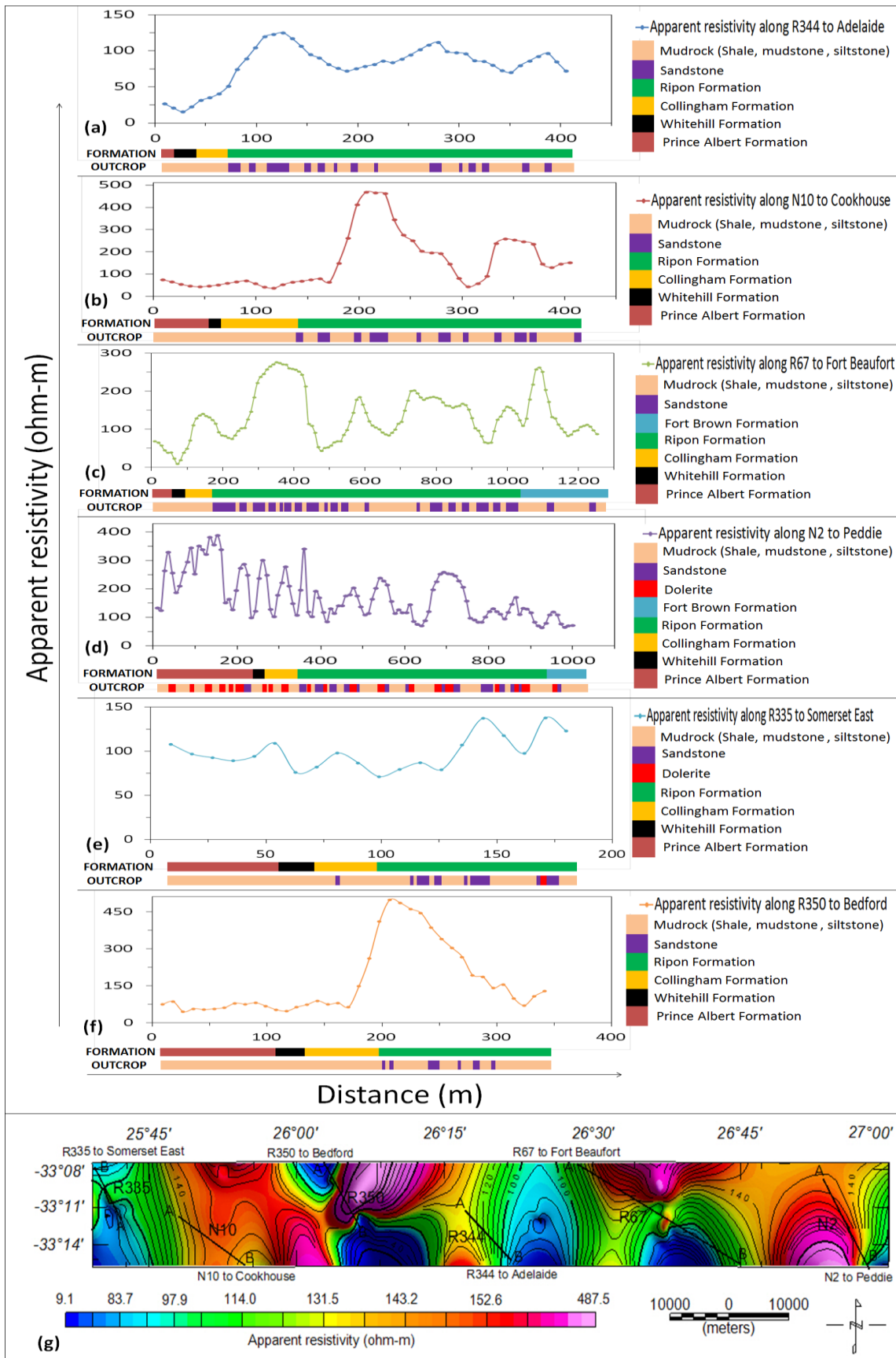
Figure 10.7: Horizontal resistivity profiling survey on road-cut exposures of the Ecca Group showing lateral variation in the apparent resistivity at a depth of about 9 m. (a-f) Graphs of apparent resistivity versus distance. (g) Isoapparent electrical resistivity map of the combined or all the profiles.

10.4.2 Vertical electrical sounding (VES)

10.4.2.1 Geoelectric models

The VES curves and the best fitting models are presented in Figures 10.8-10.13. The interpreted geoelectric sections are shown in Tables 10.3-10.8 including the inferred lithology and curve types. The geoelectric sections depicted in Figures 10.8-10.13 show four to five subsurface layers which include the topsoil, mudstone, sandstone, consolidated shale and dolerite intrusion. The topsoil is composed of dry sandy clay with resistivity values ranging between 34 Ωm and 844 Ωm. The thickness of this layer varies from 0.27 m to 2.19 m being thinnest at VES 3 along Regional roads R335 to Somerset East and R350 to Bedford, and thickest at VES 13 along Regional road R67 to Fort Beaufort. It is observed from the geoelectric sections that VES 1 and 2 along Regional road R335 to Somerset East, VES 1 along National road N10 to Cookhouse, and VES 4 along Regional road R350 to Bedford are characterized with low resistivity values varying between 34 Ωm to 77 Ωm. These low resistivity values suggest that the topsoil in these areas possibly has high clay and/or moisture content. The wide range in the resistivity values is possibly due to the different degree of compaction. The resistivity and thickness of the second layer varies from about 8 Ωm and 7009 Ωm, and 0.62 m to 5.42 m, respectively. This layer is mostly inferred to be mudstone, although in some places it has been replaced by weathered sandstone. The second layer along Regional road R335 to Somerset East is weathered dolerite intrusion with resistivity values of about 7009 Ωm. On the contrary, the apparent resistivity of the second layer (at VES 2) along Regional road R67 between Grahamstown and Fort Beaufort is 8 Ωm and it inferred to be clay. The resistivity and thickness of the third layer varies between 1 Ωm and 31601 Ωm, and 2.31 m to 19 m, respectively. In most of the VES points, based on the resistivity value, this layer is inferred to be sandstone and is weathered in some places, especially along National road N10 to Cookhouse. However, in some of the VES points, this layer is also inferred to be dolerite intrusion, mudstone, consolidated shale and clay/tuff. The fourth and fifth layers have resistivity values ranging from 35Ωm to 556996 Ωm, and 3 Ωm to 240000 Ωm, respectively. The thickness of the fifth layer is not defined since it is the last layer. Based on the resistivity values, the inferred lithologies for these layers vary from consolidated shale, dolerite intrusion, mudstone and sandstone (Tables 10.3-10.8). The curves are predominantly combination of HA, HK, KH, QH, AAK, HAA, HAK, HKH, HKQ, KHA and QHA curve-types indicating the presence of four and five layer subsurface layers.
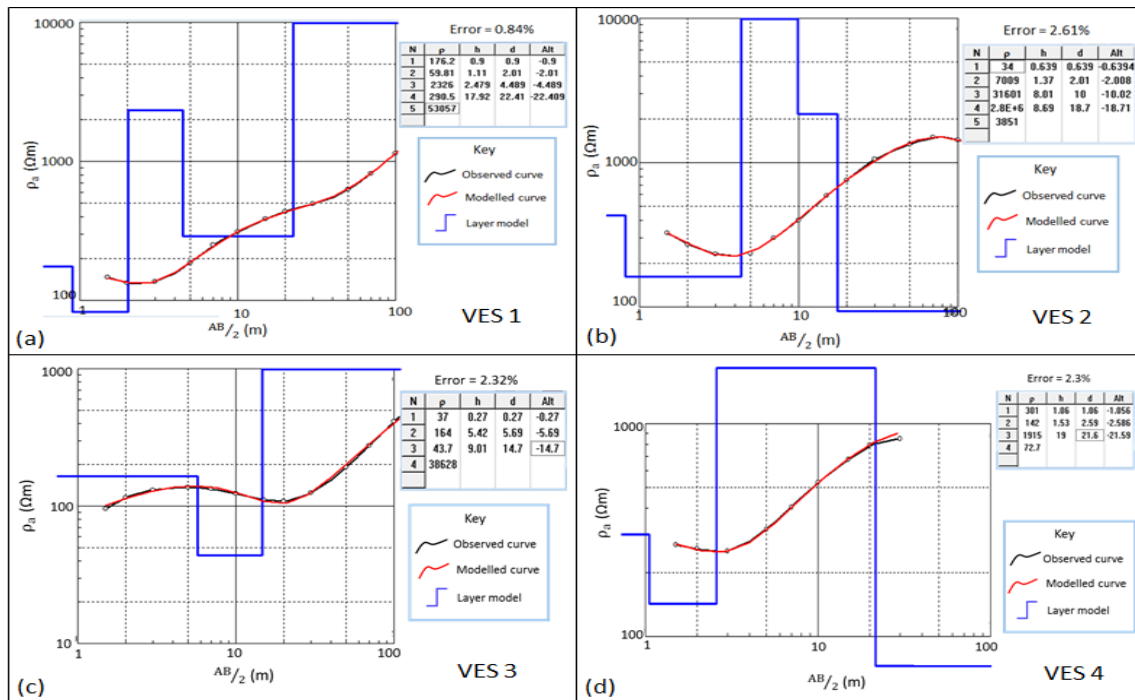
Figure 10.8: VES curves and geoelectric models for four sites along Regional road R335 between Kirkwoood and Somerset East. Note the following parameters for each of the geoelectric layers in Figures 10.8-10.13: N is the number of layers, ρ is the apparent resistivity for the layer, h is the layer thickness, and d is the depth to the top of the layer.

Table 10.3: Summary of the interpretation of VES sites 1-4 obtained along Somerset East section.

Sounding site and location	Number of layers		Resistivity (Ωm)	Thickness (m)	Depth (m)	Inferred lithology	Curve type
VES 1 25°41'42.01"E 33°10'20.55"S	5	1	176	0.90	0.90	Top soil	HKH
		2	60	1.11	2.01	Mudstone	
		3	2326	2.50	4.50	Sandstone	
		4	291	17.92	22.41	Consolidated shale	
		5	53057	∞	∞	Dolerite intrusion	
VES 2 25°40'45.10"E 33° 9'49.89"S	5	1	34	0.64	0.64	Top soil	AAK
		2	7009	1.37	2.01	Weathered dolerite intrusion	
		3	31601	8.01	10.00	Dolerite intrusion	
		4	280000	8.69	18.70	Dolerite intrusion	
		5	3851	∞	∞	Sandstone	
VES 3 25°39'21.50"E 33° 8'51.18"S	4	1	37	0.27	0.27	Top soil	KH
		2	164	5.42	5.69	Weathered sandstone	
		3	44	9.01	14.7	Mudstone	
		4	38628	∞	∞	Dolerite intrusion	
VES 4 25°37'51.11"E 33° 8'4.17"S	4	1	301	1.06	1.06	Top soil	HK
		2	142	1.53	2.59	Weathered sandstone	
		3	1915	19	21.6	Sandstone	
		4	73	∞	∞	Consolidated shale	

310
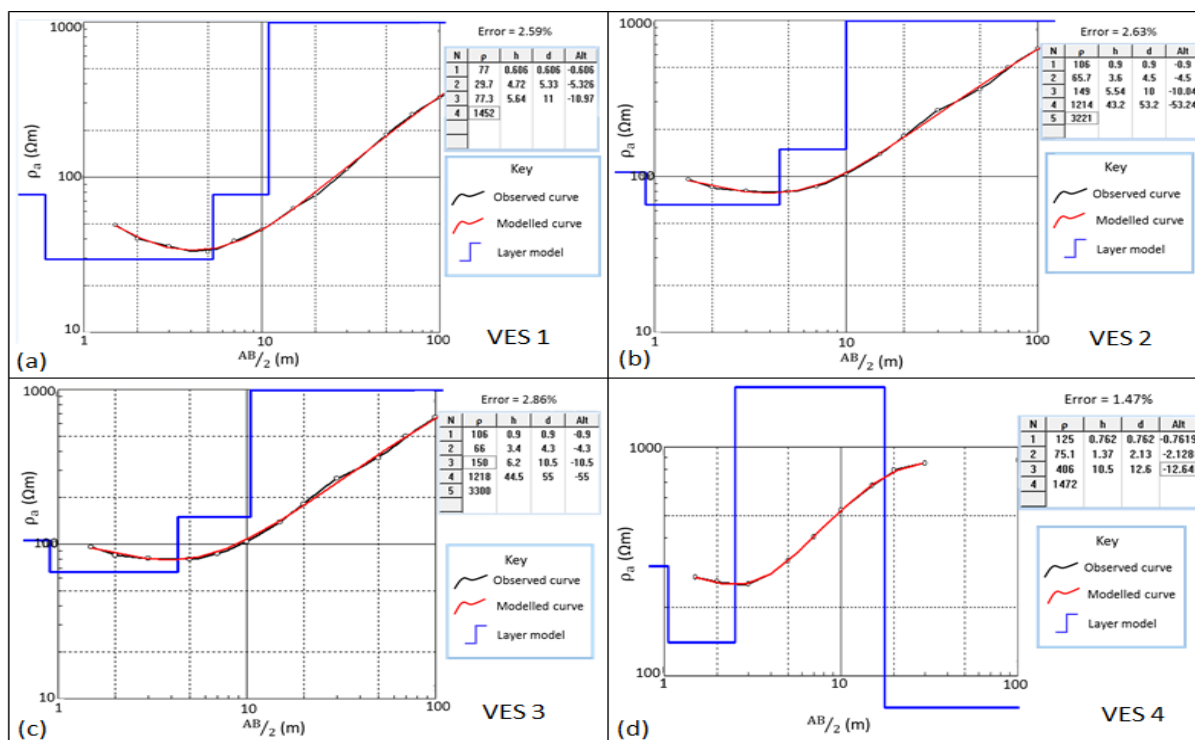
Figure 10.9: VES curves and geoelectric models for four sites along National road N10 between Cookhouse and Paterson.

Table 10.4: Summary of the interpretation of VES sites 1-4 obtained along Cookhouse section.

Sounding site and location	Number of layers		Resistivity (Ωm)	Thickness (m)	Depth (m)	Inferred lithology	Curve type
VES 1 25°52'40.96"E 33° 8'4.41"S	4	1	77	0.61	0.61	Top soil	HA
		2	30	4.72	5.33	Mudstone	
		3	77	5.64	11.00	Weathered sandstone	
		4	1452	∞	∞	Consolidated shale	
VES 2 25°52'36.58"E 33° 7'50.35"S	5	1	106	0.90	0.90	Top soil	HAA
		2	66	3.60	4.50	Mudstone	
		3	149	5.54	10.00	Weathered sandstone	
		4	1214	43.20	53.20	Consolidated shale	
		5	3221	∞	∞	Sandstone	
VES 3 25⁰52'34.9"E 33⁰07'38.7"S	5	1	106	0.90	0.90	Top soil	HAA
		2	66	3.40	4.30	Mudstone	
		3	150	6.20	10.50	Weathered sandstone	
		4	1218	44.50	55.00	Consolidated shale	
		5	3300	∞	∞	Sandstone	
VES 4 25⁰52'32.0"E 33⁰07'29.1"S	4	1	125	0.76	0.76	Top soil	HA
		2	75	1.37	2.13	Mudstone	
		3	406	10.50	12.60	Sandstone	
		4	1472	∞	∞	Consolidated shale	
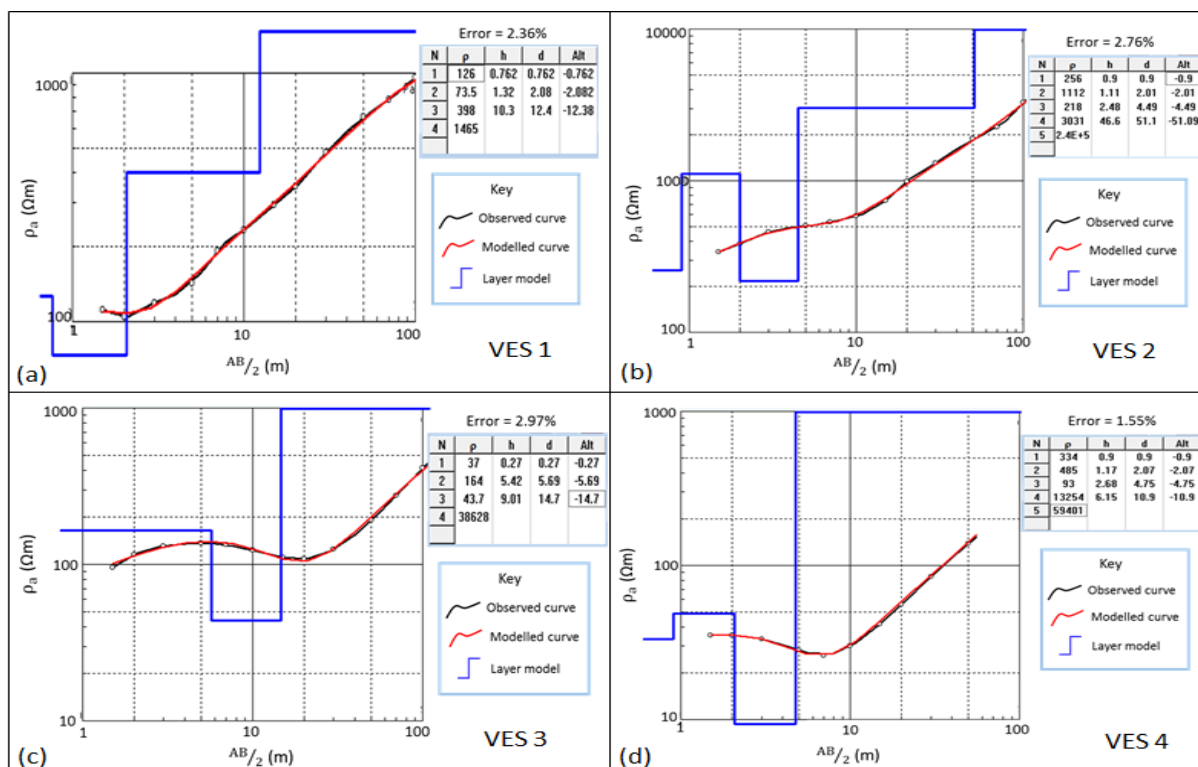
Figure 10.10: VES curves and geoelectric models for four sites along Regional road R350 between Bedford and Grahamstown.

Table 10.5: Summary of the interpretation of VES sites 1-4 obtained along Bedford section.

Sounding site and location	Number of layers		Resistivity (Ωm)	Thickness (m)	Depth (m)	Inferred lithology	Curve type
VES 1 26°21'42.95"E 33°11'53.56"S	4	1	126	0.76	0.76	Top soil	HA
		2	74	1.32	2.08	Mudstone	
		3	398	10.30	12.40	Sandstone	
		4	1465	∞	∞	Consolidated shale	
VES 2 26°21'32.40"E 33°11'46.02"S	5	1	256	0.90	0.90	Top soil	KHA
		2	1112	1.11	2.01	Sandstone	
		3	218	2.48	4.49	Consolidated shale	
		4	3031	46.6	51.10	Sandstone	
		5	240000	∞	∞	Dolerite intrusion	
VES 3 26°21'33.91"E 33°11'34.36"S	4	1	37	0.27	0.27	Top soil	KH
		2	164	5.42	5.69	Weathered sandstone	
		3	44	9.01	14.7	Mudstone	
		4	38628	∞	∞	Dolerite intrusion	
VES 4 26°21'41.23"E 33°11'26.96"S	5	1	334	0.90	0.90	Top soil	KHA
		2	485	1.17	2.07	Weathered sandstone	
		3	93	2.68	4.75	Mudstone	
		4	13254	6.15	10.90	Weathered dolerite intrusion	
		5	59401	∞	∞	Dolerite intrusion	

312
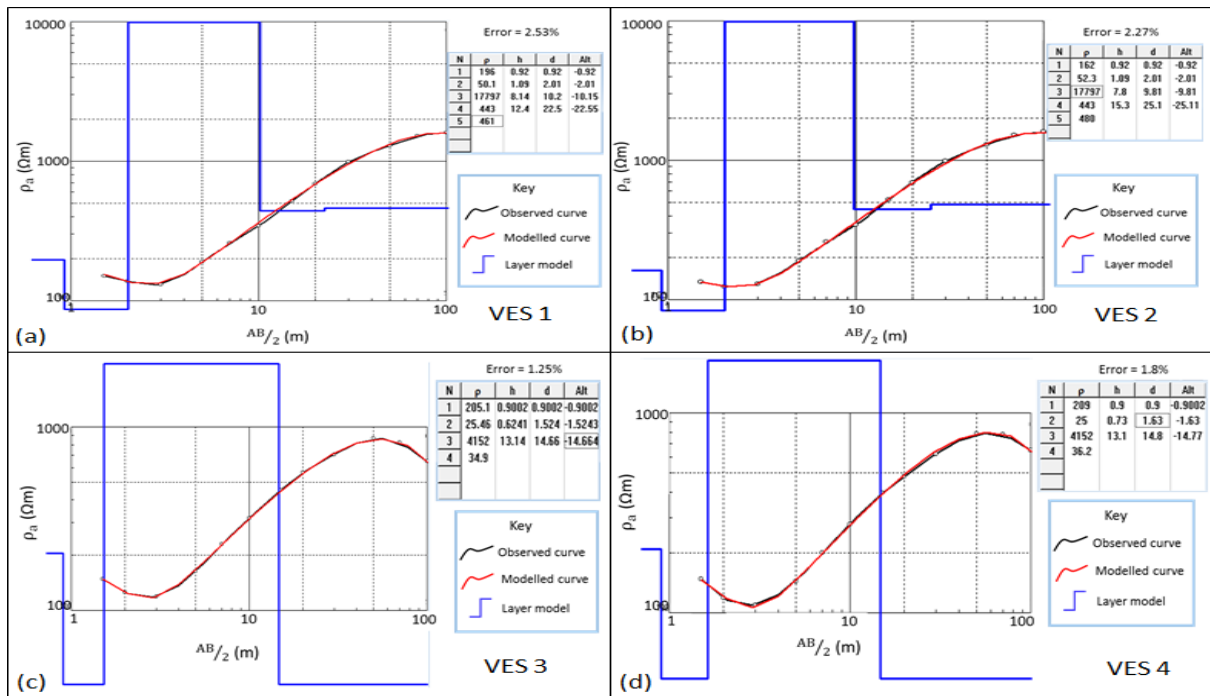
Figure 10.11: VES curves and geoelectric models for four sites along Regional road R344 between Adelaide and Grahamstown.

Table 10.6: Summary of the interpretation of VES sites 1-4 obtained along Adelaide section.

Sounding site and location	Number of layers	Resistivity (Ωm)		Thickness (m)	Depth (m)	Inferred lithology	Curve type
VES 1 26⁰24'23.2"E 33⁰12'04.6"S	5	1	196	0.92	0.92	Top soil	HKH
		2	50	1.09	2.01	Mudstone	
		3	17797	8.14	10.20	Dolerite intrusion	
		4	443	12.40	22.50	Consolidated shale	
		5	461	∞	∞	Sandstone	
VES 2 26⁰24'29.4"E 33⁰11'58.9"S	5	1	162	0.92	0.92	Top soil	HKH
		2	52	1.09	2.01	Mudstone	
		3	17797	7.80	9.81	Dolerite intrusion	
		4	443	15.30	25.10	Consolidated shale	
		5	480	∞	∞	Sandstone	
VES 3 26°24'42.64"E 33°11'51.01"S	4	1	205	0.90	0.90	Top soil	HA
		2	25	0.62	1.52	Mudstone	
		3	4152	13.14	14.66	Sandstone	
		4	35	∞	∞	Mudstone	
VES 4 26°24'50.18"E 33°11'43.53"S	4	1	209	0.90	0.90	Top soil	HK
		2	25	0.73	1.63	Mudstone	
		3	4152	13.10	14.8	Sandstone	
		4	36	∞	∞	Mudstone	
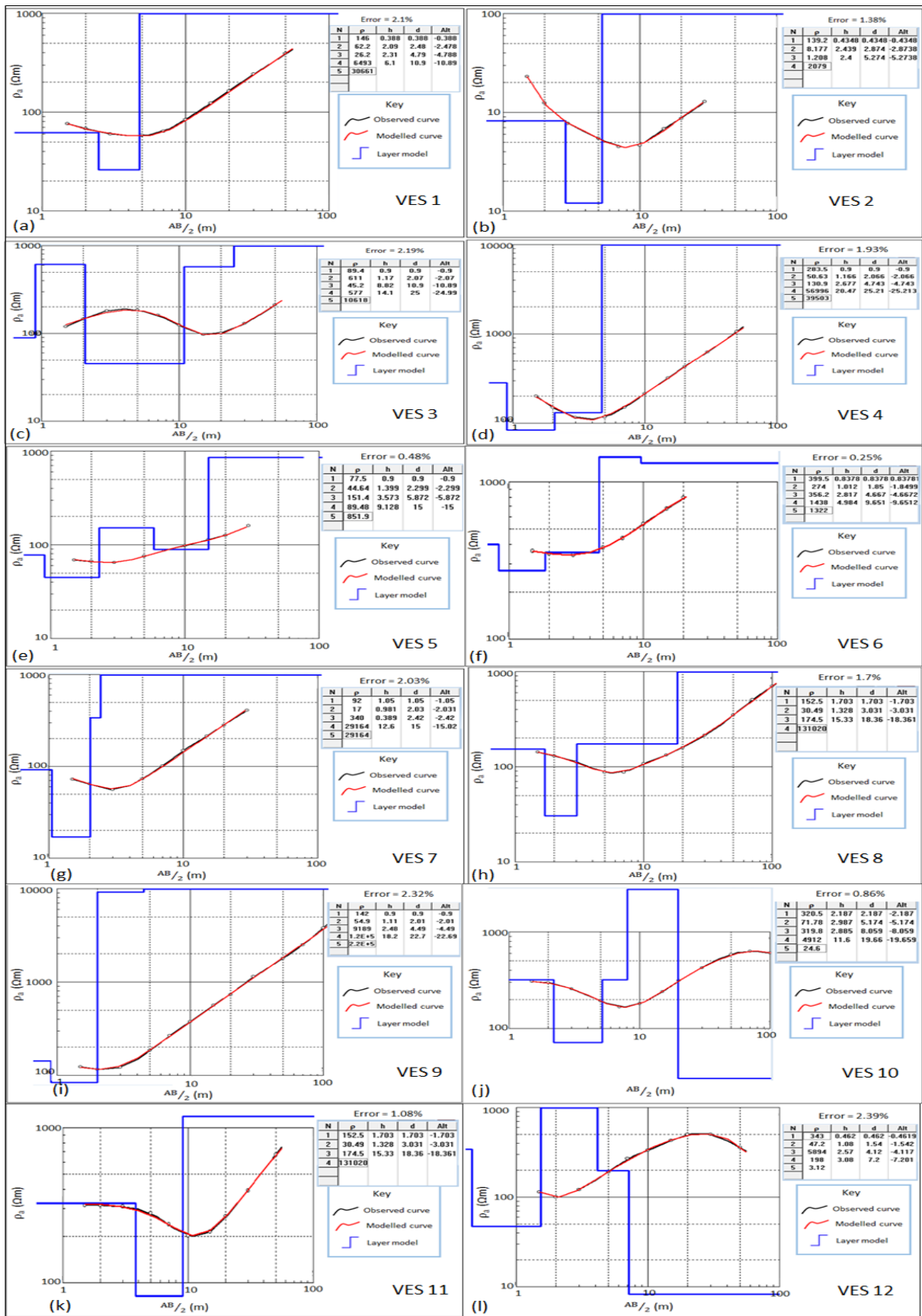
Figure 10.12: VES curves and geoelectric models for twelve sites along Regional road R67 between Grahamstown and Fort Beaufort (Ecca pass).

Table 10.7: Summary of the interpretation of VES sites 1-12 obtained along Ecca Pass section.

Sounding site and location	Number of layers		Resistivity (Ωm)	Thickness (m)	Depth (m)	Inferred lithology	Curve type
VES 1 26⁰37'38.3"E 33⁰12'59.7"S	5	1	146	0.39	0.39	Top soil	QHA
		2	62	2.09	2.48	Mudstone	
		3	26	2.31	4.79	Consolidated shale	
		4	6493	6.1	10.90	Weathered dolerite intrusion	
		5	30661	∞	∞	Dolerite intrusion	
VES 2 26⁰37'38.1"E 33⁰12'58.1"S	4	1	139	0.43	0.43	Top soil	QH
		2	8	2.44	2.87	Clays	
		3	1	2.40	5.27	Clays/tuff	
		4	2079	∞	∞	Sandstone	
VES 3 26⁰37'34.0"E 33⁰12'55.4"	5	1	89	0.90	0.90	Top soil	KHA
		2	611	1.17	2.07	Sandstone	
		3	45	8.82	10.90	Mudstone	
		4	577	14.10	25.00	Consolidated shale	
		5	10618	∞	∞	Dolerite intrusion	
VES 4 26⁰37'20.2"E 33⁰12'46.8"S	5	1	284	0.90	0.90	Top soil	HAK
		2	51	1.17	2.07	Mudstone	
		3	131	2.68	4.74	Consolidated shale	
		4	556996	20.47	25.21	Dolerite intrusion	
		5	139503	∞	∞	Dolerite intrusion	
VES 5 26⁰37'20.3"E 33⁰12'41.0"S	5	1	78	0.90	0.90	Top soil	HKH
		2	45	1.40	2.30	Mudstone	
		3	151	3.57	5.87	Weathered sandstone	
		4	89	9.13	15.00	Mudstone	
		5	852	∞	∞	Consolidated shale	
VES 6 26⁰37'21.4"E 33⁰12'38.3"S	5	1	400	0.84	0.84	Top soil	HAK
		2	274	1.01	1.85	Consolidated shale	
		3	356	2.82	4.67	Sandstone	
		4	1438	4.98	9.65	Consolidated shale	
		5	1322	∞	∞	Sandstone	
VES 7 26⁰37'19.8"E 33⁰12'37.1"S	5	1	92	1.05	1.05	Top soil	HAA
		2	17	0.98	2.03	Clays	
		3	340	0.39	2.42	Sandstone	
		4	29164	12.60	15.00	Dolerite intrusion	
		5	29165	∞	∞	Dolerite intrusion	
VE 8 26⁰37'20.0"E 33⁰12'28.1"S	4	1	153	1.70	1.70	Top soil	HA
		2	30	1.33	3.03	Mudstone	
		3	175	15.33	18.36	Sandstone	
		4	131020	∞	∞	Dolerite intrusion	
VES 9 26⁰37'15.1"E 33⁰12'14.8"S	5	1	142	0.90	0.90	Top soil	HAA
		2	55	1.11	2.01	Mudstone	
		3	9189	2.48	4.49	Weathered dolerite intrusion	

		4	120000	18.2	22.70	Dolerite intrusion	
		5	220000	∞	∞	Dolerite intrusion	
VES 10 26°37'02.6"E 33°11'43.6"S	5	1	321	2.19	2.19	Top soil	HAK
		2	72	2.99	5.17	Mudstone	
		3	320	2.89	8.06	Consolidated shale	
		4	4912	11.6	19.66	Sandstone	
		5	25	∞	∞	Mudstone	
VES 11 26°36'43.8"E 33°11'03.8"S	4	1	153	1.70	1.70	Top soil	HA
		2	30	1.33	3.03	Mudstone	
		3	174	15.33	18.36	Sandstone	
		4	131020	∞	∞	Dolerite intrusion	
VES 12 26°36'46.4"E 33°10'55.7"S	5	1	343	0.46	0.46	Top soil	HKQ
		2	47	1.08	1.54	Mudstone	
		3	5894	2.57	4.12	Weathered dolerite intrusion	
		4	198	3.08	7.20	Consolidated shale	
		5	3	∞	∞	Clays	
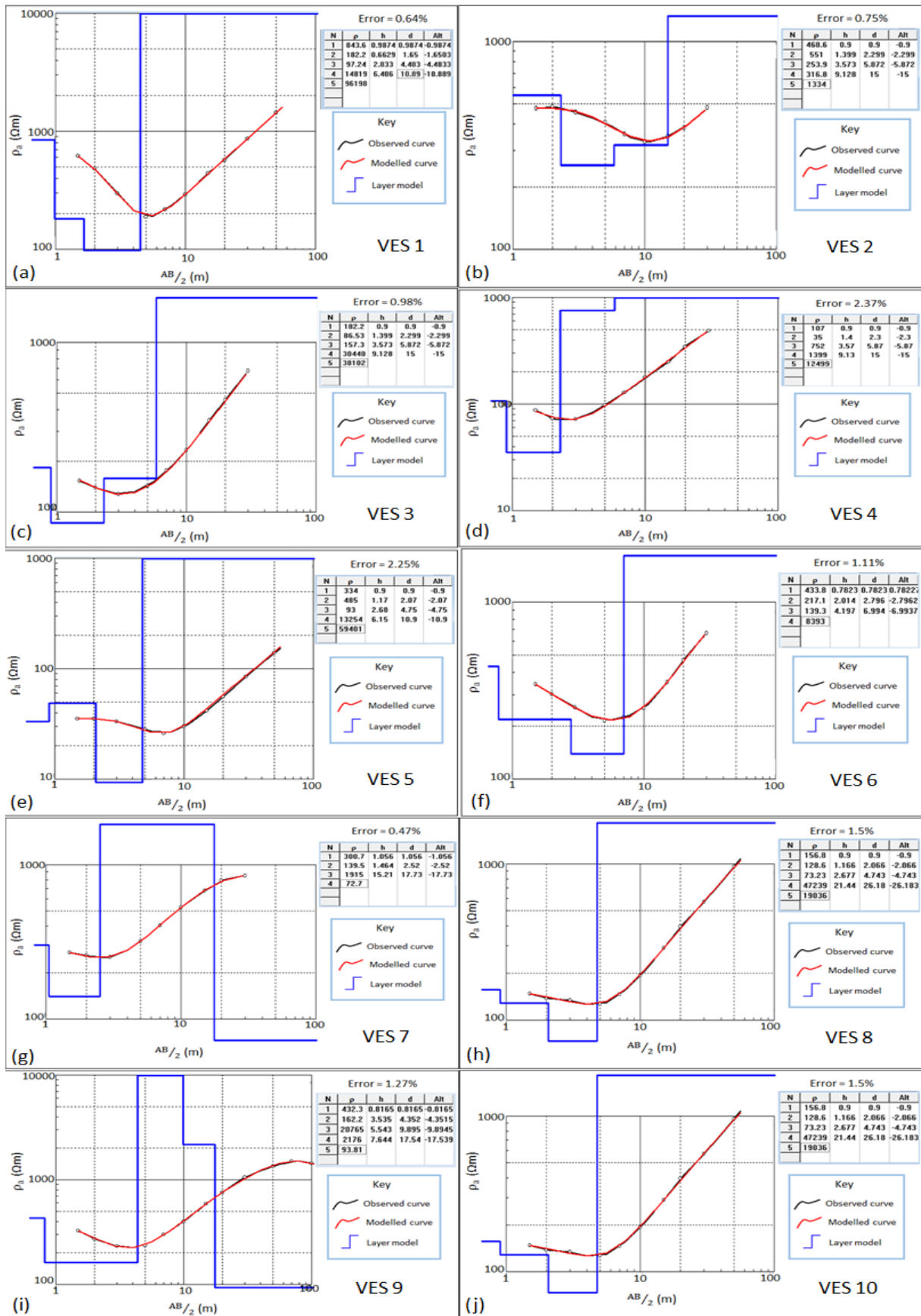
Figure 10.13: VES curves and geoelectric models for ten sites along National road N2 between Grahamstown and Peddie.

Table 10.8: Summary of the interpretation of VES sites 1-10 obtained along Peddie section.

Sounding site and location	Number of layers		Resistivity (Ωm)	Thickness (m)	Depth (m)	Inferred lithology	Curve type
VES 1 26⁰55'48.0"E 33⁰15'45.2"S	5	1	844	0.99	0.99	Top soil	QHA
		2	182	0.66	1.65	Weathered sandstone	
		3	97	2.83	4.48	Mudstone	
		4	14819	6.41	10.89	Weathered dolerite intrusion	
		5	96198	∞	∞	Dolerite intrusion	
VES 2 26⁰55'49.6"E 33⁰15'42.9"S	5	1	469	0.90	0.90	Top soil	KHA
		2	551	1.40	2.30	Consolidated shale	
		3	254	3.57	5.87	Sandstone	
		4	317	9.13	15.00	Consolidated shale	
		5	1334	∞	∞	Sandstone	
VES 3 26⁰55'51.4"E 33⁰15'41.5"S	5	1	182	0.90	0.90	Top soil	HAA
		2	87	1.40	2.30	Mudstone	
		3	157	3.57	5.87	Weathered sandstone	
		4	30440	9.13	15.00	Dolerite intrusion	
		5	38102	∞	∞	Dolerite intrusion	
VES 4 26⁰55'53.0"E 33⁰15'40.3"S	5	1	107	0.90	0.90	Top soil	HAA
		2	35	1.40	2.30	Mudstone	
		3	752	3.57	5.87	Consolidated shale	
		4	1399	9.13	15.00	Sandstone	
		5	12499	∞	∞	Weathered dolerite intrusion	
VES 5 26⁰56'02.0"E 33⁰15'32.5"S	5	1	334	0.90	0.90	Top soil	KHA
		2	485	1.17	2.07	Sandstone	
		3	93	2.68	4.75	Mudstone	
		4	13254	6.15	10.90	Weathered dolerite intrusion	
		5	59401	∞	∞	Dolerite intrusion	
VES 6 26⁰56'03.6"E 33⁰15'30.6"S	4	1	433	0.78	0.78	Top soil	QH
		2	217	2.01	2.80	Sandstone	
		3	139	4.20	6.99	Consolidated shale	
		4	8393	∞	∞	Weathered dolerite intrusion	
VES 7 26⁰56'05.4"E 33⁰15'29.3"S	4	1	301	1.06	1.06	Top soil	HK
		2	140	1.46	2.52	Consolidated shale	
		3	1915	15.21	17.73	Sandstone	
		4	73	∞	∞	Weathered sandstone	
VE 8 26⁰56'17.4"E	5	1	492	0.69	0.69	Top soil	HAK
		2	92	1.13	1.82	Weathered sandstone	

33°15'27.7"		3	19457	2.92	4.74	Weathered dolerite intrusion	
		4	86890	20.26	25.00	Dolerite intrusion	
		5	41099	∞	∞	Dolerite intrusion	
VES 9 26°56'33.9"E 33°15'26.4"S	5	1	432	0.82	0.82	Top soil	HKQ
		2	162	3.54	4.35	Weatheredsandstone	
		3	20765	5.54	9.90	Dolerite intrusion	
		4	2176	7.64	17.54	Sandstone	
		5	94	∞	∞	Consolidated shale	
VES 10 26°59'58.0"E 33°14'16.8"S	5	1	157	0.90	0.90	Top soil	QHK
		2	129	1.17	2.07	Weathered sandstone	
		3	73	2.68	4.74	Mudstone	
		4	47239	21.44	26.18	Dolerite intrusion	
		5	19036	∞	∞	Dolerite intrusion	

10.4.2.2 Apparent resistivity pseudosections

Apparent resistivity pseudosections were created by combining resistivity sounding data for several sites along the same line (Figures 10.14-10.19). The VES sites are not exactly co-linear and as such it was assumed that there is no change in geology over a small area. The inverse model (Figure 10.14c) of the data obtained along Regional road R335 to Somerset East shows a general increase in apparent resistivity with depth. The 2-D resistivity structure delineated a low resistive top layer with resistivity values of < 20 Ωm, typical of clays (top soil). This is followed by a layer of resistivity values varying between 20 Ωm and 150 Ωm and is inferred to have a composition (resistivity values) similar to mudstone and siltstone. The third layer has resistivity values varying between 150 Ωm and 200 Ωm, and is interpreted to be weathered sandstones. The resistivity of the fourth layer varies from 200 Ωm to 2000 Ωm. This layer is inferred to be consolidated shale as shown in Table 10.3. At a depth of about 12 m, and distance between 157 m and 269 m (Figure 10.14c), a more resistive body tends to compress the overlying sedimentary units as it attempts to get to the surface. This resistive body with apparent resistivity of > 2500 Ωm is inferred to be dolerite intrusion.

The pseudosection shown in Figure 10.15 is generated from data obtained on road-cut exposure of the Ecca Group along National road N10 to Cookhouse. Up to a depth of about 13 m, the sediments in the area are characterized by low apparent resistivities, varying between 30 Ωm and 3300 Ωm (Figure 10.15c). The apparent resistivity generally decreases in N-S direction along the section or profile. Between the depth of about 2 m and 5 m, and

distance of about 280 m and 305 m (Figure 10.15c), a more resistive body (> 340 Ωm; reddish colour) underlies a pocket of less resistive unit and also outcrop to the surface between the distance of 281 m and 289 m. This resistive body with apparent resistivity between 1200 Ωm and 3300 Ωm is inferred to be either consolidated shale or sandstone. Figures 10.16 and 10.17 show the 2-D resistivity structures along Regional roads R350 to Bedford and R344 to Adelaide. The inverse models for these sections in Figures 10.16c and 10.17c show a similar pattern or trend with Figure 10.14, thus they are not described to avoid repetition. The only noticeable difference in the model is that, in Figure 10.16c, the inferred third layer of resistivity values between 400-575 Ωm is exposed to the surface, whereas in Figures 10.14c and 10.17c, the layer is buried at shallow depth below the surface. The inverse model in Figure 10.18c is characterized by low and high resistivities, with high resistivities (> 3500 Ωm) predominating. The low resistive units with resistivity varying from about 1 Ωm to 2000 Ωm occurred from the surface up to an average depth of about 20 m. These units correspond to the sedimentary rocks of the Ecca Group and based on their resistivity values, they are inferred to be top soil (clays), mudstones and consolidated shale. Areas with apparent resistivity values between 2000 Ωm and 5000 Ωm are thought to be sandstones. On the other hand, the more resistive unit(s) occurring at depth of about 20 m up to 104 m and having resistivity values of > 5000 Ωm is inferred to be dolerite intrusions. The inverse model (Figure 10.19c) of the data set obtained along National road N2 to Peddie shows two low resistivity anomalies on either ends of the line (< 840 Ωm). The anomalies have been interpreted as top soil. Furthermore, Figure 10.19c also indicate high resistivity values (>4000 Ωm) and this layer is inferred to be dolerite intrusions occurringat depth of about 16 m up to 79 m below the surface.
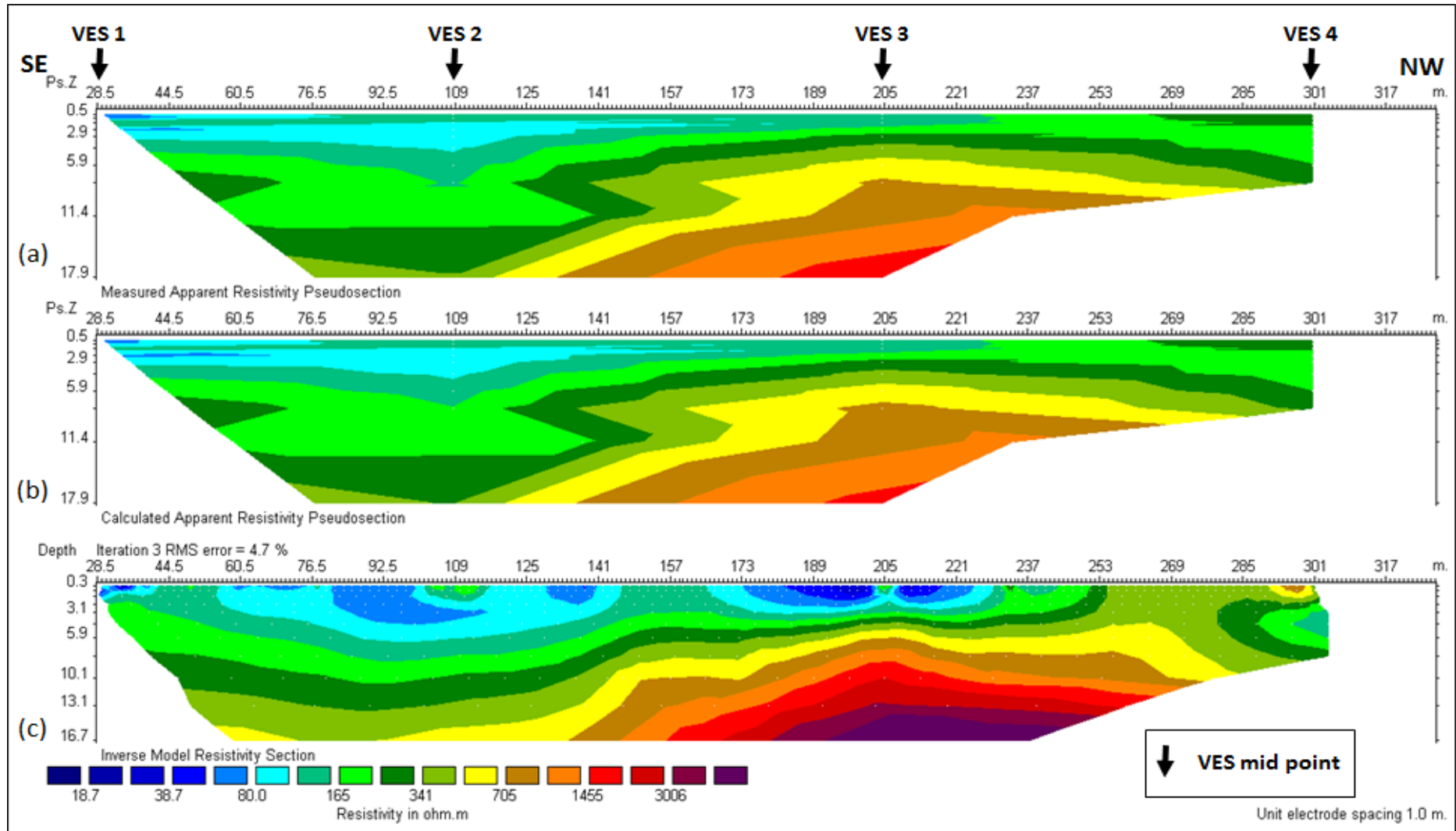
Figure 10.14: Pseudosection of the measured and calculated apparent resistivity data using a Schlumberger array on road-cut exposures of the Ecca Group along Regional road R335 between Somerset East and Kirkwood.
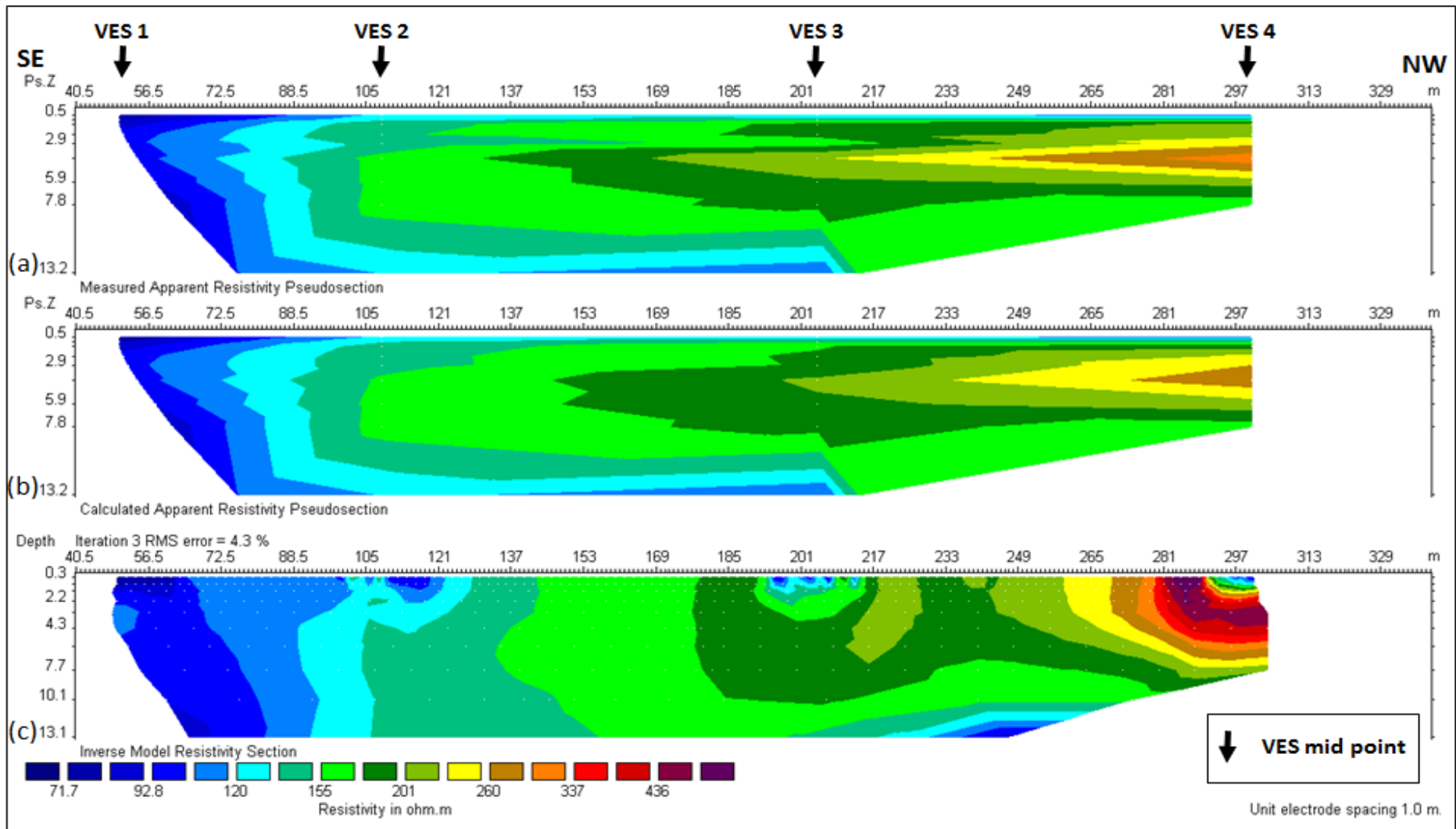
Figure 10.15: Pseudosection of the measured and calculated apparent resistivity data using a Schlumberger array on road-cut exposures of the Ecca Group along National road N10 between Paterson and Cookhouse.
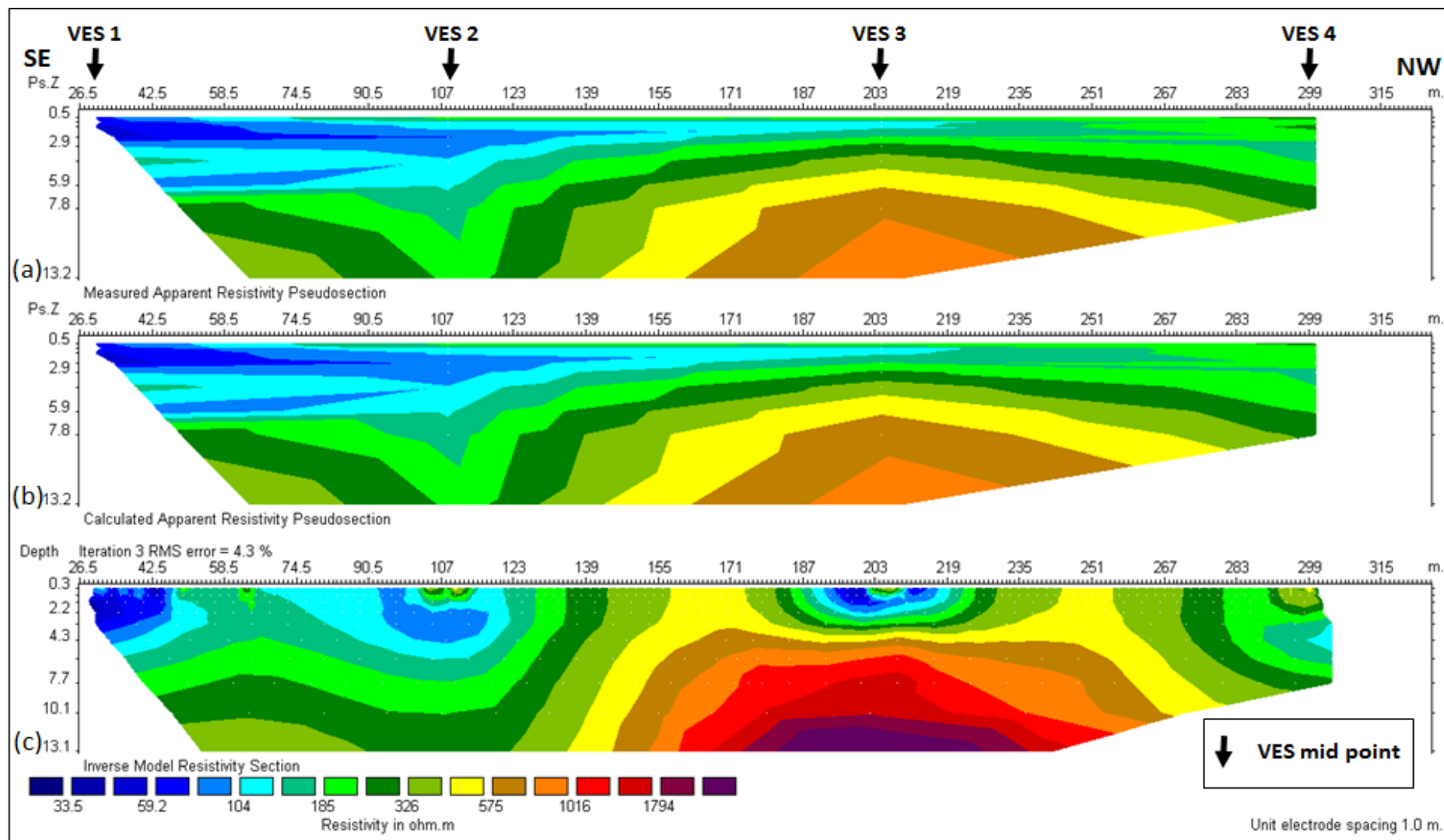
Figure 10.16: Pseudosection of the measured and calculated apparent resistivity data using a Schlumberger array on road-cut exposures of the Ecca Group along Regional road R350 between Grahamstown and Bedford.
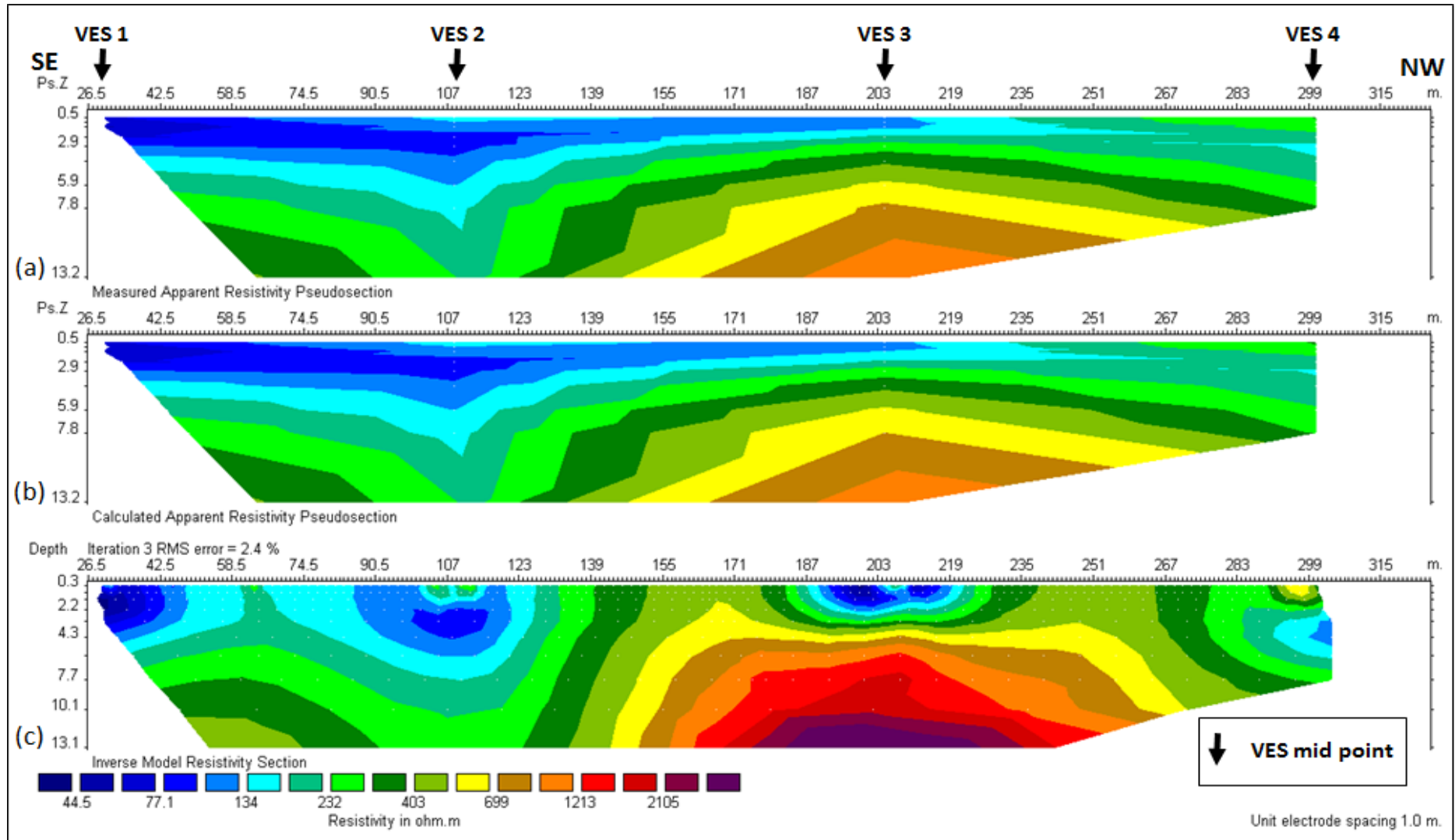
Figure 10.17: Pseudosection of the measured and calculated apparent resistivity data using a Schlumberger array on road-cut exposures of the Ecca Group along Regional road R344 between Grahamstown and Adelaide.
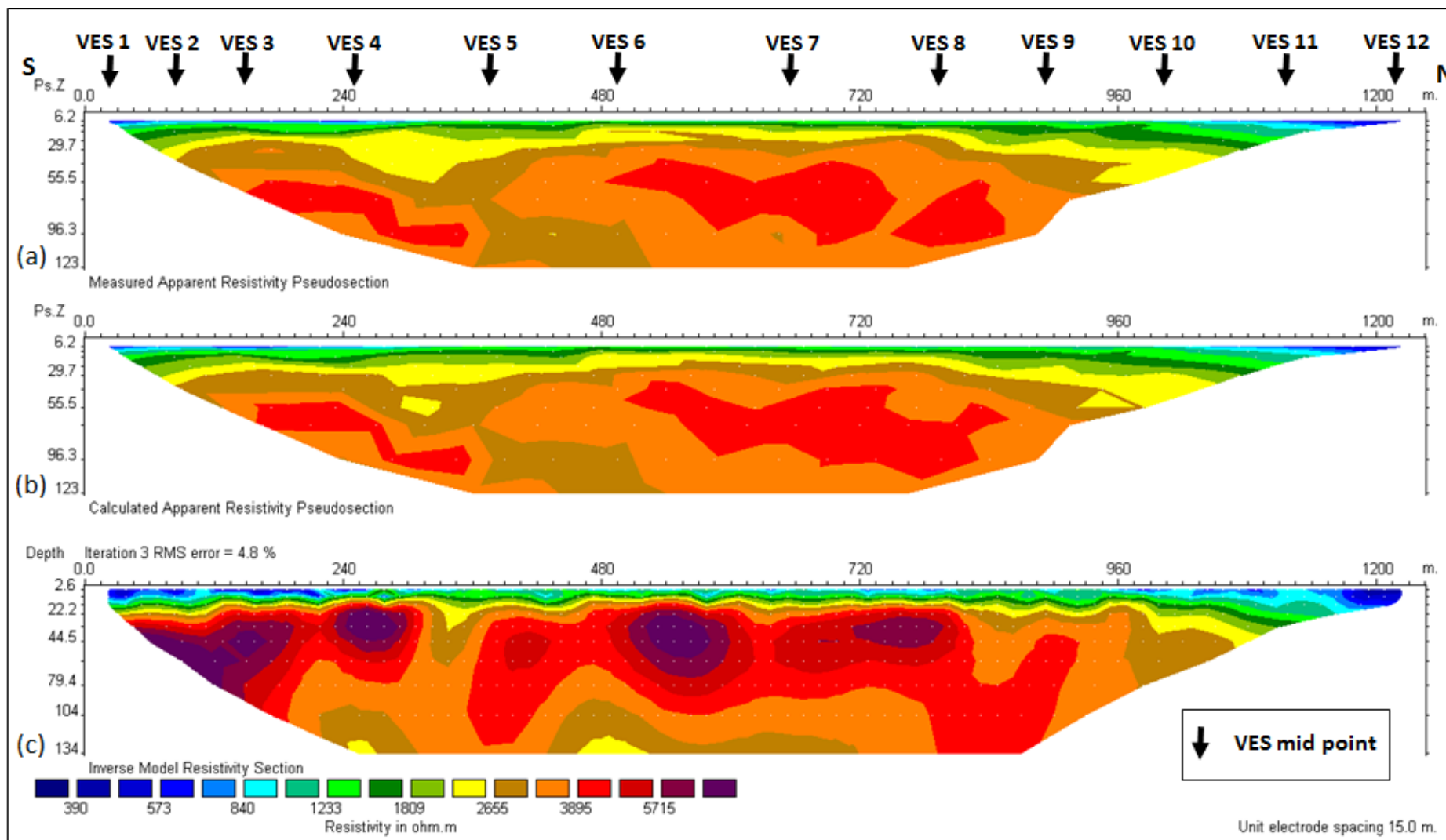
Figure 10.18: Pseudosection of the measured and calculated apparent resistivity data using a Schlumberger array on road-cut exposures of the Ecca Group along Regional road R67 between Grahaamstown and Fort Beaufort (Ecca Pass).
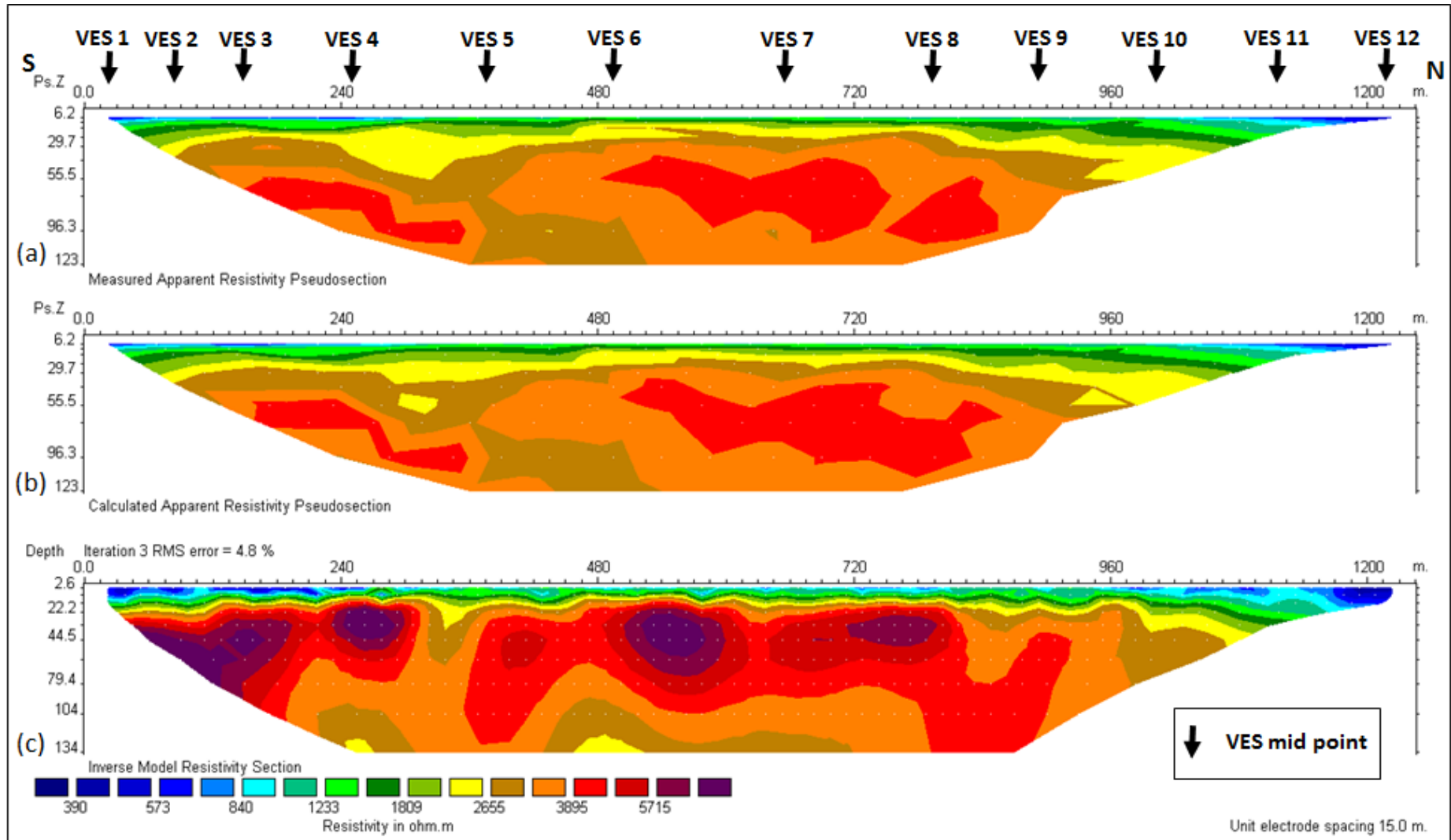
Figure 10.19: Pseudosection of the measured and calculated apparent resistivity data using a Schlumberger array on road-cut exposures of the Ecca Group along National road N2 between Grahamstown and Peddie.

The lower Ecca Group formations (Prince Albert, Whitehill and Collingham Formations) are considered to be one of the most prospective areas for shale gas exploration in South Africa. In the study area, VES 1 in Figures 10.14-10.17, and VES 1 and 2 in Figures 10.18 and 10.19 were carried out on exposure of the lower Ecca Group formations, these areas are characterised by low resistivity values compared to other areas along the same section. However, in Figures 10.14 and 10.15, the area between the distance of 180 m and 220 m in the upper Ecca Group formations (Ripon and Fort Brown Formations) have lower resistivity values than thelower Ecca Group formations. These areas outcrop to the surface along some sections and correspond to the carbonaceous shale of the Lower Grey Greywacke-Mudstone Member in the Ripon Formation (Discussed in Chapter 3). Different factors have been used to explain the low resistivity or high conductivity of the Ecca shales; these include increased pyrite content (Duba et al., 1994), enrichment in graphite (Pous et al., 2004), and enrichment in organic matter (Branch et al., 2007). Nevertheless, it is important to note that in the Karoo Basin, the Whitehill Formation is an extensive geophysical (magnetotelluric) marker that is potentially important for shale gas exploration (Weckmann et al., 2007a; 2007b).

With the exception of the Cookhouse section, all the measured sections have been intruded by dolerites. The effect of the network of dolerite intrusions on sounding curves depends on its form, dimensions, density of intrusions within it and their mode of occurrence. The general forms of these dolerite intrusions are sills, inclined sheets and dykes within a matrix of sediments (Figures 10.18-10.19). Due to the hardness and high resistivity of dolerite intrusions, they are likely to introduce a technical difficulty in the drilling stage of the hydraulic fracturing process, which will in turn reduce the recovery factor and lower the technically recoverable sources. Generally, the dolerite intrusions (mostly sills) are impermeable and act as barriers for fluid migration. As mentioned in Chapter 9, the lower Ecca Group is organically enriched, with TOC of the Prince Albert, Whitehill and Collingham Formations reaching up to 6.35 wt.%, 7.3 wt.% and 0.93 wt.%, respectively. During the intrusion of dolerites, temperatures at the contact (contact metamorphism) may have likely exceeded 1000 ℃, resulting in thermal cracking of organic matter and devolatization of water bearing minerals (Aarnes et al., 2010). The extent to which these dolerites (i.e. dykes) thermally cracked the lower Ecca shale will be important in the quantification of the natural gas that remains in the carbonaceous shale. Observations from borehole studies by Svensen et al. (2007), Aarnes et al. (2011), and this study (Chapter 9) revealed that carbonaceous shales of the lower Ecca Group at contacts with dolerites

appeared to be pale grey rather than the characteristic dark grey to black colour. In addition, the organic geochemistry results showed that the Ecca shales have lower TOC (wt.%) content in areas that are intruded by dolerites or close to dolerite intrusions. Several researchers (i.e. Rowsell and De Swardt, 1976; Svensen et al., 2007; Aarnes et al., 2011) have documented that rapid heating from multiple dolerite intrusions could be directly related to the sharp decrease in organic carbon content and increase in vitrinite reflectance in the host rocks of the lower Ecca Group.

10.5 Conclusions

HRP and VES technique have proven to be successful and highly effective in the identification and delineation of subsurface structures. Based on the results presented in this chapter, the following conclusions can be inferred:

- The isoapparent resistivity map shows five main electrical (resistivity) anomalies. Three of the anomalies (low resistivity) occurred along Regional roads R335 to Somerset East and R350 to Bedford. These areas with low apparent resistivity values are inferred to be as a result of buried rock or soil with high clay and/or moisture and water content.

- The VES curves are predominantly combination of HA, HK, KH, QH, AAK, HAA, HAK, HKH, HKQ, KHA and QHA curve-types indicating four to five geoelectric layers. These layers are topsoil, mudstone, sandstone, consolidated shale and dolerite intrusion.

- The resistivity and thickness of these layers varies between $1\Omega m$ and $556996\ \Omega m$, 0.27 m and 19 m, respectively. The inverted apparent resistivity pseudosections exhibit gradational change in resistivity with depth, indicating the different rock units.

- The lower Ecca Group is generally characterised by low resistivity values compared to the upper Ecca Group. These low resistivities (high conductivities) are thought to be as a result of high organic matter and pyrite contents in the lower Ecca shales.

- With the exception of the Cookhouse section, all the measured sections have been intruded by dolerites. The general forms of these dolerite intrusions are sills and dykes within a matrix of sediments. Due to the hardness and high resistivity of dolerite intrusions, they are likely to introduce a technical difficulty in the drilling stage of the hydraulic fracturing process, which will in turn reduce the recovery factor.

CHAPTER 11

SEDIMENTATION RATE AND SUBSIDENCE HISTORY

Abstract

Backstripping analysis has been carried out on five boreholes and one outcrop section of the Ecca Group in the Main Karoo Basin of South Africa to determine the sedimentation rate and subsidence history of the basin. The result shows that the rate of sedimentation for the Prince Albert, Whitehill, Collingham, Ripon and Fort Brown Formations range between 0.003-0.03 mm yr^{-1}, 0.02-0.05 mm yr^{-1}, 0.01-0.05 mm yr^{-1}, 0.03-0.22 mm yr^{-1}, and 0.15-0.025 mm yr^{-1}, respectively. The backstripped subsidence curves that are constructed by removing the effects of decompaction to the water column and sediment loads show subsidence rates decreasing with time, resembling the typical thermal subsidence curves of passive continental margins. Three major subsidence episodes characterised the Ecca Group, namely: (1) rapid subsidence in an extensional regime; (2) slow subsidence in the middle of basin development; and (3) another rapid subsidence in a compressional regime. The aforementioned subsidence episodes show that the southeastern Karoo Basin was located on a passive continental margin, suggesting that the subsidence was initiated and mainly controlled by mechanical (gravitational) loading or tectonic events, with little contribution of thermal events. The average rate of tectonic subsidence in the Prince Albert, Whitehill, Collingham, Ripon and Formations are 63 mMa^{-1}, 28 mMa^{-1}, 25 mMa^{-1}, 215 mMa^{-1}, and 180 mMa^{-1}, respectively. It is also inferred that the southeastern Karoo Basin evolved from a passive continental margin into an Andean-type continental foreland basin, thus portraying a complete evolved post-rift subsidence history along the southeastern Gondwana margin.

Keywords: Backstripping, sedimentation rate, tectonic subsidence, palaeobathymetry, Karoo

11.1 Introduction

Sedimentary basins provide a record of mostly vertical tectonic movement. More precisely, accumulations of marine and fluvial sediments of about 5 km thick suggest that progressive subsidence occurred to accommodate the sedimentary infill (Gallagher, 1989). A common approach used in analysing subsidence of sedimentary basin is the reconstruction of sediment accumulation as a function of time. Primarily, sedimentary basin subsidence can be attributed to three processes, namely tectonic subsidence, water and sediment loading, and sedimentary compaction. Tectonic subsidence refers to the sinking of the basement in the absence of water

and sediments. It is controlled by tectonic forces that are associated with the basin formation and evolution. The effect of water and weight of sediments in the basin is referred to as water and sediment loading, whereas sediment compaction is the decrease in sediment volume as they are buried and compacted.

Backstripping is a method used to quantitatively estimate the depth that the basement would be in the absence of sediment and water loading (Watts and Ryan, 1976). It is possible to deduce information on the basin forming mechanisms, by comparing backstripped curves to theoretical curves for basin subsidence and uplift. The main aim of backstripping is to study the subsidence history of a basin by modelling a progressive reversal of the depositional process or by stripping off the successive layers of basin fill sediment. The remaining sediments are decompacted and isostatically restored using Airy (1D) isostasy (Hirsch et al., 2010). The final restoration accounts for new load conditions, palaeowater depth, and isostatic response to the change in loads. Mathematical procedures to calculate tectonic subsidence through time from stratigraphic columns were originally described by Sleep (1971) and discussed by Watts (1978), and van Hinte (1978). Although, backstripping ismostly used in extensional basins where it is employed to determine the magnitude of lithospheric stretching from post rift subsidence rate, it can also be applied to any sedimentary basin, including platforms and foreland basins (Sclater and Christie, 1980; Cloetingh et al., 1992; Allen and Allen, 2004; Hirsch et al., 2010; Alao and Mike, 2011; Alao, 2012). To date, backstripping sediment load on the basin basement has proven to be a useful tool for revealing and reconstructing the geodynamic evolution of sedimentary basins (van Hinte, 1978; Allen and Allen, 1990).

Palaeobathymetric and stratigraphic data are employed to quantitatively estimate the depth that the basement would be in the absence of sediments and water loading. This depth allows the determination of the unknown "tectonic driving forces" that are responsible for the formation of the basin (tectonic subsidence or uplift). As a result of this, it has been termed the tectonic subsidence or uplift of the basin. To get reliable reconstructions, some constraints are needed from borehole logs and outcrop successions. First, the data (i.e. age, water depth, stratigraphic thickness and lithological parameters) needs to be corrected or confidently constrained. In addition, the units must be studied along a vertical geological section since geodynamic evolution can vary from place to place within the same sedimentary basin. Thus, it is possible to reconstruct different subsidence curves from different locations within the same sedimentary basin. Conversely, corrections must also be made for subsidence arising

from the isostatic response to sediment loading, and for sediment compaction in response to burial. The earlier stage of basin bathymetry also needs to be constrained using palaeobathymetry estimates. The isostatic response to loading is commonly calculated assuming Airy (1D) isostasy, which involves removing the effects of the sedimentary loading from the total subsidence by calculating the depth of the basin floor below sea level when an interval of sediment load is removed.

Several researchers have investigated the Ecca Group in the southern Karoo Basin (southwestern and southeastern subbasins), which led to the established stratigraphic, subsidence and seismic framework for the southeastern Karoo Basin (i.e. Visser and Loock, 1978; Kingsley, 1981; Cole, 1992; Cloetingh et al., 1992; Catuneanu et al., 1998; 2002; 2005; Johnson et al., 2006; Lindeque et al., 2007; Tankard et al., 2009). Cloetingh et al. (1992) studied the subsidence history analysis and forward modelling of the western and southeastern Cape using the South African Committee for Stratigraphy (SACS, 1980) published sedimentological and stratigraphic data of the Cape and Karoo Supergroup. The magnitude of subsidence obtained from the study of Cloetingh et al. (1992) shows lateral variation in the degree of stretching. This result signifies a shift in the main location of rifting with time, from the southwestern to southeastern Cape, and possibly resulted in the difference in geometry and structure of the Karoo subbasin depocentres at the margin of the southern (southeastern and southwestern) Karoo Basin during Ecca times. Sedimentation and subsidence rates of the southeastern Karoo subbasin are poorly understood up to now. In particular, the evolution of the southeast Gondwana margin in relation to inversion tectonics of the southeastern Karoo Basin along the margin remains unexplored. The backstripping method was applied in this study to five boreholes and 1 road-cut exposure of the Ecca Group (R67 to Fort Beaufort; Ecca Pass) in the Eastern Cape Province of South Africa (Figure 1.1).

 The water-level fluctuations in the southern Karoo Basin may be largely controlled by variations in the ice-volume covering this part of southern Gondwana during the Palaeozoic. Consequently, data from the literature are sparse or of insufficient reliability to provide good estimates of the bathymetry for the southeastern Karoo subbasin. Alao and Mike (2011) and Cloetingh et al. (1992) assumed that the effect of palaeobathymetry and water-level fluctuations on the tectonic subsidence calculations is small or contributes only small variations to the computed subsidence curves. Furthermore, non-tectonic subsidence as a result of loading and non-tectonic isostatic rebound due to removal of water is usually not considered. In this study, we carried out subsidence analysis with and without

palaeobathymetry and water depths data to compare how palaeobathymetry and water-level fluctuations would affect the subsidence curves. The work of Alao (2012) is greatly acknowledged which form the basis of this chapter.

11.2 Materials and method

The 1D Airy backstripping technique was used to reconstruct the subsidence history of the southeastern Karoo subbasin. The tectonic subsidence was computed using the OSXBackstrip program, developed by Cardozo (2012) (University of Stavanger, Norway). The program performs a "1D Airy Backstripping" based on the approach described in Watts (2001) and Allen and Allen (2004) and is used for predicting the tectonic subsidence of sedimentary basins. The backstripping procedure is intended to remove the isostatic subsidence of the basement caused by the weight of the deposited sediment loads. In order to account for the changes in the sediment supply as well as water loading in the basin, a uniform, airy type local isostasy for the lithosphere was assumed (Steckler and Watts, 1978). Nevertheless, this isostatic model is thought to be effective only in early stages of basin development, while in the later stage of basin development, flexural compensation with increasing lateral strength as a result of lithospheric cooling needs to be integrated (Frostick and Steel, 1993).

11.2.1 Data and assumption

The outcrop of the Ecca Group along the Ecca Pass and five boreholes (SC 3/67, SFT 2, CR 1/68, KWV 1 and SP 1/69) were used to quantify subsidence history of the southeastern Karoo Basin. The absence of major unconformities in this section made it possible to assume that existing overburden stresses are essentially the maximum overburden loads experienced by the sediment grains. The data input for the tectonic subsidence or geohistory computation represents five geologic formations of the Ecca Group. The average lithological compaction coefficients, initial porosity and density of the main lithological types (sandstone, siltstone, mudstone and shale) were extracted from Sclater and Christie (1980), Sawyer et al. (1982) and Schmoker and Halley (1982). The non-compacted thickness of each of the five geologic formations of the Ecca Group was calculated and backstripped using the computer program. The stratigraphic and absolute ages of the formations were extracted from literature and are depicted in Table 11.1. The Palaeowater depths during the deposition of the southern Ecca Group were taken from Johnson (1976), Visser and Loock (1978) and Kingsley (1981).

11.2.2 Age assessment

The exact or absolute age of the Ecca Group formations in the southeastern Karoo subbasin is difficult to determine and Alao (2012) documented that, it is as a result of interpreting the "diachroneity of clastic sedimentation, diachronous evolution and following foreland basin migration across the Karoo Basin". Sciunnach and Garzanti (1996) documented that the accuracy of geohistory plots largely depends on the density of biostratigraphic check points, resolution of the available biotas as well as the choice of reference timescale when converting the relative ages into numerical ages. Nonetheless, Loup (1992) reported that the discrepancies in the numerical ages between recent timescales are quite small, and the choice among them does not meaning fully affect the shape of the tectonic subsidence curve. In the present analysis, the age ranges suggested by Bangert et al. (1999), Catuneanu et al. (2005), Johnson et al. (2006), Fildani (2009), Geel et al. (2013; 2015) and McKay et al. (2015) were adopted (Table 11.1). This age range represents the best synthesis presently available and mostly employed or used.

Table 11.1: Lithostratigraphic units of the Ecca and Dwyka Groups in the Karoo Basin.

Unit	Lithology	Age (Ma) Radiometric dates, After Bangert et al.(1999), Catuneanu et al. (2005), Johnson et al. (2006), Fildani (2009), Geel et al. (2013, 2015) and McKay et al. (2015)
Fort Brown Formation	Shale Sandstone	~268-264 Ma
Ripon Formation	Shale Sandstone	~273-268 Ma
Collingham Formation	Sandstone Shale	~275-273 Ma
Whitehill Formation	Siltstone Mudstone	~276-275 Ma
Prince Albert Formation	Shale	~289-276 Ma
Dwyka Group	Diamictite Shale	~302-289 Ma

11.2.3 Decompaction

Decompaction of sediment thickness is the first step towards a correct subsidence interpretation. Undecompacted sediment curves result in the under estimation of initial subsidence, which usually hinders the correct identification of concave-upward curve tracts (i.e. the distinctive pattern of thermal subsidence curves). As documented by Alao (2012),

"decompaction is the running of a unit's compaction history in reverse, and this is achieved by considering a sedimentary rock as a mixture of sedimentary grains and interstitial pores". The volume of sediment grains remains constant, while the water is squeezed out during compaction from the overlying sediment load. The two main methods that are often used in decompaction are:

- An analytical approach to decompaction. This is based on the widely accepted expression for porosity loss with burial (Allen and Allen, 2004).
- Decompaction can also be accounted for by moving the considered layer back up empirical curves of porosity loss with burial (Hamilton, 1959; Bond and Kominz, 1984; Watts and Ryan, 1976; Corfield et al., 2005).

The procedures used in this study to decompact sediments and evaluate the removal of sediment loads on subsidence follow the backstripping or analytical method (Sleep, 1971; Van Hinte, 1978; Sclater and Christie, 1980). This method starts by restoring the original or uncompacted thickness (T_d) of the sedimentary units, beginning from the oldest unit in the stratigraphic section and considering younger units in successive steps. In addition, the method assumes that, during progressive burial in the subsiding basin, sediment compaction is depth dependent (Schmoker and Halley, 1982). The used decompaction procedure is the analytical approach to decompaction, which is based on the widely accepted expression for porosity loss with burial (Allen and Allen, 2004; equation 11.1). The decrease of porosity with depth is depicted for a number of different lithologies in Figure 11.1, which shows that porosity decreases rapidly with depth:

$$\emptyset = \emptyset_0 e^{-cz}, \qquad\qquad [11.1]$$

where $\emptyset$ is the porosity at any depth, $\emptyset_0$ is the porosity at the surface, c is the lithological compaction coefficient and z is the depth in kilometres.
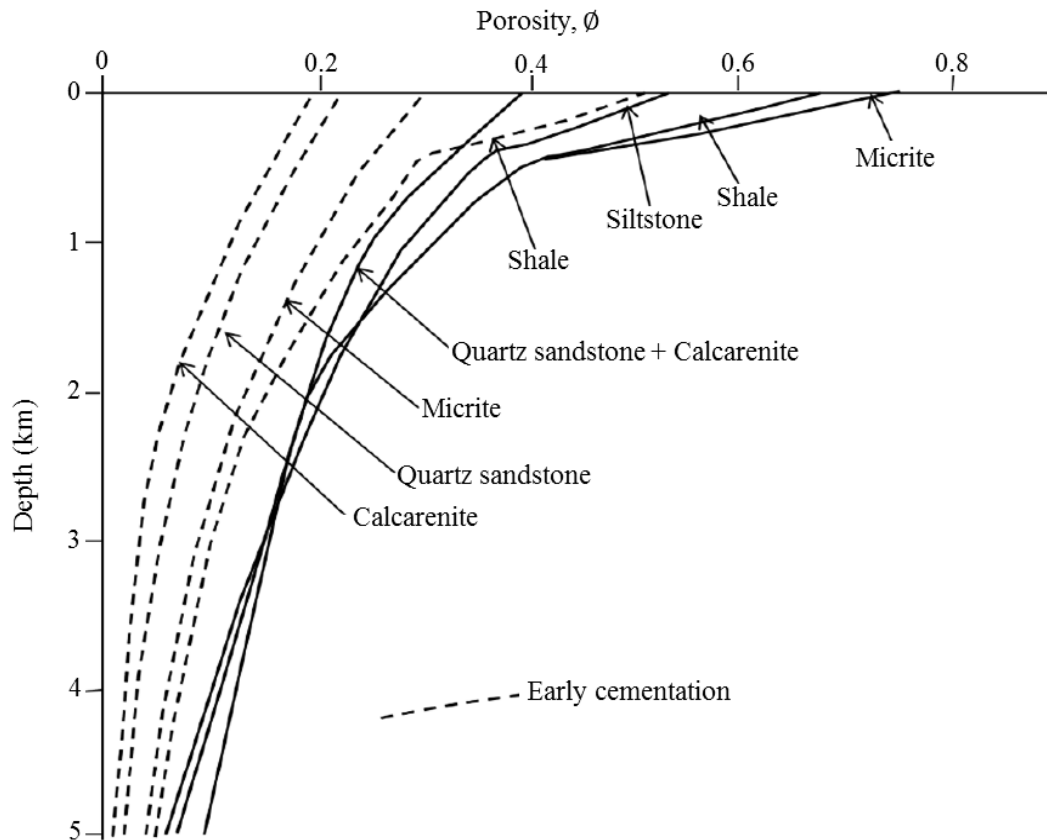
Figure 11.1: Summary of idealized porosity vs. depth curves for different lithologies. Note: the combination of sandstone and Calcarenite (a limestone with sand-grade sized grains) did not undergo early cementation; hence it is far away from the original porosity curve (Taken from Alao (2012), after Bond and Kominz, 1984).

Table 11.2: Compaction coefficients and parameters for the main lithological types (Taken from Alao (2012), after Frostick and Steel, 1993).

Lithology	Initial Porosity, $\emptyset_o$	Compaction Coefficient c (km^{-1})	Sediment grain density, ρ_{sg} (gcm^{-3})	Reference
Shale	0.63	0.51	2.72	Sawyer et al. (1982)
Sandstone	0.56	0.39	2.68	Schmoker and Halley (1982)
Limestone	0.51	0.52	2.71	Sclater and Christie (1980)
Dolomite	0.31	0.22	2.85	Sclater and Christie (1980)
Shaley sand	0.56	0.45	2.70	Sclater and Christie (1980)

To calculate the decompacted thicknesses for each formation of the Ecca Group, average lithological compaction coefficients for three main lithologies (i.e. sandstone, shale and shaley sand) were taken from Frostick and Steel (1993) as shown in Table 11.2 (Taken from

Alao, 2012) and used to calculate the decompacted thickness using equation (11.2) (After van Hinte, 1978):

$$T_d = \left[\frac{T_P(1-\varnothing)}{(1-\varnothing_0)}\right],$$ [11.2]

where T_d is the decompacted thickness, T_P is the present or compacted thickness of the vertical section; $\varnothing$ is the final/present porosity and $\varnothing_0$ is the unconsolidated/initial porosity.

The measured stratigraphic thicknesses can be decompacted by expressing the total volume V_t of the sedimentary column from equation (11.2) as:

$$V_t = V_s + V_w,$$ [11.3]

where V_s is the volume of sediment grains, which remains constant during compaction, and V_w is pore volume, which equals the volume of interstitial water in the case of a water saturated sediments.
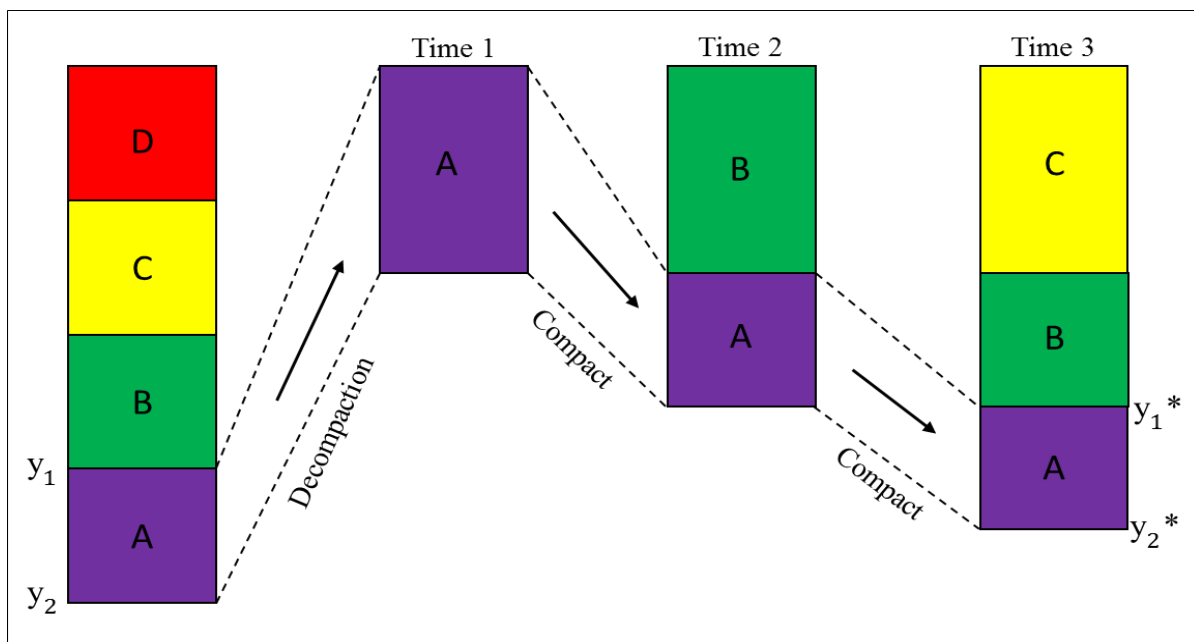
Figure 11.2: Decompaction scheme. Units A, B and C are restored to different depths and thicknesses after removal of the superposed unit D (Modified from Alao (2012), after Allen and Allen, 2004).

The total pore volume (V) of sediment between two generic depths $\mathbf{y_1}$ and $\mathbf{y_2}$ (Figure 11.2) is obtained from equation (11.4):

$$V_w = \varnothing V_t,$$ [11.4]

As the sedimentary column is decompacted (Figure 11.2), the top and bottom of a given sedimentary package are brought to the new depths y_1* and y_2* ($y_1 > y_1*$, $y_2 > y_2*$, $y_2* - y_1* > y_2 - y_1$). A new pore volume $V_w* > V_w$ can thus be calculated. From equation (11.3), the decompacted thickness (V_s plus V_w*) is obtained from equation (11.4) as shown in equations (11.5) and (11.6):

$$\Delta V = V_w(y_1) - V_w(y_2) = \emptyset_0 (e^{-cy_1} - e^{-cy_2})V_t, \qquad [11.5]$$

$$V = \emptyset_0 (e^{-cy_1} - e^{-cy_2})(V_s + V_w), \qquad [11.6]$$

The percentage of decompaction for all the lithostratigraphic units is determined as the total decompacted thickness divided by the total compacted thickness of the section. This is done in order to determine which formation decompacted the most and vice versa.

11.2.4 1D backstripping using Airy isostasy

The 1D Airy backstripping was done using a computer program based on the approach described in Allen and Allen (1990) and Watts (2001). It predicts the subsidence of a basin (a combination of basement and sediment load-driven subsidence with an exponential reduction of porosity). As documented by Alao (2012), the OSXBackstrip program works with three components for data input, namely:

- Lithobase: This comprises lithology-dependent values, including parameters for the decompaction exponential function, such as the initial porosity $\emptyset$ and the porosity reduction coefficient c.
- Strata: These are the general properties of the stratigraphic units, which are independent of the actual well (borehole, outcrop) location, such as sedimentation depth, age, sea level, name of a stratigraphic unit, well or outcrop data, local thickness of strata and lithological composition.
- Plots: The plots are backstrip and tectonic subsidence plots. The backstrip plot is where the progressive decompaction of the sediments can be observed whereas the tectonic subsidence plot is where the total thickness curve, the total subsidence (decompacted) curve, the decompacted curve corrected for sediment are observed.

The type of setting, marine or continental, affects the correction for sedimentary and water loads. In a marine basin (Type 0), any depression is filled with air which has a density approximately zero. Furthermore, in continental basin (Type 1) any depression is filled with air. The OSXBackstrip program's correction for water loading in a continental basin (Type 1)

assumes that sea-level change is the palaeo-elevation of the basin top with respect to present-day sea level. Generally, the first step in backstripping is todetermine the sediment thickness and porosity for each formation or unit, then reconstruct or restore the original sediment thicknesses (T_d) of all the stratigraphic units in a sequence for each time step, compacting the older units and decompacting the younger ones. Finally, the sediment accumulation and sedimentation rates are calculated.

11.2.4.1 Sediment accumulation rates

The rate of fill (R_m) at which the rocks of the Ecca Group accumulated during any interval of time can be calculated. According to Underschultz (1991), to measure the rate at which a particular sedimentary unit accumulated in the basin, the rate of fill, R_a can be expressed as shown below:

$$R_m = \frac{T_d \times \rho\,(1-\varnothing)}{\Delta T},$$

[11.7]

where $\varnothing$ is porosity, T_d is decompacted or present thickness (m), ρ is the rock density (kgm^{-3}),ΔT interval (Ma) during which the unit was deposited.

In addition, the accumulated sediment volume, V (m^3) is easy to calculate from the massaccumulation rate below:

$$V = \frac{R_m \times A \times \Delta T}{\rho},$$

[11.8]

where A is area in m^2

Generally, sedimentation rate (R_{sr}) can be expressed as shown in equation (11.9):

$$R_{sr} = \left[\frac{T_d}{T}\right],$$

[11.9]

11.2.4.2 Total subsidence

The total depth of the southern Karoo Basin during or just after the deposition of the Ecca sediments is the sum of the thickness of the sediments and water depth above the basin fill. The total subsidence was automatically calculated from the 1D Airy subsidence model as well as using the general backstripping equation of Steckler and Watts (1978). The mathematical expression for the general backstripping equation is depicted as:

$$S = \sum_{1}^{i} T_d + PWD_i,$$

[11.10]

where S is the total subsidence, PWD is the palaeowater depth, and T_d is the decompacted thickness.

11.2.4.3 Tectonic subsidence

The tectonic subsidence was calculated from the sediment thickness and the average density of the entire sedimentary sequence at a particular time. This technique removes from each layer the effects of sediment compaction, water and sediment loading, thus giving a tectonic subsidence curve on the time versus sediment thickness graph. Tectonic subsidence computation was done with the OSXBackstrip program. In the local loading model, the "backstripped" thickness Z of a given unit (assuming that water load is ineffective in compacting sediment) was calculated from the general backstripping equation of Steckler and Watts (1978). The mathematical expression is shown below:

$$Z_i = T_d \left[\frac{\rho_m - \rho_s}{\rho_m - \rho_w} \right] + S_L \left[\frac{\rho_m}{\rho_m - \rho_w} \right] + PWD_i, \qquad [11.11]$$

where Z_i represents depth to the tracked horizon corrected for the loading of the sediment (i.e., the amount of tectonic subsidence), T_d is the decompacted thickness, ρ_m is the mean density of the asthenosphere, ρ_s is the density of the sediment column, ρ_w is the mean density of water, S_L is the sea level and PWD_i is the paleowaterdepth for i[-th] formation. Standard values of 3330 kgm[-3] for ρ_m and 1030 kgm[-3] for ρ_w were taken as constants for all calculations. The mean density of the sedimentary column (ρ_s) changes as the thickness of the stratigraphic section changes progressively as the sedimentary units pile up due to compaction. So, it must be calculated or determined step by step, after each formation was deposited. The average density of the sedimentary column (ρ_s) was calculated after the deposition of each formation using theSteckler and Watts (1978) equation:

$$\rho_{si} = \frac{\sum_{i=1}^{i} [\emptyset_i \rho_w + (1 - \emptyset_i) \rho_{sgi}] T_{di}}{S_t}, \qquad [11.12]$$

where ρ_{si} is the mean density of the i[-th] formation, $\emptyset_i$ is the mean porosity of the formation, ρ_{sgi} is the mean sediment grain density, T_{di} is the decompacted thickness and S_t is the total decompacted thickness which is easily determined by adding up all the individual thickness for the formations. At each time-step, the depth of the basement (or total subsidence, S) is calculated by summing up the decompacted thicknesses of the deposited sediments and adopting corrections for palaeobathymetry.

11.2.4.4 Subsidence rate

The rate of subsidence (Rs) was calculated by dividing the total subsidence, S (in meters) by time interval, ΔT (age in Ma) of each formation.

$$Rs = \frac{S}{\Delta T} \qquad\qquad [11.13]$$

11.2.5 Palaeobathymetric and eustatic corrections

Palaeobathymetry or water depth during deposition is usually determined by comparing fossils with modern marine organisms. However, in most cases, the result is not accurate or poor as a result of several uncertainties (van Hinte, 1978). Depth plots for the selected basement after backstripping must be corrected based on palaeobathymetry data. Failure to carry out palaeobathymetric and eustatic corrections in the subsidence plot will lead to deviation or strong deformation of the curves. Bathymetric estimations are usually deduced from palaeoecological and palaeontological data, petrographical composition as well as sedimentary structures in rocks (Frostick and Steel, 1993). Visser and Loock (1978) documented that turbidite, black shale with chert layers, siltstones with ripple marks, limestone lenses and phosphatic nodules are the only lithological criteria that could be considered as water depth indicators in the Ecca. The Dwyka and Ecca Groups were deposited during the seaway transgression into the interior part of the southern Karoo Basin (Visser and Loock, 1978). Nevertheless, at the end of Ecca time, complete regression in the Ecca Group occurred from the limits of the preserved basin (Catuneanu et al., 1998).

The role of sea level changes in subsidence analysis is to control the base level of sedimentation by either raising or lowering the depositional base level. Vail et al. (1977) documented that relative global sea-level was low during the mid Carboniferous (330-315 Ma), which is related to termination of shelf deposition in southern Gondwana. This is reflected by a lack of marine body fossils in the southeastern Karoo subbasin. The lack of marine faunas possibly point to a partially enclosed basin. In addition, restricted oceanic circulation within the morphologically complex basin resulted in anoxic conditions within the water column (Visser, 1992). Hence, Wild (2005) proposed that the basin was not a fully open marine system. Likewise, in the southeastern Karoo subbasin, it is believed that the organic carbon-rich muds were mostly deposited under anoxic conditions, and sedimentation within the Karoo foredeep was very slow (< 10 m/Ma), thus signifying starved conditions (Alao and Mike, 2011). Several researchers like Cole (1992), Johnson et al. (1996) and Catuneanu et al. (1998) have suggested a marine depositional environment for part of the

glacial deposits of the Dwyka Group. Catuneanu et al. (1998) documented that the deeper marine glacial facies of the Dwyka Group including those of the early Ecca Group accumulated during the under-filled phase of the foreland basin. They envisaged that, in the southern part of the basin, the Dwyka succession has a uniform character with lateral continuity of layers; signifying deposition from floating ice within a large marine basin was a dominant process. In order to estimate the amount of tectonic subsidence or uplift purified from eustatic effects, sea-level changes must be quantified through the stratigraphic column, and subtracted from the backstripped subsidence curves.

Generally, it is assumed that sea level represents the uppermost possible depositional base level during sedimentation and variations in this level may be corrected to maintain a constant datum. The relative global sea level curve of Vail (1977), Hallam (1989) and Longman and Sonnenfeld (1996) were used for the sea level corrections in this study (Figure 11.3). The influence of sea-level variations on sedimentation within continental platforms, or interiors, is not obvious, and will certainly depend on the elevation of the region relative to the contemporary sea-level. Based on the global sea level during the Permian Period, as documented by Vail (1977), Hallam (1989) and Longman and Sonnenfeld (1996), an average sea level of 110 m, 90 m, 80 m, 60 m, 20 m were used for Prince Albert, Whitehill, Collingham, Ripon and Fort Brown Formations, respectively (Figure 11.3). The quality of any geohistory analysis is basically dependent upon the quality of palaeo-water depth information available (Roberts et al., 1998), as the water body gives an additional load contribution to the isostatic response of the system and, in turn, to the observed subsidence (Hirsch et al., 2010). Based on the water depths suggested by Johnson (1976), Visser and Loock (1978) and Kingsley (1981), an average water depth of 400 m, 300 m, 220 m, 180 m, 25 m were assigned for the Prince Albert, Whitehill, Collingham, Ripon and Fort Brown Formations, respectively (Figure 11.4).

| | SOUTHERN ECCA FACIES | SEA LEVEL |
| | | (m) |

The figure shows a stratigraphic column with the following units (top to bottom):

- **TRIASSIC** — BEAUFORT GROUP
- **PERMIAN** — ECCA GROUP:
  - FORT BROWN FORMATION
  - RIPON FORMATION
  - COLLINGHAM FORMATION
  - WHITEHILL FORMATION
  - PRINCE ALBERT FORMATION
- **CARBONIFEROUS** — DWYKA GROUP

Sea level axis (m): -100, 0, 100, 200

Curves labelled:
- Longman and Sonnenfeld (1996)
- Hallam (1989)
- After Vail (1977)

Figure 11.3: Relative global sea level change during the deposition of the southern Ecca Group (After Vail, 1977; Hallam, 1989; Longman and Sonnenfeld, 1996).
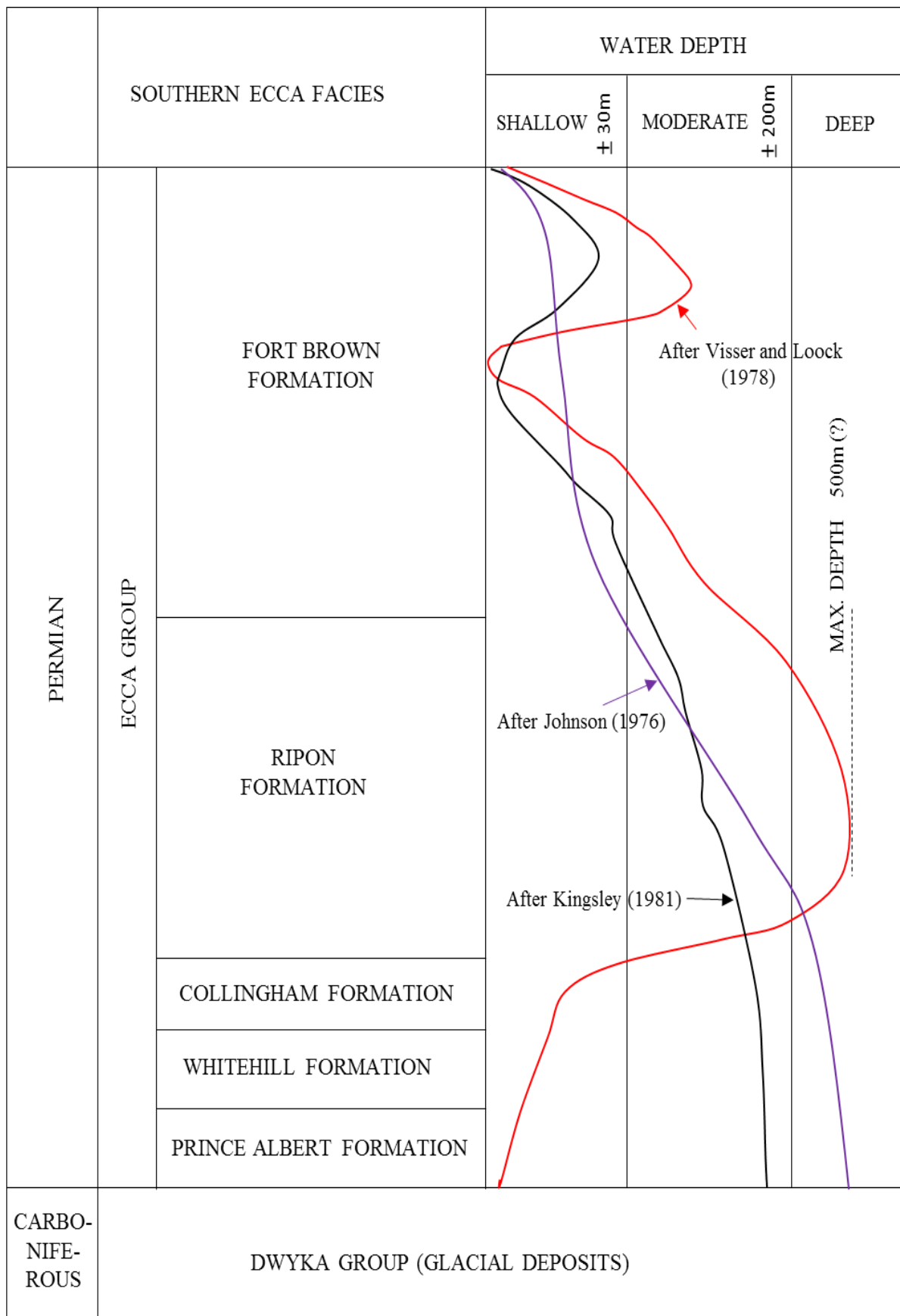
Figure 11.4: Relative water depths during the deposition of the southern Ecca Group (After Johnson, 1976; Visser and Loock, 1978; Kingsley, 1981).

11.2.6 Sources of error

The combined effect of approximations in the input values for $\emptyset_0$ and c was ensured not to exceed $\pm$ 5% of the calculated value for the decompacted thickness (Gallagher, 1989). The layer thickness is measured from well data and outcrops (i.e. stratigraphic sections). Alao (2012) stated that "uncertainties are derived from the unknown amount of erosion or from an erroneous stratigraphic classification". This could result in inaccuracy of the age, based on either "biostratigraphy or chronostratigraphic correlations or geochronology" (Alao, 2012). Quantification of lithological parameters (i.e. porosity, lithology) is often derived from geochemical and sedimentological analyses and geophysical well logs. Therefore, these factors are dependent on the quality of the measurements or analyses. However, the results, although presented quantitatively in this chapter, are believed to be reliable only in a semi quantitative sense, because of the many sources of uncertainty associated with several basic assumptions (i.e. time frame, palaeowater depth, eustasy, choice of a physical model for lithospheric stretching and isostasy versus flexure).

11.3 Results and interpretation

11.3.1 Compaction and decompaction estimates

The calculated compaction and decompaction estimates obtained using equation (4) for porosity at any depth (van Hinte, 1978) are shown in Tables 11.3-11.8. The percentage compaction and porosity at depth were calculated to demonstrate how average porosity of sandstones and shales reduces with depth. Percentage of compaction and decompaction were plotted for each formation to depict the difference in thicknesses between the compacted and decompacted sections of the Ecca formations (Figures 11.5-11.14). The percentage decompaction graph for borehole SC 3/67 (Figures 11.5 and 11.6) shows that, in the Ecca Group, the shales of the Prince Albert, Whitehill and Collingham Formations decompacted the most at 251.6%, 248.4% and 247.8%, respectively. The sandstones lithostratigraphic units of the Fort Brown and Ripon Formations are observed to have a lower percentage decompaction of 145.6% and 205.2%, respectively. However, when considering the percentage compaction, the Fort Brown Formation with the lowest percentage decompaction has the highest percentage compaction at 68.7% and the porosity at any depth (φ) is calculated to be 0.094. Conversely, the Prince Albert Formation with the highest percentage decompaction has the lowest percentage compaction at 39.7% and the porosity at any depth (φ) is calculated to be 0.069. In borehole SFT 2 (Figures 11.7 and 11.8), the Prince Albert

Formation has the lowest percentage compaction and highest percentage decompaction of approximately 81% and 124%, respectively.

In addition, the Ripon Formation has the highest percentage compaction and lowest percentage decompaction of approximately 92% and 109%, respectively. The porosity at any depth varies from about 0.52 to 0.56. In borehole CR 1/68, a percentage compaction ranging from 41 to 56% is calculated for the Ecca Group formations, and the porosity range from 0.092 to 0.132 (Figures 11.9 and 11.10). The percentage compaction, percentage decompaction and porosity ranges from 47.5 to 61.3%, 163.2 to 210.5% and 0.22 to 0.40, respectively, in the Ecca Pass section (Figures 11.11 and 11.12). In borehole KWV 1, the Prince Albert Formation is the most decompacted with percentage decompaction of 218.7%, while the Fort Brown is the most compacted with percentage compaction of about 61% (Figures 11.13 and 11.14). The percentage decompaction graph for borehole SP 1/69 (Figures 11.15 and 11.16) shows that, in the Ecca Group, the Prince Albert Formation has the lowest percentage compaction and highest percentage decompaction of 41% and 245%, respectively. The Ripon Formation has the highest percentage compaction and lowest percentage decompaction of 49% and 203%, respectively. However, when considering the porosity at any depth, the Fort Brown Formation has the highest porosity of about 0.16. Generally, the percentage decompaction is seen to increase with depth, while the calculated porosity decreases with depth.

Table 11.3: Calculated results for porosity at specific depths, decompacted thickness, percent compaction and decompaction, and thickness difference for lithostratigraphic units in borehole SC 3/67. *φ_0 values are from Table 11.2.

Units	Depth to top and bottom (km)	Compacted thickness (m)	Lithology	Porosity at surface φ_0	Porosity at any depth φ	Decompacted thickness (m)	Compaction (%)	Decompaction (%)	Thickness difference (m)
Beaufort Group	0.000-2.684	2684	Shale Sandstone	0.560	0.167	5081	53	189	2397
Fort Brown Formation	2.684-3.734	1007	Shale Sandstone	0.630	0.094	1466	69	146	459
Ripon Formation	3.734-3.901	550	Sandstone Shale	0.560	0.097	1129	49	205	579
Collingham Formation	3.901-3.972	70	Siltstone Mudstone	0.630	0.083	173	40	248	103
Whitehill Formation	3.972-4.023	51	Shale	0.630	0.081	127	40	248	76
Prince Albert Formation	4.023-4.346	323	Shale	0.630	0.069	813	40	252	490
Dwyka Group	4.346-5.343	997	Diamictite	0.560	0.051	2150	46	216	1153
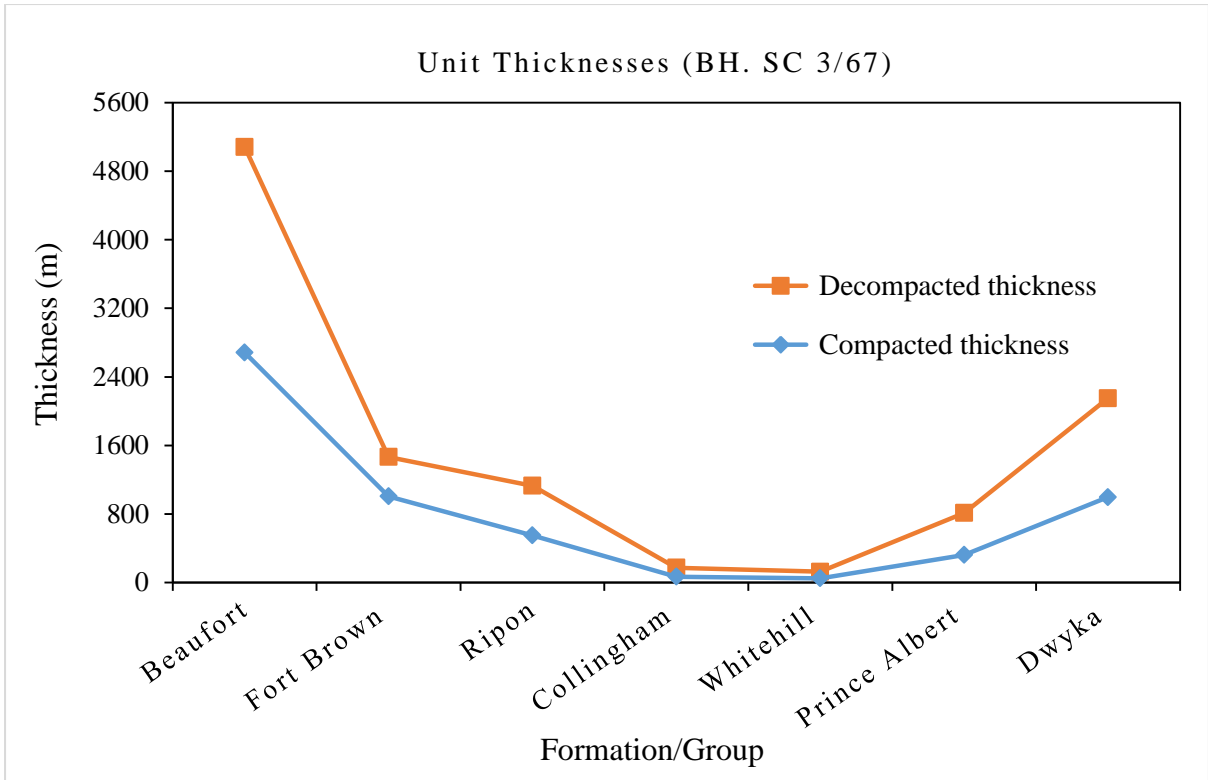
Figure 11.5: The thicknesses of compacted segments compared to decompacted segments in borehole SC 3/67.
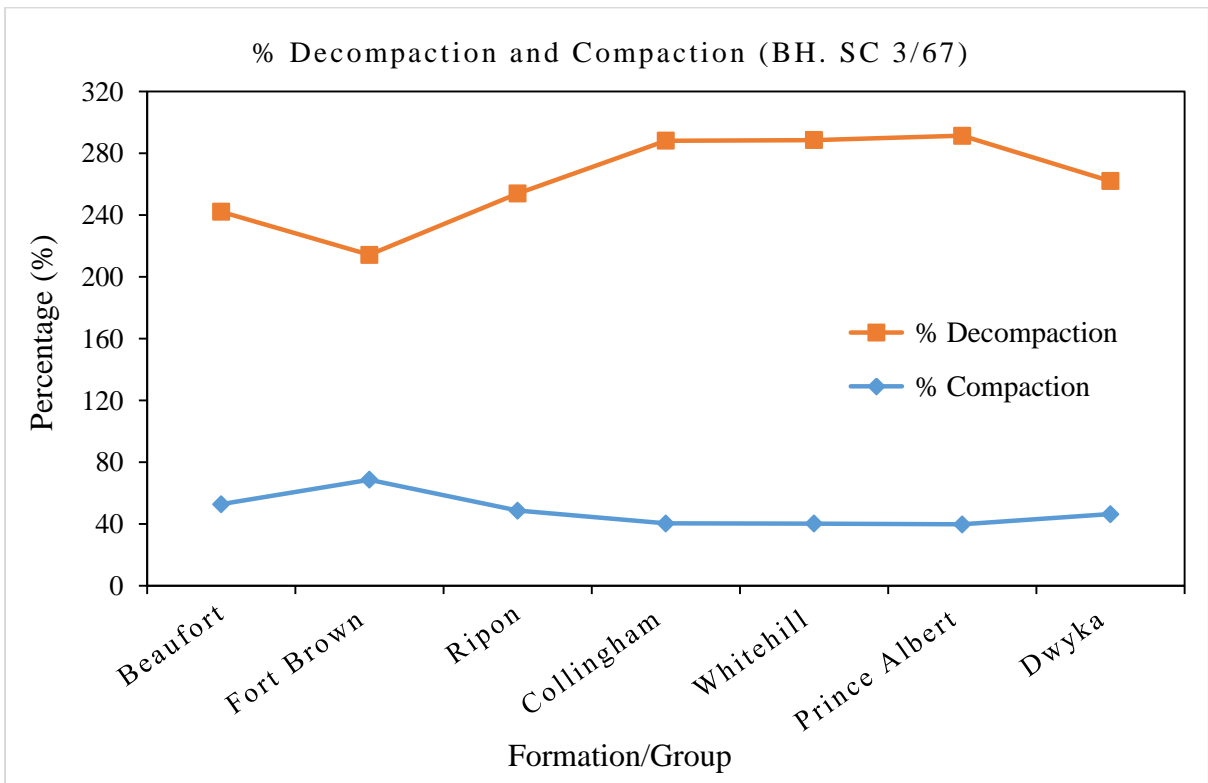
Figure 11.6: The percentage decompaction compared to percentage compaction per formation in borehole SC 3/67.

Table 11.4: Calculated results for porosity at specific depths, decompacted thickness, percent compaction and decompaction, and thickness difference for lithostratigraphic units in borehole SFT 2. $*\varphi_0$ values are taken from Table 11.2 and the thickness values are extracted from Black et al. (2016).

Units	Depth to top and bottom (km)	Compacted thickness (m)	Lithology	Porosity at surface φ_0	Porosity at any depth φ	Decompacted thickness (m)	Compaction (%)	Decompaction (%)	Thickness difference (m)
Ripon Formation	0.000-0.165	165	Sandstone Shale	0.560	0.520	180	92	109	15
Collingham Formation	0.165-0.200	35	Siltstone Mudstone	0.630	0.569	41	86	116	6
Whitehill Formation	0.200-0.226	26	Shale	0.630	0.562	31	84	118	5
Prince Albert Formation	0.226-0.291	65	Shale Mudstone	0.630	0.543	80	81	124	15
Dwyka Group	0.291-0.300	>9	Diamictite Shale	0.560	0.481	11	85	118	2
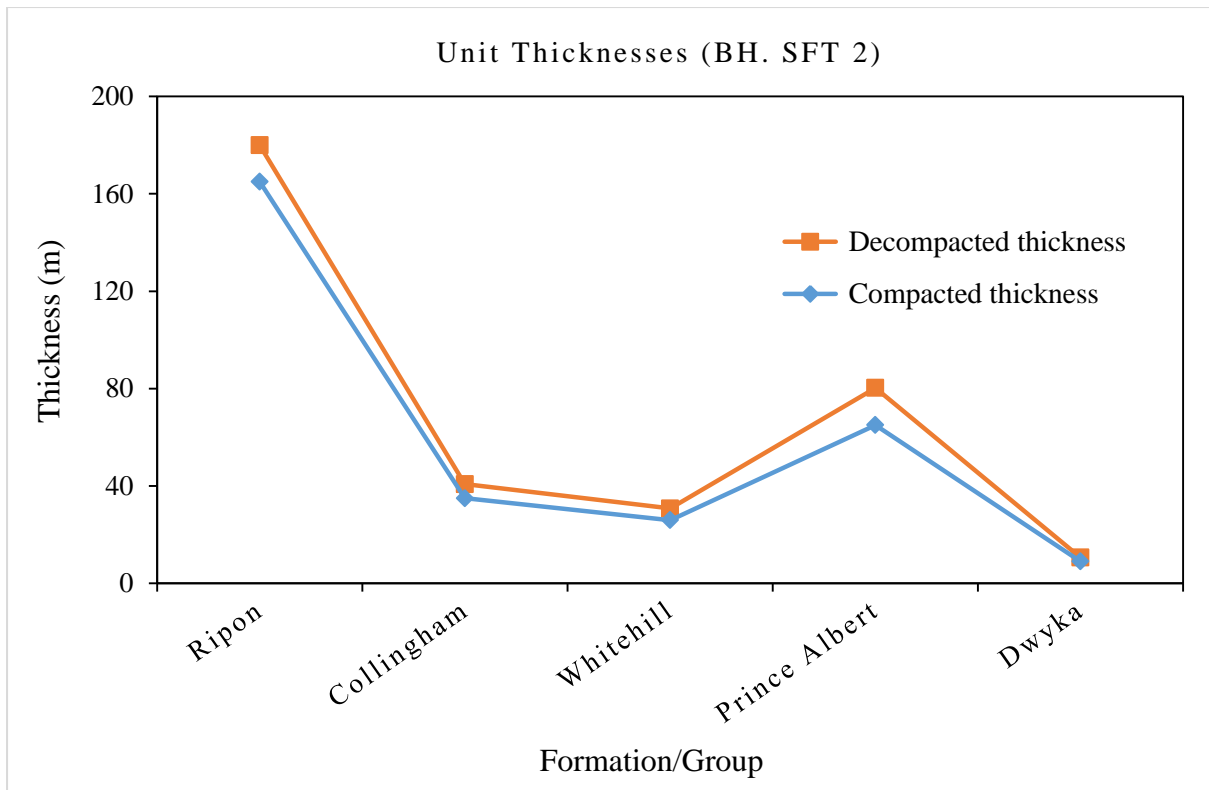
Figure 11.7: The thicknesses of compacted segments compared to decompacted segments in borehole SFT 2 (Data extracted from Black et al., 2016).
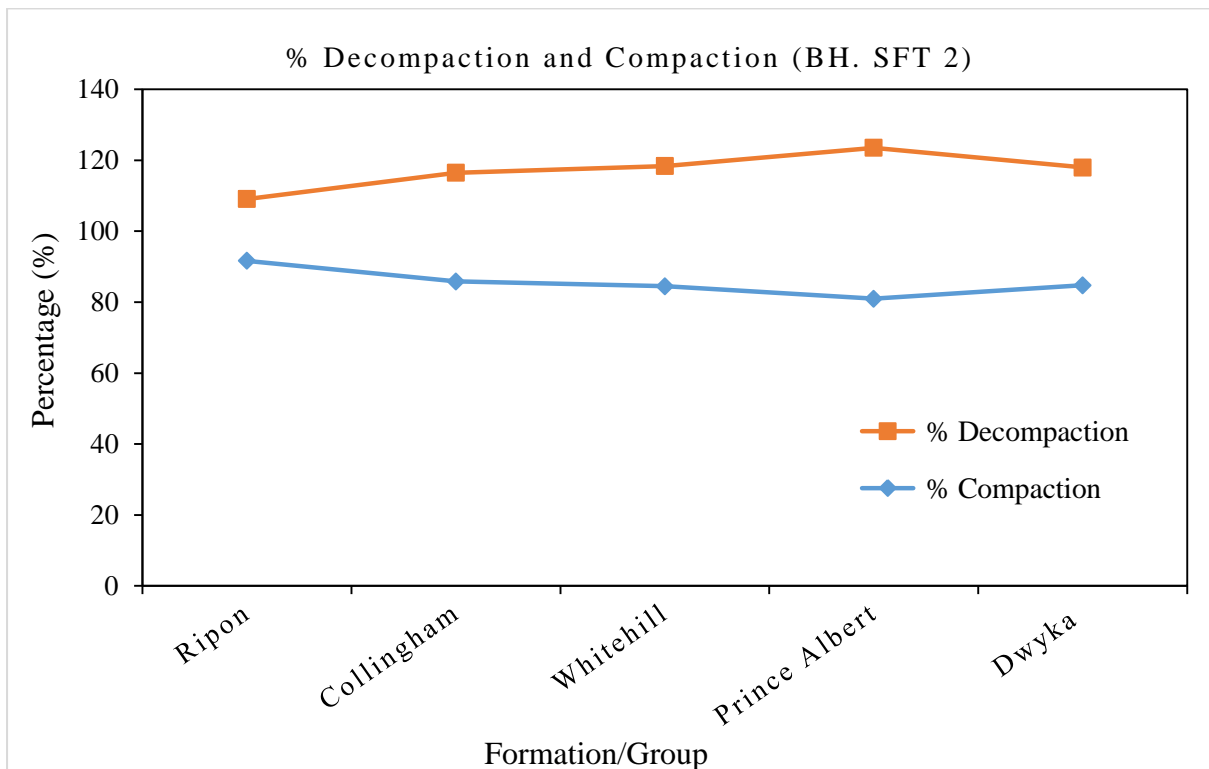
Figure 11.8: The percentage decompaction compared to percentage compaction per formation in borehole SFT 2 (Data extracted from Black et al., 2016).

Table 11.5: Calculated results for porosity at specific depths, decompacted thickness, percent compaction and decompaction, and thickness difference for lithostratigraphic units in borehole CR 1/68. *φ_0 values are from Table 11.2.

Units	Depth to top and bottom (km)	Compacted thickness (m)	Lithology	Porosity at surface φ_0	Porosity at any depth φ	Decompacted thickness (m)	Compaction (%)	Decompaction (%)	Thickness difference (m)
Beaufort Group	0.000-2.140	2140	Shale Sandstone	0.560	0.214	3823	56	179	1683
Fort Brown Formation	2.140-3.070	930	Shale Sandstone	0.630	0.132	2182	43	235	1252
Ripon Formation	3.070-3.630	560	Sandstone Shale	0.560	0.109	1134	49	203	574
Collingham Formation	3.630-3.670	40	Siltstone Mudstone	0.630	0.097	98	41	244	58
Whitehill Formation	3.670-3.705	35	Shale	0.630	0.095	86	41	245	51
Prince Albert Formation	3.705-3.780	75	Shale	0.630	0.092	184	41	245	109
Dwyka Group	3.780-4.283	503	Diamictite	0.560	0.081	1051	48	209	548
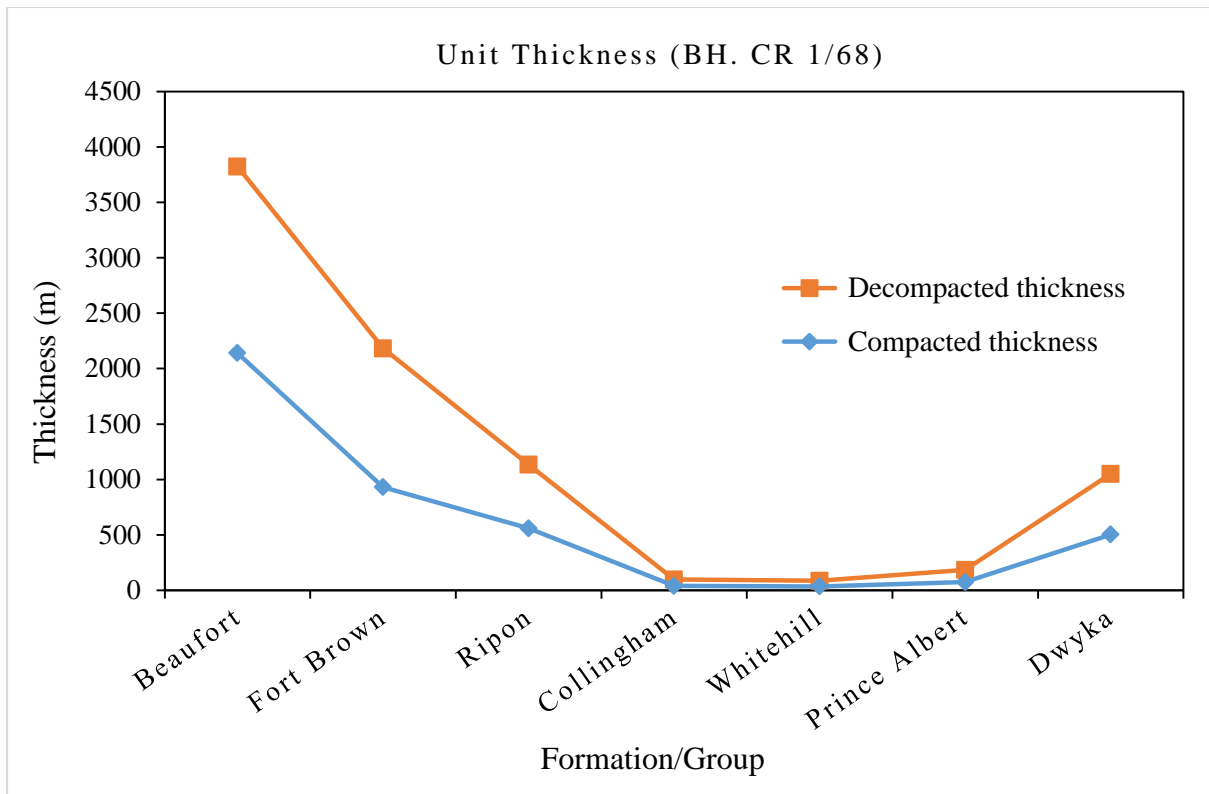
Figure 11.9: The thicknesses of compacted segments compared to decompacted segments in borehole CR 1/68.
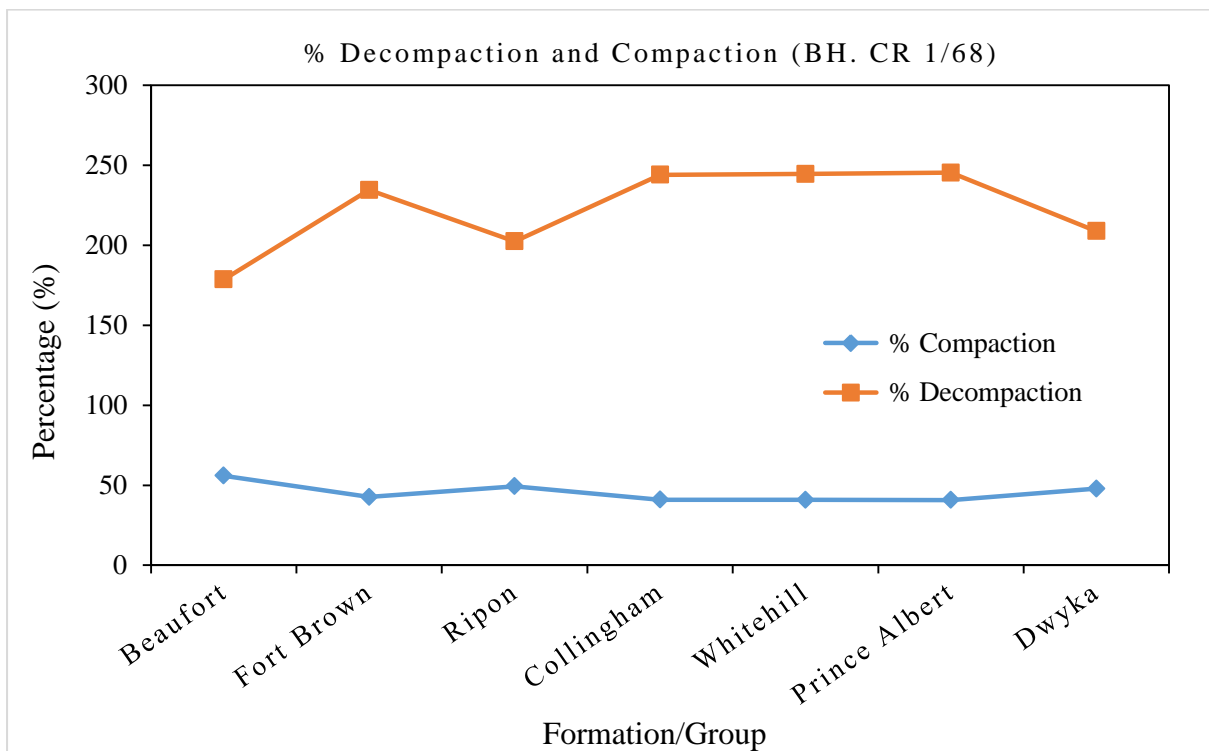
Figure 11.10: The percentage decompaction compared to percentage compaction per formation in borehole CR 1/68.

Table 11.6: Calculated results for porosity at specific depths, decompacted thickness, percent compaction and decompaction, and thickness difference for lithostratigraphic units in the Ecca Pass Section. *φ_0 values are from Table 11.2.

Units	Compacted thickness (m)	Depth (km)	Lithology	Porosity at surface φ_0	Porosity at any depth φ	Decompacted thickness (m)	Compaction (%)	Decompaction (%)	Thickness difference (m)
Fort Brown Formation	910	0.910	Shale Sandstone	0.630	0.396	1486	61	163	576
Ripon Formation	900	1.810	Sandstone Shale	0.560	0.248	1538	59	171	638
Collingham Formation	64	1.874	Siltstone Mudstone	0.630	0.242	131	49	205	67
Whitehill Formation	41	1.915	Shale	0.630	0.237	85	48	206	44
Prince Albert Formation	142.7	2.058	Shale	0.630	0.221	300	47	211	158
Dwyka Group	> 150	2.208	Diamictite	0.560	0.207	270	55	180	120
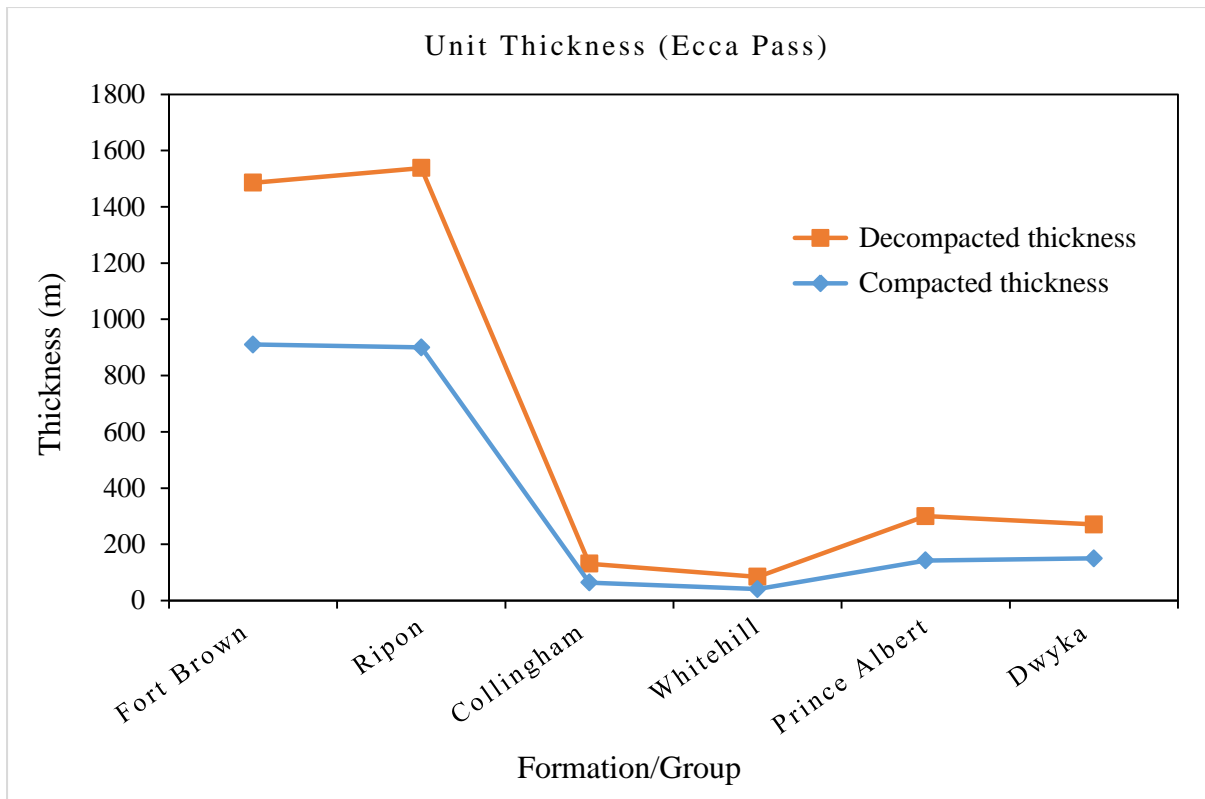
Figure 11.11: The thicknesses of compacted segments compared to decompacted segments in the exposure along the Ecca Pass.
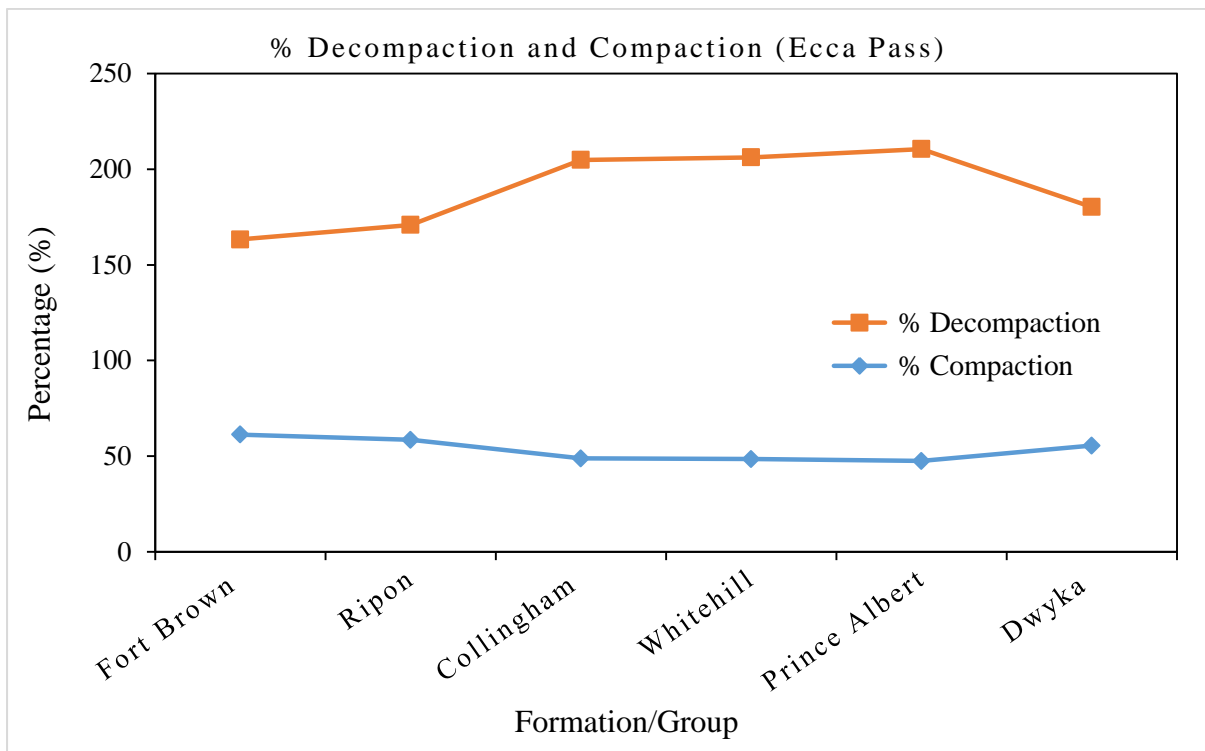
Figure 11.12: The percentage decompaction compared to percentage compaction per formation in the exposure along the Ecca Pass.

Table 11.7: Calculated results for porosity at specific depths, decompacted thickness, percent compaction and decompaction, and thickness difference for lithostratigraphic units in borehole KWV 1. *φ_0 values are from Table 11.2.

Units	Depth to top and bottom (km)	Compacted thickness (m)	Lithology	Porosity at surface φ_0	Porosity at any depth φ	Decompacted thickness (m)	Compaction (%)	Decompaction (%)	Thickness difference (m)
Beaufort Group	0.000-0.265	264.5	Shale Sandstone	0.560	0.497	302	87	114	39
Fort Brown Formation	0.265-0.919	654.7	Shale Sandstone	0.630	0.394	1072	61	164	418
Ripon Formation	0.919-2.205	1082.8	Sandstone Shale	0.560	0.208	1949	56	180	866
Collingham Formation	2.205-2.295	90	Siltstone Mudstone	0.630	0.195	196	46	218	106
Whitehill Formation	2.295-2.308	17.10	Shale	0.630	0.194	37	46	218	20
Prince Albert Formation	2.308-2.340	27.55	Shale	0.630	0.191	60	46	219	33
Dwyka Group	2.340-2.758	418	Diamictite	0.560	0.162	796	53	190	378

Note: thickness of the dolerite intrusions was removed.
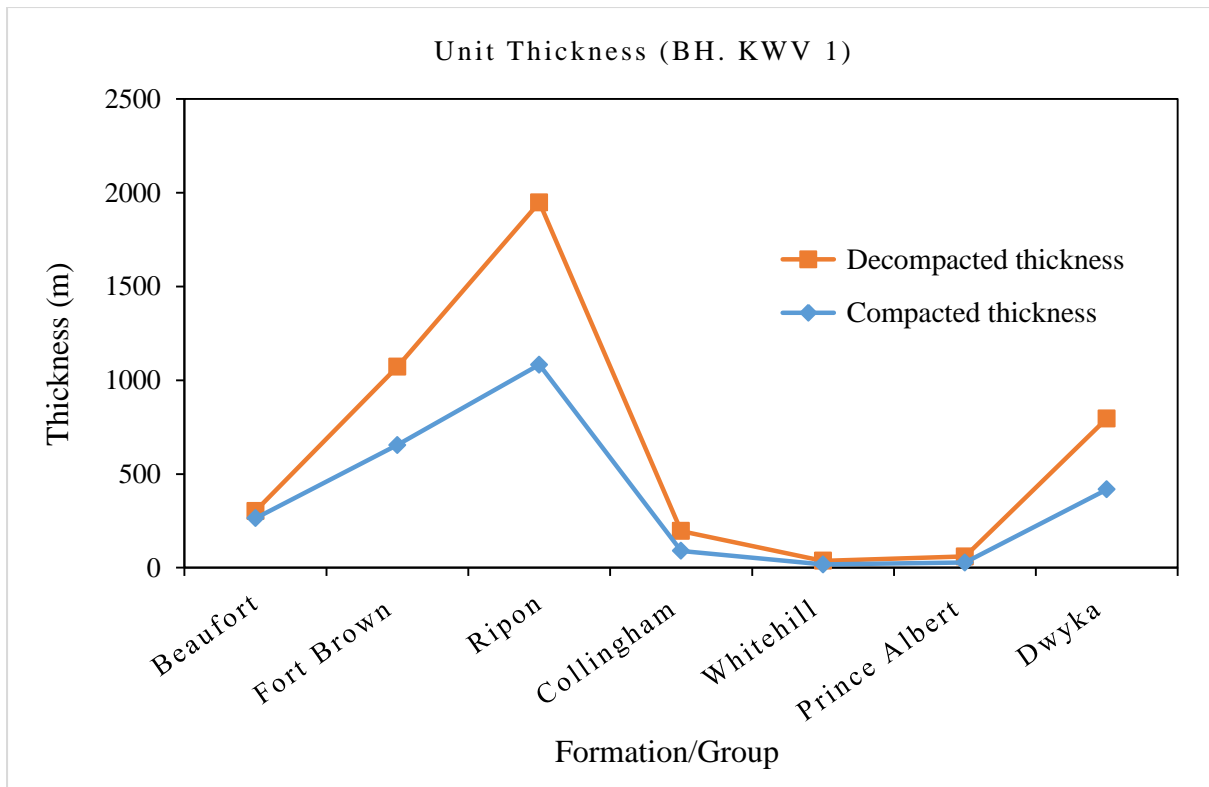
Figure 11.13: The thicknesses of compacted segments compared to decompacted segments in borehole KWV 1.
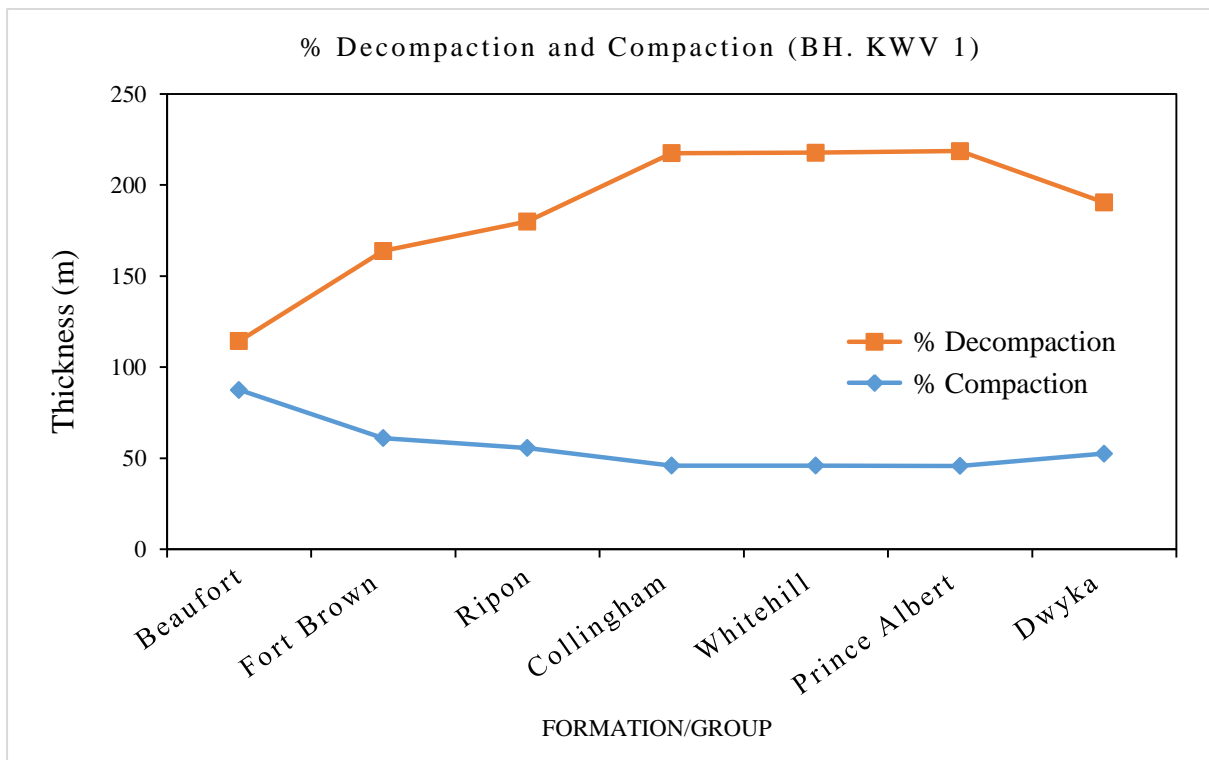
Figure 11.14: The percentage decompaction compared to percentage compaction per formation in Borehole KWV 1.

Table 11.8: Calculated results for porosity at specific depths, decompacted thickness, percent compaction and decompaction, and thickness difference for lithostratigraphic units in borehole SP 1/69. *φ_0 values are from Table 11.2.

Units	Depth to top and bottom (km)	Compacted thickness (m)	Lithology	Porosity at surface φ_0	Porosity at any depth φ	Decompacted thickness (m)	Compaction (%)	Decompaction (%)	Thickness difference (m)
Beaufort Group	0.000-2.100	2100	Shale Sandstone	0.560	0.194	3847	55	183	1747
Fort Brown Formation	2.100-2.702	602	Shale Sandstone	0.630	0.159	1368	44	227	766
Ripon Formation	2.702-3.630	928	Sandstone Shale	0.560	0.109	1879	49	203	951
Collingham Formation	3.630-3.653	23	Siltstone Mudstone	0.630	0.098	56	41	244	33
Whitehill Formation	3.653-3.688	35	Shale	0.630	0.096	86	41	244	51
Prince Albert Formation	3.688-3.728	40	Shale	0.630	0.094	98	41	245	58
Dwyka Group	3.728-4.248	520	Diamictite	0.560	0.083	1084	48	208	564
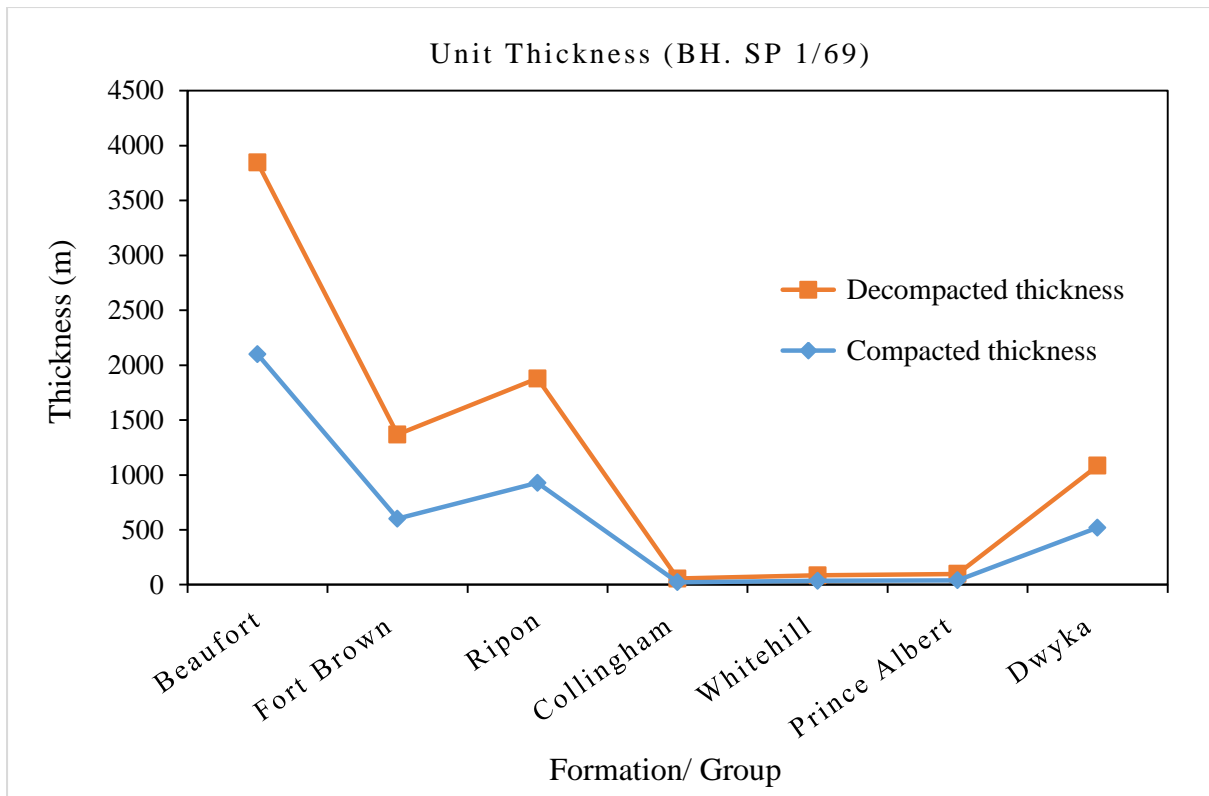
Figure 11.15: The thicknesses of compacted segments compared to decompacted segments in borehole SP 1/69.
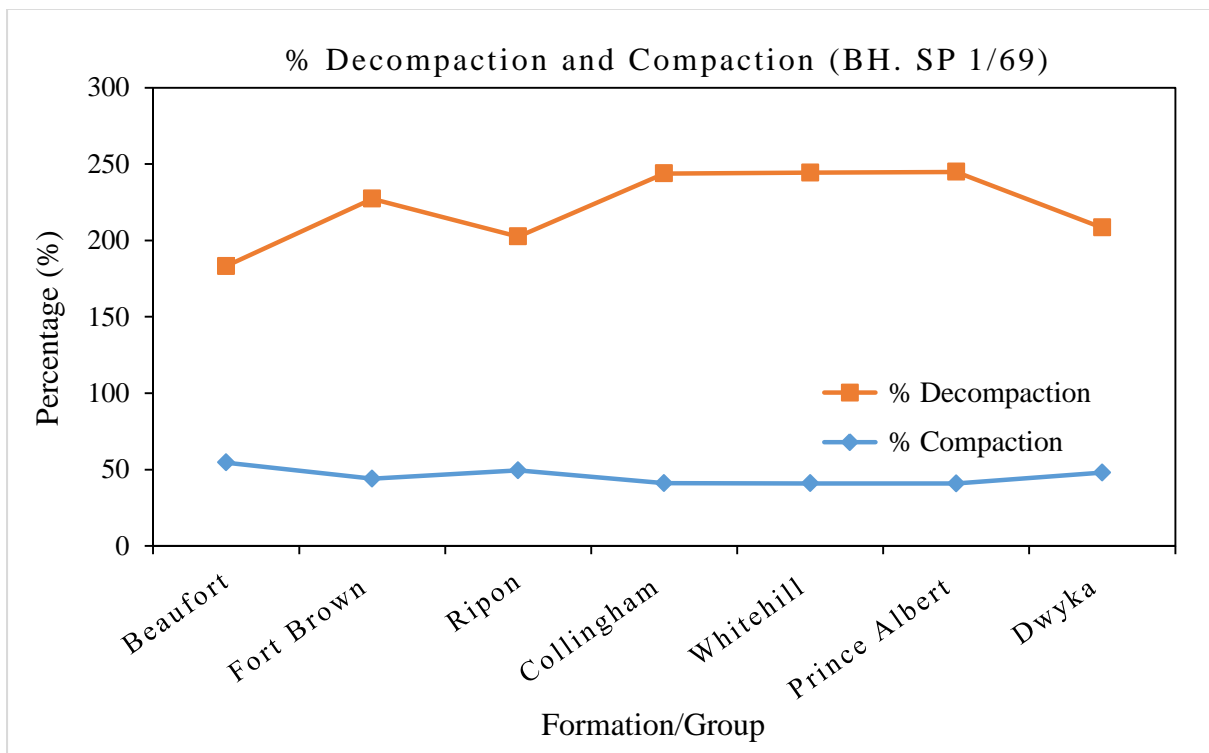
Figure 11.16: The percentage decompaction compared to percentage compaction per formation in borehole SP 1/69.

11.3.2 Sedimentation rate

The sedimentation rate results for the Ecca formations are represented in Tables 11.9-11.14 and Figures 11.17-11.22. In borehole SC 3/67, a relatively low sedimentation rate (8×10^{-2} mm yr^{-1}) is estimated during deposition of the Dwyka Group (Figure 11.17). Afterwards, there was a decrease in sedimentation rate during the deposition of the Prince Albert Formation (3×10^{-2} mm yr^{-1}) and it increases to 5×10^{-2} mm yr^{-1} during the deposition of the Whitehill Formation. Subsequently, the sedimentation rate decreases to 4×10^{-2} mm yr^{-1} during the deposition of the Collingham Formation and increases gradually to 1.1×10^{-1} mm yr^{-1} and 2.5×10^{-1} mm yr^{-1} during the deposition of the Ripon and Fort Brown Formations, respectively in the Late Permian.

On the other hand, the accumulated sediment volume decreases from 940×10^{-3} km^3 during the deposition of the Dwyka Group to 31.3×10^{-3} km^3 during the deposition of the Prince Albert Formation, and 1×10^{-4} km^3 during the deposition of the Whitehill Formation. Thereafter, it increases to 3×10^{-4} km^3, 150×10^{-3} km^3 and 922×10^{-4} km^3 during the deposition of Collingham, Ripon and Fort Brown Formations, respectively.

Table 11.9: Total sediment volumes and accumulation rates in borehole SC 3/67. *Area for each lithostratigraphic unit is obtained by multiplying the decompacted thicknesses (in km) by the borehole thickness. The radiometric dates are from Bangert et al.(1999), Catuneanu et al. (2005), Johnson et al. (2006), Fildani (2009), Geel et al. (2013, 2015) and McKay et al. (2015).

Units	Age span (Ma)	Time span ΔT (Ma)	Compacted Thickness, T_d (m)	Density (kgm^{-3})	Mass accumulation rate, Rm $(kgm^{-2} Ma^{-1})$ x 10^3	Borehole thickness (km) x 10^{-1}	*Area A (km^2) x 10^{-2}	Accumulated sediment volume, V (km^3) x 10^{-3}	Sedimentation rate, $R_{sr} \left[\frac{T_d}{\Delta T}\right]$ $(mm\ yr^{-1})$ x 10^{-2}
Fort Brown Formation	~268-264	4	1007	2720	618.34	10.07	101.4	922	25
Ripon Formation	~273-268	5	550	2700	268.19	5.50	30.3	150	11
Collingham Formation	~275-273	2	70	2700	86.66	0.70	0.5	0.3	4
Whitehill Formation	~276-275	1	51	2720	127.48	0.51	0.3	0.1	5
Prince Albert Formation	~289-276	13	323	2720	62.92	3.23	10.4	31.3	3
Dwyka Group	~302-289	13	997	2600	189.23	9.97	99.4	940	8

where T_d is decompacted or present thickness (m)
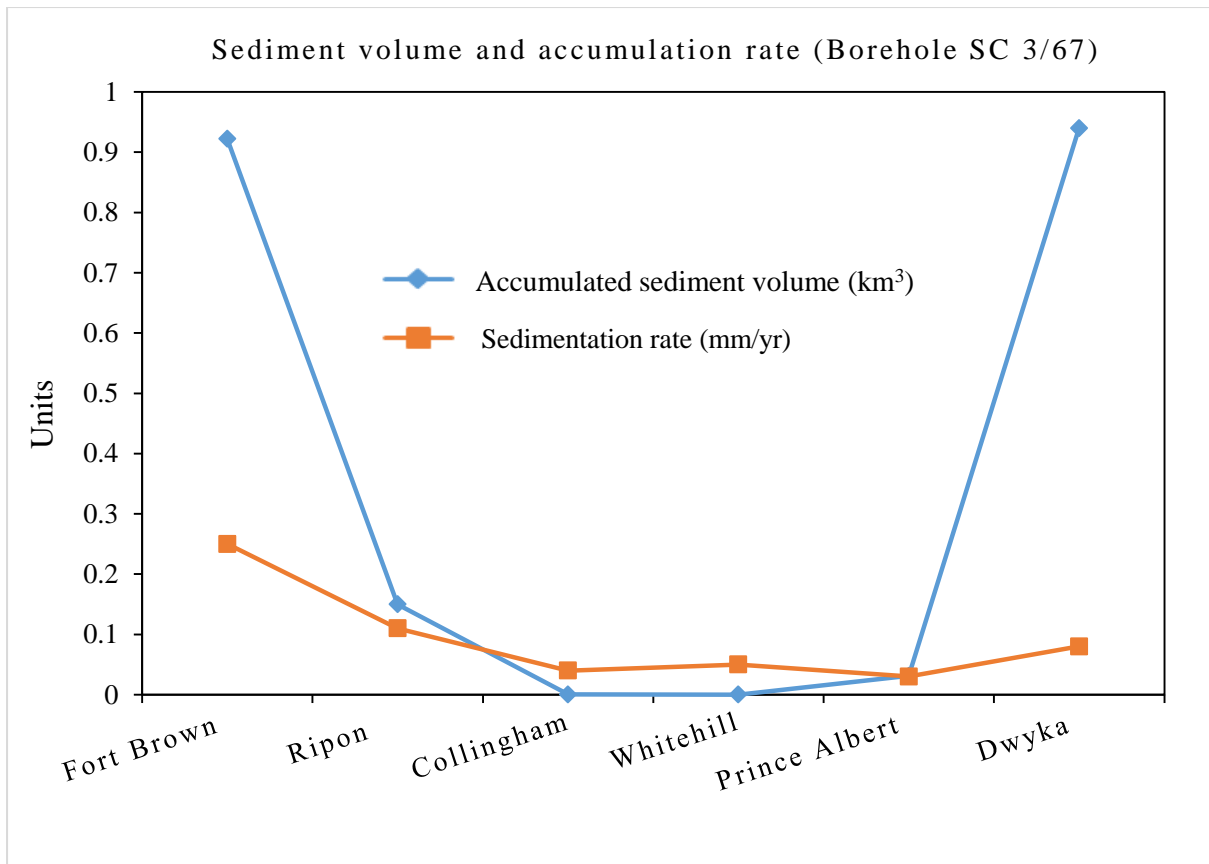
Figure 11.17: Comparison of sedimentation rate and accumulated sediment volume in the southeastern Karoo subbasin (Borehole SC 3/67) during the Permian Period.

The accumulated sediment volume in borehole SFT 2 decreases from 5.2×10^{-4} km^3 during the deposition of the Dwyka Group to 1.3×10^{-4} km^3 and 1×10^{-5} km^3 the deposition of the Prince Albert and Whitehill Formations, respectively. Thereafter, the volume increases to 2×10^{-5} km^3 and 2.16×10^{-3} km^3 during the deposition of Collingham and Ripon Formations, respectively. The sedimentation rate is low during deposition of the Dwyka Group and Prince Albert Formation, approximately 1×10^{-2} mm/yr (Figure 11.18). This sedimentation rate gradually decreases to 3×10^{-2} mm/yr during the deposition of the Whitehill Formation in the Early Permian. Thereafter, the sedimentation rate increases from 2×10^{-2} mm/yr during the deposition of the Collingham Formation to 3×10^{-2} mm/yr during the deposition of the Ripon Formation.

Table 11.10: Total sediment volumes and accumulation rates in borehole SFT 2. *Area for each lithostratigraphic unit is obtained by multiplying the decompacted thicknesses (in km) by the borehole thickness. The radiometric dates are from Bangert et al.(1999), Catuneanu et al. (2005), Johnson et al. (2006), Fildani (2009), Geel et al. (2013, 2015) and McKay et al. (2015).

Units	Age span (Ma)	Time span ΔT (Ma)	Compacted Thickness, T_d (m)	Density (kgm^{-3})	Mass accumulation rate, Rm (kgm^{-2} Ma^{-1}) x 10^3	Borehole thickness (km) x 10^{-1}	*Area A (km^2) x10^{-2}	Accumulated sediment volume,V (km^3) x 10^{-3}	Sedimentation Rate,R$_{sr}$ $\left[\frac{T_d}{\Delta T}\right]$ (mm yr^{-1}) x 10^{-2}
Ripon Formation	~273-268	5	165	2700	42.77	1.65	2.72	2.16	3
Collingham Formation	~275-273	2	35	2700	20.36	0.35	0.12	0.02	2
Whitehill Formation	~276-275	1	26	2720	30.98	0.26	0.07	0.01	3
Prince Albert Formation	~289-276	13	65	2720	6.22	0.65	0.42	0.13	1
Dwyka Group	~302-289	13	>100	2600	10.38	10	01.0	0.52	1
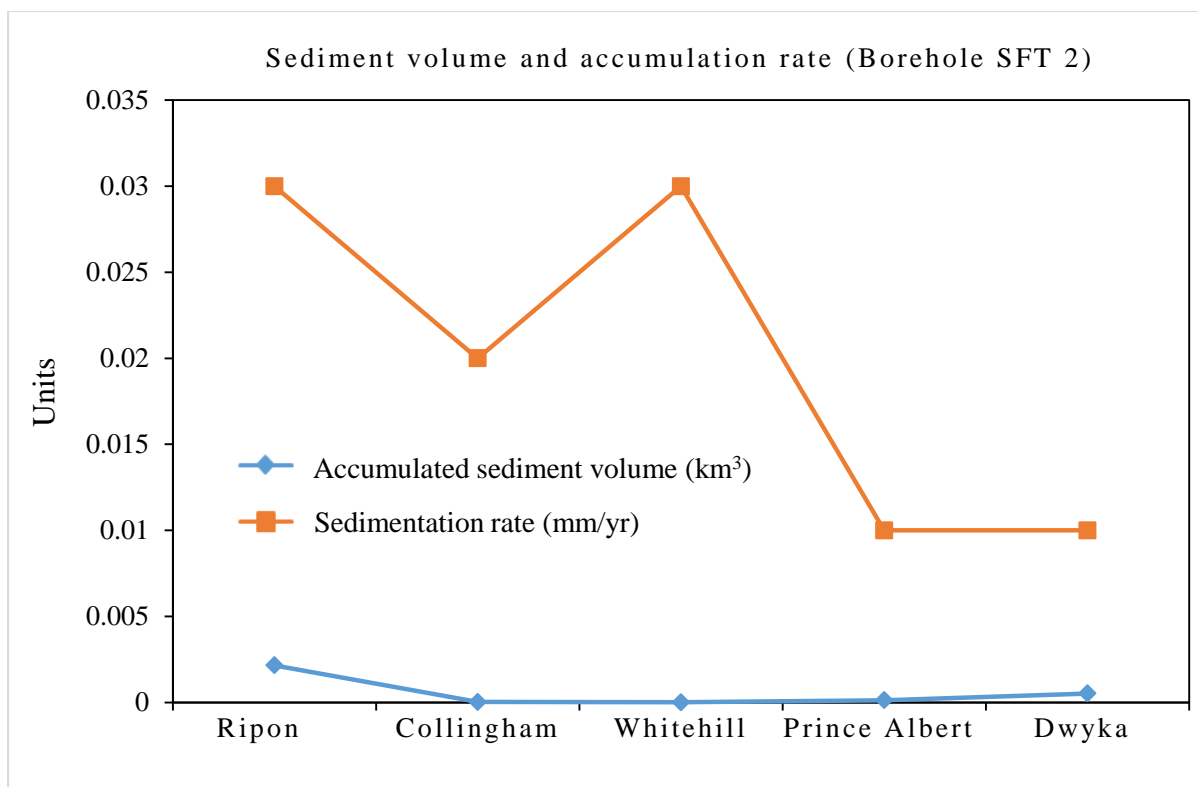
Figure 11.18: Comparison of sediment rate and accumulation rate in the southeastern Karoo subbasin (Borehole SFT 2) during the Permian Period.

In borehole CR 1/68, sedimentation rate of about 0.04 mm/yr is estimated during deposition of the Dwyka Group as shown in Figure 11.19. The sedimentation rate decreases to 1×10^{-2} mm/yr during the deposition of the Prince Albert Formation. Subsequently, the sedimentation rate gradually increases to 4×10^{-2} mm/yr during the deposition of the Whitehill Formation. Then, the sedimentation rate decreases to 2×10^{-2} mm/yr during the deposition of the Collingham Formation and further decreases to 1.1×10^{-1} mm/yr during the deposition of the Ripon Formation. Thereafter, the sedimentation rate gradually increases to 2.3×10^{-1} mm/yr during the deposition of the Fort Brown Formation. Conversely, the accumulated sediment volume decreases from 116.96×10^{-3} km^3 during the deposition of the Dwyka Group to 3.8×10^{-4} km^3 during the deposition of the Prince Albert Formation. Thereafter, it increases to 4×10^{-5} km^3, 6×10^{-5} km^3, 156.47×10^{-3} km^3 and 698.18×10^{-3} km^3 during the deposition of the Whitehill, Collingham, Ripon and Fort Brown Formations, respectively.

Table 11.11: Total sediment volumes and accumulation rates in borehole CR 1/68. *Area for each lithostratigraphic unit is obtained by multiplying the decompacted thicknesses (in km) by the borehole thickness. The radiometric dates are from Bangert et al.(1999), Catuneanu et al. (2005), Johnson et al. (2006), Fildani (2009), Geel et al. (2013, 2015) and McKay et al. (2015).

Units	Age span (Ma)	Time span ΔT (Ma)	Compacted Thickness, T_d (m)	Density (kgm^{-3})	Mass accumulation rate, Rm $(kgm^{-2}\,Ma^{-1}) \times 10^3$	Borehole thickness (km) $\times 10^{-1}$	*Area A $(km^2) \times 10^{-2}$	Accumulated sediment volume, V $(km^3) \times 10^{-3}$	Sedimentation rate,$R_{sr}\left[\frac{T_d}{\Delta T}\right]$ $(mm\,yr^{-1}) \times 10^{-2}$
Fort Brown Formation	~268-264	4	930	2720	548.92	9.3	86.49	698.18	23
Ripon Formation	~273-268	5	560	2700	269.44	5.6	31.36	156.47	11
Collingham Formation	~275-273	2	40	2700	48.76	0.4	0.16	0.06	2
Whitehill Formation	~276-275	1	35	2720	86.16	0.35	0.12	0.04	4
Prince Albert Formation	~289-276	13	75	2720	14.25	0.75	0.56	0.38	1
Dwyka Group	~302-289	13	503	2600	92.45	5.03	25.30	116.96	4

Figure 11.19: Comparison of sedimentation rate and accumulated sediment volume in the southeastern Karoo subbasin (Borehole CR 1/68) during the Permian Period.

In the Ecca Pass section, the calculated sedimentation rates during deposition of the Dwyka Group (1×10^{-2} mm/yr) and Prince Albert Formation (1×10^{-2} mm/yr) are generally low as depicted in Figure 11.20. Thereafter, the sedimentation rate increases to 4×10^{-2} mm/yr during the deposition of the Whitehill Formation and gradually decreases to 3×10^{-2} mm/yr during the deposition of the Collingham Formation.Subsequently, the sedimentation rate increases to 1.8×10^{-1} mm yr^{-1} and 2.3×10^{-1} mm yr^{-1} during the deposition of the Ripon and Fort Brown Formations, respectively. On the other hand, the accumulated sediment volume gradually decreases from 2.68×10^{-3} km^3 during the deposition of the Dwyka Group until the deposition of the Whitehill Formation (5×10^{-5} km^3). Thereafter, it increases to 2×10^{-4} km^3 and 548.21×10^{-3} km^3 during the deposition of Collingham and Ripon Formations, respectively. The accumulated sediment volume later decreases to 455.16×10^{-3} km^3 during the deposition of the Fort Brown Formation.

Table 11.12: Total sediment volumes and accumulation rates along the Ecca Pass Section. *Area for each lithostratigraphic unit is obtained by multiplying the decompacted thicknesses (in km) by the borehole thickness. The radiometric dates are from Bangert et al.(1999), Catuneanu et al. (2005), Johnson et al. (2006), Fildani (2009), Geel et al. (2013, 2015) and McKay et al. (2015).

| Units	Age span (Ma)	Time span ΔT (Ma)	Compacted Thickness, T_d (m)	Density (kgm^{-3})	Mass accumulation rate, Rm ($kgm^{-2} Ma^{-1}$) x 10^3	Borehole thickness (km) x 10^{-1}	*Area A (km^2) x 10^{-2}	Accumulated sediment volume, V (km^3) x 10^{-3}	Sedimentation rate, $R_{sr} \left[\frac{T_d}{\Delta T}\right]$ ($mm\ yr^{-1}$) x 10^{-2}
Fort Brown Formation	~268-264	4	910	2720	373.76	9.1	82.81	455.16	23
Ripon Formation	~273-268	5	900	2700	365.47	9	81	548.21	18
Collingham Formation	~275-273	2	64	2700	65.49	0.64	0.41	0.20	3
Whitehill Formation	~276-275	1	41	2720	85.09	0.41	0.17	0.05	4
Prince Albert Formation	~289-276	13	142.7	2720	23.26	1.43	2.04	2.26	1
Dwyka Group	~302-289	13	> 150	2600	23.79	1.50	2.25	2.68	1
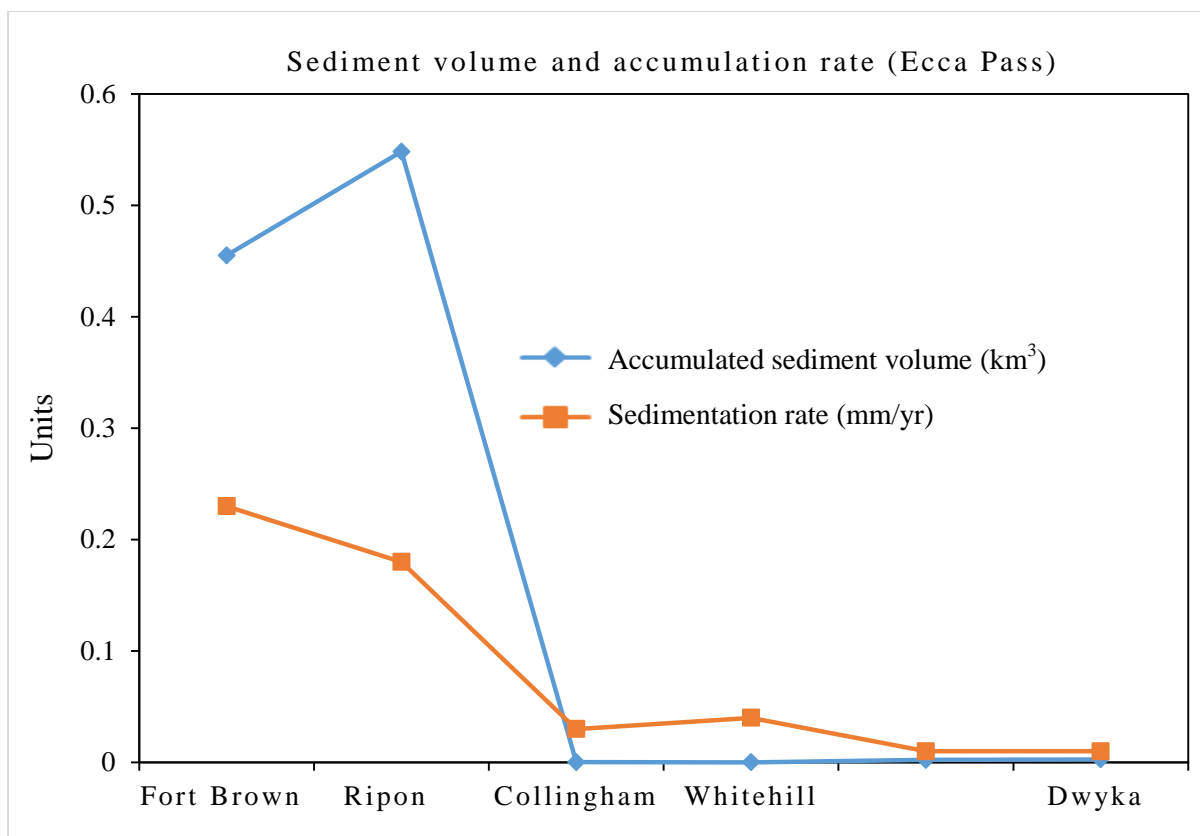
Figure 11.20: Comparison of sedimentation rate and accumulated sediment volume in the southeastern Karoo subbasin (Ecca Pass) during the Permian Period.

In borehole KWV 1, the accumulated sediment volume decreases from 6126.03×10^{-3} km^3 during the deposition of the Dwyka Group until the deposition of the Whitehill Formation (4×10^{-6} km^3). Thereafter, it increases to 5.9×10^{-4} km^3 and 1005.47×10^{-3} km^3 during the deposition of the Collingham and Ripon Formations, respectively. The accumulated sediment volume later decreases to 170.06×10^{-3} km^3 during the deposition of the Fort Brown Formation. A relatively low sedimentation rate of approximately 3×10^{-2} mm/yr is observed during deposition of the Dwyka Group as shown in Figure 11.21. Afterwards, the sedimentation rate decreases to 2×10^{-3} mm/yr during the deposition of the Prince Albert Formation. Thereafter, the sedimentation rate gradually increases from 2×10^{-2} mm/yr during the deposition of the Whitehill Formation to 5×10^{-2} mm/yr and 2.2×10^{-1} mm/yr during the deposition of the Collingham and Ripon Formations, respectively. Thereafter, it decreases to 1.6×10^{-1} mm/yr during the deposition of the Fort Brown Formation.

Table 11.13: Total sediment volumes and accumulation rates in borehole KWV 1. *Area for each lithostratigraphic unit is obtained by multiplying the decompacted thicknesses (in km) by the borehole thickness. The radiometric dates are from Bangert et al.(1999), Catuneanu et al. (2005), Johnson et al. (2006), Fildani (2009), Geel et al. (2013, 2015) and McKay et al. (2015).

Units	Age span (Ma)	Time span ΔT (Ma)	Compacted Thickness, T_d (m)	Density (kgm^{-3})	Mass accumulation rate, Rm $(kgm^{-2} Ma^{-1})$ x 10^3	Borehole thickness (km) x 10^{-1}	*Area, A (km^2) x 10^{-2}	Accumulated sediment volume, V (km^3) x 10^{-3}	Sedimentation rate,$R_{sr} \left[\frac{T_d}{\Delta T}\right]$ $(mm\ yr^{-1})$ x 10^{-2}
Fort Brown Formation	~268-264	4	654.7	2720	269.79	6.55	42.86	170.06	16
Ripon Formation	~273-268	5	1082.8	2700	463.09	10.83	117.25	1005.47	22
Collingham Formation	~275-273	2	90	2700	97.801	0.9	0.81	0.59	5
Whitehill Formation	~276-275	1	17.10	2720	37.49	0.17	0.03	0.004	2
Prince Albert Formation	~289-276	13	27.55	2720	4.66	0.28	0.08	0.02	0.2
Dwyka Group	~302-289	13	418	2600	70.06	4.18	17.47	612.03	3
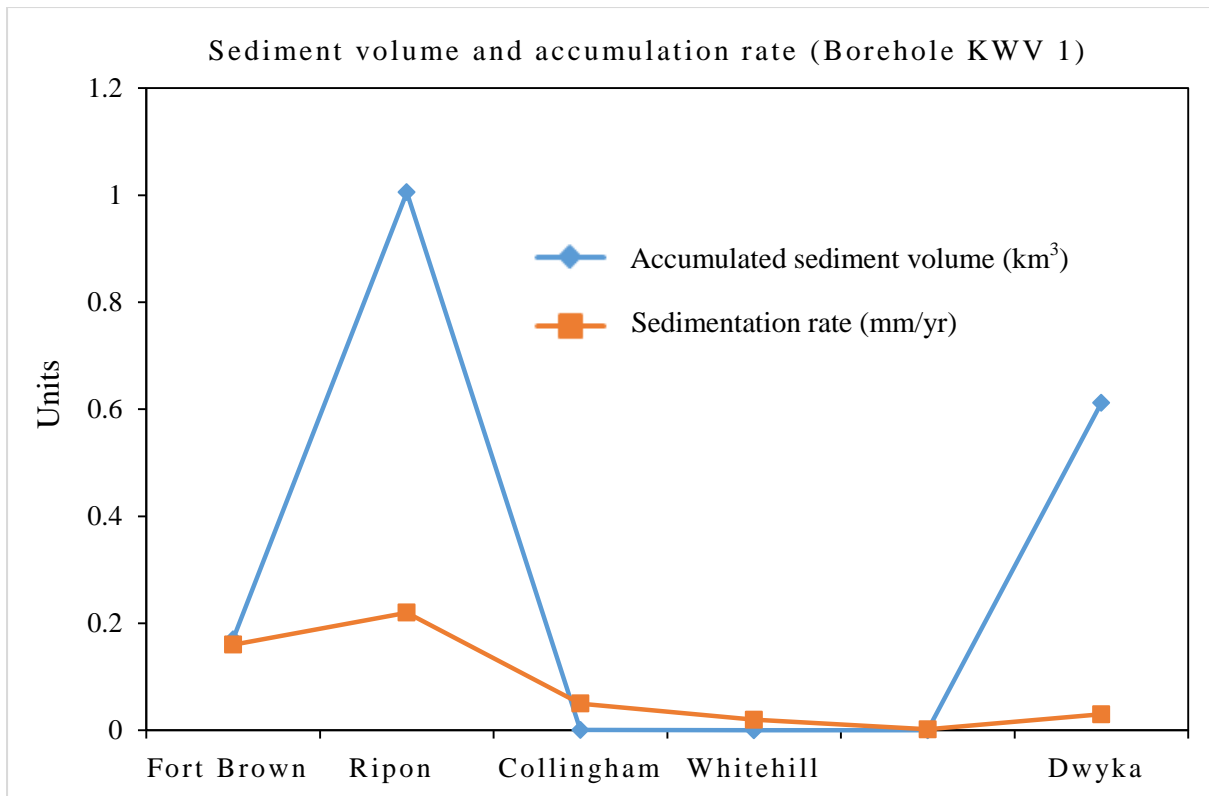
Figure 11.21: Comparison of sedimentation rate and accumulated sediment volume in the southeastern Karoo subbasin (Borehole KWV 1) during the Permian Period.

Sedimentation rate of approximately 4×10^{-2} mm/yr is observed during deposition of the Dwyka Group in borehole SP 1/69 (Figure 11.22). Subsequently, the sedimentation rate decreases to 3×10^{-2} mm/yr during the deposition of the Prince Albert Formation and gradually increases to 4×10^{-2} mm/yr during the deposition of the Whitehill Formation. Thereafter, the sedimentation rate decreases to 1×10^{-2} mm/yr during the deposition of the Collingham Formation and increases to 1.9×10^{-1} mm/yr during the deposition of the Ripon Formation. Then it decreases to 1.5×10^{-1} mm/yr during the deposition of the Fort Brown Formation. On the other hand, the accumulated sediment volume decreases from 128.94×10^{-3} km^3 during the deposition of the Dwyka Group to 6×10^{-5} km^3, 4×10^{-5} km^3 and 1×10^{-4} km^3 during the deposition of the Prince Albert, Whitehill and Collingham Formation, respectively. Thereafter, it increases to 712×10^{-3} km^3 during the deposition of the Ripon Formation and then decreases to 183.48×10^{-3} km^3 during the deposition of Fort Brown Formation.

Table 11.14: Total sediment volumes and accumulation rates in borehole SP 1/69. *Area for each lithostratigraphic unit is obtained by multiplying the decompacted thicknesses (in km) by the borehole thickness. The radiometric dates are from Bangert et al.(1999), Catuneanu et al. (2005), Johnson et al. (2006), Fildani (2009), Geel et al. (2013, 2015) and McKay et al. (2015).

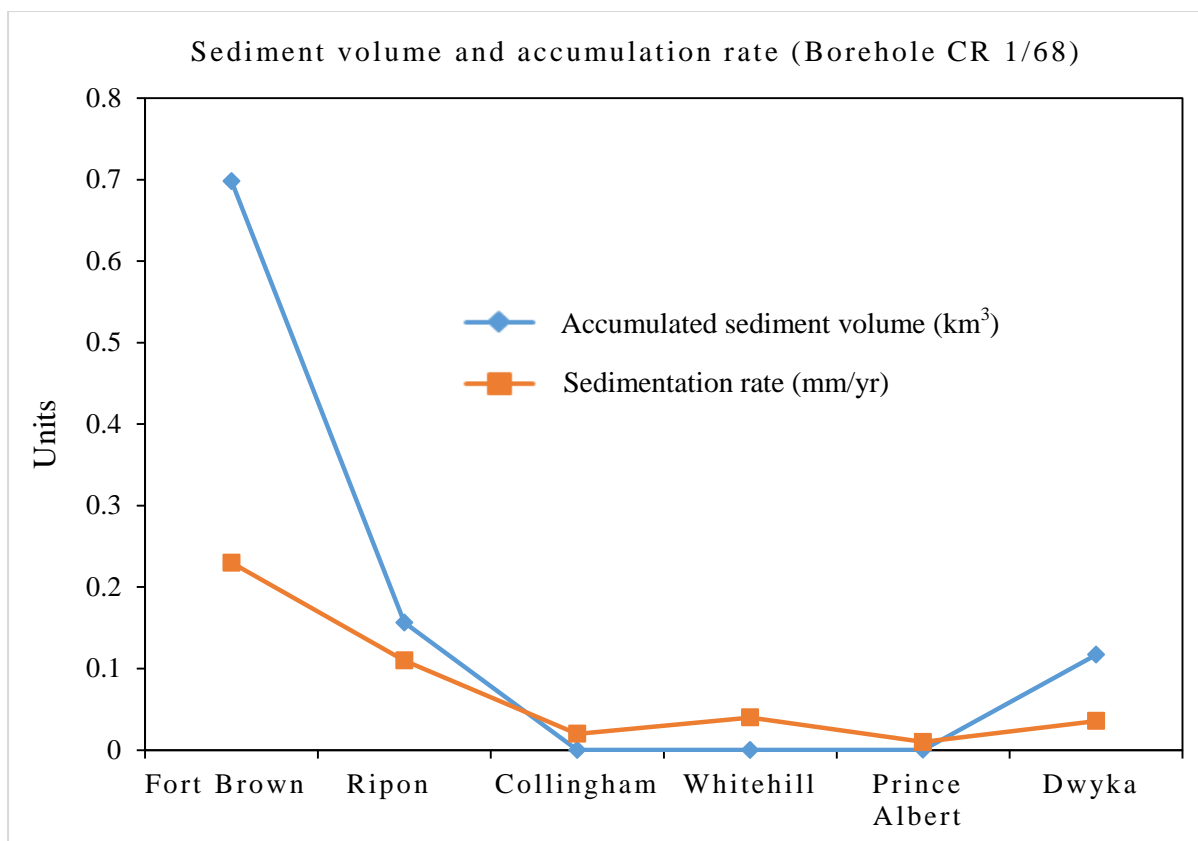| Units	Age span (Ma)	Time span ΔT (Ma)	Compacted Thickness, T_d (m)	Density (kgm^{-3})	Mass accumulation rate, Rm $(kgm^{-2}Ma^{-1})$ x 10^3	Borehole thickness (km) x 10^{-1}	*Area A (km^2) x 10^{-2}	Accumulated sediment volume, V (km^3) x 10^{-3}	Sedimentation rate,$R_{sr}\left[\frac{T_d}{\Delta T}\right]$ $(mm\ yr^{-1})$ x 10^{-2}
Fort Brown Formation	~268-264	4	602	2720	344.27	6.02	36.24	183.48	15
Ripon Formation	~273-268	5	928	2700	446.50	9.28	86.12	712.07	19
Collingham Formation	~275-273	2	23	2700	28.01	0.23	0.05	0.01	1
Whitehill Formation	~276-275	1	35	2720	86.06	0.35	0.12	0.04	4
Prince Albert Formation	~289-276	13	40	2720	7.58	0.40	0.16	0.06	0.3
Dwyka Group	~302-289	13	520	2600	95.37	5.20	27.04	128.94	4
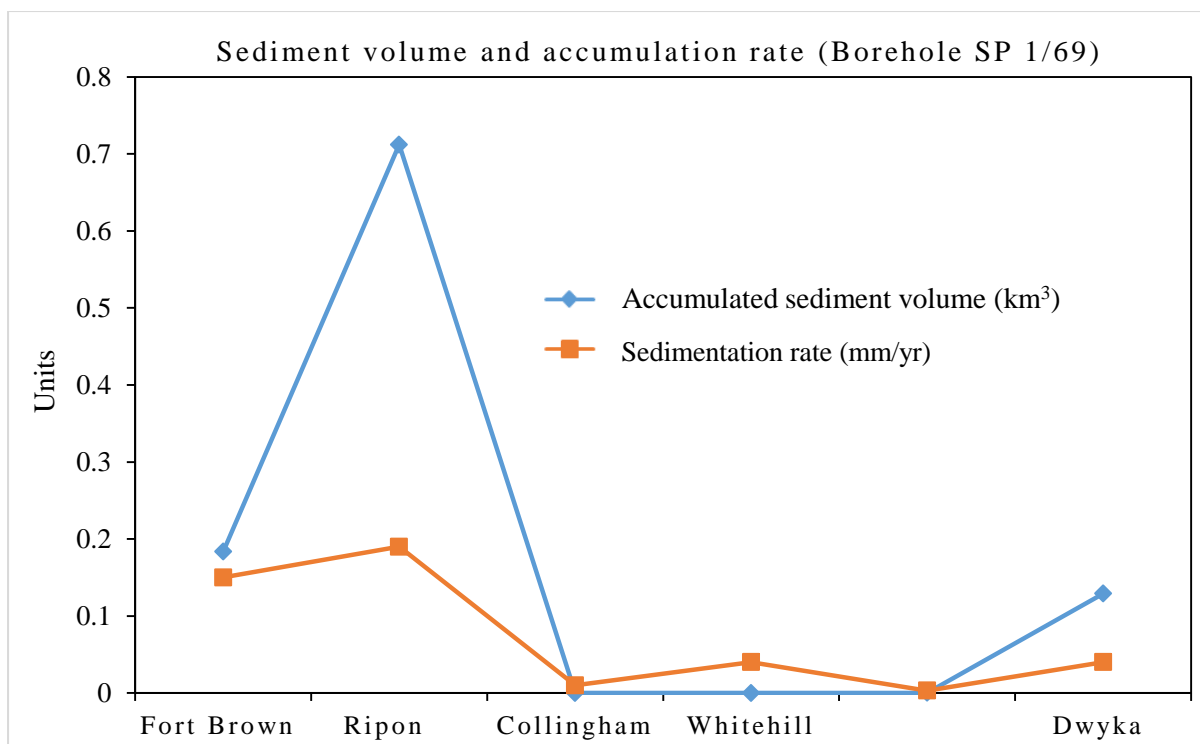
Figure 11.22: Comparison of sedimentation rate and accumulated sediment volume in the southeastern Karoo subbasin (Borehole SP 1/69) during the Permian Period.

11.3.3 1D Airy subsidence model

Backstripped and subsidence curves for the five lithostratigraphic units in the Ecca Group (Tables 11.4-11.8) during the Permian time are shown in Figures 11.23-11.28. In this study, the Airy model is used and changes in the supply of sediments as well as water-loading in the basin are accounted for by (1) assuming a homogeneous local, airy-type isostatic adjustment for the lithosphere, and (2) using existing palaeobathymetry data from literature to correct the backstripping model. The results from both models (using (1) and (2)) were compared to see how the effects of palaeobathymetry and water-level fluctuations would affect the subsidence curves. Alao (2012) documented that the subsidence curves are the results from the backstripping inverse model and not direct observation, and should therefore be interpreted with more emphasis on relative rather than absolute values. Furthermore, interpretations of the curves are based on the shape and timing of representative subsidence curves and the major events of all the curves are described in section 11.3.3.1-11.3.3.3. The tectonic subsidence curveswere compared with the previous work of Cloetingh et al. (1992) in order to check the reliability of the subsidence curves.

11.3.3.1 Late Carboniferous-Early Permian subsidence

The compacted, backstripped and total subsidence curves during the Late Carboniferous to Early Permian (302-289 Ma) are linear in profile (Figures 11.23-11.28). This linear subsidence curve has an average subsidence rate of about 272 mMa^{-1} (Table 11.15; arrow 1 in Figures 11.23-11.28) and resulted in the deposition of the diamictite Dwyka Group. The phase is related to the initial extensional fault controlled subsidence of the basin. This subsidence phase continued into the Early Permian with a decreasing subsidence rate, ranging between 22 and 117 mMa^{-1} and corresponds to deposition of the Prince Albert Formation during the interval of 289-276 Ma (Figures 11.23-11.28). Generally, subsidence phase for the Late Carboniferous-Early Permian correlates well with the linear profile at the onset of subsidence in episode 3 of Cloetingh et al. (1992). The Karoo sedimentation appears to have been fault-controlled from the onset.

11.3.3.2 Mid Permian subsidence

The mid Permian subsidence (arrow 2 in Figures 11.23-11.28) brought about a change in the basin configuration as shown on the subsidence curves by straight and convex-upward profiles. This two-fold change in subsidence pattern points to flexural subsidence in Karoo foreland basin, which agreeswith the tectonic model of Visser (1993). The tectonic model of Visser (1993) revealed that the Karoo Basin changed from a back-arc to a foreland basin during the late Early to Mid Permian, causing a major change in the basin configuration. The straight and convex-upward profiles are noticed on the subsidence curves during the interval of 276-273 Ma signifying a short phase of slow subsidence. This subsidence rate gradually decreases through time at an average rate of 28 m Ma^{-1} and 25 m Ma^{-1} and corresponds to the deposition of the Whitehill and Collingham Formations respectively. At the time interval of 273-265 Ma, another gradually decreasing straight profile is noticed on the subsidence curves. This straight profile also indicates a short and relatively rapid flexural subsidence phase with the subsidence rate ranging between 36 mMa^{-1} and 399 mMa^{-1} and corresponds to the deposition of Ripon Formation (Table 11.15, arrow 2 in Figures 11.23-11.28). The mid Permian subsidence phase is also related to the fault controlled subsidence of the basin. This interpretation is based on a characteristic features documented in Allen et al. (1986) that at a rapid subsidence stage, curves are either straight or convex upwards. The mid Permian subsidence phase in the southeastern Karoo subbasin also agrees with the subsidence model produced by Cloetingh et al. (1992) for the southeastern Cape Province.

11.3.3.3 Late Permian subsidence

The last phase is characterised by a decelerating subsidence which possibly represents the post-rift thermal subsidence (arrow 3 in Figures 11.23-11.28). During the Late Permian time, another straight profile is seen on the subsidence curves during the interval of 268-264 Ma. This Late Permian subsidence is interpreted as rapid flexural subsidence with an average subsidence rate of approximately 180 mMa^{-1} and corresponds to the deposition of Fort Brown Formation. Generally, the decelerating subsidence pattern of the Ecca Group is comparable to predictive models of foreland basin subsidence. Decelles and Giles (1996) documented that foreland basins show straight and convex-upwards subsidence curves as a result of subsequent increasing subsidence rates through time. This is due to the migration of a supracrustal orogenic load towards the foreland basin. In addition, Allen et al. (1986) reported that subsidence rates in foreland basins increase towards or decrease away from the orogenic load, and are usually higher than those in extensional basins. Hence, a compressional setting is suggested for the Late Permian subsidence phase, with subsidence resulting from the development of a significant supra-crustal load that is probably related to thrust tectonics from the adjacent Cape Fold Belt (CFB), and the Karoo foreland basin system development during the Late Permian.

Table 11.15: Subsidence rates over time across the study area.

Formation	Location (Boreholes and Outcrop)						Average subsidence rate (mMa^{-1})
	CR 1/68 (mMa^{-1})	SC 3/67 (mMa^{-1})	SFT 2 (mMa^{-1})	Ecca Pass (mMa^{-1})	KWV 1 (mMa^{-1})	SP 1/69 (mMa^{-1})	
Fort Brown	222	208	-	200	134	134	180
Ripon	185	36	65	317	399	290	215
Collingham	21	22	17	23	56	13	25
Whitehill	19	17	14	89	8	20	28
Prince Albert	45	38	38	117	22	24	63
Dwyka Group	324	561	5	119	291	333	272
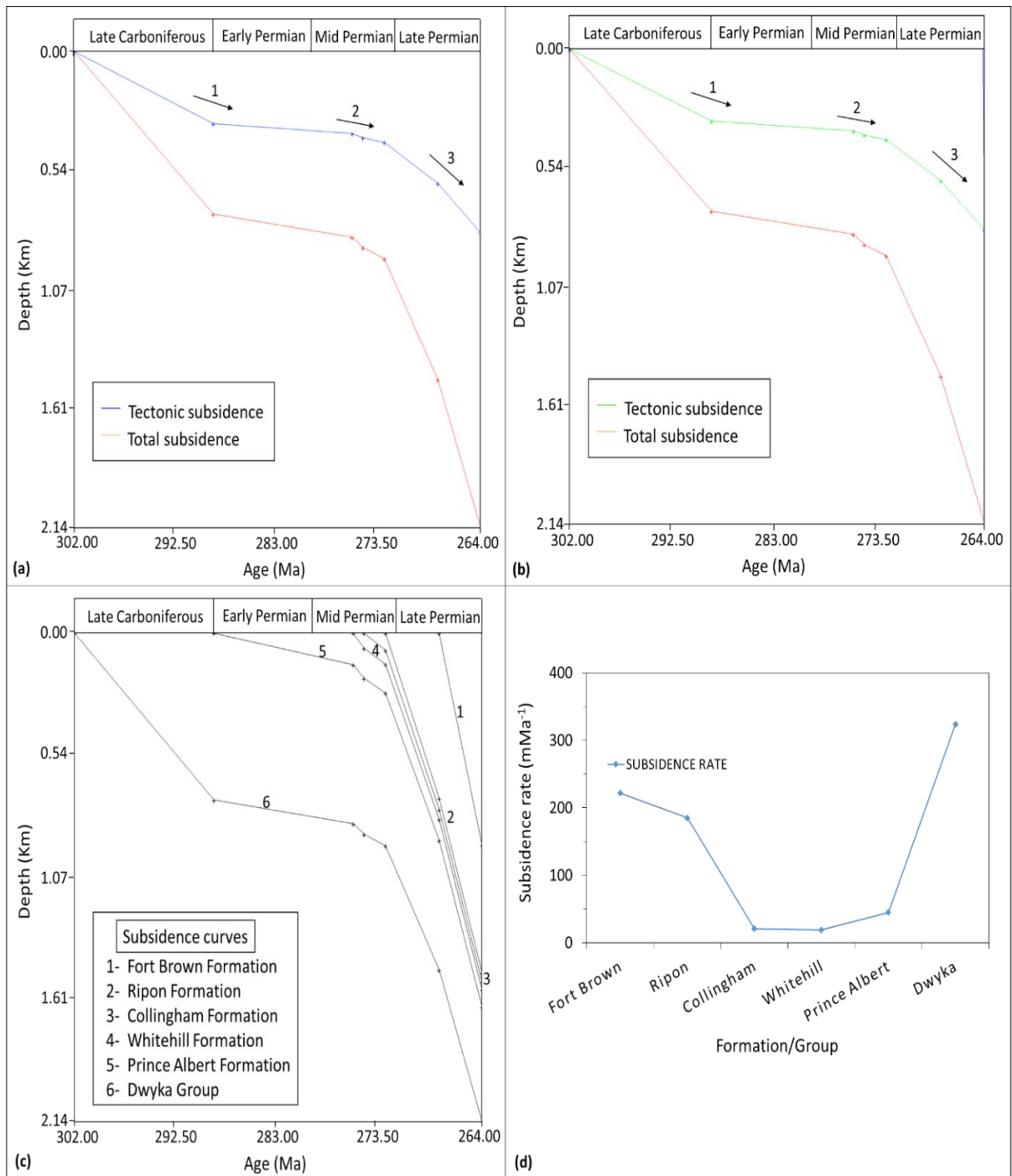
Figure 11.23: 1D Airy subsidence model of the Ecca Group in borehole CR 1/68 showing: (a) Tectonic subsidence curves of the Ecca Group, assuming a homogeneous local, airy-type isostatic adjustment for the lithosphere (Note the three phases indicated by black arrows). (b) Tectonic subsidence curves of the Ecca Group in the Main Karoo Basin, using existing palaeobathymetry data from literature to correct the backstripping model. (c) Backstripping plots of the Ecca Group in the Main Karoo Basin. Boundaries of the five to six selected horizons are recognized on the subsidence curves with ages corresponding to the age of the top surface of each horizon. (d) Subsidence rates over time and corresponding to lithostratigraphic units.
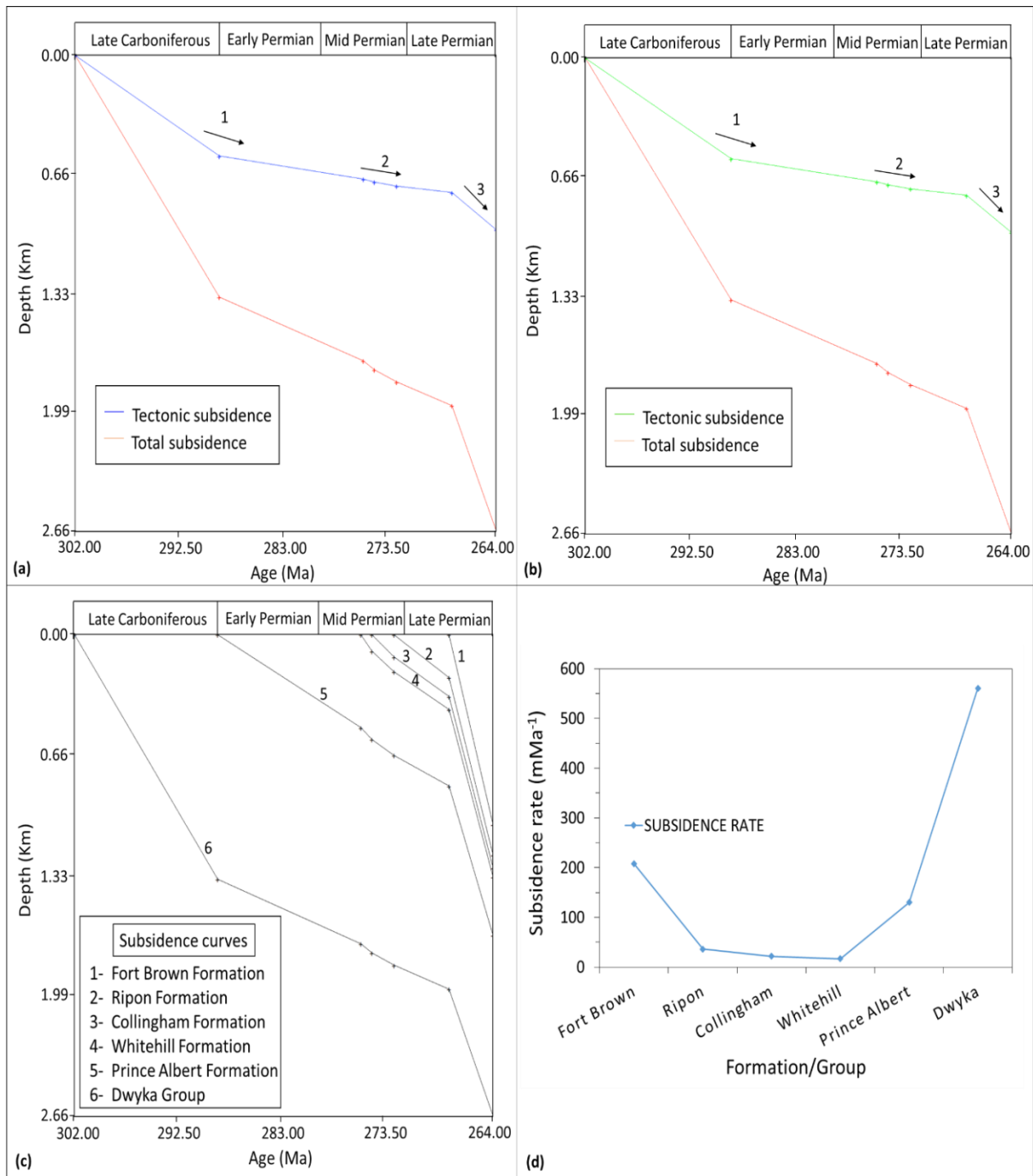
Figure 11.24: 1D Airy subsidence model of the Ecca Group in borehole SC 3/67 showing: (a) Tectonic subsidence curves of the Ecca Group, assuming a homogeneous local, airy-type isostatic adjustment for the lithosphere (Note the three phases indicated by black arrows). (b) Tectonic subsidence curves of the Ecca Group in the Main Karoo Basin, using existing palaeobathymetry data from literature to correct the backstripping model. (c) Backstripping plots of the Ecca Group in the Main Karoo Basin. Boundaries of the five to six selected horizons are recognized on the subsidence curves with ages corresponding to the age of the top surface of each horizon. (d) Subsidence rates over time and corresponding to lithostratigraphic units.
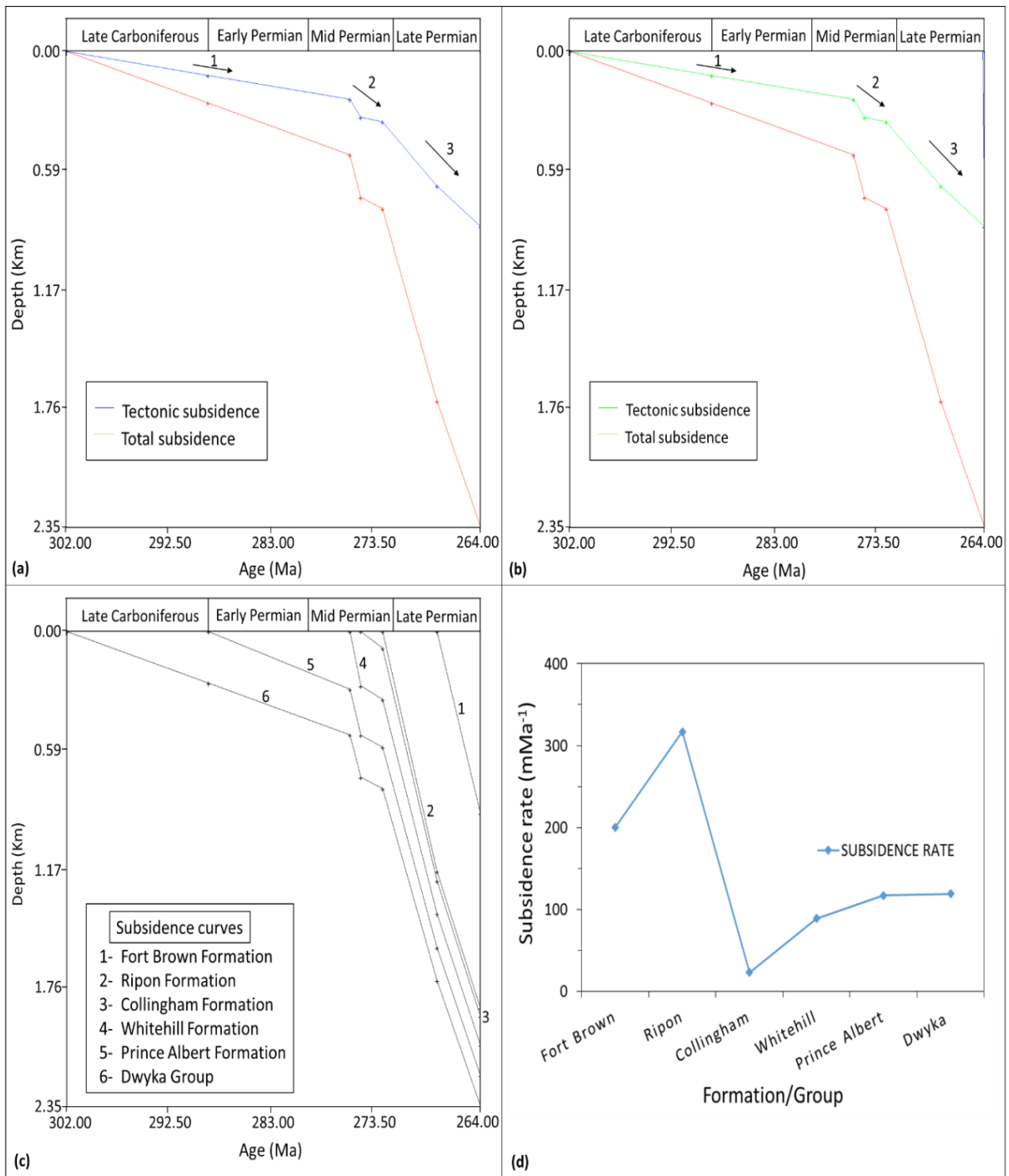
Figure 11.25: 1D Airy subsidence model of the Ecca Group along Ecca Pass Section showing: (a) Tectonic subsidence curves of the Ecca Group, assuming a homogeneous local, airy-type isostatic adjustment for the lithosphere (Note the three phases indicated by black arrows). (b) Tectonic subsidence curves of the Ecca Group in the Main Karoo Basin, using existing palaeobathymetry data from literature to correct the backstripping model. (c) Backstripping plots of the Ecca Group in the Main Karoo Basin. Boundaries of the five to six selected horizons are recognized on the subsidence curves with ages corresponding to the age of the top surface of each horizon. (d) Subsidence rates over time and corresponding to lithostratigraphic units.

375
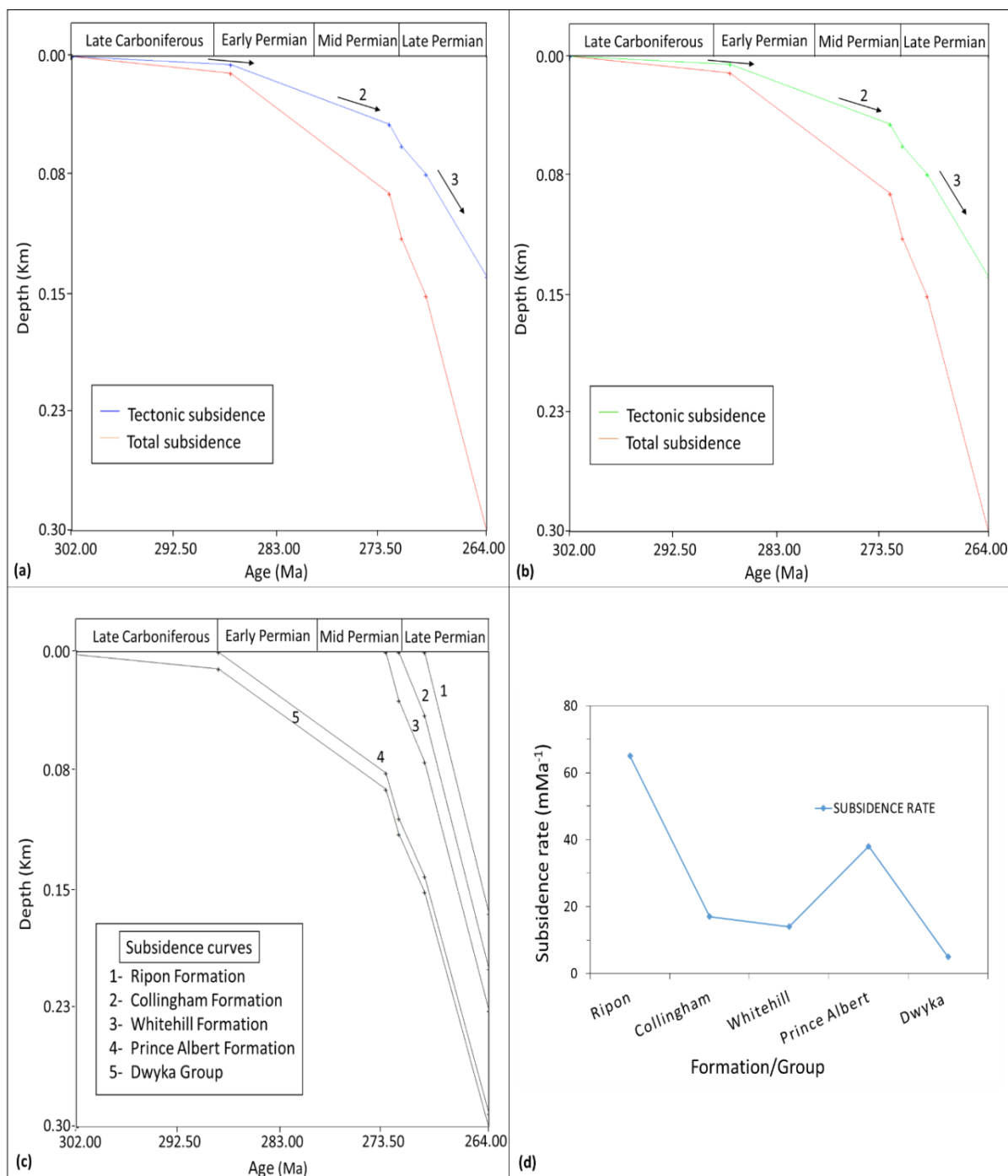
Figure 11.26: 1D Airy subsidence model of the Ecca Group in borehole SFT 2 showing: (a) Tectonic subsidence curves of the Ecca Group, assuming a homogeneous local, airy-type isostatic adjustment for the lithosphere (Note the three phases indicated by black arrows). (b) Tectonic subsidence curves of the Ecca Group in the Main Karoo Basin, using existing palaeobathymetry data from literature to correct the backstripping model. (c) Backstripping plots of the Ecca Group in the Main Karoo Basin. Boundaries of the five to six selected horizons are recognized on the subsidence curves with ages corresponding to the age of the top surface of each horizon. (d) Subsidence rates over time and corresponding to lithostratigraphic units.

376
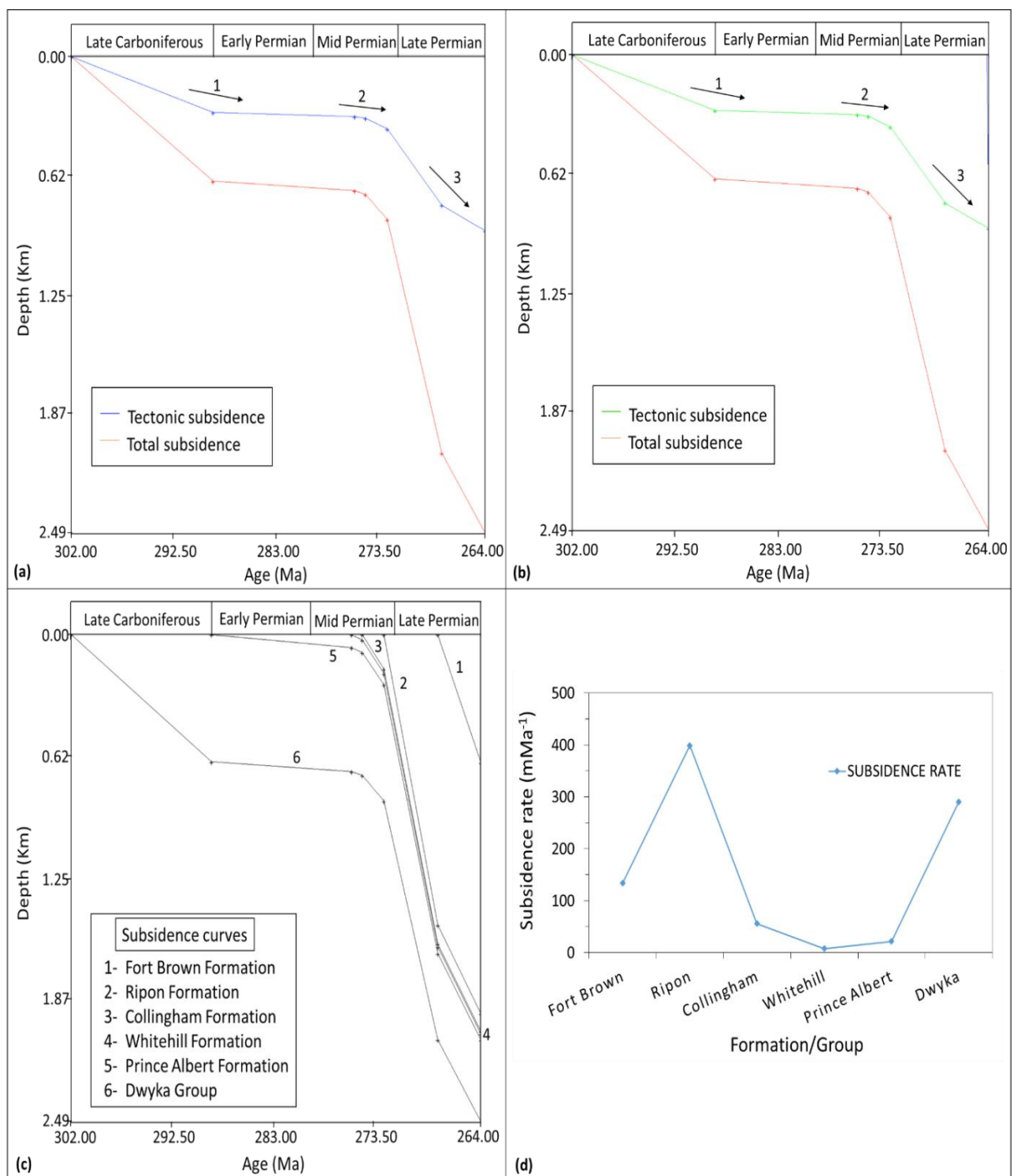
Figure 11.27: 1D Airy subsidence model of the Ecca Group in borehole KWV 1 showing: (a) Tectonic subsidence curves of the Ecca Group, assuming a homogeneous local, airy-type isostatic adjustment for the lithosphere (Note the three phases indicated by black arrows). (b) Tectonic subsidence curves of the Ecca Group in the Main Karoo Basin, using existing palaeobathymetry data from literature to correct the backstripping model. (c) Backstripping plots of the Ecca Group in the Main Karoo Basin. Boundaries of the five to six selected horizons are recognized on the subsidence curves with ages corresponding to the age of the top surface of each horizon. (d) Subsidence rates over time and corresponding to lithostratigraphic units.

Figure 11.28: 1D Airy subsidence model of the Ecca Group in borehole SP 1/69 showing: (a) Tectonic subsidence curves of the Ecca Group, assuming a homogeneous local, airy-type isostatic adjustment for the lithosphere (Note the three phases indicated by black arrows). (b) Tectonic subsidence curves of the Ecca Group in the Main Karoo Basin, using existing palaeobathymetry data from literature to correct the backstripping model. (c) Backstripping plots of the Ecca Group in the Main Karoo Basin. Boundaries of the five to six selected horizons are recognized on the subsidence curves with ages corresponding to the age of the top surface of each horizon. (d) Subsidence rates over time and corresponding to lithostratigraphic units.

378

11.4 Discussion

The calculated compaction and decompaction estimates show that average porosity and percentage compaction of the sandstones and shales reduce with depth. On the other hand, percentage decompaction increases with depth. Generally, in the Ecca Group, the shales of the Prince Albert, Whitehill and Collingham Formations decompacted the most, whereas the sandstones lithostratigraphic units of the Fort Brown Formation are observed to have lowest percentage decompaction and highest percentage compaction. The rate of sedimentation in the Prince Albert, Whitehill, Collingham, Ripon and Fort Brown Formations range between 0.003-0.03 mm yr^{-1}, 0.02-0.05 mm yr^{-1}, 0.01-0.05 mm yr^{-1}, 0.03-0.22 mm yr^{-1}, and 0.15-0.025 mm yr^{-1}, respectively. The thickness of the geologic formations does not increase or decrease in a particular trend or direction, i.e. thickness increases or decreases from E-W and vice versa. In most boreholes, the formation with the highest sedimentation rate (maximum sediments thickness) also has the highest subsidence. This could possibly be due to the fact that the amount of preserved sediment was directly dependent on the amount of basement subsidence. Low and moderate accumulation rates correspond to the deposition of the lower Ecca Group shale and mudstones (Prince Albert, Whitehill and Collingham Formations) and Dwyka Group diamictites. The highest sediment accumulation rates which occurred during times of greatest subsidence correspond to the deposition of the Ripon and Fort Brown Formations. The Early Permian sedimentation is thought to represent the onset of foreland basin deposition.

Tectonic subsidence models were generated for the studied boreholes and outcrop of the Ecca Group by (1) assuming a homogeneous local, airy-type isostatic adjustment for the lithosphere, and (2) using existing palaeobathymetry data from literature to correct the backstripping model. Based on the observations on the subsidence curves, the result from both models (using (1) and (2)) does not show any appreciable variations in terms of the subsidence curves. This possibly suggests that palaeobathymetry and water-level fluctuations do not have significant effects on the tectonic subsidence of the basin during the Permian time. The subsidence plots in Figures 11.23-11.28 show linear, concave and/or convex-upward curves with the subsidence rates decreasing early on and thereafter slightly increase and decrease through the Permo-Carboniferous period. McKenzie (1978) documented that these concave-upward subsidence curves are typical features of tectonic and thermal stages of lithospheric extension (Figure 11.29) that involves mechanical-stretching, while subsequent

delay in subsidence possibly reveals the cooling phases. Using this theory in the context of the southeastern Gondwana, subduction of the paleo-Pacific oceanic plate underneath the Gondwana plate perhaps during the mid Carboniferous, which formed a magmatic arc might have initiated stretching as well as slow thermal subsidence of the lithosphere. In addition, thermal thinning of the lithosphere in the mid Carboniferous time, could have led to the formation of a back-arc basin. This back-arc activity must have resulted in substantial extension followed by thermal subsidence. In this regard, it is suggested that the interior part of the basin was superimposed on a passive continental margin (mechanically extended and thermally subsided lithosphere). This indicates that the subsidence was initiated and thermally controlled by tectonic events, with little contribution of thermal events, which also agrees with the work Visser and Praekelt (1996) and Catuneanu et al. (1998; 2005).
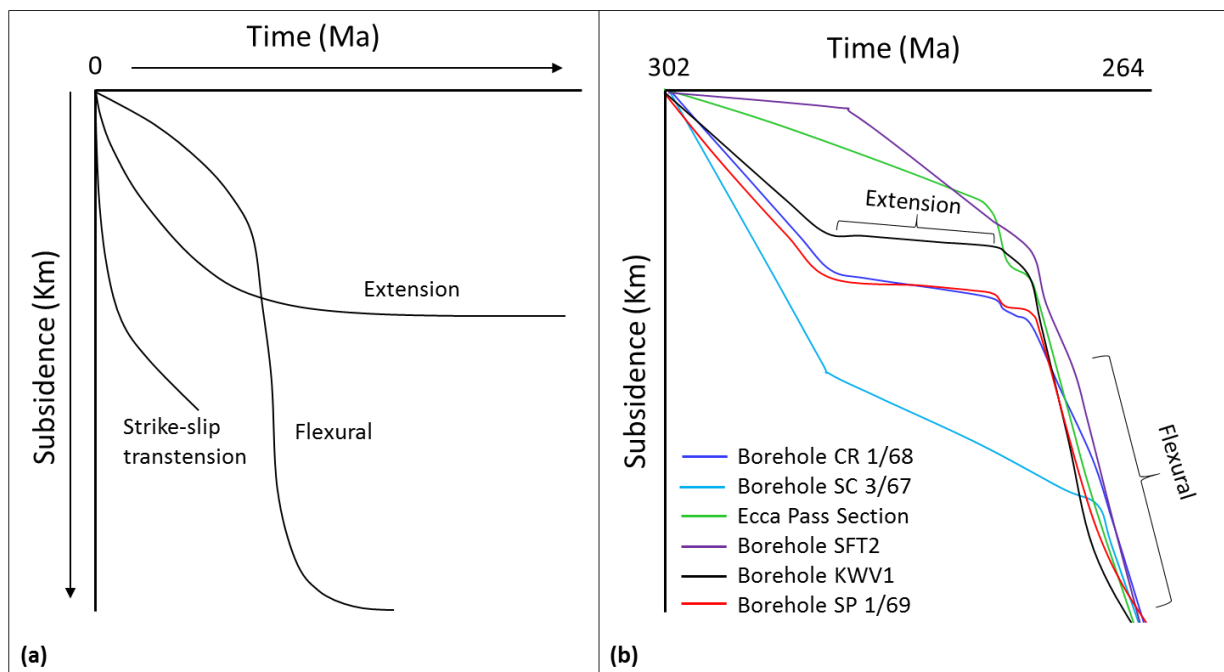
Figure 11.29: Comparison between the tectonic subsidence curves obtained in this study and a simplified diagram depicting the visual expression of basin-generating mechanisms on various subsidence curve patterns (Modified from Alao, 2012). Note: No absolute vertical scale is implied, although relative timescales (horizontals) vary but are often found as shown in Figure 11.29a (Modified after Pitman and Andrews, 1985; Kneller, 1991; Alao, 2012).

Catuneanu et al. (2005) documented that tectonism was the main control on accommodation in the Karoo Basin, with subsidence mechanisms ranging from flexural in the south, in

relation to processes of subduction and orogenesis along the paleo-Pacific margin, to extensional in the north, propagating southwards from the divergent Tethyan margin. The tectonic subsidence of the Ecca Group during the Permian can be subdivided into two major episodes, namely, extensional and compressional episodes (Figure 11.30).
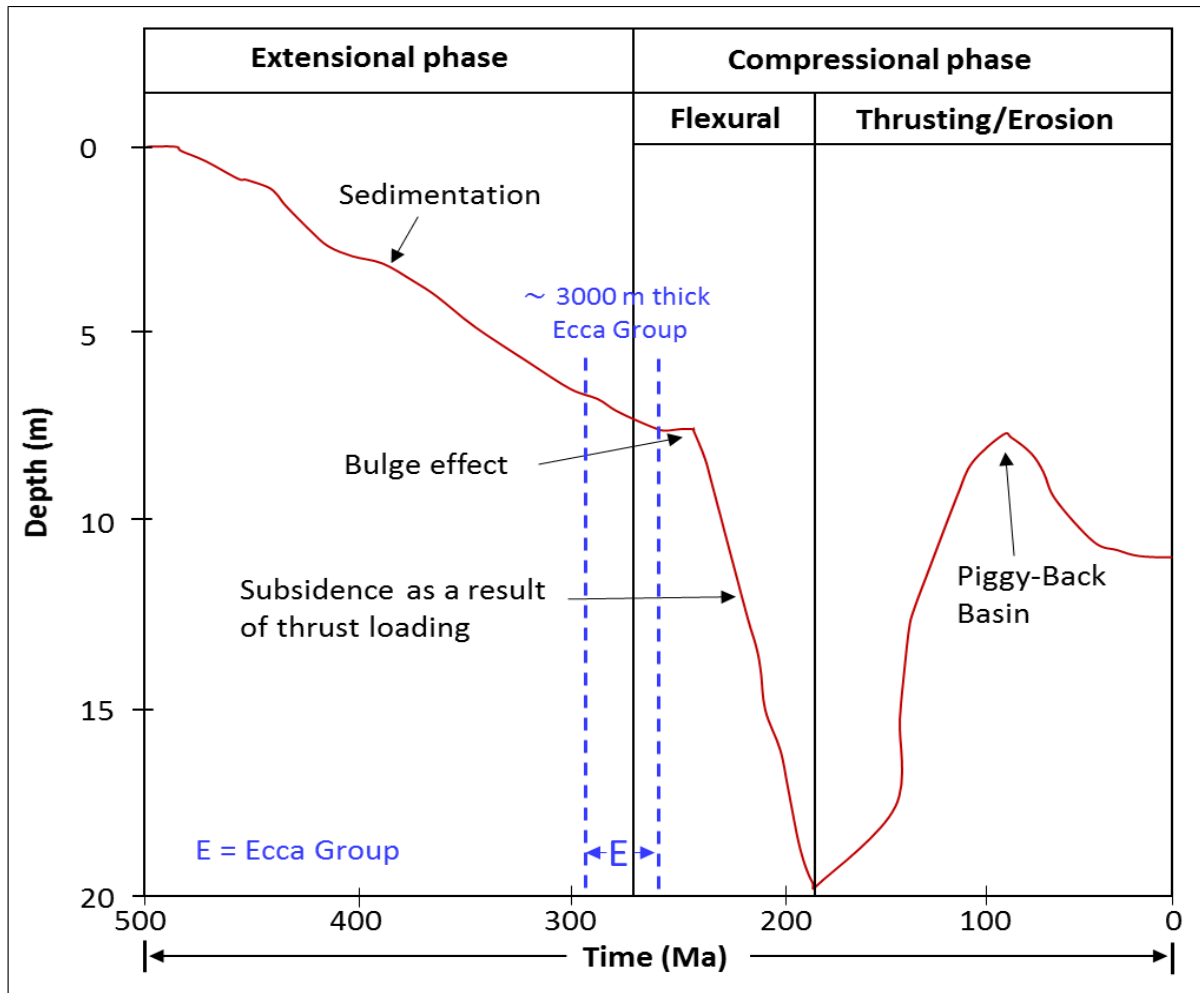
Figure 11.30: Hypothetical illustration of tectonic subsidence of the Ecca Group during the Permian. Note: the piggy-back basin caused by uplift and erosion later on during the compressional phase as expressed would occur craton-ward (i.e. NE direction and distal to the Cape Fold Belt (CFB) (Taken from Alao, 2012).

The extensional episode that occurs between 289-275 Ma involves subsidence that are caused by sedimentation (Figure 11.30). The compressional setting (273-264 Ma) is related to the substratum-upper plate, whereby thrust-faults loading of the CFB induced subsidence of the substratum, which in turn influenced the elastic thickness of the underlying lithosphere.

381

However, Tankard et al. (2012) reported that regional thickness and stratigraphic variation in the Cape and Karoo basins reveal the control of first-order crustal faults and asymmetric subsidence of the intervening basement blocks. Furthermore, the Ecca subsidence between these crustal faults were uniform and without the characteristics diagnostic of significant upper-plate extension, such as normal basin-forming faults, syn-rift sedimentary wedges or unconformities.

Alao (2012) documented that the "early occurrence of extensional tectonics as well as the development of a passive margin shows that the subsidence was initiated and mainly controlled by mechanical (i.e. detachment faults of basement blocks that occurred during rifting), rather than thermal geologic events (i.e. sediment burial)". Also, as overthrusting continues, the orogenic belt progressively loads more rigid lithosphere on the landward side of the former passive margin. Furthermore, variations in the flexural rigidity along the strike of the basin perhaps resulted in the irregular lateral changes in the subsidence history (Figures 11.23c, 11.24c, 11.25c 11.26c, 11.27c and 11.28c). The flexural subsidence during the interval of 273 to 264 Ma observed on the subsidence curves (Figure 11.23-11.28) also concur with the tectonic model of Visser (1993). Visser (1993) proposed that, during the Late Carboniferous to Early Permian, a major change in basin configuration for the Karoo Basin involving the transition from a back-arc to a foreland basin occurred. The source of the sedimentary fill in the Karoo Basin is related to the mountain belt in the paleo-Pacific southwestern Gondwana when rifting of the Gondwana supercontinent began, also referred to as the flexural subsidence stage (Johnson, 1991; Cole, 1992; Duncan et al., 1997).

11.5 Conclusions

The backstripping technique has been applied to five boreholes and one road-cut exposure (outcrop) of the Permian Ecca Group in the Eastern Cape Province of South Africa. The results presented in this study show that the average rate of sedimentation in the Prince Albert, Whitehill, Collingham, Ripon and Formations are 0.01 mm yr^{-1}, 0.04 mm yr^{-1}, 0.03 mm yr^{-1}, 0.14 mm yr^{-1}, and 0.20mm yr^{-1}, respectively. The subsidence curves show subsidence rates decreasing with time, resembling the typical thermal subsidence curves of passive continental margins. Three major subsidence episodes characterised the Ecca Group, namely, (1) rapid subsidence in an extensional regime, (2) slow subsidence in the middle of basin development, and (3) another rapid subsidence in compressional regime. In the Late

Carboniferous to Early Permian, rapid initial subsidence was observed on the subsidence curves during the deposition of Dwyka Group and Prince Albert Formation. This rapid subsidence in an extensional regime (mechanical stretching) is interpreted to be due to heating of the lithosphere. In the mid Permian, slow subsidence was driven under the effect of sedimentary weight, when Whitehill and Collingham Formations were deposited. After that, rapid subsidence happened in the Late Permian during the deposition of Ripon and Fort Brown Formation, which possibly reflects regional compressional event, perhaps foreland compression. In the mid Permian, the slow subsidence rate points to a cooling phase that succeeds the initial heating. The average rate of tectonic subsidence in the Prince Albert, Whitehill, Collingham, Ripon and Formations are 63 mMa^{-1}, 28 mMa^{-1}, 25 mMa^{-1}, 215 mMa^{-1}, and 180 mMa^{-1}, respectively. The tectonic subsidence analysis with and without palaeobathymetry and water depth corrections show very small or no variations to the computed subsidence curves. Consequently, it is inferred that effect of palaeobathymetry and water-level fluctuations on tectonic subsidence of southeastern Karoo Basin is negligible when using 1D airy isostatic model and can be ignored in further tectonic subsidence study in the area.

CHAPTER 12
SUMMARY

The stratigraphy of the Ecca Group in the study area was previously subdivided into five formations, namely the Prince Albert, Whitehill, Collingham, Ripon and Fort Brown Formations (Rossouw, 1953; Johnson 1976; Kingsley, 1977; Johnson et al., 2006). These

formations have now been further subdivided into stratigraphic members based on their lithological features and sedimentary structures. The Prince Albert Formation is subdivided into the Lower Grey Mudrock Member and Upper Khaki Mudrock Member. Succeeding the Prince Albert Formation is the Whitehill Formation, which is subdivided into the Lower Black Shale-Chert Member and Upper Grey Mudrock Member. The contact between the Whitehill Formation and Prince Albert Formation is disconformity, rather than conformity as was suggested in the previous studies. The Collingham Formation is subdivided into the Lower Black Rhythmite Member and Upper Grey Mudrock Member. The overlying Ripon Formation is subdivided into the Lower Greywacke-Mudrock Member, Middle Black Mudrock Member and Upper Grey Mudrock-Sandstone Member. From the bottom to the top, the three members correspond to the Pluto's Vale, Wonderfontein and Trumpeters Members that were named by Kingsley (1977, 1981). The Fort Brown Formation is subdivided into the Lower Grey Varved Rhythmite Member and Upper Grey Sandstone-Mudrock Member. The above mentioned stratigraphic Members are newly established Members of the Ecca Group.

The grain size parameters of the Ecca Group sandstones show that most of the sandstones are very fine to fine grained, poorly to moderately sorted, mostly near-symmetrical and mesokurtic in nature. The linear discriminant function (LDF) analyses are dominantly indicative of turbidity current deposits under marine environment for samples from the Prince Albert, Collingham and Ripon Formations, while those samples from the Fort Brown Formation are deltaic deposits. The CM pattern shows a clustered distribution of sandstones in the PQ and QR segments, indicating that the sandstones were deposited mostly by suspension and rolling/saltation. The log probability grain-distribution curves indicate the variability of hydraulic depositional conditions for the Ecca Group sandstones. Saltation is the major process of transportation, although suspension and traction also played some role during deposition of the finer sediments.

A total of fourteen major lithofacies were identified in the Ecca Group, which can be grouped into seven distinct facies associations (FAs), which are: Shale and mudstones intercalated with siltstones (FA 1), carbonaceous shale, mudstone with chert beds (FA 2), mudstones-claystone rhythmite with lenticular siltstone (FA 3), greyish medium bedded sandstone intercalated with laminated mudstone (FA 4), dark-grey medium to thick bedded mudstone and siltstone (FA 5), thin to medium bedded sandstone alternated with thin bedded carbonaceous mudstone (FA 6), and varved mudstone rhythmite intercalated with siltstone

and sandstone (FA 7). The Ecca Group is interpreted to have progressively changed upwards from deep marine environment (FA 1, FA 2, FA 3, FA 4 and FA 5) to shallow marine environment (FA 6), and finally to lacustrine environment (FA 7).

The petrographic study of Ecca sandstones revealed that they are generally poorly to moderate sorted, and texturally and compositionally immature. Modal composition analyses of the sandstones show that the detrital components of the sandstones are dominated by monocrystalline quartz, feldspar (mostly K-feldspar) and lithic fragments. The sandstones can be classified as feldspathic wacke and lithic wacke. The QFL ternary diagrams reveal a dissected and transitional arc provenance pointing to an active margin and uplifted basement. This is an indication that the sandstones were derived from a magmatic arc and metamorphic provenances. The detrital modal compositions of these sandstones are related to back arc to island and continental margin arc.

Geochemical compositions of the sandstones and shales were analysed to identify provenance, paleoweathering conditions and ancient tectonic environment characteristics of the Karoo Basin. The geochemical data of major and trace elements show that the studied sandstone and shales have the same source. The discriminant function plots indicated that the sandstones and shales are mostly of quartzose sedimentary provenance, suggesting that they were derived from a cratonic interior or recycled orogen. The cross plot and ternary plots of the geochemical data revealed that the shales and sandstones were derived from felsic igneous rocks. A-CN-K ternary diagram and indices of weathering revealed that the granitic source rocks underwent moderate to high degree of chemical weathering. The tectonic setting discrimination diagrams support passive continental margin setting of provenance.

The organic geochemical investigations of Ecca Group shales indicate the presence of gas-prone potential source rocks with fair to excellent hydrocarbon source potential. The Tmax and vitrinite reflectance values indicate immature to over maturity of the shales, which are variable with localities. Binary plots of HI against OI, and HI versus Tmax shows that the shales are of Type II and mixed Type II-III kerogen, which are capable of generating both gas and minor oil. Based on the geochemical data, it can be inferred that source rocks are immature to over-matured and have potential of producing gas in present-day. The Whitehill Formation is generally comparable to the Marcellus and Barnett Shales. This further supports

the assumption that the Whitehill Formation has a high probability of being a profitable shale gas play, but only when explored in dolerite-free area.

The diagenetic process in the Ecca Group rocks had passed through early, burial and uplift diagenetic stages. In the early diagenetic stages, sediments mainly underwent cementation, authigenesis and lithification. Mechanical compaction, recrystallization, pressure solution, dissolution by pore fluids, mineral replacement, clay-mineral conversion, mineral deformation and pressure-solution are the main diagenetic processes during burial diagenesis. Uplift-related diagenesis comprises of decementation, mineral replacement, oxidation of ferromagnesian minerals, saussuritization and weathering. Quartz, calcite, hematite, clay matrix and authigenic clay minerals are the five cement types with feldspar as a minor cement type identified in the rocks of the Ecca Group. Petrophysically, potential reservoir quality of the Ecca Group is poor to medium. The presence of fractured and dissolution pores tend to enhance reservoir quality.

HRP and VES technique of the electrical resistivity method has proven to be successful and highly effective in the identification and delineation of subsurface structures. The HRP result revealed that the resistivity of the subsurface varies laterally between 2 Ωm and 500 Ωm. The VES curves indicate four to five geoelectric layers. The resistivity pseudosections (inverse models) exhibit gradational change in resistivity with depth, indicating the different rock units. The 2-D resistivity pseudosections revealed that the lower Ecca Group rocks are generally characterised by low resistivity compared to the upper Ecca Group rocks. These low resistivities (high conductivities) are thought to be as a result of the high organic matter and pyrite contents in the lower Ecca Group shales. The general forms of these dolerite intrusions are sills and dykes within a matrix of sediments. Due to the hardness and high resistivity of dolerite intrusions, they are likely to introduce a technical difficulty in the drilling stage of the hydraulic fracturing process.

Backstripping analysis has been carried out on five boreholes and one outcrop section of the Ecca Group in the Main Karoo Basin. The result shows that rapid subsidence in an early extensional regime, slow subsidence in the middle of basin development, and another late rapid subsidence in compressional regime are the three major subsidence episodes that characterised the Ecca Group. The decelerating subsidence pattern of the Ecca Group is generally comparable to predictive models of foreland basin subsidence.

This study has identified the Ecca Group as a potential unconventional gas reservoir, which is important for future shale gas exploration. Geophysical and subsidence studies have revealed the basin architecture, which will provide a reference for future exploration projects in the study area. Furthermore, the geophysical results have revealed the extensive network of dolerite sills and dykes throughout the study area, which has drawn attention to fracking operations. The datasets used in this study provide a foundation on which new knowledge can be built.

REFERENCES

- Aarnes, I., Svensen, H., Polteau, S. and Planke, S. (2011). Contact metamorphic devolatilization of shales in the Karoo Basin, South Africa, and the effects of multiple sill intrusions. Chemical Geology, 281(3), 181-194.

- Aarnes, I., Svensen, H., Conolly, J.A.D. and Podladchikov, Y.Y. (2010). How contact metamorphism can trigger global climate changes: Modeling gas generation around igneous sills in sedimentary basins. Geochimica et Cosmochimica Acta, 74, 7179-7195.

- Adams, J. (1977). Sieve size statistics from grain measurement. Journal of Geology, 85, 209-227.

- Advance Resource International, (2013). Shale gas and oil assessment in Karoo Basin, South Africa. In: EIA/ARI World Shale Gas and Shale Oil Resource Assessment, 1-14. http://www.adv-res.com/pdf/19_XIX_EIA_ARI__S%20Africa_June_2013.pdf

- Ahzegbobor, P.A. (2010). 2D and 3D Geoelectrical Resistivity Imaging: Theory and Field Design. Scientific Research and Essays, 5(23), 3592-3605.

- Ajdukiewicz, J.M. and Lander, R.H. (2010). Sandstone reservoir quality prediction: the state of the art. American Association of Petroleum Geologists Bulletin, 94 (8), 1083-1091.

- Alao, A.O. (2012). Basin-fill of the Permian Tanqua Depocentre, Sw Karoo Basin, South Africa. MSc dissertation (Unpublished). Stellenbosch University, South Africa, 168pp.

- Alao, A.O. and Mikes, D. (2011). Subsidence analysis of the Permian Tanqua depocentre, Southwestern Karoo Basin, South Africa. South Africa Journal of Geology, 114, 325-328.

- Al-Ghadban, A.N. (1990). Holocene sediments in a shallow bay, southern coast of Kuwait, Arabian Gulf. Marine Geology, 92, 237-254.

- Allen, P.A., Homewood, P. and Williams, G.D. (1986). Foreland basins: an introduction. In: P.A. Allen, and P. Homewood (Eds). "Foreland Basins". Special Publications International Association of Sedimentologists, 8, 3-12.

- Allen, P.A. and Allen, J.R. (1990). Basin Analysis: Principles and Applications, Blackwell Scientific Publications, Oxford, 449pp.

- Allen, P.A. and Allen, J.R. (2004). Basin Analysis: Principles and Applications. 2nd edition, Blackwell, Scientific Publications, Oxford, 560pp.

- Almond, J.E. (2013). Palaeontological Heritage Study: Combined desktop and field based Assessment. Natura Viva cc, Cape Town, 33pp.

- American Society for Testing and Materials, ASTM D7708-14 (2014). Standard Test Method for Microscopical Determination of the Reflectance of Vitrinite Dispersed in Sedimentary Rocks, ASTM International, West Conshohocken, PA, 14pp.

- Amy, L.A., Peachy, S.A., Gardiner, A.A. and Talling P.J. (2009). Prediction of hydrocarbon recovery from turbidite sandstones with linked-debrite facies: Numerical flow simulation studies. Marine and Petroleum Geology, 26, 2032-2043.

- Andersson, P.O.D., Johansson, A. and Kumpulainen, F. (2003). Sm-Nd isotope evidence for the provenance of the Skoorsteenberg Formation, Karoo Supergroup, South Africa. Journal of African Earth Science, 36, 173-183.

- Angusamy, N. and Rajamanickam, G.V. (2006). Depositional environment of sediments along the southern coast of Tamil Nadu, India. Oceanologia, 48 (1), 87-102.

- Araújo, C.E.G., Pinéo, T.R.G., Caby, R., Costa, F.G., Cavalcante, J.C., Vasconcelos, A.M. and Rodrigues, J.B. (2010). Provenance of the Novo Oriente Group, Southwestern Ceará Central Domain, Borborema Province (NE-Brazil): A dismembered segment of a magma-poor passive margin or a restricted rift-related basin. Gondwana Research, 18, 497-513.

- Armstrong-Altrin, J.S. (2009). Provenance of sands from Cazones, Acapulco, and Bahía Kino beaches, Mexico. Revista Mexicana de Ciencias Geológicas, 26(3), 764-782.

- Armstrong-Altrin, J.S., Lee, Y.I., Verma, S.P. and Ramasamy, S. (2004) Geochemistry of sandstones from the Upper Miocene Kudankulam Formation, southern India: implication for provenance, weathering and tectonic setting. Journal of Sedimentary Research, 74, 285-297.

- Bamford, M.K. (2000). Fossil wood of Karoo age deposits in South Africa and Namibia as aid in biostratigraphical correlation. Journal of African Earth Sciences, 31, 119-132.

- Bamford, M.K. (2004). Diversity of the woody vegetation of Gondwana, Southern Africa. Gondwana Research, 7, 153-164.

- Bangert, B., Stollhofen, H., Lorenz, V. and Armstrong, R. (1999). The geochronology and significance of ash-fall tuffs in the glaciogenic Carboniferous-Permian Dwyka Group of Namibia and South Africa. Journal of African Earth Sciences, 29, 33-49.

- Barker, C. (1996). Thermal Modelling of Petroleum Generation: Theory and Applications, Elsevier, New York, 62pp.

- Bartolini, C., Berlato, S. and Bortolotti, V. (1975). Upper Miocene shallow-water turbidites from western Tuscany. Sedimentary Geology, 14, 77-122.

- Basu, A. (2003). A perspective on quantitative provenance analysis, in Valloni, R., Basu, A. (Eds.), Quantitative Provenance Studies in Italy: Memorie Descrittive Della Carta Geologica dell'Italia, 61, 11-22.

- Basu, A.S., Suttner, L.J., James, W.C. and Mack, G.H. (1975). Re-evaluation of the use of undulatory extinction and crystallinity in detrital quartz for provenance interpretation. Journal of Sedimentary Petrology, 45, 873-882.

- Bauluz, B., Mayayo, M.J., Fernandez-Nieto, C. and Gonzalez-Lopez, J.M. (2000). Geochemistry of Precambrian and Paleozoic siliciclastic rocks from the Iberian Range (NE Spain): implications for source-area weathering, sorting, provenance, and tectonic setting. Chemical Geology, 168, 135-150.

- Bauluz, B., Nieto, F., Mata, P., Giorgetti, G., Arkai, P. and Peacor, D. (2005). Retrograde diagenesis: A widespread process on a regional scale. Clay Minerals, 1, 93-104.

- Beaumont, C., Quinlan, G.M. and Stockmal, G.S. (1993). The evolution of the western interior basin: causes, consequences and unsolved problems. In: W.G.E. Caldwell, E.G. Kauffman (Eds.). Evolution of the Western Interior Basin. Geological Association of Canada Special Paper, 39, 97-117.

- Beukes, N.J. (1970). Stratigraphy and sedimentology of the Cave Sandstone Stage, Karoo System. In: S.H. Haughton (Ed.). Proceedings 2nd IUGS Symposium on Gondwana Stratigraphy and Palaeontology, CSIR, Pretoria, South Africa, 321-341.

- Bhat, M.S., Chavadi, V.C. and Hegde, V.S. (2002). Morphological and textural characteristics of Kudle beach, Karnataka, central west coast of India. Lour. Geological Society of India, 59, 125-131.

- Bhatia, M.R. (1983). Plate tectonics and geochemical composition of sandstones. Journal of Geology, 91, 611-627.

- Bhatia, M.R. and Crook, K.A.W. (1986). Trace element characteristics of greywacke and tectonic setting discrimination of sedimentary basins. Contributions to Mineralogy and Petrology, 92, 181-193.

- Bipartisan Policy Center, (2012). Shale gas: new opportunities, new challenges, Bipartisan Policy Center Energy Report, 26pp.

- Bjorlykke, K. (1988). Diagenesis, I, Development in Sedimentology. In: G.V. Chilingarian and K.H. Wolf (Eds.). Elsevier, Amsterdam, 41, 555-588.

- Bjorlykke, K. (1989). Sedimentology and Petroleum Geology. Springer-Verlag, New York, 263pp.

- Bjorlykke, K., Elverhoi, A. and Malm, O. (1979). Diagenesis in Mesozoic Sandstones from Spitzbergen and the North Sea – a comparison. Geologische Rundschau Journal, 68, 1152-1171.

- Black, D.E., Booth, P.W.K. and de Wit, M.J. (2016). Petrographic, geochemical and petro-physical analysis of the Collingham Formation near Jansenville, Eastern Cape, South Africa – potential cap rocks to shale gas in the Karoo. South African Journal of Geology, 119 (1), 171-186.

- Blakey, R.C. (2008). Gondwana palaeogeography from assembly to breakup - A 500 m.y. odyssey. The Geological Society of America Special Paper, 441, 1-28.

- Blatt, H., Middleton, G. and Murray, R. (1980). Origin of Sedimentary Rocks. Prentice-Hall, New Jersey, 782pp.

- Bloch, S., Lander, R. H., and Bonell, L. (2002). Anomalously high porosity and permeability in deeply buried sandstones reservoirs. Origin and predictability. American Association of Petroleum Geologists Bulletin, 86, 301-328.

- Blott, S.J. and Pye, K. (2001). Gradistat: A Grain Size Distribution and Statistics Package for The Analysis of Unconsolidated Sediments. Earth Surface Processes and Landforms, 26, 1237-1248.

- Boggs, S.J. (1995). Principles of Sedimentology and Stratigraphy, 2nd Edition. Prentice Hall, Upper Saddle River, New Jersey, 774pp.

- Boggs, S.J. (2001). Principles of Sedimentology and Stratigraphy, 3rd Edition. Prentice Hall, New Jersey, 726pp.

- Boggs, S.J. (2006). Principles of Sedimentology and Stratigraphy, 4th Edition. Prentice Hall, Upper Saddle River, New Jersey, 774pp.

- Boggs S. J. (2009). Petrology of sedimentary rocks. 2nd Edition. Cambridge University Press, Cambridge, 600pp.

- Bond, G.C. and Kominz, M.A. (1984). Construction of tectonic subsidence curves for the early Palaeozoic miogeocline, southern Canadian Rocky Mountains: Implications for subsidence mechanisms, age of breakup, and crustal thinning. Geological Society of America Bulletin, 95, (2), 155-173.

- Bouma, A. H. (1962). Sedimentology of Some Flysch Deposits: Amsterdam (Elsevier): Amsterdam, 168pp.

- Bordy, E.M., Hancox, P.J. and Rubidge, B. (2004). Provenance studies of the Late Triassic-Early Jurassic Elliot formation, Main Karoo Basin, South Africa. South Africa Journal of Geology, 107, 587-602.

- Bordy, E.M., Hancox, P.J. and Rubidge, B. (2005). The contact of the Molteno and Elliot Formations through the Main Karoo Basin, South Africa: A second-sequence boundary. South Africa Journal of Geology, 108, 351-364.

- Bordy, E.M. and Catuneanu, O. (2001). Sedimentology of the Upper Karoo fluvial strata in the Tuli Basin, South Africa. Journal of African Earth Sciences, 33, 605-629.

- Bowden, L.L. (2014). A comparative study of detrital zircon ages from river sediment and rocks of the Karoo Supergroup (Late Carboniferous to Jurassic), Eastern Cape Province, South Africa: Implications for the tectono-sedimentary evolution of Gondwanaland's southern continental margin. MSc dissertation (Unpublished). University of Johannesburg, South Africa, 321pp.

- BP Statistical Energy Survey (2012). BP Statistical Review of World Energy, 1-45. http://www.bp.com/content/dam/bp/pdf/Statistical-Review 2012/

- Bracciali, L., Marroni, M., Pandolfi, L. and Rocchi, S. (2007). Geochemistry and petrography of Western Tethys Cretaceous sedimentary covers (Corsica and Northern Apennines): From source area to configuration of margins. In: J. Arribas, S. Critlli, M.J. Johanson, (Eds.). Sedimentary provenance and petrogenesis: Perspectives from petrography and geochemistry. Geological Society of America, Special Paper, 420, 73-93.

- Branch, T., Ritter, O., Weckmann, U., Sachsenhofer, R. and Schilling, F. (2007). The Whitehill Formation- a high conductivity marker horizon in the Karoo Basin. South African Journal of Geology, 110, 465-476.

- Bruner, K.R. and Smosna, R. A. (2011). Comparative Study of the Mississippian Barnett Shale, Fort Worth Basin and Devonian Marcellus Shale, Appalachian Basin. U.S. Department of Energy (DOE). National Energy Technology Laboratory, 118pp.

- Burgess, P.M., Gurnis, M. and Moresi, L. (1997). Formation of sequences in the cratonic interior of North America by interaction between mantle, eustatic, and stratigraphic processes. Geological Society of America Bulletin, 108 (12), 1515-1535.

- Burhanuddin, M. (2007). Textural analysis in interpreting the depositional environmental of Lower Gondwana Sandstone in central part of Godavari basin, Andhra Pradesh. Journal of the Geological Society of India, 69, 1335-1341.

- Burke, K. and Dewey, J.F. (1973). Plume generated triple junctions: key indicators in applying plate tectonics to old rocks. Journal of Geology, 81, 406-433.

- Burley, S.D. and Worden, R.H. (2003). Sandstone diagenesis: The evolution of sand to stone. In: S.D. Burley and R.H. Worden (Eds.), Sandstone Diagenesis; Recent and Ancient: Blackwell Publishing, Malden, MA, International Association of Sedimentologists Reprint Series, 4, 3-44.

- Bruner, K.R. and Smosna, R. (2011). A Comparative Study of the Mississippian Barnett Shale, Fort Worth Basin and Devonian Marcellus Shale, Appalachian Basin. U.S. Department Energy, National Energy Technology Laboratory, DOE/NETL/2011/1478, 106pp.

- Burwood, R., de Witte, S.M., Mycke, B. and Paulet, J. (1995). Petroleum geochemical characterisation of the lower Congo coastal basin bucomazi formation. In: B.J. Katz, (ed.), Petroleum Source Rocks. Springer- Verlag, Berlin, 235-263.

- Business Day live (2014). South Africa petroleum agency's Karoo shale-gas estimate 'far lower'.http://www.bdlive.co.za/business/energy/2014/02/21/sapetroleumagencys-karoo-shale-gas-estimate-far-lower.html

- Bustin, M.R., Bustin, A., Chamlmers, G., Murthy, V., Laxmi, C. and Cui, X. (2009). Shale gas opportunities and challenges. Search and Discovery Article No. 40382, 18-27.

- Cadle, A.B., Cairncross, B., Christie, A.D.M. and Roberts, D.L. (1993). The Karoo Basin of South Africa: type basin for the coal-bearing deposits of southern Africa. International Journal of Coal Geology, 23, 117-157.

- Cairncross, B. (2001). An overview of the Permian (Karoo) coal deposits of southern Africa. Journal of African Earth Sciences, 33, 529-562.

- Catuneanu, O. (2004). Retroarc foreland systems-evolution through time. Journal of Earth Sciences, 38, 225-242.

- Catuneanu, O. and Elango, H.N. (2001). Tectonic control on fluvial styles: the Balfour Formation of the Karoo Basin, South Africa. Sedimentary Geology, 140, 291-313.

- Catuneanu, O., Beaumont, C. and Waschbusch, P. (1997). Interplay of static loads and subduction dynamics in foreland basins: Reciprocal stratigraphies and the ''missing'' peripheral bulge. Geology, 25 (12), 1087-1090.

- Catuneanu, O., Hancox, P.J. and Rubidge, B.S. (1998). Reciprocal flexural behavior and contrasting stratigraphies: A new basin development model for the Karoo retroarc foreland system, South Africa. Basin Research, 10, 417-439.

- Catuneanu, O., Hancox, P.J., Cairncross, B. and Rubidge, B.S. (2002). Foredeep submarine fans and forebulge deltas: Orogenic off-loading in the underfilled Karoo Basin. Journal of African Earth Sciences, 35, 489-502.

- Catuneanu, O., Sweet, A.R. and Miall, A.D. (1999). Concept and styles of reciprocal stratigraphies: Western Canada foreland basin. Terra Nova, 11, 1-8.

- Catuneanu, O., Sweet, A.R. and Miall, A.D. (2000). Reciprocal stratigraphy of the Campanian-Paleocene Western Interior of North America. Sedimentary Geology, 134 (3-4), 235-255.

- Catuneanu, O., Wopfner, H., Eriksson, P.G., Cairncross, B., Rubidge, B.S., Smith, R.M.H. and Hancox, P.J. (2005). The Karoo basins of south-central Africa. Journal of African Earth Sciences, 43, 211-253.

- Chapelle, F.H. (1993). Ground-water Microbiology and Geochemistry. John Wiley and Sons, New York, 448pp.

- Chevalier, L., Goedhart, M. and Woodford, A.C. (2001). The influence of dolerite sill and ring complexes on the occurrence of groundwater in Karoo Fractured Aquifers: a morpho-tectonic approach. WRC Report No. 937/1/01.

- Chevallier, L. and Woodford, A.C. (1999). Morpho-tectonics and mechanism of emplacement of the dolerite rings and sills of the western Karoo, South Africa. South African Journal of Geology, 102, 43-54.

- Cloetingh, S., Lankreijer, A., de Wit, M.J. and Martinez, I. (1992). Subsidence history analysis and forward modelling of the Cape and Karoo super groups. In: M.J. de Wit and I.G.D. Ransome (Eds.). Inversion Tectonics of the Cape Fold Belt, Karoo and Cretaceous Basins of Southern Africa. Balkema, Rotterdam, 239-248.

- Cole, D.I. (1992). Evolution and development of the Karoo Basin. In: M.J. de Wit and I.D.G. Ransome, (Eds.). Inversion Tectonics of the Cape Fold Belt, Karoo and Cretaceous Basins of Southern Africa, Balkema, Rotterdam, Netherlands, 87-99.

- Cole, D.I. and Smith, R.M.H. (2008). Fluvial architecture of the Late Permian Beaufort Group deposits, S.W. Karoo Basin: Point bars, crevasse splays, paleosols, vertebrate fossils and uranium. Field Excursion Guidebook, American Association of Petroleum Geologists International Conference, Cape Town, FT02, 1-110.

- Condie, K.C. (1991). Another look at rare earth elements in shales. Geochim. Cosmochim. Acta, 55, 2527-2531.

- Condie, K.C. (1993). Chemical composition and evolution of the upper continental crust: contrasting results from surface samples and shales. Chemical Geology, 104, 1-37.

- Condie, K.C., Lee, D. and Farmer, G.L. (2001). Tectonic setting and provenance of the Neoproterozoic Uinta Mountain and Big Cottonwood groups, northern Utah: Constraints from geochemistry, Nd isotopes and detrital modes. Sedimentary Geology, 141, 443-464.

- Condie, K.C. and Wronkiewicz, D.J. (1990). The Cr/Th ratio in Precambrian pelites from the Kaapvaal craton as an index of craton evolution. Earth and Planetary Science Letters, 97, 256-267.

- Cook, P., Beck, V., Brereton, D., Clark, R., Fisher, B., Kentish, S., Toomey, J. and Williams, J. (2013). Engineering energy: unconventional gas production. Report for the Australian Council of Learned Academies, 251pp. www.acola.org.au.

- Corfield, R.I., Watts, A.B. and Searle, M.P. (2005). Subsidence of the North Indian Continental Margin, Zanskar Himalaya, NW India. Journal of the Geological Society of London, 162, 135-146.

- Cornell, D.H., Thomas, R.J., Moen, H.F.G., Reid, D.L., Moore, J.M. and Gibson, R.L. (2006). The Namaqua-Natal Province. In: M.R. Johnson, C.R. Anhaeusser, and R.J. Thomas (Eds.). The Geology of South Africa. Geological Society of South Africa and Council for Geoscience, 325-379.

- Council for Geoscience (1995). Geological Map of South Africa 1:250000, Sheet 2922 Prieska, Geological Survey of South Africa, Pretoria.

- Council of Canadian Academies (2014). Environmental Impacts of Shale Gas Extraction in Canada: The expert panel on harnessing science and technology to understand the environmental impacts of shale gas extraction, Council of Canadian Academies, Ottawa (ON), 262pp.

- Coward, M.P. (1983). Thrust tectonics, thin skinned or thick skinned, and the continuation of thrusts to deep in the crust. Journal of Structural Geology, 5, 113-123.

- Cox, K.G. (1988). The Karoo Provence. In: J.D. Macdougall (Ed.). Continental Flood Basalts. Kluwer Academic Publishers, Dordrecht, 239-271.

- Cox, R., Low, D.R. and Cullers, R.L. (1995). The influence of sediment recycling and basement composition on evolution of mudrock chemistry in the southwestern United States. Geochimica et Cosmochimica Acta, 59(14), 2919-2940.

- Crook, K.A.W. (1974). Lithogenesis and geotectonics: the significance of compositional variation in flysch arenites (greywackes). Society of Economic, Palaeontology and Mineralogy Special Publication, 19, 304-310.

- Cullers, R.L. (1994a). The chemical signature of source rocks in size fractions of Holocene stream sediment derived from metamorphic rocks in the Wet Mountains region, USA. Chemical Geology, 113, 327-343.

- Cullers, R.L. (1994b). The controls on the major and trace element variation of shales, siltstones, and sandstones of Pennsylvanian-Permian age from uplifted continental blocks in Colorado to platform sediment in Kansas, USA. Geochimica et Cosmochimica Acta, 58, 4955-4972.

- Cullers, R.L. (2002). Implications of elemental concentrations for provenance, redox conditions, and metamorphic studies of shales and limestones near Pueblo, CO, USA. Chemical Geology, 191(4), 305-327.

396

- Cullers, R.L., Barrett, T., Carlson, R. and Robinson, B. (1987). Rare earth element and mineralogic changes in Holocene soil and stream sediment: a case study in the Wet Mountains, Colorado, USA. Chemical Geology, 63, 275-297.

- Cullers, R.L., Basu, A. and Suttner, L. (1988) Geochemical signature of provenance in sand-size material in soils and stream sediments near the Tobacco Root batholith, Montana, USA. Chemical Geology, 70, 335-348.

- Curtis, C.D. (1977). Sedimentary geochemistry: environments and processes dominated by involvement of an aqueous phase. Philosophical Transactions of the Royal Society, 286, 272-353.

- Curtis, J.B. (2002). Fractured shale-gas systems. American Association of Petroleum Geologists Bulletin, 11, 1921-1938.

- Clayton, C. J. (1994). Microbial and organic processes. In: A. Parler, and B.W. Sellwood (Eds.). Quantitative diagenesis: Recent developments and applications to reservoir Geology. Kluwer Dordrecht, 125-160.

- Dabbagh, M.E., and Rogers, J.J. (1983). Depositional environments and tectonic significance of the Wajid sandstone of southern Saudi Arabia. Journal of African Earth Sciences, 24, 47-57.

- Damiani, R.J. (2004). Temnospondyls from the Beaufort Group (Karoo Basin) of South Africa and their biostratigraphy. Gondwana Research, 7(1), 165-173.

- Dapples, E.C. (1967). Diagenesis of sandstones. Developments in Sedimentology, 8, 91-125.

- Das, B.K., AL-Mikhlafi, A.S. and Kaur, P. (2006). Geochemistry of Mansar Lake sediments, Jammu, India: Implication for source-area weathering, provenance, and tectonic setting. Journal of Asian Earth Sciences, 26, 649-668.

- De Beer, C.H. (1992). Structural evolution of the Cape Fold Belt syntaxis and its influence on syntectonic sedimentation in the SW Karoo Basin. Inversion tectonics of the Cape Fold Belt, Karoo and Cretaceous Basins of southern Africa, Balkema, Rotterdam, 197-206.

- DeCelles, P.G. and Giles, K.A. (1996). Foreland basin systems. Basin Research, 8, 105-123.

- Decker, J.E. (2013). The shale gas potential of the Main Karoo Basin, South Africa. In South African Geophysical Association 13th Biennial Conference, Skukuza, 83-84.

- Decker, J. and Helmold, K.P. (1985). The effect of grain size on detrital modes: a test of the Gazzi-Dickison point counting method. Discussion, 618-620.

- Decker, J. and Marot, J. (2012). Investigation of hydraulic fracturing in the Karoo of South Africa. Annexure A, Resource Assessment, Petroleum Agency SA. Available at: http://www.dmr.gov.za/publications/viewdownload/182/854.html.

- Dembicki, H. Jr. (2009). Three common source rock evaluation errors made by geologists during prospect or play appraisals. American Association of Petroleum Geologists Bulletin, 93, 341-356.

- De Wit, M.J., Jeffery, M., Nicolaysen, L.O.N. and Bergh, H. (1988). Explanatory Notes on the Geologic Map of Gondwana. American Association Petroleum Geology, Tulsa, 7-13.

- De Wit, M.J. and Ransome, I.G. (1992). Regional inversion tectonics along the southern margin of Gondwana. In: M.J. de Wit, and I.G. Ransome, (Ed.). Inversion tectonics of the Cape Fold Belt, Karoo and Cretaceous Basins of Southern Africa. Rotterdam, 15-22.

- De Wit, M.J. (2011). The great shale debate in the Karoo. South African Journal of Science, 107, 7, 1-9.

- Dickinson, W. (1974). Plate Tectonics and Sedimentation. In W. Dickinson (Ed.), Tectonics and Sedimentation. Special Publication of the Society of Economic Paleontologists and Mineralogists, 22, 1-27.

- Dickinson, W.R. (1985). Interpreting provenance relations from detrital modes of sandstones. In: G. Zuffa (Ed.). Provenance of Arenites. Reidel, Dordrecht, 333-361.

- Dickinson, W.R. (1988). Provenance and sediment dispersal in relation to paleotectonics and paleogeography of sedimentary basins. In: Kleinspehn, K.L., Poala, C. (Eds.). New prespectives in basin analysis. Springer-Verlag, New York, 2-25.

- Dickinson, W.R., Suczek, C. (1979). Plate tectonics and sandstone composition. American Association of Petroleum Geologists Bulletin, 63, 2164-2194.

- Dickinson, W.R., Beard, S., Brakenbridge, F., Erjavec, J., Fergusion, R., Inman, K., Knepp, R., Linberg, P. and Ryberg, P. (1983). Provenance of the North American Phanerozoic sandstones in relation to tectonic setting. Geological Society of America Bulletin, 64, 222-235.

- Dott, R.H., 1964. Wackes, greywacke and matrix: what approach to immature sandstone classification? Journal of Sedimentary Petrology, 34, 625-632.

- Duba, A., Heikamp, S., Meurer, W., Nover, G. and Will, G. (1994). Evidence from borehole samples for the role of accessory minerals in lower-crustal conductivity. Nature, 367, 59-61.

- Duncan, A.R., and Marsh, J.S. (2006). The Karoo Igneous Province. In: M.R. Johnson, C.R. Anhaeusser and R.J. Thomas (Eds.). The Geology of South Africa. Geological Society of South Africa, Johannesburg, 501-520.

- Duncan, R.A., Hooper, P.R., Rehacek, J., Marsh, J.S. and Duncan, A.R. (1997). The timing and duration of the Karoo igneous event, southern Gondwana. Journal of Geophysical Research, 102, 18127-18138.

- Du Toit, A.L. (1920). The Karoo dolerites of South Africa: A study in hypabyssal injection. Transactions of the Geological Society of South Africa, 23, 1-42.

- Du Toit, J.C.O. and O'Connor, T.G. (2014). Changes in rainfall pattern in the eastern Karoo, South Africa, over the past 123 years. Water Research Commission of South Africa, 40, 453-460.

- Edwards, A.C. (2001). Grain size and sorting in modern beach sands. Journal of Coastal Research, 17, 38-52.

- Eriksson, P.G., (1984). A palaeoenvironmental analysis of the Molteno Formation in the Natal Drakensberg. Transactions Geological Society of South Africa, 87, 237-244.

- Faure, K. and Cole, D. (1999). Geochemical evidence for lacustrine microbial blooms in the vas Permian Main Karoo, Parana, Falkland Islands and Huab basins of the southwestern Gondwana. Palaeogeography, Palaeoclimatology, Palaeoecology, 152, 189-213.

- Fedo, C.M., Young, G.M. and Nesbitt, H.W. (1997). Paleoclimate control on the composition of the Paleoproterozoic Serpent formation, Huronian Supergroup, Canada, a greenhouse to icehouse transition. Precambrian Research, 86, 201-223.

- Fedo, C.M., Nesbitt, H.W. and Young, G.M. (1995). Unravelling the effects of potassium metasomatism in sedimentary rocks and paleosols, with implications for paleoweathering conditions and provenance. Geology, 23, 921-924.

- Fildani, A., Weislogel, A., Drinkwater, N. J., McHargue, T., Tankard, A., Wooden, J., Hodgson, D. and Flint, S. (2009). U-Pb zircon ages from the southwestern Karoo

Basin, South Africa: Implications for the Permian-Triassic boundary. Geology, 37, 719-722.

- Flint, S.S., Hodgson, D.M., Sprague, A.R., Brunt, R.L., Van der Merwe, W.C., Figueiredo, J., Prélat, A., Box, D., Di Celma, C., and Kavanagh, J.P. (2011). Depositional architecture and sequence stratigraphy of the Karoo basin floor to shelf edge succession, Laingsburg depocentre, South Africa. Marine and Petroleum Geology, 28, 658-674.

- Flint, S., Wild, R. and Hodgson, D. (2009). Stratigraphic evolution of the upper slope and shelf edge in the Karoo Basin, South Africa. Basin Research, 21, 502-527.

- Floyd, P.A. and Leveridge, B.E. (1987) Tectonic environment of the Devonian Gramscatho basin, south Cornwall: Framework mode and geochemical evidence from turbiditic sandstones. Journal of the Geological Society London, 144, 531-542.

- Floyd, P.A., Winchester, J.A. and Park, R.G. (1989) Geochemistry and tectonic setting of Lewisian clastic metasediments from the Early Proterozoic Loch Maree Group of Gairloch, N.W. Scotland. Precambrian Research, 45 (1-3), 203-214.

- Folk, R.L. (1966). A review of grain size parameters. Sedimentology, 6, 73-93.

- Folk, R.L. (1974). Petrology of sedimentary rocks: Hemphill Publishing Company, Austin TX, 182pp.

- Folk, R.L. and Ward, W. (1957). Brazos river bar: a study in the significance of grain size parameters. Journal of Sedimentary Petrology, 27, 3-26.

- Folk, R.L. (1980). Petrology of sedimentary rocks. Hemphill, Austin, Texas, 182pp.

- Friedman, G.M. (1961). Distinction between dune, beach and river sands from their textural characteristics. Journal of Sedimentary Petrology, 31, 514-529.

- Friedman, G.M. (1967). Dynamic processes and statistical parameters compared for size frequency distribution of beach and river sands. Journal of Sedimentary Petrology, 37, 327-354.

- Friedman, G.M. (1979). Differences in size distribution of populations of particles among sands of various origin, Sedimentology, 26, 859-862.

- Frohlich, R.K., Fisher, J.J. and Summerly, E. (1996). Electric-hydraulic conductivity correlation in fractured crystalline bedrock: Central Landfill, Rhode Island, USA. Journal of Applied Geophysics, 35, 249-259.

- Frostick, L.E. and Steel, R.J. (1993). Tectonic controls and signatures in sedimentary successions: special publication of the International Association of Sedimentologists, Published by Blackwell Scientific Publications, 20, 139-142.

- Galerne, C.Y., Galland, O., Neumann, E.R. and Planke, S. (2011). 3-D relationships between sills and their feeders: evidence from the Golden Valley Sill Complex (Karoo basin) and experimental modelling. Journal of Volcanology and Geothermal Research, 202, 189-199.

- Gallagher, K. (1989). An examination of some uncertainties associated with estimates of sedimentation rates and tectonic subsidence. Basin Research, 2, 97-114.

- Gastaldo, R.A., Neveling, J., Clark, C.K., and Newbury, S.S. (2009). The terrestrial Permian–Triassic boundary event bed is a non-event. Geology, 37, 199-202.

- Geel, C., Schulz, H.M., Booth, P., de Wit, M.J. and Horsfield, B. (2013). Shale gas characteristics of Permian black shales in South Africa: Results from recent drilling in the Ecca Group (Eastern Cape). Energy Procedia, 40, 256-265.

- Geel, C., de Wit, M., Booth, P., Schulz, H.M. and Horsfield, B. (2015). Palaeo-environment, diagenesis and characteristics of Permian black shales in the lower Karoo Supergroup flanking the Cape Fold Belt near Jansenville, Eastern Cape, South Africa: Implications for the shale gas potential of the Karoo Basin. South African Journal of Geology, 118(3), 249-274.

- Goswami, B. and Ghosh, D. (2011). Understanding the transportational and depositional setting of Panchet Formation, Purulia and Bankura districts of West Bengal, India - Evidence from grain size analysis. Frontiers of Earth Science, 5(2), 138-149.

- Gresse, P.G., Theron, J.N., Fitch, F.J. and Miller, J.A. (1992). Tectonic inversion and radiometric resetting of the basement in the Cape Fold Belt. In: M.J. de Wit and I.G.D. Ransome (Eds.). Inversion Tectonics of the Cape Fold Belt, Karoo and Cretaceous Basins of Southern Africa, 217-228.

- Gressly, A. (1838). Observations géologiques sur le Jura soleurois. Nouveaux mémoires de la Société Helvetique des Sciences Naturelles, Neuchâtel, 349 (2), 1-14.

- Gromet, L.P., Dymek, R.F., Haskin, L.A. and Korotev, R.L. (1984). The North American shale composite. Its compilation, major and trace element characteristics. Geochim.Cosmochim. Acta 48, 2469-2482.

- Giles, M.R. and Marshall, J.D. (1986). Constraints on the development of secondary porosity in the subsurface: Re-evaluation of processes. Marine and Petroleum Geology, 3, 243-255.

- Griffiths, D.H., Turnbull, J. and Olayinka, A.I. (1990). Two-dimensional resistivity mapping with a computer- controlled array. First Break, 8, 121-129.

- Griffiths, D.H. and Barker, R.D. (1993). Two-dimensional resistivity imaging and modelling in areas of complex geology. Journal of Applied Geophysics, 29, 211-226.

- Hälbich, I.W., Fitch, F.J. and Miller, J.A. (1983). Dating the Cape orogeny, In: A.P.G. Söhnge and I.W. Hälbich (Eds.). Geodynamics of the Cape Fold Belt. Special Publications of the Geological Society of South Africa, 12, 149-164.

- Hälbich, I.W. (1992). The Cape Fold Belt Orogeny: State of the art 1970s-1980s. In: M.J. de Wit and I.G.D. Ransome (Eds.). Inversion Tectonics of the Cape Fold Belt, Karoo and Cretaceous Basins of Southern Africa, 141-158.

- Hälbich, I.W. (1993). Global Geoscience Transect 9. The Cape Fold Belt - Agulhas Bank transect across Gondwana Suture, Southern Africa. American Geophysical Union Special Publication, 202, 1-18.

- Hackett, D.P., Byrd, M.J., Davis, L.J., Sanders, D.B. and De Doe, D.R. (2012). Shale gas – environmental law and regulation, Global Environment SG-ELR, Baker and McKenzie, U.S., 9pp.

- Hallam, A. (1989). The case for sea-level change as a dominant causal factor in mass extinction of marine invertebrates. Philosophical Transactions of the Royal Society of London (Series B), 325, 437-455.

- Hamilton, E.L. (1959). Thickness and consolidation of deep-sea sediments. Bulletin of the Geological Society of America, 70, 1399-1424.

- Hanamgond, P.T. and Chavadi, V.C. (1998). Sedimentological study of Kwada and Belekeri bay beaches, Uttara Kannada, west coast, India. Journal of the Geological Society of India, 51, 193-200.

- Hansma, J., Eric Tohver, E., Jourdan, F., Schrank, C. and David Adams, D. (2015). The timing of the Cape Orogeny: New 40Ar/39Ar age constraints on deformation and cooling of the Cape Fold Belt, South Africa. Gondwana Research, 32, 122-137.

- Harder, H. (1980). Synthesis of glauconite at surface temperatures. Clays and Clay Minerals, 28, 217-222.

- Hartnady, C., Joubert, P. and Stowe, C. (1985). Proterozoic crustal evolution in south western Africa. Episodes, 8, 236-244.

- Harnois, L. (1988). The CIW index: A new chemical index of weathering. Sedimentary Geology 55(3/4), 319-322.

- Hayashi, K., Fujisawa, H., Holland, H. and Ohmoto, H. (1977). Geochemistry of ~1.9 Ga sedimentary rocks from northeastern Labrador, Canada. Geochimica et Cosmochimica Acta, 61(19), 4115-4137.

- Hedberg, H.D. and Moody, J.O. (1979). Petroleum prospects of deep offshore. American Association of Petroleum Geologists Bulletin, 63, 286-300

- Hirsch, K.K., Scheck-Wenderoth, M., van Wees, J.D., Kuhlman, G. and Paton, D.A. (2010). Tectonic subsidence history and thermal evolution of the Orange basin. Journal of Marine and Petroleum Geology, 27, 565-584.

- Hoelke, J.D. (2011). Chemostratigraphy and Paleoceanography of the Mississippian Barnett Formation, Southern Fort Worth Basin, Texas, USA. Master of Science Degree, University of Texas, Arlington, 96pp.

- Honarmand, J. and Amini, A. (2012). Diagenetic processes and reservoir properties in the ooid grainstones of the Asmari Formation, Cheshmeh Khush Oil Field, SW Iran. Journal of Petroleum Science and Engineering, 81, 70-79.

- Horsfield, B., and Schulz, H.M. (2010). Shale Gas Research: the way forward for Europe. Oilfield Technology, 4, 14-18.

- Huggins, P. (2007) Heterogeneity and flow barriers in turbidites, Foinaven Field, UKCS. 69th EAGE Conference and Exhibition, WO11 North Sea Core Workshop, 24pp.

- Hunt, J. M. (1979). Petroleum Geochemistry and Geology. Freeman and Company, San Francisco, 617pp.

- Hunter, D.R. and Reid, D.L. (1987). Mafic dike swarms in Southern Africa. In: H. C. Halls and W. F. Fahrig (Eds.). Mafic Dike Swarms. Geological Association of Canada Special Paper, 34, 445-456.

- Hurst, A. and Irwin, H. (1982). Geological Modelling of Clay Diagenesis in Sandstones. Clay Minerals, 17, 5-22.

- Ingersoll, R.V., Bullard, T.F., Ford, R.L., Grimm, J.P., Pickle, J.D. and Sares, S.W. (1984). The effect of grain size on detrital modes: A test of the Gazzi-Dickinson point counting method. Journal of Sedimentary Petrology, 54, 103-116.

- International Organization for Standardization (ISO) 7404-5 (2009). Methods for the petrographic analysis of coal-Part 5: Method of determining microscopically the reflectance of vitrinite, 13pp.

- International Organization for Standardization (ISO) 7404-2 (2009). Methods for the petrographic analysis of coals-Part 2: Methods of preparing coal samples, 12pp.

- James D. E., Niub, F. and Rokosky, J. (2003). Crustal structure of the Kaapvaal craton and its significance for early crustal evolution. Lithos, 71, 413-429.

- Jarvie, D.M., Hill, R.J., Ruble, T.E. and Pollastro, R.M. (2007). Unconventional shale-gas systems: The Mississippian Barnett Shale of north-central Texas as one model for thermogenic shale-gas assessment. American Association of Petroleum Geologists Bulletin, 91, 475-499.

- Johnson, M.R. (1976). Stratigraphy and Sedimentology of the Cape and Karoo Sequences in the Eastern Cape. PhD Thesis (Unpublished). Rhodes University, Grahamstown, South Africa, 267pp.

- Johnson, M.R. (1991). Sandstone petrography, provenance and plate tectonic setting in Gondwana context of the south-eastern Cape Karoo basin. South African Journal of Geology, 94, 137-154.

- Johnson, M.R. (1994). Thin section grain size analysis revisited. Sedimentology, 41, 985-999.

- Johnson, D.D. and Beaumont, C. (1995). Preliminary results from a planform kinematic model of orogen evolution, surface processes and the development of clastic foreland basin stratigraphy. In: S.L. Doborek, G.M. Ross (Eds.). Stratigraphic Evolution of Foreland Basins. Special Publication of the Society of Economic Paleontologists and Mineralogists, 52, 3-24.

- Johnson, M.R., van Vuuren, C.J., Hegenberger, W.F., Key, R. and Shoko, U. (1996). Stratigraphy of the Karoo Supergroup in southern Africa: an overview. Journal of African Earth Sciences, 23, 3-15.

- Johnson M., van Vuuren C., Visser J., Cole D., de Wickens H., Christie A. and Roberts D. (1997). The Foreland Karoo Basin, South Africa., In: R. Selley (Editor). African Sedimentary Basins of the World, Elsevier, Amsterdam, 3, 269-317.

- Johnson, M.R., van Vuuren, C.J., Visser, J.N.J., Cole, D.I., Wickens, H. DeV, Christie, A.D.M., Roberts, D.L. and Brandl, G. (2006). Sedimentary rocks of the Karoo Supergroup. In: M. R. Johnson, C. R. Anhaeusser and R. J. Thomas (Eds.). The Geology of South Africa, Geological Society of South Africa and Council for Geoscience, 461-499.

- Karpeta, W.P. and Johnson, M.R. (1979). The geology of Umtata area. Exploration to 1:250000 geology sheet 3128 Umtata, Council for Geoscience, Pretoria, 16pp.

- Katemaunzanga, D. and Gunter, C.J. (2009). Lithostratigraphy, sedimentology and provenance of the Balfour Formation, Beaufort Group in the Fort Beaufort Alice area, Eastern Cape Province, South Africa. Acta Geologica Sinica (English Edition), 83(5), 902-916.

- Katz, B.J. (2006). Significance of ODP results on deep-water hydrocarbon exploration–eastern equatorial Atlantic region. Journal of African Earth Sciences, 46, 331-345.

- Kearey, P. and Brooks, M. (2002). An Introduction to Geophysical Exploration (3rd Edition), Blackwell, London.

- Kingsley, C. S. (1977). Stratigraphy and sedimentology of the Ecca Group in the Eastern Cape Province, South Africa. PhD thesis (Unpublished), University of Port Elizabeth, South Africa, 290pp.

- Kingsley, C.S. (1981). A composite submarine fan-delta-fluvial model for the Ecca and lower Beaufort Groups of Permian age in the Eastern Cape Province, South Africa. Transaction of the Geological Society of South Africa, 84, 27-40.

- Kneller, B.C. (1991). A foreland basin on the southern margin of Iapetus. Journal of the Geological Society, London, 148, 207-210.

- Kovacs, J. (2008). Grain size analysis of the Neogene red clay formation in the Pannonian Basin. International Journal of Earth Sciences (Geol Rundsch), 97, 171-178.

- Kulkarni, S. J., Deshbhandaria, P. G. and Jayappaa, K.S. (2015). Seasonal Variation in Textural Characteristics and Sedimentary Environments of Beach Sediments, Karnataka Coast, India. Aquatic Procedia, 4, 117-124.

- Kumar, S. and Singh, I.B., (1978). Sedimentological study of Gomti river sediments, Uttar Pradesh, India. Senckenbergiana marit., 10 (4/6), 145-211.

- Kumon, F., Kiminami, K., Adachi, M., Bessho, T., Kusunoki, T., Mishimura, T., Okada, H., Okami, K., Suzuki, S. and Teraoka, Y. (1992). Modal compositions of representative sandstones from the Japanese Islands and their tectonic implications. Memoir Geological Society of Japan, 38, 385-400.

- Kunetz, G. (1966). Principles of Direct Current Resistivity Prospecting. Gebrüder Borntraeger, Berlin, 103pp.

- Kuuskraa, V., Stevens, S., Van Leeuwen, T. and Moodhe, K. (2011). World shale gas resources: An initial assessment prepared for US Energy Information Administration. World Shale Gas Resources: An initial assessment of 14 regions outside the United States. Available at: http://www.eia.doe.gov/analysis/studies/worldshalegas.

- Lecompte, B., Hursn, G., and Hughes, B. (2010). Quantifying source rock maturity from logs. How to get more than TOC from Delta Log R, SPE Ann. Tech. Confer. Exhibit. Held in Florence, Italy, 19-22.

- Lee, J.I., Park, B.K., Jwa, Y.J., Yoon, H.I., Yoo, K.C. and Kim, Y. (2005). Geochemical characteristics and the provenance of sediments in the Bransfield Strait, West Antarctica. Marine Geology, 219, 81-98.

- Levinson, A.A. (1974). Introduction to Exploration Geochemistry, Applied Publishing, Illnois, 56pp.

- Lewin, J.C. (1971). The dissolution of Silica from Diatom walls. Geochim. Cosmochim. Acta, 21, 182-198.

- Lewis, C.A. (2008). Geomorphology of the Eastern Cape, South Africa. NISC, South Africa, 188pp.

- Lindeque, A., de Wit, M.J., Ryberg, T., Weber, M. and Chevallier, L. (2011). Deep crustal profile across the Southern Karoo basin and Beattie magnetic anomaly, South Africa: An integrated interpretation with tectonic implications. South Africa Journal of Geology, 114, 265-292.

406

- Lindeque, A.S., Ryberg, T., Stankiewicz, J., Weber, M.H. and de Wit, M.J. (2007). Deep Crustal Seismic Reflection Experiment across the Southern Karoo Basin, South Africa. South African Journal of Geology, 110, 419-438.

- Lindsey, D.A. (1999). An evaluation of alternative chemical classifications of sandstones. United States Geological Survey Open File Report, 23pp.

- Linol, B., de Wit, M.J., Milani, E.J., Guillocheau, F. and Scherer, C. (2014). Chapter 7b: New Regional Correlations between the Congo, Paraná and Cape-Karoo Basins of southwest Gondwana. In: de Wit, M.J. and Guillocheau, F. (Eds.). The Geology and Resource Potential of the Cango Basin. Regional Geology Reviews, Springer- Verlag, 245-268.

- Linol, B., de Wit, M.J., Barton, E., Guillocheau, F., de Wit, M.J.C. and Colin J.P. (2015). Chapter 7a: Paleogeography and tectono-stratigraphy of Carboniferous-Permian and Triassic 'Karoo-like' sequences of the Congo Basin. In: de Wit, M.J., Guillocheau, F., de Wit, M.J.C. (Eds.). The Geology and Resource Potential of the Congo Basin, Regional Geology Reviews, Springer-Verlag, 111-134.

- Liu, K.W. and Greyling E.H. (1996). Grain size distribution and cementation of the Cretaceous Mzamba Formation of Eastern Cape, South Africa: A case study of a storm influenced offshore sequence. Sedimentary Geology, 107, 83-97.

- Loke, M.H. (1999). Time-lapse resistivity imaging inversion. Proceedings of the 5th Meeting of the Environmental and Engineering Geophysical Society European Section, Em1, 2pp.

- Loke, M.H. and Barker, R.D. (1996). Rapid least-squares inversion of apparent resistivity pseudosections using a quasi-Newton method. Geophysical Prospecting, 44, 131-152.

- Longman M.W. and Sonnenfeld, M.D. (1996). Paleozoic Systems of the Rocky Mountain Region: Introduction and Overview, Rocky Mountain Section, Journal of Sedimentary Research, 85, 1-10.

- Lopez-Gamundi, O.R. (2006). Permian plate margin volcanism and tuffs in adjacent basins of west Gondwana: Age constraints and common characteristics. Journal of South American Earth Sciences, 22, 227-238.

- Loup, B. (1992). Evolution de la partie septentrionale du domaine helvétique en Suisse occidentale au Trias et au Lias: Contrôle par subsidence thermique et variations du niveau marin. PhD thesis (Unpublished), Université de Genève, 298pp.

- Lowrie, W. (1997). Fundamentals of Geophysics. Cambridge University Press, 1-354.

- Lurie, J. (1981). South African geology for mining, metallurgical, hydrological and civil engineering. 3rd Edition ed. Johannesburg: McGraw-Hill Book Company, 65pp.

- Mackenzie, F.T. (2005). Diagenesis and sedimentary rocks. In: Treatise on Geochemistry (2nd Edition), Elsevier, Oxford, UK. 446pp.

- Macmullin, A. (2013). Treasury to introduce carbon tax, effective from 2015-Gordhan. Business Day live. http://www.bdlive.co.za/national/science/2013/02/27/treasury-tointroduce-carbon-tax-effective-from-2015-gordhan.

- Macquaker, J.H.S., Taylor, K.G., Keller, M. and Polya, D. (2014). Compositional controls on early diagenetic pathways in fine-grained sedimentary rocks: Implications for predicting unconventional reservoir attributes of mudstones. American Association of Petroleum Geologists Bulletin, 93, 587-603.

- Madhavaraju, J. and Lee, Y.I. (2010). Influence of Deccan volcanism in the sedimentary rocks of Late Maastrichtian-Danian age of Cauvery basin South-eastern India: constraints from geochemistry. Current Science, 98, 528-537.

- Madukwe, H.Y. (2016). Granulometric analysis of the sandstone facies of the Ise Formation, Southwestern Nigeria. Journal of Multidisciplinary Engineering Science and Technology, 3 (2), 3909-3919.

- Mahlstedt, N. and Horsfield, B. (2012). Metagenetic methane generation in gas shales I. screening protocols using immature samples. Marine and Petroleum Geology, 31 (1), 27-42.

- Maravelis, A. and Zelilidis, A. (2010). Organic geochemical characteristics of the Late Eocene-Early Oligocene submarine fan and shelf deposits on Lemons Island, NE Greece. Journal of Petroleum Science and Engineering, 9, 25-40.

- Martini A.M., Walter L.M. and McIntosh J.C. (2008). Identification of microbial and thermogenic gas components from Upper Devonian black shale cores, Illinois and Michigan basins. American Association of Petroleum Geologists Bulletin, 92(3), 327-339.

- Martins, L. R. (2003). Recent sediments and grain size analysis. Gravel, 1, 90-105.

- Mbendi Information Services (2014). Electrical power in South Africa. http://www.mbendi.com/indy/powr/af/sa/p0005.html.

- McBride, E.F. (1963). A classification of common sandstones. Journal of Sedimentary Petrology, 33, 664-669.

- McBride E. F. (1989). Quartz cement in sandstones: A review. Earth-Science Reviews, 26(2), 69-112.

- McCann, T. (1991). Petrological and geochemical determination of provenance in the southern Welsh Basin. In: A.C. Morton, S.P., Todd and P.D.W. Haughton (Eds.). Developments in Sedimentary Provenance. Geological Society Special Publication, 57, 215-230.

- McCarthy, T. and Rubidge, B. (2005). The story of Earth and life: a southern African perspective on a 4.6-billion-year journey. Struik, Cape Town, 334pp.

- McCarthy, K., Rojas, K., Niemann, M., Palmowski, D., Peters, K. and Stankiewicz, A. (2011). Basic petroleum geochemistry for source rock evaluation. Oil Field Review, 23(2), 32-43.

- McKay, M.P., Weislogel, A.L., Fildani, A., Rufus L., Brunt, R.L., David M. Hodgson, D.M. and Flint, S.S. (2015). U-PB zircon tuff geochronology from the Karoo Basin, South Africa: implications of zircon recycling on stratigraphic age controls. International Geology Review, 57, 393-410.

- McKenzie, D. (1978). Some remarks on the development of sedimentary basins. Earth and Planetary Science Letters, 40, 25-32.

- McLennan, S.M., Hemming, S., McDaniel, D.K. and Hanson, G.N. (1993). Geochemical approaches to sedimentation, provenance and tectonics. In: M.J. Johnson and A. Basu, (Eds.). Processes controlling the composition of clastic sediments. Geological Society of American Special Paper, 32, 21-40.

- McLennan, S.M., Simonetti, A. and Goldstein, S.L. (2000). Nd and Pb isotopic evidence for provenance and post-depositional alteration of the Paleoproterozoic Huronian Supergroup, Canada. Precambrian Research, 102, 263-278.

- Miall, A.D. (1988a). Facies architecture in clastic sedimentary basins. In: K. Kleinspehn and C. Paola (Eds.). New Perspectives in basin analysis: Springer-Verlag, New York, 63-81.

- Miall, A.D. (1988b). Architectural elements and bounding surfaces in channelized clastic deposits: notes on comparisons between fluvial and turbidite systems. In: A. Taira and F. Masuda (Eds.). Sedimentary facies in the active plate margin. Terra Scientific Publishing Company, Tokyo, Japan, 3-15.

- Miall, A.D. (1995). Description and interpretation of fluvial deposits: A critical perspective (Discussion). Sedimentology, 42, 379-384.

- Miall, A.D. (1996). The Geology of Fluvial Deposits: Sedimentary Facies, Basin Analysis and Petroleum Geology, Springer, New York, USA, 22pp.

- Miall, A.D. (1997). A review of the braided river depositional environment. Earth Science Reviews, 13, 1-62.

- Middleton, G.V. and Hampton, M.A. (1976). Subaqueous sediment transport and deposition by sediment gravity flows. In: D.J. Stanley and D.J.P. Swift (Eds.). Marine sediment transport and environmental management, Wiley, New York, 197-218.

- Milani, E.J. and de Wit M.J. (2008). Correlations between the classic Paraná and Cape Karoo sequences of South America and southern Africa and their basin infills flanking the Gondwanides: du Toit revisited. In: R.J. Pankurst, R.A.J. Trouw, B.B. Brito Neves, and M.J. de Wit (Eds.). West Gondwana: Pre-Cenozoic Correlations across the South Atlantic Region. Geological Society of London Special Publications, 294, 319-342.

- Milliken, K.L. (2006). Understanding diagenetic controls on sandstone reservoir quality: A compendium of influential papers. Compiled on CD-ROM. Getting Started 4.

- Millot, G. (1970). Geology of Clays. Springer-Verlag, New York, 429pp.

- Miola, R.J. and Weiser, D. (1968). Textural parameters: an evaluation. Journal of Sedimentary Petrology 38, 45-53.

- Molenaar, N. (1998). Origin of low-permeability calcite-cemented lenses in shallow marine sandstones and $CaCO_3$ cementation mechanisms, an example from the Lower Jurassic Luxemburg sandstones, Luxemburg. In: S. Morad (Ed.). Carbonate cementation in sandstones. International Association of Sedimentologists Special Publication, 26, 193-211.

- Montgomery S.L., Jarvie D.M., Bowker K.A. and Pollastro R.M. (2005). Mississippian Barnett Shale, Fort Worth Basin, North-Central Texas: Gas-shale play

with multi-trillion cubic foot potential. American Association of Petroleum Geologists Bulletin, 89, 155-175.

- Moore (1949). Meaning of facies. Memoir Geological Society of America, 39, 1-34.

- Morton, A.C. (1985). Heavy minerals in provenance studies. In: G.G. Zuffa (Ed.). Provenance of Arenites. Reidel Publication, Dordrecht, 249-277.

- Murali, A.V., Parthasarathy, R., Mahadevan, T.M. and Sankar Das, M. (1983). Trace element characteristics, REE patterns and partition coefficients of zircons from different geological environments-A case study on Indian zircons. Geochimica et Cosmochimica Acta, 47, 2047-2052.

- Murkute, Y.A. (2001). Textural parameters and petrography of Kamthi Sandstone around Minijhari, Chandrapur district, Maharashtra. Journal of Indian Association of Sedimentologists, 20, 97-108.

- Murkute, Y.A. (2002). Lithofacies analysis, petrography and textural parameters of Kamthi Sandstone from Umrer coalfield, Nagpur district, Maharashtra. Gondwana geological magazine, 17, 19-32.

- Murphy, J. B. (2000). Tectonic influence on sedimentation along the southern flank of the late Paleozoic Magdalen basin in the Canadian Appalachians: Geochemical and isotopic constrains on the Horton Group in the St. Marys basin, Nova Scotia. Geological Society of America Bulletin, 112, 997-1011.

- Mutti, E. and Ricci Lucchi, F. (1972). Turbidites of the northern Apennines: Introduction to facies analysis (English translation by T.H. Nilson, 1978). International Geology Review, 20, 125-166.

- Mutti, E., Tinterri, R., Remacha, E., Mavilla, N., Angella, S. and Fava, L. (1999). An introduction to the analysis of ancient turbidite basins from an outcrop perspective. The American Association of Petroleum Geologists Continuing Education Course Note, Series 39, 4-90.

- Nesbitt, H.W. and Young, G.M. (1982). Early Proterozoic climates and plate motions inferred from major element chemistry of lutites. Nature, 299, 715-717.

- Nesbitt, H.W. and Young, G.M. (1984). Prediction of some weathering trends of plutonic and volcanic rocks based upon thermodynamic and kinetic consideration. Geochimica et Cosmochimica Acta, 48, 1523-1534.

- Nesbitt, H.W. and Young, G.M. (1989). Formation and diagenesis of weathering profiles. Journal of Geology, 97, 129-147.

- Nesbitt, H.W. and Young, G.M. (1996). Petrogenesis of sediments in the absence of chemical weathering: effects of abrasion and sorting on bulk composition and mineralogy. Sedimentology, 43, 341-358.

- Nesbitt, H.W., Fedo, C.M. and Young, G.M. (1997). Quartz and feldspar stability, steady and non-steady state weathering and petrogenesis of siliciclastic sands and muds. Journal of Geology, 105, 173-191.

- Noh, J. and Lee, I. (1999). Diagenetic pore fluid evolution in the Pohang Miocene sediments: oxygen isotopic evidence of septarian carbonate concretions and authigenic mineral phases. Geosciences Journal, 3, 141-149.

- Normark W.R. (1970). Growth patterns of deep-sea fans. American Association of Petroleum Geologists, 54, 2170-2195.

- Nuñez-Betelu, L. and Baceta, J.I. (1994). Basics and application of Rock-Eval/TOC Pyrolysis: An example from the uppermost Paleocene/lowermost Eocene in the Basque Basin, Western Pyrenees. Munibe Natural Sciences - Natur Zientziak, 46, 43-62.

- Nyathi, N. (2014). Stratigraphy, sedimentary facies and diagenesis of the Ecca Group, Karoo Supergroup in the Eastern Cape, South Africa. MSc. dissertation (Unpublished), University of Fort Hare, South Africa, 142pp.

- Olivier, H.J. (1972). Geohydrological investigation of the flooding at Shaft 2, Orange-Fish Tunnel, North-Eastern Cape Province. Transactions of the Geological Society of South Africa, 75, 197-224.

- Pángaro, F. and Ramos, V.A. (2012). Palaeozoic crustal blocks of onshore and offshore central Argentina: New pieces of the southwestern Gondwana collage and their role in the accretion of Patagonia and the evolution of Mesozoic south Atlantic sedimentary basins. Marine and Petroleum Geology, 37, 150-162.

- Passega, R. (1957). Texture as characteristics of clastic deposition. American Association of Petroleum Geologists Bulletin, 41, 1952-1984.

- Passega, R. (1964). Grain size representation by C-M pattern as a geological tool. Journal of Sedimentary Petrology, 34, 830-847.

- Paton, A.D., Di Primio, R., Kuhlmann, G., Van der Spuy, D. and Horsfield, B. (2006). Insight into the petroleum system evolution of the Southern Orange Basin, South Africa. South Africa Journal of Geology, 110, 261-274.

- Peters, K.E. (1986). Guidelines for evaluating petroleum source rock using programmed analysis. The American Association of Petroleum Geologists Bulletin, 70, 318-329.

- Peters K.E., and Cassa, M.R. (1994). Applied source rock geochemistry. In Magoon, L.B., and Dow, W.G., (Eds.). The petroleum system -from source to trap. American Association of Petroleum Geologists, 60, 93-120.

- Pettijohn, F.J. (1957). Sedimentary Rocks (2nd Edition). Harper and Row, New York, 718pp.

- Pettijohn, F.J., Potter, P.E. and Siever, R. (1972). Sand and Sandstones. Springer-Verlag, New York, 587pp.

- Pettijohn, F.G., Potter, P.E. and Siever, R. (1973). Sand and Sandstone. Springer-Verlag, 618pp.

- Pettijohn, F.J., Potter, P.E. and Siever, R. (1987). Sand and Sandstone. Springer, New York, 553pp.

- Pitman, W.C. and Andrews, J.A. (1985). Subsidence and thermal history of small pull-apart basins. In: K.T. Biddle and N. Christie-Blick (Eds.). Strike-Slip Deformation, Basin Formation and Sedimentation. Special Publications of the Society of Economic Palaeontologists and Mineralogists, 37, 45-49.

- Potter, P.E. and Pettijohn, F.J. (1963). Palaeocurrent and Basin analysis: Springer-Verlag, Berlin, 296pp.

- Potter, P.E. and Pettijohn, F.J. (1977). Paleocurrents and Basin Analysis (2nd Edition). Springer-Verlag, Berlin, 413pp.

- Pous, J., Munoz, G., Heise, W., Melgarejo, J.C. and Quesada, C. (2004). Electromagnetic imaging of Variscan crustal structures in southwest Iberia: the role of interconnected graphite. Earth and Planetary Science Letters, 217, 435-450.

- Pysklywec, R.N. and Mitrovica, J.X. (1999). The role of subduction-induced subsidence in the evolution of the Karoo Basin. Journal of Geology, 107, 155-164.

- Rajamanickam, G.V. and Muthukrishnan, N. (1995). Grain size distribution in the Gadilam river basin, northern Tamil Nadu. Journal of Indian Association of Sedimentologists, 14, 55-66.

- Rajesh, E., Anbarasu, K. and Rajamanickam, G.V. (2007). Grain size distribution of silica sand in and around Marakkanam coast of Tamil Nadu. Journal of the Geological Society of India, 69, 1361-1368.

- Rajganapathi, V.C., Jitheshkumar, N., Sundararajan, M., Bhat, K.H. and Velusamy, S. (2013). Grain size analysis and characterization of sedimentary environment along Thiruchendur coast, Tamilnadu, India. Arabian Journal of Geosciences, 6, 4717-4728.

- Ramanamurthy, B.V. (1985). Gondwana sedimentation in Ramagundam-Mantheni area, Godavari valley basin. Journal of the Geological Society of India, 26, 43-55.

- Ramanathan, A.L., Rajkumar, K., Majumdar, J., Singh, G., Behera, P.N., Santra, S.C. and Chidambaram, S. (2009). Textural characteristics of the surface sediments of a tropical mangrove Sundarban ecosystem, India. Indian Journal of Marine Sciences, 38(4), 397-403.

- Rao, T.C.S., Machado, X.T. and Murthy, K.S.R. (2005). Topographic features over the continental shelf off Visakhapatnam. Mahasagar-Bulletin National Institute of Oceanography, 13, 83-89.

- Ratner, M. and Tiemann, M. (2015). An overview of unconventional oil and natural gas: Resources and Federal Actions. CSR Report, 27pp.

- Raymond, L.A. (1995). The Study of Igneous, Sedimentary and Metamorphic Rocks. Wm.C. Brown Communication Inc., United States of America, 264-388.

- Reading, H.G. (1978). Sedimentary environments and facies. Oxford: Black Scientific Publications, 557pp.

- Reading, H.G. and Levell, B. K. (1996). Controls on the sedimentary rock record. In: H.G. Reading (Ed.). Sedimentary environments: processes, facies and stratigraphy (third edition). Blackwell Science, Oxford, 5-36.

- Reed, J.S., Eriksson, K.A. and Kowalewski, M. (2005). Climatic, depositional and burial controls on diagenesis of Appalachian Carboniferous sandstones: qualitative and quantitative methods. Sedimentary Geology, 176, 225-246.

- Ricci Lucchi, F. (1975a). Depositional cycles in two turbidite formations of northern Apennines (Italy). Journal Sedimentary Petrology, 45, 3-43.

- Ricci Lucchi, F. (1975b). Miocene paleogeography and basin analysis in Periadriatic Apennines: Guidebook to the Geology of Italy, Tripoli, Libya, 33pp.

- Riley, T.R. and Knight, K.B. (2001). Review age of pre-break-up Gondwana magmatism. Antarctic Science, 13, 99-110.

- Roberts, A.M., Kusznir, N.J., Yielding, G. and Styles, P. (1998). 2D flexural backstripping of extensional basins: the need for a sideways glance. Petroleum Geoscience, 4, 327-338.

- Rollinson, H.R. (1993). Using geochemical data: evaluation, presentation, interpretation, Essex. Longman Scientific Technical, 344pp.

- Roser, B.P. and Korsch, R.J. (1986). Determination of tectonic setting of sandstone-mudstone suites using SiO_2 content and K_2O/Na_2O ratio. Journal of Geology, 94, 635-650.

- Roser, B.P. and Korsch, R.J. (1988). Provenance signature of sandstone mudstone suite determined using discriminant function analysis of major element data. Chemical Geology, 67, 119-139.

- Roser, B.P., Cooper, R.A., Nathan, S. and Tulloch, A.J. (1996). Reconnaissance sandstone geochemistry, provenance and tectonic setting of the Lower Palaeozoic terranes of the West Coast an Nelson, New Zealand. New Zealand. Journal of Geology and Geophysics, 39, 1-16.

- Roswell, D.M. and de Swart, A.M.J. (1976). Diagenesis in Cape and Karroo sediments, South Africa, and its bearing on their hydrocarbon potential. Transactions of the Geology Society of South Africa, 79, 81-145.

- Rossouw, P.J. (1953). General Geology: the southern Karoo in results of an investigation into the possible presence of oil in Karoo rocks in parts of the Union of South Africa, Memoirs of the Geological Survey of South Africa, 45, 14-36.

- Rubidge, R. N. (1858). Notes on the geology on some parts of South Africa. Quarterly Journal of the Geological Society of London, 12, 237-238. In: O. Catuneanu, H. Wopfner, P.G. Eriksson, B. Cairncross, B.S. Rubidge, R.M.H. Smith, P.J. Hancox (2005). The Karoo Basins of South-Central Africa. Journal of African Earth Sciences, 43, 211-253.

- Rubidge, B.S. (1995). Biostratigraphy of the Beaufort Group (Karoo Supergroup), South Africa, 1. South African Committee for Stratigraphy, SACS Biostratigraphic Series, Council for Geoscience, 40-46.

- Rubidge, B.S., Hancox, P.J. and Catuneanu, O. (2000). Sequence analysis of the Ecca-Beaufort contact in the Southern Karoo of South Africa. South Africa Journal of Geology, 103, 81-96.

- Rudnick, R.L. and Gao, S. (2003). Composition of the continental crust. Treatise of Geochemistry, 3, 1-64.

- Rust, I.C. (1975). Tectonic and sedimentary framework of Gondwana Basins in southern Africa. Third Gondwana Symposium, 5, 554-564.

- Ryan, P.J. (1967). Stratigraphic and palaeocurrent analysis of the Ecca Series and lowermost Beaufort Beds in the Karroo basin of South Africa, Ph.D. thesis (unpublished), University of the Witwatersrand, 210pp.

- SACS, South African Committee for Stratigraphy (1980). Stratigraphy of South Africa. Part 1: Lithostratigraphy of the Republic of South Africa, South West Africa/Namibia and the Republics of Bophuthatswana, Transkei and Venda (Compiled by Kent, L.E.). Geological Survey of South Africa. Handbook 8, 690pp.

- Sagoe, K.M.O. and Visher, G.S. (1977). Population breaks in grain size distributions of sand - a theoretical model. Journal of Sedimentary Petrology, 47(1), 285-310.

- Sahu, B.K. (1962). Environments of deposition from the size analysis of clastic sediments. PhD. thesis, University of Wisconsin, Madison, Wisconsin, 99pp.

- Sahu, B.K. (1964). Depositional mechanism from the size analysis of elastic sediments. Journal of Sedimentary petrology, 34(1), 73-83.

- Salem, A.M., Ketzer, J.M., Morad, S., Rizk, R.R. and Al-Aasm, I.S. (2005). Diagenesis and Reservoir-Quality Evolution of Incised-Valley Sandstones: Evidence from the Abu Madi Gas Reservoirs (Upper Miocene), the Nile Delta Basin, Egypt. Journal of Sedimentary Research, 75, 572-584.

- Sawyer, D.S., Toksöz, M.N., Sclater, J.G. and Swift, B.A. (1982). Thermal evolution of the Baltimore Canyon trough and Georges Bank basin. In: J.S. Watkins and D.L. Drake (Eds.). Studies in Continental Margin Geology. American Association of Petroleum Geologists Memoir, 34, 743-764.

- Scheiber-Enslin, S. E., Webb, S. J. and Ebbing, J. (2014). Geophysically plumbing the Main Karoo Basin, South Africa, South African Journal of Geology, 117(2), 275-300.

- Schmidt, V. and McDonald, D.A. (1979a). Texture and recognition of secondary porosity in sandstones. In: A. Peter, P.R. Schluger (Eds.). Aspects of Diagenesis. Society of Economic Palaeontologists and Mineralogists, Special Publication, 26, 209-225.

- Schmidt, V. and McDonald, O.A. (1979b). The role of secondary porosity in the course of sandstone diagenesis. In: P.A. Scholle, P.R. Schluger (Eds.). Aspects of Diagenesis. Society for Sedimentary Geology Special Publication, 26,175-207.

- Schmoker, J.W. and Halley, R.B. (1982). Carbonate porosity versus depth: a predictable relation for South Florida. American Association of Petroleum Geologists Bulletin, 66, 2561-2570.

- Sciunnach, D. and Garzanti, E. (1996). Sedimentary record of Late Paleozoic rift and breakup in Northern Gondwana (Thini Chu Group and Tamba-Kurkur Fm.; Dolpo Tethys Himalaya, Nepal). Geodinamica Acta, 9, 41-56.

- Sclater, J.G. and Christie, P.A.B. (1980). Continental stretching: an explanation of the post mid Cretaceous subsidence of the Central North Sea basin, Journal of Geophysical Research, 85, 3711-3739.

- Segwabe, T. (2008). The Geological Framework and Depositional Environments of the Coal-Bearing Karoo Strata in the Central Kalahari Karoo Basin, Botswana. M.Sc thesis (unpubl.), Rhodes University, South Africa, 121pp.

- Selley, R.C. (1997). Elements of Petroleum Geology. Academic Press, 16pp.

- Selvaraj, K. and Ram Mohan V. (2003). Textural Variation and Depositional Environments of Innershelf Sediments, off Kalpakkam, Southeast Coast of India. Journal Geological Society of India, 61, 449-462.

- Sharda, Y.P. and Verma, V.K. (1977). Paleo environment during Muree and Siwalik sedimentation around Udhampur, Jammy Himalaya. Publication of the centre of advanced study in Geology No. II, Punjab University, Chandigarh, 1-24.

- Shen, S-Z., Schneider, J.W., Angiolini, L. and Henderson, C.M. (2013). The international Permian timescale: March 2013 update. The Carboniferous-Permian transition. New Mexico Museum of Natural History and Science Bulletin, 60, 411-416.

- Singh, K.P. (2005). Non-linear estimation of aquifer parameters from surficial resistivity measurements. Hydrology and Earth System Sciences Discuss, 2, 917-938.

- Skaberne, D. (1996). Interpretation of Depositional Environment Based on Grain Size Distribution of Sandstones of the Val Gardena Formation in the Area Between Cerkno and Smrečje, Slovenia. Geologija, 39, 193-214.

- Sleep, N.H. (1971). Thermal effects of the formation of Atlantic continental margins by continental break up. Geophysical Journal of the Royal Astronomical Society, 24, 325-348.

- Smith, R.A. (1984). The lithostratigraphy of the Karoo Supergroup in Botswana. Bulletin of the Geological Survey Botswana, 26, 239pp.

- Smith, R.M.H. (1980). The lithology, sedimentology and taphonomy of flood-plain deposits of the Lower Beaufort (Adelaide Subgroup) strata near Beaufort West. Transactions of the Geological Society of South Africa, 83, 399-413.

- Smith, R.M.H. (1987). Morphology and depositional history of exhumed Permian point bars in the southwestern Karoo, South Africa. Journal of Sedimentary Petrology, 57, 19-29.

- Smith, R.M.H. (1990). A review of the stratigraphy and sedimentary environments of the Karoo basin of South Africa. Journal of African Earth Sciences, 10, 117-137.

- Smith, R.M.H. (1995). Changing fluvial environments across the Permian-Triassic boundary in the Karoo Basin, South Africa, and possible causes of tetrapod extinctions. Palaeogeography, Palaeoclimatology, Palaeoecology, 117, 81-104.

- Smith, R.H.M. and Ward, P.D. (2001). Pattern of vertebrate extinction across an event bed at the Permian-Triassic boundary in the Karoo Basin of South Africa. Marine and Petroleum Geology, 29, 1147-1150.

- Smith, R.M.H., Eriksson, P.G. and Botha, W.J. (1993). A review of the stratigraphy and sedimentary environments of the Karoo-aged basins of Southern Africa. Journal of African Earth Sciences, 132 (16), 143-169.

- Srinivasa Rao, P., Krishna Rao, G., Durga Prasada Rao, N.V.N. and Swamy, A.S.R. (1990). Sedimentation and sea level variations in the Nizampatnam Bay, east coast of India. Indian Journal of Marine Science, 19, 261-264.

- Srivastava, A.K. and Mankar, R.S. (2009). Grain Size Analysis and Depositional Pattern of Upper Gondwana Sediments (Early Cretaceous) of Salbardi Area, Districts

Amravati, Maharashtra and Betul, Madhya Pradesh. Journal Geological Society of India, 73, 393-406.

- Srivastava, A.K., Khare, N. and Ingle, P.S. (2010). Textural characteristics, distribution pattern and provenance of heavy minerals in glacial sediments of Schirmacher Oasis, East Antarctica. Journal of the Geological Society of India, 75, 393-402.

- Srivastava, A.K., Ingle, P.S., Lunge, H.S. and Khare, N. (2012). Grain size characteristics of deposits derived from different glacigenic environments of the Schirmacher Oasis, East Antarctica. Geologos, 18(4), 251-266.

- Stavrakis, N. (1980). Sedimentation of the Katberg sandstone and adjacent formations in the south-eastern Karoo Basin. Transactions of the Geological Society of South Africa, 83, 361-374.

- Steckler, M.S. and Watts, A.B. (1978). Subsidence of the Atlantic-type continental margin off New York. Earth and Planetary Science Letters, 41, 1-10.

- Stettler, E.H., De Beer, J. and Blom, M.P. (1989). Crustal domains in the northern Kaapvaal craton as defined by magnetic lineaments. Precambrian Research, 45, 263-276.

- Stewart, H.B. (1958). Sedimentary reflection on depositional environment, in San Mignellagoon, Baju California, Mexico. American Association of Petroleum Geologists, 42, 2567-2618.

- Steyl, G. and van Tonder, G.J. (2013). Hydrochemical and hydrogeological impact of hydraulic fracturing in the Karoo, South Africa, Effective and Sustainable Hydraulic Fracturing, In Tech, 213-237. Available at: http://dx.doi.org/10.5772/56310.

- Suarez-Ruiz I., Flores D., Graciano Mendonca Filho J. and Hackley P.C. (2012). Review and update of the applications of organic petrology: Part 1, geological applications. International Journal of Coal Geology, 99, 54-112.

- Sutherland, R.A. and Lee, C. (1994). Discrimination between coastal subenvironments using textural characteristics. Sedimentology, 41, 1133-1145.

- Suttner, L.J. and Dutta, P.K. (1986). Alluvial sandstone composition and palaeoclimate: I. Framework mineralogy. Journal of Sedimentary Petrology, 56, 329-345.

- Svensen, H., Bebout, G., Kronz, A., Li, L., Planke, S., Chevallier, L., Jamtveit, B. (2008). Nitrogen geochemistry as a tracer of fluid flow in a hydrothermal vent complex in the Karoo Basin, South Africa. Geochimica et Cosmochimica Acta, 72 (20), 4929-4947.

- Svensen, H., Corfu, F., Ploteau, S., Hammer, O., and Planke, S. (2012). Rapid magma emplacement in the Karoo Large Igneous Province. Earth and Planetary Science Letters, 325-326, 1-9.

- Svensen, H., Planke, S., Chevallier, L., Malthe-Sørenssen, A., Corfu, F. and Jamtveit, B. (2007). Hydrothermal venting of greenhouse gases triggering Early Jurassic global warming. Earth and Planetary Science Letters, 256(3), 554-566.

- Tankard, A.J., Jackson, M.P.A., Eriksson, K.A., Hobday, D.K., Hunter, D.R. and Minter, W.E.L., (1982). Crustal Evolution of Southern Africa, 3.8 Billion Years of Earth History, Springer-Verlag, New York, 523pp.

- Tankard, A., Welsink, H., Aukes, P., Newton, R. and Stettler, E. (2009). Tectonic evolution of the Cape and Karoo basins of South Africa. Marine and Petroleum Geology, 26, 1379-1412.

- Tankard, A., Welsink, H., Aukes, P., Newton, R. and Stettler, E. (2012). Geodynamic interpretation of the Cape and the Karoo basins, South Africa. Phanerozoic Passive Margins, Cratonic Basins and Global Tectonics Maps, 869-876.

- Taylor, S.R. and McLennan, S.M. (1985) The Continental Crust: Its Composition and Evolution. Blackwell Scientific Publications, 312pp.

- Telford, W.M., Geldart, I.P. and Sheriff, R. E. (1990). Applied Geophysics (2nd Edition), New York. Cambridge University Press, 770pp.

- Tissot, B.P. and Welte, D.H. (1978). Petroleum Formation and Occurrence, first ed. Springer-Verlag, New York, 538pp.

- Tissot, B. and Welte, D.H. (1984). Petroleum formation and occurrence. Springer Verlag, Berlin, 699pp.

- Thomas, R.J., von Veh, M.W. and McCourt, S. (1993). The tectonic evolution of southern Africa: an overview. Journal of African Earth Sciences, 16(2), 5-24.

- Toulkeridis, T., Clauer, N., Kröner, A., Reimer, T. and Todt, W. (1999). Characterization, provenance, and tectonic setting of Fig Tree greywackes from the

Archaen Barberton Greenstone Belt, South Africa. Sedimentary Geology, 124, 113-129.

- Trewin, N.H., Macdonald D.I.M. and Thomas, C.G.C. (2002). Stratigraphy and sedimentology of the Permian of the Falkland Islands: Lithostratigraphic and palaeoenvironmental links with South Africa. Journal of the Geological Society of London, 159, 5-19.

- Tucker, M.E. (2001). Sedimentary Petrology (3rd Edition). Blackwell Publishing Company, Oxford, 262pp.

- Turekan, K.K., and Wedepohl, K.H. (1961). Distribution of the elements in some major. Units of the Earth's crust. Geological Society of America Bulletin, 72, 175-191.

- Turner, B.R. (1975). The stratigraphy and sedimentary history of the Molteno Formation in the Main Karoo Basin of South Africa and Lesotho. Ph.D. thesis (unpubl.), Univ. Witwatersrand, 314pp.

- Turner, B.R. (1980). Braid plain deposition of the Upper Triassic Molteno Formation in the Main Karoo (Gondwana) Basin, South Africa. Sedimentology, 30, 77-89.

- Turner, B.R. (1999). Tectono-stratigraphical development of the Upper Karoo foreland basin: Orogenic unloading versus thermally-induced Gondwana rifting. Journal of Africa Earth Science, 28, 215-238.

- Udden, J.A. (1914). Mechanical composition of clastic sediments. Geological Society of America Bulletin, 25, 655-744.

- Underschultz, J.R. (1991). Tectonic loading, sedimentation, and sea-level changes in the foreland basin of north-west Alberta and north-east British Columbia, Canada. Basin Research, 3, 165-174.

- Vail, P.R., Mitchum, R.M. and Thompson, S. (1977). Seismic stratigraphy and global changes of sea level. In: C.E. Payton (Ed.). Seismic stratigraphy – Applications to hydrocarbon exploration. American Association of Petroleum Geologists Memoir, 26, 83-97.

- Van Hinte, J.E. (1978). Geohistory analysis-application of micropaleontology in exploration geology. Bulletin of the American Association of Petroleum Geologists, 62, 201-222.

- Van Zijl, J.S.V. (2006a). A review of the resistivity structure of the Karoo Supergroup, South Africa, with emphasis on the dolerites: A study in anisotropy. South African Journal of Geology, 109, 315-328.

- Van Zijl, J.SV. (2006b). Physical characteristics of the Karoo sediments and mode of emplacement of the dolerites. South Africa Journal of Geology, 109, 329-334.

- Veevers, J.J., Cole, D.I. and Cowan, E.J. (1994). Southern Africa: Karoo Basin and Cape Fold Belt. In: J.J. Veevers and C. McA. Powell (Eds.). Permian-Triassic Pangean Basins and Fold belts along the Pathalassan Margin of Gondwanaland. Boulder Colorado. Geological Society of America Memoir, 184, 223-279.

- Vengosh, A., Jackson, R.B., Warner, N., Darrah, T.H. and Kondash, A. (2014). A critical review of the risks to water resources from unconventional shale gas development and hydraulic fracturing in the United States. Environmental Science and Technology, 47(22), 13141-13150.

- Vermeulen, P.D. (2012). A South Africa perspective on shale gas hydraulic fracturing. International Mine Water Association, Annual Conference, 149-156.

- Viljoen, J.H.A. (1994). Sedimentology of the Collingham formation, Karoo Supergroup, South Africa. Journal of Geology, 97, 167-183.

- Visher, G.S. (1969). Grain size distributions and depositional processes. Journal of Sedimentary Petrology, 39, 1074-1106.

- Visser, J.N.J. (1991). Geography and Climatology of the late Carboniferous to Jurassic Karoo basin in Southwestern Gondwana. Annals of the South African Museum, 99, 415- 431.

- Visser, J.N.J. (1992). Basin tectonics in south-western Gondwana during the Carboniferous and Permian. In: M.J. de Wit and I.G.D. Ransome (Eds.). Inversion Tectonics of the Cape Fold Belt, Karoo and Cretaceous Basins of Southern Africa, 109-115.

- Visser, J.N.J. (1993). Sea-level changes in a back-arc foreland transition-the Late Carboniferous-Permian Karoo Basin of South Africa. Sedimentary Geology, 83, 115-131.

- Visser, J.N.J. (1995). Post-glacial Permian stratigraphy and geography of southern and central Africa; boundary conditions for climatic modelling. Palaeogeography, Palaeoclimatology, Palaeoecology, 118, 213-243.

- Visser, J.N.J. (1997). Deglaciation sequences in the Permo-Carboniferous Karoo and Kalahari basins of southern Africa: A tool in the analysis of cyclic glaciomarine basin fills. Sedimentology, 44, 507-521.

- Visser, J.N.J. (1986). Lateral lithofacies relationships in the glacigene Dwyka Formation in the western and central parts of the Karoo Basin. Transactions of the Geological Society of South Africa, 89, 373-384.

- Visser, J.N.J. and Botha, B.J.V. (1980). Meander belt, point bar, crevasse splay and aeolian deposits from the Elliot Formation in Barkly Pass, northeastern Cape. Transactions of the Geological Society of South Africa, 83, 55-62.

- Visser, J.N.J. and Dukas, B.A. (1979). Upward fining fluviatile megacycles in the Beaufort Group, north of Graaff-Reinet, Cape Province. Transactions of the Geological Society of South Africa, 82, 149-154.

- Visser, J.N.J. and Loock, J.C. (1978). Water depth in the main Karoo Basin in South Africa during Permian sedimentation. Transaction of the Geological Society of South Africa, 81, 185-191.

- Visser, J.N.J. and Praekelt, H.E. (1996). Subduction, mega-shear systems and Late Palaeozoic basin development in the African segment of Gondwana. Geologische Rundschau, 85, 632-646.

- Vorster, C. (2013). Laser ablation ICP-MS age determination of detrital zircon age population in the Phanerozoic Cape and lower Karoo Supergroups (South Africa) and correlatives in Argentina. PhD Thesis (Unpublished). University of Johannesburg, South Africa, 648pp.

- Von Brunn, V. (1994). Glaciogenic deposits of the Permo-Carboniferous Dwyka Group in the eastern region of the Karoo basin, South Africa, 60-69. In: M. Deynoux, J.M.G. Miller, E.W. Domack, N. Eyles, I. Fairchild, and G.M. Young (Eds.). Earth's Glacial Record. Cambridge, UK, Cambridge University Press, 266pp.

- Walker R.G. (1967). Turbidite sedimentary structures and their relationship to proximal and distal depositional environments. Journal of Sedimentary Petrology, 37 (1), 25-37.

- Walker, R.G. (1978). Deep-Water Sandstones Facies and Ancient Submarine Fans: Models for Exploration for Stratigraphic Traps. American Association of Petroleum Geologists, 62, 932-966.

- Walker, T.R. (1967). Formation of red beds in modern and ancient deserts. Geological Society of America Bulletin, 78, 353-368.

- Wanas, H.A. and Abdel-Maguid, N.M. (2006). Petrography and geochemistry of the Cambro–Ordovician Wajid Sandstone, southwest Saudi Arabia: Implications for provenance and tectonic setting. Journal of Asian Earth Sciences, 26, 1-14.

- Ward, P.D., Botha, J., Buick, R., De Kock, M.O., Erwin, D.H., Garrison, G., Kirschvink, J. and Smith, R.H.M. (2005). Abrupt and gradual extinction among Late Permian land vertebrates in the Karoo Basin, South Africa. Science, 307, 79-714.

- Watts, A.B. (1978). An analysis of isostasy in the world's oceans: 1. Hawaiian-Emperor Seamount Chain. Journal of Geophysical Research, 83, 5989-6004.

- Watts, A.B. (2001). Isostasty and flexure of the lithosphere. Cambridge University press, 1-26.

- Watts, A.B. and Ryan, W.B.F. (1976). Flexure of the lithosphere and continental margin basins. Tectonophysics, 36, 25-44.

- Weaver, C.E. (1989). Clays, muds and shales. Amsterdam, Elsevier, 818pp.

- Weckmann, U., Ritter, O., Jung, A., Branch, T. and de Wit M.J. (2007a). Magnetotelluric measurements across the Beattie magnetic anomaly and the Southern Cape Conductive Belt, South Africa. Journal of Geophysical Research, 112, 416-426.

- Weckmann, U., Jung, A., Branch, T. and Ritter, O. (2007b). Comparison of electrical conductivity structures and 2D magnetic modelling along two profiles crossing the Beattie Magnetic Anomaly, South Africa. South African Journal of Geology, 110, 449-464.

- Weckmann, U., Ritter, O., Chen, X., Tietze, K. and de Wit, M.J. (2012). Magnetotelluric image across the Cape Fold Belt, South Africa. Terra Nova, 24, 207-212.

- Wei, G.J., Liu, Y., Li, X.H., Shao, L. and Fang D. (2004). Major and trace element variations of the sediments at ODP Site 1144, South China Sea, during the last 230ka and their paleoclimate implications. Palaeogeography, Palaeoclimatology, Palaeoecology, 212, 331-342.

- Weltje, G.J. (2002). Quantitative analysis of detrital modes: statistically rigorous confidence regions in ternary diagrams and their use in sedimentary petrology. Earth Science Reviews, 57, 211-253.

- Wentworth, C.K. (1922). A scale of computing mechanical composition types in sediments. Geological Society of America Bulletin, 40, 760-771.

- White, R.S. (1997). Mantle plume origin for the Karoo and Ventersdorp flood basalts, South Africa. South African Journal of Geology, 100(4), 271-282.

- Wickens, H. DeV. (1994). Basin Floor Fan Building Turbidites of the South-western Karoo Basin, Permian Ecca Group, South Africa. PhD thesis (Unpublished), University of Port Elizabeth, South Africa, 233pp.

- Wild, R.J. (2005). Sedimentology and Sequence Stratigraphy of a Permian Lower Slope to Shelf Succession, Tanqua Depocentre, SW Karoo Basin, South Africa. PhD thesis (Unpublished), University of Liverpool, UK, 182pp.

- Williamson, I.T. (1996). The geology of the area around Mmamabula and Dibete: including an account of the Greater Mmamabula Coalfield. District Memoir 6. Geological Survey, Botswana, 239pp.

- Winter, H. de La R. and Venter, J.J. (1970). Lithostratigraphic correlation of recent deep boreholes in the Karroo-Cape Sequence. In: Proceedings and papers, Second Gondwana Symposium. Council for Scientific and Industrial Research, 395-408.

- Woodford, A.C. and Chevallier, L. (2002). Regional characterization and mapping of Karoo fractured aquifer systems - an integrated approach using a geographical information system and digital processing. Water Research Commission Report, 653/1/02, 192pp.

- Wopfner, H. (2002). Tectonic and climatic events controlling deposition in Tanzanian Karoo basins. Journal of African Earth Sciences, 34, 167-177.

- Wright, V.P. (1993). Sedimentology Review 1. Blackwell Publishing, Oxford, 152pp.

- Wronkiewicz, D. J. and Condie, K. C. (1987). Geochemistry of Archean shales from the Witwatersrand Supergroup, South Africa: Source-area weathering and provenance. Geochimica et Cosmochimica Acta, 51, 2401-2416.

- Wronkiewicz, D.J. and Condie, K.C. (1990). Geochemistry and mineralogy of sediments from the Ventersdorp and Transvaal Supergroups, South Africa: cratonic evolution during the early Proterozoic. Geochimica et Cosmochimica Acta, 54, 343-354.

- Yan, Y., Xia, B., Lin, G., Cui, X., Hu, X., Yan, P. and Zhang, F. (2007). Geochemistry of the sedimentary rocks from the Nanxiong Basin, South China and

implications for provenance, paleo-environment and paleoclimate at the K/T boundary. Sedimentary Geology, 197, 127-140.

- Yerino, L.N. and Maynard, J.B. (1984). Petrography of modern marine sands from the Peru-Chile Trench and adjacent areas. Sedimentology, 31, 83-89.

- Zoback, M.D. and Arent, D.J. (2014). The opportunities and challenges of sustainable shale gas development. Elements, 10, 251-253.

- Zou, C., Zhu, R., Liu, K., Su, L., Bai, B., Zhang, X., Yuan, X. and Wang, J. (2012). Tight gas sandstone reservoirs in China: Characteristics and recognition criteria. Journal of Petroleum Science and Engineering, 88, 82-91.

APPENDICES

Appendix A: Grain size analysis
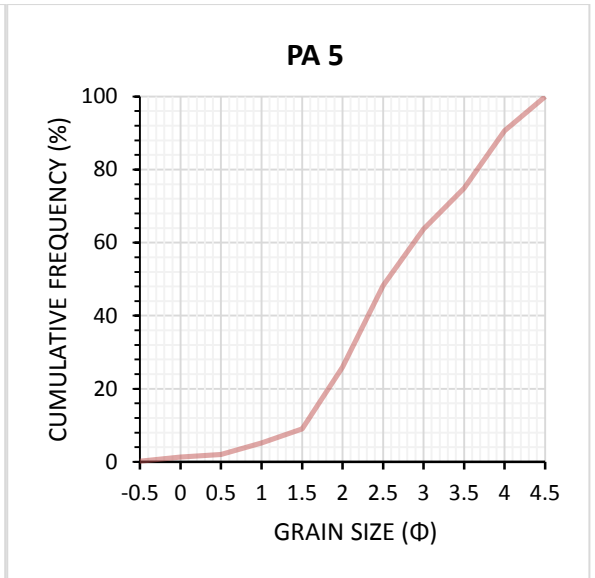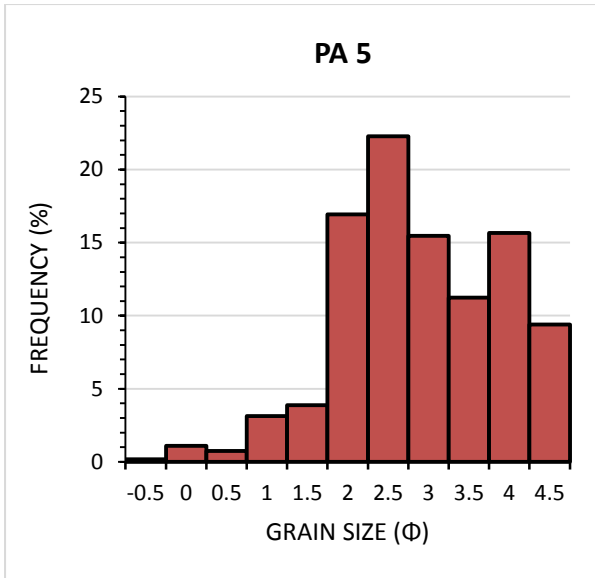
Table A1: Sample identification for the grain size plots.

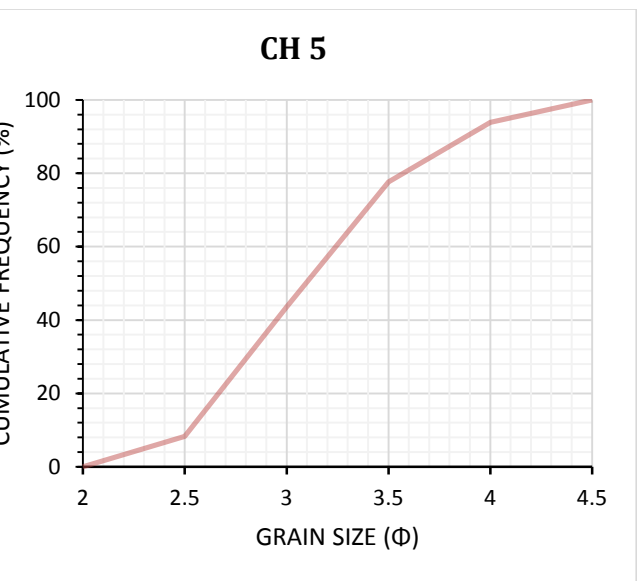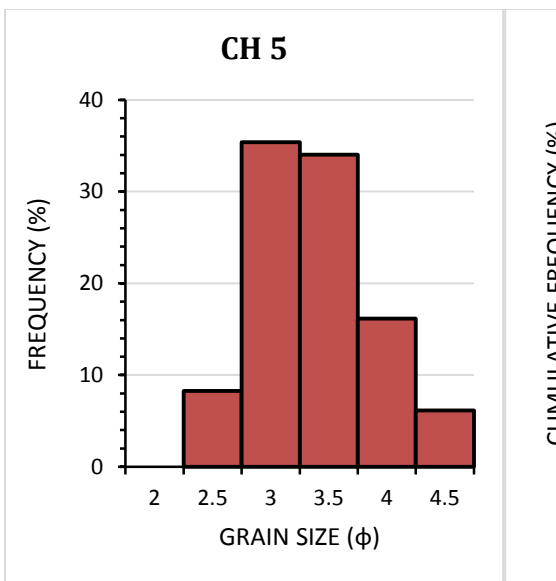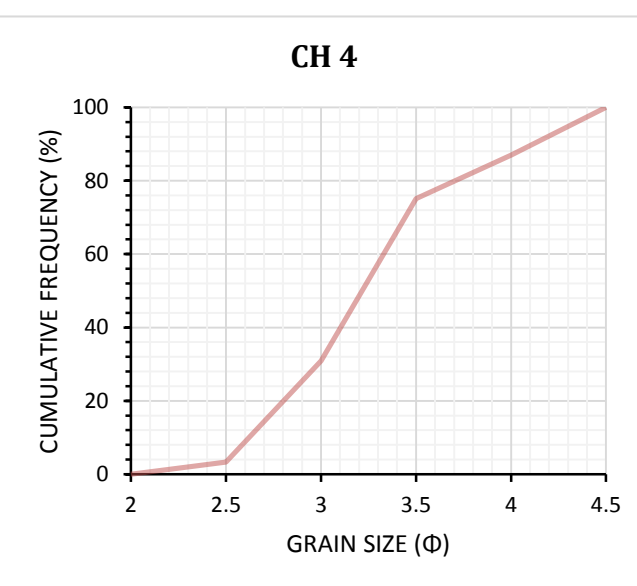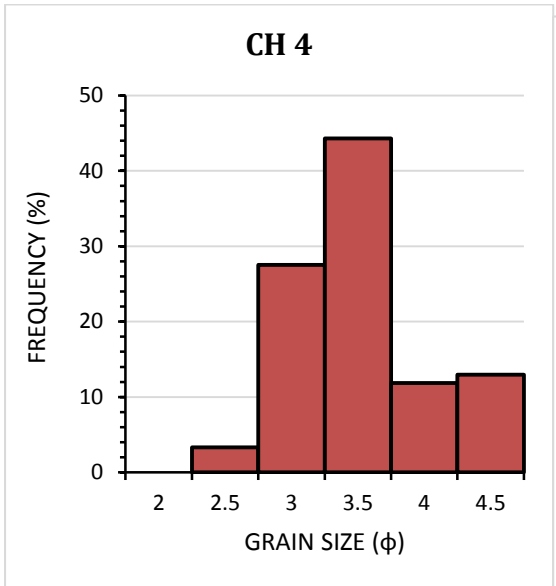| Sample ID	Formation	Sample ID	Formation
PA 1-5	Prince Albert	RB, RC, RP, ZN02L and ZN02K	Ripon
CH 1-5	Collingham	R 1A, R 2A and R 5A	Ripon
R 1-11	Ripon	FB 1-6	Fort Brown

Grain size frequency histograms (left) and cumulative frequency curve (right) plotted for the analysed Ecca samples.

CH 3

CH 3

CH 4

CH 4

CH 5

CH 5

430

431

433

434

R2A

R2A

R 6

R 6

R 4

R 4

435

R 10

R 10

FB 1

FB 1

FB 2

FB 2

438

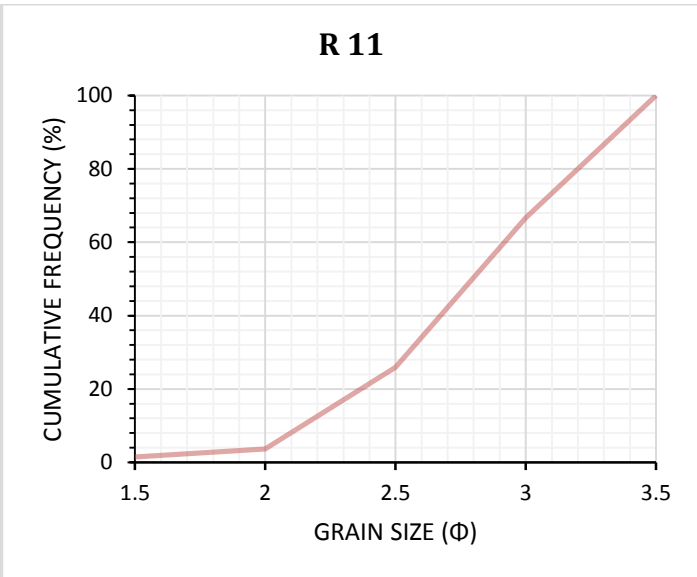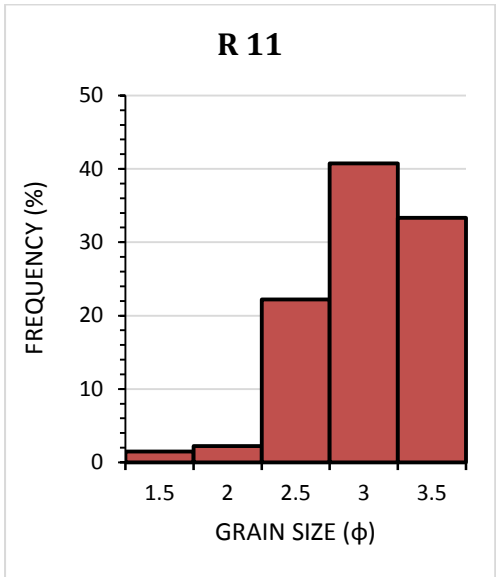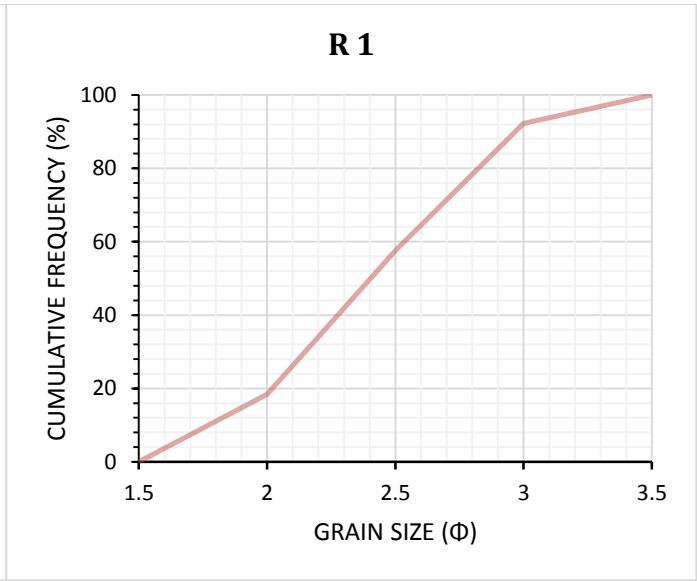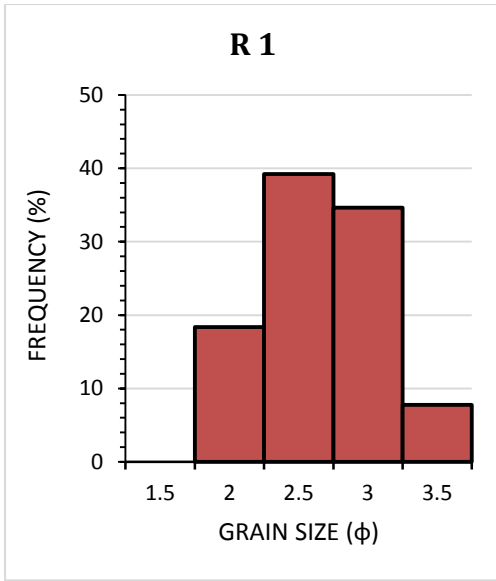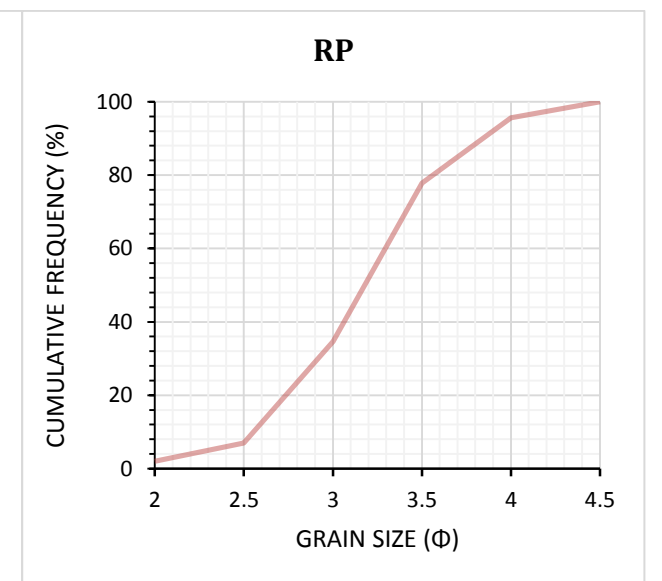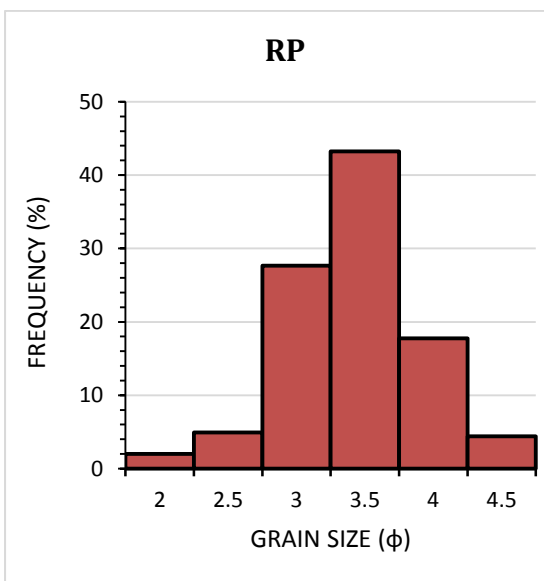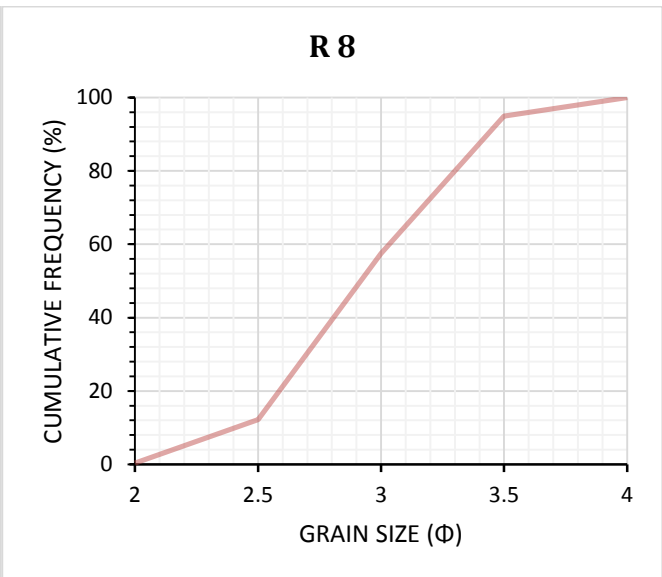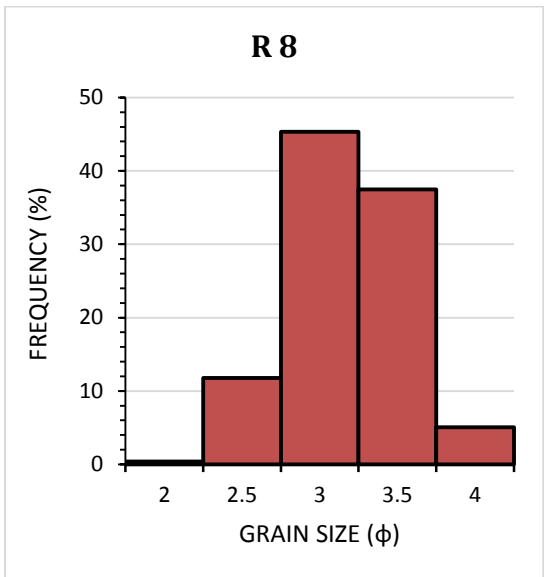**FB 6** (Frequency histogram) — FREQUENCY (%) vs GRAIN SIZE (φ)

FB 6 (Cumulative curve) — CUMULATIVE FREQUENCY (%) vs GRAIN SIZE (Φ)
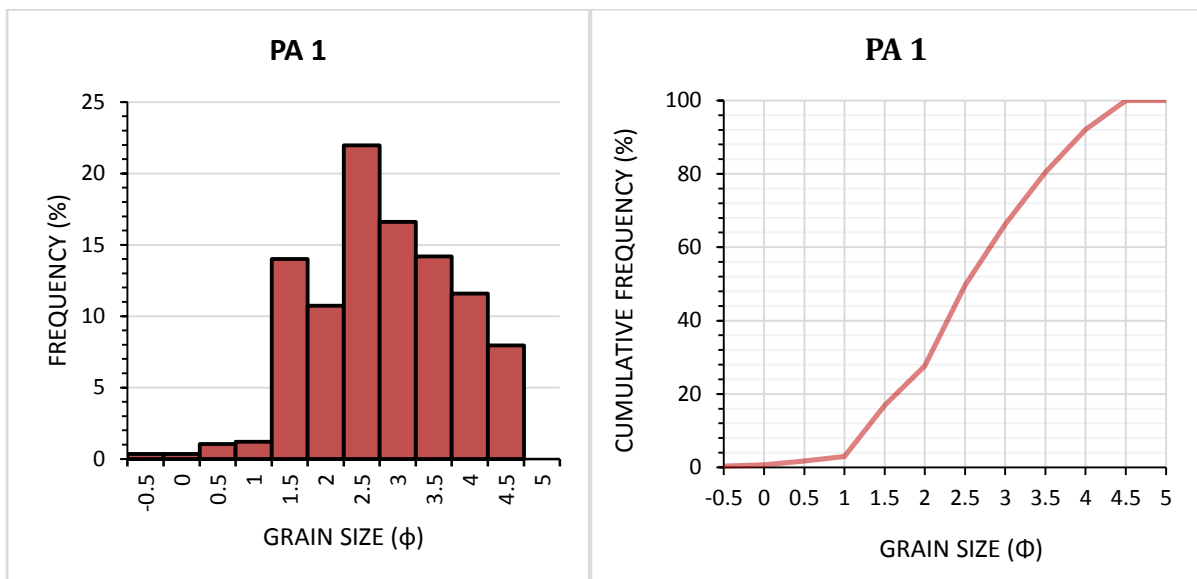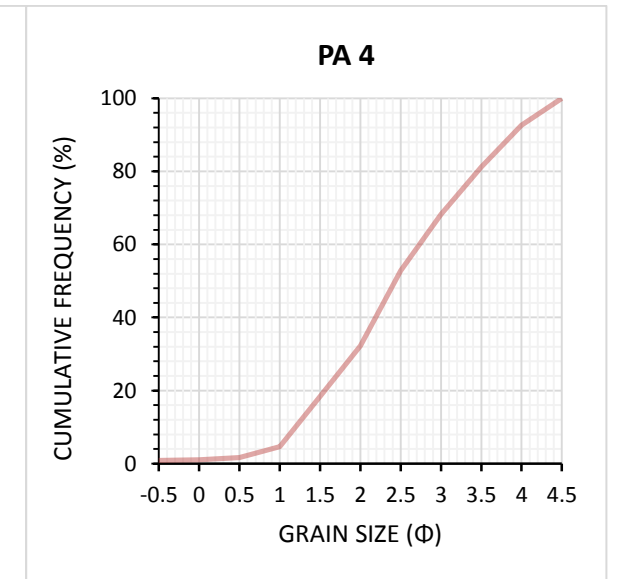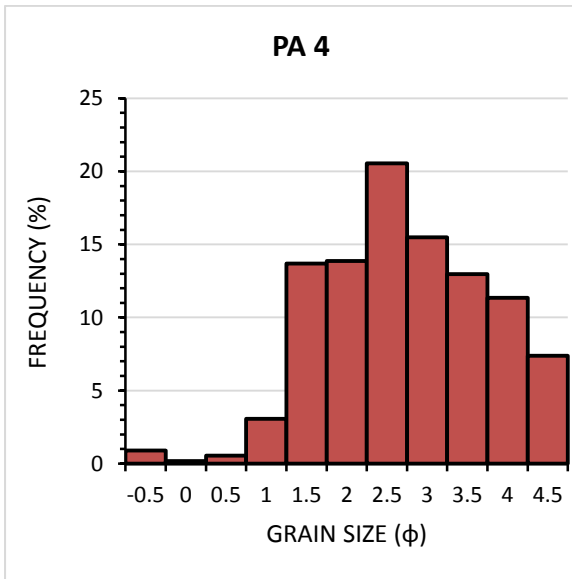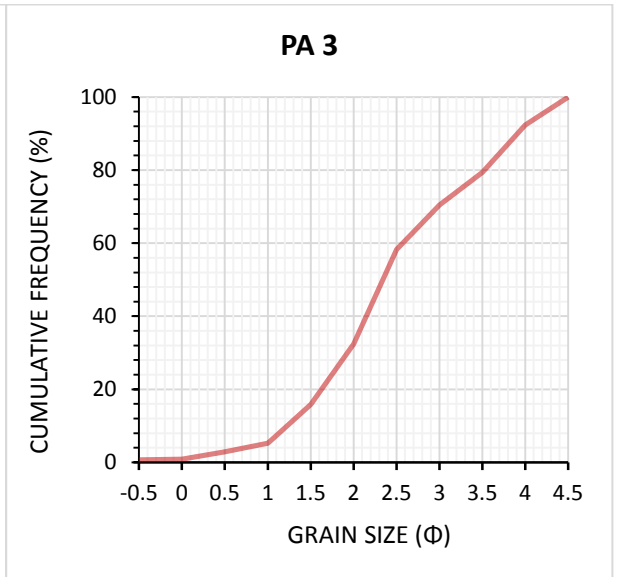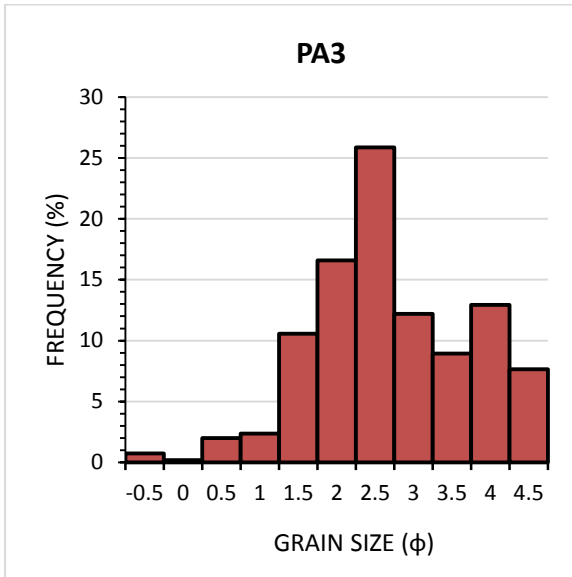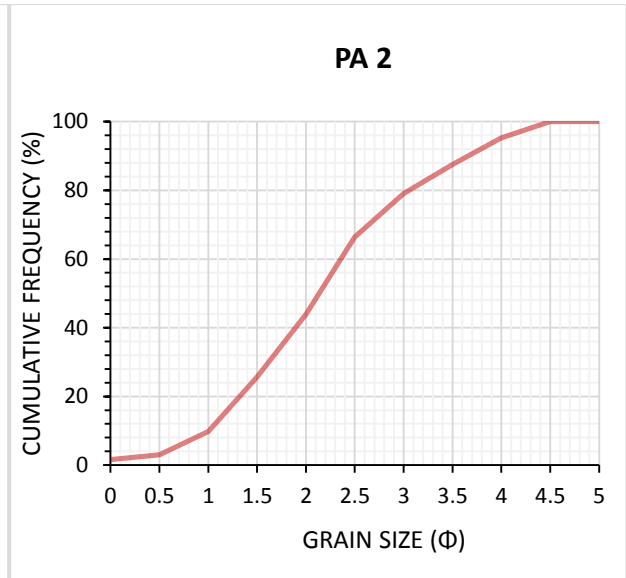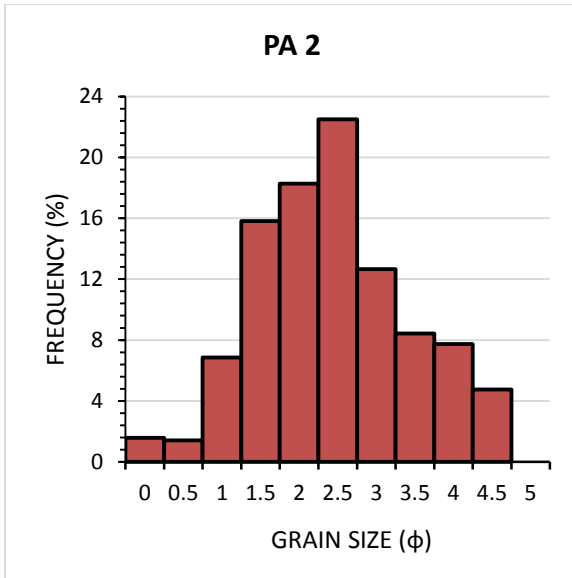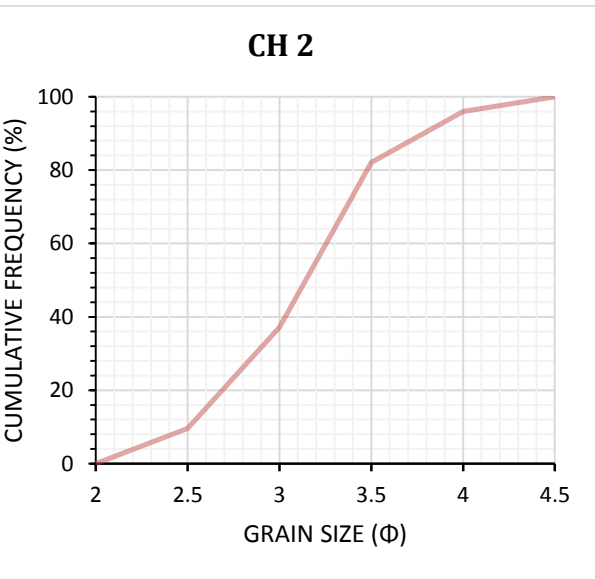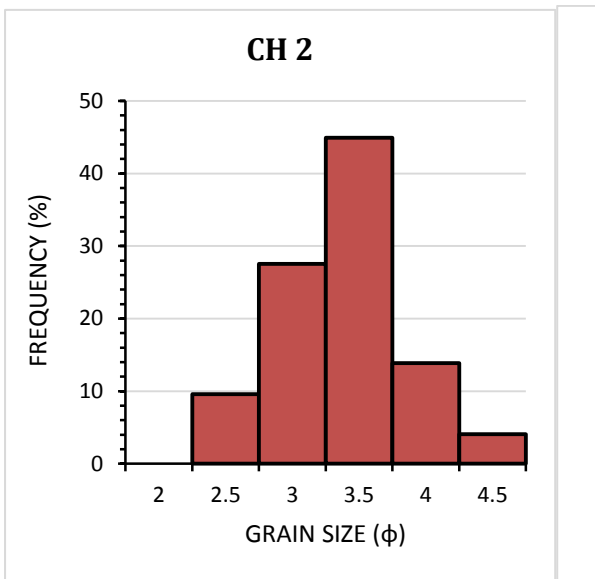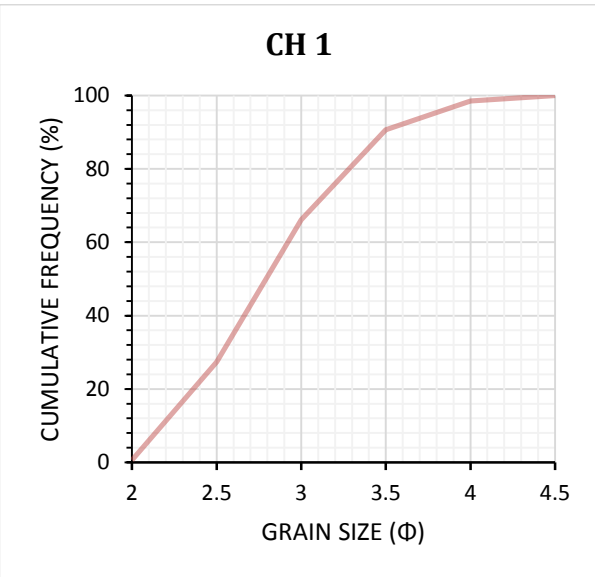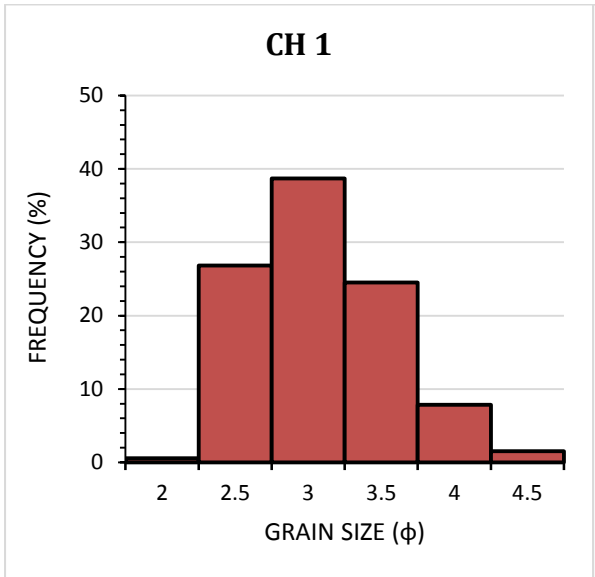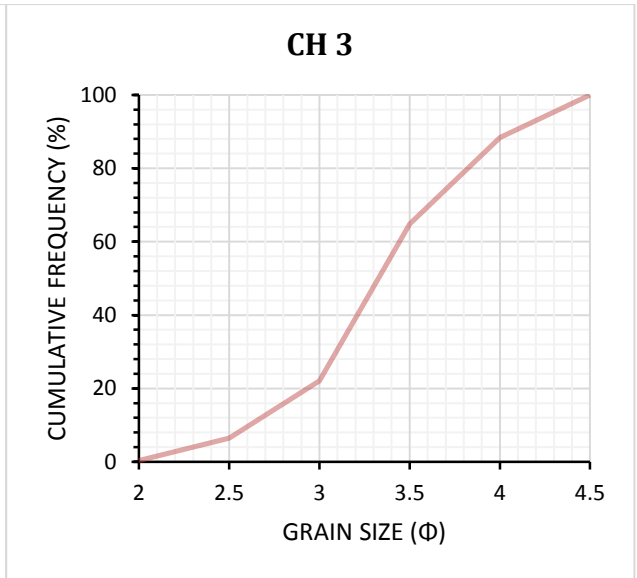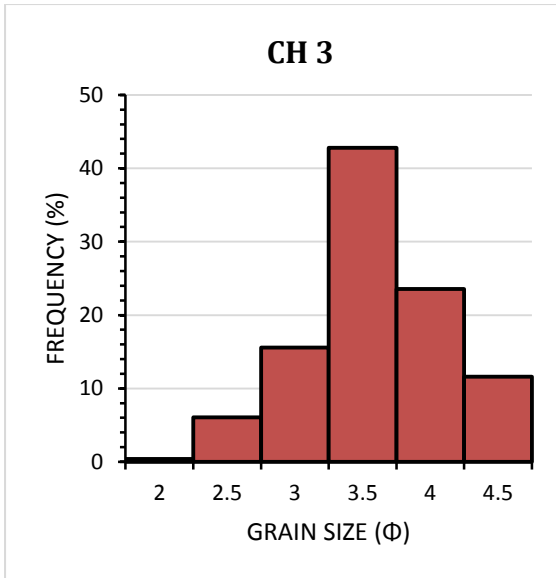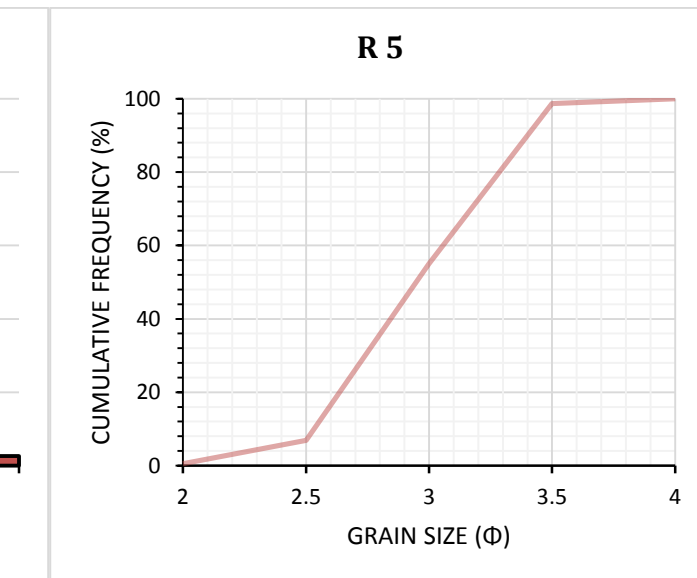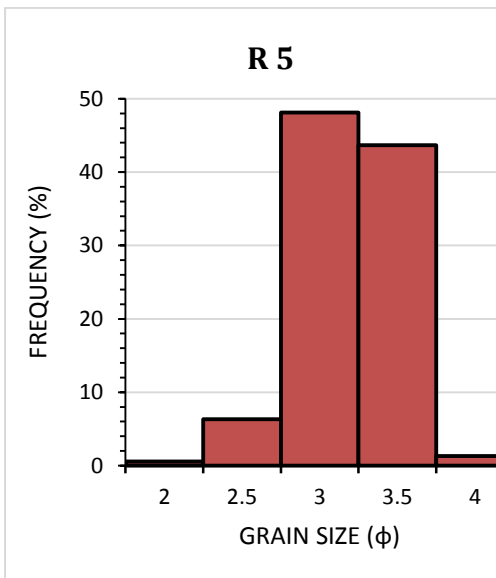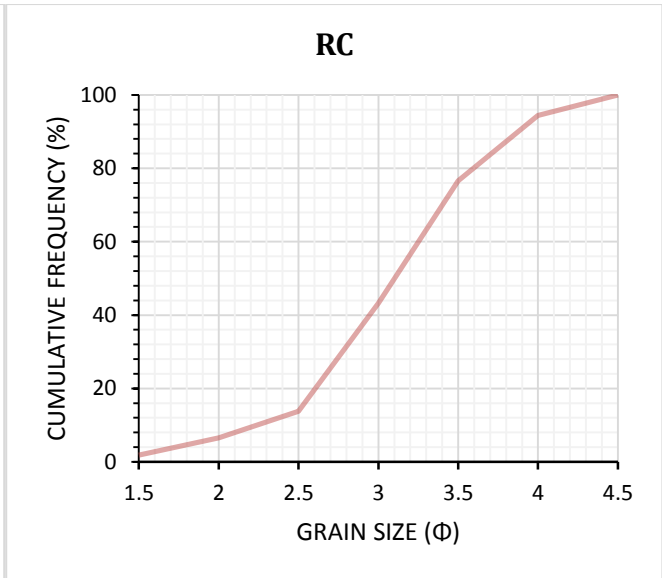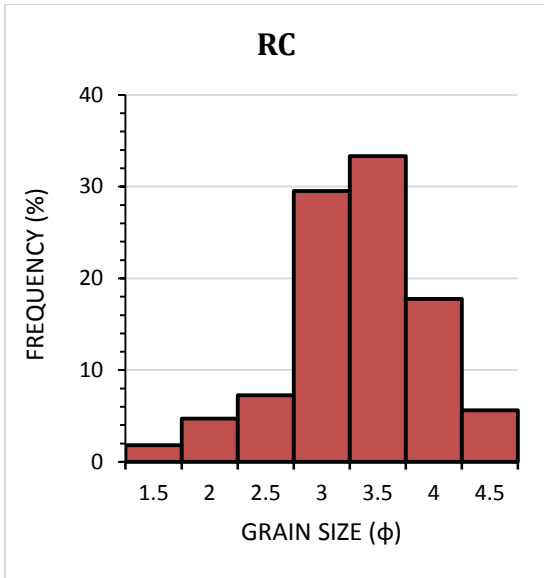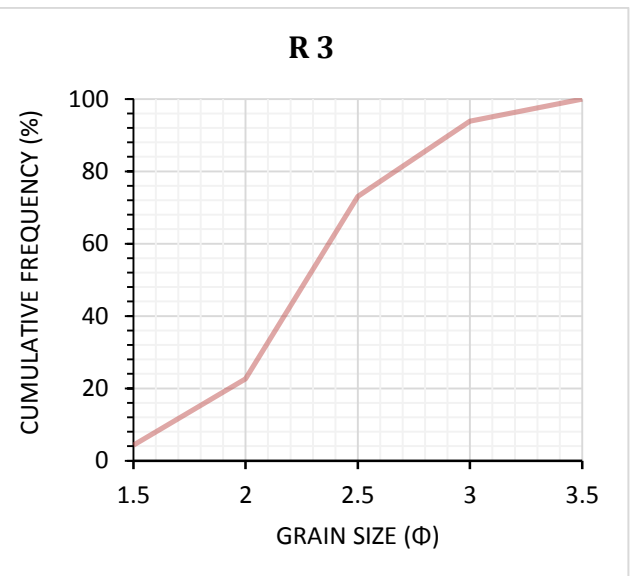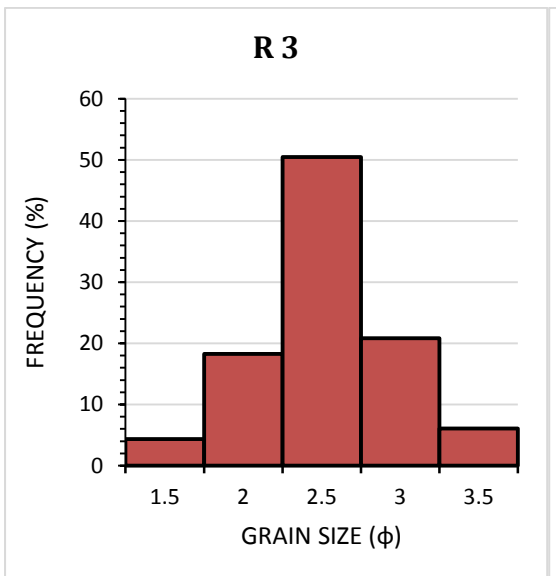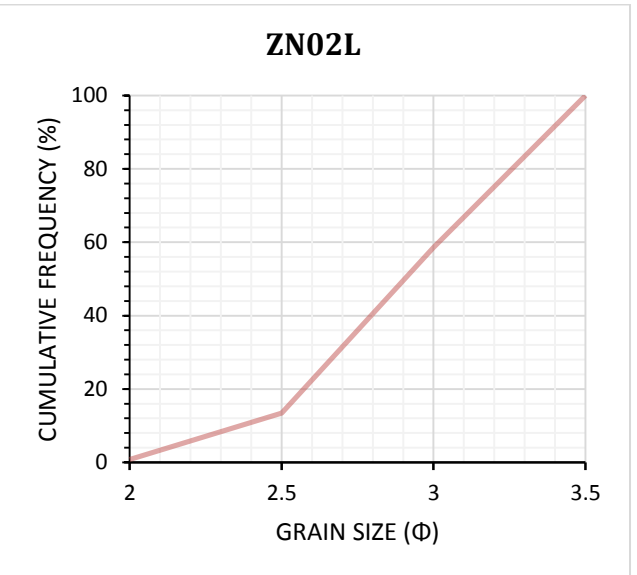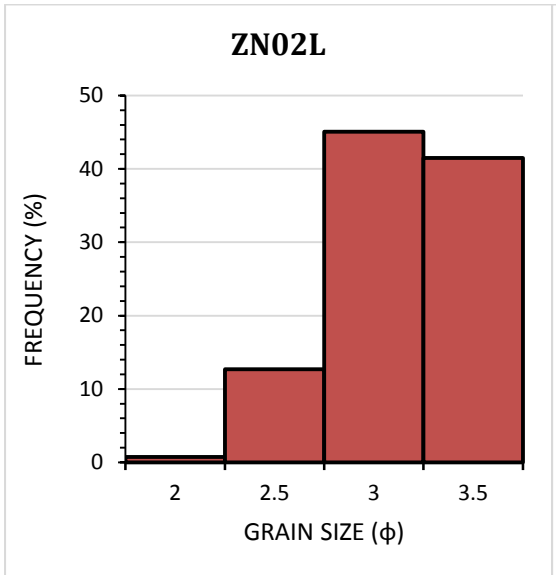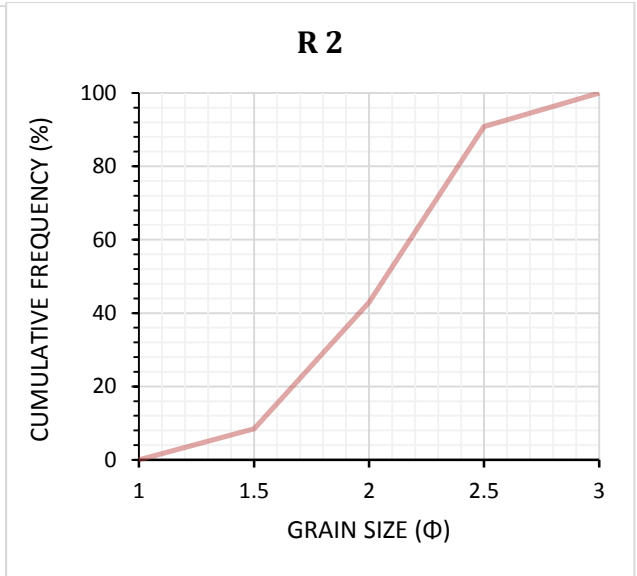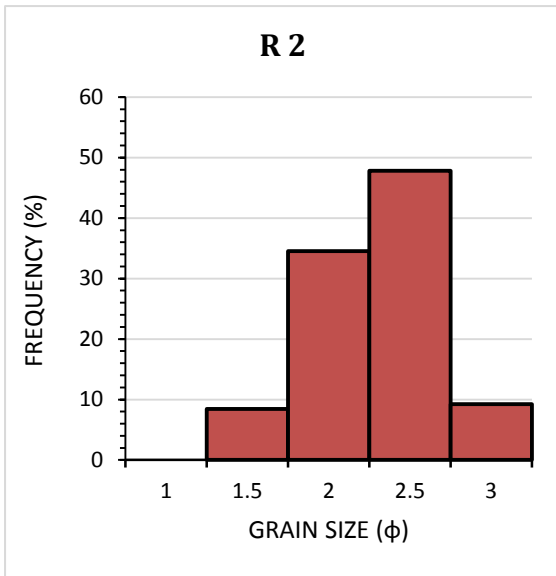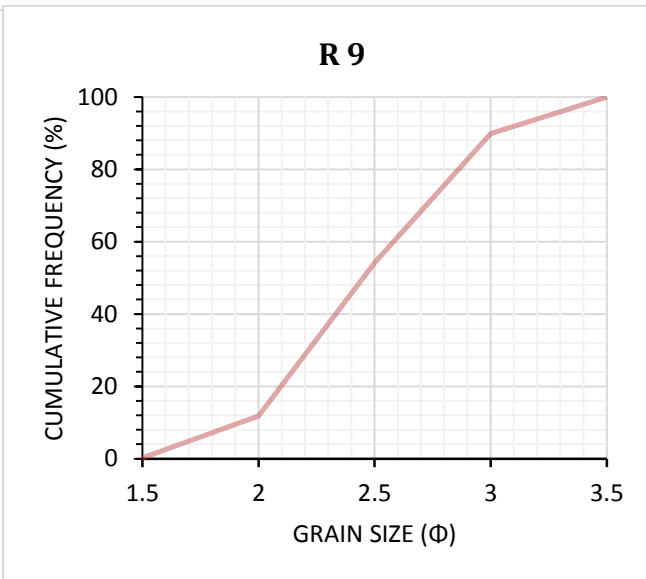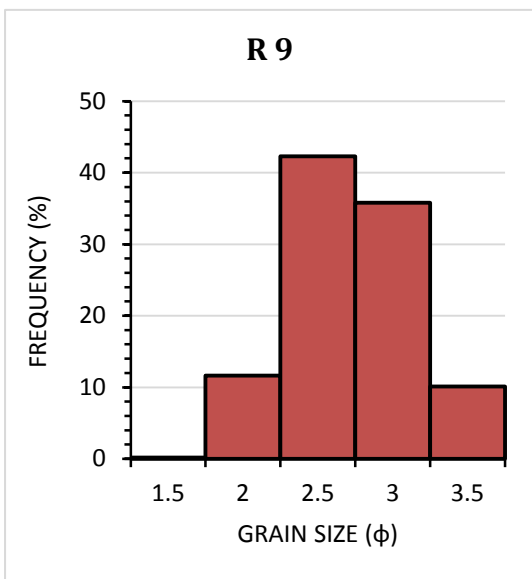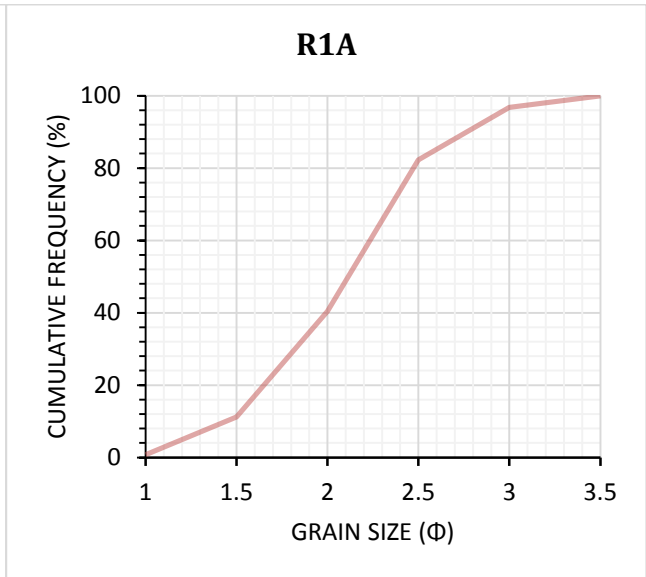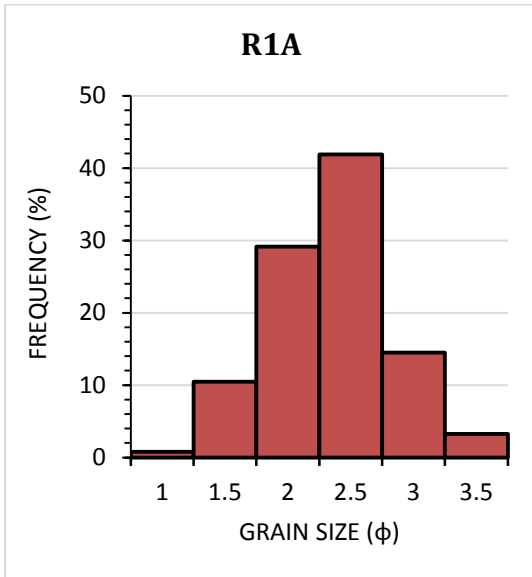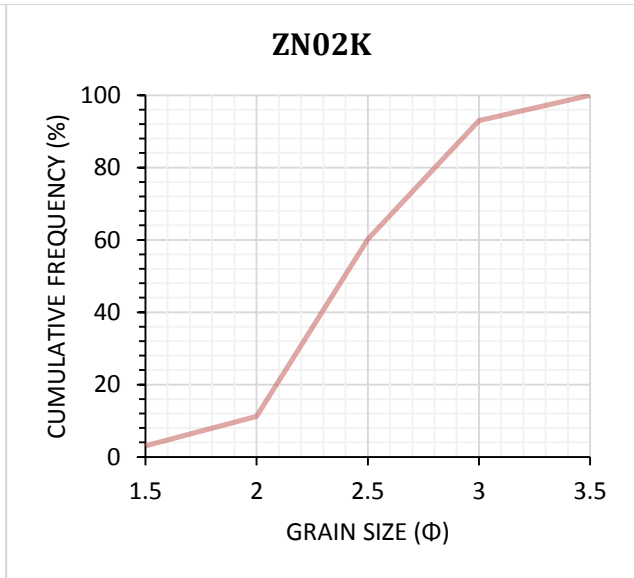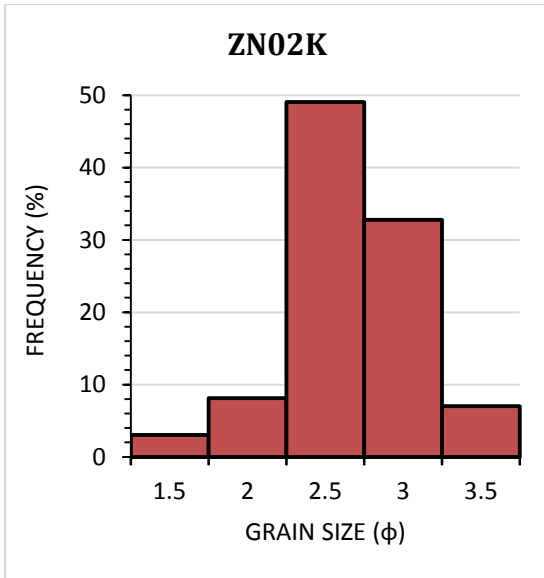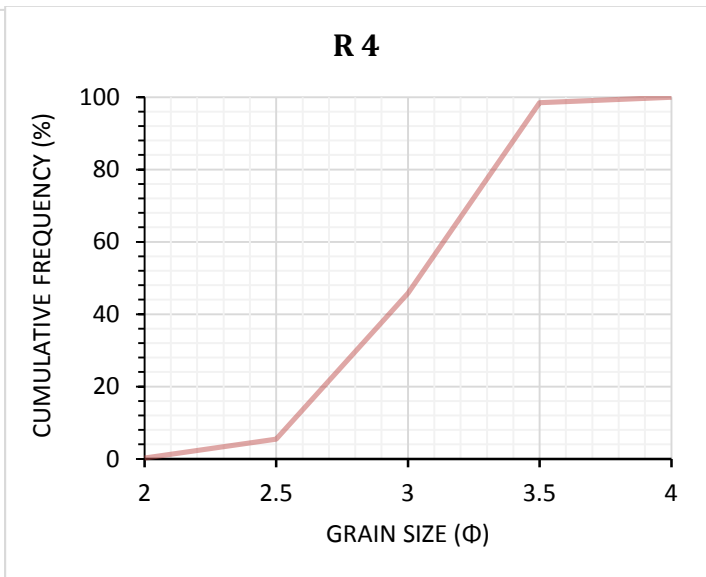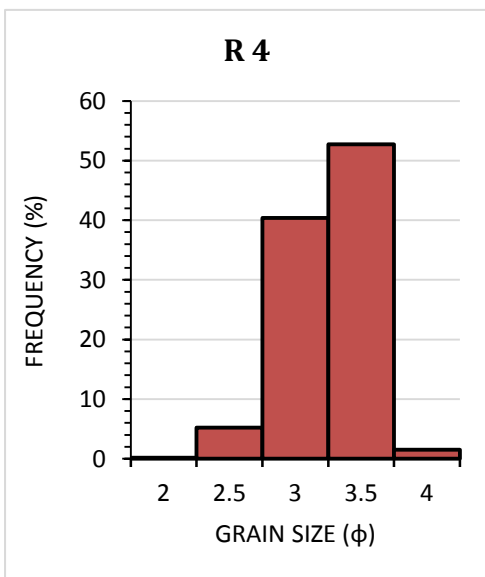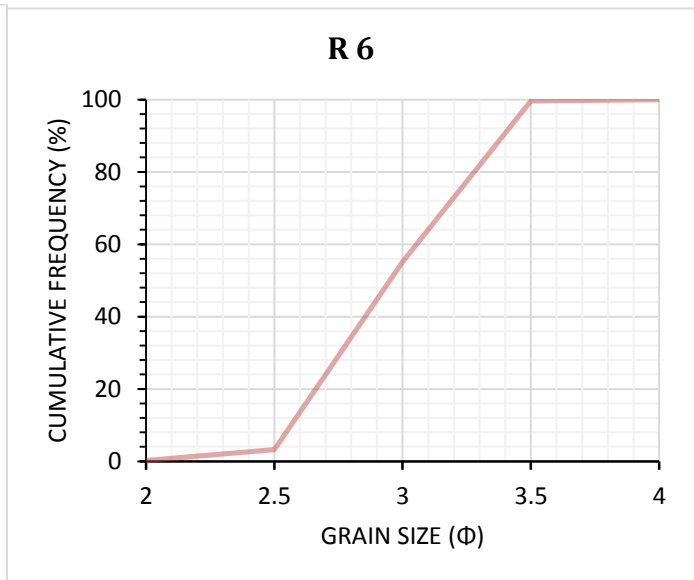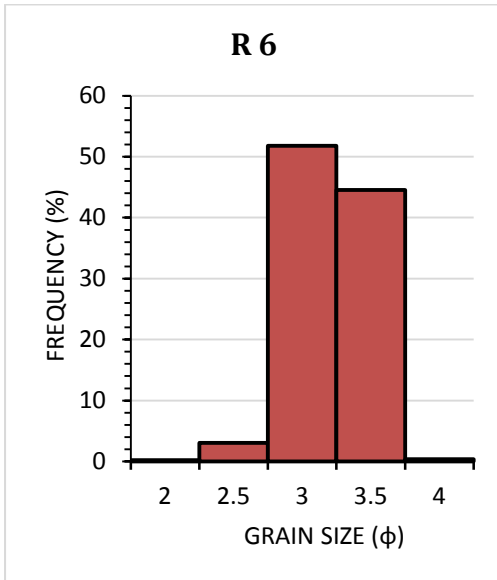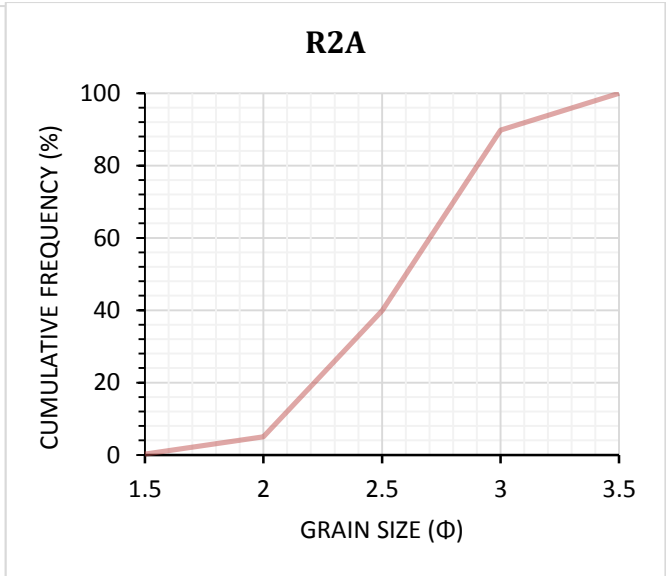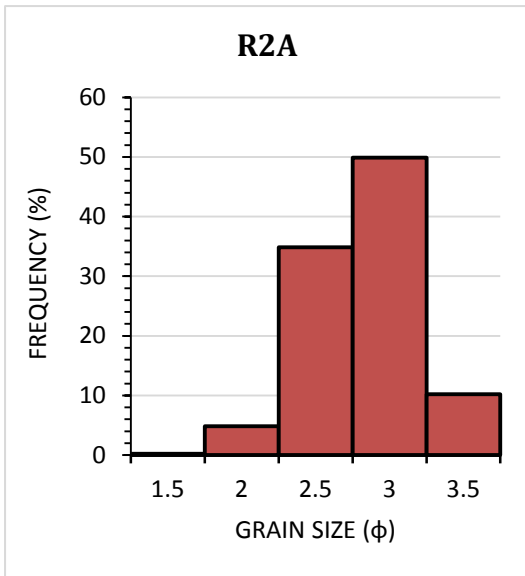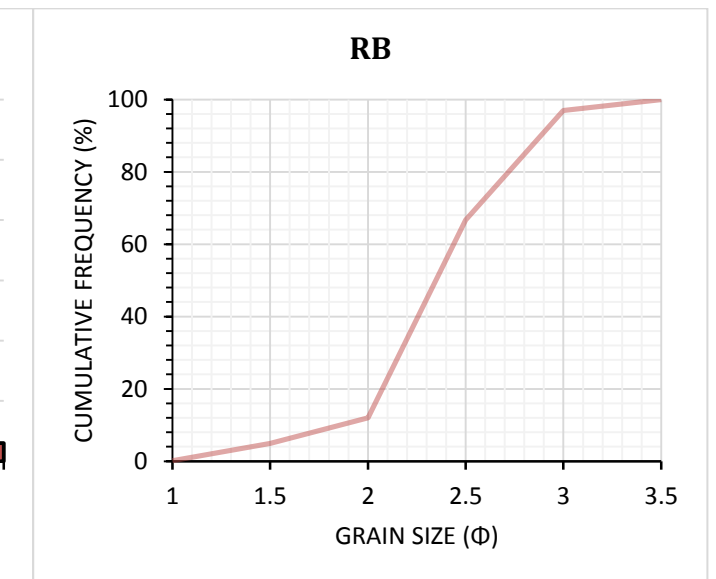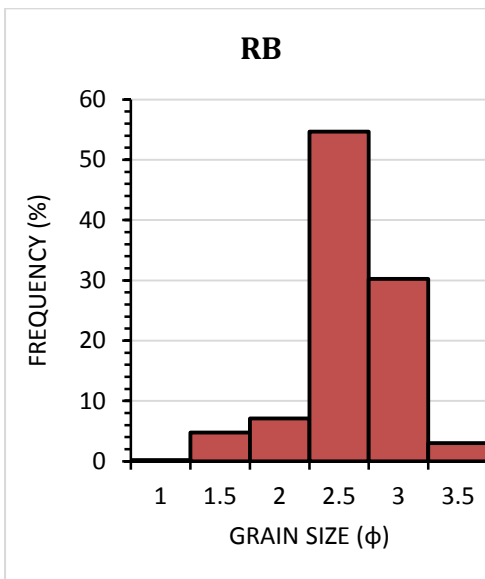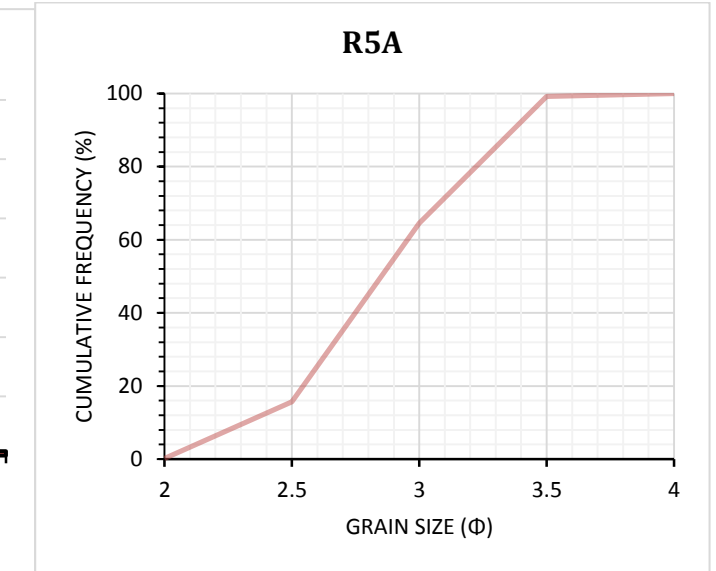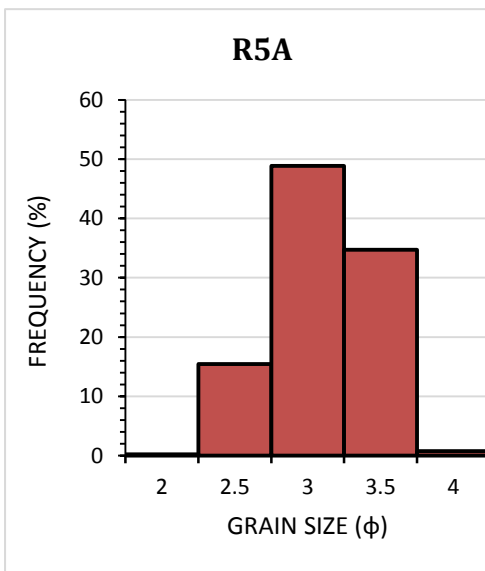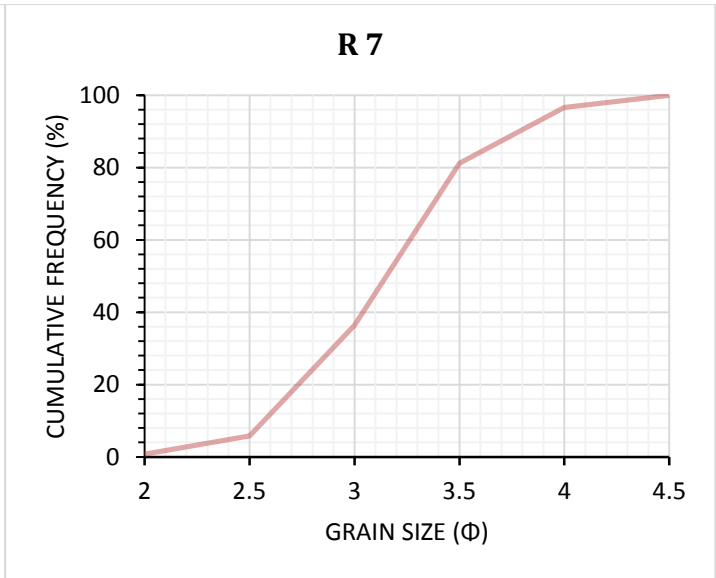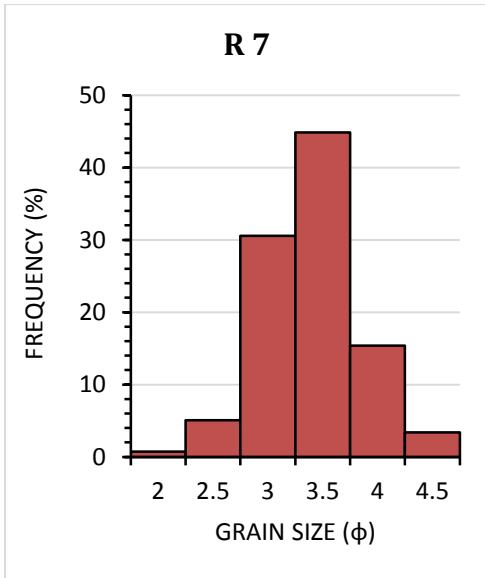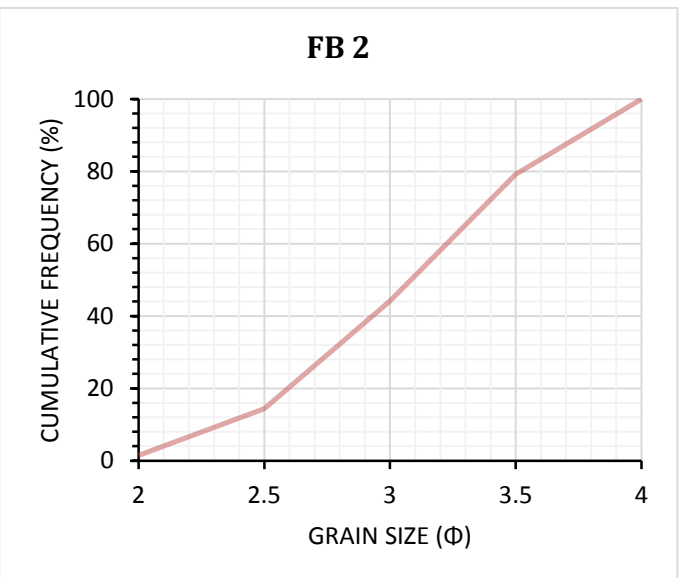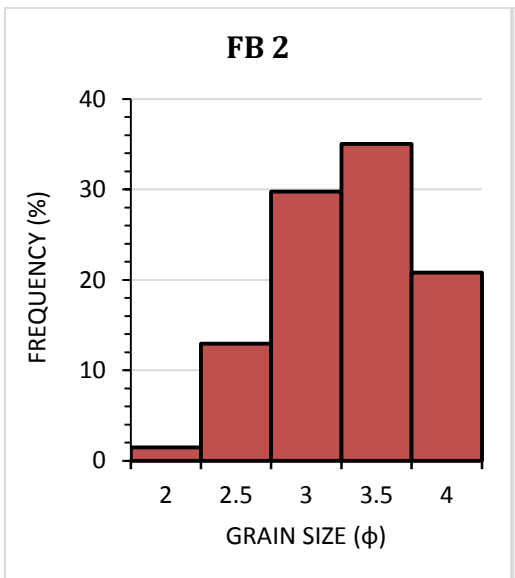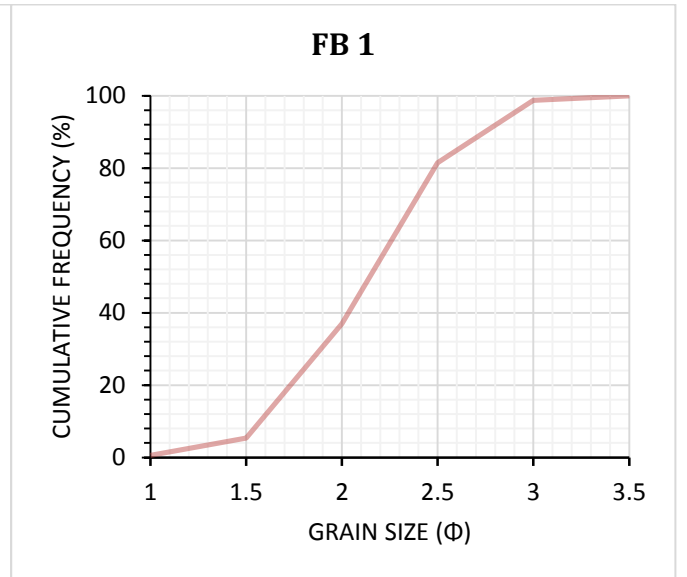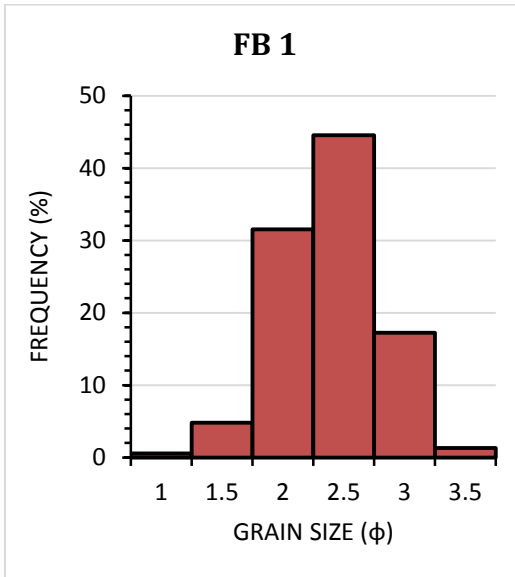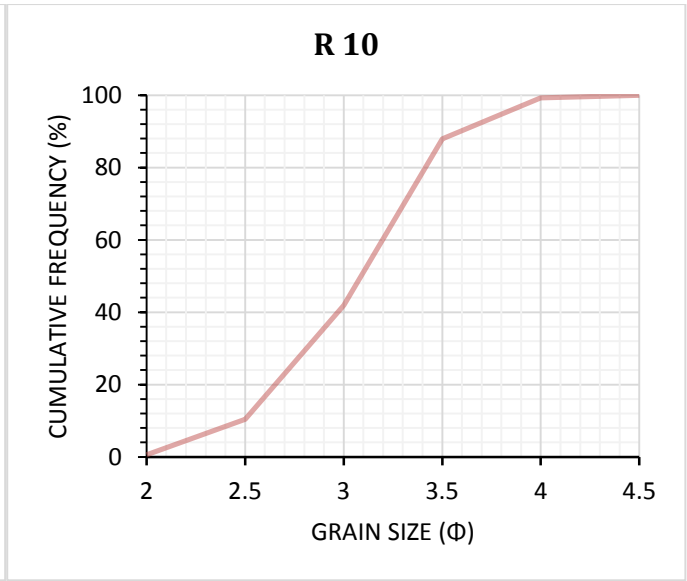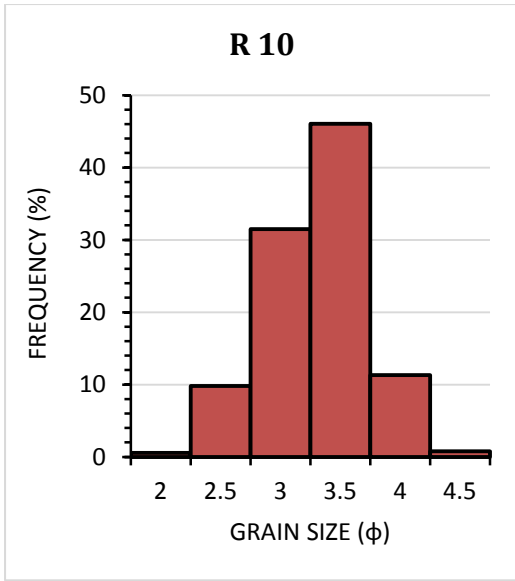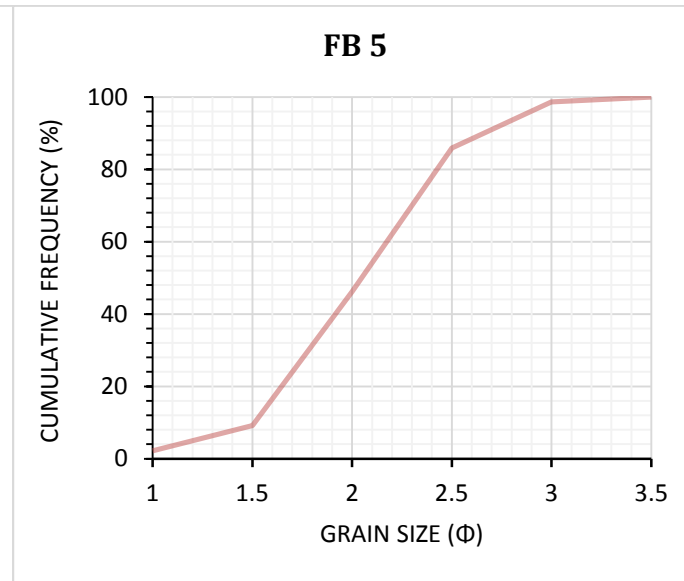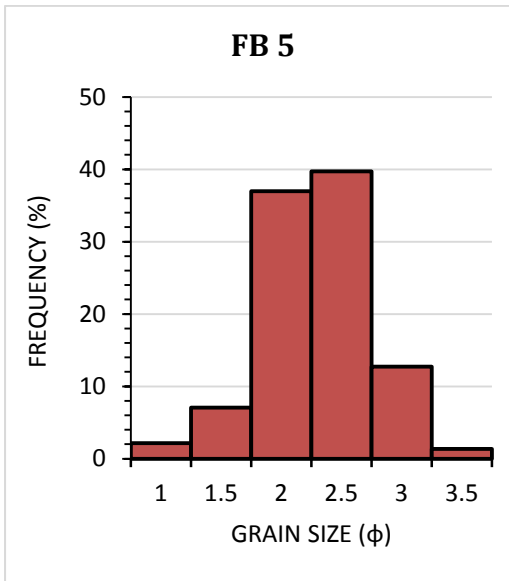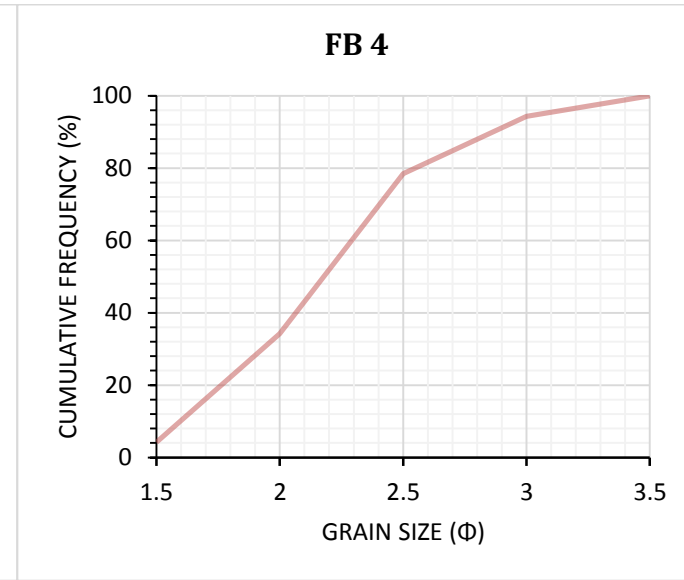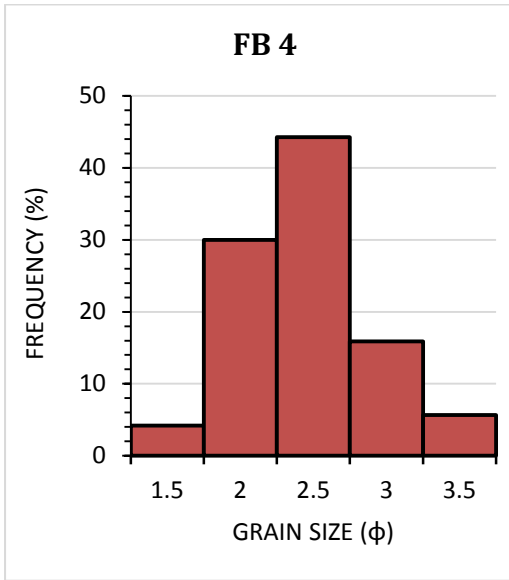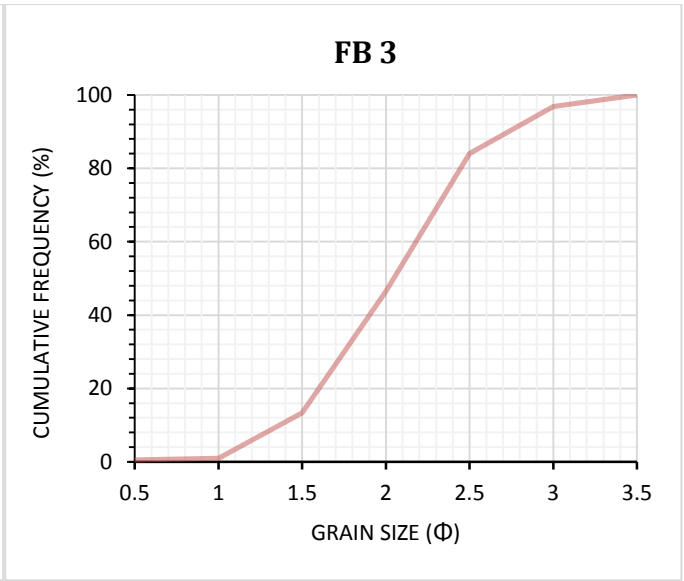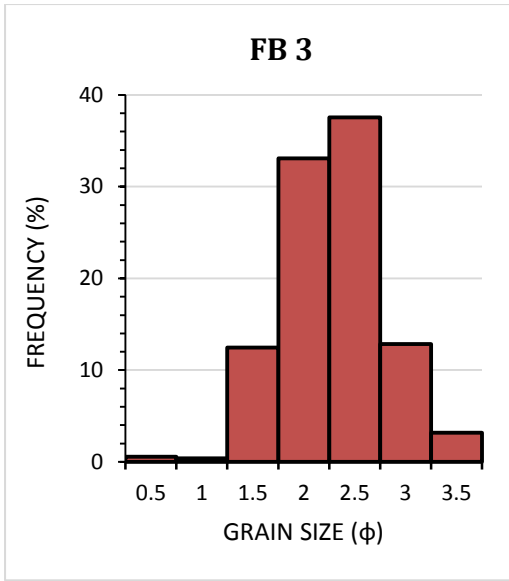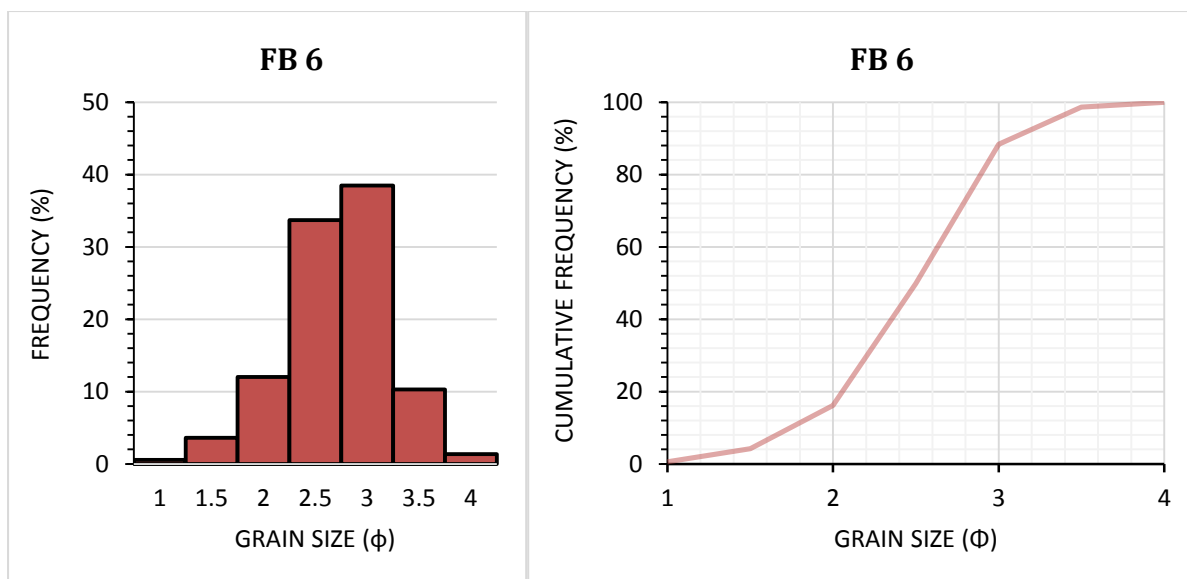
Appendix B: Mineralogical and Geochemical Results

Table B1: Results of X-ray Diffraction (XRD).

Formation	Sample ID	Plagioclase (%)	Microcline (%)	Quartz (%)	Illite (%)	Chlorite (%)	Mica (%)	Smectite (%)	Talc/pyrophyllite (%)	Sericite (%)	Hematite (%)	Pyrite (%)	Dolomite (%)	Garnet (%)	Zircon (%)	Zeolite (%)
Fort Brown	FB2 (Sst)	26	1	31	4	4	1	24	8	-	tc	-	-	tc	tc	tc
Fort Brown	FB1 (Sst)	30	2	29	6	5	2	20	5	-	tc	-	-	tc	tc	tc
Fort Brown	FB (Mds)	28	2	30	6	6	2	18	7	-	tc	-	-	tc	tc	tc
Ripon	RPP (Sst)	20	3	38	7	3	5	17	6	-	-	-	-	-	tc	tc
Ripon	RC (Sst)	16	tc	21	30	10	8	12	2	-	-	tc	-	tc	tc	tc
Ripon	R11 (Sst)	17	tc	18	28	9	6	18	3	-	-	-	-	tc	-	-
Ripon	R 10 (Sst)	12	tc	25	26	11	4	20	1	-	-	-	-	tc	-	tc
Ripon	R9 (Sst)	10	2	32	25	14	17	tc	-	-	-	-	-	-	-	-
Ripon	R8 (Sst)	10	tc	36	18	9	26	-	-	-	-	-	-	tc	-	-
Ripon	R7 (Mds)	20	-	27	6	11	tc	35	tc	-	tc	tc	-	tc	tc	-
Ripon	R6 (Sh)	19	tc	16	26	9	8	16	5	-	-	-	-	tc	-	-
Ripon	R5 (Sh)	28	4	40	7	3	5	2	11	-	-	-	-	-	-	-
Ripon	R4 (Sst)	25	tc	30	6	4	6	28	-	tc	tc	-	-	-	-	-
Ripon	R3 (Sst)	18	3	34	6	1	9	23	5	-	-	-	-	-	tc	tc
Ripon	R2 (Mds)	25	tc	32	5	8	2	25	2	tc	tc	tc	-	tc	tc	tc
Ripon	R 1 (Mds)	19	-	28	7	10	1	34	tc	-	tc	tc	-	tc	tc	-
Ripon	RP* (Mds)	23	3	34	7	6	11	13	tc	2	-	-	-	tc	-	-

Collingham	CH2 (Sh)	12	4	32	13	10	5	23	-	-	-	tc	-	tc	tc	-
Collingham	CH1 (Sh)	13	-	30	11	13	4	28	-	-	-	tc	-	tc	-	-
Collingham	CH (Sh)	11	-	40	12	8	16	12	-	-	-	-	-	tc	tc	-
Whitehill	WH3 (Sh)	23	-	37	9	6	14	8	-	tc	-	2	-	-	-	-
Whitehill	WH2 (Sh)	9	-	28	14	4	18	12	-	-	-	9	6	-	-	-
Whitehill	WH1 (Sh)	12	-	32	26	-	2	tc	-	tc	-	5	22	-	-	-
Whitehill	WH (Sh)	7	tc	30	16	8	15	6	-	tc	tc	7	9	-	-	-
Prince Albert	PA2 (Mds)	10	2	25	18	6	3	30	-	5	tc	tc	-	tc	tc	-
Prince Albert	PA1 (Mds)	15	tc	20	14	8	4	31	-	7	tc	tc	-	tc	tc	-
Prince Albert	PA (Mds)	13	tc	23	16	4	6	33	-	3	tc	tc	-	tc	tc	-

Note: sst, mds, sh, tc and - represent sandstone, mudstone, shale, minerals identified in traces and not detected, respectively.

Table B2: Results of major elements (wt%) analysed by X-ray fluorescence spectrometry.

Sample ID	Lith.	SiO_2	TiO_2	Al_2O_3	Fe_2O_3 (t)	MnO	MgO	CaO	Na_2O	K_2O	P_2O_5	Cr_2O_3	LOI	Total	H_2O^-
FB	Sh	66.88	0.77	15.43	5.36	0.06	1.46	0.77	2.46	2.91	0.23	0.02	3.26	99.61	0.35
RPP	Sh	68.83	0.63	15.12	4.87	0.05	1.47	0.87	2.15	3.19	0.18	0.01	2.85	100.22	0.30
RC	Sh	66.50	0.71	16.22	5.14	0.04	1.58	0.73	2.03	3.50	0.21	0.03	3.37	100.07	0.34
R 10	Sh	65.74	0.67	14.44	5.15	0.04	1.58	0.85	2.79	3.47	0.22	0.01	3.03	97.99	0.41
R 7	Sh	63.49	0.60	16.13	5.02	0.08	1.51	2.71	2.32	3.48	0.22	0.03	4.40	99.99	0.39
CH1	Sh	78.53	0.35	10.63	1.70	0.05	0.49	1.57	0.68	2.36	0.11	0.02	3.47	99.96	0.48
CA	Sh	57.56	0.80	19.83	7.62	0.06	2.22	0.34	0.80	4.42	0.17	0.05	4.71	98.57	0.57
WH1	Sh	70.31	0.17	10.84	1.52	0.20	0.36	6.59	0.38	2.35	0.09	0.00	7.42	100.23	0.39
WH	Sh	87.99	0.35	5.91	0.47	0.00	0.27	0.06	0.17	1.41	0.09	0.01	2.64	99.37	0.64
PA2	Sh	67.63	0.46	14.98	3.58	0.10	1.10	2.76	0.58	3.50	0.11	0.01	5.52	100.33	0.71
PA1	Sh	67.30	0.74	15.90	4.31	0.03	1.49	0.80	2.89	3.02	0.18	0.02	3.41	100.09	0.48
PA	Sh	63.90	0.69	15.65	6.88	0.06	1.81	0.82	2.26	3.31	0.22	0.02	3.87	99.49	0.82
FB2	Sst	77.78	0.50	8.25	7.78	0.09	1.13	0.11	0.54	0.95	0.09	0.01	2.47	99.70	0.31
RP*	Sst	77.84	0.13	10.73	2.79	0.11	0.50	1.62	0.31	2.22	0.10	0.02	3.86	100.23	0.47
R 11	Sst	55.94	0.54	6.22	2.71	0.18	0.31	16.67	1.13	1.46	0.05	0.04	12.03	97.28	0.34
R 9	Sst	81.65	0.45	8.55	4.26	0.04	0.67	0.17	1.08	1.30	0.08	0.01	1.81	100.06	0.23
R 8	Sst	85.29	0.29	6.71	1.99	0.01	0.25	0.10	1.23	1.35	0.06	0.01	1.01	98.30	0.20
R 6	Sst	66.95	0.54	6.81	2.55	0.18	0.27	10.98	0.86	1.18	0.06	0.01	9.85	100.24	0.23
R 5	Sst	87.32	0.68	5.91	2.04	0.02	0.25	0.06	1.06	0.98	0.06	0.04	1.00	99.41	0.15
R 4	Sst	67.61	0.74	15.48	5.44	0.03	1.09	0.51	3.15	2.38	0.20	0.01	3.38	100.02	0.64
R 3	Sst	80.86	0.34	8.74	3.78	0.03	0.57	0.14	1.41	1.44	0.07	0.01	1.56	98.95	0.24
R 2	Sst	82.74	0.50	7.78	3.29	0.07	0.50	0.71	1.59	1.14	0.08	0.01	1.74	100.15	0.22
R 1	Sst	86.32	0.25	6.93	2.32	0.01	0.35	0.12	1.17	1.16	0.06	0.01	1.15	99.85	0.27
CH	Sst	66.91	0.56	16.10	4.42	0.03	1.20	0.65	3.27	3.30	0.16	0.02	3.53	100.14	0.64

Certified		45.42	1.54	16.62	9.73	0.18	8.15	10.93	3.65	0.70	0.26	0.07	2.50	99.75	0.18
Result		45.83	1.52	17.05	9.68	0.18	7.84	10.59	3.68	0.72	0.27	0.08	2.74	100.18	0.13

Note: Lith- lithology; LOI - Loss on ignition; Sh- shale; Sst- sandstones; $Fe_2O_3(t)$ as total iron, 12/76 is a secondary amphibolite reference material; GSS-1-soil reference material from IGGE, China.

Table B3: Results of trace elements (ppm) analysed by X-ray fluorescence spectrometry.

Sample	Lith.	Ag	As	Ba	Bi	Br	Cd	Ce	Co	Cr	Cs	Cu	Ga	Ge	Hf	La	Mo	Nb	Nd
FB	Sh	<2	19	501	<5	<3	<4	78	6.2	54	<5	23	19	<2	5.8	42	<2	15	41
RPP	Sh	<2	6.3	612	<5	<3	<4	53	3	47	6.8	21	19	<2	5.1	32	<2	13	34
RC	Sh	<2	4.3	545	<5	3.6	<4	48	4.4	45	<5	26	21	<2	6.9	34	<2	15	34
R 10	Sh	<2	7.7	435	<5	3.1	<4	60	5.6	42	<5	19	19	<2	2	29	<2	13	30
R 7	Sh	<2	9.5	614	<5	<3	<4	76	8.2	40	6.9	19	21	<2	8	43	<2	15	40
CH1	Sh	<2	<3	670	<5	<3	<4	78	<2	17	<5	26	12	<2	7.7	44	<2	15	35
CA	Sh	<2	7.9	910	<5	<3	<4	74	10	85	5.8	29	26	<2	5.6	38	<2	17	40
WH1	Sh	<2	11	474	<5	<3	<4	41	<2	3.4	12	6.8	10	<2	6.1	18	<2	5	24
WH	Sh	<2	3.6	303	<5	6.1	<4	68	<2	19	6.1	15	11	<2	5.9	34	<2	9.8	32
PA2	Sh	<2	<3	605	<5	<3	<4	94	<2	85	11	54	19	<2	6.6	53	<2	13	48
PA1	Sh	<2	19	506	<5	9.5	<4	77	6.9	40	<5	51	21	<2	8.9	42	<2	15	44
PA	Sh	<2	7.7	546	<5	<3	<4	48	11	43	6.9	47	21	<2	4.3	19	<2	14	23
FB2	Sst	<2	8.1	285	<5	<3	<4	62	15	51	<5	5.3	10	<2	7.7	32	<2	11	35
RP*	Sst	<2	12	414	<5	<3	<4	46	<2	4.8	6.9	<2	11	<2	3	15	<2	5.5	20
R 11	Sst	<2	7.3	272	<5	<3	<4	46	<2	28	5.2	2.2	6.4	<2	14	24	<2	10	27
R 9	Sst	<2	16	507	<5	<3	<4	68	6	40	<5	11	18	<2	8.2	34	<2	12	37
R 8	Sst	<2	4.8	279	<5	<3	<4	16	<2	22	<5	3.5	7.9	<2	8.1	8.7	<2	6.2	13
R 6	Sst	<2	5.1	310	<5	<3	<4	50	4	28	9	2.5	6.5	<2	12	22	<2	9.7	25
R 5	Sst	<2	3.5	208	<5	<3	<4	55	2.8	53	<5	3	5.9	<2	19	24	<2	12	29
R 4	Sst	<2	11	506	<5	<3	<4	66	7.2	51	<5	10	18	<2	8.7	34	<2	12	35
R 3	Sst	<2	3.7	301	<5	<3	<4	24	8.1	22	<5	2.5	10	<2	5	10	<2	8.3	17
R 2	Sst	<2	7.2	317	<5	<3	<4	42	5	28	<5	4.2	8.7	<2	10	29	<2	10	26
R 1	Sst	<2	<3	280	<5	<3	<4	15	3.3	15	5.3	4.8	8.6	<2	5.4	7.9	<2	6.3	9.4
CH	Sst	<2	8.8	909	<5	<3	<4	73	8.7	26	<5	11	20	<2	5.9	43	<2	11	40
Certified		0.4	33.5	590	1.2	2.9	4.3	70	14	62	9.0	21	19.3	1.3	6.8	34	1.4	16.6	28
Result		<2	37	595	<5	<3	6	67	13	62	5.9	16	18	<2	6.4	31	<2	15	30

441

	Lith.																		
Average	Sh		560.1				66.3		43.37		28.07	18.25		6.08	35.7		13.3	35.4	
Average	Sst		382.3				46.9		30.73			10.92		8.92	23.6		9.5	26.1	
UCC			628			17	92		28	17.5		5.3			12				
PAAS			650			23	110		50	20		5			19				

Note: Lith- lithology; Sh- shale; Sst- sandstones; UCC- Upper Continental Crust; PAAS- Post Archean Australian Shale; 12/76 is a secondary amphibolite reference material; GSS-1-soil reference material from IGGE, China.

Table B4: Results of trace elements (ppm) analysed by X-ray fluorescence spectrometry.

Sample	Lith.	Ni	Pb	Rb	Sb	Sc	Se	Sn	Sr	Ta	Th	Tl	U	V	W	Y	Yb	Zn	Zr
FB	Sh	22	23	125	<3	13	<2	<3	106	<2	18	<2	3.6	85	<5	35	<4	89	187
RPP	Sh	21	21	139	<3	13	<2	<3	133	<2	15	2.8	4.2	73	<5	30	<4	81	148
RC	Sh	20	21	158	<3	14	<2	<3	125	<2	17	<2	4.1	85	<5	29	<4	85	151
R 10	Sh	20	19	131	<3	12	<2	<3	110	<2	14	<2	3.7	73	<5	30	<4	95	139
R 7	Sh	18	26	153	<3	14	<2	<3	210	<2	19	<2	4.1	73	<5	35	<4	83	201
CH1	Sh	5.9	11	89	<3	6.4	<2	<3	174	<2	19	2.1	5.3	39	<5	24	<4	21	158
CA	Sh	34	18	197	<3	16	<2	<3	84	<2	22	<2	3.8	124	<5	30	<4	121	136
WH1	Sh	9.2	9.1	66	<3	5.3	<2	<3	277	<2	21	2.4	3.6	6.4	<5	29	<4	16	128
WH	Sh	2.1	30	77	<3	8.2	<2	<3	145	<2	17	<2	4.7	34	<5	21	<4	<2	164
PA2	Sh	9.6	14	149	<3	12	<2	<3	100	<2	16	<2	4.5	56	<5	35	<4	70	188
PA1	Sh	19	38	144	<3	16	<2	<3	152	<2	19	<2	4.6	96	<5	35	<4	77	221
PA	Sh	21	23	159	<3	13	<2	<3	135	<2	17	<2	5	96	<5	32	<4	112	166
FB2	Sst	31	13	37	<3	6.6	<2	<3	46	<2	9.4	2.1	2.3	46	<5	24	<4	57	270
RP*	Sst	4.5	16	62	<3	3	<2	<3	112	<2	23	<2	3.5	7.7	<5	17	<4	18	109
R 11	Sst	6.9	12	44	<3	9.2	<2	<3	135	<2	10	<2	2.5	24	<5	30	<4	21	442
R 9	Sst	16	24	92	<3	13	<2	<3	96	<2	12	2.1	3.4	88	<5	22	<4	73	232
R 8	Sst	8.6	12	47	<3	4.8	<2	<3	23	<2	3.8	<2	<2	16	<5	9.1	<4	12	186
R 6	Sst	9.7	12	46	<3	11	<2	<3	94	<2	8	<2	2.7	26	<5	27	<4	16	392
R 5	Sst	8.3	16	39	<3	5.8	2.1	<3	24	<2	12	<2	<2	28	<5	23	<4	28	652
R 4	Sst	16	24	93	<3	13	<2	<3	97	<2	14	<2	3.1	90	<5	21	<4	73	238
R 3	Sst	15	22	49	<3	5.5	<2	<3	29	<2	4.3	<2	<2	25	<5	11	<4	32	102
R 2	Sst	12	23	46	<3	6.8	<2	<3	46	<2	7.7	<2	<2	30	<5	18	<4	27	301
R 1	Sst	11	13	45	<3	3.6	<2	<3	28	<2	2.8	<2	<2	21	<5	8.1	<4	23	108
CH	Sst	13	20	128	<3	13	<2	<3	340	<2	15	<2	3.1	76	<5	26	<4	65	174
Certified		20	98	140	0.9	11.2	0.14	6.1	155	1.4	11.6	1.0	3.3	86	3.1	25	2.7	680	245

Result		22	91	140	<3	12	<2	<3	156	<2	9.3	<2	<2	86	<5	24	<4	674	249
Average	Sh	17	21	132		11.9			145.9		17.8		4.27	70		30.4			166
Average	Sst	13	17	60.7		7.94			89.17		10.2			39.8		19.7		37.08	267
UCC		47	17	84		14			320		10.5		2.7	97		21		67	193
PAAS		55	20	160		16			200		14.6		3.1	150		27		85	210

Note: Lith- lithology; Sh- shale; Sst- sandstones; UCC- Upper Continental Crust; PAAS- Post Archean Australian Shale; 12/76 is a secondary amphibolite reference material; GSS-1-soil reference material from IGGE, China.

APPENDIX C: Organic Geochemistry

C (i) Vitrinite reflectance (colour images on the left and monochromatic images on the right)
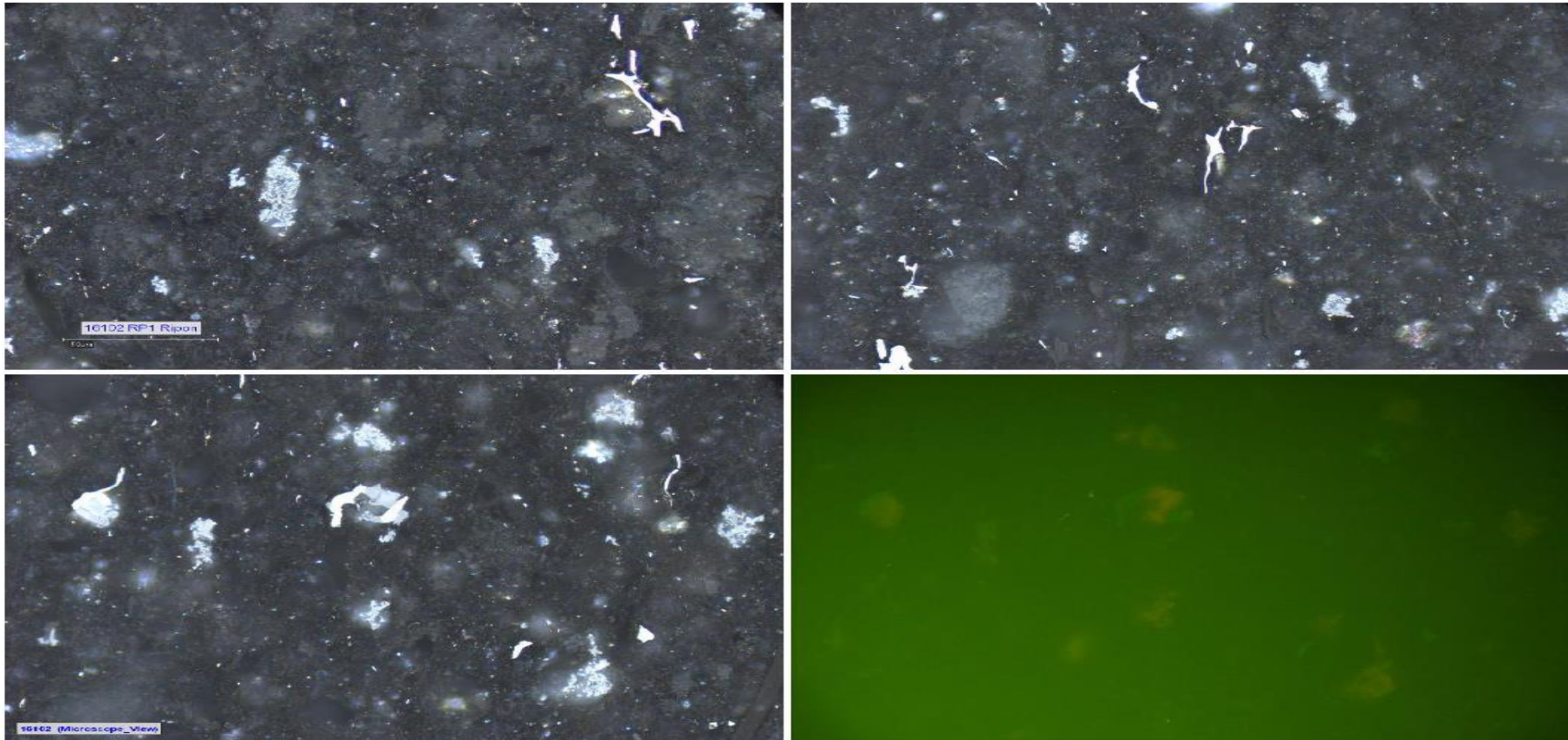
Figure C1: Dispersed organic matter assessment for sample RK6 (Ripon Formation) from borehole KWV 1. TOC: 0.68 wt.%.

Comments: No vitrinite determined; rare inertinite fragments; some fluorescence determined (bottom; Right), most likely carbon. Very fine grained mudstone with carbonaceous materials.
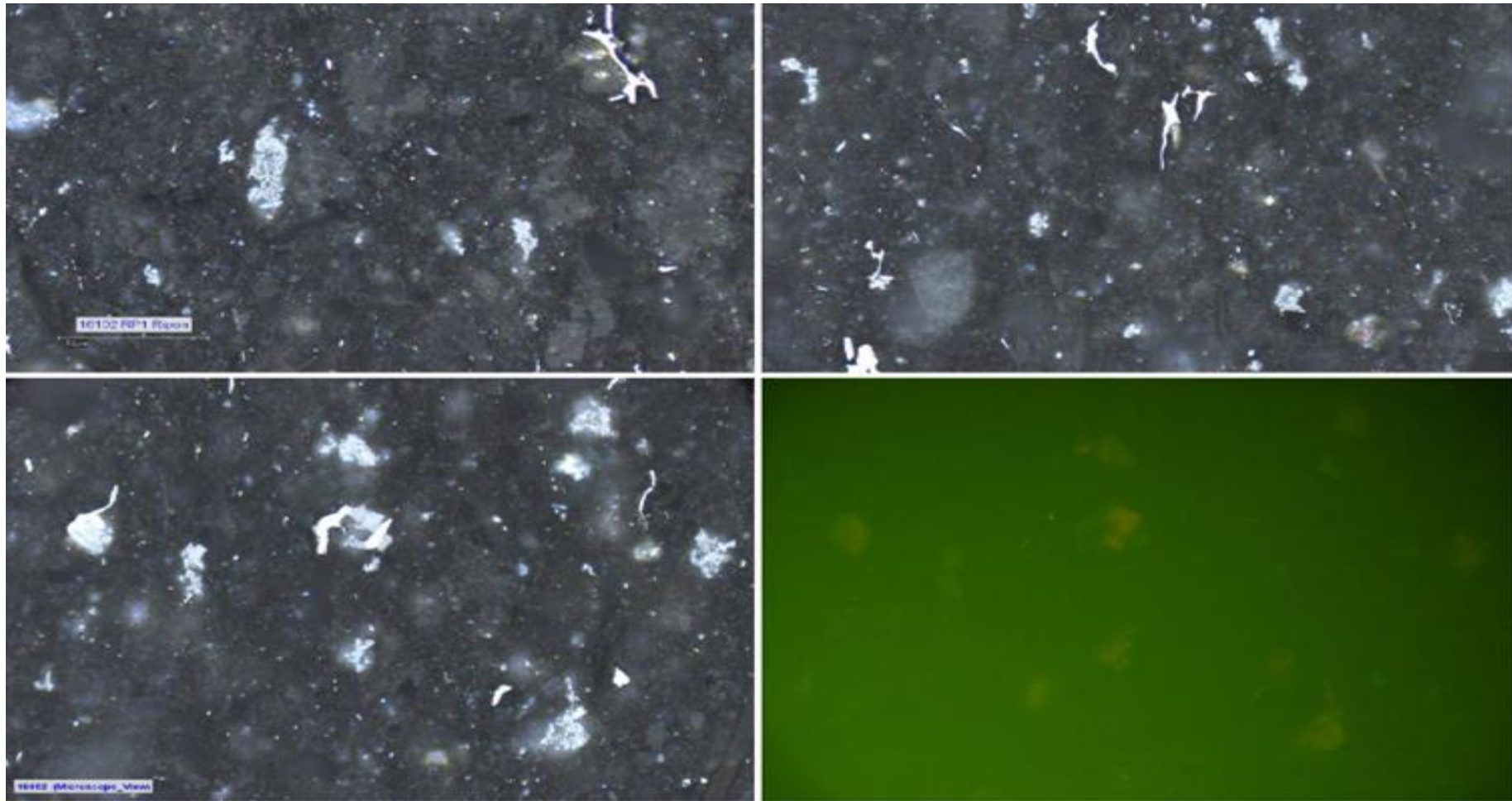
Figure C2: Dispersed organic matter assessment for sample RK5 (Ripon Formation) from borehole KWV 1. TOC: 0.52 wt.%.

Comments: No vitrinite determined; very rare inertinite fragments; no fluorescence determined. Very fine grained mudstone with carbonaceous materials.
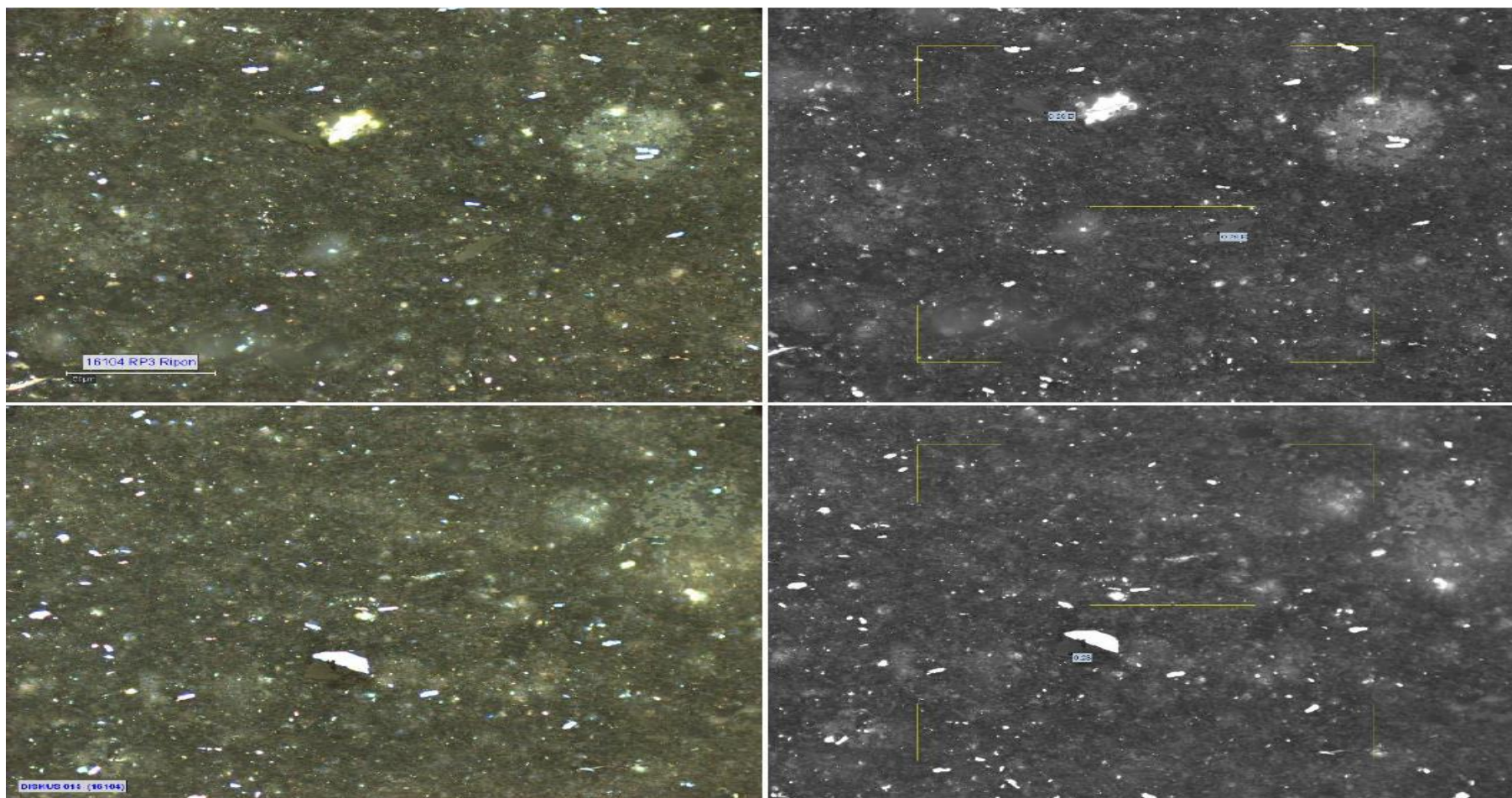
Figure C3: Dispersed organic matter assessment for sample RK4 (Ripon Formation) from borehole KWV 1. TOC: 0.51 wt.%.

Comments: Very fine grained mudstone with carbonaceous materials. No vitrinite determined; very rare inertinite fragments; no fluorescence determined.
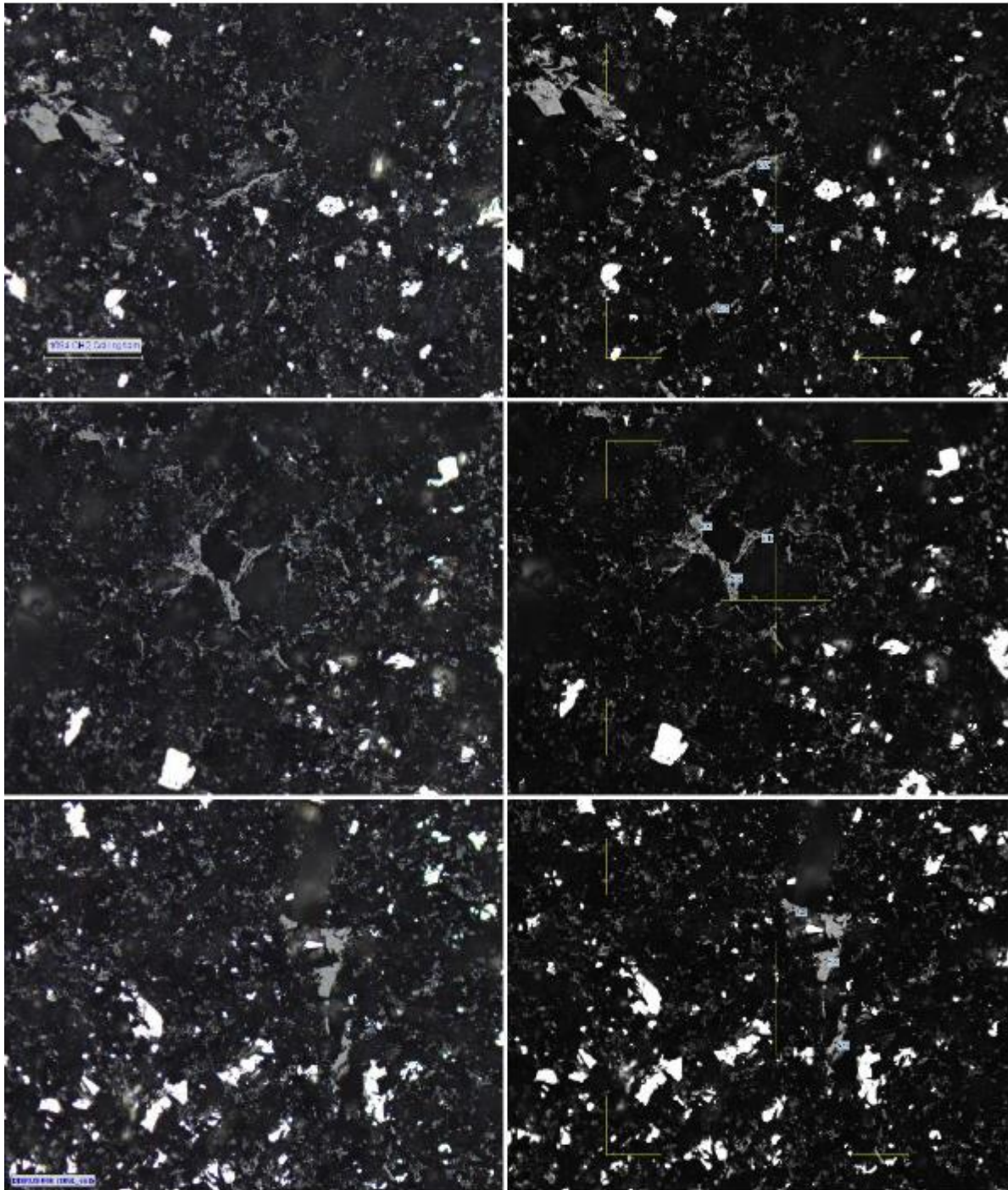
Figure C4: Dispersed organic matter assessment for sample RK2 (Collingham Formation) from borehole KWV 1. TOC: 1.18 wt.%.

Comments: Possibly no vitrinite determined as reflectance readings are very high – range 4.633 – 6.369%. Lots of pyrite and carbon materials and highly fragmented organic matter.
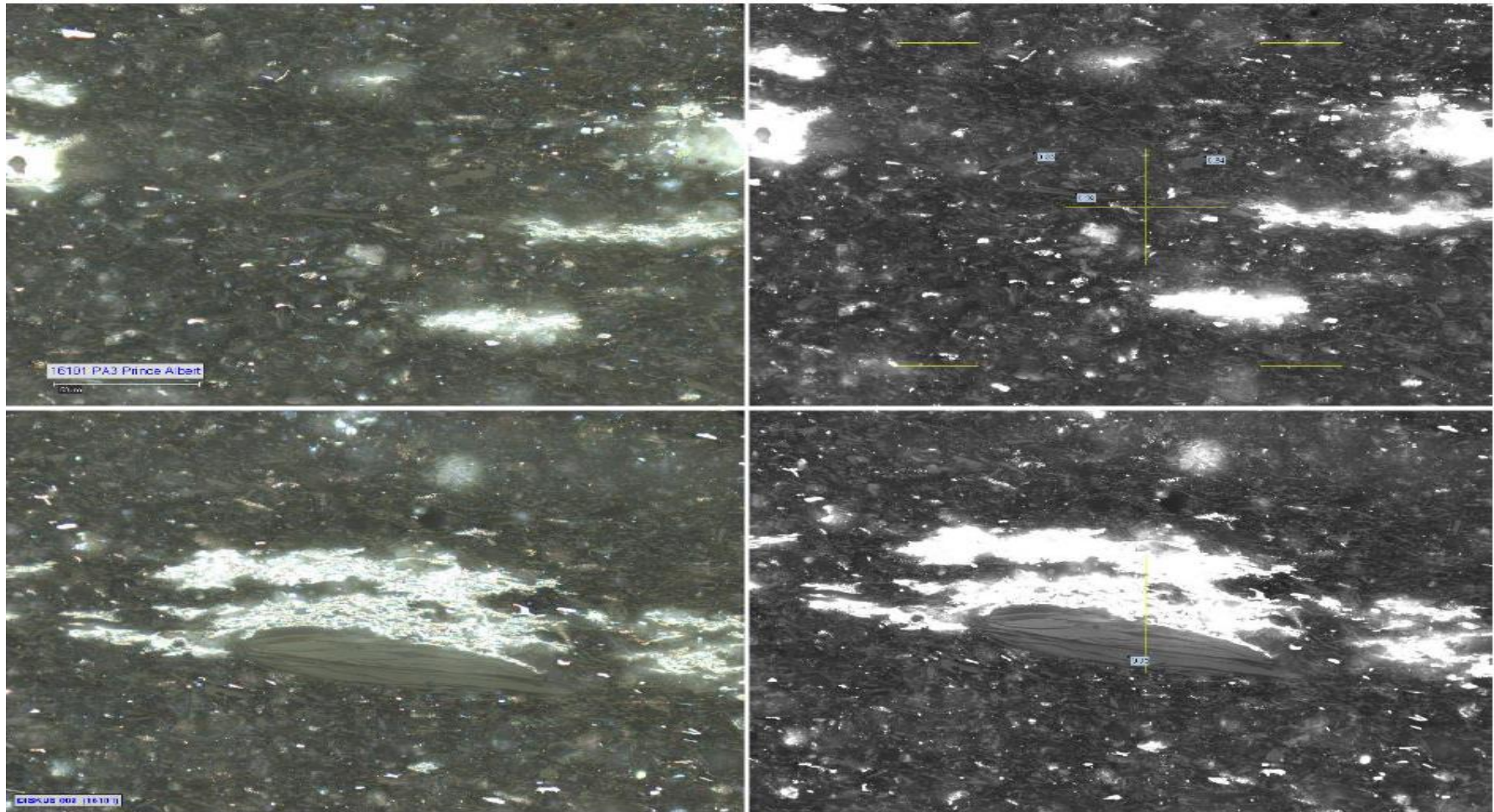
Figure C5: Dispersed organic matter assessment for sample RK 1 (Ripon Formation) from borehole KWV 1. TOC: 0.68 wt.%.

Comments: Fine mudstone with 'woody' fragments, and unusual inclusions. Inertinite fragments – rare - , but no vitrinite.

Figure C6: Dispersed organic matter assessment for sample WK8 (Whitehill Formation) from borehole KWV 1. TOC: 2.36 wt.%. Average %Ro: 3.437, %Ro standard deviation: 0.427. %Ro range: 2.431– 4.291%.

Comments: More organic matter than sample above (Figure C5). This is also confirmed by higher TOC. Mesh network of organic matter, possibly a bitumen mat. Very low fluorescence. Pyrite appears more crystalline.
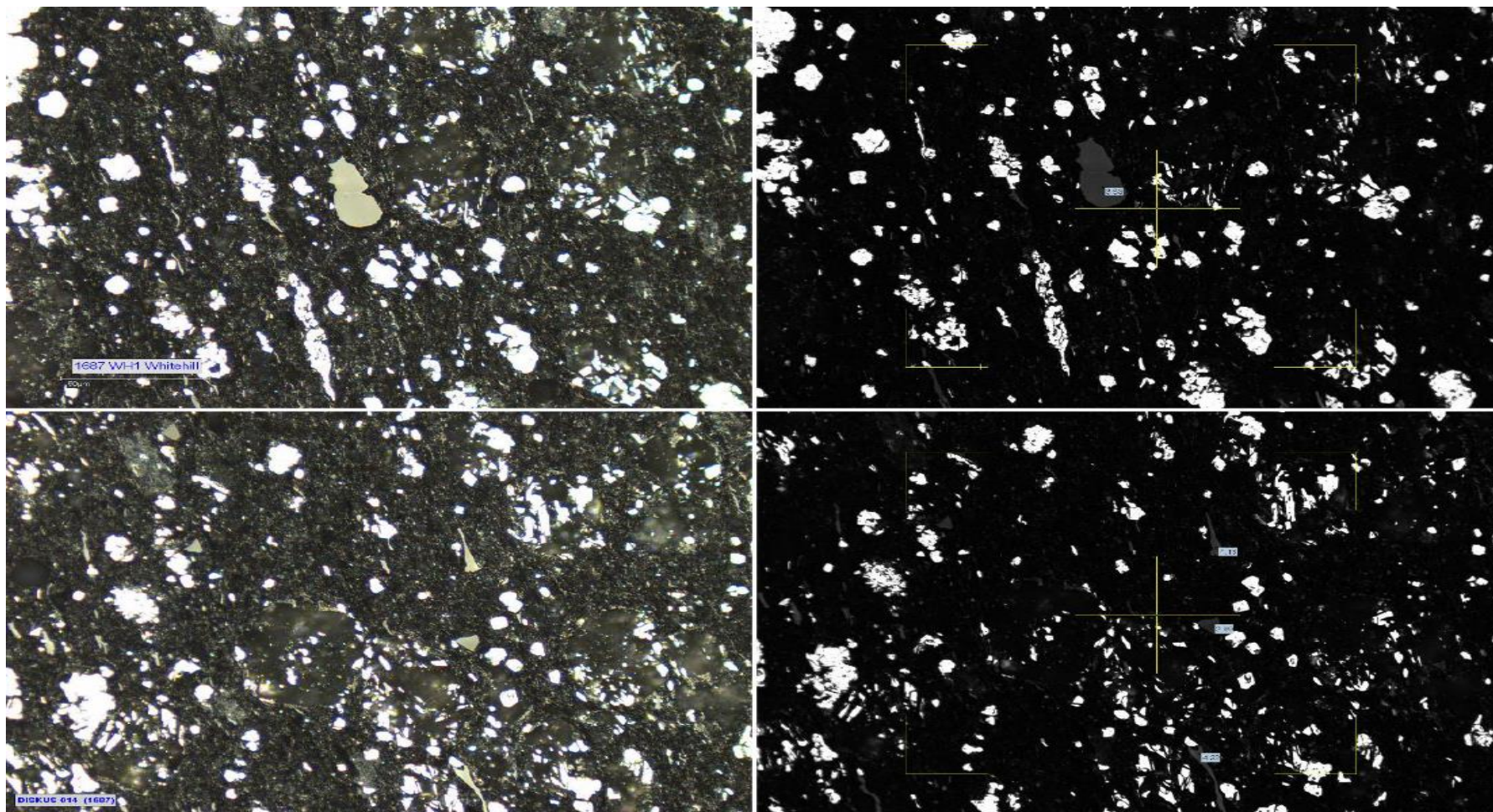
Figure C7: Dispersed organic matter assessment for sample WK7 (Whitehill Formation) from borehole KWV 1. TOC: 2.07 wt.%. Average %Ro: 3.55, %Ro standard deviation: 0.486, %Ro Range: 2.52 – 4.468%.

Comments: Lots of pyrite; readings possibly not taken only on vitrinite due to limited number of particles and difficult to discern vitrinite.
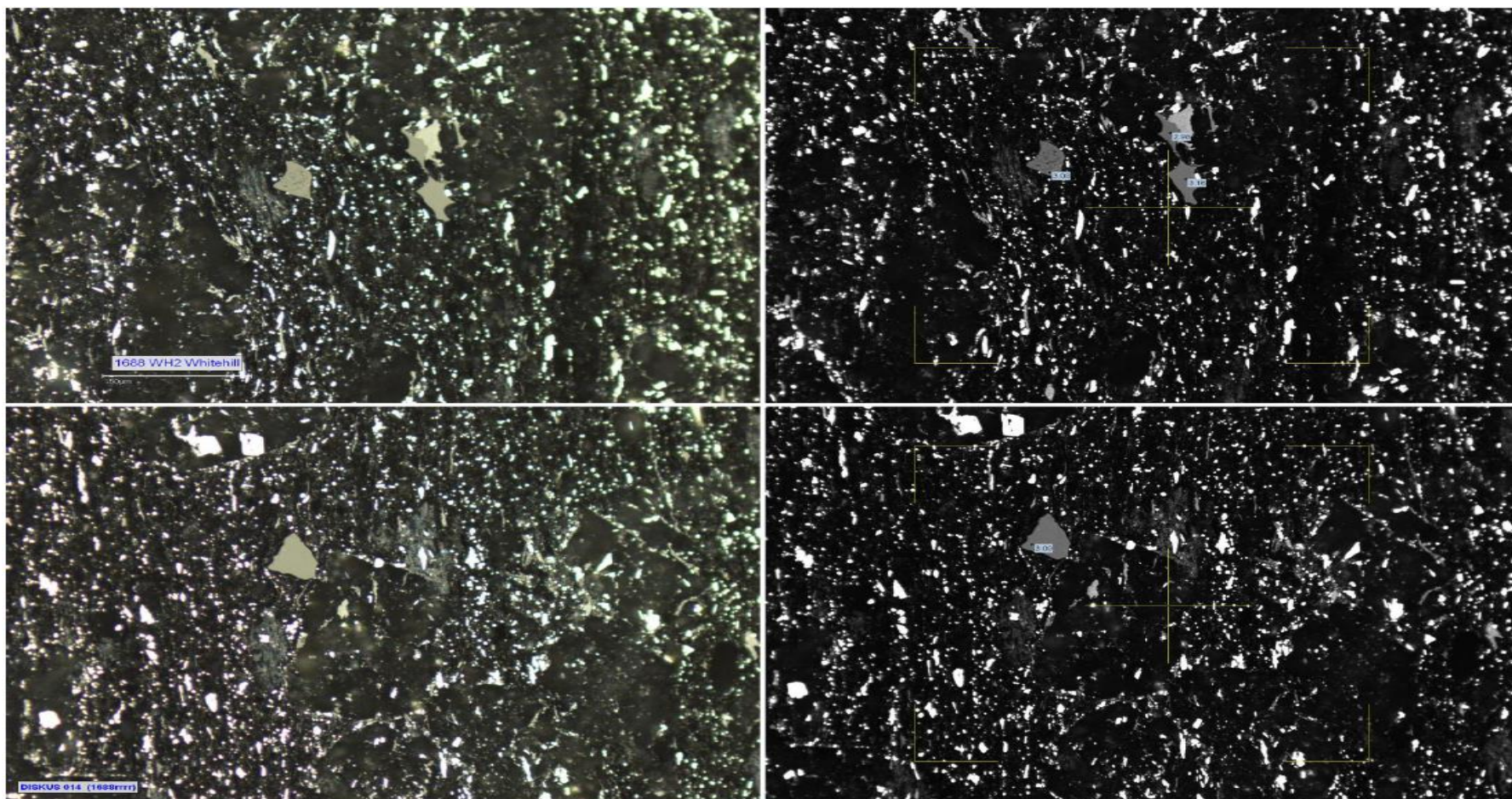
Figure C8: Dispersed organic matter assessment for sample WK6 (Whitehill Formation) from borehole KWV 1. TOC: 2.28 wt.%. Average %Ro: 3.489, %Ro standard deviation: 0.303, %Ro range: 2.93 – 4.21%.

Comments: Lots of pyrite; readings possibly not taken only on vitrinite due to limited number of particles and difficult to discern vitrinite.
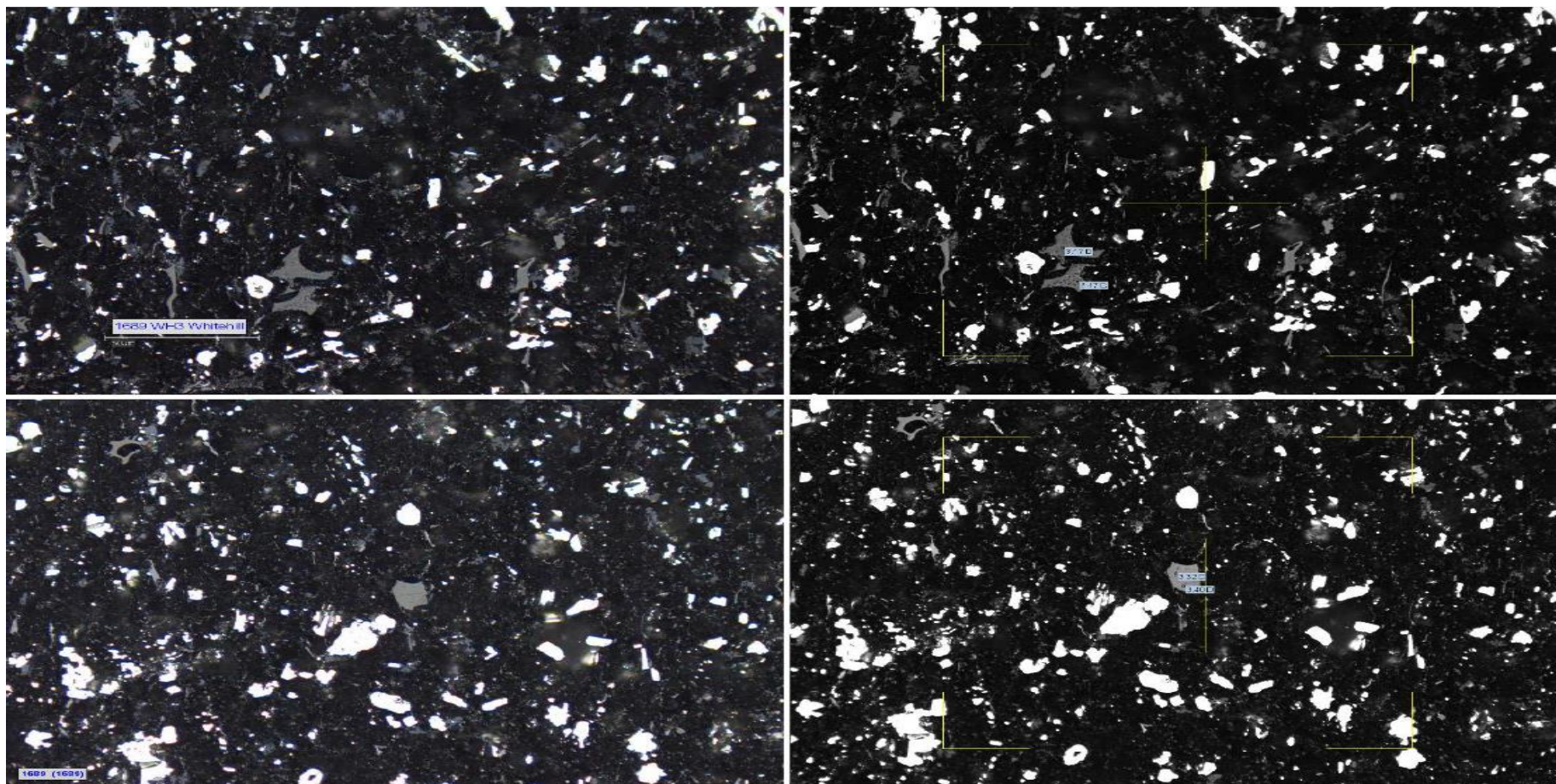
Figure C9: Dispersed organic matter assessment for sample WK5 (Whitehill Formation) from borehole KWV 1. TOC: 2.06 wt.%. Average %Ro: 3.692, %Ro standard deviation: 0.333, %Ro range: 1.756 – 4.179%.

Comments: Lots of small, finely disseminated pyrite; blobs of solid bitumen. Rare evidence of possible devolatilisation in vitrinite-like particles, with pore development (top two images). Network of bitumen.
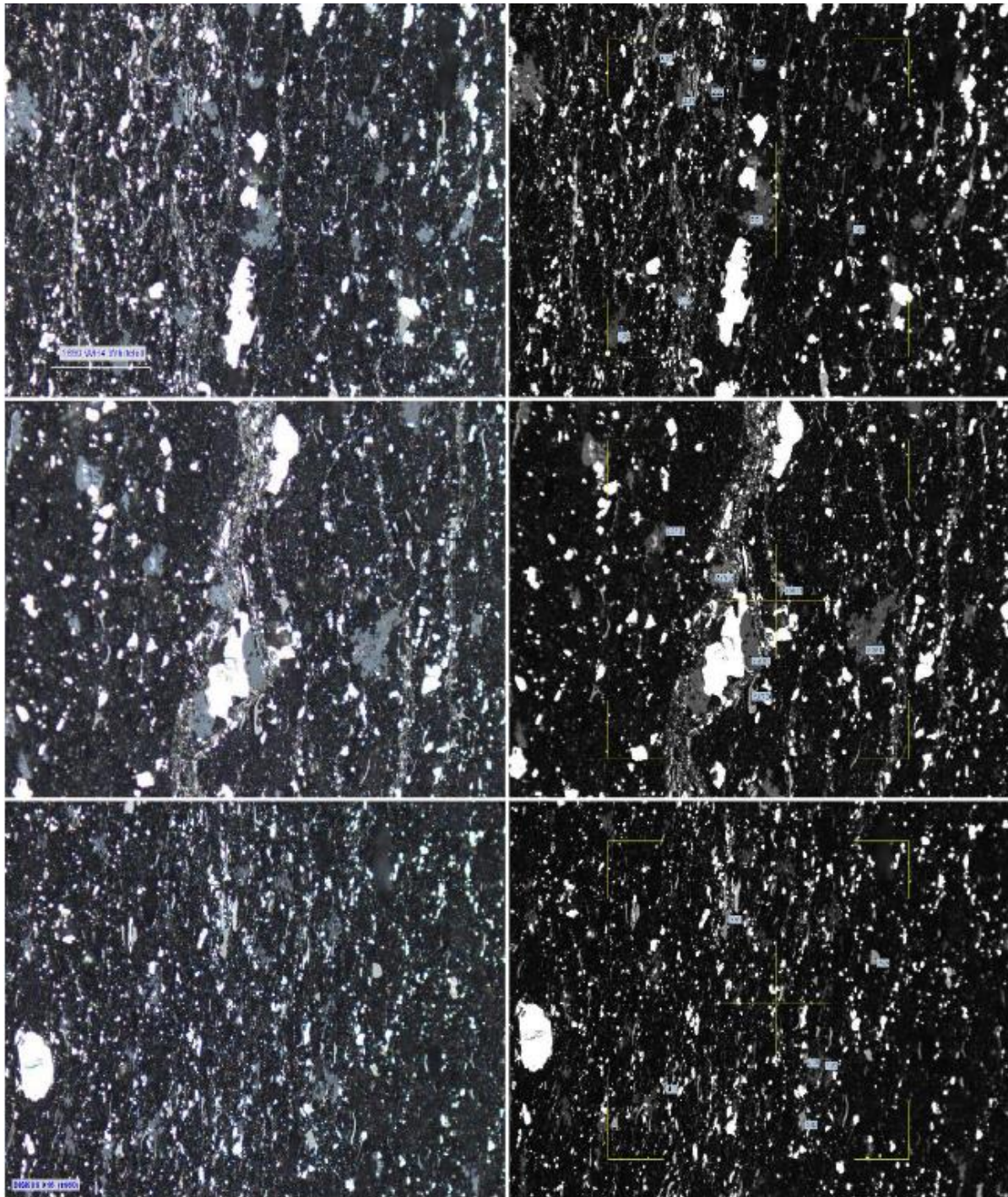
Figure C10: Dispersed organic matter assessment for sample WK4 (Whitehill Formation) from borehole KWV 1. TOC: 1.72 wt.%. Average %Ro: 2.216, %Ro standard deviation: 0.243. %Ro range: 1.655 – 2.586%.

Comments: Lots of pyrite; organic matter differs from above samples. Lots of solid bitumen (bluish colour) not observed in samples above. Lot of organic fragments, possibly limited vitrinite. Lower Ro value may be due to readings taken on solid bitumen and not vitrinite.
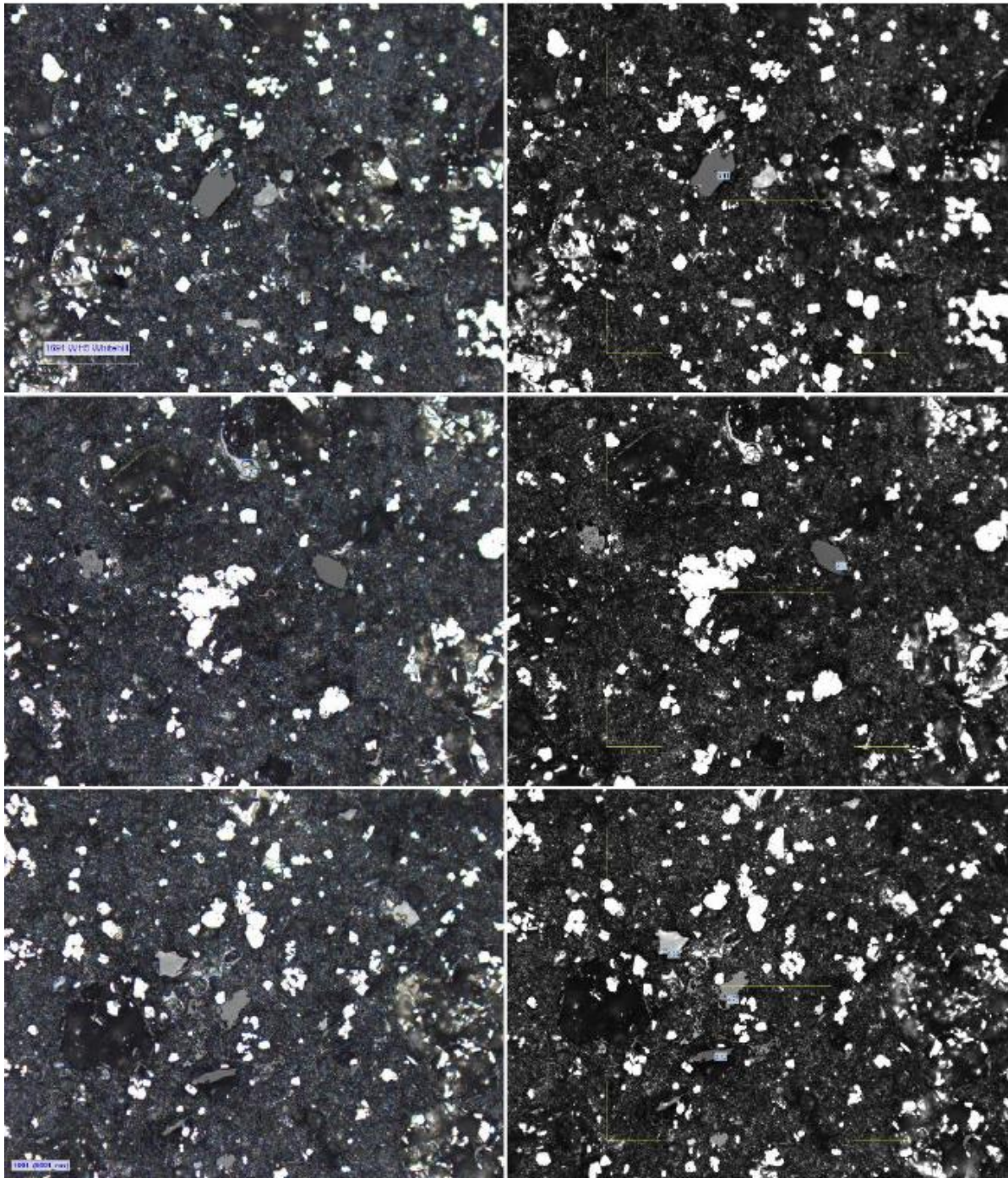
Figure C11: Dispersed organic matter assessment for sample WK2 (Whitehill Formation) from borehole KWV 1. TOC: 2.42 wt.%. Average %Ro: 3.241, %Ro standard deviation: 0.280. %Ro range: 2.671-4.457%.

Comments: Lots of pyrite; possibly a reworked solid bitumin matrix. No blue solid bitumen observed, but clear differentiation between organic matter – inertinite and vitrinite. Possibly the only sample with clear vitrinite.
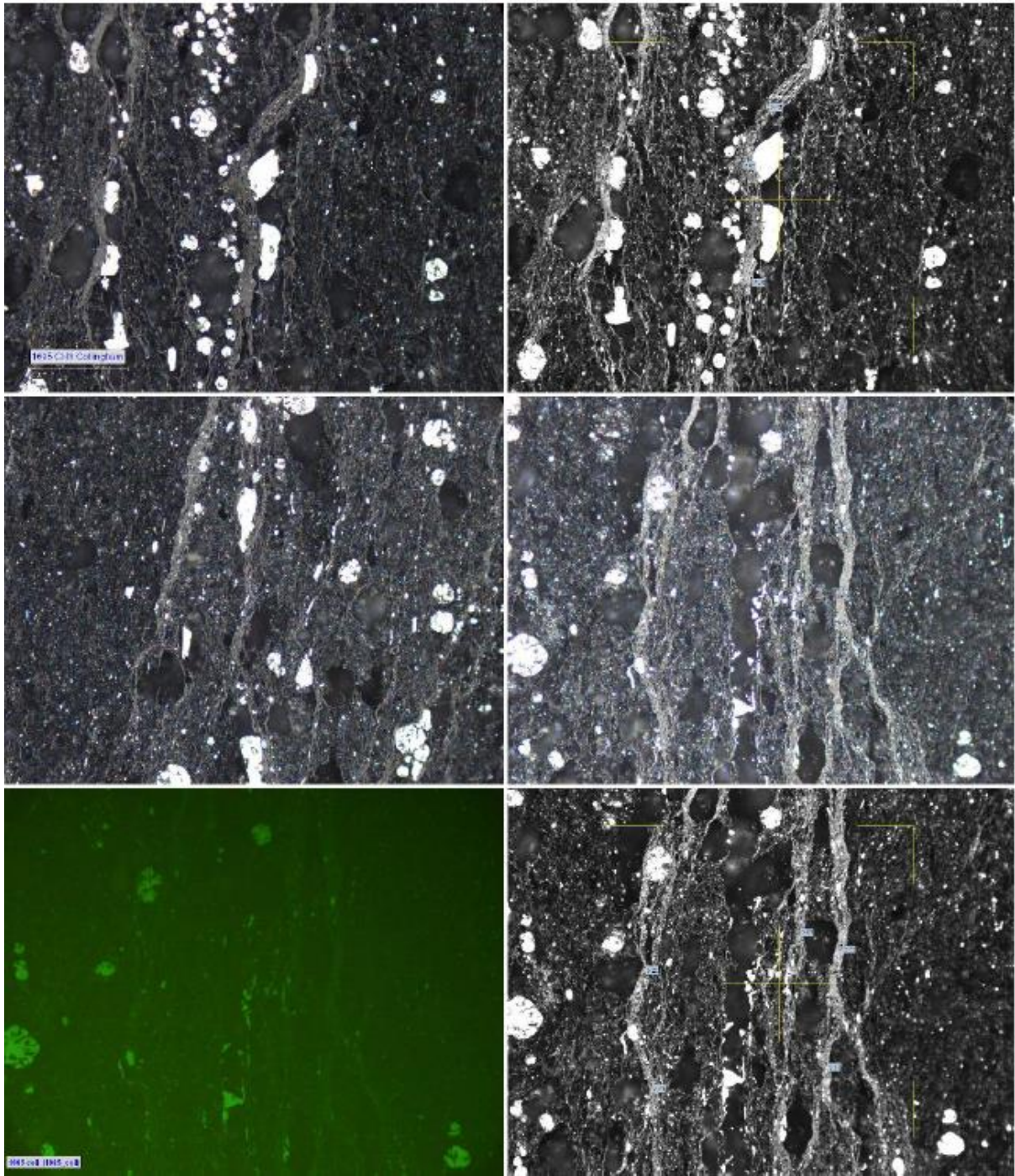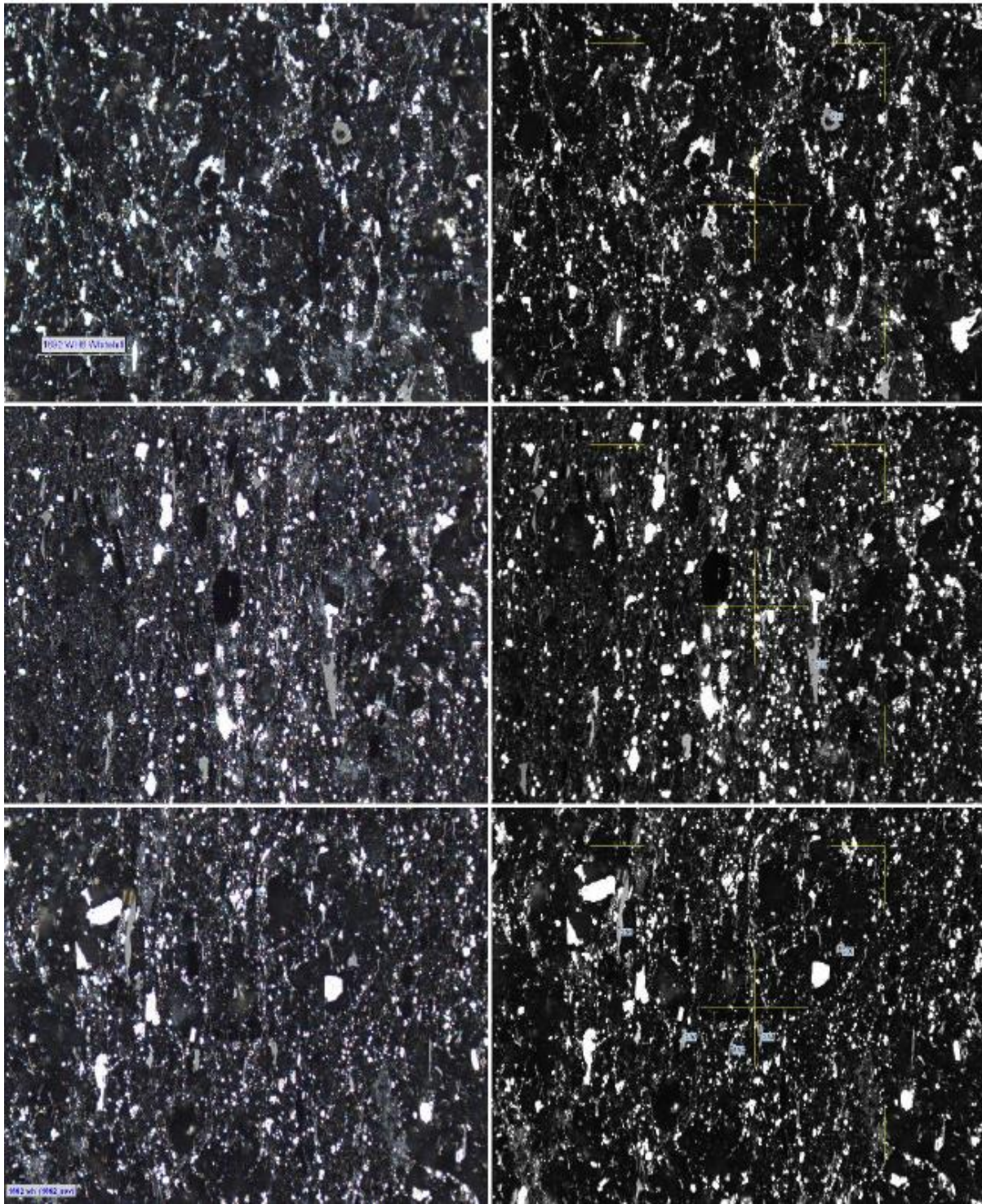
Figure C12: Dispersed organic matter assessment for sample WK1 (Whitehill Formation) from borehole KWV 1. TOC: 3.02 wt.%. Average %Ro: 3.526, %Ro standard deviation: 0.276. %Ro range: 2.97 – 4.017%.

Comments: Lots of small, finely disseminated pyrite; blobs of solid bitumen. Rare evidence of possible devolatilisation in vitrinite-like particles, with pore development (top two images). Network of bitumen.
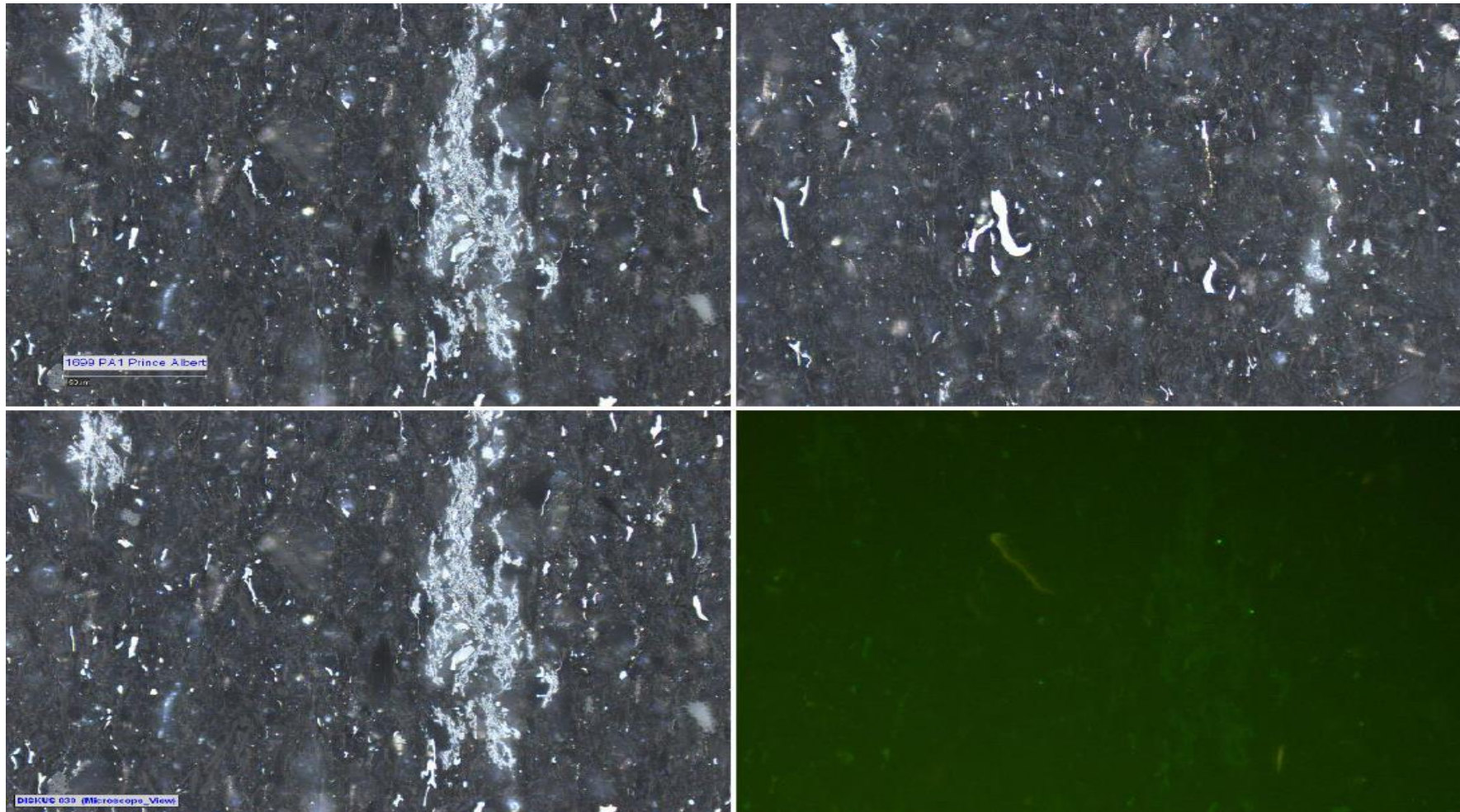
Figure C13: Dispersed organic matter assessment for sample PK 3 (Prince Albert Formation) from borehole KWV 1. TOC: 1.04 wt.%.

Comments: Inertinite fragments – rare - , but no vitrinite. Fine mudstone with unusual white mineral inclusions.
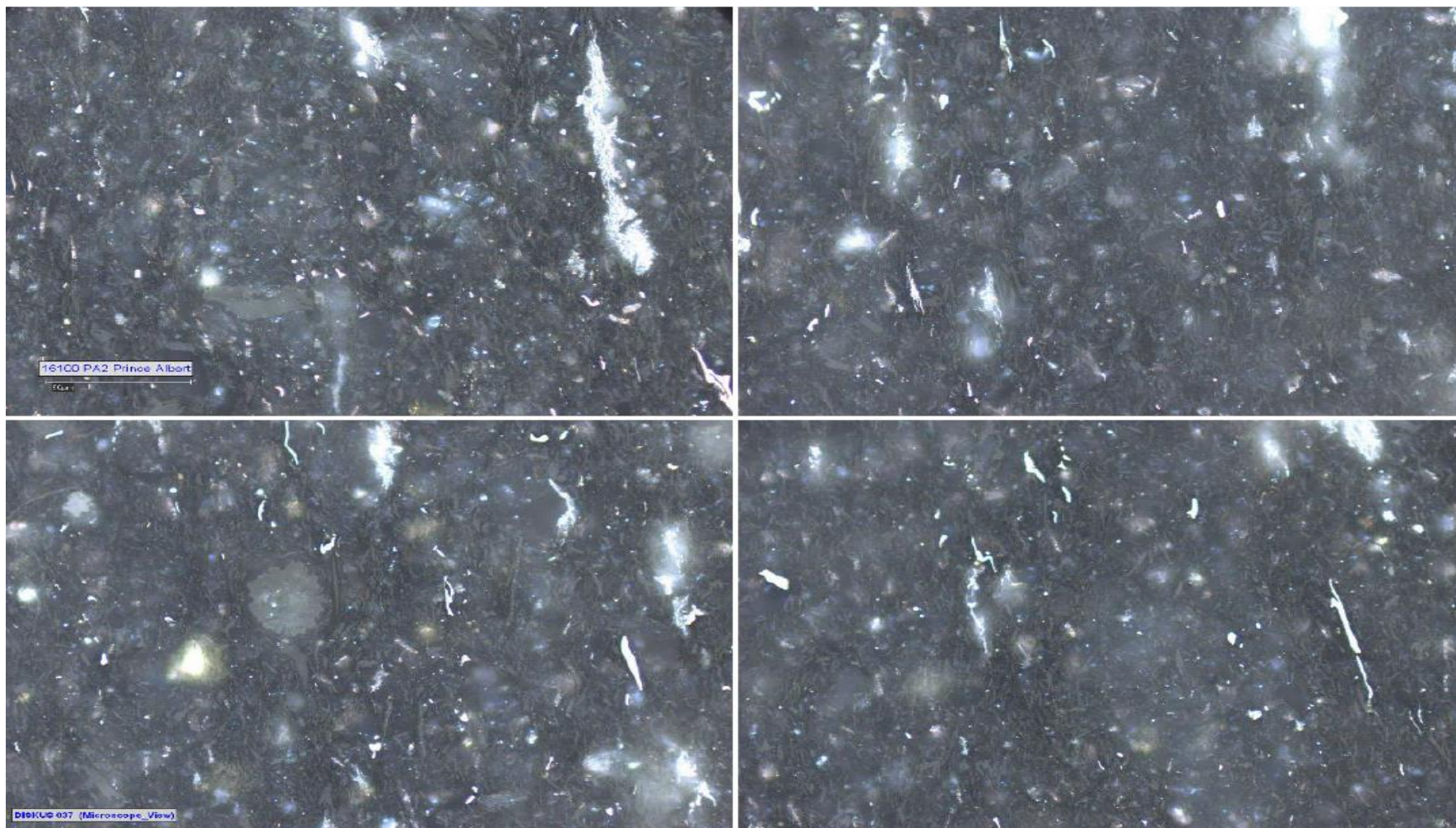
Figure C14: Dispersed organic matter assessment for sample PK 2 (Prince Albert Formation) from borehole KWV 1. TOC: 0.98 wt.%.

Comments: Inertinite fragments – rare - , but no vitrinite. Fine mudstone with carbon and quartz inclusions.

Figure C15: Dispersed organic matter assessment for sample RS2 (Ripon Formation) from borehole SP 1/69. TOC: 1.72 wt.%.

Comments: No vitrinite determined; no fluorescence determined. Similar "woody fragments" as the Prince Albert Formation. Rare inertinite particle. Lots of worm holes, some infilled with minerals. Very fine mudstone with quartz inclusions. Possible solid bitumen occurrence.
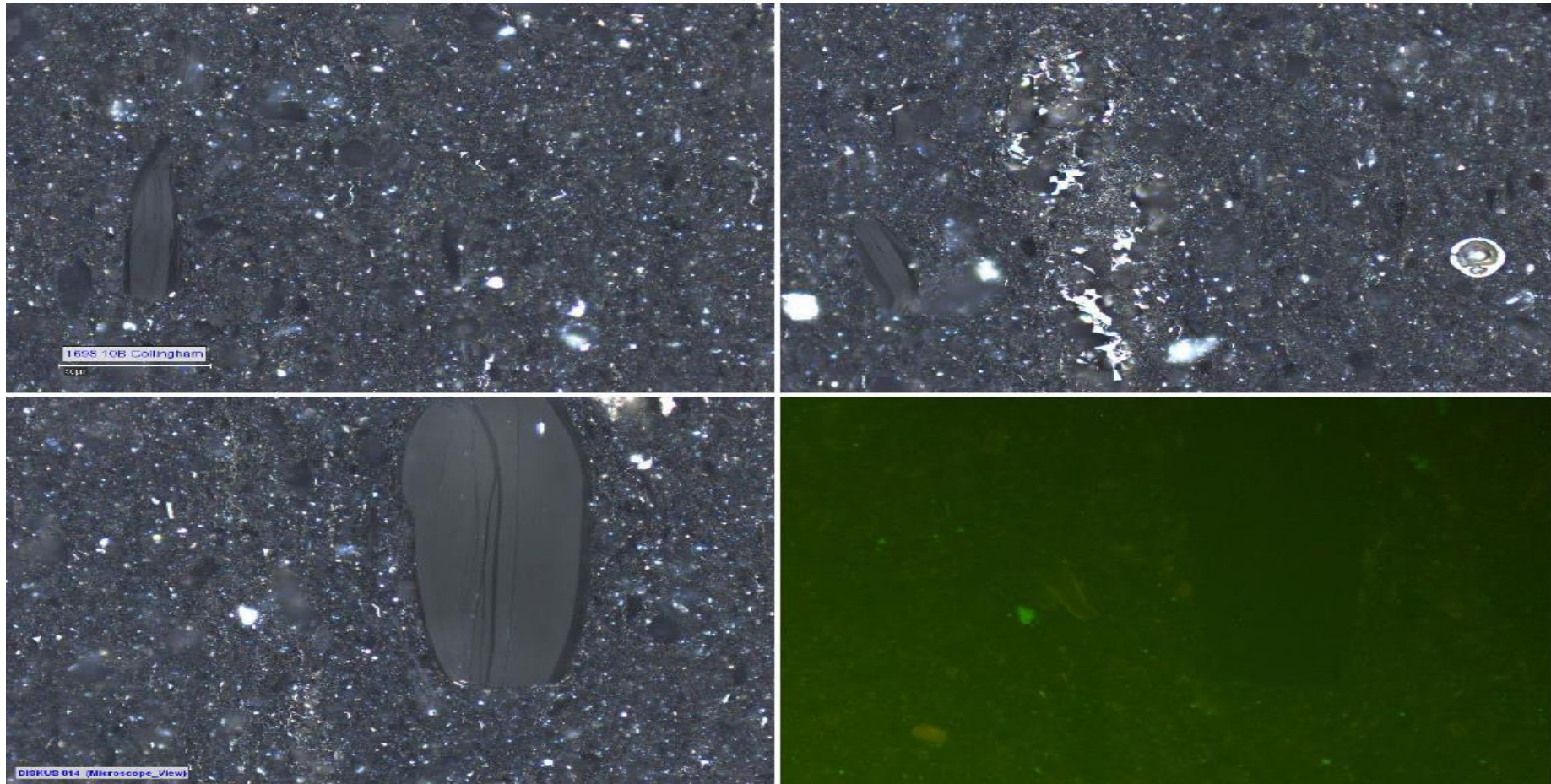
Figure C16: Dispersed organic matter assessment for sample CS1 (Collingham Formation) from borehole SP 1/69. TOC: 0.93 wt.%.

Comments: Less organic matter than above sample, but no apparent vitrinite. Rare inertinite fragments. Fluorescence component possibly carbon minerals. Interesting inclusions, possibly carbonates. Similar inclusion seen in sample RS2.
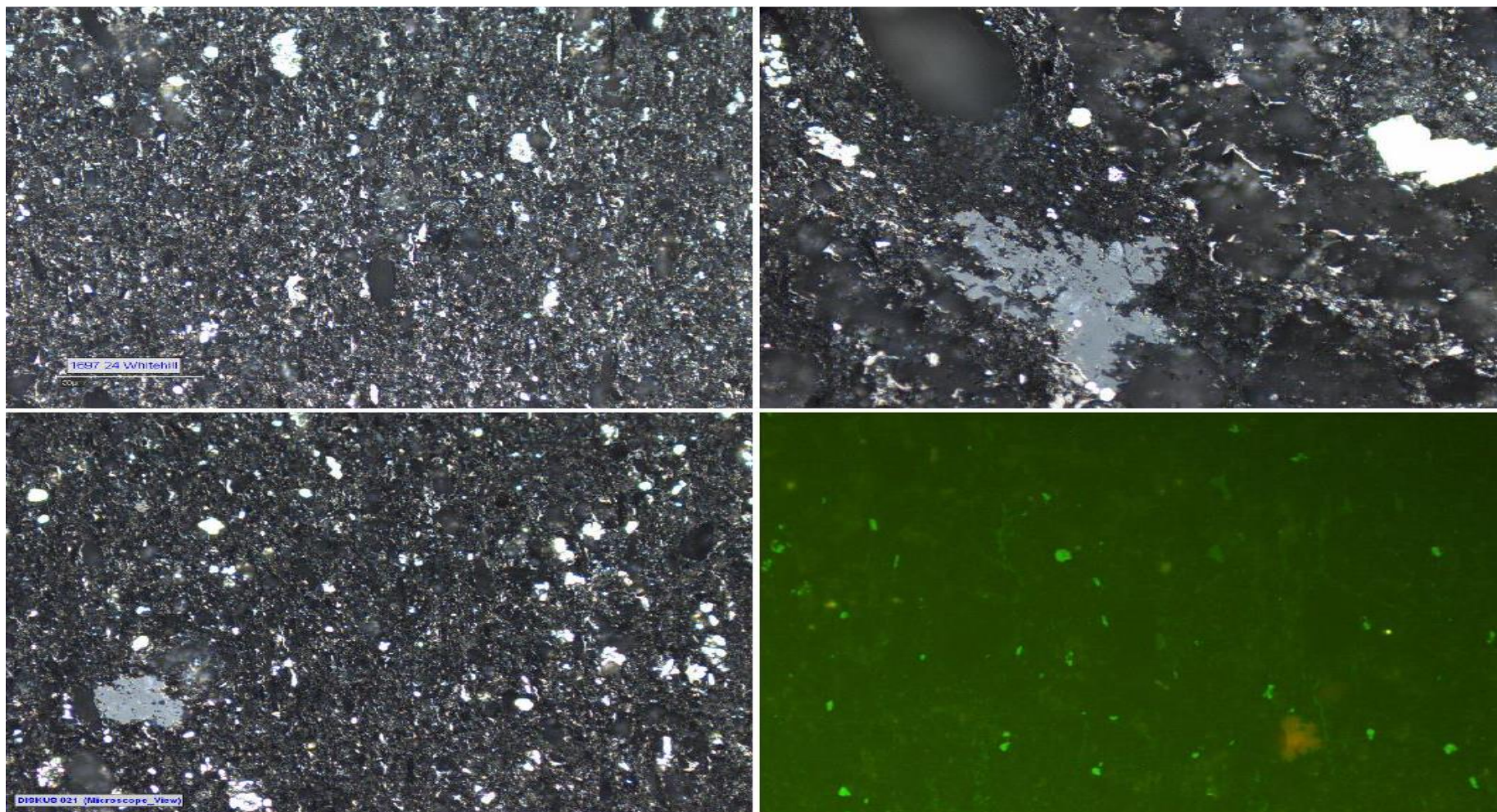
Figure C17: Dispersed organic matter assessment for sample WS2 (Whitehill Formation) from borehole SP 1/69. TOC: 5.60 wt.%.

Comments: Lots of organic matter, but no apparent vitrinite. Inertinite fragments and large solid bitumen, which does fluoresce as shown above.
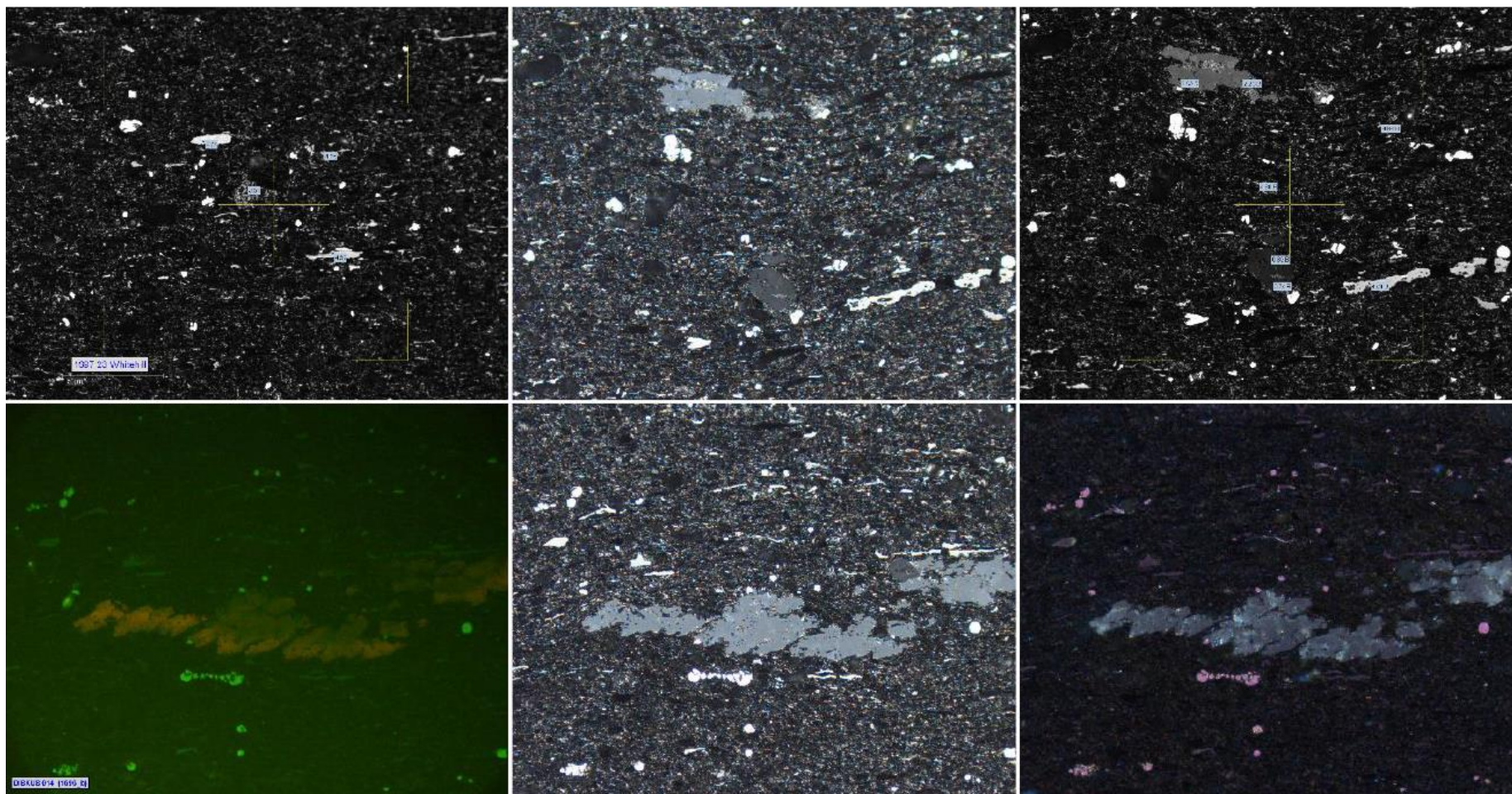
Figure C17: Dispersed organic matter assessment for sample WS1 (Whitehill Formation) from borehole SP 1/69. TOC: 7.30 wt.%.

Comments: Lots of organic matter than sample above (WS2), but no vitrinite. Inertinite fragments and large solid bitumen which does fluoresce as shown above.

461

C (ii) Rock Eval-6 pyrograms

RK6 (BOREHOLE KWV1)

RK5 (BOREHOLE KWV1)

RK4 (BOREHOLE KWV1)

WK7 (BOREHOLE KWV1)

WK1 (BOREHOLE KWV1)

WK8 (BOREHOLE KWV1)

WK6 (BOREHOLE KWV1)

WK5 (BOREHOLE KWV1)

462
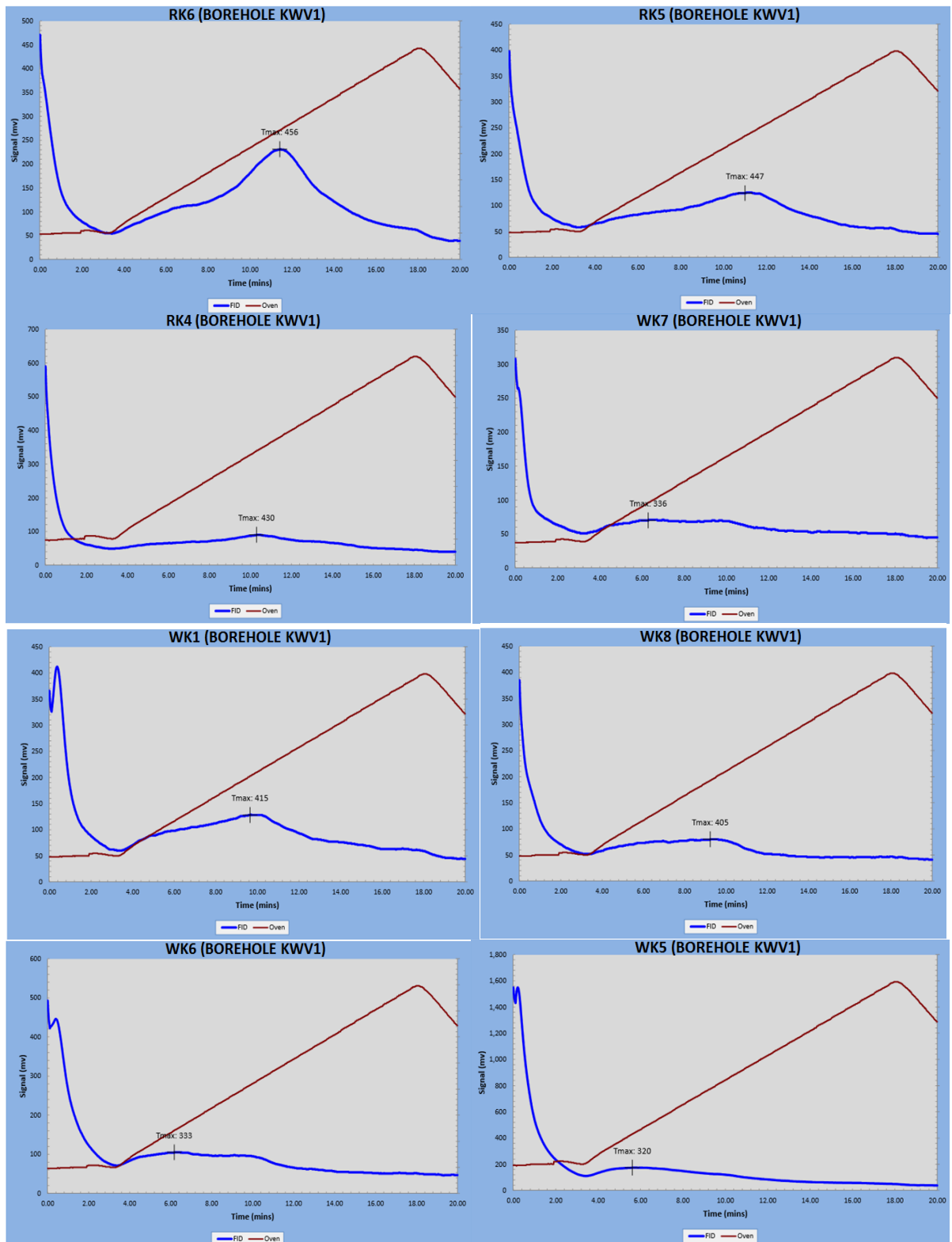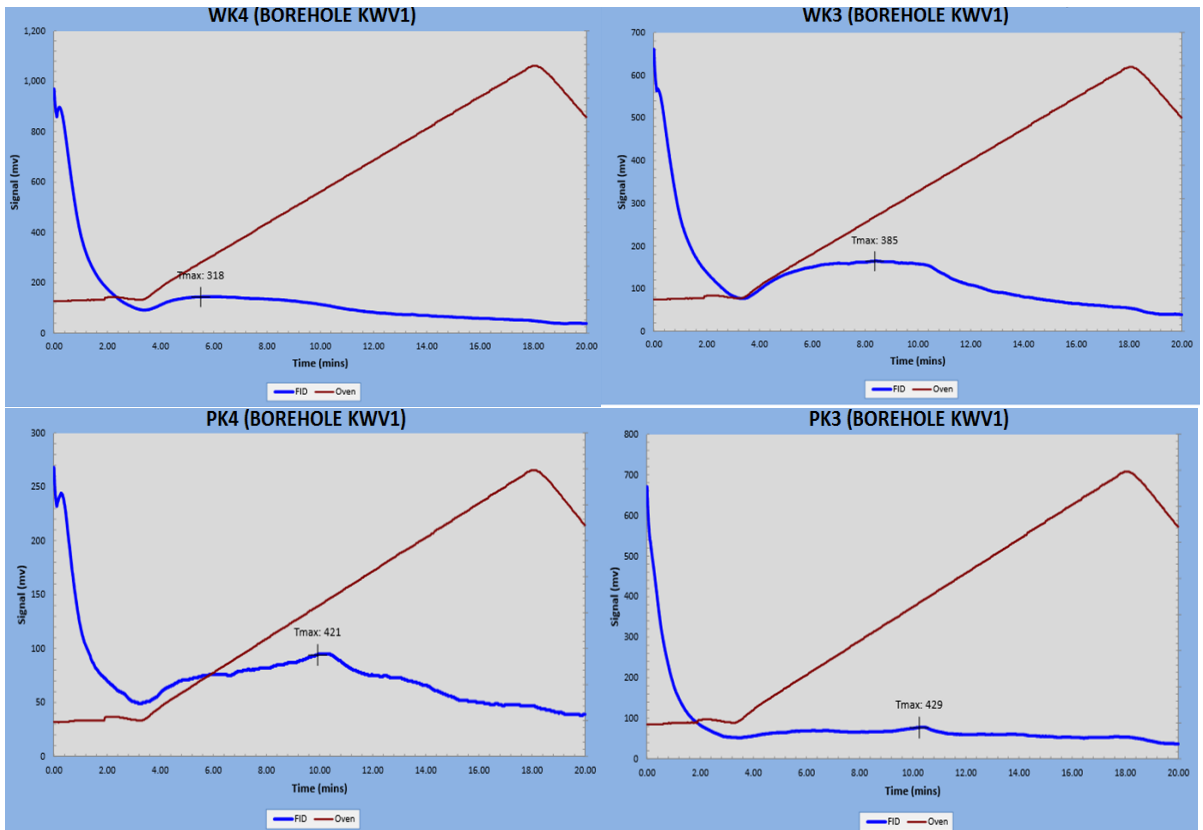
Rock Eval-6 pyrograms for some Ecca shale samples from the borehole KWV 1

APPENDIX D: Subsidence Analysis

Data input

Bases should be deeper than tops, and the depth, age, sea level and water depths at the base of a given unit are equal to the depth, age, sea level and water depth at the top of the unit immediately below (see table below).

- Unit base (base) and top (top) as depths (km) from the ground surface.
- The age of unit base (Ageb) and the unit top (Aget) in Ma
- Sea-level at the time of deposition of the unit base (SLb) and top (SLt) in km sediment load.
- The sea-level is reported relative to present sea-level, positive numbers indicate above present sea-level, while negative numbers below sea
- Water depth at the time of deposition of the unit base (WDb) and top (WDt) in Km, WD should be positive numbers
- Porosity coefficient (C) in Km^{-1} is between 0-1.
- Grain density (ρc) in Kgm^{-3}. The dry density is a positive number.
- Surface porosity ($\emptyset_0$) as percentage %, between 0-100.

Table D1: Data input table for borehole CR 1/68 (without palaeobathymetric corrections) for the backstripping and plotting of the subsidence curve on OSXBackstrip programme.

Name	Base	Ageb	SLb	WDb	Top	Aget	SLt	WDt	ρc	c	$\emptyset_0$	type
Dwyka	4.283	302	0	0	3.780	289	0	0	2600	0.45	56%	1
Prince Albert	3.780	289	0	0	3.705	276	0	0	2720	0.51	63%	1
Whitehill	3.705	276	0	0	3.670	275	0	0	2720	0.51	63%	1
Collingham	3.670	275	0	0	3.630	273	0	0	2720	0.51	63%	1
Ripon	3.630	273	0	0	3.070	268	0	0	2700	0.45	56%	1
Fort Brown	3.070	268	0	0	2.140	264	0	0	2720	0.51	63%	1

Table D2: Data input table for borehole CR 1/68 (with palaeobathymetric corrections) for the backstripping and plotting of the subsidence curve on OSXBackstrip programme.

Name	Base	Ageb	SLb	WDb	Top	Aget	SLt	WDt	ρc	c	$\emptyset_o$	type
Dwyka	4.283	302	140	500	3.780	289	110	400	2600	0.45	56%	1
Prince Albert	3.780	289	110	400	3.705	276	90	300	2720	0.51	63%	1
Whitehill	3.705	276	90	300	3.670	275	80	220	2720	0.51	63%	1
Collingham	3.670	275	80	220	3.630	273	62	180	2720	0.51	63%	1
Ripon	3.630	273	60	180	3.070	268	20	30	2700	0.45	56%	1
Fort Brown	3.070	268	20	30	2.140	264	0	0	2720	0.51	63%	1

Table D3: Data input table for borehole SC 3/67 (without palaeobathymetric corrections) for the backstripping and plotting of the subsidence curve on OSXBackstrip programme.

Name	Base	Ageb	SLb	WDb	Top	Aget	SLt	WDt	ρc	c	$\emptyset_o$	type
Dwyka	5.343	302	0	0	4.346	289	0	0	2600	0.45	56%	1
Prince Albert	4.346	289	0	0	4.023	276	0	0	2720	0.51	63%	1
Whitehill	4.023	276	0	0	3.972	275	0	0	2720	0.51	63%	1
Collingham	3.972	275	0	0	3.901	273	0	0	2720	0.51	63%	1
Ripon	3.901	273	0	0	3.734	268	0	0	2700	0.45	56%	1
Fort Brown	3.734	268	0	0	3.684	264	0	0	2720	0.51	63%	1

Table D4: Data input table for borehole SC 3/67 (with palaeobathymetric corrections) for the backstripping and plotting of the subsidence curve on OSXBackstrip programme.

Name	Base	Ageb	SLb	WDb	Top	Aget	SLt	WDt	ρc	c	$\emptyset_o$	type
Dwyka	5.343	302	140	500	4.346	289	110	400	2600	0.45	56%	1
Prince Albert	4.346	289	110	400	4.023	276	90	300	2720	0.51	63%	1
Whitehill	4.023	276	90	300	3.972	275	80	220	2720	0.51	63%	1
Collingham	3.972	275	80	220	3.901	273	62	180	2720	0.51	63%	1
Ripon	3.901	273	60	180	3.734	268	20	30	2700	0.45	56%	1
Fort Brown	3.734	268	20	30	3.684	264	0	0	2720	0.51	63%	1

Table D5: Data input table Ecca Pass section (without palaeobathymetric corrections) for the backstripping and plotting of the subsidence curve on OSXBackstrip programme.

Name	Base	Ageb	SLb	WDb	Top	Aget	SLt	WDt	ρc	c	$\emptyset_o$	type
Dwyka	2.358	302	0	0	2.208	289	0	0	2600	0.45	56%	1
Prince Albert	2.208	289	0	0	2.058	276	0	0	2720	0.51	63%	1
Whitehill	2.058	276	0	0	1.915	275	0	0	2720	0.51	63%	1
Collingham	1.915	275	0	0	1.874	273	0	0	2720	0.51	63%	1
Ripon	1.874	273	0	0	0.910	268	0	0	2700	0.45	56%	1
Fort Brown	0.910	268	0	0	0.010	264	0	0	2720	0.51	63%	1

Table D6: Data input table for Ecca Pass section (with palaeobathymetric corrections) for the Backstripping and plotting of the subsidence curve on OSXBackstrip programme.

Name	Base	Ageb	SLb	WDb	Top	Aget	SLt	WDt	ρc	c	$\emptyset_o$	type
Dwyka	2.358	302	140	500	2.208	289	110	400	2600	0.45	56%	1
Prince Albert	2.208	289	110	400	2.058	276	90	300	2720	0.51	63%	1
Whitehill	2.058	276	90	300	1.915	275	80	220	2720	0.51	63%	1
Collingham	1.915	275	80	220	1.874	273	62	180	2720	0.51	63%	1
Ripon	1.874	273	60	180	0.910	268	20	30	2700	0.45	56%	1
Fort Brown	0.910	268	20	30	0.010	264	0	0	2720	0.51	63%	1

Table D7: Data input table for borehole SFT 2 (without palaeobathymetric corrections) for the Backstripping and plotting of the subsidence curve on OSXBackstrip programme.

Name	Base	Ageb	SLb	WDb	Top	Aget	SLt	WDt	ρc	c	$\emptyset_o$	type
Dwyka	0.300	302	0	0	0.291	289	0	0	2600	0.45	56%	1
Prince Albert	0.291	289	0	0	0.226	276	0	0	2720	0.51	63%	1
Whitehill	0.226	276	0	0	0.200	275	0	0	2720	0.51	63%	1
Collingham	0.200	275	0	0	0.165	273	0	0	2720	0.51	63%	1
Ripon	0.165	273	0	0	0.000	268	0	0	2700	0.45	56%	1

Table D8: Data input table for borehole SFT 2 (with palaeobathymetric corrections) for the Backstripping and plotting of the subsidence curve on OSXBackstrip programme.

Name	Base	Ageb	SLb	WDb	Top	Aget	SLt	WDt	ρc	c	$\emptyset_o$	type
Dwyka	0.300	302	140	500	0.291	289	110	400	2600	0.45	56%	1
Prince Albert	0.291	289	110	400	0.226	276	90	300	2720	0.51	63%	1
Whitehill	0.226	276	90	300	0.200	275	80	220	2720	0.51	63%	1
Collingham	0.200	275	80	220	0.165	273	62	180	2720	0.51	63%	1
Ripon	0.165	273	60	180	0.000	268	20	30	2700	0.45	56%	1

Table D9: Data input table for borehole KWV 1 (with palaeobathymetric corrections) for the Backstripping and plotting of the subsidence curve on OSXBackstrip programme.

Name	Base	Ageb	SLb	WDb	Top	Aget	SLt	WDt	ρc	c	$\emptyset_o$	type
Dwyka	2.758	302	140	500	2.340	289	110	400	2600	0.45	56%	1
Prince Albert	2.340	289	110	400	2.308	276	90	300	2720	0.51	63%	1
Whitehill	2.308	276	90	300	2.295	275	80	220	2720	0.51	63%	1
Collingham	2.295	275	80	220	2.205	273	62	180	2720	0.51	63%	1
Ripon	2.205	273	60	180	0.919	268	20	30	2700	0.45	56%	1
Fort Brown	0.919	268	20	30	0.265	264	0	0	2720	0.51	63%	1

Table D10: Data input table for borehole KWV 1 (without palaeobathymetric corrections) for the Backstripping and plotting of the subsidence curve on OSXBackstrip programme.

Name	Base	Ageb	SLb	WDb	Top	Aget	SLt	WDt	ρc	c	$\emptyset_o$	type
Dwyka	2.758	302	0	0	2.340	289	0	0	2600	0.45	56%	1
Prince Albert	2.340	289	0	0	2.308	276	0	0	2720	0.51	63%	1
Whitehill	2.308	276	0	0	2.295	275	0	0	2720	0.51	63%	1
Collingham	2.295	275	0	0	2.205	273	0	0	2720	0.51	63%	1
Ripon	2.205	273	0	0	0.919	268	0	0	2700	0.45	56%	1
Fort Brown	0.919	268	0	0	0.265	264	0	0	2720	0.51	63%	1

Table D11: Data input table for borehole SP 1/69 (with palaeobathymetric corrections) for the Backstripping and plotting of the subsidence curve on OSXBackstrip programme.

Name	Base	Ageb	SLb	WDb	Top	Aget	SLt	WDt	ρc	c	$\emptyset_o$	type
Dwyka	4.248	302	140	500	3.728	289	110	400	2600	0.45	56%	1
Prince Albert	3.728	289	110	400	3.688	276	90	300	2720	0.51	63%	1
Whitehill	3.688	276	90	300	3.653	275	80	220	2720	0.51	63%	1
Collingham	3.653	275	80	220	3.630	273	62	180	2720	0.51	63%	1
Ripon	3.630	273	60	180	2.702	268	20	30	2700	0.45	56%	1
Fort Brown	2.702	268	20	30	2.100	264	0	0	2720	0.51	63%	1

Table D12: Data input table for borehole SP 1/69 (without palaeobathymetric corrections) for the Backstripping and plotting of the subsidence curve on OSXBackstrip programme.

Name	Base	Ageb	SLb	WDb	Top	Aget	SLt	WDt	ρc	c	$\emptyset_o$	type
Dwyka	4.248	302	0	0	3.728	289	0	0	2600	0.45	56%	1
Prince Albert	3.728	289	0	0	3.688	276	0	0	2720	0.51	63%	1
Whitehill	3.688	276	0	0	3.653	275	0	0	2720	0.51	63%	1
Collingham	3.653	275	0	0	3.630	273	0	0	2720	0.51	63%	1
Ripon	3.630	273	0	0	2.702	268	0	0	2700	0.45	56%	1
Fort Brown	2.702	268	0	0	2.100	264	0	0	2720	0.51	63%	1

The subsidence of a sedimentary basin can be attributed to three processes: tectonic subsidence, water and sediment loading, and sediment compaction. These three components of subsidence can be estimated from a stratigraphic section using a procedure called "backstripping" (Allen and Allen, 1990). Backstripping removes from each sedimentary layer the effects of sediment compaction, water and sediment loading; thus extracting from the section tectonic subsidence curve. OSXBackstrip is a program to perform "1D Airy backstripping with exponential reduction of porosity". Stratigraphic units can be easily input in a table, and backstripping and tectonic subsidence plots and tables can be rapidly produced (Figure D1).
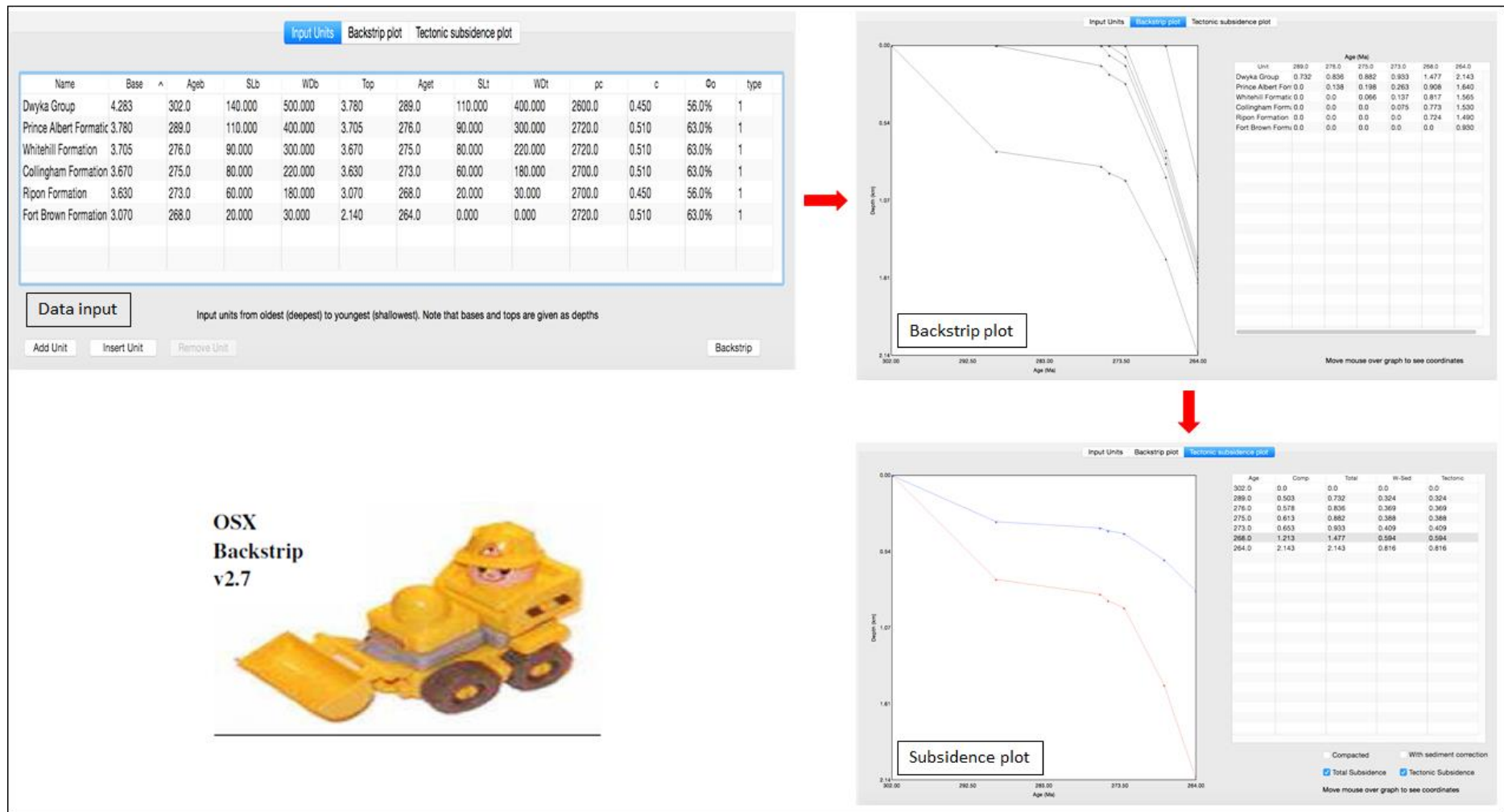
Figure D1: The OSXBackstrip Program description and work flow (http://homepage.mac.com/nfcd/work/programs.html). The software formulas are based on Allen and Allen (1990), and Watts (2001).